Technical Memorandum:

Delta Risk Management Strategy (DRMS) Phase 1

Topical Area:

Water Analysis Module (WAM)

Draft 2

Prepared by:
URS Corporation/Jack R. Benjamin & Associates, Inc.

Prepared for:
California Department of Water Resources (DWR)

June 15, 2007

June 15, 2007

Mr. Ralph R. Svetich, P.E.
Delta Risk Management Strategy Project Manager
Department of Water Resources
Division of Flood Management
Delta-Suisun Marsh Office
901 P Street, Suite 313A
Post Office Box 942836
Sacramento, CA 94236-0001

Subject: Delta Risk Management Strategy
Phase 1 Draft 2 Technical Memorandum – Water Analysis Module (WAM)

Dear Mr. Svetich,

Please find herewith a copy of the subject technical memorandum. Members of the Steering Committee's Technical Advisory Committee and agency staff have reviewed the draft technical memorandum and this second draft addresses their comments.

The document was prepared by Will B. Betchart (Jack R. Benjamin and Associates), Walter Bourez (MBK Engineers), John DeGeorge (Resource Management Associates / RMA), Michael Dias and Stacy K. Tanaka (Watercourse Engineering, Inc.), Edward Gross, Michael MacWilliams, and Nicholas Nidzieko (Bay Modeling Hydrodynamics), and Elizabeth Nielsen (URS Corporation). Drs. Said Salah-Mars (URS) and Marty McCann (JBA) reviewed this technical memorandum. Internal peer review was provided in accordance with URS' quality assurance program, as outlined in the (DRMS) project management plan.

Sincerely,

URS Corporation

Said Salah-Mars, Ph.D., P.E.
URS Engineering Division Manager
DRMS Project Manager
1333 Broadway Ave, Suite 800
Oakland, CA 94612
Ph. 510-874-3051
Fax: 510-874-3268

Jack R. Benjamin & Associates, Inc.

Martin W. McCann, Jr., Ph.D.
President JBA
DRMS Technical Manager
530 Oak Grove Ave., Suite 202
Menlo Park, CA 94025
Ph. 650-473-9955

Topical Area: Water Analysis Module (WAM)

Preamble

The Delta Risk Management Strategy (DRMS) project was authorized by DWR to perform a risk analysis of the Delta and Suisun Marsh (Phase 1) and to develop a set of improvement strategies to manage those risks (Phase 2) in response to Assembly Bill 1200 (Laird, Chaptered, September 2005). The Technical Memorandum (TM), is one of 12 TMs (2 topics are presented in one TM: hydrodynamics and water management) prepared for topical areas for Phase 1 of the DRMS project. The topical areas covered in the Phase 1 Risk Analysis include:

1. Geomorphology of the Delta and Suisun Marsh
2. Subsidence of the Delta and Suisun Marsh
3. Seismic Hazards of the Delta and Suisun Marsh
4. Global Warming Effects in the Delta and Suisun Marsh
5. Flood Hazard of the Delta and Suisun Marsh
6. Wind Wave Action of the Delta and Suisun Marsh
7. Levee Vulnerability of the Delta and Suisun Marsh
8. Emergency Response and Repair of the Delta and Suisun Marsh Levees
9. Hydrodynamics of the Delta and Suisun Marsh
10. Water Management and Operation of the Delta and Suisun Marsh
11. Ecological Impacts of the Delta and Suisun Marsh
12. Impact to Infrastructure of the Delta and Suisun Marsh
13. Economic Impacts of the Delta and Suisun Marsh

Note that the Hydrodynamics and Water Quality topical area was combined with the Water Management and Operations topical area because they needed to be considered together in developing the model of levee breach water impacts for the risk analysis. The resulting team is the Water Analysis Module (WAM) Team and this TM is the Water Analysis Module TM.

The work product described in these TMs will be used to develop the integrated risk analysis of the Delta and Suisun Marsh. The results of the integrated risk analysis will be presented in a technical report referred to as:

14. Risk Analysis – Report

The first draft of this report was made available to the DRMS Steering Committee in April 2007.

Assembly Bill 1200 amends Section 139.2 of the Water Code, to read, “The department shall evaluate the potential impacts on water supplies derived from the Sacramento-San Joaquin Delta based on 50-, 100-, and 200-year projections for each of the following possible impacts on the delta:

1. Subsidence.
2. Earthquakes.
3. Floods.
4. Changes in precipitation, temperature, and ocean levels.
5. A combination of the impacts specified in paragraphs (1) to (4) inclusive.”

In addition, Section 139.4 was amended to read: (a) The Department and the Department of Fish and Game shall determine the principal options for the delta. (b) The Department shall evaluate and comparatively rate each option determined in subdivision (a) for its ability to do the following:

1. Prevent the disruption of water supplies derived from the Sacramento-San Joaquin Delta.
2. Improve the quality of drinking water supplies derived from the delta.
3. Reduce the amount of salts contained in delta water and delivered to, and often retained in, our agricultural areas.
4. Maintain Delta water quality for Delta users.
5. Assist in preserving Delta lands.
6. Protect water rights of the "area of origin" and protect the environments of the Sacramento- San Joaquin river systems.
7. Protect highways, utility facilities, and other infrastructure located within the delta.
8. Preserve, protect, and improve Delta levees.…"

In meeting the requirements of AB 1200, the DRMS project is divided into two parts. Phase 1 involves the development and implementation of a risk analysis to evaluate the impacts to the Delta of various stressing events. In Phase 2 of the project, risk reduction and risk management strategies for long-term management of the Delta will be developed.

Definitions and Assumptions

During the Phase 1 study, the DRMS project team developed various predictive models of future stressing events and their consequences. These events and their consequences have been estimated using engineering and scientific tools readily available or based on a broad and current consensus among practitioners. Such events include the likely occurrence of future earthquakes of varying magnitude in the region, future rates of subsidence given continued farming practices, the likely magnitude and frequency of storm events, the potential effects of global warming (sea level rise, climate change, and temperature change) and their effects on the environment. Using the current state of knowledge, estimates of the likelihood of these events occurring can be made for the 50-, 100-, and 200-year projections with some confidence.

While estimating the likelihood of stressing events can generally be done using current technologies, estimating the consequences of these stressing events at future times is somewhat more difficult. Obviously, over the next 50, 100, and 200 years, the Delta will undergo changes that will affect what impact the stressing events will have. To assess those consequences, some assumptions about the future "look" of the Delta must be established.

To address the challenge of predicting impacts under changing conditions, DRMS adopted the approach of evaluating impacts absent changes in the Delta as a baseline.

This approach is referred to as the "business-as-usual" (BAU) scenario. Defining a business-as-usual Delta is required, since one of the objectives of this work is to estimate whether 'business-as-usual' is sustainable for the foreseeable future. Obviously changes from this baseline condition can occur; however, as a basis of comparison for risks and risk reduction measures, the BAU scenario serves as a consistent standard rather than as a "prediction of the future" and relies on existing agreements, policies, and practices to the extent possible.

In some cases, there are instances where procedures and policies may not exist to define standard emergency response procedure during a major (unprecedented) stressing event in the Delta or restoration guidelines after such a major event. In these cases, prioritization of action will be based on: (1) existing and expected future response resources, and (2) highest value recovery/restoration given available resources.

This study relies solely on available data. Because of the limited time to complete this work, no investigation or research were to be conducted to supplement the state of knowledge.

Perspective

The analysis results presented in this technical memorandum do not represent the full estimate of risk for the topic presented herein. The subject and results are expressed whenever possible in probabilistic terms to characterize the uncertainties and the random nature of the parameters that control the subject under consideration. The results are the expression of either the probable outcome of the hazards (earthquake, floods, climate change, subsidence, wind waves, and sunny day failures) or the conditional probability of the subject outcome (levee failures, emergency response, water management, hydrodynamic response of the Delta and Suisun Marsh, ecosystem response, and economic impacts) given the stressing events.

A full characterization of risk is presented in the Risk Analysis Report. In that report, the integration of the probable initiating events, the conditional probable response of the Delta levee system, and the expected probable consequences are integrated in the risk analysis module to develop a complete assessment of risk to the Delta and Suisun Marsh.

Consequently, the subject areas of the technical memoranda should be viewed as pieces contributing to the total risk, and their outcomes represent the input to the risk analysis module.

Table of Contents

1. Introduction 1
1.1 WAM Purpose 1
1.2 Approach 2
1.3 Overall WAM Calculation Flow Chart 5
2. Input, Output, and Submodel Summaries – 2005 Conditions 9
2.1 WAM Input Data 9
2.1.1 Base Data Sets 9
2.1.2 Levee Breach Event Sequence Data 9
2.2 Net Delta Area Losses 10
2.3 Delta Water Operations 11
2.4 Upstream and South of Delta Reservoir Management 12
2.5 Hydrodynamics and Water Quality 13
2.6 WAM Outputs 15
2.1.3 The 2005 Base Case (with No Breaches) 15
2.1.4 For Each 2005 Base Case Condition and Levee Breach Sequence 15
3. Input, Output, and Submodel Modifications for Future Year Conditions (2030, 2050, 2100, and 2200) 15
3.1 WAM Input Data 15
3.1.1 Base Data Sets 15
3.1.2 Levee Breach Event Sequence Data 17
3.2 Net Delta Area Losses (NDAL) 17
3.3 Delta Water Operations 17
3.4 Upstream and South of Delta Reservoir Management 18
3.5 Hydrodynamics and Water Quality 18
3.6 WAM Outputs 18
4. Concluding Observations 18
4.1 Status 18
4.2 Model Review and Evaluation 18
4.3 Uncertainties 19
4.1.1 Aleatory Uncertainty 19
4.1.2 Epistemic Uncertainty 19

4.4 wam extensions needed 20
4.5 Conclusion 20
5. References 20

Figures

1-1 Position of the Water Analysis Module in the Risk Analysis Framework
1-2 Overall Water Analysis Module (WAM) Flow Chart
2-1 Simplified Hydrodynamic/Water Quality Submodel Schematic (showing example islands only)

Appendices

A Net Delta Area Losses
B Delta Water Operations
C Reservoir Management
D Hydrodynamics and Water Quality
E Hydrodynamic and Salinity Calibration
F Future Conditions – Hydrologic and Water Supply Impacts of Climate Change
G Future Conditions – Precipitation, Temperature, and CO_2 Concentration Impacts on Water Supply and Use
H Three-Dimensional Modeling of Hydrodynamics and Water Quality for Existing Conditions and Sea Level Rise Scenarios
H1 Parameterization of Mixing Using a Three-Dimensional Hydrodynamic Model
H2 UnTRIM San Francisco Bay–Delta Model Calibration Report
H3 Three-Dimensional Salinity Simulations of Sea Level Rise Scenarios
I Organic Carbon

Acronyms and Abbreviations

BAU	business as usual
CalSim	California Water System Simulation Model (DWR & USBR)
cfs	cubic feet per second
CO_2	carbon dioxide
CVP	(federal) Central Valley Project
DOC	Dissolved Organic Carbon
DRMS	Delta Risk Management Strategy
DWR	California Department of Water Resources
dss	data storage system
HD	hydrodynamic submodel
ITF	Initial Technical Framework
JBA	Jack R. Benjamin & Associates, the DRMS risk analysis consultant
NDAL	Net Delta Area Losses (or Net Delta Consumptive Water Use)
OC	Organic Carbon
RMA	Resource Management Associates, the DRMS hydrodynamics consultant
SWP	State Water Project
SWRCB	State Water Resources Control Board
TAF	thousand acre-feet
TM	Technical Memorandum
TOC	Total Organic Carbon
umhos/cm	micro-mhos per centimeter – Electrical Conductivity, a measure of salinity
URS	URS Corporation, the DRMS prime consultant
USBR	United States Bureau of Reclamation
WAM	Water Analysis Module or Model

1. Introduction

1.1 WAM Purpose

One or more Delta levee breaches that result in island flooding will impact Delta water quality (most obviously salinity) and water operations. A substantial amount of saline water may be drawn in from the Bay depending on the initial salinity of the river/Delta/ Bay system, river inflows at the time of the breach event, and the number, size and locations of the breaches and flooded islands. Subsequently, salinity may be dispersed and degrade Delta water quality for a prolonged period due to the complex inter-relationship between ongoing Delta inflows, tidal mixing, and the breach repair schedule.

For a given levee breach scenario considered in the Delta Risk Management Strategy (DRMS) risk analysis, the Water Analysis Module (or WAM) simulates direct, water-quality-related consequences of levee breach events. Specifically, WAM incorporates initial island flooding, upstream reservoir management response, Delta water operations, water quality (salinity) disruption of Delta irrigation, Delta net losses (or net consumptive water use), hydrodynamics, water quality (initially represented by salinity), and water export. The module is central to the risk analysis, receiving the description of each breach scenario (e.g., resulting from a seismic or other event) and details of the levee repair process from the emergency response and repair part of the analysis. The model produces hydrodynamic, water quality, and water supply consequences for use in the economic and ecosystem modules (Figure 1-1). Water quality consequences of levee failures in the Delta are dependent, not only on the initial state of the Delta at the time of failure, but also on the time series of tides, inflows, exports, other uses, and on the water management decisions that influence these factors. Thus, WAM tracks water management and the Delta's water quality response starting before the initial breach event and proceeding through the breach, emergency operations, repair, and recovery period. The model is a key link in facilitating assessment of ecosystem and economic consequences and associated risks.

This Technical Memorandum (TM) provides an overview of the WAM framework and describes the detailed submodels and related aspects that pertain to accomplishing the above assignment in the context of DRMS. The approach taken in developing the WAM was presented in two Initial Technical Framework (ITF) papers (DRMS, 2006a, 2006b):

- Upstream Reservoir Management / Delta Water Operations / Delta Island Water Use
- Hydrodynamics / Water Quality

These ITF papers are available on the DRMS website. There have been refinements to the approaches described in these initial documents, but the basic concepts remain unchanged. The role of WAM in the Risk Analysis Framework is shown in Figure 1-1.

This is a summary of WAM's basic attributes and context for use. More details on technical concepts, relationships, and assumptions/simplifications are included as appendices. Those wishing to explore particular submodels should understand that WAM development was responsive to the need for an adequate overall simulation tool – one that is accurate enough to provide meaningful and useful results, but also computationally efficient. These were essential requirements because thousands of levee breach events must be considered in the risk analysis. This necessitated considerable simplification of more sophisticated submodels.

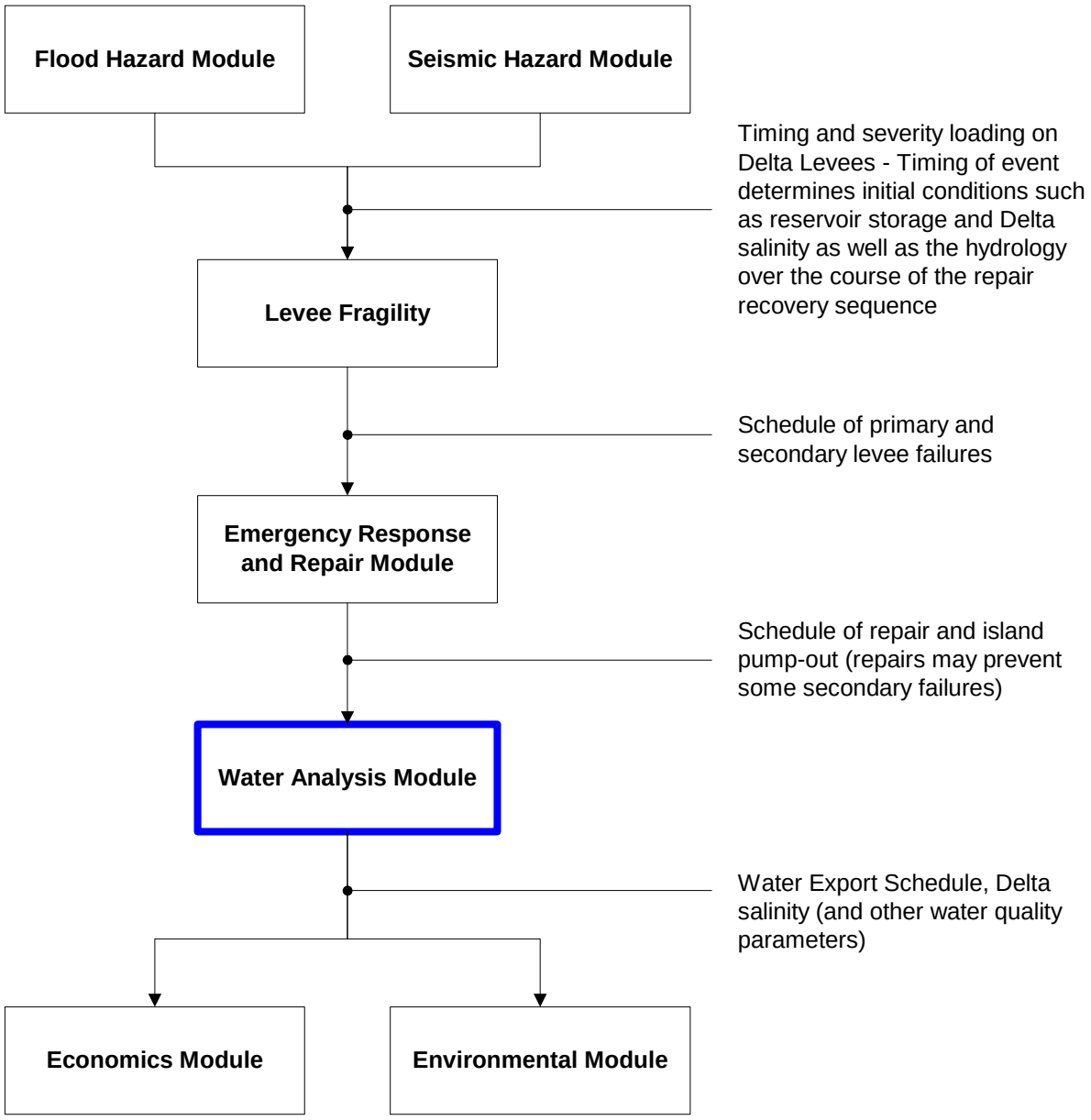

Figure 1-1 Position of the Water Analysis Module in the Risk Analysis Framework

1.2 Approach

Because there is a complex inter-relationship between reservoir operations upstream of the Delta, hydrodynamics and water quality within the Delta, and the ability to use or export water from the Delta, these features of WAM within the risk analysis framework are combined into a single module. When an emergency occurs, decisions will be made to manage ongoing reservoir releases and Delta exports based on the water quality of the Delta, so it is not possible to set release or export strategies without simultaneously evaluating the evolution of Delta water quality. In WAM, water quality conditions are initially represented by salinity.

Topical Area: Water Analysis Module (WAM)

The following are important concepts or principals that have guided our approach.

Hydrodynamics is the branch of science that addresses the dynamics (changes through time) of fluids in motion, especially incompressible fluids such as water. It is based on the physical conservation laws of mass, momentum, and energy. It addresses not only the movement of the fluid, but also the transport and mixing of fluid constituents. In the Delta, water inflows, withdrawals and the tides are the primary drivers of water movement. There are many interesting water constituents, but the dominant phenomenon in the Delta is the freshness of the inflows, the salinity of the tidally active downstream boundary, and the resultant mixing and gradual transition of salinity concentrations as the two meet and interact.

Initially, WAM addresses and models only salinity as a water quality characteristic. This is the essential first step in developing a useful model for evaluating the dominant impacts of a levee breach event and the resultant island flooding. Especially from flooding of multiple islands, these impacts can be as severe as tens of thousands mg/l of dissolved solids making Delta water unfit for use for either municipal or agricultural purposes. The unfit for use condition can last for months or years. The salinity impacts are relevant to the ecosystem as well as to water supply. The first question of importance is “What is the magnitude of the salinity impact?” and the second is “How long does unfit for use last?” WAM was specifically developed to answer those questions and does so successfully and efficiently. Because of schedule constraints, it has not been possible yet to include other water quality parameters into WAM. Other water quality parameters, such as organic carbon, can be included in the model when DWR’s schedule requirements allow for the necessary work.

Because of its potential importance, the project performed a preliminary analysis of organic carbon to obtain initial estimates of increases in water exports due to contact of flood waters with the organic soils on flooded islands. The analysis is presented in Appendix I. Although the analysis was based on many assumptions, did not include any effort to manage island dewatering to minimize organic carbon impacts and did no hydrodynamic tracking of organic carbon discharges, it did provide valuable preliminary information. For cases with only a few levee breaches (less than ten), it indicated that organic carbon concentrations are likely to be manageable and treatable. For more severe cases, more detailed modeling and management approaches are needed because impacts could be severe. Thus it is very important to extend WAM in a next phase of model development.

The decision submodels incorporated into WAM calculate Delta water operations, upstream reservoir releases, and exports immediately following a breach event and throughout the repair/recovery period. The submodels are based, to the extent possible, on operating rules included in existing models of the California water system, water rights and water quality standards, contractual requirements, and operating guidelines. The California Water System Simulation Model (CalSim) is an example of an existing model that includes operations components. However, because CalSim does not consider levee breach emergencies, different operating rules than are currently included in CalSim are required to manage water operations in response to such an emergency. Considerable input was required from operators and policy makers responsible for managing the State and Federal water systems in order to develop the decision submodels. The initial versions of the models reflect this input, but the amount of input was constrained by our limited schedule. Additional input is needed and will be reflected in future versions of the models.

Topical Area: Water Analysis Module (WAM)

The overall simulation of a levee breach scenario has been subdivided into three phases to reflect the dramatically different hydrodynamic and water management situations that define each phase. The phases in WAM simulation are:

- **Island Flooding.** The rush of water filling an island(s) immediately following a levee breach dominates Delta water flow or hydrodynamics (especially after multiple, approximately simultaneous levee breaches). Island flooding may take up to several days. The water needed to fill the islands comes mainly from adjacent Delta channels, but the effect will be felt at an ever-expanding spatial scale. Ultimately, the total volume required to fill the islands and restore overall balance will come from river inflows and/or flow from Suisun Bay. The hydrodynamics submodel considers the initial flow and salinity conditions in the Delta (as obtained from CalSim results for the selected event initiation time); calculates the sources, amounts and distribution routes of the required inflows; and characterizes the resulting Delta salinity distribution at the time a stable flow situation reestablishes (post-flooding). The "flooding" phase of WAM accomplishes this task.
- **Flushing.** During the flushing period, WAM's focus is on the Delta fresh water inflows, tidal mixing, dispersion, and dilution of salinity, and the gradual movement or reestablishment of a fresh water / saline water interface at a more normal downstream location (normal being indicated by CalSim results for the selected event initiation time). Upstream reservoir management and flushing releases are primary considerations. Flushing releases are limited by reservoir low-level outlet capacity and available water. Flow in the Sacramento River at the Delta Cross Channel is kept below 25,000 cfs so the Cross Channel gates can remain open. The hydrodynamics and water quality submodel is focused on characterizing the distribution and timing of water quality improvements that result from flushing. Pumping for export is greatly reduced or suspended since it may exacerbate the situation by drawing saline water into the south Delta, where previous modeling (JBA, 2005) suggests a degraded water quality condition and prolonged disruption could result. Limitations under such conditions would include violation of water quality standards for both local uses and export.
- **Limited Pumping.** When Delta water quality is sufficient to allow export pumping, WAM focus shifts to maintenance of the Delta's water quality and calculating how much export pumping can occur. These decisions are not straightforward. Maintaining Delta water quality when several islands are still flooded requires more than the usual inflow of fresh water because of the extra volume of tidal flow under breach conditions and the resultant increased mixing. This is because when an island is flooded and the breach is open, the volume of water flowing into and out of the Delta on each tidal cycle is increased; a portion of it goes into and out of each flooded island. This causes additional tidal mixing and more fresh water inflow is required to repulse salinity. When pumping starts, the additional water (over and above the amount of pumping) required in order to prevent quality degradation (i.e., carriage water) will also increase. If poor decisions are made, upstream reservoir storage may be exhausted or opportunities for additional export could be missed. The WAM calculator concentrates on using the normal inflows of water as wisely as possible. It simulates Delta inflows and pumping decisions and conformance with water quality and other requirements until Delta levee repairs are completed and both pumping and reservoir storage return to normal.

WAM simulates water-quality consequences of the levee breach occurrence, repair and water management responses, Delta inflows, Delta hydrodynamics, and water quality through time—in some cases, through an extended period of time. To avoid iteration—a computationally intensive process—WAM calculations for the current time step rely only on the previous calculation period results. WAM is designed to operate overall on a monthly time step. Internally, some processes (such as flooding and flushing) must be addressed on a daily basis. However, the overall results of Delta water quality, changes in reservoir storage, exports, and other actions are reported monthly.

At all time steps, the model includes tidal averaging simplifications as an approach to achieve computational efficiency. This is made possible by using dispersion coefficients to capture the impacts of tidal mixing and other causes of salt intrusion. The dispersion coefficients were estimated by analysis of three-dimensional TRIM and UnTRIM model results, as discussed in Appendix H, and two-dimensional RMA Bay-Delta Model results. The RMA Bay-Delta Model also provided datasets used in the simpler tidally-averaged model. The RMA Delta Model uses a 7.5-minute time step and a higher resolution grid, but requires too much computer time for direct use in WAM.

1.3 Overall WAM Calculation Flow Chart

The overall flow chart for WAM calculations is shown in Figure 1-2. Each calculation period begins with updating the calculation variables, as needed, for the current time step. WAM then determines whether there are new breaches that flood new islands and, if so, proceeds with a flooding calculation. Next, the model evaluates whether the Delta salinity distribution (at the start of the time step or after flooding is complete) requires flushing releases from upstream storage. If so, a request for flushing water is generated, all or a portion of the requested water is released from upstream reservoirs and the water quality change due to the increased inflows (when they arrive in one to five days) is calculated. If enough water can be released to complete flushing during a calculation step, WAM begins to consider how much pumping can occur. Delta inflows are allocated first for in-Delta uses, for water quality maintenance, and Net Delta Outflow. Pumping can occur if sufficient water is available for both pumping and the associated carriage water. Subsequently, Delta water quality, as influenced by the pumping, is calculated for the end of the time step.

A more detailed examination of the flow chart conveys the following basic logic of the Water Analysis Module:

- At initiation, information is gathered from base data sets to fully describe the initial state of the Delta, all upstream reservoirs, and the hydrology for the entire simulation period. If several years are involved, different sequences of water years can be considered and this will require multiple simulations.
- At initiation and at the beginning of every time interval, the model updates the levee breach state, as affected by secondary breaches and repair progress.
- If new islands are flooded, the model simulates immediate emergency water operations and the evolution of the salinity distribution for the number of days it takes to fill the islands (i.e., flooding).

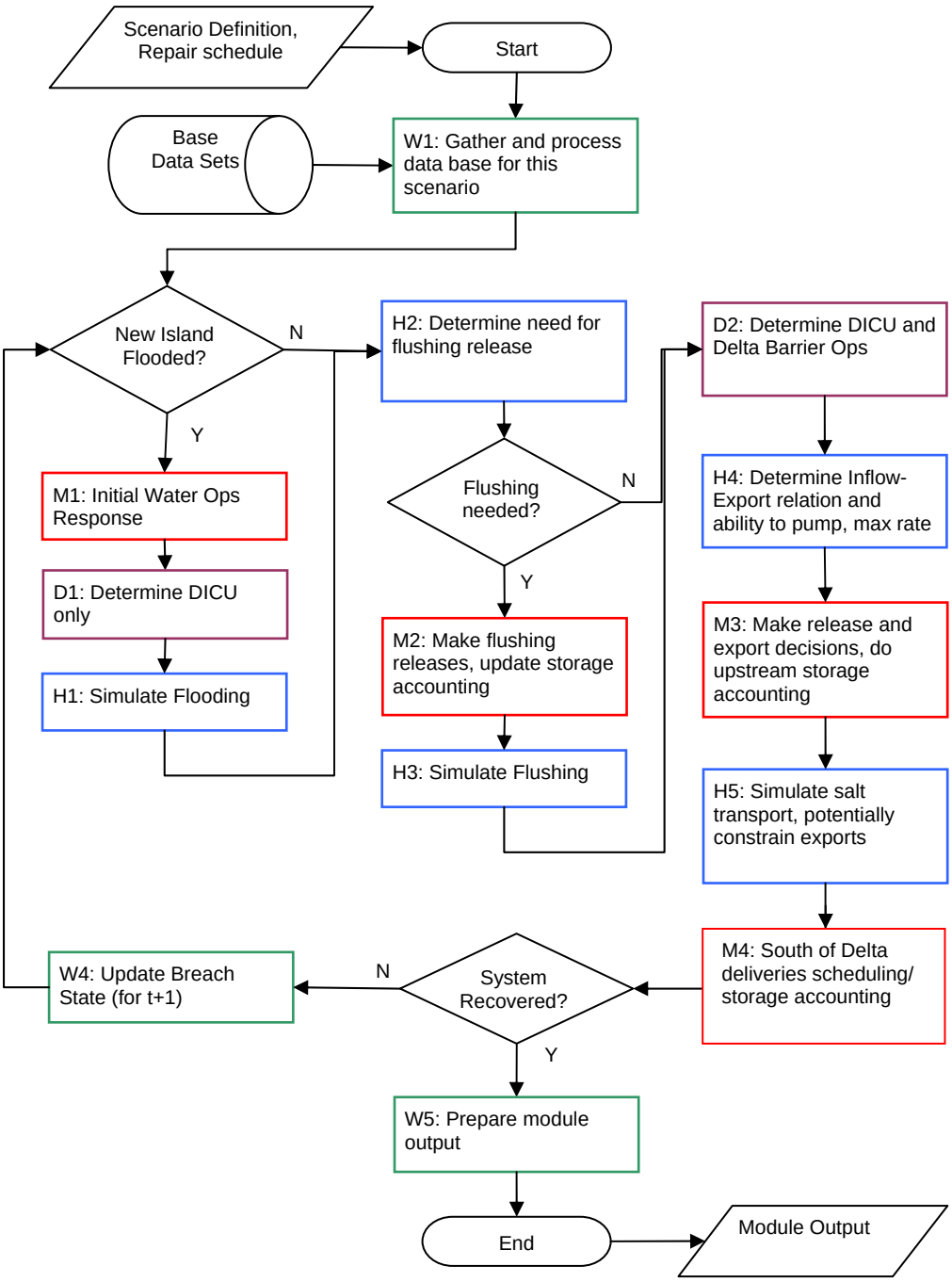

Figure 1-2 Overall Water Analysis Module (WAM) Flow Chart

- Based on estimated conditions when the islands have filled, the model calculates whether flushing releases are needed to satisfy Delta salinity criteria. If flushing releases are needed, the water management component makes releases, to the extent possible, based on water availability. The model then simulates the evolution of Delta salinity for the number of days that flushing occurs.
- Net Delta Area Losses (NDAL or Net Delta Consumptive Water Use) are revised based on the Delta salinity distribution (which affects Delta irrigation) and island breach state. These calculations consider evaporation from flooded islands and the decreased evapotranspiration when channel water is too salty to irrigate unflooded islands.
- The ability to pump for export, based on salinity criteria, is evaluated and the required inflows to support various amounts of exports are estimated.
- The water management component considers storage availability and Delta inflows for the remainder of the time step, establishes export targets and updates the reservoir storage accounting.
- The hydrodynamics/water quality component simulates salinity transport, dilution, and dispersion over the remainder of the time step and updates the salinity distribution. Exports may be constrained if salinity criteria are not met.

If the system is recovered, simulation is complete. Otherwise the module proceeds to the next time step. The system is recovered when the upstream reservoirs and San Luis Reservoir have returned to normal operation and the Delta has returned to a state where normal export pumping can occur.

There are seven key elements in the WAM—important because they are the most difficult and represent crucial innovations that have been necessary for success of WAM. These include five parts that apply a simplified hydrodynamics/water quality model and two that manage upstream reservoirs to provide Delta inflow and, at the same time, retain enough storage upstream to provide for future needs.

The key hydrodynamic/water quality elements are:

H1: Simulate island flooding – The model must simulate the impact of island flooding on the salinity distribution in the Delta. This impact is primarily a function of the island volume to be filled. Time required to fill the islands was estimated based on the 1, 3, 10, and 50 breach scenarios developed as a part of an earlier study (JBA, 2005). Given the time-to-fill estimate, net flow rates can be determined for each island that is flooding. The salinity distribution can then be simulated with net flows and tidally averaged dispersion.

H2: Estimate the volume required to flush high salinity water from the Sacramento and San Joaquin Rivers in the central Delta – If island flooding leads to a salinity distribution in the central Delta that precludes exports, then a flushing volume is estimated to push the salinity gradient seaward. An estimate of the flushing volume is developed based on the volume of water in the main channels that must be displaced to move the salinity gradient downstream the required distance plus the flow over the flushing period required to compensate for the tidally averaged dispersive flux that tends to push salt upstream. Tidally averaged dispersive flux is a quantitative measure of how much

salinity a tidal cycle carries upstream and leaves farther upstream than it was when the cycle started.

H3 Simulate salinity transport during flushing period – This considers Delta inflow and NDAL flows as well as net salt flux in/out of breached islands. The dispersion coefficients used in WAM increase with increased horizontal salinity gradients to account for strengthened gravitational circulation.

H5: Determine whether pumping is possible and estimate needed inflow to support various amounts of export – The ability to pump will be a function of Delta salinity and available inflow. Conditions that constrain pumping are the following:

- Salinity standards in the central Delta are exceeded such that export pumping will draw salt into the south Delta where it is difficult to flush,
- The net salt flux out of flooded islands along the conveyance corridor is sufficient to drive the salinity of exported water above standards, or
- The total salt mass in channels south of the San Joaquin River is too much for south of Delta water users to accept.

If the salinity in the south Delta channels is above standards, but pumping is allowable by other criteria, it may be permissible to begin exports in an effort to flush the south Delta. This is only allowable if the salt load in the south Delta channels can be accepted by south of Delta water users. Provisional criteria for deciding to send this residual salinity south have been formulated.

This submodel must also estimate the relationship between desired exports and required inflow that is appropriate for the current breach state. This relation will vary depending on the number and location of breached islands. In general, the more islands that are actively filling and draining with the tides, the more tidal mixing occurs, resulting in a greater need for net Delta outflow to offset dispersion of salt upstream in the Delta. Thus, more inflow will be required to support a given amount of export.

H6: Simulate salinity transport – This will consider Delta inflow, exports (if any), and NDAL flows as well as net salt flux in/out of breached islands and pump out of flooded islands that have been repaired. If salinity standards at the pumps or elsewhere in the Delta are exceeded, exports may be curtailed. The dispersion coefficients used to represent salt intrusion processes vary spatially, to account for the effects of Bay-Delta geometry on salt transport, and temporally, to account for effects of changing salinity gradients, net Delta outflow and sea level rise on salt transport.

The key water/reservoir management routines are:

M2: Decide what flushing releases can be provided responsive to the H2 request – This algorithm considers the type of water year, time of year, available storage, and prospective needs in future months.

M3: Decide how to manage Delta inflows – These inflows must be sufficient for NDAL, Delta outflow, and any exports – considering the type of water year, time of year, available storage, the relationship between exports and inflow provided by H5, and prospective needs for stored water or progress on Delta repairs in coming months. Part

of the decision is how much upstream storage must be conserved for future needs and whether and how much to export this period.

In the following section, each major submodel is summarized together with its input requirements and outputs generated. These summaries focus on simulation of the base case – 2005 conditions assuming Business as Usual (BAU). Additional details on each submodel are provided in appendices.

Finally, in the subsequent section, modifications needed to simulate the Delta's water-quality-related response to levee breach incidents under future conditions are described. These descriptions are also supported by additional detail in appendices.

2. Input, Output, and Submodel Summaries – 2005 Conditions

2.1 WAM Input Data

To perform the required calculations, WAM requires an extensive collection of input data. The following items are read by the program and assembled into an accessible electronic library.

2.1.1 Base Data Sets

The base data sets include:

- Island identification numbers, names, areas, and floodable volumes.
- Potential breach identification numbers (by island), locations, and sizes. Each potential breach is described in the basic data set, but it does not occur unless it is "activated" by a specific levee breach sequence.
- CalSim input and output for the no breaches base case including reservoir storages, reservoir releases, Delta salinity, inflow, outflow, pumping, and project deliveries – namely, the CalSim Run for 2005 Level of Development, extended hydrology, D-1641, and B-2 (the most current, available 2005 version from the Common Assumptions Model Package). CalSim input and output is required for the entire 82-year CalSim hydrologic sequence derived from the historic record. This is because WAM has the flexibility to use the beginning of any CalSim month as the levee breach initiation time and uses the CalSim state-of-the-system at that time as its starting condition. WAM then uses the CalSim hydrologic conditions for the next several years as the input hydrology for the duration of the event.

2.1.2 Levee Breach Event Sequence Data

Note that WAM is designed to calculate the water related impacts for any combination of possible Delta levee breaches and resulting flooded islands. WAM can accept the first day of any CalSim month as the event initiation date. WAM can also calculate the impacts from several or all potential CalSim start times (82 X 12 = 984 potential start times). A selection of CalSim start times can also be specified; for example, WAM only uses months with large floods as start times for levee breach incidents caused by floods.

The levee breach sequence is determined by previous modules in the risk analysis framework – the Seismic and Flood Hazard modules, the Levee Fragility module and the Emergency

Response and Repair module. Data describing a particular combination of breaches and a repair schedule (from these previous modules) includes:

- SEQNAME – Sequence Name
- SEQCODE – Sequence Code used to identify sequence output file names and *.dss (data storage system) paths
- SEQTYPE – Sequence Type Integer: 0=blue sky, 1=seismic, 2 =flood (including size of flood)
- Breach – Day of Event; Island Id; Breach Id (for all islands and breaches)
- Repair – Day of Event, Island Id; Breach Id (for all islands and breaches)
- PumpOutStrt – Day of Event, Island Id, Rate (cubic feet per second [cfs]; for all islands)
- Recovered – Day of Event, Island Id. (this is the date that pump out is completed, for all islands)

2.2 Net Delta Area Losses

Within WAM, the net Delta area consumptive use or Net Delta Area Losses submodel (referred to herein as NDAL) determines the return flow, return flow salinity and net channel withdrawals for each island and/or groupings of islands. Net consumptive use is total consumptive use minus precipitation. Net Delta Area Losses and net channel withdrawals are the same as net consumptive use, because consumptive use is supplied by either precipitation or water from Delta channels.

To represent NDAL within WAM, the Delta is divided into groups. Initially the Delta is divided into five groups representing each of the major Delta flow paths as defined by the hydrodynamics (HD) submodel. These flow paths convey water from major Delta inlets to the export locations. The 142 sub-areas (defined by California Department of Water Resources [DWR] for tabulating Delta net evapotranspiration) are assigned to groups and these groupings are used to report the NDAL output to the HD calculator. Each of the sub-areas is assigned to an evapotranspiration group, an evaporation group, and a precipitation group. The HD calculator maps the original 142 islands to the island tabulation of 184 islands addressed in the DRMS project

The first call to NDAL reads the configuration files, initializes the variables, and gets the basic data. The second call to NDAL initializes the variables that change for each simulation. The third call to NDAL obtains the time step specific data, determines the status of the area, and then computes the net channel withdrawals, return flow, and return flow salinity needed by the HD submodel.

In sum, NDAL assesses in-Delta water demands based on normal irrigation net consumptive use, breach event details, islands flooded, channel salinity, and repair progress. If an island is flooded, irrigation demand ceases for that island, as does seepage through or underneath the levees, and return flows from the island's drainage system. These variables are zero, at least until the island is repaired and pumped out. Further, there is no evapotranspiration from a flooded island, but evaporation occurs instead. For this version of NDAL, net loss from a breached island's free water surface evaporation was approximated by evapotranspiration.

When an island is repaired, seepage and return flow are restarted. Irrigation can commence, as well, if adjacent channel salinity is of appropriate quality. For an unbreached or a repaired island, NDAL checks channel salinity calculated by the HD submodel and determines whether water quality conditions are sufficient to provide irrigation water. If water quality is unsatisfactory, irrigation does not occur until water quality conditions become satisfactory.

2.3 Delta Water Operations

In the event of a Delta levee breach incident with island flooding, Delta water operations may be substantially altered – gate positions may be changed (including the Delta Cross Channel gates and the South Delta barriers), export pump operations may be curtailed (e.g., emergency shutdowns), in-Delta diversions may cease (for Delta island irrigation) and, potentially, upstream reservoir releases may occur to counteract salinity intrusion during island flooding. The purpose of the Delta Water Operations Submodel is to represent these operations as they are expected to occur in a BAU response to a Delta levee breach incident. This is necessary because they will impact Delta hydrodynamics and salinity concentrations.

The operations submodel is subdivided into three phases in coordination with the hydrodynamics and upstream reservoir management submodels. The phases for Delta Water Operation actions are: 1) immediate response (during flooding), 2) flushing, and 3) limited pumping.

The operations submodel reflects standard project operating procedures that existed in 2005 together with additional details that could be inferred from discussions with operators. In general, operations are tightly controlled by the water quality standards established by the State Water Resources Control Board (SWRCB) and set forth in Water Rights Decision 1641 (SWRCB, 2000). Our assumption under BAU is that the projects would not intentionally violate a requirement of D-1641.

To the extent the projects can be operated with discretion, such actions often require consultation with federal and state fish and wildlife agencies under their respective Endangered Species Act provisions. These consultations require some time to formulate a request, discuss conditions and concerns, and agree on an action. Thus, the operations submodel assumes that any action requiring consultation will not be immediately available (within hours), but will require at least three days for formulation of a proposed action, discussion, agreement, and implementation. Consequently, such actions will typically be initiated during the flushing phase. Another assumption is that consultation will generally not allow compromises of intended protections for endangered species. Similarly, adjustment of upstream reservoir releases under present procedures requires a period of analysis and consultation with upper management. This is also assumed (under the BAU scenario) to require three days. Only project reservoirs with stored water under project control are considered for extra releases. These are Folsom, Oroville and Shasta. Essentially all stored water in New Melones is controlled by senior water rights holders (per Central Valley Project [CVP] Operators).

During the limited pumping phase, normal D-1641 provisions are assumed to be in force.

Additional detail on Delta water operations is provided in Appendix B.

2.4 Upstream and South of Delta Reservoir Management

Depending on the severity of the levee breach scenario, the management of upstream and south of Delta reservoirs may be substantially altered. A small event, like Jones Tract, may require only slight modifications. But in a larger event, there may be a prolonged period of reduced or no pumping with an associated need to ration south of Delta supplies. There will also be a need for managed Delta inflows to provide flushing and additional Delta outflow to maintain water quality. After adequate flushing is achieved, the quantity of inflow required to maintain water quality will include normal Delta outflow and an increased amount based on the larger tidal prism due to tidal flow into and out of unrepaired, flooded islands. Finally, when limited export pumping can be reestablished, residual Delta inflow can be pumped provided that sufficient normal and supplemental carriage water is available to maintain water quality.

The reservoir management submodel makes emergency reservoir operating decisions related to the levee breach incident in order to balance the amount of water released from storage while the emergency and repairs progress with the need to conserve water for other and future uses. This is distinct from flood control emergency operations, which are assumed to proceed as required by the existing reservoir flood control rules.

South of Delta reservoir management means balancing deliveries that respond to water users' needs with the need to conserve water in south of Delta reservoirs in case the disruptions last longer than expected or the projects encounter dry or critical years. North of Delta this means balancing releases to reestablish through-Delta conveyance with the need to conserve in upstream reservoirs, so that other needs can be served, drought protection is provided and, when export pumping is reestablished, there is water available to pump.

The basic approach used north of Delta is to receive daily requests from the HD submodel indicating the amounts of Delta inflow needed to reestablish or maintain required water quality. Separately, the HD submodel indicates the extra amount required to facilitate any given amount of pumping. These requests are then considered in light of the time of year, stored water available, the quantity requested and the releases programmed for normal (non-breach) conditions. A set of decision rules is incorporated into the submodel to operate reasonably while saving enough water in storage to get through the incident and be in a position to recover toward normal operations, even encountering dry years. These daily operations are accumulated in order to report monthly amounts of Delta inflow, Delta exports, and end of month upstream storage.

For south of Delta storage, the approach is similar. Deliveries may be made for federal CVP and State Water Project (SWP) contractors after considering and balancing available stored water, normal allocations, anticipated limited pumping during the rest of the incident, and the intensity of needs from the earlier cuts that are part of the incident. These water contractor deliveries are apportioned in full conformance with existing contracts. Again, the decision rules are crafted to get through the incident without implementing even more drastic cuts (due to running out of water) and then being able to rebuild deliveries in a reasonable way when pumping from the Delta is reestablished. Monthly amounts of deliveries and end of month storage are reported.

Additional detail on reservoir operation modeling is provided in Appendix C.

2.5 Hydrodynamics and Water Quality

The challenge for the hydrodynamics and water quality has been somewhat different – it has not been to balance decisions, but to have a working interaction with the water management decisions in order to calculate the Delta salinity resulting from the water management decisions in the context of the specific levee breach scenario. There are already very sophisticated models for doing this – e.g., Delta Simulation Model 2 (DSM2), the RMA Bay-Delta Model. However, it takes hours to days of real time for these models to simulation large-scale levee breach scenarios, so it is not feasible to use it for each of several thousand scenarios. A simplified hydrodynamics/water quality submodel has therefore been developed as part of the WAM. The following approach has been implemented:

- Use existing physically based numerical models (RMA Bay Delta Model and TRIM/UnTrim 3D models) to explicitly evaluate hydrodynamic, salinity, and other water quality impacts for a limited number of specific breach events as well as to characterize the dynamics of the system, and
- Analyze scenario simulations conducted using existing multi-dimensional models to estimate dispersion coefficients that quantify the strength of salt intrusion processes,
- Create a new tidally averaged flow and salinity transport model using a one-dimensional network approximation system reaching from the central San Francisco Bay to the upstream limits of the Sacramento-San Joaquin Delta to rapidly evaluate salinity impacts of levee breach events and interact with the water management decision-making component of WAM.

The primary challenge in developing the simplified hydrodynamic/water quality model has been to represent enough of the physics to provide sufficient accuracy while maintaining the computational speed needed to simulate many thousands of levee breach events. The primary outputs of WAM are monthly average quantities including export volumes and salinity, and in-Delta salinity at selected locations. Therefore, it is not necessary for the simplified model to explicitly represent flow and transport on the tidal time scale or variations in flow velocity or salinity concentrations across a channel cross section. The simplified model is therefore a one-dimensional, tidally-averaged transport model. This type of model considers the impacts of net flow, mixing by tidal and other currents, and vertical stratification by relying on dispersion coefficients to calculate the mixing effects and then provides a cross-section average value of salinity. Thus, the model provides depth-averaged, across-the-channel-averaged, and tidal-cycle-averaged flow, water surface elevation, and salinity concentration. The dispersion coefficients are derived from full dynamic models of the system. The simplified model then interacts with the water management component of WAM during the course of simulation, both providing input to the water management decision making component and receiving calculated inflows and exports. Figure 2-1, illustrates the basic conceptual structure of the simplified model.

The WAM HD is a one-dimensional tidally averaged model and therefore does not represent tidal currents or vertical variability in salinity. The effect of tidal currents, gravitational circulation and other processes on salt intrusion is represented in the WAM by dispersion coefficients. The parameterization of dispersive transport (salt intrusion) processes was accomplished through the application of multi-dimensional models to several scenarios, spanning different net Delta outflow conditions. At 28 cross-sections in the Bay-Delta, the

three-dimensional model results were analyzed to estimate dispersion coefficients for each scenario simulated.

The estimated dispersion coefficients are based primarily on three-dimensional TRIM model results, which are discussed in Appendix H1. The dispersion coefficients are partitioned into components associated with different physical processes, and the variability of the component associated with gravitational circulation is specified and a function of a non-dimensional parameter called the horizontal Richardson number, which varies with horizontal salinity gradients such that the dispersion coefficients increase strongly as horizontal salinity gradients increase.

The UnTRIM model was developed to allow simulations further into the Delta than the TRIM model allowed. In Appendix H2, the UnTRIM model is shown to accurately predict water surface elevation, flow and salinity in the Bay-Delta under a wide range of conditions. This model will also be used in uncertainty analysis for the WAM.

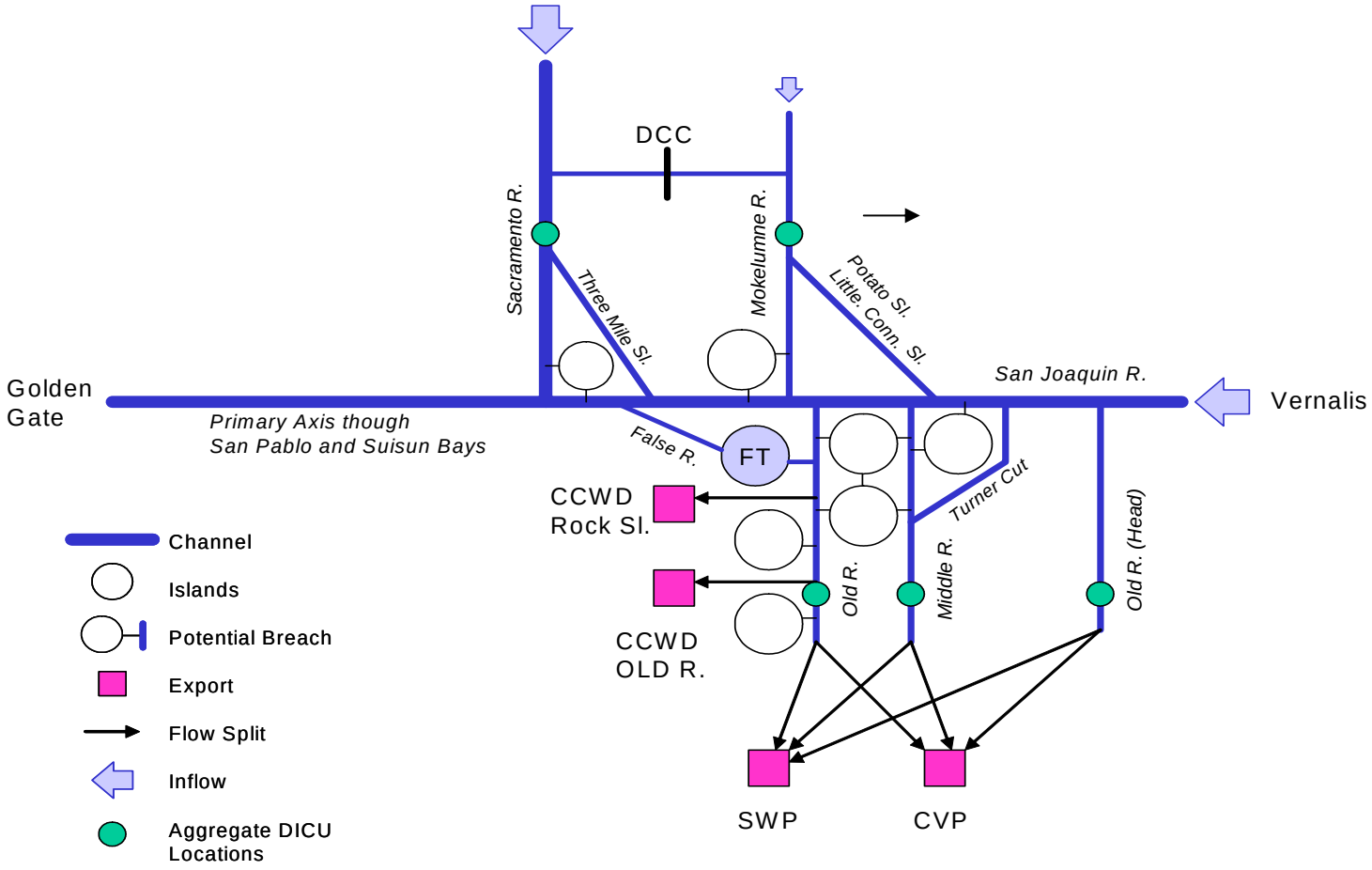

Figure 2-1 Simplified Hydrodynamic/Water Quality Submodel Schematic (showing example islands only)

Additional details on the hydrodynamic and water quality submodel are provided in Appendix D. The calibration of the submodel is documented in Appendix E.

2.6 WAM Outputs

WAM outputs will include the items listed in the following subsections.

2.1.3 The 2005 Base Case (with No Breaches)

Outputs will be a set of 82 x 12 files (for each CalSim water year and month) including:

- Year / Month – (Calendar Year)
- Water Year Types (Sacramento Index, 1=Wet, through 5=Critical)
- Reservoir Storage (end of month, for each CalSim reservoir requested, thousand acre-feet [TAF])
- Water Delivery (monthly, for each SWP and CVP contractor requested)
- Ambient Delta Water Quality (end of month, for a reference point for each island requested, micro-mhos per centimeter [umhos/cm])

2.1.4 For Each 2005 Base Case Condition and Levee Breach Sequence

Outputs for each breach sequence will be a set of up to 82 x 12 output files (each representing a different event initiation date), each file including:

- Event Start Time (in CalSim Trace) – Year / Month
- Disruption Duration – Months Until Return to Normal
- Reservoir Storage (end of month, for each modeled reservoir, TAF)
- Water Delivery (monthly, for each SWP and CVP contractor requested)
- Ambient Delta Water Quality (end of month, for a reference point for each island requested, umhos/cm).

3. Input, Output, and Submodel Modifications for Future Year Conditions (2030, 2050, 2100, and 2200)

To address future years, the WAM calculations need specific modifications. The modifications needed for the submodels themselves are identified in the respective submodel sections below (Subsections 3.2 through 3.5). However, they are modest; the most significant changes in the calculation and the results will be from preparation and use of revised input data. Thus, Section 3.1 focuses on these changed input data needs and this is the most important consideration for characterizing future years.

3.1 WAM Input Data

To perform a “Business as Usual” analysis for any future year, the input data identified in Section 2.1 will need to be adjusted in several ways as outlined below.

3.1.1 Base Data Sets

- **Island identification numbers, names, areas, and floodable volumes:** Island identification numbers and names would be assumed to remain unchanged. Island areas

and especially their floodable volumes would need to be adjusted for the future year being analyzed in response to the expected amounts of subsidence and sea level rise compared with 2005.

- **Potential breach identification numbers (by island), locations, and sizes:** These inputs will likely remain unchanged, although one could argue for increasing breach sizes due to the increased water level differential during island flooding (due to subsidence and sea level rise). Such a change may be considered. Each potential breach is described in input data, but the breach does not occur unless it is "activated" in a specific levee breach sequence.
- **CalSim input and output for the no breaches base case:** The major input changes for WAM future years need to be reflected in the hydrologic, water quality, and water management inputs that are used. Two main drivers create the need for substantial changes. These two drivers are population/economic growth and climate change.

The DRMS project has made a management decision to not make population and economic projections where no data and/or state policy/guidance exists. Thus, the available population and associated economic projections only extend to 2030, as produced for and incorporated in Bulletin 160 – "The California Water Plan Update 2005" (DWR, 2005). These population and economic conditions are then reflected in the DWR 2030 Level of Development CalSim run (DWR, 2006a). This CalSim input and output (as adjusted for climate change – see below) would be used as the basis for any future year WAM analyses performed.

Climate change may have dramatic future effects on California hydrology and water management and on Delta sea level. A major impact is expected in the form of less snowfall and snowpack accumulation and more winter rainfall and runoff instead. That change has been quantified in simulations of unimpaired streamflow made available to the DRMS Climate Change Team (DRMS, 2006c). Those results can be interpreted and used to adjust the CalSim streamflow inputs (rim flows) and new CalSim runs can be made to obtain the modified outputs that WAM can use as inputs (see Appendix F). Climate change inputs for such analyses are currently available for 2030, 2050, and 2100.

Further, CalSim modifications may be required to reflect the impacts of altered temperature and precipitation on the Sacramento Valley floor. This would address Delta watershed areas downstream from the streamflow simulation locations identified above. The resulting changes in evaporation, transpiration, runoff, and upstream water diversions may substantially affect water availability for Delta inflow. Further exploration is required to define a practical means of incorporating such CalSim adjustments within an acceptable schedule and budget (see Appendix G). Similarly, precipitation and temperature changes will impact Net Delta Area Losses (Delta area net consumptive use).

The alterations in precipitation, temperature, and carbon dioxide (CO_2) can be used directly by the NDAL submodel in WAM (see Appendix A and Section 3.2).

Finally, climate change will result in sea level rise and this will require increased CalSim water allocations to Delta outflow. The modified 2030 CalSim runs must incorporate this increased water requirement since it will mean less water available in storage or for exports in the base case simulations and thus less available for addressing levee breach incidents.

Climate Change impacts are available for 2030, 2050, and 2100. Useable information is not presently available for 2200.

3.1.2 Levee Breach Event Sequence Data

These input data are generated by preceding modules in the risk analysis. They will be altered by those modules in response to changes incorporated to reflect future year conditions. For example, the seismic hazard is expected to increase over time due to increasing strain accumulation. Similarly climate change may alter the characteristics of floods. A given earthquake or flood may have more impact due to sea level rise. If there is more or different damage, times of repair may also differ. The WAM module will not need to make special allowances for these data changes unless the changes are so substantial that they cause the application to go beyond its initial, practical scope limits. This will simply be monitored in reviewing input and output.

- SEQNAME – Sequence Name
- SEQCODE – Sequence Code used to identify sequence output file names and dss paths
- SEQTYPE – Sequence Type Integer: 0=blue sky, 1=seismic, 2 =flood (including size of flood)
- Breach – Day of Event; Island Id; Breach Id (for all islands and breaches)
- Repair – Day of Event, Island Id; Breach Id (for all islands and breaches)
- PumpOutStrt – Day of Event, Island Id, Rate (cubic feet per second [cfs]; for all islands)
- Recovered – Day of Event, Island Id (this is the date that pump out is completed, for all islands).

3.2 Net Delta Area Losses (NDAL)

The NDAL submodel includes the ability to read and incorporate climate changes in the form of Delta area precipitation changes, temperature increases and CO_2 concentration increases. Precipitation increases result in a corresponding decrease in NDAL. The opposite is true for precipitation decreases. Temperature increases would increase evaporation and plant transpiration. CO_2 increases, on the other hand, are believed to decrease water use for transpiration (DWR, 2006b) and will thus dampen the effect of future temperature increases. The relationships are explained more fully in Appendix A.

3.3 Delta Water Operations

Since the future year analyses are to be for a “Business as Usual” base case, 2005 Delta water operations approaches, and rules will remain unchanged. The one potential exception (included in the 2030 California Water Plan) is inclusion of the proposed operable south Delta barriers. A decision on whether to assume they have been installed may be unnecessary. It is not clear that barrier operation in a levee breach emergency would be any different than that assumed for the 2005 case with temporary barriers. For now, we will assume that BAU means barrier operation as it now would occur for the temporary barriers.

3.4 Upstream and South of Delta Reservoir Management

Refinements of the upstream reservoir management submodels for future years will generally be avoided in the spirit of providing a BAU analysis. Flood control operating rules will be assumed to stay the same. This may not actually occur for future years, but it is a reasonable place to start thinking about the future. There are reasons to change flood space allocations in either direction – to provide more reservoir space to control larger, more frequent floods or to dedicate more winter space to water supply because of decreased snow pack storage.

Water supply operating rules will be altered as necessary in the CalSim runs (used as WAM input) to develop reasonable base cases. The objective will be to ensure that reservoirs are not unrealistically drawn down in the "no breaches" case used as a baseline. Follow up refinements of WAM water supply operating rules may be required to avoid similar drawdown in levee breach events.

3.5 Hydrodynamics and Water Quality

The hydrodynamics and water quality model will reflect future changes in two substantial ways. First the sea level rise attributed to the analysis year will be incorporated. As described in Appendix H, this will change Delta hydrodynamics and require recalibration of the dispersion coefficients used in the simplified hydrodynamics model. In Appendix H3, dispersion coefficients are found to increase weakly with sea level rise in most of the Bay-Delta, but in Suisun Bay and the western Delta, dispersion coefficients increase substantially with sea level rise. The increase in dispersion coefficients indicates an increase in landward salt intrusion in these areas with increasing sea level rise.

Secondly, when a levee breach with island flooding occurs, a larger volume will be flooded due both to the higher flood water level (higher sea level) and due to lower island surfaces where subsidence has occurred (see input data in Section 3.1).

3.6 WAM Outputs

WAM output structure and data fields will not be changed unless it is essential for some reason that is presently unforeseen, i.e., only the results are expected to change.

4. Concluding Observations

4.1 Status

As of the date of this report, the WAM calculator is producing reasonable results. Only limited review of the full working model's internal relationships and assumptions, as well as output, has been completed to date. To ensure a sufficient level of confidence in model performance and results, additional review is underway.

4.2 Model Review and Evaluation

With additional review, testing, and refinement, WAM will provide technically solid information for 2005 BAU risk analysis and related decisions. The specific additional work that is needed includes:

- Internal (Project Team) review of decision criteria, operating rules, and relationships imbedded in the WAM calculator.
- Performance and review of several more test runs to refine calibration of the model and ensure that reasonable results are produced throughout the range of potential applications.
- Performance of verification runs, with independent tests of result validity, to the extent possible.
- Presentation of model operating rules and initial results to state and federal project operators and stakeholders to achieve buy-in and acceptance, or, if needed, to receive substantive suggestions for improvements.

To provide useful results for future years (2030, 2050, and 2100), some additional model refinements are required and substantial work is needed to generate appropriate input data. These needs are described more fully in Section 3. As stated in Section 3, useable data regarding the year 2200 does not appear to be available at this time.

4.3 Uncertainties

Several types of uncertainty are inherent parts of any modeling effort such as WAM. In the context of the broader risk analysis they are usually discussed as either aleatory or epistemic uncertainties.

4.1.1 Aleatory Uncertainty

The natural randomness or aleatory uncertainties are a major factor in WAM modeling. The most dramatic example is the year-to-year hydrologic variability together with the variety of sequences in which hydrologic years can occur. Typical of most simulation models, WAM is limited to the collection of historic data that are available, and the historic sequence of hydrologic years that we have experienced. Although the 82-year CalSim data sequence would be considered an exceptionally rich data resource by past generations of analysts, the record would be much improved if it were extended, especially, by including a greater variety of three to five year sequences that could be used for analyzing Delta levee breach events. A quantitative estimate of these aleatory uncertainties is to be performed in collaboration with the risk analyst.

4.1.2 Epistemic Uncertainty

The epistemic uncertainty, generally the modeling uncertainty in representing the physical system with a particular level of mathematical relationships, is also significant. One of the basic precepts of the WAM model was to simplify more complex (and accurate) models in order to achieve computational efficiency. The price that is paid is larger epistemic uncertainty. These uncertainties come most obviously through the simplified hydrodynamic and water quality model, which can be compared to the more sophisticated and accurate RMA model and even more sophisticated 3D models. They also stem from the relationships used in the NDAL consumptive use model and the operating rules created in the upstream reservoir management model. A quantitative estimate of these uncertainties is to be performed in collaboration with the risk analyst.

4.4 wam extensions needed

Although a great deal has been accomplished in developing WAM to its present state in the limited time available, implementation of some features was postponed, due to schedule constraints. The two most significant needs for additional model development work are:

- Inclusion of organic carbon as a second water quality variable (in addition to salinity)
- Extension of the model to future year conditions by developing needed revised inputs and calibrations to reflect altered hydrology, sea level rise, island flooding volumes (due to subsidence and sea level rise) and increased hydrodynamic dispersion (due to sea level rise).

Both of these further developments are practical and achievable, given availability of sufficient time to do the work.

4.5 Conclusion

In summary, the first version of WAM is an appropriate calculator for its intended use. It represents a new and valuable computational tool for assessing the direct salinity-related impacts of Delta levee breaches within the context of a probabilistic risk analysis. It is computationally efficient, so it is practical to evaluate several thousand levee breach events. With review, testing, and some refinement, it is a tool that can be used with confidence in Delta risk analyses and that deserves and will inspire trust from the technical community and decision makers. With extension, its usefulness will be further enhanced.

5. References

DRMS, 2006a. Delta Risk Management Strategy (DRMS). Initial Technical Framework Paper: Upstream Reservoir Management / Delta Water Operations / Delta Island Water Use. Prepared by URS Corporation/Jack R. Benjamin & Associates, Inc. Prepared for Department of Water Resources. September, 2006.

DRMS, 2006b. Delta Risk Management Strategy (DRMS). Initial Technical Framework Paper: Hydrodynamics / Water Quality. Prepared by URS Corporation/Jack R. Benjamin & Associates, Inc. Prepared for Department of Water Resources. September, 2006.

DRMS, 2006c. Technical Memorandum: Delta Risk Management Strategy (DRMS) Phase 1, Topical Area: Climate Change. Prepared by URS Corporation/Jack R. Benjamin & Associates, Inc. Prepared for Department of Water Resources. October, 2006 (Draft).

DWR, 2005. “The California Water Plan Update 2005.” California Department of Water Resources Bulletin 160-05. December 2005.

DWR, 2006a. CalSim 2030: Common Assumptions Base Case for 2030 Level of Development. Walter Bourez, MBK Engineers, Personal Communication.

DWR, 2006b. “Progress on Incorporating Climate Change into Management of California’s Water Resources.” Technical Memorandum Report. California Department of Water Resources. July, 2006.

JBA, 2005. "Preliminary Seismic Risk Analysis Associated with Levee Failures in the Sacramento – San Joaquin Delta." Prepared for California Bay-Delta Authority and California Department of Water Resources. Prepared by Jack R. Benjamin & Associates, Inc. in association with Resource Management Associates and Economic Insights. June, 2005.

SWRCB, 2000. "Revised Water Rights Decision 1641." State Water Resources Control Board. March 15, 2000.

Appendix A
Net Delta Area Losses

Table of Contents

A1. Net Delta Area Consumptive Use or Net Delta Area Losses A-1
A2. NDAL Overview A-1
A3. System Representation and Data Needs A-1
A3.1 Base Data: DWR 'DICU' Model A-1
A3.2 Pre-Processing: Delta Area Groups A-2
A3.3 Inputs A-3
A3.4 Outputs A-3
A4. NDAL Calculator A-3
A5. References A-6
Personal Communications A-6

Figures

A-1. Delta Area Groupings (grey shading has no significance).
A-2. ComputeNDAL routine flow chart.

Acronyms and Abbreviations

CU	Consumptive Use
DICU	Delta Island Consumptive Use (Net of Precipitation)
DRMS	Delta Risk Management Strategy
DWR	California Department of Water Resources
HD	Hydrodynamic Submodel
NDAL	Net Delta Area Losses Submodel
WAM	Water Analysis Module or Model

A1. Net Delta Area Consumptive Use or Net Delta Area Losses

Within the Water Analysis Module (WAM) the net Delta area consumptive use or Net Delta Area Losses calculator (referred to herein as NDAL) determines the return flow, return flow salinity, and net channel withdrawals for each island and/or groupings of islands. Net consumptive use is total consumptive use minus precipitation. Net Delta Area Losses and net channel withdrawals are the same as net consumptive use, because consumptive use is supplied by either precipitation or water from Delta channels.

A2. NDAL Overview

NDAL calculates the net channel withdrawals, return flow, and return flow salinity for each of the Delta island/area groups. NDAL assesses in-Delta water demands based on normal irrigation net consumptive use, breach event details, islands flooded, channel salinity, and repair progress. If an island is flooded, irrigation demand ceases, as does seepage, and return flow. There is no evapotranspiration, but evaporation occurs from the free water surface and precipitation inputs are included. For this version of NDAL, net loss from a breached island free water surface evaporation was approximated by evapotranspiration. When an island is repaired, seepage and return flow are restarted. Irrigation can commence, as well, if adjacent channel salinity is of appropriate quality. For an unbreached or a repaired island, NDAL checks channel salinity calculated by the Simplified Hydrodynamic/ Water Quality (HD) submodel and determines whether water quality conditions are sufficient to provide irrigation water. If water quality is unsatisfactory, irrigation does not occur until water quality conditions become satisfactory.

A3. System Representation and Data Needs

A3.1 Base Data: DWR DICU Model

The Department of Water Resources (DWR) identifies 142 sub-areas (Figure A-1) within the Delta (DWR, 1995), which encompasses the approximately 70 islands in the Delta plus some additional areas. The HD calculator maps the original 142 islands to the latest island tabulation of 184 islands currently employed in the DRMS project. DWR has estimated the monthly diversions and seepage to each sub-area from Delta channels and drains (return flows to Delta channels) from each sub-area. This is done using DWR's Delta Island Consumptive Use (DICU) model. These values were subsequently used by DWR to represent monthly diversions, drainage, and seepage within the DSM2 model.

The data used to drive the WAM module is from the CalSim model. In the case where no levee breaches occur, net Delta consumptive use calculated by NDAL should be the same as the CalSim results. The two models use slightly different data ("DICU" model versus the CalSim "CU" [Consumptive Use] model). Therefore, a "calibration" flow was determined to ensure that the DICU and CU models are compatible. There are two types of calibration flows included in NDAL. The first type resolves the overall net Delta consumptive use represented in the NDAL data set to match DWR's DICU model output. The second set of calibration flows is to make the net Delta consumptive use match the overall consumptive use represented in CalSim. These calibration flows are applied to

each group as non-changing values (i.e., they are the same for any given analysis year conditions, regardless of the breach sequence).

A3.2 Pre-Processing: Delta Area Groups

To represent NDAL within WAM, the Delta is divided into groups. Initially the Delta is divided into five groups representing each of the major Delta flow paths (Figure A-1) as defined by the HD submodel. The 142 sub-areas are assigned to a group and these groupings are used to report the NDAL output to the HD calculator. Each of the sub-areas is correlated to a DWR/DSM2 sub-area and then assigned to a group, an evaporation group, and a precipitation group.

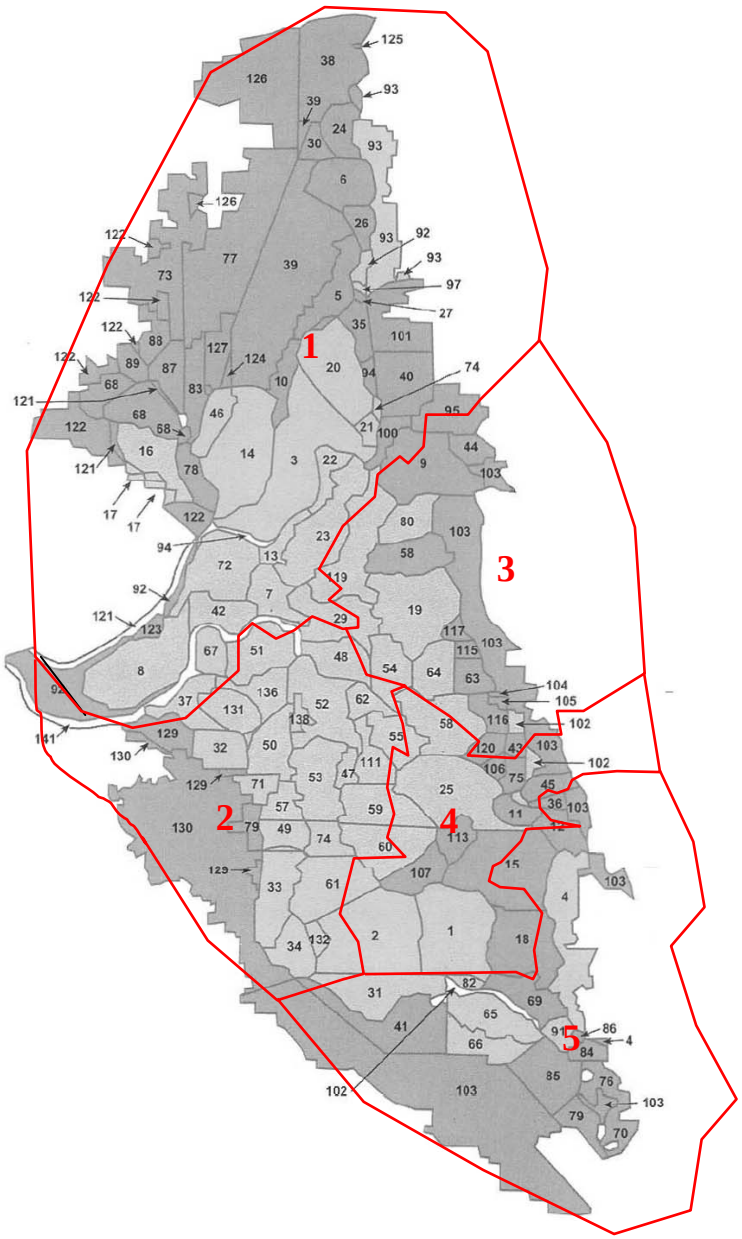

Figure A-1. Delta Area Groupings (gray shading has no significance)

A3.3 Inputs

NDAL requires monthly information for each area (*i* = 1 to 142, in Figure A-1) included in WAM. (The term "area" is used in lieu of "island" to avoid confusion. "Area" refers to a computational unit within the NDAL structure. For example, Sherman Island is an area, as is Franks Tract.) NDAL addresses all relevant Delta areas. This includes irrigated areas, temporarily flooded areas, permanently flooded areas, wetlands, and waterways, but does not include unirrigated uplands.

Information is provided to the NDAL model from two main sources: pre-processed text files (see below) and other WAM/DRMS components. The text files provide a wide variety of information, including, but not limited to simulation specific information or system configuration information; area diversion, seepage rates, drainage rates, allowable irrigation water salinity, etc., data; group parameters and data; evaporation and precipitation data, and other basic information. These files must be prepared prior to simulations and follow specific formats. These files provide information used by NDAL that is not necessarily needed by other WAM components.

Other input required is provided by the HD submodel. Specifically, the HD submodel provides the channel salinity concentration for each area to the NDAL calculator at the beginning of each time step.

Finally, other groups within the DRMS project will provide the global data information, such as flooded water surface area, pump out rate, precipitation change, CO_2 concentration increase, air temperature increase, and breach sequence specifics (which can be incorporated into the text files or passed directly to the module). For future analysis years, NDAL has the ability to include precipitation changes and to model reduced transpiration due to increased atmospheric CO_2 concentration and increased evaporation and transpiration due to air temperature increases. For current (2005) conditions, these changes are set to zero.

A3.4 Outputs

The NDAL submodel produces outputs for each area that include the diversions, seepage (normal and due to a breach repair), drainage, evaporative losses, precipitation change, net evaporation, pumpage, return flow, return flow salinity, and net channel withdrawals. The individual area values are then aggregated into groups (red numbers 1 through 5 in Figure A-1). The return flow, return flow salinity, and net channel withdrawals are then reported to the HD submodel.

A4. NDAL Calculator

The NDAL calculator is a FORTRAN program (FORTRAN) composed of ten subroutines. The WAM model within the DRMS project runs on a daily time step. The NDAL calculator is called by the WAM model at three points within a simulation.

The initial call (the **ReadNDALConfig** routine) opens and reads the configuration files, initializes variables, and reads basic data. This occurs prior at the inception of the WAM model and only happens once (and applies to all levee breach events for a given analysis year [e.g., 2005 conditions]). The second call (the **InitNDALSim** routine) occurs at the start of each simulation sequence. The third call (the **ComputeNDAL** routine) is by the

HD calculator in each time step. The **ComputeNDAL** routine contains the subroutines that actually calculate the outputs requested by the HD calculator and other calculators within the WAM model. It is composed of multiple subroutines and is called upon in each time step (Figure A-2).

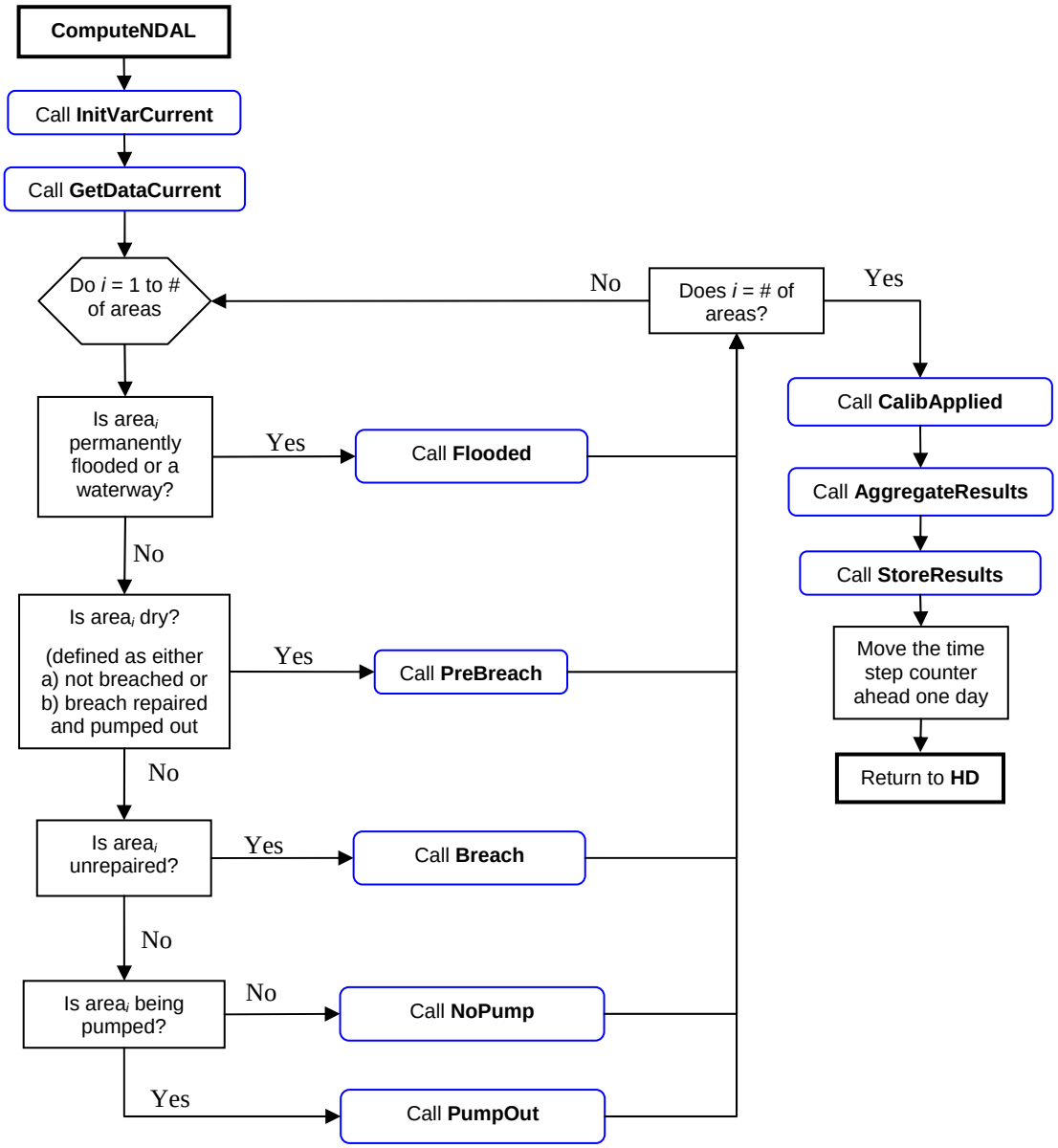

Figure A-2. ComputeNDAL routine flow chart

InitVarCurrent initializes the variables that change value in each time step.

GetData Current populates the variables that change value in every time step. Recall that the input data are monthly average, but that the WAM is running on a daily time

step. The channel salinity concentration is obtained from the HD calculator. Finally the area status and breach information are obtained for the current time step.

EvapCorrection correct the evaporation rate from the flooded water surface area due to changes in salinity concentrations, and uses either channel salinity or the salinity of the water trapped within the area (for repaired islands).

Flooded determines net evaporative losses from and precipitation to the free water surfaces of the permanently flooded areas and waterways based on surface area. Losses depend on the net evaporation rate, the surface area of the free water surface and the salinity of the water in the channel. Flooded areas receive no irrigation diversion, so diversions, seepage, and drainage are all zero. For this version of NDAL, net loss from a breached island free water surface evaporation was approximated by evapotranspiration.

PreBreach determines the output values for an area that is dry (defined as either not breached or repaired and fully pumped out Two general conditions are modeled: irrigation is allowed, or irrigation is terminated due to excessive channel salinity adjacent to the island.

- If the salinity concentration in the channel is below the threshold, irrigation is allowed occur. In this case – based on known diversions, seepage, and drainage rates – the net consumptive use for area *i* is calculated as the difference between inflows to and outflows from the area. For a dry area there are no free water surface net evaporative losses or pump out volumes, only net consumptive use. The return flow is composed of the drainage and the return flow salinity concentration is directly equal to the drainage salinity concentrations.
- When an area is not flooded, but irrigation is terminated due to excessive salinity at diversion points on the periphery of the area, diversion, seepage, drain, return flows and NDAL are all assumed zero (to ensure proper calculation of salinity concentration at the group level). This effectively assumes that consumptive use equals precipitation for these areas, which introduces an underestimate of NDAL in summer and an overestimate in winter. These assumptions will be reviewed during model refinement and verification.

The **Breach** subroutine determines evaporation from the free water surface of a breached area based on known island areas. The area is assumed to be flooded and irrigation has ceased, thus there is no return flow from this area. Salinity of the water trapped in the area is assumed equal to the channel salinity at the time of levee repair. At this point in the logic, the area has been repaired, but still contains water.

The **NoPump** subroutine assesses conditions with irrigation absent and only evaporation and precipitation occurring. Because there is no return flow to the channel via pumping or drainage, the return flow and return flow salinity are negligible. Seepage may be occurring if there is enough of a head differential. Seepage may be occurring through two types of levees: a normal levee and a repaired breach. The volume of water trapped in the area will change depending on the evaporation and precipitation rate and the seepage volume. The volume and salinity of the remaining water are determined. Evaporation does not remove any of the salt in the island and precipitation does not add any, while seepage adds salt. The volume of water in the island at the start of the time period is used

to determine the salt mass in the area at the start of the time step. The volume of water that entered the area from seepage is used to determine the salt added by seepage. The total salt mass in the area is divided by the volume of water in the island at the end of the time period to determine the new salinity concentration. In the current version of the code, evaporation rate is not modified to account for increasing salinity. If volume change due to evaporation (minus precipitation) is greater than the volume of water available then evaporation rates are reduced.

Subsequently the **PumpOut** subroutine defines the process of pumping out the island. There is no irrigation, diversions, or any drainage from the area during pump out. Precipitation continues to occur at the specified rate. Seepage may occur if there is sufficient head differential similar to the **NoPump** subroutine.

The **CalibApplied** subroutine applies the calibration flows (due to the DICU model and CalSim) to each group.

The **AggregateResults** subroutine aggregates the individual area results into the pre-defined groups and reports the results to the HD calculator. The first step is to aggregate the individual area results into their appropriate groupings (based on area group assignments). The HD calculator requires the return flow, return flow salinity, and net channel withdrawals for each group in each time step.

The **StoreResults** subroutine is to store the results from each time step. While not used directly by the WAM, the results could be provided as output if necessary.

A5. References

California Department of Water Resources (DWR). 1995. Estimation of Delta Island Diversions and Return Flows. February.

Marvin Jung and Associates, Inc. 2000. Revision of Representative De3lat Island Return Flow Quantity for DSM2 and DICU Model Runs. Prepared for the CALFED Ad-Hoc Workgroup To Simulate Historical Water Quality Conditions in the Delta. MWQI-CR#3. December.

Personal Communications

J Wilde, California Department of Water Resources (July, 2006)

Appendix B
Delta Water Operations

Table of Contents

B.1 Introduction B-1

B.2 Basic Approach B-1

B.3 State and Federal Project Standard Operating Procedures B-2

B.4 In-Delta Diversions B-2

B.5 References B-2

Tables

B-1 Delta Water Operations in Levee Breach Events – Facilities

B-2 Delta Water Operations in Levee Breach Events – Maximum E/I Ratio

B-3 Delta Water Operations in Levee Breach Events – Net Delta Outflow Index (NDOI) per D-1641

Acronyms and Abbreviations

BAU	Business as Usual
CVP	Federal Central Valley Project
D-1641	SWRCB Water Rights Decision 1641 (2000)
DRMS	Delta Risk Management Strategy
DWR	California Department of Water Resources
E/I Ratio	The ratio of Delta Exports to Inflow, as defined by D-1641
ITF	Initial Technical Framework
SWP	State Water Project
SWRCB	State Water Resources Control Board
WAM	Water Analysis Module or Model

B.1 Introduction

In event of a Delta levee breach incident with island flooding, Delta hydrodynamics and salinity concentrations will be impacted by Delta water operations – gate positions (including the Delta Cross Channel gates and the South Delta barriers), export pump operations (e.g., emergency shutdowns), in-Delta diversions (for Delta island irrigation) and, potentially, upstream reservoir releases to counteract salinity intrusion during island flooding. These factors were recognized and discussed in the Water Analysis Module (WAM) Initial Technical Framework (ITF) paper (DRMS, 2006, see ITF Appendix D). The purpose of this Appendix B is to document the Delta water operations submodel that has been adopted to represent the "Business as Usual" (BAU) response to a Delta levee breach incident within the WAM calculator.

B.2 Basic Approach

The operations submodel reflects the standard project operating procedures that existed in 2005, together with additional details inferred from discussions with operators. In general, operations are closely regulated by the water quality standards established by the State Water Resources Control Board (SWRCB) and set forth in Water Rights Decision 1641 (SWRCB, 2000). Our assumption under BAU is that the federal and state water projects would not intentionally violate a requirement of D-1641. To the extent the projects can be operated with discretion, such actions often require consultation with federal and state fish and wildlife agencies under their respective Endangered Species Act provisions. These consultations require some time to formulate a request, discuss conditions and concerns, and agree on an action. Thus, the operations submodel assumes that any action requiring consultation will not be immediately available (within hours), but will require several days for agreement and implementation.

The operations submodel is subdivided into three phases in coordination with the hydrodynamic and upstream reservoir management submodels (see Appendices D and C, respectively, for additional detail). The phases for Delta Water Operation actions are:

1. **Immediate Response** – Standard operation responses implemented within three hours of event initiation. These operations do not require consultation, although endangered species agencies and the SWRCB would usually be informed as a courtesy. The hydrodynamic submodel will assume these actions are effective during the flooding period – that is, during the period that breached islands are filling.
2. **Flushing** – During the flushing period, as defined in the hydrodynamic submodel, additional operating actions may occur that are discretionary but require time for implementation or that require consultation. An example would be breaching of South Delta agricultural barriers to improve circulation and flushing. The operations submodel assumes BAU means that, even with consultations, actions would not occur if they would compromise the intended protection of endangered species.
3. **Limited Pumping** – When Delta water quality is sufficient to allow export pumping, WAM assumes that normal operating requirements (e.g., relative to gates and barriers) would apply. Per discussions with operators, sufficient water quality is

defined as chloride concentrations that do not exceed 250 mg/l in the pumped water, as is required by the D-1641 standards.

The details of the Delta water operations submodel are presented in Tables B-1 (Water Operations – Facilities), B-2 (Maximum E/I Ratio), and B-3 (Net Delta Outflow Index).

B.3 State and Federal Project Standard Operating Procedures

Actions that qualify as standard operating procedures and would be implemented automatically within three hours of event initiation are few. Most defined procedures are inspection, monitoring, and communications with central operation offices. Those that affect the movement of water are reduction or cessation of export pumping at Tracy and Banks. More specifically:

1. The CVP Tracy Pumping Plant, if it were operating, would reduce pumping to one pump, or approximately 900 cfs.
2. The SWP Banks Pumping Plant would close the Clifton Court Forebay gates if they were open and operational, thereby eliminating any draw on the Delta. If the gates were open and not operational, pumping at Banks would be stopped with a similar, but somewhat delayed, result.

Other actions that are discretionary and could be implemented immediately include emergency releases from upstream reservoirs. Neither the CVP nor the SWP has predefined procedures for implementing such releases. Accordingly, consultations with higher management would occur and such actions would not be immediately implemented. The WAM calculator will not include such responses within the first three days of the flooding phase of the BAU model. Within the flushing phase, such releases would be expected – indeed they may be essential. Generally, the releases described in the latest “Emergency Operations Plan” (DWR, 1986) are used as a starting point and the upstream reservoir operations submodel modifies those releases as warranted by storage available, type of water year, time of year, and other commitments. Again, no increase in releases would occur within the first three days after event initiation (see Appendix C).

B.4 In-Delta Diversions

Per consultations with state and federal project operators and Delta water user interests, there is no clear authority or an institutional mechanism to quickly and effectively manage in-Delta diversions in response to a levee breach incident. Accordingly, no response actions by in-Delta users are detailed in the BAU water operations submodel.

B.5 References

DRMS, 2006. ITF Paper: Upstream Water Management/Delta Water Operations / Delta Island Water Use. Prepared by URS Corporation/Jack R. Benjamin & Associates, Inc., Prepared for Department of Water Resources. September, 2006.

DWR, 1986. Sacramento-San Joaquin Delta Emergency Water Plan – Report to the Legislature, Department of Water Resources. December, 1986.

SWRCB, 2000. Revised Water Right Decision 1641. March, 2000.

Table B-1 Delta Water Operations in Levee Breach Events – Facilities

2005 Base Case (Business as Usual) -- Super Simplified for Simplified Hydrodynamic Submodel							
Facility	**Applicable Control Period**	**Damage State**	**Start of Event Status**	**Immediate Response (within 3 hrs)**	**Flooding Period (after third day) & Flushing Period**	**Limited Pumping**	**Comments**
Gates & Barriers							
Cross Channel	All With High Sac Flow >25,000 cfs	All	Closed	Keep Closed	Keep Closed	Keep Closed Until Flow Decreases and Gates Fixed, if failed	Assumes 25,000 cfs is firm limit for avoiding interior Delta flooding and erosion around gate structure. Assumes gates are both opened or closed; no partial opening.
	Dec 17 - June 3; Closed	All	Closed	Keep Closed	Request Open; Can't Open: Stds Prohibit	Request Open; Can't Open: Stds Prohibit	Consolidates variable closed/open periods in fall and spring into equivalent day for day extensions of winter closed period (up to 45 days in Nov thru Jan – assume closed Dec 17 - Jan 31 and for 14 days May 21 thru June 15 – assume closed through Jun 3).
	June 4 - Dec 16; Norm Open	OK	Open	Keep Open	Keep Open	Keep Open	
Clifton Court Forebay	All	All					Lump with Banks under pumps
Suisun Marsh Salinity Control	All	All					The Suisun Marsh Salinity Control Gates have little impact on Delta salinity. They will not be included in the simplified model.
South Delta Temporary Ag Barriers (3)	Installed Period; April 16 - Nov 15	N/A	Closed	No Change, Closed	Request Open; Assume Open	Request Open?; Assume Closed	If pumps are off (for Delta flushing), water levels should be adequate for South Delta agricultural users and improved circulation should result from breaching barriers. When pumping starts, assume the barriers are restored.

Table B-1 Delta Water Operations in Levee Breach Events – Facilities

2005 Base Case (Business as Usual) -- Super Simplified for Simplified Hydrodynamic Submodel							
Facility	**Applicable Control Period**	**Damage State**	**Start of Event Status**	**Immediate Response (within 3 hrs)**	**Flooding Period (after third day) & Flushing Period**	**Limited Pumping**	**Comments**
	Open Period; Nov 16 - April 15	N/A	Open	No Change, Open	Keep Open	Keep Open	
Head of Old River Temp Fish Barrier	Installed Periods; April 16 - May 15, Sept 16 - Nov 15	N/A	Closed	No Change, Closed	Request Open; Assume Closed for Fish	Request Open?; Assume Closed	Assume barrier still provides significant enhancement for San Joaquin River fish and must be maintained. The three ag barriers are not necessary for the fish barrier to be effective (per DWR ops, TH).
	Open Periods; May 16 - Sept 15, Nov 16 - April 15	N/A	Open	No Change, Open	Keep Open	Keep Open	
Pumping Plants							
Banks	Any	All	All	Off	Keep Off	On As Needed, If Clifton Court OK or Repaired and Banks OK or Repaired*	For Clifton Court and Banks, assume if there is one gate, pump, or power failure all is shut down. Note that this is because we are not really concerned about individual equipment problems; we are concerned about massive environmental loadings (e.g., earthquakes) that will affect all similar equipment in similar ways. * is for E/I ratio and min NDOI. See next sheets.

Table B-1 Delta Water Operations in Levee Breach Events – Facilities

2005 Base Case (Business as Usual) -- Super Simplified for Simplified Hydrodynamic Submodel							
Facility	**Applicable Control Period**	**Damage State**	**Start of Event Status**	**Immediate Response (within 3 hrs)**	**Flooding Period (after third day) & Flushing Period**	**Limited Pumping**	**Comments**
Tracy	Any	OK	On	Reduce to One Pump (900 cfs)	Keep to One Pump (900 cfs); Off if Salty	On As Needed*	Criteria for turning off final pump during flooding or flushing is chloride > 250 mg/l; WQ Std. *See next sheets for E/I Ratio & NDOI.
		Fail (stops if on)	All	Off	Keep Off	On As Needed, If Repaired*	Assume if one fails, all fail. *See next sheets for E/I Ratio & NDOI.
CCWD Old River	Any	OK	On	No Change	Off if Salty	On As Needed	For Jones Tract, CCWD suspended pumping one day at Old River (6/6, three days after event initiation), but this seems to have been a precaution. Assume chloride > 250 mg/l is stop criterion; WQ Std. CCWD is not included in E/I Ratio calc or April/May diversion limit, but its diversions subtract from NDOI. It limits diversions from March 15 to May 31 for fish (no diversion in April), but this seems to be voluntary.
		Fail (stops if on)	All	Off	Keep Off	On As Needed, If Repaired	

Table B-1 Delta Water Operations in Levee Breach Events – Facilities

2005 Base Case (Business as Usual) -- Super Simplified for Simplified Hydrodynamic Submodel							
Facility	**Applicable Control Period**	**Damage State**	**Start of Event Status**	**Immediate Response (within 3 hrs)**	**Flooding Period (after third day) & Flushing Period**	**Limited Pumping**	**Comments**
CCWD Rock Slough	Any	OK	On	No Change	Off if Salty	On As Needed	No lessening of pumping for Jones Tract. Assume chloride > 250 mg/l is shut down criterion. See above.
		Fail (stops if on)	All	Off	Keep Off	On As Needed, If Repaired	
North Bay Aqueduct	Any	OK	On	No Change	Off if Salty	On As Needed	No immediate lessening of pumping for Jones Tract. Some decrease in pumping 6/6 through 6/10. Assume chloride > 250 mg/l is shut down criterion; WQ Std). NBA diversions subtract from NDOI.
		Fail (stops if on)	All	Off	Keep Off	On As Needed, If Repaired	
Upstream Reservoir Releases							
New Melones	Wet Year	OK	All	None	Up to 2,000cfs for up to 0 days	None	2,000 cfs as indicated in 1986 report. Water availability limited per USBR because senior water rights holders (rather than the CVP) control essentially all the stored water. Assume none is available, per USBR operators instruction.
	All Other Years	OK	All	None	None	None	Bureau indicates water not available.

Table B-1 Delta Water Operations in Levee Breach Events – Facilities

2005 Base Case (Business as Usual) -- Super Simplified for Simplified Hydrodynamic Submodel							
Facility	**Applicable Control Period**	**Damage State**	**Start of Event Status**	**Immediate Response (within 3 hrs)**	**Flooding Period (after third day) & Flushing Period**	**Limited Pumping**	**Comments**
Friant/Millerton	Any	OK	All	None	Only if ordered by SWRCB	As required to meet Exchange Contractor water rights	Need to review criteria for Bureau decision to tap for Exchange Contractors and Refuges or SWRCB order for Delta WQ mitigation and flow rate and duration
San Luis	Any	OK	All	None	Only to prime pumping; assume none	None	Need to review criteria for "priming pumping"
Folsom	Any	OK	All	None	Up to 5,000 cfs; assume for up to 2 weeks	None	5,000 cfs as indicated in 1986 report. Review availability draw rule. Assume up to 2 weeks = 140,000 af, but decrease Folsom as Oroville and Shasta arrive to keep Sac River flow <25,000 cfs.
Oroville/Thermalito	Any	OK	All	None	Up to 3,000 cfs; assume for up to 2 months	As Needed	3,000 cfs as indicated in 1986 report. Review draw rules in order to confirm or adjust the assumed maximum period of availability.
Shasta/Trinity/ Whiskeytown/ Keswick	Any	OK	All	None	Up to 4,000 cfs; assume for up to 2 months	As Needed	4,000 cfs as indicated in 1986 report. Review draw rules in order to confirm or adjust the assumed maximum period of availability.

Note:
It would be logical to have different operation responses for different situations, such as high versus low flows and one or two islands flooded versus three or four islands versus five or more. This type of pre-planning is not now formalized. The only impact of high flows is closure of the Cross Channel Gates.

Table B-2 Delta Water Operations in Levee Breach Events – Maximum E/I Ratio

Time (Month)	Water Year Type	Maximum E/I Ratio	
Oct	All	0.65	
Nov	All	0.65	
Dec	All	0.65	
Jan	All	0.65	
Feb	All	0.35	
Mar	All	0.35	
Apr 1-14	All	0.35	
Apr 15-30	All	0.35	E limit is 1,500 cfs Actual limit is more complex; assume 1,500 cfs for WAM
May 1-15	All	0.35	E limit is 1,500 cfs Actual limit is more complex; assume 1,500 cfs for WAM
May 16-31	All	0.35	
June	All	0.35	
July	All	0.65	
Aug	All	0.65	
Sept	All	0.65	

Note:
For the 2005 Base Case (Business as Usual); simplified for the simplified hydrodynamic submodel but based on D-1641, Table 3.
E = Exports (defined only for E/I calc) = Tracy PP + (Clifton Court Forebay Diversions net of Byron-Bethany ID)
Note that this number is less than total exports; it doesn't include CCWD or NBA.
Byron-Bethany ID diversion actually occurs through Clifton Court but is included in DICU.
I = Delta Inflow = Sac Riv + Sac Reg Waste TP + Yolo + San Joa Riv + East (Mok, Cos, Calav)
Misc (BearCr, DryCr, StocktonDivCan, FrenchCmpSl, MarshCr, & MorrisonCr)

Table B-3 Delta Water Operations in Levee Breach Events – Net Delta Outflow Index (NDOI) per D-1641

	Water Year Type						
Time (Month)	**All**	**Wet**	**Above Norm**	**Below Norm**	**Dry**	**Critical**	
cfs; this is a monthly target for ave of daily numbers; compliance ok if 7-day ave is within 1,000 cfs							
Oct		4,000	4,000	4,000	4,000	3,000	Note that for Oct through Dec, Water Year Type is for the previous water year.
Nov		4,500	4,500	4,500	4,500	3,500	
Dec		4,500	4,500	4,500	4,500	3,500	
Jan	4,500	4,500	4,500	4,500	4,500	4,500	Increase to 6,000 if Eight River Index for Dec is > 800 TAF
Feb	7,100	7,100	7,100	7,100	7,100	7,100	
Mar	7,100	7,100	7,100	7,100	7,100	7,100	Considered satisfied if daily or 14-day ave EC at Collinsville is ≤ 2.64 mmhos/cm
Apr	7,100	7,100	7,100	7,100	7,100	7,100	(Simplified model just use the number from the table.)
May		7,100	7,100	4,000	4,000	4,000	The table is a simplification of the standard for May and June
June		7,100	7,100	4,000	4,000	4,000	
July		8,000	8,000	6,500	5,000	4,000	Note that there are also Sacramento and San Joaquin flow requirements
Aug		4,000	4,000	4,000	3,500	3,000	
Sept	3,000	3,000	3,000	3,000	3,000	3,000	

Note:
It is not clear whether "precipitation runoff" is different from precipitation.
NDAL must include Byron-Bethany and Delta depletions due to any other miscellaneous diversions (e.g., the Vallejo intake on Cache Slough).
2005 Base Case (Business as Usual) – Simplified for Simplified Hydrodynamic Submodel
NDOI = Delta Inflow - Net Delta Consumptive Use - Delta Exports
Delta Inflow = I = Same as defined for E/I ratio
= Sac Riv + Sac Reg Waste TP + Yolo + San Joa Riv + East (Mok, Cos, Calav) + Misc (BearCr, DryCr, StocktonDivCan, FrenchCmpSl, MarshCr, & MorrisonCr)
Delta Exports = Elarger = E (for E/I ratio) + CCWD + NBA
Net Delta Consumptive Use = GDEPL – PREC
GDEPL = Delta gross channel depletion for the previous day based on water year type using DWR's latest land use study.
PREC = Real-Time Delta precipitation runoff for the previous day estimated from stations within the Delta

Appendix C
Reservoir Management

Table of Contents

C.1 Physical System C-1
C.2 Available Water Management Models C-2
C.3 Submodel Functions C-4
C.4 Boundary Conditions and Basic Data C-4
C.5 Normal Operations C-6
C.6 Approach Implemented to Model Reservoir Management C-9
C.6.1 Model Procedure C-9
C.6.2 Operation Rules C-10
C.6.3 Definition of Available Upstream Supply C-11
C.6.4 Reservoir Descriptions C-11
C.6.4.1 Folsom Reservoir C-12
C.6.4.2 Oroville Reservoir C-12
C.6.4.3 Shasta Reservoir C-12
C.6.4.4 Trinity Reservoir C-12
C.6.4.5 New Melones Reservoir C-12
C.6.4.6 Proximity to the Delta C-13
C.6.5 Definition of Maximum Upstream Release C-13
C.6.6 Sharing of Delta Supplies C-13
C.6.7 South of Delta Reservoir Management C-13
C.6.7.1 CVP South of Delta Storage C-13
C.6.7.2 SWP South of Delta Storage C-14
C.6.8 South of Delta Water Allocations C-14
C.6.8.1 CVP South of Delta Allocations C-14
C.6.8.2 SWP South of Delta Allocations C-15
C.6.9 Balance of North of Delta Storage with Starting South of Delta Storage and Normal Needs C-16
C.6.9.1 Balance of North of Delta Storage with South of Delta Conditions and Desire for Flushing Flows C-16
C.6.9.2 Rules Included to Determine Export Levels Based on Delta Salinity C-16
C.6.10 Rules to address upstream storage deficits C-16
C.6.11 Determining the End of the Recovery Period C-17

C.6.12 Reservoir Management Submodel Characteristics C-17
C.6.13 Reservoir Management Submodel Sample Results C-18

Tables

C-1 Water Analysis Module (WAM) Computational Processes for Reservoir Management Submodel
C-2 Sample Reservoir Level Table

Figures

C-1 Water Analysis Module Basic Logic Flow Chart
C-2 WAM Submodels Data Exchange Points
C-3 CalSim Output Viewer
C-4 CVP Exports
C-5 SWP Exports
C-6 Total South of Delta deliveries
C-7 SWP Delivery to MWD
C-8 SWP Delivery to M&I (other than MWD)
C-9 SWP Delivery to Agriculture
C-10 SWP Delivery to Article 21
C-11 CVP Delivery to Agricultural Service Contractors
C-12 CVP Delivery to M&I Contractors
C-13 CVP Delivery to Refuges
C-14 CVP Delivery to Exchange Contractors
C-15 CVP Delivery to Friant Agricultural Service Contractors
C-16 Total South of Delta Storage
C-17 Storage in CVP Portion of San Luis
C-18 Storage in SWP Portion of San Luis
C-19 SWP South of Delta “Terminal Reservoir” Storage

Acronyms and Abbreviations

CalSim	California Water System Simulation Model (DWR & USBR)
CALVIN	CALifornia Integrated Value Network
cfs	cubic feet per second
CVP	Federal Central Valley Project

DMC	Delta Mendota Canal
DRMS	Delta Risk Management Strategy
DWR	California Department of Water Resources
EC	Electrical Conductivity
HD	The WAM Hydrodynamic / Water Quality Submodel
ITF	Initial Technical Framework
M&I	Municipal and Industrial
MAF	Million Acre-Feet
NDAL	Net Delta Area Losses (or Net Delta Consumptive Water Use)
SOD	South of Delta
SWP	State Water Project
SWRCB	State Water Resources Control Board
TAF	Thousand Acre-Feet
TM	Technical Memorandum
USBR	United States Bureau of Reclamation
WAM	Water Analysis Module or Model
WY	Water Year

C.1 Physical System

Following occurrence of a levee failure, particularly during events that involve multiple breaches and more than one flooded island, decisions must be made to manage Delta inflows and outflows. Hydrodynamic model simulations suggest these decisions are critical to both short-term and long-term water quality in the Delta. The impact on water quality then directly affects the consequences of ultimate concern – water exports, Delta island water availability, ecosystem functions, and economic disruption. Similarly water management decisions must be made about the management of water delivered to customers.

The most difficult water management responses focus on upstream and South of Delta reservoirs. The appropriate reservoir management responses are not always obvious.

- Should freshwater flows into the Delta be increased?
- If increases are desired, what quantity and on what schedule?
- How should the need for additional flushing water be balanced with the need to save water for environmental needs, other water users, future exports and protection against dry years?
- Should South of Delta stored water be delivered now or saved, in case of a prolonged disruption of Delta exports?

For any given levee breach event, water project reservoir operators will be faced with several reasonable options, each with some likelihood of being most appropriate and at the same time some uncertainty regarding its short-term effects and long-term benefit. Thus, as a levee breach event unfolds, reservoir managers will have to choose a particular course of action.

Such operating decisions will either shorten or prolong periods of high salinity that inhibit or prevent water export and may intensify or mitigate other consequences such as stress on critical Delta species and water supplies available for basic municipal health and safety needs. Even the simplest concepts of “reservoir management response” imply a description of the considerations and rules used in decision-making and the related action or inaction relative to water flows.

Resulting Delta inflows are a critical input to assessing the hydrodynamic response of the Delta and the estimated water quality impacts are quite sensitive to the inflows used. To quantify the ultimate consequences, it is necessary to have estimates of what the Delta inflows will be throughout an incident and during the recovery period. Hydrodynamic simulations of levee failures indicate that reservoir management decisions concerning Delta water inflows have a marked effect on water quality and effects are particularly important early in the incident.

Also the allocation of available supplies south of the Delta for delivery during various periods throughout the duration of the incident require careful decisions so that overly restrictive rationing is avoided but sufficient reserves are maintained to avoid more drastic cuts later in the incident.

Each levee breach incident is, in principal, unique, with its consequences depending in large part on the reservoir management decisions and resulting Delta inflows and deliveries to contractors. Thus, the reservoir management submodels must effectively consider several factors including, but not limited to:

- Potential duration of the incident (e.g., the number of breaches and flooded islands, the resulting repair period, and when in the repair sequence partial pumping might begin),
- Stored water available for use as Delta inflows,
- Need to reduce storage at particular times for flood protection,
- Need to retain storage at other times for future pumping and drought protection, and
- Need for critical benefits such as health and safety or protection of endangered species.

Such needs have varying importance depending on specific incident circumstances. The submodels discussed here include allowances for such variations. However, the submodels are simple and are focused on the big picture. They are first generation. Since they are to address each levee breach incident in a practical manner, they are not expected to predict all factors that affect reservoir management decisions and Delta inflows.

C.2 Available Water Management Models

Presently available California water management models include CalSim and CALVIN. CALVIN is an optimization model oriented toward policy decisions that interact with the state's water system under normal circumstances. CalSim is the statewide water operations model presently used by the state and federal projects to simulate reservoir and other aspects of project management. CalSim is also designed to simulate operation under normal conditions.

With a levee breach incident in the Delta, conditions become abnormal (perhaps even extremely abnormal) and operating strategies must change. Significantly different operating rules are required to manage reservoir operation responses to a major levee failure emergency. Submodels must focus on those reservoir operation responses and interact with the submodels simulating hydrodynamics and water quality in the Delta. The CalSim structure does not lend itself to that application. Thus, special submodels have been developed for the specific applications indicated in Figure C-1. Water managers do have important criteria or rules that are implicitly used in their decision making. These have been described, extended, and formalized into workable submodels for a levee breach incident. Some components from the existing models incorporate such rules and they have been adapted, extended, and applied where possible.

Due to computation effort, simple tools are required. CalSim or other "heavy" lifting models do not meet this need. The form selected for the submodels is therefore water-balance models that are constrained primarily by physical factors and operating rules. Interviews with operators and input from others have been used to initially represent and constrain reservoir operations. Existing, complex models, such as CalSim, have been

used to assist in developing the essential, simplified relationships for creating reservoir management submodels that satisfy WAM needs.

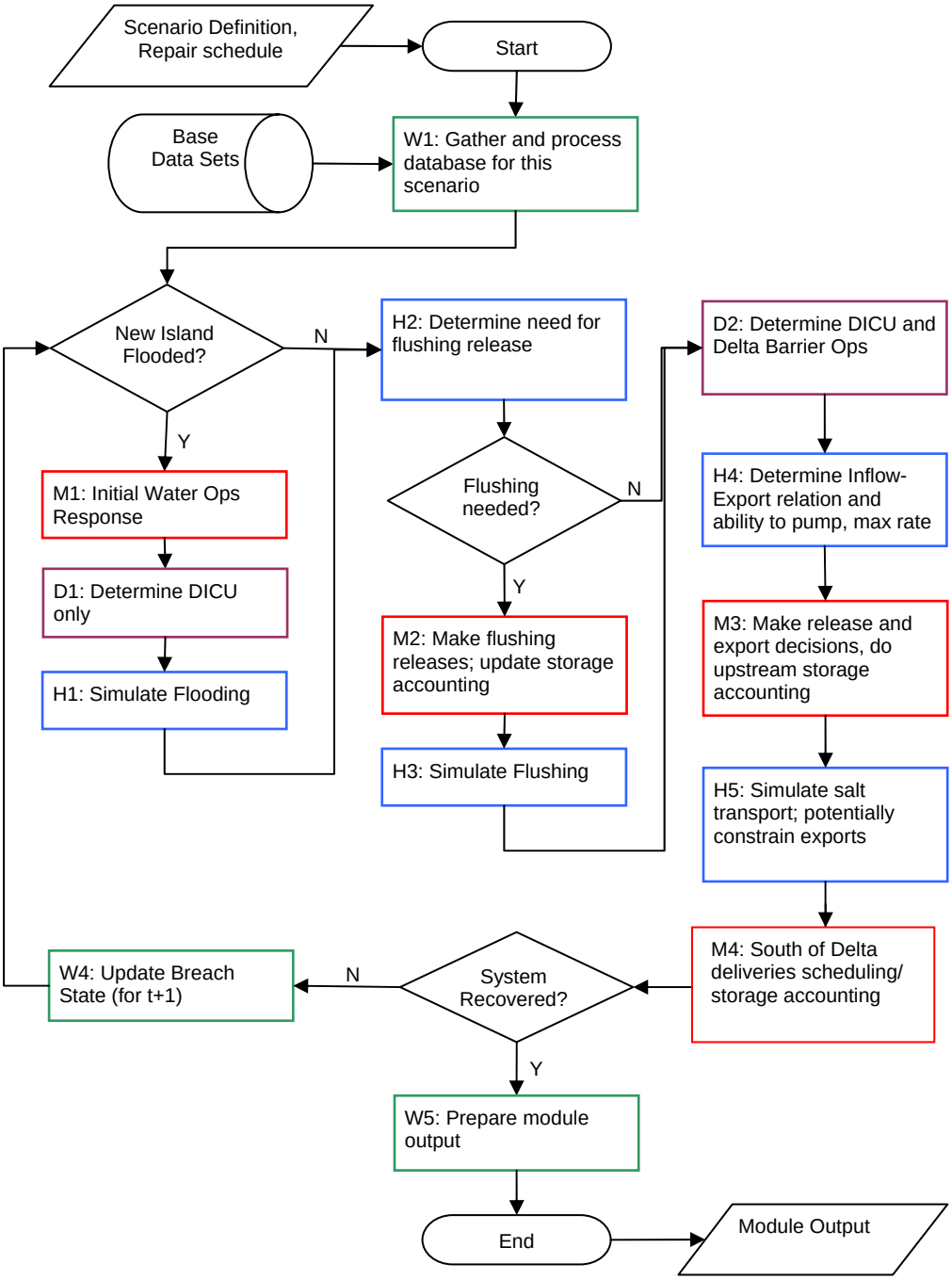

Figure C-1 Water Analysis Module Basic Logic Flow Chart
(Reservoir Management Submodel is responsible for Steps M1, M2, M3, and M4.)

C.3 Submodel Functions

Reservoir management ("M") submodels are to simulate these decisions, responsive to the distinct stages of the incident – flooding, flushing, and limited pumping – as outlined in Figure C-1. The four reservoir management submodels indicated are highlighted in red and are:

- M1 – Flooding Period Reservoir Releases
- M2 – Flushing Period Reservoir Releases
- M3 – Repair/Recovery Period Reservoir Releases
- M4 – South of Delta Scheduling of Deliveries

The first three "M" submodels address Delta inflows. Other submodels address water quality, in-Delta water use, and Delta water operations. The fourth "M" submodel considers the tradeoffs South of Delta between delivering available supplies now versus saving them for later. The calculation protocol for each submodel is given in Table C-1.

The water/reservoir management submodels are:

M1: Decide whether to adjust releases immediately on incident initiation to respond to the island flooding phase. The present approach is to hold releases constant. Decisions to change releases take some time and then flows take time to reach the Delta. In all but severe events changed reservoir releases will arrive too late to affect the flooding phase.

M2: Decide what flushing releases can be provided responsive to the H2 request, considering the type of water year, time of year, available storage, and prospective needs in future months. The earlier this decision can be made, the better. Presently, the submodel includes a three day period for consultation and decision making prior to actual release changes.

M3: Decide what releases to provide to Delta inflow (for NDAL, Delta outflow and exports), considering the type of water year, time of year, available storage, the required Delta outflow versus for various amounts of exports provided by H4, and prospective storage reserves needed or Delta repair progress in coming months.

M4: Decide on scheduling of south of Delta deliveries, based on anticipated incident duration, available stored water, user needs, and available upstream storage.

C.4 Boundary Conditions and Basic Data

The state of the water resource system upstream and the Delta inflows at the time of the incident are essential inputs for the water management submodels. Also, the state of the resource south of the Delta, particularly storage, at the time of the incident is an essential input to south of Delta delivery scheduling and affects north of Delta water management.

Since WAM is designed to work with a wide variety of levee breach initiation dates, this information is required for each water year and incident initiation date modeled. To achieve this compatibility, WAM is designed to use the first day of any month in the CalSim 82-year historic sequence as an event initiation date. This provides (82 X 12 =) 984 possible event initiation dates. In addition, basin and reservoir inflow hydrologic data

Table C-1 Water Analysis Module (WAM) Computational Processes for Reservoir Management Submodel

	Description	Input	Output
M1	Initial estimate for reservoir operations response – hold releases	Scenario description Hydrology Reservoir states	Delta inflows and exports during period of flooding
M2	Make flushing releases and update storage accounting. Releases may be less than requested by hydro model.	Scenario description Hydrology Reservoir states Requested flushing volume (Flow-Volume relation)	Delta inflows and exports during period of flushing
M3	Make release and export decisions, perform storage accounting for upstream reservoirs considering the inflow-export relationship determined by hydro model	Scenario description Estimated duration Hydrology Reservoir states Delta outflow-exports relationship	Delta inflows and exports during period Updated upstream reservoir storage
M4	Make South of Delta water delivery allocations to SWP and CVP contractors	Estimated duration South of Delta Storage Accumulated Delivery Cuts	Deliveries to Contractors Updated South of Delta Storage

are required for the years being used (both north and south of the Delta). Antecedent conditions are expected to be particularly important in calculating the water availability, thus they receive close consideration. The inputs and outputs of CalSim provide the hydrology and water system data that are needed to drive WAM's water management submodels, thus the WAM submodels have been designed to draw on CalSim inputs and outputs as the fundamental source of hydrologic data.

Boundary conditions include reservoir storage, river flows, and water deliveries throughout the CVP/SWP system and the Delta. CalSim outputs are used to establish these boundary conditions at the time an event in the Delta occurs. CalSim output is also used to establish boundary conditions for the Delta hydrodynamic/ water quality model. Figure C-2 contains a graphic depicting main Delta channels and indicates the locations of boundary condition flows provided by CalSim. Key reservoir storage and flows that have been extracted from CalSim are displayed in a CalSim output viewer in Figure C-3.

Hydrologic conditions are characterized by water year type using one of the recognized indices such as the Sacramento River Index. Antecedent water year type and the incident water year type are incorporated by maintaining the CalSim water year sequence. The index influences the reservoir management submodel in the first instance though the CalSim base case. When an event start time is specified, it is specified in terms of a CalSim year and month. Thus, for example, it may be specified as June, 1977. The reservoir management model then extracts the CalSim output data for June 1, 1977 and those data become the boundary conditions with which WAM starts. The fact that 1977 was a Critically Dry year is used in managing the upstream and South of Delta reservoirs. The fact that the preceding year was also critically dry is reflected in the base case and is also part of the basic information used to calculate the way that WAM responds to the incident.

C.5 Normal Operations

Normal operations, in absence of the levee-breach incident, from the time of the event to the end of the water year as indicated by the CalSim operating rules provides a starting point for considering what reservoir operation modifications would be helpful and prudent. This depends strongly on the water year type and the hydrologic record, but reservoir management decision making is not able to "look ahead" at the upcoming hydrologic record. Depending on the event initiation date, there may be relatively good information about water available for the next several months, or (especially in late fall) there may be substantial uncertainty. The hydrologic conditions (e.g., wet, normal, or dry) due to the upcoming wet season are not yet known and operations are likely to be similar regardless of the next water year type. An important aspect of this is recognition of reservoir draw down requirements in preparation for the upcoming flood season. These normal operations are needed to make sure that the WAM reservoir operation rules converge with those actually used in "no breach" situations. They are also needed to provide a "without event" baseline for economic analyses.

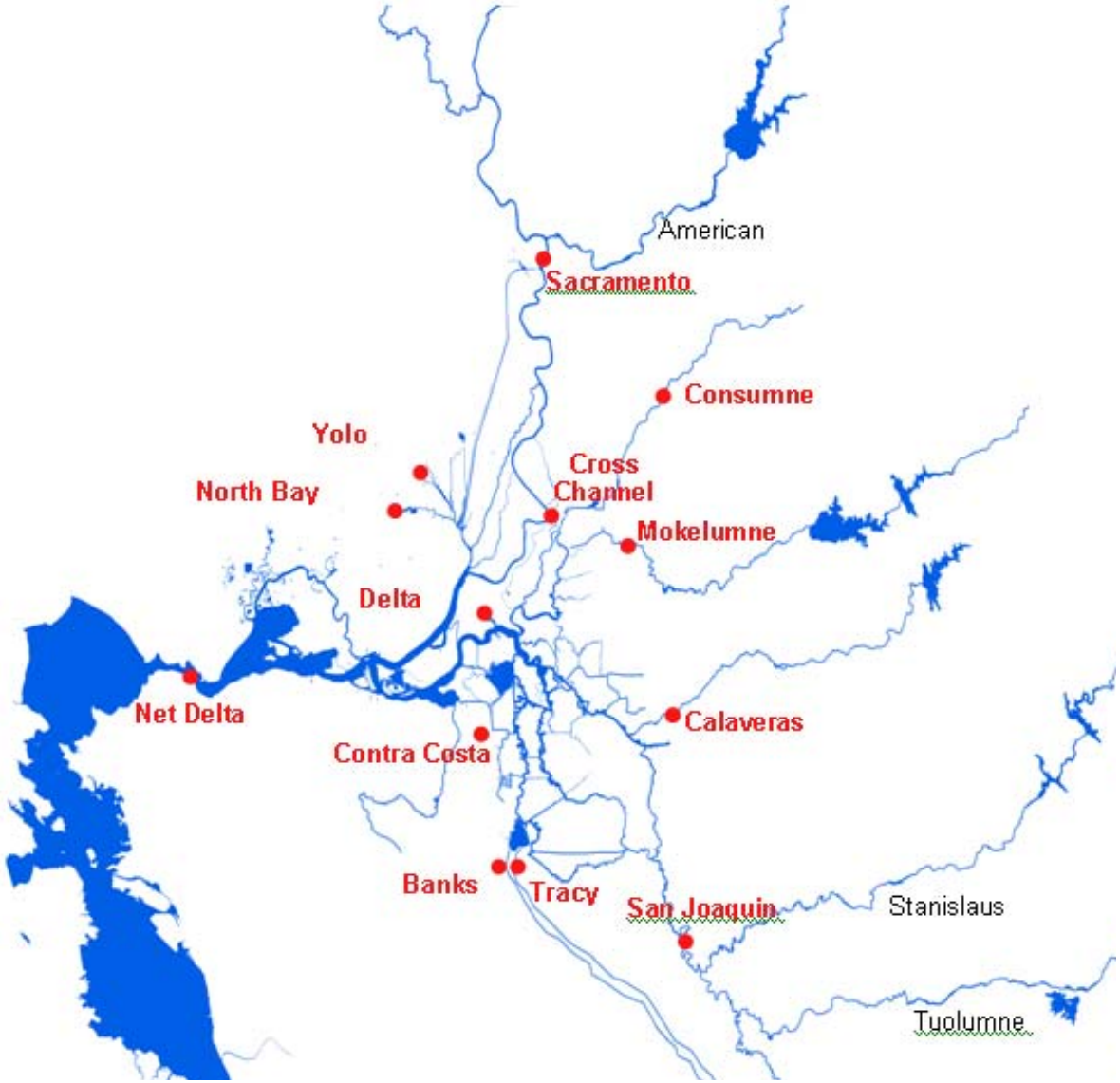

Figure C-2 WAM Submodels Data Exchange Points

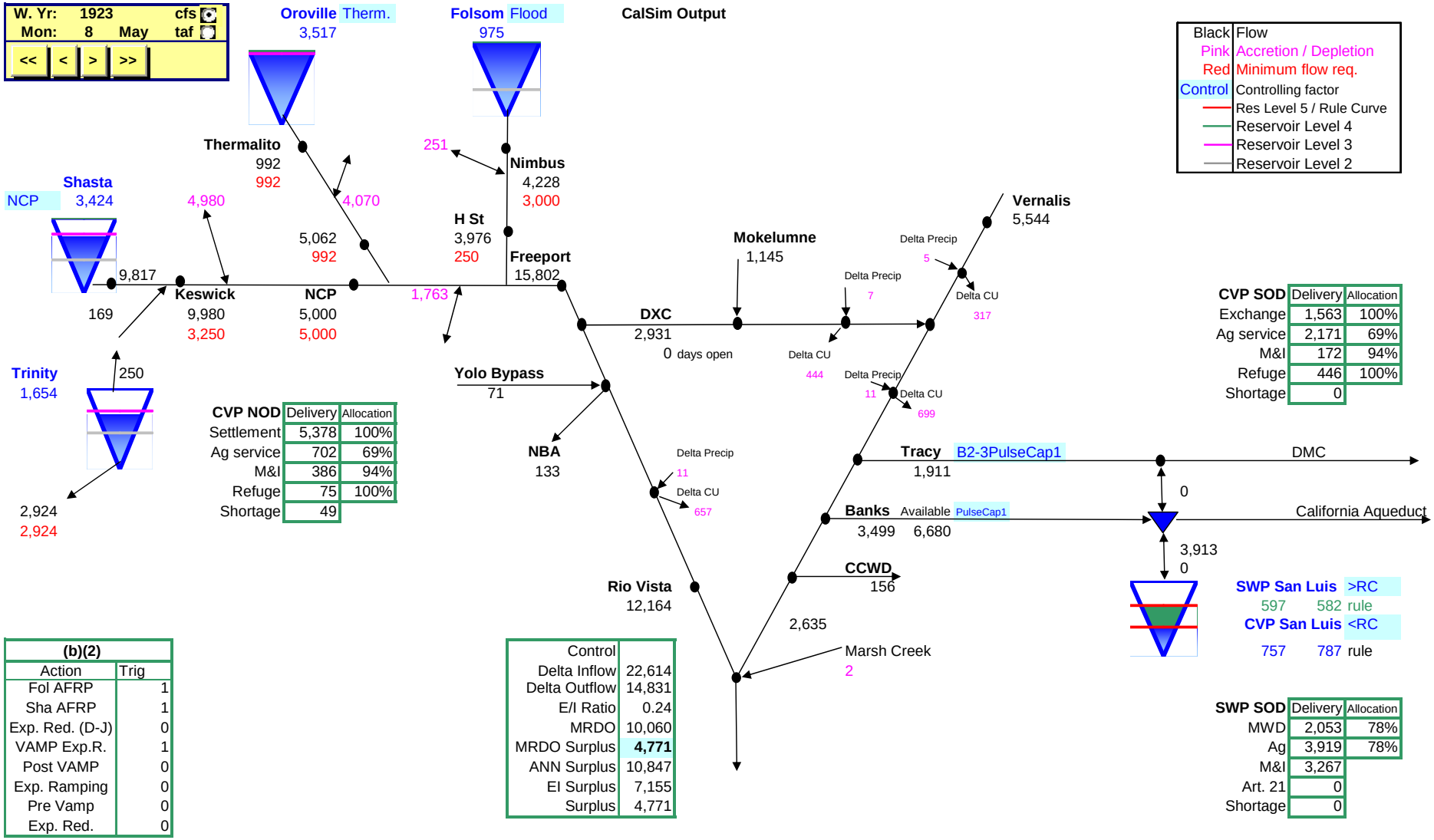

CVP NOD	Delivery	Allocation
Settlement	5,378	100%
Ag service	702	69%
M&I	386	94%
Refuge	75	100%
Shortage	49	

CVP SOD	Delivery	Allocation
Exchange	1,563	100%
Ag service	2,171	69%
M&I	172	94%
Refuge	446	100%
Shortage	0	

(b)(2)	
Action	Trig
Fol AFRP	1
Sha AFRP	1
Exp. Red. (D-J)	0
VAMP Exp.R.	1
Post VAMP	0
Exp. Ramping	0
Pre Vamp	0
Exp. Red.	0

Control	
Delta Inflow	22,614
Delta Outflow	14,831
E/I Ratio	0.24
MRDO	10,060
MRDO Surplus	**4,771**
ANN Surplus	10,847
EI Surplus	7,155
Surplus	4,771

SWP SOD	Delivery	Allocation
MWD	2,053	78%
Ag	3,919	78%
M&I	3,267	
Art. 21	0	
Shortage	0	

Figure C-3 CalSim Output Viewer

The outputs of primary interest from this projection of routine operations are:

- Reservoir storages upstream of the Delta
- Delta inflows
- Normal exports

The above data and projections are independent of the incident; they depend only on the antecedent conditions, type of water year, and the incident start date.

The basin/reservoir inflow hydrology is used as input to drive the WAM. In modeling response to the incident, water normally exported is available for reallocation to Delta flushing, retention in storage, or partial pumping (if pumping is feasible based on water quality achieved in managing the incident). Additional water might be used based on reducing end-of-year carryover storage and anticipated limitations on pumping during the next water year.

C.6 Approach Implemented to Model Reservoir Management

The reservoir operations model is responsible for determining reservoir releases and target exports following a breach event and throughout the repair/recovery period. This model relies on hydrologic data from CalSim along with information from the hydrodynamic/water quality model, and is based on operating rules to balance upstream storage with Delta needs, the needs of other beneficial uses, and export needs. This only includes simulation of CVP/SWP facilities and the river systems affecting or affected by their operation.

C.6.1 Model Procedure

The basic modeling procedure can be characterized in five basics steps:

1. Boundary conditions for a specified hydrologic year type and month are read in from consolidated CalSim results.
2. The event occurs and desired flushing flows, export limits, altered NDAL, and/or an outflow-export relationship from the hydrodynamic/water quality consequence model are read in as appropriate.
3. Delta export targets and supporting upstream reservoir releases are calculated based on water availability, the temporal context, prospective future needs, perceived export needs, and Delta conditions.
4. South of the Delta reservoirs are operated and CVP / SWP allocations are revised based on ability to export and water available in storage.
5. Releases are made from Friant Dam when CVP Exchange contractor demands can not be satisfied from the Delta

The submodels are designed to respond to conditions calculated by the hydrodynamic/water quality model. They recognize and respond to initial flushing, prolonged periods of no pumping, partial pumping or operations during the repair/recovery period. The submodels include various rules to operate reservoirs for

releasing flushing flows and the substantial increases in carriage water required to support export operations in the context of a levee breach incident.

C.6.2 Operation Rules

Operating rules are used to manage the emergency responses to the various stages of a full range of levee failure incidents, from single breaches to multiple, simultaneous breaches. Considerable input has been obtained from the operators and policy makers responsible for managing the State's water system so the decision model actually simulates their likely response to the emergency. Several rules have input variables to control the operations. Rules are structured in terms of the following categories or concepts, which have varying applicability to the submodels:

- Available upstream supply is based on reservoir storage levels and minimum levels required to ensure adequate water remains upstream to meet prospective environmental requirements and upstream water deliveries. In addition, this parameter recognizes the need for meeting flood control space requirements in the fall and establishes reserves for carryover to potential dry periods.
- Maximum upstream release from each reservoir is variable and based on physical constraints, upstream fishery requirements, hydropower needs, and the needs of water users between the reservoir and the Delta. In the unusual situation when the factors above indicate that available water is less than would be needed for minimum releases, the minimum release is assumed. In the very rare instance when dead pool is reached, a deficit account is maintained. Allocation of deficits to downstream beneficial uses (north of Delta contractors and fish flows) has not yet been accomplished in the model. This is recognized as a loose end that needs to be addressed in further work.
- Rules are included to balance available upstream water supply with flushing flow requirements within Submodel M2
- Rules are included to determine export levels based on Delta current state of repair (as reflected by carriage water costs) and prospective improvements of conditions and share available Delta supplies based on the Coordinated Operating Agreement (COA).
- Rules govern use of CVP and SWP south of the Delta storage and balance storage between SWP San Luis and SWP terminal reservoirs.
- Rules are use to allocate water to CVP and SWP contractors south of the Delta based on water availability, type of water use, and contracts.
- Rules are included to balance north of Delta storage with south of Delta normal needs, cumulative deficits, and the duration to date of export disruptions. If exports are possible, Submodel M3 attempts to meet "baseline" export levels considering upstream water availability, the outflow-export relationship ("carriage water" cost), and accumulated deficits.

- Rules have been developed to address deficits in upstream storage caused by increased releases in previous months to flush the Delta
- Additional rules have been included, as necessary, to produce a reasonable simulation of the way in which water projects operate under current (2005) policies.

Actual rules and input parameters are to be adjusted based on initial model results, which are now being reviewed. For example, if releases to satisfy Delta needs result in adverse environmental upstream impacts or cause unacceptable reduction in upstream water deliveries, input rules will be refined to avoid the undesirable consequences.

The approach used for developing the various types of rules is presented in more detail below.

C.6.3 Definition of Available Upstream Supply

This definition is based on reservoir storage levels and minimum levels required to ensure adequate water remains upstream to meet environmental requirements and upstream water deliveries. In addition, reserves are established for project carryover to protect against potential dry periods.

Each upstream reservoir in the CVP/SWP has a unique physical makeup, location relative to the Delta, hydrologic properties, environmental requirements, agricultural demands, and M&I demands. Although the unique nature of each reservoir is considered in the operating rules and parameters, the form of the rule is similar for each reservoir. The storage rule takes the form shown in Table C-2, where the values represent minimum acceptable reservoir levels after making additional releases.

Table C-2 Sample Reservoir Level Table

Year Type	Oct	Nov	Dec	Jan	Feb	Mar	Apr	May	Jun	Jul	Aug	Sep
Wet	100	110	120	130	140	150	150	150	150	140	130	120
Above Normal	95	105	115	125	135	145	145	145	145	135	125	115
Below Normal	90	100	110	120	130	140	140	140	140	130	120	110
Dry	85	95	105	115	125	135	135	135	135	125	115	105
Critical	80	90	100	110	120	130	130	130	130	120	110	100

C.6.4 Reservoir Descriptions

The following descriptions of upstream reservoirs are the basis of rules governing additional releases during and after an event in the Delta.

C.6.4.1 Folsom Reservoir

Folsom is a CVP reservoir that holds about 974 TAF with an average annual inflow of about 2.7 MAF. Because the inflow is almost 3 times the storage capacity it has a high probability of refill each year. Folsom is operated to meet instream flows and temperature requirements, provide releases for Delta needs, and meet large M&I demands in the American River basin. Before additional releases can be made from Folsom consideration is given to instream fisheries, where flow fluctuations can cause significant damage to spawning salmon and steelhead. In addition to fishery considerations, adequate carryover is maintained to provide drought protection to urban water users.

C.6.4.2 Oroville Reservoir

Oroville is a SWP reservoir that holds about 3.5 MAF with an average annual inflow just under 4 MAF. Oroville is the only major upstream water supply source for the SWP and is used to satisfy large upstream agricultural demands, local M&I demands, instream flow needs, and drought year reliability for the entire SWP.

C.6.4.3 Shasta Reservoir

Shasta is a CVP reservoir that holds about 4.5 MAF with an average annual inflow of about 5.7 MAF. Shasta is the largest storage facility in the CVP/SWP system. In terms of flexibility, its operation is considered to be one of the most constrained. There are flow requirements just below Shasta at Keswick to protect endangered fish species and there are flow requirements down stream, just upstream from the confluence with the Feather River. There are also temperature requirements in the Sacramento River that require management of the cold water pool in Shasta in conjunction with releases. Shasta also has high carryover storage requirements (1.9 MAF) to protect endangered species. Shasta releases are also made to provide flows to senior water right holders along the Sacramento River. Operating levels for Shasta consider the constrained nature of its operation and balance those constraints with Delta needs.

C.6.4.4 Trinity Reservoir

Trinity is a CVP reservoir that holds about 2.4 MAF with an average annual inflow of about 1.2 MAF. Annual imports from the Trinity River to the Sacramento River basin are approximately 540 TAF, based on the most recent CalSim simulations. There are significant instream flow requirements in the Trinity River leaving little flexibility for meeting additional Delta needs. Currently, Trinity Reservoir operations are not altered by WAM in response to Delta outages.

C.6.4.5 New Melones Reservoir

New Melones is a CVP project reservoir located on the Stanislaus River. Essentially all its water is allocated to senior water rights holders and little, if any, is available for addressing Delta levee breach incidents. Currently, New Melones Reservoir operations are not altered by WAM in response to Delta outages.

C.6.4.6 Proximity to the Delta

New Melones is the reservoir that is closest to the Delta (flow time of about a half a day) and it also has the unique advantage of providing Delta inflow via the San Joaquin River. However, since little water is available, it does not receive primary attention in our models. Folsom Reservoir is the next closest project reservoir to the Delta, releases from Folsom take approximately 1 day to reach the Delta. For this reason Folsom is generally the first reservoir called on to provide flushing flows. Oroville is the next closest reservoir with a travel time of about 3 days, and Shasta releases take about 5 days to reach the Delta. Rules balance response time to an event in the Delta with water available in each upstream reservoir.

C.6.5 Definition of Maximum Upstream Release

Maximum releases from each reservoir are variable in the submodels and based on physical constraints, upstream fishery requirements, hydropower needs, and other needs. The first objective is to prevent releases that are so high there are adverse impacts on facilities, property, or fisheries. The next objective is to prevent releases so high there are lost hydropower benefits. This rule considers maximum flow and changes in flow from baseline. It is also based on water year types.

C.6.6 Sharing of Delta Supplies

Delta water supplies are first used to meet agricultural demands within the Delta, environmental requirements, and regulatory flow and quality requirements; supply available after satisfying these needs can be used to support Delta exports. Water available to support exports is determined in WAM by first using Delta Supplies to satisfy in-Delta diversions, D1641 flow and quality standards, and 3406 (b)(2) requirements. Once available Delta water available to support exports is determined, water is shared between State and Federal projects according to the Coordinated Operating Agreement (COA). The shared water must be allocated to additional Delta outflow (i.e., additional carriage water) as well as exports. The COA is only considered to when allocating water among exporters and is not considered when making emergency releases for flushing the Delta.

C.6.7 South of Delta Reservoir Management

During an outage in the Delta reservoirs in the export area are operated in WAM to maintain deliveries to the extent possible. WAM only considers the main CVP / SWP reservoirs and does not address local reservoirs or ground water supplies when allocating water.

C.6.7.1 CVP South of Delta Storage

The federal share in San Luis Reservoir is 972,000 AF in CalSim and WAM; this is the only significant Federal reservoir south of the Delta (except Friant). San Luis may be drawn down to dead pool to maintain baseline CVP deliveries.

C.6.7.2 SWP South of Delta Storage

There are six reservoirs considered when operating the SWP:

- San Luis Reservoir (1,067,000 AF)
- Castaic Lake (324,000 AF)
- Del Valle Lake (77,000 AF)
- Lake Perris (131,000 AF)
- Pyramid Lake (171,000 AF)
- Silverwood Lake (75,000 AF)

WAM operates SWP share of San Luis as an individual reservoir, but addresses the five "terminal" reservoirs as a single reservoir. After a Delta outage San Luis Reservoir is relied upon to satisfy SWP baseline deliveries, when available supply in San Luis Reservoir is insufficient to meet demands terminal reservoirs are used. Storage in each of the five terminal reservoirs is used in proportion to available storage in each, and refill occurs after San Luis recovers.

C.6.8 South of Delta Water Allocations

Water is allocated to both CVP and SWP contractors based on existing agreements and contracts. WAM does not address deliveries to individual contractors, but aggregates users of similar use categories and with similar contract provisions.

C.6.8.1 CVP South of Delta Allocations

South of Delta CVP deliveries are aggregated into 4 categories based on demand type and contracts:

- CVP Exchange (875,000 AF, including Schedule II water rights)
- CVP Refuge (256,000 AF 2005 LOD and 300,000 AF 2030 LOD)
- CVP Ag service (1,885,000 AF)
- CVP M&I (148,000 AF)

WAM allocates water to these four groups based on current operating criteria to the extent possible:

1. First check if it's a Shasta critical year, if it is then Settlement Contracts, Exchange Contracts and Refuge Contracts are cut from 100% to 75%.
2. Cut CVP Ag service contractors to 75% without reducing M&I
3. Reduced Ag and M&I by the same amount (%) until CVP Ag service contractors to reach 50% and M&I reach 75%
4. Reduced Ag until CVP Ag service contractors reach 25% (M&I stays unchanged at 75%)

5. Reduced Ag and M&I by the same amount (%) until CVP Ag service contractors reach 0% and M&I reach 50%
6. Reduced M&I to 0%
7. Reduce Refuge Contracts allocations reach 0%
8. Reduced Exchange Contracts until allocations reach 72%
9. Reduced Friant deliveries to keep Exchange Contractor allocations at 72%

Definition of Shasta Critical Year

1. The forecasted full natural inflow to Shasta Lake for the current water year, as such forecast is made by the United States on or before February 15, and reviewed as frequently thereafter as conditions and information warrant, is equal to or less than three million two hundred thousand (3,200,000) acre-feet; or
2. The total accumulated actual deficiencies below four million (4,000,000 acre-feet in the immediately prior water year or series of successive prior water years each of which had inflow of less than four million (4,000,000 acre-feet, together with the forecasted deficiency for the current water year, exceed eight hundred thousand (800,000) acre-feet.

CVP Friant Division

Although the Friant Division does not directly rely on Delta exports for supply, it is obligated to satisfy Exchange Contractors when their demands cannot be satisfied from the Delta. WAM assumes that Friant is obligated to release enough water to keep the Exchange Contractors monthly allocation to a minimum of 72%. Losses are assumed to occur in the San Joaquin River from Gravelly Ford to Mendota Pool based on loss rates assumed in CalSim. WAM assumes that required releases from Friant Dam are limited to inflow to Millerton Lake. Millerton is not operated in WAM, which may result in a slight inaccuracy in estimating of delivery reductions for the Friant Division.

C.6.8.2 SWP South of Delta Allocations

Although the SWP delivers water to a very large geographic area, SWP deliveries are aggregated into 4 categories:

- SWP MWD (Table A entitlement 1,911,500 AF)
- SWP AG (Table A entitlement 1,032,100 AF)
- SWP other M&I (Table A entitlement 1,226,500 AF)
- SWP Article 21 (up to 1,408,000 AF)

Allocation to SWP contractors in WAM is based on the Monetary Agreement, where allocation to both agricultural and M&I contractors is equal. Article 21 deliveries only occur when SWP south of Delta reservoirs are full, conveyance capacity exists at Banks and in the Aqueduct, and Delta surplus is available.

C.6.9 Balance of North of Delta Storage with Starting South of Delta Storage and Normal Needs

This is the most complex and important rule included is the submodels. This rule combines information on upstream water availability and maximum releases, previously described, with information from the hydrodynamic/water quality consequence model and conditions south of the Delta (SOD). The model attempts to meet “baseline” export levels considering conditions described in these rules.

C.6.9.1 Balance of North of Delta Storage with South of Delta Conditions and Desire for Flushing Flows

In addition to considering conditions south of the Delta, rules are included to balance available upstream water supply with flushing flow requirements. There are similar issues in balancing upstream conditions with desired flushing flows as with balancing upstream conditions with SOD conditions. Rules for determining how much water should be released to flush the Delta also consider the time-value of flushing flows. In many cases initial high levels of flushing flows are beneficial to longer-term water supply, while in other cases they are adverse to long-term water supply.

C.6.9.2 Rules Included to Determine Export Levels Based on Delta Salinity

In some cases it is beneficial to maintain some level of export to improve water quality in the central and southern Delta. Export of higher EC water could be very short-term or could last for a season. Ability to export water higher in EC depends on ability and desire of agricultural users on the DMC to use this water; their use of higher EC water depends on length of time higher EC water would be applied, status of their crops, and potential supply for blending.

C.6.10 Rules to address upstream storage deficits

When a levee breach occurs in the Delta WAM may call for releases from upstream reservoirs based on rules described in Section C6.3. Increased releases result in lower reservoir storage in subsequent months that may either be refilled during times of surplus or result in decreases in future water deliveries, if followed by dry periods. Depending on a myriad of conditions, decreases in water deliveries may be allocated to upstream agricultural deliveries, urban agencies, or environmental uses. Reduction in upstream reservoir storage may also cause reduction in Delta inflows that can result in decreases in Delta water quality and/or exports.

In actual operations available water supplies would be allocated considering all the complexities associated with water allocations. For the purpose of WAM deficits in upstream reservoirs are characterize by a volume of supply needed to maintain storage at minimum acceptable levels. Upstream deficits in WAM are simply added to reservoir storage and accounted as decreases in deliveries. These decreases are not yet allocated by WAM to specific categories of users or beneficiaries.

C.6.11 Determining the End of the Recovery Period

From an upstream reservoir operations standpoint recovery is based on recovery of storage north of the Delta and a return to a normal level of delivery. There also is recognition of recovery needs south of the Delta. This is based on providing excess Delta exports for the period needed until south of Delta storage has recovered.

C.6.12 Reservoir Management Submodel Characteristics

The reservoir management submodels have been designed to be suitable for use in the risk analysis computation, adapted to the Delta/upstream water system, fit into the WAM calculation flow, and applicable to the full range of levee breach incidents. They were developed in close collaboration with operation managers and include an articulation of the criteria and rules for operating decisions. A group of federal and state project operators, contingency planners, and water contractors has been assembled to provide input on example breach incidents. They will now have opportunity to review the management rules/guidelines for levee incident reservoir operations.

Reservoir management modeling establishes the relevant relationships for each hazard that is considered, (e.g., seismic, flood), the timing of the incident (high or low flows, season), the magnitude and potential duration of the incident. The submodels are formatted to be used efficiently in evaluating each incident. The water management submodel is defined based on its role in the risk analysis, the inputs available, and outputs desired.

Robust reservoir management decision submodels have been developed. As part of the Delta risk analysis, there are thousands (possibly tens of thousands) of levee breach incidents involving various combinations of levee breaches and island flooding. In principal, each sequence is unique. Furthermore, each may occur during any type of water year and at various times during that year. The resource state and response in managing Delta inflows varies. The objective of each reservoir management submodel is to provide the inflow time series required for hydrodynamic and water quality modeling – for each incident and start time. The inflows are responsive to both the water resource state at the time of the incident and the damage caused to water export capabilities. It simulates the reservoir management decisions that would be taken in each incident in order to respond. A specific reservoir operation strategy (for use in modeling) is developed for simulating Delta inflows during the duration of the repair and recovery period.

Consider the following widely varying set of circumstances and markedly different events. For example, a breach event might occur during a period of low net Delta outflow and a significant volume of high salinity water could be drawn into the western and central Delta from Suisun Bay. In this case, the submodels indicate increases in reservoir releases for a short period of time, responsive to the approach described in the "Sacramento-San Joaquin Delta Emergency Water Plan: Report to the Legislature" (California DWR, 1986). Once salinity intrusion from the initial island flooding has been repulsed, reservoir releases are decreased to save the water that would have been exported until sufficient repairs have been completed to use the water to further flush the

Delta and resume pumping. On the other hand, if sufficient water is available the releases are maintained at a higher level to enhance or accelerate flushing.

As another example, the event might occur during the wet season with relatively high Delta outflows. For a modest number of levee breaches, there may have been little intrusion of saline water. In that case no increase in reservoir releases would be provided.

C.6.13 Reservoir Management Submodel Sample Results

WAM produces time-series output for Delta exports, south of Delta water deliveries, south and north of Delta storage, and north of Delta flow and delivery changes. The following figures contain output from a sample WAM simulation – a preliminary version of a multi-island breach case beginning in August of 1992. Note that the only purpose of this simulation and the results presented is to illustrate the way WAM may react to a breach scenario and to indicate the types of output information that will be generated.

The following two figures contain traces indicating Delta exports for the baseline (without disruption) and for the preliminary multi-island breach case. Figures C-4 and C-5 contain Delta exports for each month for the WAM simulation. Both CVP and SWP exports are halted during the flooding and flushing period after the breach and resume after seven months.

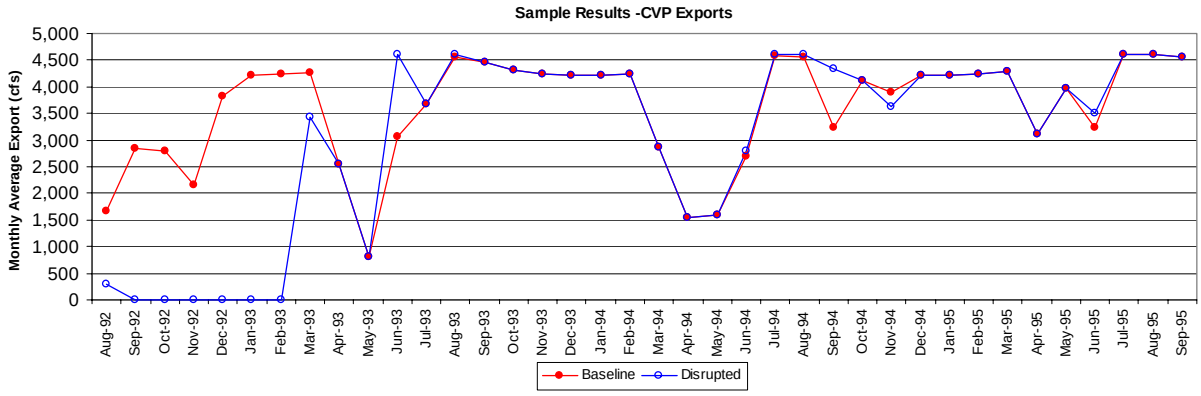

Figure C-4 CVP Exports

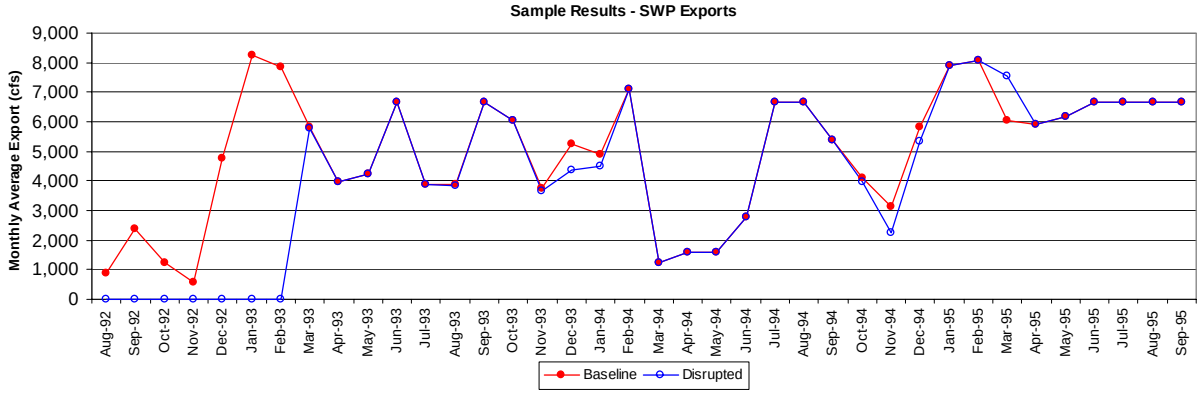

Figure C-5 SWP Exports

Figures C-6 through C-15 contain plots of SWP and CVP south of Delta deliveries. WAM allocates water to each group of contractors of the SWP and CVP based on contract priority. Figure C-6 contains a plot showing total south of Delta deliveries and total delivery reduction due to disruption; the total reduction in delivery is about 2.8 MAF.

Figures C-7 through C-10 contain SWP deliveries. SWP delivery allocations are maintained at the same percentage for all SWP contractors, therefore reductions follow similar patterns for each group of contractors. Article 21 deliveries are only made when the SWP has surplus water available, during the disruption these deliveries are reduced to zero due to the absence of surplus.

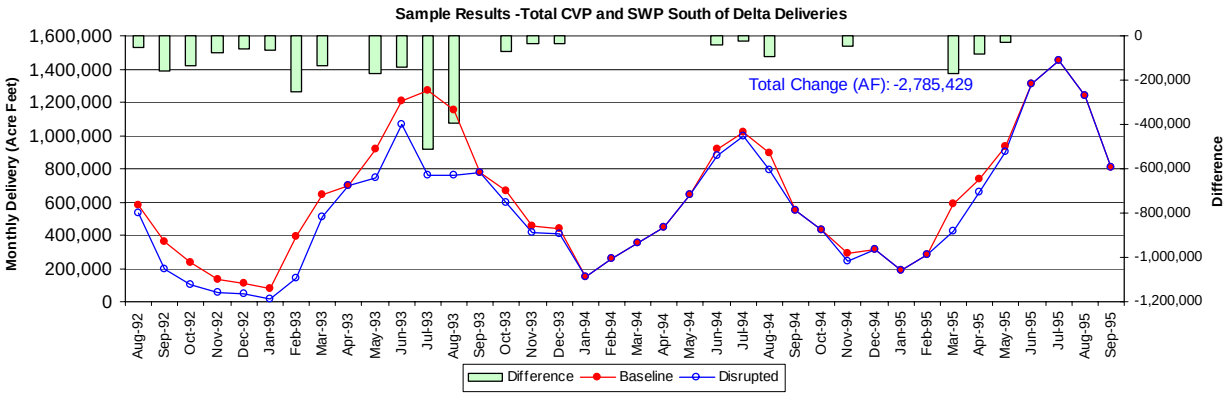

Figure C-6 Total South of Delta deliveries

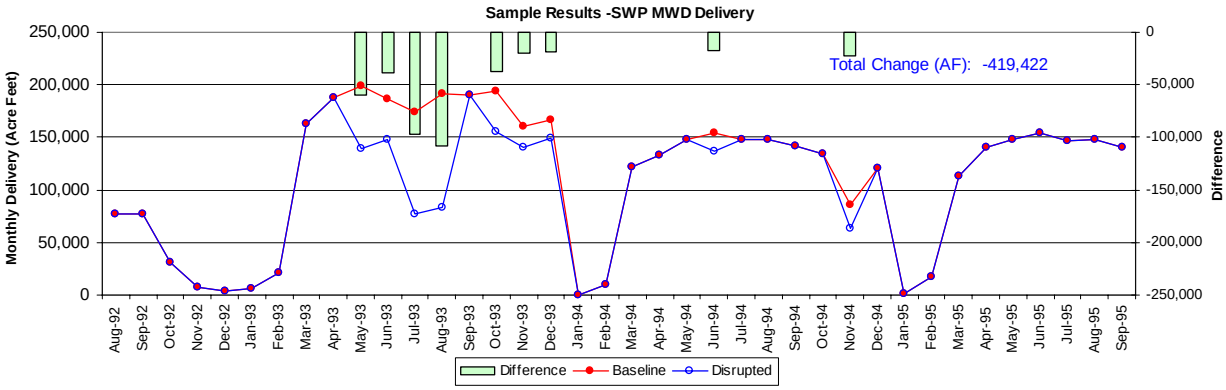

Figure C-7 SWP Delivery to MWD

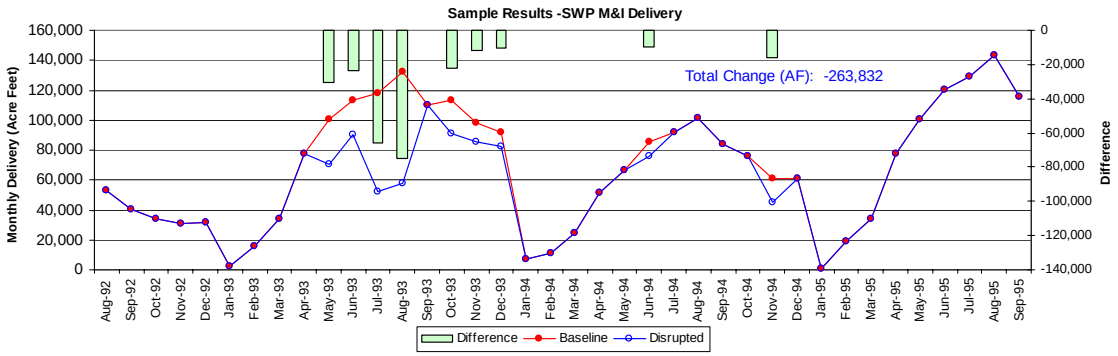

Figure C-8 SWP Delivery to M&I (other than MWD)

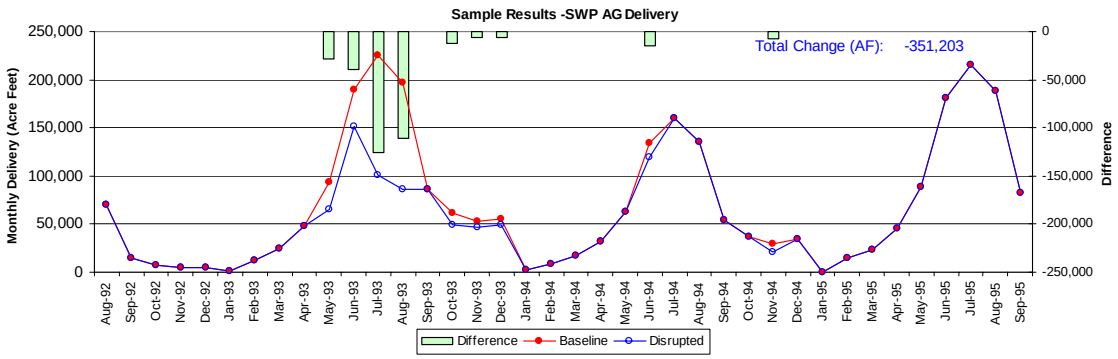

Figure C-9 SWP Delivery to Agriculture

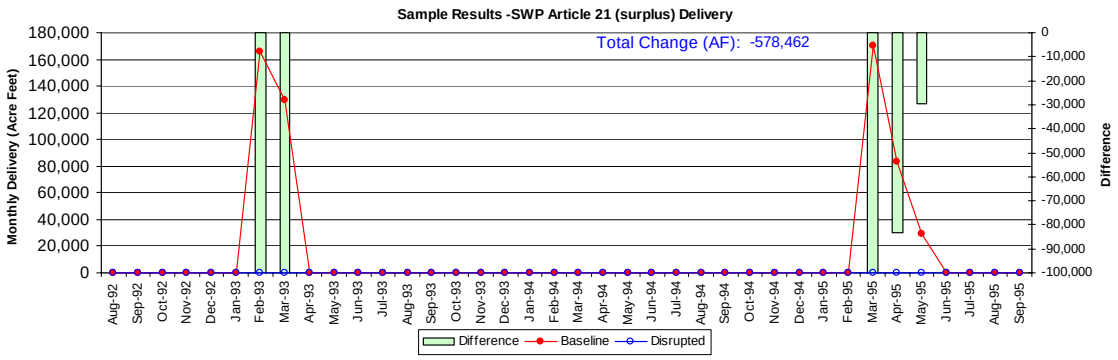

Figure C-10 SWP Delivery to Article 21

Figures C-11 through C-15 contain CVP deliveries.

Deliveries to CVP contractors are made based on priority presented in Section C6.8.1, the following plots show deliveries based on these priorities. Agricultural service contractors are the first to be cut while the Exchange contractors, the most senior water right holders,

are the last. Deliveries to the Friant Division are reduced only when it is necessary to maintain Exchange contractor deliveries at 72%.

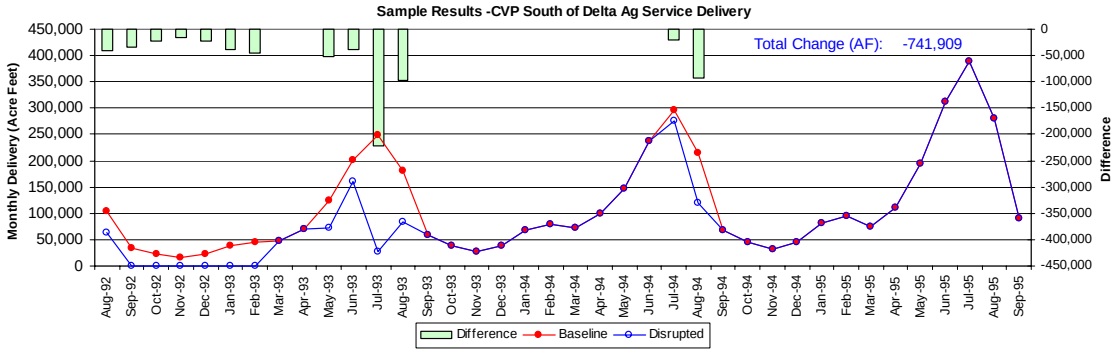

Figure C-11 CVP Delivery to Agricultural Service Contractors

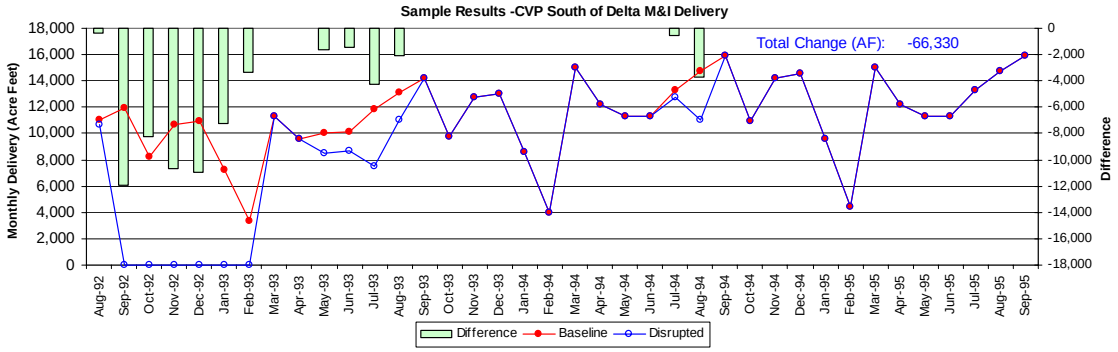

Figure C-12 CVP Delivery to M&I Contractors

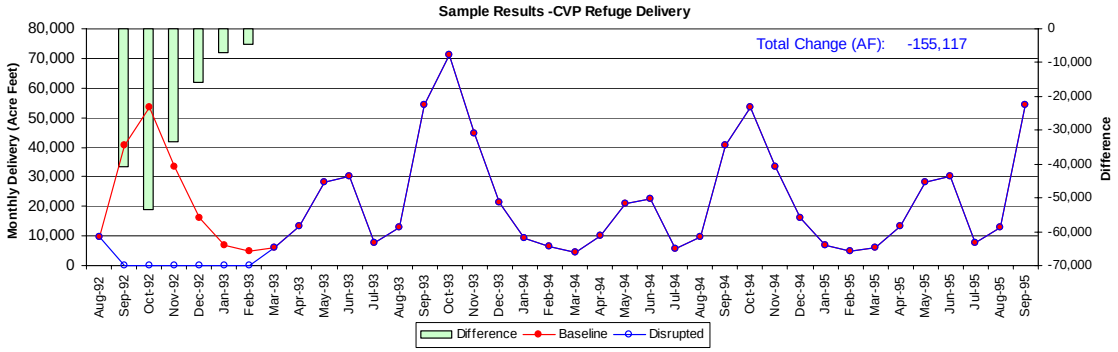

Figure C-13 CVP Delivery to Refuges

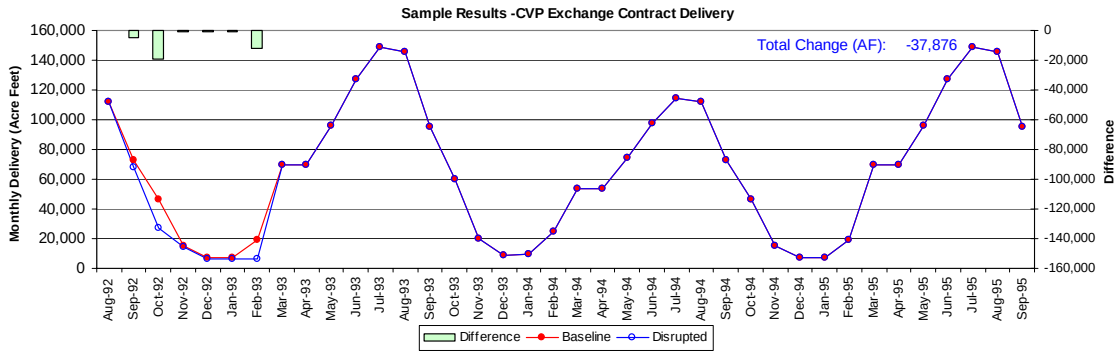

Figure C-14 CVP Delivery to Exchange Contractors

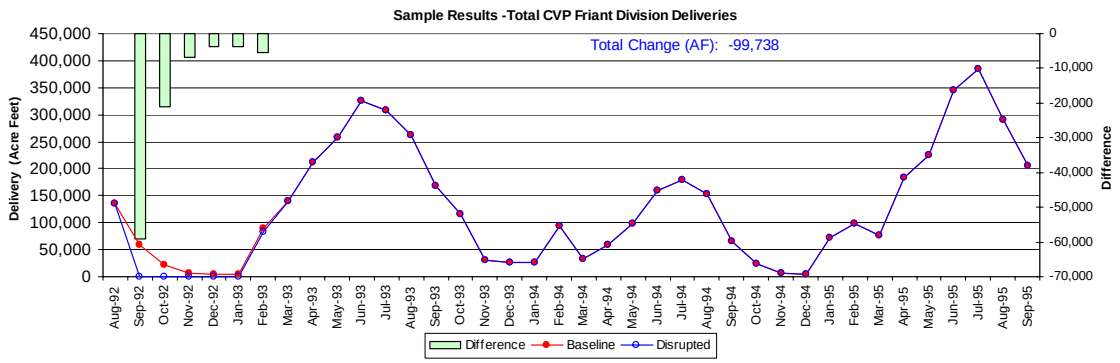

Figure C-15 CVP Delivery to Friant Agricultural Service Contractors

Figures C-16 through C-19 contain plots of storage south of the delta. During this model simulation south of Delta storage dropped by approximately 2 MAF.

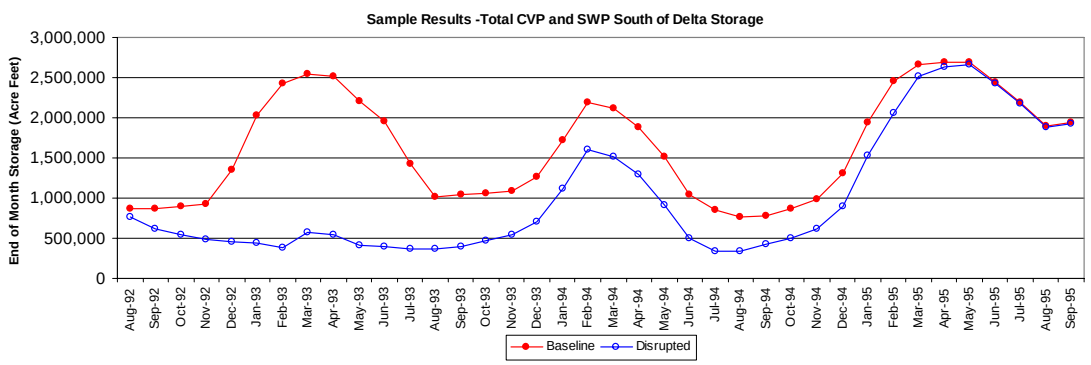

Figure C-16 Total South of Delta Storage

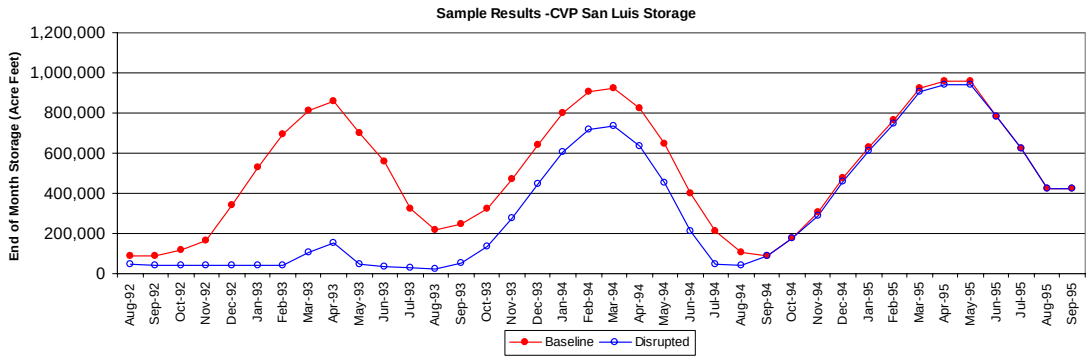

Figure C-17 Storage in CVP Portion of San Luis

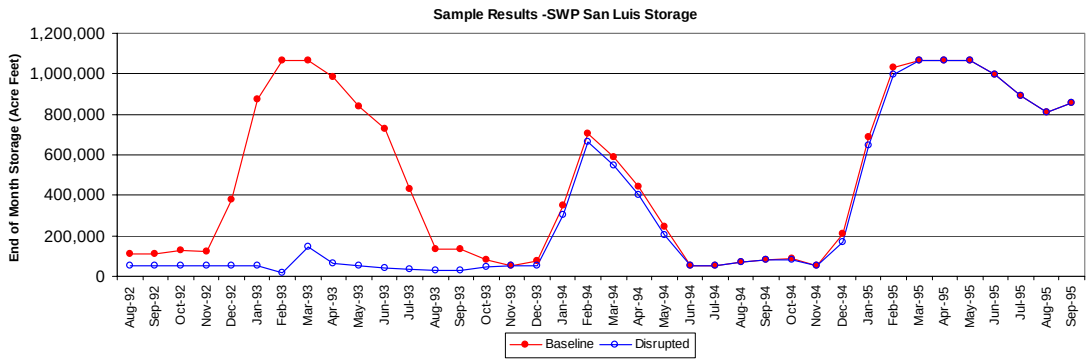

Figure C-18 Storage in SWP Portion of San Luis

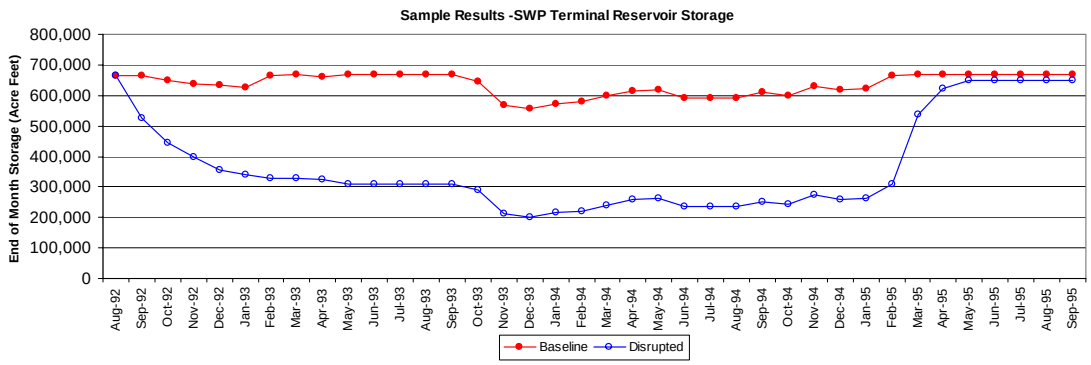

Figure C-19 SWP South of Delta "Terminal Reservoir" Storage

Appendix D
Hydrodynamics and Water Quality

Table of Contents

Executive Summary **1**

D.1 Introduction **2**

D.2 Objective **3**

D.3 Physical System **3**

D.3.1 Physical and Operational Issues Related to Delta Levee Breach Events 3

D.3.2 Evaluating Hydrodynamic and Water Quality Consequences 6

D.3.3 Criteria for HD Submodel Acceptability in the WAM 6

D.4 Approach and Product **7**

D.4.1 Multi-Dimensional Simulations of Select Levee Breach Events 8

D.4.2 Development of the Simplified Hydrodynamic/Water Quality Consequence Submodel 8

D.4.3 Hydrodynamic/Water Quality Simulation Tasks Within the Water Analysis Module 9

D.4.4 Simplified Model Configuration 13

D.4.5 Representation of Transport Processes 17

D.4.6 Calibration/Verification of the Simplified Model 19

D.4.7 Example Results 19

D.5 Assumptions, Constraints, Limitations **23**

D.6 Pertinent Prior Work **24**

Tables

D-1 Water Analysis Module (WAM) Computational Processes (Simple Hydrodynamics/Water Quality Model Component)

Figures

D-1 Water Analysis Module Basic Logic Flow Chart.

D-2 Simplified HD Submodel Schematic

D-3 WAM HD Model Configuration: 1-Dimensional RMA Finite Element Network with 500m Elements (note that 1-D element width for channels and island segments are drawn centered on the elements)

D-4 WAM HD Model Configuration: Boundary Conditions

D-5 WAM HD Model Configuration: Dispersion Zones

D-6 EC impact at Jersey Point resulting from 20 Island Breach Events starting on the first of each month from January through December 1993.

D-7 EC impact at Jersey Point resulting from 20 Island Breach Events starting each July 1 from 1992 through 2002.

D-8 Export deficit at time exports are initially resumed based on starting breach events on the first of each month from January 1986 through October 1998, Risk Analysis Event Sequences 2-6.

D-9 Exceedance probability of export deficit at time exports are initially resumed based on starting breach events on the first of each month from January 1923 through October 1998, Risk Analysis Event Sequences 2-6.

Acronyms and Abbreviations

BAU	Business as Usual
CalSim	California Water System Simulation Model (DWR & USBR)
cfs	cubic feet per second
CO_2	Carbon Dioxide
CVP	Federal Central Valley Project
DRMS	Delta Risk Management Strategy
DWR	California Department of Water Resources
dss	Data storage system
EC	Electrical Conductivity
HD	The WAM Hydrodynamic / Water Quality Submodel
ITF	Initial Technical Framework
JBA	Jack R. Benjamin & Associates, the DRMS risk analysis consultant
MWH	MegaWatt Hours
NDAL	Net Delta Area Losses (or Net Delta Consumptive Water Use)
RMA	Resource Management Associates, the DRMS hydrodynamics consultant
SWP	State Water Project
SWRCB	State Water Resources Control Board
TAF	Thousand Acre-Feet
TM	Technical Memorandum
µmhos/cm	Micro mhos per centimeter – Electrical Conductivity, a measure of salinity
URS	URS Corporation, the DRMS prime consultant
USBR	United States Bureau of Reclamation
WAM	Water Analysis Module or Model
WY	Water Year

Executive Summary

This document describes the design and development of the Hydrodynamic and Water Quality analysis submodel (HD) of the WAM. Calibration of the HD is discussed in Appendix E.

The objective of WAM is to rapidly evaluate consequences of levee breach sequences in terms of salinity and the impact on water operations.

The physical problem involves flooding, flushing, operating to standards, and determining recovery. Key physical processes are the advection and tidal dispersion of salt in the system. Other water quality constituents such as organic carbon are also important, but, for this version of the risk analysis, have not been included in the WAM HD and are addressed separately in a limited fashion. It would be possible to add other constituents to the WAM HD at a later date.

A one-dimensional, tidally averaged, advection-dispersion model is created for the HD component of WAM. Net flow and dispersion are modeled with a constant downstream stage boundary and variable rim flows, exports, and Delta consumptive use. Internal flow boundaries are used to force flow splits that are driven by tidal dynamics and gate operations.

The model utilizes the RMA2/RMA11 computational engines. Conceptually, another computational engine could be substituted for the RMA2/RMA11 engine.

Geometry is based on a transport corridor concept balancing computational requirements and detail of the model configuration. Volumes are based on RMA Bay Delta Model. One-dimensional channels are trapezoidal sections with off channel storage.

Bed friction parameters are taken from average from RMA Bay-Delta model. Friction is not particularly important because it is a tidally averaged model. Friction does come into play during island flooding due to breaches because internal net flow boundaries are relaxed during periods when islands are flooding.

Internal flows at important connecting channels are specified by multiple linear regression fits to observed data and, where necessary, RMA Bay-Delta Model results.

Boundary conditions include rim flows, stage at central San Francisco Bay, NDAL (or net Delta consumptive use), and exports. All inflows are assigned salt concentration. NDAL provides return flow and return flow salinity at five locations representing aggregated island response.

Dispersion coefficients are developed from simulations with the RMA Bay-Delta (2D) and the TRIM and UnTRIM 3D models. Use of TRIM and UnTRIM are described in Appendices H and H1 through H3. Base condition (no breaches) dispersion coefficients for the central bay through the western Delta are primarily from the TRIM 3D model. K is represented as three components of gravitational circulation, 2D horizontal mixing, and unsteady shear. In the HD, K is a function horizontal Richardson number for gravity circulation. 2D horizontal mixing and unsteady shear are combined and estimated as functions of net Delta outflow.

Dispersion in and out of islands is estimated by area of the island and tidal range and an exchange efficiency. The exchange efficiency has been estimated based on flushing of islands in RMA Bay Delta model.

Changes in dispersion (after Delta islands have been flooded) are very complex. The changes in dispersion are related to changes in tidal dynamics. Adding tidal prism changes the propagation of the tidal signal into the system and is dependent on the breach location, island tidal prism, channel breached, and size of breach. Through several numerical experiments, it appears that the breaches increase excursion near the breach, but may decrease excursion in areas far from the breach. Most interestingly, flooded islands in the Delta may decrease excursion in Suisun Bay. The aggressive schedule imposed on the Phase 1 risk analysis has not provided enough time to fully resolve this issue.

Interaction with the water management component of the WAM is accomplished through evaluation of a subset of the D1641 water quality standards and computing a flush volume and balance flow. The WAM is calibrated to the ANN when there are no breaches. When there are breaches there is pump shutdown to minimal export, then full shutdown on reaching an EC limit.

Simulation construct involves daily interaction with the water management and NDAL components of the WAM. Outputs include tidally averaged EC and flow at stations corresponding to monitoring stations. Each simulation outputs number of days to export resumption and Delta recovery. Delta recovery is achieved when salinity and dispersion are reasonably normal.

A single simulation is run for the entire CalSim hydrologic period using CalSim Delta inflows and exports directly to establish initial salinity conditions at the beginning of each month. Because the WAM operation for the non-breached state does not precisely mimic the base CalSim simulation (due to differences in flow requirements derived from HD relative to ANN), simulations are performed for no breach cases starting each month with no deviation from the CalSim characterization.

With the CalSim record of 1922 through 2003, allowing for spinup and runout, WAM sequence start times may occur from January 1923 through September 1998.

The HD requires the majority of the computer execution time in WAM. With minimum output on Intel Pentium 3 GHz processor, WAM requires approximately 75 sec per 60-month simulation. Multiple WAM instances may be run on multicore machines. On a dual processor, dual core machine, three instances of the WAM may be run simultaneously. On a dual processor, quad core machine up to six instances may be run simultaneously. Performance is enhanced if results are written to separate physical disks.

D.1 Introduction

This document describes the Hydrodynamic and Water Quality Analysis submodel (HD submodel) of the Water Analysis Module (WAM) of the Delta Risk Management Strategy (DRMS) Risk Analysis.

WAM encompasses water management decision making and Delta hydrodynamic/ water quality response related to levee breach events and subsequent repair and recovery period. The water management submodel is presented in a separate appendix.

The water quality transport model incorporated into the WAM is responsible for determining salinity distribution in the Delta. Because the full risk analysis requires evaluation of thousands or tens of thousands of discrete levee breach events, the WAM must provide very rapid calculation of consequences related to any given breach event. Dynamic simulation of the hydrodynamic and water quality impacts of levee breaches using the best currently available models is very time consuming, requiring hours to days of computation time to fully evaluate a multi-breach event where the repair/recovery period may span several years. A critical aspect of this work has been development of a reasonable and defensible simplified representation of water quality transport within the Delta to be used within the WAM. This has been accomplished by characterizing the response of the Delta to a range of levee breach sequences using existing Delta models and then using that characterization to construct a tidally averaged advection-dispersion model.

D.2 Objective

During the risk analysis phase (first phase) the WAM has been developed to produce estimates of water export disruptions and environmental conditions based on a wide range of explicit levee breach sequences for the current Delta configuration and generally accepted range of “Business as Usual” operating procedures. The specific primary objectives of the WAM HD submodel in Phase 1 have been:

- To simulate the hydrodynamic and water quality responses to levee breach incidents and resulting inflow/export management – in particular salinity – as needed for input to other WAM submodels and ultimately to estimate salinity and water export impacts for use by the economic and environmental consequence modules.
- To calculate inflow needs and export constraints for Delta island flooding, flushing, and support of export pumping, for use by the WAM reservoir management submodel.

D.3 Physical System

D.3.1 Physical and Operational Issues Related to Delta Levee Breach Events

The Sacramento-San Joaquin Delta is a complex estuary that is carefully managed for fresh water conveyance, agricultural water use, and environmental quality. Management of the Delta involves balancing upstream reservoir releases with in-Delta water use and water exports, as well as operation of a variety of control structures such as the Delta Cross Channel. Levee breach events can have a dramatic and immediate impact on Delta water quality as high salinity water is drawn in from the seaward boundary to fill breached islands. Levee breach events can also have very important long-term water quality impacts during the protracted repair and recovery process associated with multiple breach scenarios. Thus, the time scale of the problem is on the order of months

or years. The significance of economic and environmental consequences associated with a levee breach event depends upon the ability to compensate for the physical changes in the system by modifying management of the system. In some cases, there is sufficient management flexibility that economic and environmental consequences are minimal. However, with multiple levee breaches it is likely that significant economic or environmental consequences will occur. The following is a listing of operational issues and physical processes related to Delta levee breach events, most of which affect hydrodynamics and water quality and, thus, have necessarily been included in the HD submodel:

- **Initial Flooding:** Breached islands fill with water from the neighboring channels, river inflows, and (potentially) high salinity water drawn from Suisun Bay and San Pablo Bay. The salinity impact on the Delta of the initial flooding depends on the location and volume of the breached islands, the initial geometry and evolution of the breaches, river inflow rate, and the salinity distribution in Suisun and San Pablo Bays. Since the fresher water in Delta channels fills the islands and is replaced in the channels by saltier water from the Bay, salinity tends to be higher in Delta channels than in flooded islands during the initial flooding phase.
- **Suspension of Exports:** At the time of the event, exports are typically drastically reduced or suspended to inspect the facilities and to evaluate the salinity distribution in the Delta and avoid drawing salty water toward the pumps.
- **Flushing Releases:** If the initial flooding brings high salinity water into the western Delta, it is important to flush the channels with additional reservoir releases before the high salinity water mixes into Franks Tract or the breached islands.
- **Gate Operations:** The operation of the Delta Cross Channel and south Delta barriers is considered and possibly changed to enhance effectiveness of flushing releases.
- **Emergency Procedures:** If the initial flooding is severe, emergency procedures may be required such as modified operation of permanent operable gates (the Delta Cross Channel gates). Temporary south Delta Barriers may need to be removed.
- **Initial Tidal Mixing:** Following the initial flooding, the salinity distribution in the Delta is far from equilibrium. The strong salinity gradients present following the initial flooding gradually weaken over a period of weeks as a result of tidal mixing. The salinity distribution from the western Delta through Suisun Bay will move toward a new equilibrium determined by the Net Delta Outflow and tidal exchange that is now modified by the breached islands. During this period of initial tidal mixing, high salinity water in the channels mixes in and out of flooded islands, increasing the salinity in the islands. Due to strong horizontal salinity gradients during this period, Delta channels and flooded islands may become stratified.
- **Levee Repair:** As soon as possible following the event, levee breaches may be capped to prevent widening. Then, based on the availability of materials, equipment, and personnel, breaches are repaired over a period of months to years depending on the number of breaches. Ideally, the breach closures are prioritized to most effectively facilitate restoration of Delta exports, although other issues may override export water

quality concerns. As levees are repaired, the active tidal prism in the Delta returns toward that of the original Delta configuration.

- **Secondary Failures:** Secondary levee failures may occur due to damage from the flood or seismic event, or due to wind induced wave action resulting from the large wind fetch over the surface of newly flooded islands. Secondary failures may flood additional islands drawing additional high salinity water into the Delta.
- **Reservoir Management:** Throughout the repair and recovery period reservoir release decisions will be based on managing the salinity in the Delta, providing for Delta exports if possible, meeting flood control requirements and providing for water users upstream of the Delta. Managing salinity in the Delta involves balancing Net Delta Outflow with tidal mixing to meet water quality standards in conjunction with operation of in Delta barriers. Tidal mixing will be strongly affected by the un-repaired breaches because they will allow exchange between flooded island and channels and alter the tidal currents in Delta channels.
- **Export Decision Making:** The ability to export water from the Delta for agricultural or municipal use is dependent on the quality of water. Salinity is the primary constituent of concern. With careful management, it may be possible to export before the breaches are completely repaired, perhaps at a limited rate. If the repair period spans a high runoff period, there may be opportunities to intermittently export water.
- **Delta Area Net Consumptive Use:** Diversions and returns associated with in-Delta agriculture are a very important component of the summer time water balance and strongly influence the Delta salinity distribution due to the high salinity of return flows. When an island is flooded, evapotranspiration is replaced by evaporation, which may be more consumptive. Depending on the severity of a levee breach scenario, channel salinities may be so high that water use on other islands is eliminated or curtailed during the repair and recovery period.
- **Island Pump Out:** Once levee repairs are complete on an island, water from the island is pumped back into the adjacent Delta channels. Pump flow will have a small effect on the overall water balance, but may have significant impact on Delta salinity.
- **Salt Transport:** Salt transport in the system is a function of tidal flows through the complex network of interconnected Delta channels and flooded islands as well as the net flows determined by tributary inflows, in-Delta consumptive use, and Delta exports. Newly breached islands add tidal prism to the Delta, increasing tidal flow between the flooded islands and the seaward boundary. This increased tidal flow leads to increased dissipation of tidal energy and damping of tidal range throughout the system, reducing tidal flow landward of the flooded islands. These changes in tidal flow affect the salt flux from Suisun Bay into the western Delta and mixing within the Delta. In addition, levee breaches will alter the path of tributary flows take through the Delta. Changes in tidal flows and residual flows in the Delta channels will alter the Net Delta Outflow required to maintain water quality standards.

The HD submodel necessarily incorporates the water movement and salinity impacts that result from the above listed physical phenomena.

D.3.2 Evaluating Hydrodynamic and Water Quality Consequences

Simulating tidal hydrodynamics and salinity in the Delta is challenging due to the complex branching channel structure of the Delta, strong tidal flows and exchange with Suisun Bay, variable tributary flows and complex operations. Accurate representation of the geometry and bathymetry of Delta channels, junctions, flooded islands, marsh areas, and structures is one essential step in achieving accurate predictions. Models also require a large number of boundary condition data describing salinity and tidal conditions at the seaward boundary, freshwater inflows, diversions, wind velocities, precipitation, and evaporation. Hydrodynamic processes in the Delta are complex with large spatial variability in salinity, current speeds, tidal amplitude and phase, and residual flow direction and magnitude. Furthermore, these quantities vary in time over the spring-neap cycle and with tributary flows. In addition to the spatial variability along and between channels, Suisun Bay and the western Delta are often stratified during conditions with significant salinity in the Delta, which are the conditions of interest in the DRMS study.

During and following any levee failure event, hydrodynamic conditions in the Delta change, primarily as a result of tidal exchange between the channels and flooded islands. Flooded islands with multiple breach locations will also introduce new flow paths for tidally-averaged flows. Changes in tidal and tidally-averaged flow magnitude in any one channel affect neighboring channels.

The changes in Delta hydrodynamics may greatly influence salinity in the Delta. Due to initial filling of flooded island and increased tidal exchange between islands and channels, the salinity of the Delta will increase, probably leading to stratified conditions in some channels and flooded islands. Changes in tidally-averaged flows in each channel will also affect salinity. In some channels the seaward flow magnitudes will decrease leading to decreased ability to flush salt from these channels. Increased tidal prism will affect the tidal excursion leading to potentially significant impacts on dispersion.

The hydrodynamics and transport mechanisms in the Delta are further complicated by the evolution of bathymetry resulting from increased tidal prism near (seaward of) levee breaches. As channels deepen and, possibly, widen to reach equilibrium with the increased tidal prism, the tendency for salt to mix into the Delta will increase because tidally-averaged velocities will decrease in inverse proportion to the increase in channel area, leading to decreased flushing of salt from the Delta by tributary flows. Deeper channels are also much more likely to become stratified because bottom friction is less effective in mixing deeper water columns leading to increased gravitational circulation. For the same reasons sea level rise is likely to increase salinity and stratification in the Delta. Monismith et al. (2002) indicate that moderate increases in water depth may lead to quite large increases in salinity and stratification.

D.3.3 Criteria for HD Submodel Acceptability in the WAM

Evaluation of hydrodynamic and water quality consequences within the DRMS risk analysis framework requires the HD submodel to achieve the following:

- Link the water management decision model with water quality simulation,
- Develop an appropriate and defensible approach to evaluating hydrodynamic and salinity impacts that can be used for the full range of levee breach events that are considered in the risk analysis, and

Many physical and operational issues associated with levee breach events are reasonably well represented with existing hydrodynamic simulation modeling tools. However, a model that includes coupling between water quality and emergency management for levee breach events (reservoir releases, exports, and gate/barrier operations) had not been developed previously. Further, the tools available for fully dynamic simulation of flow and salt transport during multiple levee breach events are complex and numerically intensive models so it is not possible to use them directly to evaluate hundreds, let alone thousands of breach events.

To meet the needs of the DRMS risk analysis component, a tool – WAM – has been developed that couples water management decision making with a submodel of hydrodynamics and salt transport in the Delta that allows rapid estimates of water quality consequences. The simplified HD submodel discussed in the following sections provides tidally-averaged estimates of Delta salinity in response to managed inflows and flooded island hydrodynamics.

As discussed above, the water management and hydrodynamic/water quality response to levee breach sequences evolves over time, necessitating a time step simulation approach as opposed to a static evaluation of impacts. The WAM receives time series input and generates time series output. The primary inputs to WAM are the levee breach, repair, and pump-out schedules. Also critical to WAM is the hydrology during the repair/ recovery period, which describes the time history of inflows to reservoirs upstream of the Delta and tributary flows directly entering the Delta. As these inflows are managed, the HD submodel estimates the evolution of Delta salinity and the feasibility of exports.

There are time dependent outputs that should be passed to the economic and environmental consequence modules. In particular, it is very likely that many breach incidents will reduce the ability to export water at intermittent periods during the repair and recovery period rather than completely preventing exports. In this situation reporting a single value for time of export disruption is a very poor estimate of the water supply consequences of the event. Therefore, it is necessary to compute and pass on to the economic module a time series of exports during the repair/recovery period.

Perhaps the most important physical data influencing the impact of initial flooding is the Delta Island topography, which determines the flood volume. The data currently available is not believed to adequately represent existing conditions, with errors potentially on the order of five to ten feet vertically.

D.4 Approach and Product

This section describes the approach taken to simulating hydrodynamic and water quality consequences within the WAM and the submodel that was produced. The HD submodel was developed by:

- Using existing physically based numerical models of the system to explicitly evaluate hydrodynamic, salinity, and other water quality impacts of a limited number of specific breach events as well as to characterize the dynamics of the system, and
- Creating a new numerical tool to rapidly evaluate salinity impacts of levee breach events and interact with the water management decision-making submodels of WAM.

D.4.1 Multi-Dimensional Simulations of Select Levee Breach Events

The RMA Bay-Delta model has previously been used to simulate the Jones Tract levee failure in 2004 and, through the Preliminary Delta Levee Seismic Risk Assessment Project, 1-, 3-, 10-, 30-, and 50-breach cases. A description of the RMA Bay-Delta Model can be found in the recent calibration report prepared for the Flooded Islands Pre-Feasibility Study, which is available on line at http://www.rmanet.com/zip/FloodedIslandsCalibrationFinalReport-2005-06-30.zip. Description of modeling work performed for the preliminary Delta Levee Risk Assessment is also available on-line at http://calwater.ca.gov/Programs/LeveeSystemIntegrity/LeveeDeltaSeismic.shtml. Flow, stage, and salinity results from the RMA Bay-Delta model have provided a resource for testing of HD submodel salinity estimates. These result sets have also been utilized to provide information to the Environmental Consequences Team regarding changes in salinity distributions, velocity fields, and residence time.

Additional work has been performed as part of the DRMS study utilizing the three dimensional hydrodynamics and salt transport models TRIM3D and UnTRIM/3D as described in WAM Appendix H.

D.4.2 Development of the Simplified Hydrodynamic/Water Quality Consequence Submodel

The primary challenge in developing the HD submodel was representing enough of the physics to provide sufficient accuracy while maintaining the computational speed needed to simulate many thousands of levee breach events. The primary outputs of WAM are monthly average quantities including export volumes and salinity, and in-Delta salinity at selected locations. As such, it is not necessary for the simplified model to explicitly represent the tidal flow and transport provided the net transport is simulated with reasonable accuracy. The approach taken has be to develop a tidally-averaged salt transport model which utilizes net flow and tidal mixing (tidal dispersion and turbulent diffusion) relations derived from full dynamic models of the system. The simplified model has been developed to interact on a daily basis with the water management component of the WAM during the course of simulation, both providing input to the water management decision making component and receiving calculated inflows and exports. The main uses of the simplified HD submodel within WAM are shown in the flow chart in Figure D-1.

D.4.3 Hydrodynamic/Water Quality Simulation Tasks Within the Water Analysis Module

In the WAM flow chart (Figure D-1), the simplified hydrodynamic/water quality model contributes to five of the tasks. Input and output data for each of these tasks are summarized in Table D-1.

H1: Simulate island flooding – the model simulates the impact of island flooding on the salinity distribution in the Delta. This impact is primarily a function of the island volume filled. While the time required to fill the islands is an important consideration, it is sufficient to derive an estimated time based on the 1-, 3-, 10-, 30-, and 50-breach events. Given the time to fill estimate, net flow rates are determined for each island that is flooding. Using the estimated flows to fill the islands along with the initial salinity distribution, Delta inflow, Cross Channel gate status, and pumping status, the simplified model is used to determine the salinity distribution when the islands have filled.

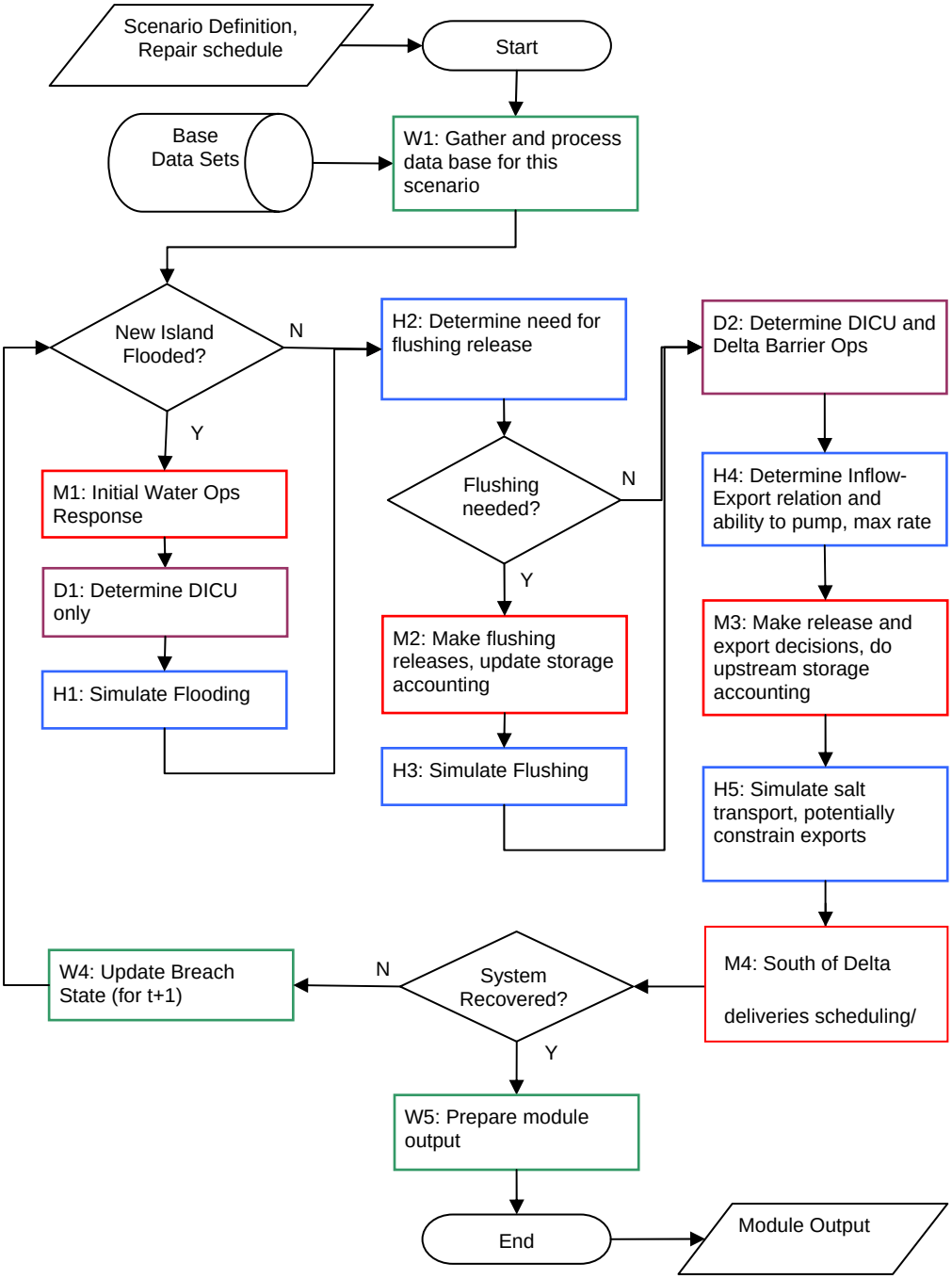

Figure D-1 Water Analysis Module Basic Logic Flow Chart.

Simplified Hydrodynamic/Water Quality Model Is Responsible for Steps H1, H2, H3, H4, and H5.

Table D-1
Water Analysis Module (WAM) Computational Processes (Simple Hydrodynamics/Water Quality Model Component)

Process	Description	Input	Output
H1	Simulate impact of island flooding on salinity distribution. The simulation period is be determined by the time required to fill the breached islands.	Levee breach state DICU, Inflow, Exports Control Structure Operation (DCC) Salinity Distribution	Salinity distribution at time when all breached islands have filled. Requested changes in Water Operations (pumps, gates, releases)
H2	Determine need for adjusted flushing releases (after flooding) with the intention of reducing salinity in central Delta to make pumping possible. The volume required to flush the Delta is a function of the release flow rate	Levee breach state DICU Salinity Distribution	Request for flushing release as a Flow-Volume function
H3	Simulate salinity response to flushing releases. The period of simulation is determined by the reservoir management flushing release decision	Levee breach state DICU, Inflow, Exports Control Structure Operation (DCC) Salinity Distribution	Salinity distribution at end of flushing period
H4	Determine Inflow-Export relation and ability to pump based on the predicted salinity distribution and damage to pumps	Levee breach state Salinity Distribution WQ Standards Pump damage state	Inflow-Export function (determines required net Delta outflow) Ability to pump at each export location
H5	Simulate salinity and potentially constrain exports if WQ standards are not met	Levee breach state DICU, Inflow, Exports Control Structure Operation (DCC) Salinity Distribution	Salinity distribution at end of time period Actual export volume from each location

H2: Estimate volume required to flush high salinity water from the Sacramento and San Joaquin Rivers in the central Delta – If island flooding leads to a salinity distribution in the central Delta that precludes exports, then a flushing volume in addition to expected Delta inflows is estimated to push the salt gradient seaward. An estimate of the flushing volume is developed based on the volume of water in the main channels that must be displaced to move the salinity gradient seaward the required distance plus the flow over the flushing period required to compensate for the tidally-averaged dispersive flux tending to transport salt landward. The release rate for flushing is determined by the reservoir operation component of the WAM. When flushing of the Delta is required, the Delta Cross Channel is opened unless it must be kept closed due to regulatory constraints.

H3: Simulate salt transport during the flushing period – Simulation of salt transport considers Delta inflow, exports (if any), and NDAL flows as well as net salt flux into/out of breached islands.

H4: Estimate net Delta outflow required, for various export amounts to maintain salinity standards and determine the ability to pump – The ability to pump is controlled by Delta salinity and pump damage. Conditions that constrain pumping include the following:

- A pump has suffered damage due to seismic activity or flooding,
- Salinity standards in the central Delta are exceeded such that export pumping would draw salt into the south Delta where it is difficult to flush,
- The net salt flux out of flooded islands along the conveyance corridors is sufficient to drive the salinity of exported water above standards, or
- The salinity in channels south of the San Joaquin River is too high for south of Delta water users to accept.

If the salinity in south Delta channels is above standards, but pumping is allowable by the other criteria, it may be permissible to begin exports in an effort to flush the south Delta. This is only allowable if the salt load in the south Delta channels can be accepted by south of Delta water users. The Delta operations Submodel includes provisions for making this decision and proposed rules are to be reviewed with state and federal project operators.

The model also estimates the amount of net Delta outflow required for various amounts of exports to keep salinity low enough in the central Delta so that exports are possible. This varies depending on the number and location of breached islands. In general, tidal mixing (dispersion) increases with the number (area) of islands that are actively filling and draining. Therefore, each additional levee breach that results in island flooding results in a greater need for net Delta outflow to counteract tidal mixing of salt into the Delta.

H5: Simulate salt transport – Simulation of salt transport considers Delta inflow, net Delta outflow, exports (if any), and DICU flows as well as net salt flux in/out of breached islands and pump out of flooded islands that have been repaired. If salinity standards at the pumps are exceeded, exports are curtailed.

D.4.4 Simplified Model Configuration

The simplified model is a tidally-averaged, advection-diffusion model with net flow and tidal dispersion properties derived from the multi-dimensional models. The simplified model configuration contains enough spatial resolution to reasonably represent salinity variability in the system. It also represents key control structures (including the Delta Cross Channel), aggregate NDAL locations, and all Delta islands with breaches.

Conceptually the simplified model represents the transport of fresh water from north to south through the Delta, across the San Joaquin River. The basic model configuration to accomplish this includes the primary flow axis from the Golden Gate/Central Bay up through the north Bay and Suisun Bay up through the San Joaquin River to Vernalis. The model also includes the Delta flow corridors from the north that bring fresh water to the San Joaquin River and flow corridors to the south that bring water to the pumps.

The schematic for the simplified model is show in Figure D-2. The primary flow axis runs from the Golden Gate up the San Joaquin River to Vernalis. Stratification has been considered within the simple model by using tidally averaged longitudinal dispersion coefficients which include the influence of gravitational circulation based on horizontal Richardson number. This parameterization is derived from TRIM/UnTrim three-dimensional model simulations.

Flow corridors from the north include the Sacramento and Mokelumne Rivers. The Delta Cross Channel moves flow from the Sacramento to the Mokelumne. Threemile Slough splits some of the Sacramento flow and Potato Slough/Little Connection Slough splits some of the Mokelumne flow. Conveyance of all other channels north of the San Joaquin are included as part of the principal channels. For example, flow in Georgiana Slough is effectively included in Mokelumne flow.

Flow corridors south of the San Joaquin include Old River, Middle River, and Old River at Head. Turner Cut brings additional flow to Middle River from a point farther upstream on the San Joaquin. The complex channel connections in the south Delta and south Delta barriers are included as necessary to adequately calculate flows and salinities. To determine salinity at the pumps, flow splits are evaluated from the multi-dimensional models and the quality of exports is derived from the quality of the three primary flow corridors – Old River (northern section adjacent to Franks Tract), Middle River, and Old River at Head.

Five aggregate NDAL locations are included, one on each of the principal flow corridors north and south of the San Joaquin River.

The islands considered in the risk analysis are included (only examples are shown in Figure D-2). Because the submodel is operated with tidally-averaged flows, exchange with islands and channels through breaches must be analyzed with the multi-dimensional models and exchange estimates are given to the simplified model so that net salt flux can be determined. Islands are allowed to have multiple breaches, in which case flow through islands may occur. In the simplified model, Franks Tract is treated in the same manner as other islands except that it is always flooded.

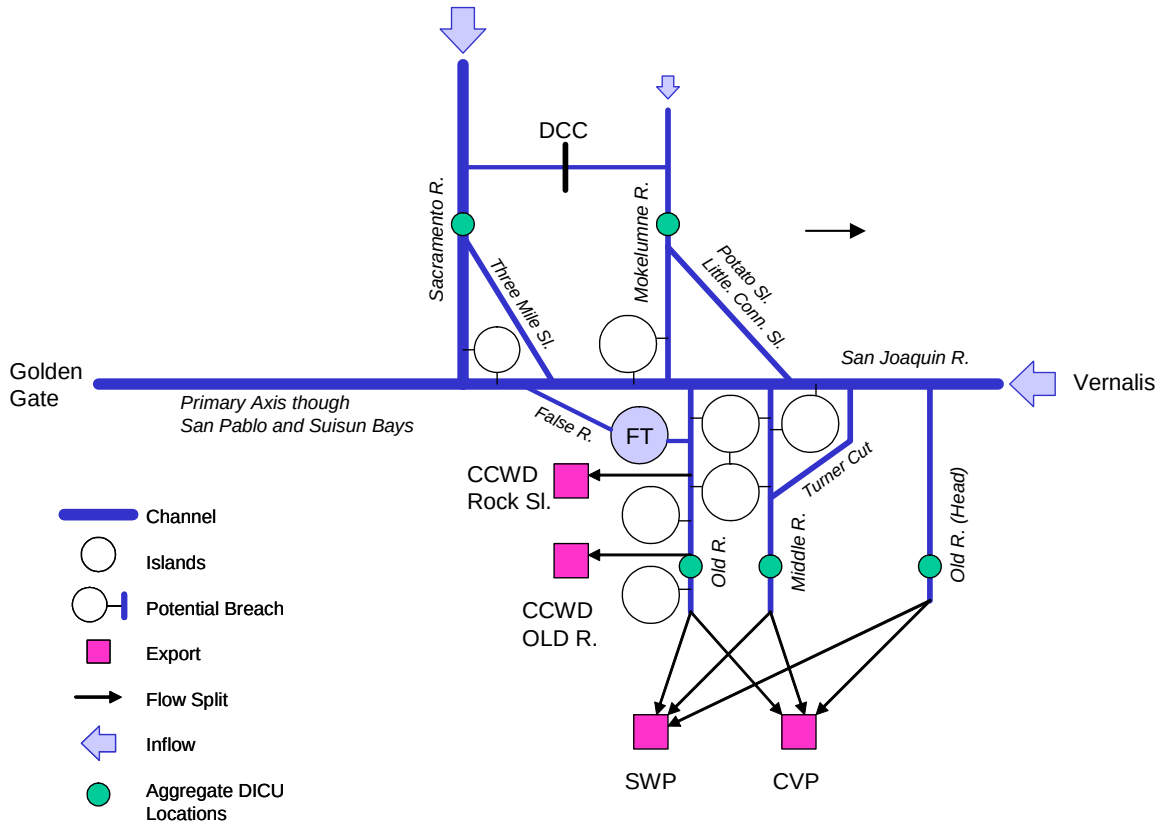

Figure D-2 Simplified HD Submodel Schematic (only example islands shown)

The HD has been implemented as a one-dimensional RMA finite element model as shown in Figure D-3. The RMA finite element modeling framework is a generalized tool for multi-dimensional simulation of surface water systems, which includes the RMA2 and RMA11 computational engines for simulation of hydrodynamics and water quality transport as well has RMA10 for stratified flow and a variety of pre and post processing tools. The framework supports computational networks which include a combination of 1, 2, and 3-dimensional elements. The full RMA Bay-Delta model is a specific application of the RMA finite element modeling system for the San Francisco Bay /Sacramento-San Joaquin Delta that represents the majority of the system with two-dimensional depth averaged elements and smaller tributary streams and Delta channels as one-dimensional cross-sectionally averaged elements. The RMA Bay-Delta Model simulates tidal dynamics typically using a time step of 7.5 minutes. The WAM HD uses only one-dimensional elements and operates on a tidally averaged (daily) time step.

The HD model geometry has been constructed to approximate the conveyance and storage of the system with the objective of minimizing computational demand. The simplified model uses 500m elements with trapezoidal cross-section. Because the objective of the WAM HD is to provide reasonable salinity distributions with very low computation time, not all channels in the Delta are explicitly represented in the simplified model configuration. Where possible parallel channels where combined into a single channel will similar total conveyance capacity. For example, conveyance capacity of

Steamboat and Sutter Sloughs where combined with the upstream reaches of the Sacramento River and the conveyance capacity of Dutch Slough was combined with False River. Minor connecting channels and Sloughs where included as off-channel storage in the primary channels. Overall volume of each reach in the HD was checked against the equivalent reaches in the RMA Bay-Delta Model including and found to be generally within 2 to 5 percent. It is likely that the quality of the WAM HD calibration would improve if more of the Delta channels were explicitly represented in the model configuration at the expense of longer computation time.

Locations where boundary conditions are applied are shown in Figure D-4. Boundary conditions include river inflows, exports, internal flow boundaries, grouped DICU locations, and the downstream boundary. Grouping the Delta Island diversions and returns and local precipitation into five discrete locations is a significant simplification. If there is an opportunity to improve the WAM HD for future use, providing a better distribution of DICU flows would be a valuable enhancement.

Dispersion parameters used by the WAM HD vary by zones as shown in Figure D-5. Dispersion zones have been selected to represent regions of similar mixing characteristics.

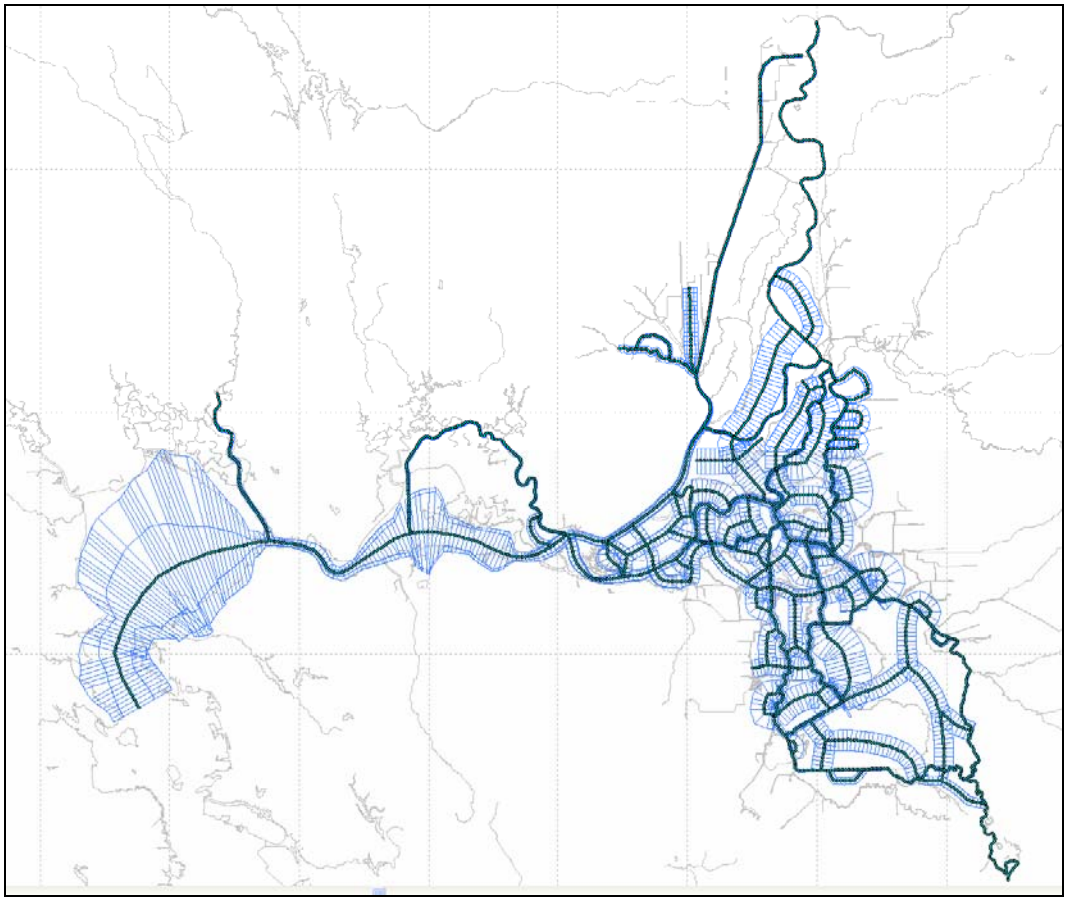

Figure D-3 WAM HD Model Configuration: 1-Dimensional RMA Finite Element Network with 500m Elements

(Note that 1-D element width for channels and island segments are drawn centered on the elements.)

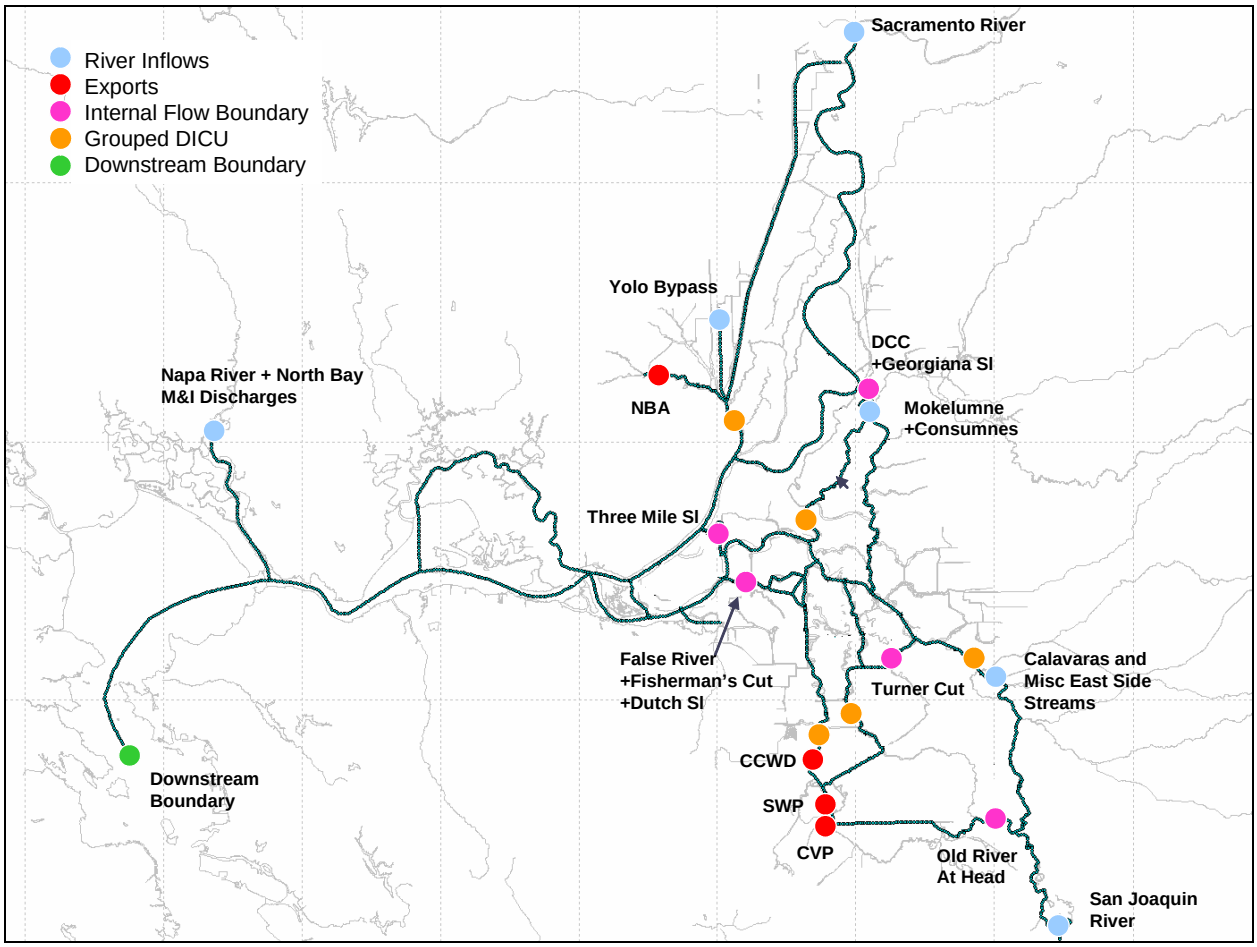

Figure D-4 WAM HD Model Configuration: Boundary Conditions

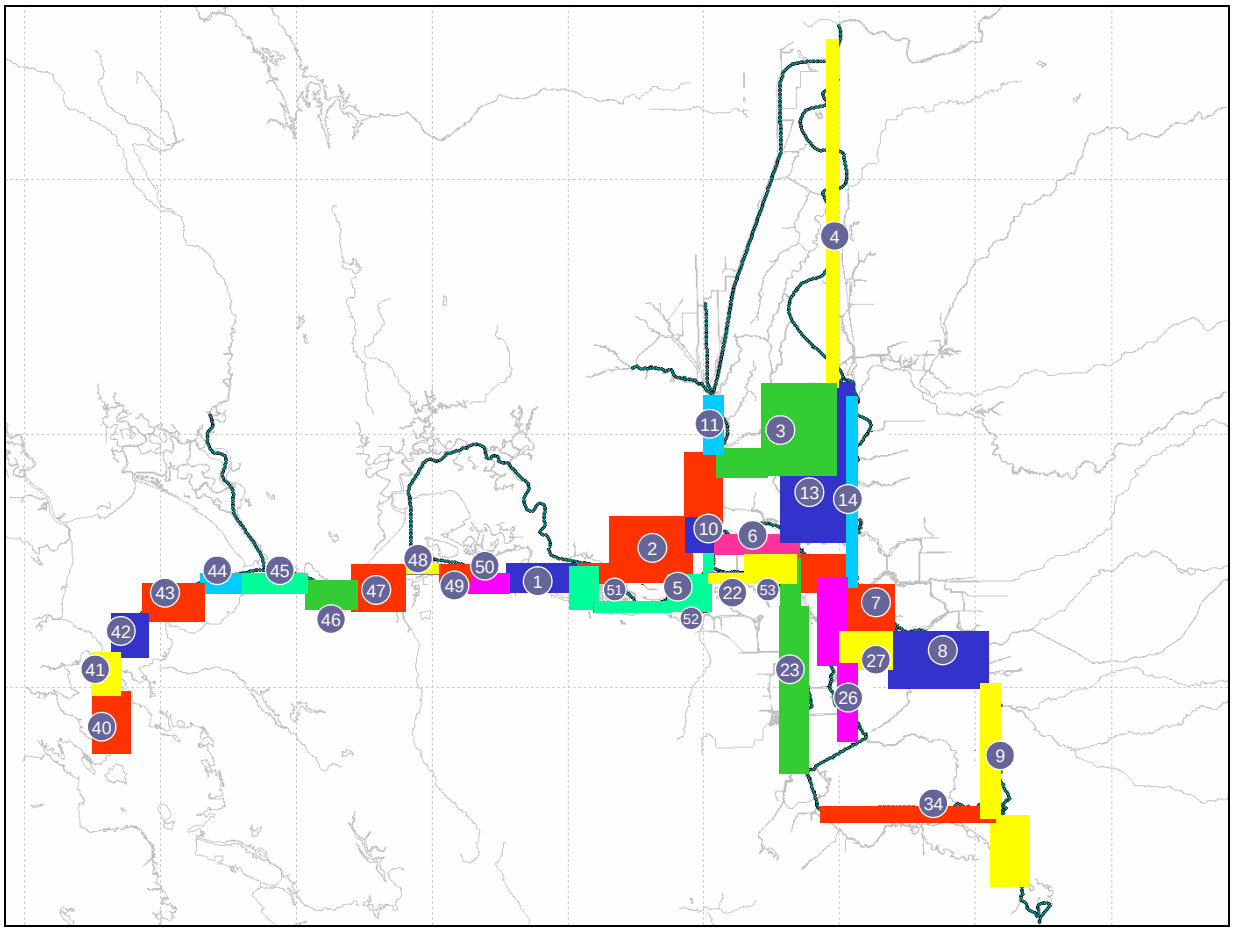

Figure D-5 WAM HD Model Configuration: Dispersion Zones

D.4.5 Representation of Transport Processes

Key aspects of the simplified model include the following.

- The geometry has appropriate volume and conveyance areas.
- Net flows are distributed appropriately across the channel network.
- Tidally-averaged mixing coefficients are representative of the dynamic tidal mixing.
- Net salt flux between Delta channels and flooded islands accounts for daily tidal exchange and horizontal variability in salinity within the islands. The flooded island representation allows net flow through the flooded islands when multiple breaches are present.

Configuration and calibration of the simplified model is based on existing multi-dimensional models of the system, specifically the RMA Bay-Delta and TRIM3D models. The geometric configuration was discussed in the previous section.

Direct simulation of net flows in the Delta without simulating tidal dynamics does not yield the correct flow distribution because the propagation of the tides and operation of

flow control structures causes some channels to be favored on flood flows and others on ebb flows. To provide a better representation of net flows in the system, internal flow boundary conditions are applied at important connecting channels within the Delta to represent the influence of tidal flows and gate operation. Internal flows are set by means of multiple linear regressions that relate net daily total inflow to four quadrants (Northeast, Northwest, Southeast, and Southwest) of the Delta to the each internal flow location. Where internal flows are strongly influenced by gate operations, different regression relationships are developed with and without gate operations. Internal flow boundaries are relaxed while islands are flooding.

Water surface elevation is part of the net flow hydrodynamic simulation; however, because the model is operating on a daily time step tidal highs and lows in water surface elevation are not represented. So concerns regarding extreme lower-low water cannot be evaluated with the WAM HD. In the first day(s) following a breach event, the HD may predict low water surface elevations as islands are filling. These low water surface elevations do not directly influence export constraints as the pumps are assumed to not be operated during the initial flooding regardless of water surface elevation. In the physical system after the islands have filled, the addition of newly flooded islands will generally decrease the tidal range and water surface elevations are not expected to constrain pumping operation.

The approach to parameterization of tidally averaged dispersion in the HD is based on the TRIM3D analysis presented in WAM Appendix H. The total dispersion coefficient for each dispersion reach is computed as the sum of a gravitational component that varies with salinity distribution and a combined 2D horizontal/vertical unsteady shear term that varies with net Delta outflow. Because the geometry of the WAM HD does not precisely match the geometry of the TRIM3D model it is was not expected that the dispersion parameterization from the TRIM3D analysis would work directly in the WAM HD. Calibration was performed primarily regarding the flow dependence of the combined 2D horizontal/vertical unsteady shear term while maintaining parameters in the range of those presented in the TRIM3D analysis. Additional information was gleaned from particle track experiments using the RMA Bay-Delta Model.

Tidally averaged dispersion following breaching and flooding of Delta islands may be expected to change from the base, un-breached condition. At the outset of the DRMS study it was expected that the change in tidal mixing would be very significant. While developing the WAM HD, several numerical experiments where performed with the RMA Bay-Delta model in attempt to quantify the change in mixing characteristics associated with single and multiple levee breach cases. In the time available for this study no conclusive relationship was determined. While local increases in mixing near the breaches was observed, in many cases mixing apparently decreased in regions away from the breach site so that the overall affect was difficult to quantify. This issue should be pursued further in future studies.

The net salt flux between channels and flooded islands is parameterized as a function of the active tidal prism in the island, volume of the island, number of breaches on the island, and a calibration coefficient related to the effective exchange of channel water and island water during over the course of a flood/ebb cycle. The exchange coefficient was

adjusted manually based on results from breach scenarios simulated with the RMA Bay-Delta Model.

Further discussion of representation of transport processes is provided in Appendix E of the WAM TM.

D.4.6 Calibration/Verification of the Simplified Model

Calibration and limited verification of the WAM HD is described in Appendix E. The HD was calibrated against the historic period of October 1992 through September 2003. Calibration was accomplished manually, with the primary effort involving adjustment of flow dependent tidally averaged dispersion parameters related to 2D horizontal/unsteady shear dispersion. Calibration of the exchange coefficient for mixing in flooded islands was based on the RMA Bay-Delta Model of a 50-breach event with 20 flooded islands. The 2004 Jones Tract levee failure event in 2004 was simulated as a limited verification. The salinity impact associated with Jones Tract flooding was very small, so additional verification for breached conditions would need to utilized simulation results from the RMA Bay-Delta Model or other models.

Because the WAM HD runs very rapidly, it may be very useful to implement an automated calibration procedure as a future enhancement. At that time the available historic data should be more formally divided into calibration and verification data sets.

Results of the base case calibration show that RMS (root mean squared) difference between computed and observed EC values are generally within 15% of the peak summer salinity at any given Delta location.

It is expected that initial runs of the risk analysis will identify important breach events that were not explicitly simulated using the RMA Bay-Delta Model. These events may be important either due to particularly high probability of occurrence, or due to potentially high damages. To validate the results of the simplified hydrodynamic/water quality submodel, important “bookend” cases will be simulated with the RMA Bay-Delta Model. In this way the simplified model embedded in the WAM acts as a screening tool to assist in identifying the levee breach events that warrant fully dynamic simulation. The full simulations will then serve as additional data sets for model verification or refinement.

D.4.7 Example Results

This section presents example results that illustrate use of the WAM HD to evaluate salinity consequences of levee breach sequences. Within the Risk Assessment Framework, the WAM receives information from the Emergency Repair and Response Module identifying individual levee breach sequences. Because consequences of a levee breach sequence are dependent both on antecedent and subsequent hydrology, for each levee breach sequence the WAM performs multiple simulations. Five years has been selected as the maximum length of simulation period for any given run to complete repair and recovery following the event start date. The WAM works within the CALSIM hydrologic time window with allowance for spin-up and run-out and may perform simulations starting on the first of any month between January 1923 and September 1998, which results in 909 possible event start dates.

In preparation for analysis of breach cases, the entire CALSIM hydrologic period is simulated continuously with out over-riding reservoir releases or exports to establish a baseline Delta salinity distribution. The baseline salinity distribution is used as the initial salinity condition for subsequent runs.

Because the WAM HD does not exactly duplicate the behavior of the ANN model used with CALSIM, the WAM reservoir operations without any breach event may diverge from the reference CALSIM run. To avoid confusing differences in operations caused by behavior of the WAM HD relative to the ANN verses differences related to breach cases, WAM is run with a no-breach case for each possible event start date. This set of five year simulations becomes the basis of comparison when evaluating breach cases.

To illustrate the importance of breach event start date on salinity intrusion, example EC time series at Jersey Point are presented in Figures D-6 and D-7. In Figure D-6 results are shown for a 20 island levee failure sequence that was run 12 separate times, starting on the first each month in 1993. Note that events that occur during late winter and spring have a lower salinity impact than do events that occur during fall. This is because high flows during the late winter and spring push the salinity gradient farther downstream, so that when a breach occurs, less salt water is drawn in to the central Delta. Over the course of the year, the system is managed for minimum required net Delta outflow, allowing the salinity gradient to move upstream. So when breach events occur in the fall, the impact is more severe.

Beyond simple seasonal variation, variation in hydrology from year to year will influence the severity of levee events. EC at Jersey Point resulting from separate breach events occurring each July 1st from 1992 through 2003 are shown in Figure D-7. Wet years such as 1995 and 1997 have low impact even for a July event, while drier years such as 1991 and 2002 show considerably greater impact.

The amount of salt drawn into the Delta following a breach event is one of the most important factors affecting the length of time that export operations are disrupted. A second important factor is the water available both at the time of the breach and over the coming months to flush salt from the Delta. The severity of the disruption in terms of water management depends both on the length of time exports curtailed and on the volume of export water that was expected during that period. Export deficit is one of the outputs of the WAM calculation. The export deficit at the time exports are first resumed is useful parameter to illustrate the variation of impact with hydrology. Exports are stopped at time of the event. Exports do not resume until salinity in the central Delta drops below acceptable levels (1000 μmhos/cm). The volume of water exported during the base simulation that was not exported is the deficit. The magnitude of the deficit is therefore a function of both the amount of time that pumping cannot be continued due to high salinity as well as the export rate for that period that would have occurred had there been no breach. If a breach occurs following a high runoff period, the deficit will tend to be small as there is less high salt water drawn into the Delta. If the breach occurs toward the end of a drought period, exports from the delta may have already been constrained such that outage due to salinity intrusion does not necessarily cause a large export deficit. The greatest deficit occurs during relatively dry periods when base case exports are large.

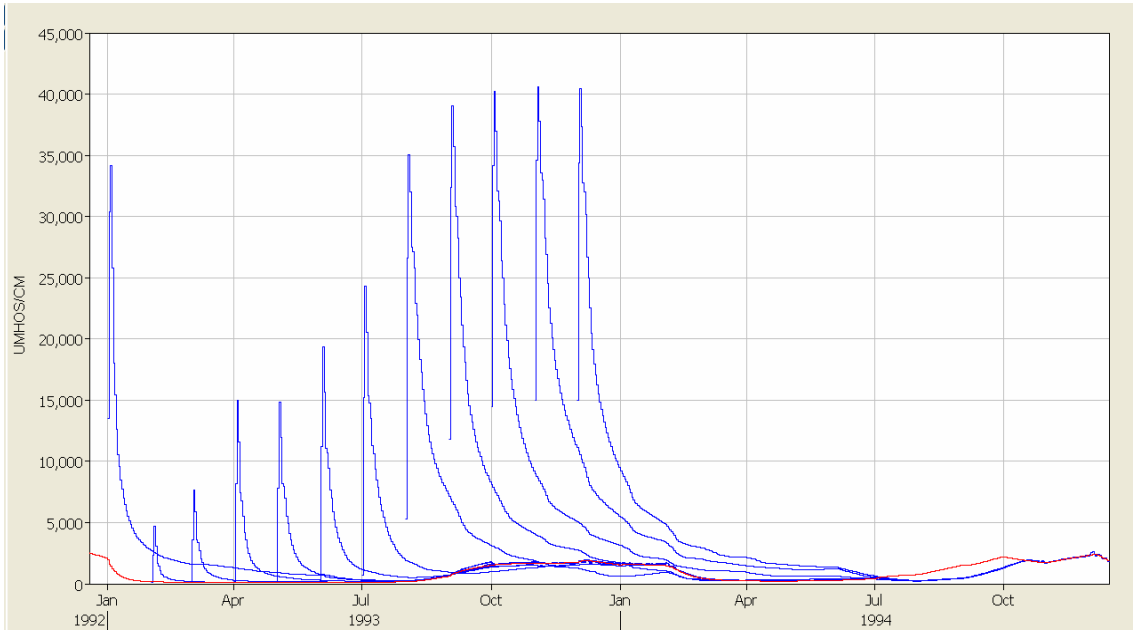

Figure D-6 EC impact at Jersey Point resulting from 20 Island Breach Events starting on the first of each month from January through December 1993.

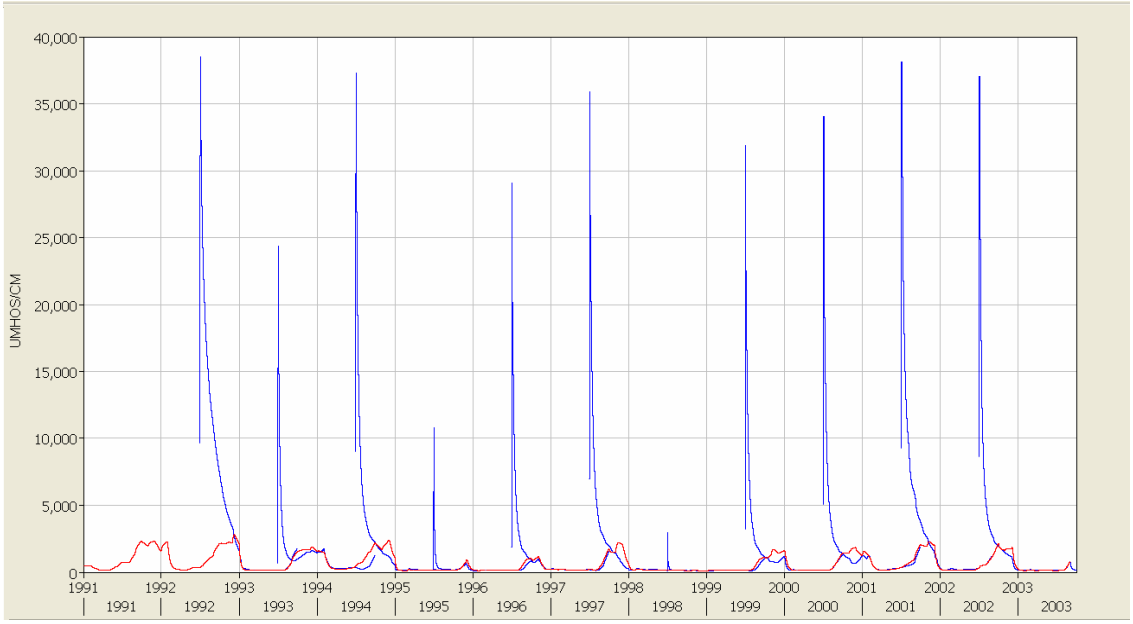

Figure D-7 EC impact at Jersey Point resulting from 20 Island Breach Events starting each July 1 from 1992 through 2002.

Export deficit results for a set of example breach sequences related to seismic events from the risk analysis are shown in Figures D-8 and D-9. The event sequences include the following.

- Run 2, 3 Island Case
- Run 3, 3 Island Case, alternate repair schedule
- Run 4, 10 Island Case
- Run 5, 20 island Case
- Run 6, 30 Island Case

The breach sequences were simulated at each of the event start dates and run until the system recovered or a maximum of five years (over 20,000 years of Delta salinity simulation in total).

Figure D-8 shows the export deficit for events occurring between January 1986 and September 1998. Figure D-9 shows the exceedance probability for all start times from January 1923 through September 1998. Even with the 20 and 30 island breach cases there are some start dates that result in very low export deficits. For the Run 5, the 20 island case, the 50 % exceedance export deficit is on the order of 5 million acre feet.

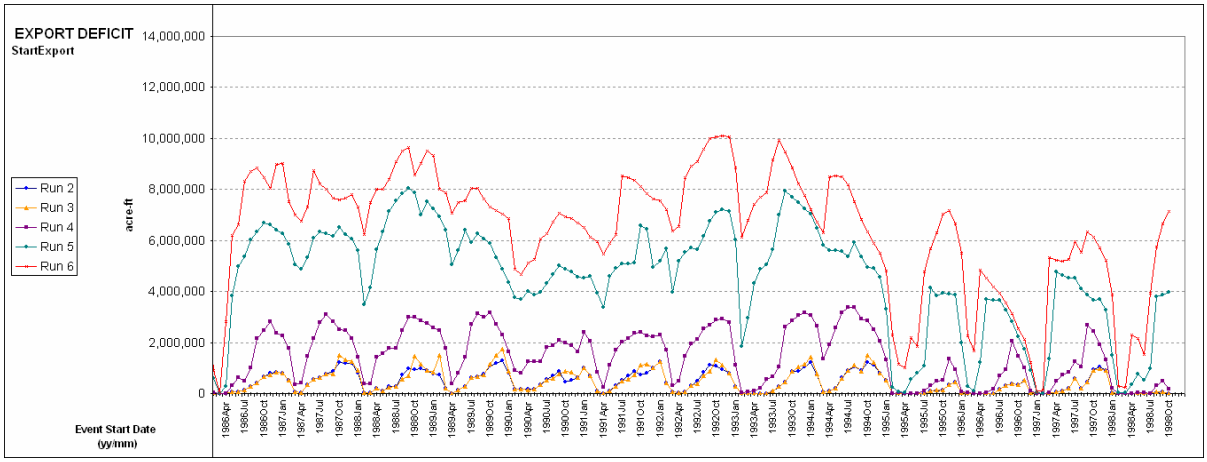

Figure D-8 Export deficit at time exports are initially resumed based on starting breach events on the first of each month from January 1986 through October 1998, Risk Analysis Event Sequences 2-6.

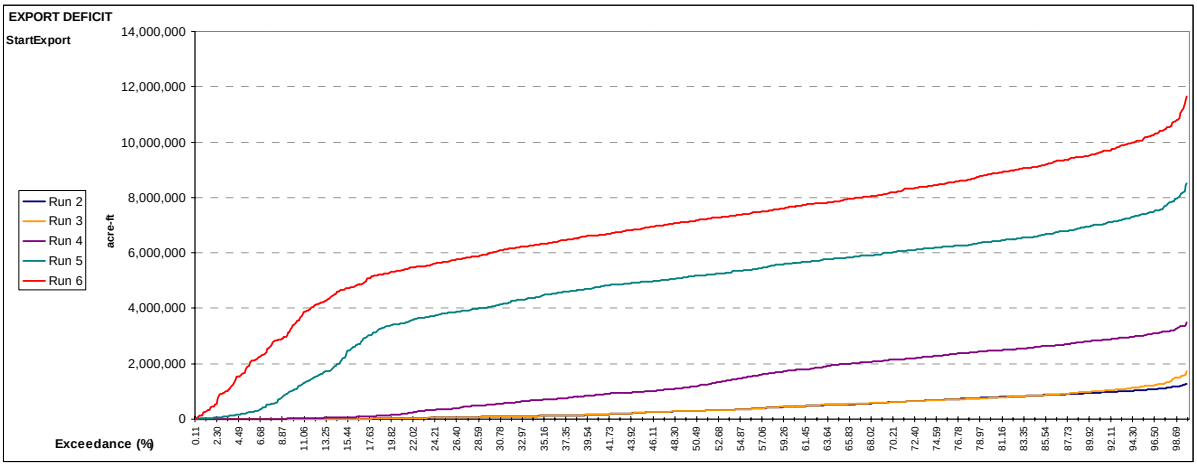

Figure D-9 Exceedance probability of export deficit at time exports are initially resumed based on starting breach events on the first of each month from January 1923 through October 1998, Risk Analysis Event Sequences 2-6.

D.5 Assumptions, Constraints, and Limitations

The simplified HD submodel is limited in several ways. Many of these limitations follow from assumptions of the analysis while other limitations are time available for initial development of the WAM.

The bathymetry of San Francisco Bay, San Pablo Bay and Suisun Bay is assumed to not change in configuration during a breach event. The WAM assumes no changes in current Delta operations. This includes no new barriers and gates and no major changes in operation of existing infrastructure.

A key limitation of the salinity analysis is that Delta bathymetry and topography are based upon best available data. They are assumed to be known accurately. Available data are actually limited and often inaccurate, particularly on the Delta Islands. Quantification of the effect of the uncertainties in island topography on the simulations rely on error estimates in island volumes from DWR and DRMS project team GIS analysis. The fundamental Delta channel network geometry and bathymetry are assumed static. The submodel does not account for geomorphic evolution of the channels due to levee failure. In reality, a very significant seismic event may breach large sections of levees in a way that fundamentally changes the flow paths in the Delta. While flow through islands breached on more than one side is considered, wholesale changes to the major flow paths (in Delta channels) that might accompany significant scour are not considered.

The levee failure details are inputs to the water module and are not affected by the results of WAM. In reality, both secondary levee failures and breach geometry are related to hydrodynamics. Secondary levee failures may occur due to sudden drawdown in water surface elevation when flooded islands fill or due to wind wave action over the long fetch of a flooded island acting on the inside of an island levee or for other reasons. In addition, breach geometry evolves as breaches scour due to strong currents through the breaches.

Because coupling the levee fragility and water modules would increase the complexity and computational expense of the overall DRMS analysis, these modules are not coupled.

Due to limited time there has been a shortage of sensitivity and validation. From calibration it appears that the RMS Difference between computed and observed on the order of 15% of the peak summer EC values. What is not well determined is the accuracy of operations with reservoirs. There is work on-going to compare results to DSM2 for a CALSIM sequence and to look comparison of WMA HD reservoir operation for the un-breached condition.

Filling and draining of breached islands in the Delta will impact tidal dispersion, however, work to date has not provided well defined relationship that can be implemented in the WAM HD. Numerical experiments with the RMA Bay-Delta model suggest that dispersion increases in the neighborhood of levee breaches, but may be unchanged or decrease in regions of the Delta away from the breach. If dispersion increases in the western and central Delta significantly, it is likely that carriage water requirements would increase. Further investigation is required to better understand this issue.

D.6 Pertinent Prior Work

Casulli, V., and E. Cattani. 1994. Stability, accuracy and efficiency of a semi-implicit method for three-dimensional shallow water flow. Computers Math. Applic. 27(4), 99-112.

Casulli, V., and R.A. Walters. 2000. An unstructured, three-dimensional model based on the shallow water equations, International Journal for Numerical Methods in Fluids 2000, 32: 331 - 348.

Cheng, R.T., and V. Casulli. 2001. Evaluation of the UnTRIM model for 3-D Tidal Circulation. Reprint from: Proceedings of the 7-th International Conference on Estuarine and Coastal Modeling, St. Petersburg, FL, November 2001, p. 628-642.

Chow, V.T. 1959. Open-channel Hydraulics. McGraw-Hill Inc., New York.

Denton, R.A. 1993. Accounting for antecedent conditions in sea-water intrusion modeling – applications to the San Francisco Bay-Delta. Hydraulic Engineering ‘93, H.W. Shen, S.T. Su, and F. Wen, Eds., ASCE, 448-453.

Gross, E.S., J.R. Koseff, and S.G. Monismith. 1999. Evaluation of advective schemes for estuarine salinity simulations. Journal of Hydraulic Engineering 125 (1): 32-46.

Gross, E.S., M.L. MacWilliams, and W. Kimmerer. In press. Simulating periodic stratification in the San Francisco Estuary. Proceedings of the 9th Estuarine and Coastal Modeling Conference.

Monismith, S.G., W. Kimmerer, J.B. Burau, and M.T. Stacey. 2002. Structure and flow-induced variability of the subtidal salinity field in Northern San Francisco Bay, Journal of Physical Oceanography, 3003-3019.

Resource Management Associates. 2005. Flooded Islands Pre-Feasibility Study: RMA Delta Model Calibration Report. Project report prepared for California Department of Water Resources for submittal to California Bay-Delta Authority.

Uncles, R.J., and D.H. Peterson. 1995. A computer model of long-term salinity in San Francisco Bay: Sensitivity to Mixing and Inflows. Environmental International 21(5): 647-656.

Warner, J.C., C.S. Sherwood, H.G. Arango and R.P. Signell. 2005. Performance of four turbulence closure models implement using a generic length scale method, Ocean Modeling, 8, 81-113.

Appendix E
Hydrodynamic and Salinity Calibration

Table of Contents

E1. Introduction.....1

E2. Base Condition Calibration Using Dayflow Boundary Conditions.....1

E.2.1 Calibration Period 1

E.2.2 Boundary Conditions..... 2

E.2.3 Observed Data Sources 3

E.2.4 Calibration Methodology 3

E.2.5 Flow Comparisons..... 4

E.2.2 Salinity (EC) Comparisons..... 14

E3. Comparison to RMA Bay-Delta Model 50 Breach Simulation.....16

E4. 2004 Jones Tract Event 39

E5. Discussion.....46

Figures

E-1 Net Delta Outflow and Observed EC variation over 1991-2003 Calibration Period and Typical Summer EC Spatial Distribution

E-2 Flow Comparison Stations for 1991-2003 Calibration Period

E-3 Tidally Averaged and Monthly Averaged Net Delta Outflow – Calibration to Dayflow Boundary Conditions

E-3a Tidally Averaged and Monthly Averaged Net Delta Outflow, Summer 2002 – Calibration to Dayflow Boundary Conditions

E-4 Tidally Averaged and Monthly Averaged Flow at Station RSAC101 – Calibration to Dayflow Boundary Conditions

E-5 Tidally Averaged and Monthly Averaged Flow at Station SLTRM004 – Calibration to Dayflow Boundary Conditions

E-6 Tidally Averaged and Monthly Averaged Flow at Station RSAN018 – Calibration to Dayflow Boundary Conditions

E-7 Tidally Averaged and Monthly Averaged Flow at Station ROLD024 – Calibration to Dayflow Boundary Conditions

E-8 Tidally Averaged and Monthly Averaged Flow at Station RMID015 – Calibration to Dayflow Boundary Conditions

E-9 EC Comparison Stations for 1991-2003 Calibration Period

E-10 Tidally Averaged and Monthly Averaged EC at Station RSAC054 – Calibration to Dayflow Boundary Conditions

E-11 Tidally Averaged and Monthly Averaged EC at Station RSAC075 – Calibration to Dayflow Boundary Conditions

E-12 Tidally Averaged and Monthly Averaged EC at Station RSAC081 – Calibration to Dayflow Boundary Conditions

E-13 Tidally Averaged and Monthly Averaged EC at Station RSAC092 – Calibration to Dayflow Boundary Conditions

E-14 Tidally Averaged and Monthly Averaged EC at Station RSAC101 – Calibration to Dayflow Boundary Conditions

E-15 Tidally Averaged and Monthly Averaged EC at Station RSAN007 – Calibration to Dayflow Boundary Conditions

E-16 Tidally Averaged and Monthly Averaged EC at Station RSAN008 – Calibration to Dayflow Boundary Conditions

E-17 Tidally Averaged and Monthly Averaged EC at Station RSAN018 – Calibration to Dayflow Boundary Conditions

E-18 Tidally Averaged and Monthly Averaged EC at Station RSAN032 – Calibration to Dayflow Boundary Conditions

E-19 Tidally Averaged and Monthly Averaged EC at Station RSAN058 – Calibration to Dayflow Boundary Conditions

E-20 Tidally Averaged and Monthly Averaged EC at Station RSAN072 – Calibration to Dayflow Boundary Conditions

E-21 Tidally Averaged and Monthly Averaged EC at Station RSAN087 – Calibration to Dayflow Boundary Conditions

E-22 Tidally Averaged and Monthly Averaged EC at Station ROLD014 – Calibration to Dayflow Boundary Conditions

E-23 Tidally Averaged and Monthly Averaged EC at Station RMID023 – Calibration to Dayflow Boundary Conditions

E-24 Tidally Averaged and Monthly Averaged EC at Station SWP Export – Calibration to Dayflow Boundary Conditions

E-25 Tidally Averaged and Monthly Averaged EC at Station CVP Export – Calibration to Dayflow Boundary Conditions

E-26 Comparison of RMA Bay Delta Model and WAM HD Model for 20 Island Breach Case – Time of Peak Salinity Intrusion

E-27 Comparison of RMA Bay Delta Model and WAM HD Model for 20 Island Breach Case – One Month After Event

E-28 Comparison of RMA Bay Delta Model and WAM HD Model for 20 Island Breach Case – EC Time Series At Antioch (Station RSAN008), Franks Tract, and Station ROLD034

E-29 Breach locations on Bacon Island in the RMA Bay-Delta Model and the WAM HD as used for the 20 Island Breach Case

E-30 EC Comparison Station for 2004 Jones Tract Breach Simulation

E-31 Computed and Observed EC at Station RSAC054 – Jones Tract Event

E-32 Computed and Observed EC at Station RSAC075 – Jones Tract Event

E-33 Computed and Observed EC at Station RSAC092 – Jones Tract Event

E-34 Computed and Observed EC at Station RSAN007 – Jones Tract Event

E-35 Computed and Observed EC at Station RSAN018 – Jones Tract Event

E-36 Computed and Observed EC at Station SLTRM004 – Jones Tract Event

E-37 Computed and Observed EC at Station ROLD014 – Jones Tract Event

E-38 Computed and Observed EC at Station RMID023 – Jones Tract Event

E-39 Computed and Observed EC at Station SWP Export – Jones Tract Event

E-40 Computed and Observed EC at Station CVP Export – Jones Tract Event

E1. Introduction

This document presents the calibration of the Hydrodynamic and Water Quality submodel (HD) of the Water Analysis Module (WAM). The model was calibrated for the un-breached condition using observed data from the period of October 1991 through September 2003. The 50 breach (with 20 islands flooded) previously simulated with the RMA Bay-Delta Model for the Preliminary Delta Risk Assessment was used to calibrate dispersion between channels and flooded islands in the WAM HD. Simulation of the historic 2004 Jones Tract breach event is used as a limited verification for them model.

E2. Base Condition Calibration Using Dayflow Boundary Conditions

Given the short time frame allowed for development of the WAM HD, a manual calibration exercise was conducted with the objective of reasonably reproducing monthly variation in salinity from the western Delta to the export locations in the southern Delta for a wide range of hydrologic years.

E.2.1 Calibration Period

The period ranging from October 1991 to October 2003 was selected for calibration. This period includes both very dry and wet years and historic flow and EC observations are available for much of the Delta. The variation of net Delta outflow and EC over the calibration period is illustrated in Figure E-1. January 1991 through September 1991 was used as a spin-up period.

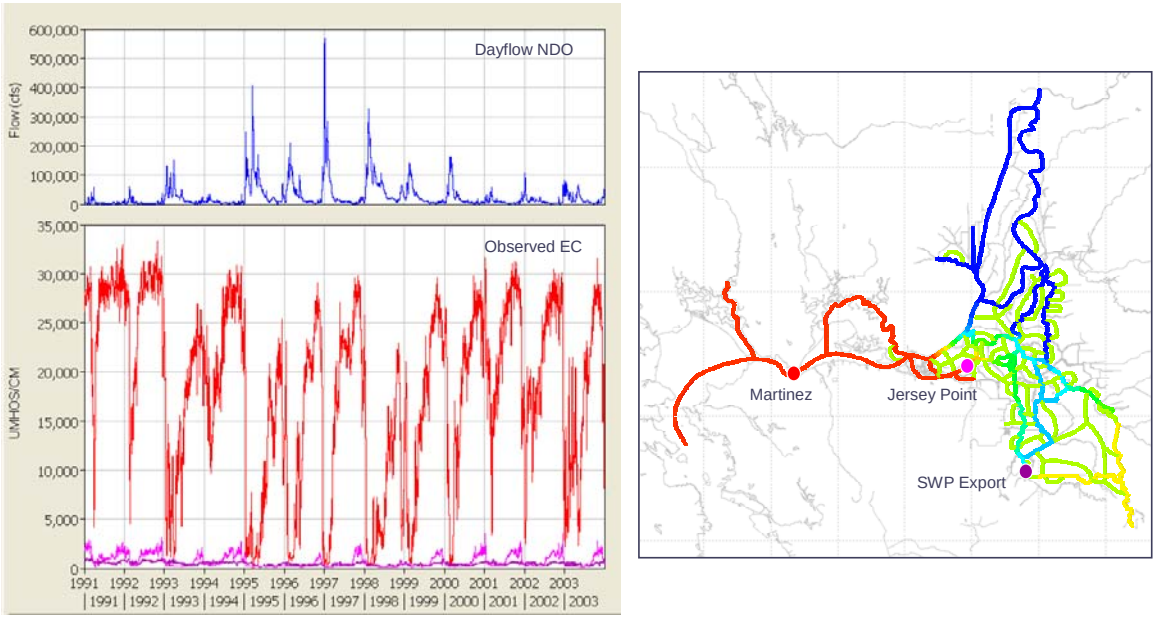

Figure E-1 Net Delta Outflow and Observed EC variation over 1991-2003 Calibration Period and Typical Summer EC Spatial Distribution (red=50,000 μmhos/cm, blue=100 μmhos/cm, log contour scale)

E.2.2 Boundary Conditions

Flow boundary conditions are taken from the Dayflow database (http://wwwiep.water.ca.gov/dayflow/) managed by the Interagency Ecological Program (IEP). Flow boundaries conditions include the following.

- Sacramento Inflow
- San Joaquin Inflow
- Yolo By-Pass Inflow
- Mokelumne + Consumnes Inflows
- Miscellaneous East Side Inflows
- North Bay Aqueduct Export
- Contra Costa Water District (CCWD) Export
- State Water Project (SWP) Export
- Central Valley Project (CVP) Export
- Channel Diversions and Returns/Precipitation

The CCWD export was treated as a single withdrawal and removed from Old River. Channel Diversions and Returns were divided and applied at five locations as described in the appendix discussing the NDAL component of the WAM.

EC is specified for all inflow boundaries as well as the downstream boundary in the central Bay.

- Sacramento Inflow – constant EC = 150 μmhos/cm
- San Joaquin Inflow – Observed Daily Average EC
- Yolo By-Pass Inflow – constant EC = 150 μmhos/cm
- Mokelumne + Consumnes Inflows – constant EC = 200 μmhos/cm
- Miscellaneous East Side Inflows – set equal to San Joaquin Inflow EC
- Channel Returns/Precipitation – computed by NDAL
- Downstream Boundary at Central Bay – constant EC = 50,000 μmhos/cm

Internal flow boundary conditions are applied at important connecting channels within the Delta to represent the influence of net tidal flow and gate operation. Most internal flows are determined by a multiple linear regression that relates the net daily inflow to four quadrants (Northeast, Northwest, Southeast, and Southwest) of the Delta as determined by boundary conditions to the desired internal flow. In some cases the different regressions are developed with and without gate operations. Internal flow locations include the following.

- Delta Cross Channel + Georgiana Slough – represents operation of DCC as well as net tidal flow from Sacramento River to the Mokelumne River through Georgiana Slough, for calibration run this flow is set to XGEO record from Dayflow.
- Threemile Slough – represents net tidal flow between the Sacramento and San Joaquin rivers through Threemile Slough, flow is determined by two separate multiple linear regressions derived from observed Threemile Slough flow depending on whether the DCC is open or closed.

- False River – represents net tidal flow between the San Joaquin River and Old River via False River and Franks Tract, flow is determined by a multiple linear regression derived from RMA Bay-Delta Model results.
- Turner Cut – represents net tidal flow between the San Joaquin River and Middle River via Turner Cut, flow is determined by a multiple linear regression derived from RMA Bay-Delta Model results.
- Old River at Head – represents net tidal flow from the San Joaquin to Old River at Head with consideration for operation of temporary south Delta barriers, flow is determined by two separate multiple linear regression relations developed from RMA Bay-Delta Model results with and without operation of the temporary barrier at Grantline Canal with modification for spring and fall operation of the temporary barrier on Old River at Head.

E.2.3 Observed Data Sources

Observed data has been collected from the online IEP (http://www.iep.ca.gov/data.html) and CDEC (http://cdec.water.ca.gov/) databases. Data collected at intervals less than one day was filtered using a two-pass 24.75 hour running average to generate tidally averaged flow or EC and resampled at a one day interval for comparison against WAM HD daily results. Monthly averaged data is derived by averaging over calendar months.

E.2.4 Calibration Methodology

Calibration of the WAM HD focused on adjustment of dispersion parameters to match observed EC time-series. Before beginning adjustment of dispersion parameters, net flows were checked to ensure reasonable operation of the multiple linear regressions for internal flows. One key flow location is Jersey Point where reverse net flows can occur during periods of low net Delta outflow. The salinity distribution in the central Delta is dramatically impacted when net flow at Jersey Point is up stream. Correctly representing the net flow at Jersey requires that the net flow in Threemile Slough be correct. Another key net flow location is Old River at Head, which impacts the distribution of San Joaquin water between the SWP and CVP export locations. When gate operations cause less San Joaquin River water to pass through Old River at Head and more San Joaquin water to pass through Turner Cut, the SWP export location receives more of the salt load from the San Joaquin. Providing different multiple linear regression parameters to represent different gate operation states improved the representation of internal net flows.

Tidally averaged dispersion parameters used in the WAM HD have been based primarily on the 3D dispersion analysis of the TRIM model results with additional information derived from 2D particle tracking simulations using the RMA Bay-Delta Model. Because the WAM HD uses significantly simplified channel geometry, the dispersion parameters were allowed to vary from the explicit estimates provided by the 3D model analysis.

The 3D model analysis separated tidally averaged dispersion coefficients for each dispersion region into components related to gravitation circulation, 2D horizontal dispersion, and unsteady shear dispersion. The relationship for calculation of the gravitational circulation component is based on a horizontal Richardson number and

utilizes the local estimate of salinity gradient, channel depth, and shear velocity. For each dispersion region in the WAM HD, typical channel depth and root means square shear velocity was estimated from a representative simulation using the RMA Bay-Delta Model. The salinity gradient is calculated at each time step in the WAM HD as the average gradient over each dispersion region. The 3D model analysis provided estimates of 2D horizontal and unsteady shear dispersion components for a range of net Delta outflow. The WAM HD uses a dispersion term that represents the combined 2D horizontal and unsteady shear dispersion components from the 3D analysis. The combined term is allowed to vary with net Delta outflow when the dispersion component value is specified at three values of net Delta outflow. Calibration for EC was accomplished by manually varying the three reference values for the combined 2D horizontal and unsteady shear dispersion component within the range of values developed by the 3D analysis. Adjustment of parameters proceeded from the central Bay upstream toward the export locations.

After initial review by the DWR Delta modeling section, additional calibration was performed to improve performance of the model in the south Delta. Match between computed and observed daily averaged EC at the SWP and CVP export locations was improved by three adjustments to the model. First, the observed daily EC at Vernalis was used for the San Joaquin EC boundary condition in place of the CALSIM monthly-averaged Vernalis EC record. Second, the impact of the temporary barrier on Grantline Canal was more accurately represented in establishing the net flow through Old River at Head. And third, the multiple linear regression relationship for estimating flow through Turner Cut was improved

As described in a following section, the year 2004 has been simulated without adjustment of parameters and includes the Jones Tract breach event. With additional time a further simulation of 2005 and 2006 could be made as validation tests. Ultimately, if the WAM HD is to receive wider use, implementation of an automated calibration process would be valuable. At that time, the historic period could be formally separated into calibration and validation sets.

E.2.5 Flow Comparisons

Comparisons of computed and observed net flow are presented in figures E-3 to E-8. Flow comparison locations are shown in Figure E-2. Each figure shows time series of tidally averaged and monthly averaged flow from October 1991 through September 2003. Scatter plots of computed verses observed are presented with each time series plot and include the following error statistics.

- Linear regression with intercept forced to zero
- Coefficient of determination (r2)
- Mean difference - $\frac{1}{n}\sum_{i=1}^{n}\left(C_i - O_i\right)$
- Mean absolute difference - $\frac{1}{n}\sum_{i=1}^{n}\left|C_i - O_i\right|$

- RMS (root mean squared) difference - $\sqrt{\frac{1}{n}\sum_{i=1}^{n}\left(C_i - O_i\right)^2}$

where C_i and O_i are corresponding computed and observed values and n is the number of number of values in the observed time series.

Comparison of the Net Delta Outflow (NDO) from Dayflow and computed WAM HD flow near Martinez (Figure E-3) serves as a check on the applications of boundary conditions. The minor variation between the Dayflow NDO and computed flow is primarily a result of routing boundary conditions through the system (Figure E-3a).

Net flow in the Sacramento River near Rio Vista (RSAC101, Figure E-4) ranges from a few thousand cubic feet per second (cfs) to hundreds of thousands of cfs during storm runoff periods. The RSAC101 flow in the WAM is a function of the Sacramento River and Yolo Bypass inflows less the flow that is diverted through the Delta Cross Channel (DCC) and Georgiana Slough, North Bay Aqueduct export, and the northwest DICU group. Given the large range of flow at this station the RMS difference of 6869 cfs, linear regression slope of 1.06, and r2 of 0.953 for daily flow show that the model is performing well. However, small errors in summer net flow are important with regard to the salt transport simulation. The EC result at RSAC101 during 1992 is significantly high. While there is no observed flow data available for 1992, It is very likely that the net flow is too low, which is probably due to incorrect allocation of DICU flow to the northwest group.

Flow in Threemile slough is shown in Figure E-5. In the HD Threemile flow is forced by a multiple linear regression relation as described in section 2.2 above. Net flow in Threemile slough is a critical factor in determining the net flow in the San Joaquin and Jersey Point and the summer salinity at Jersey Point. There is a distinct shift in the observed net flow in Threemile in 2001 when the USGS recalibrated the Threemile Slough gage. It appears that the recent data underestimates the net flow toward the San Joaquin in summer. In calibrating the WAM HD, it was found that ignoring the post 2001 summer Threemile slough data and tuning the multiple linear regression to the pre-2001 data provided a better overall result, both in terms of net flow at Jersey point and summer EC in the central delta. This issue warrants further investigated in cooperation with USGS staff.

Flow in the San Joaquin River at Jersey Point (RSAN018) is shown in Figure E-6. As noted above, the Jersey Point flow is very sensitive to the net flow in Threemile Slough, and balancing net flow across Sacramento and San Joaquin is critical to getting a good result for summer salinity intrusion. While the r2 at this station is 0.964, the computed flow is generally lower than the observed flow by 1800 cfs. A small part of this difference is because Dutch Slough is not explicitly in the model and the flow that would have moved through Dutch Slough travels upstream passed Jersey Point and through False River. The summer net flows tend to be too low, which will increase the rate of salinity intrusion up the San Joaquin. Any future flow calibration effort should focus on improving the summer net flow result at this station.

The flow comparisons for Old River (ROLD024) and Middle River (RMID015) are shown in Figures E-7 and E-8. In the WAM HD the flow split between old and middle

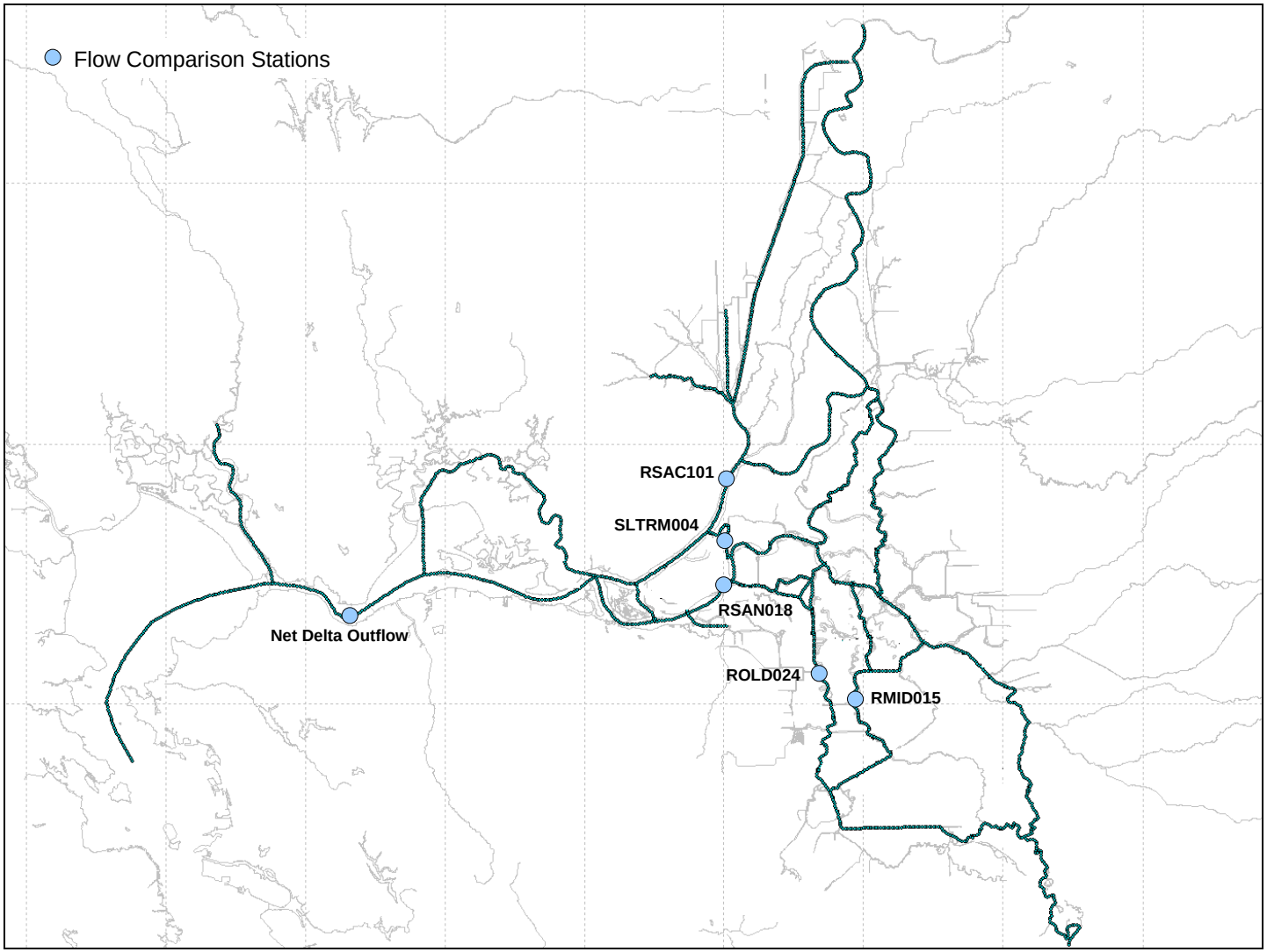

Figure E-2 Flow Comparison Stations for 1991-2003 Calibration Period

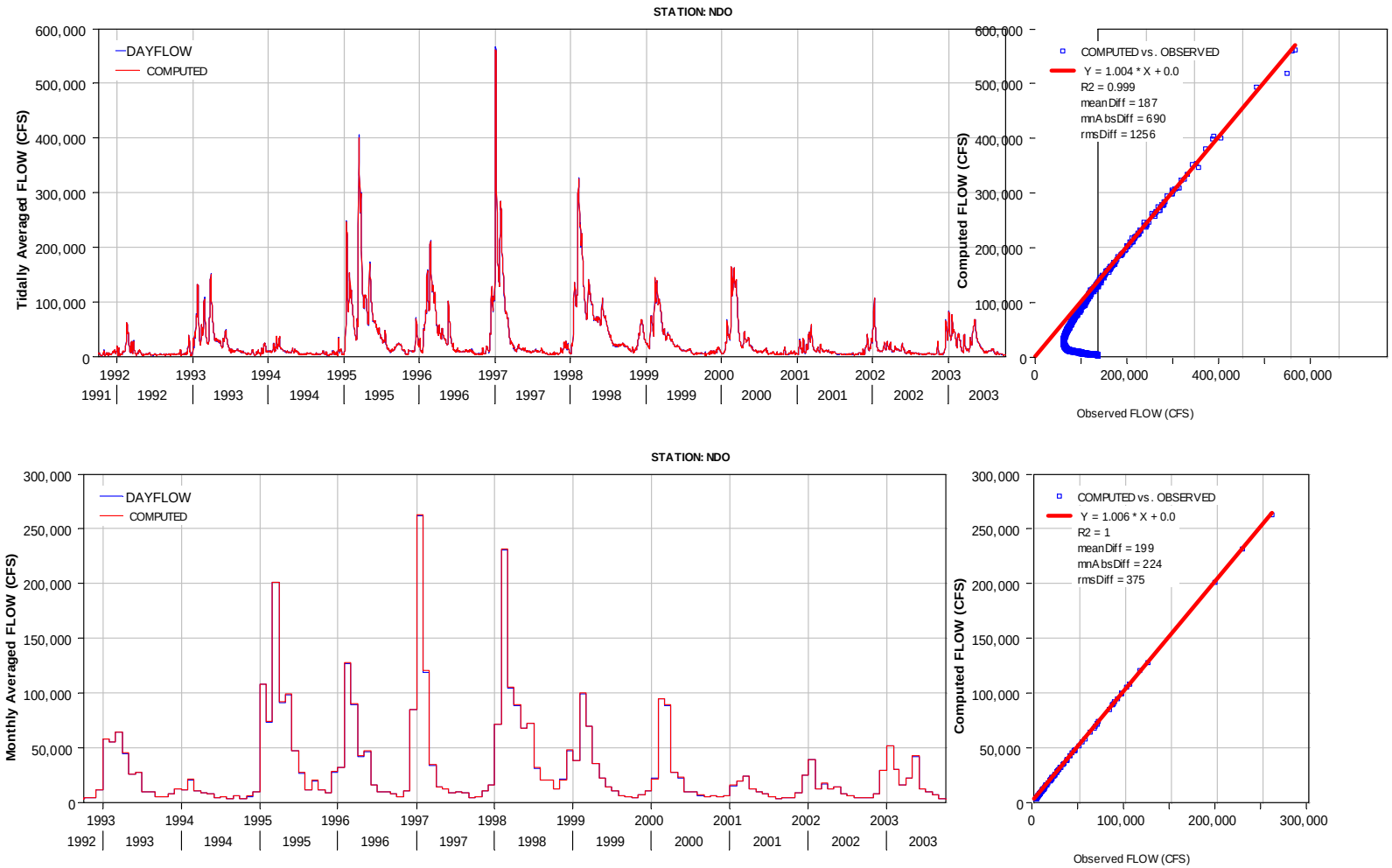

Figure E-3 Tidally Averaged and Monthly Averaged Net Delta Outflow – Calibration to Dayflow Boundary Conditions

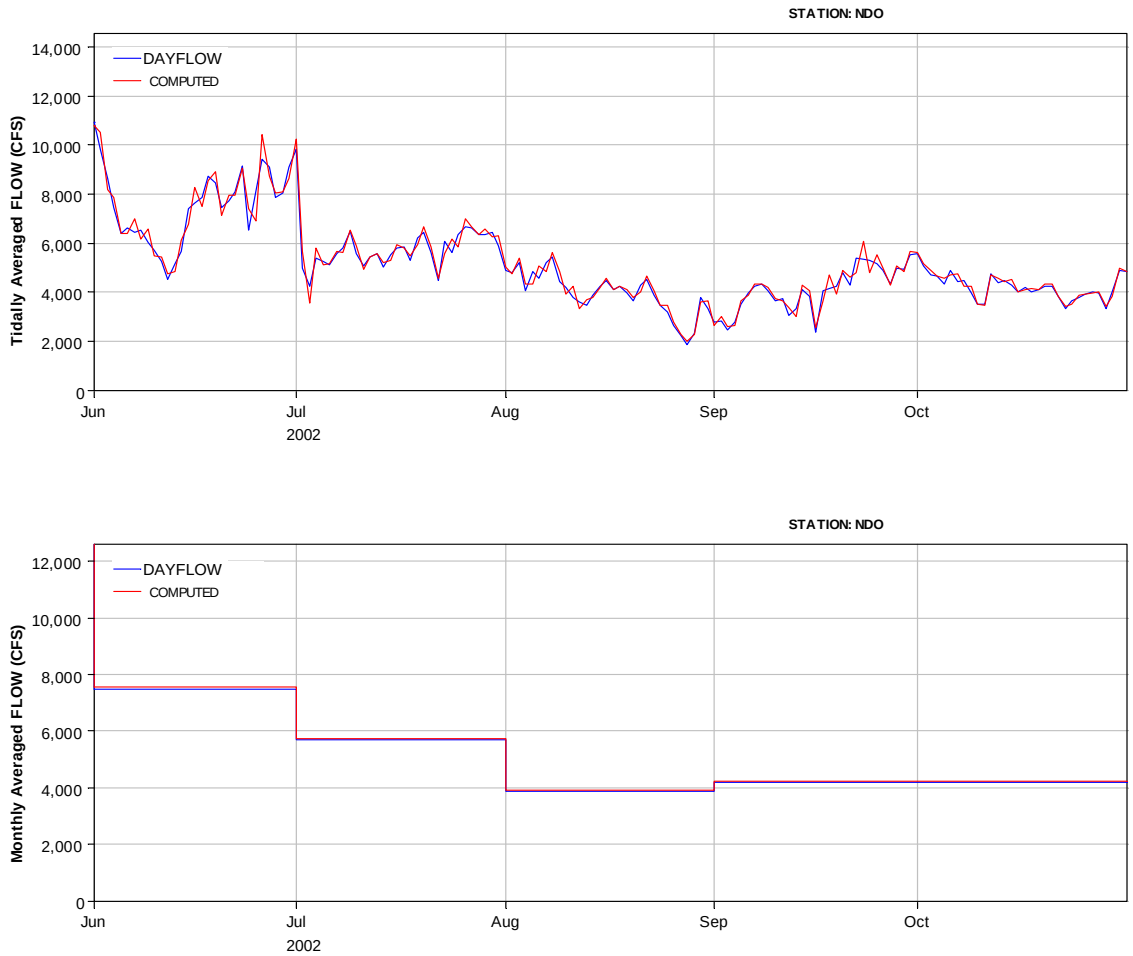

Figure E-3a Tidally Averaged and Monthly Averaged Net Delta Outflow, Summer 2002 – Calibration to Dayflow Boundary Conditions

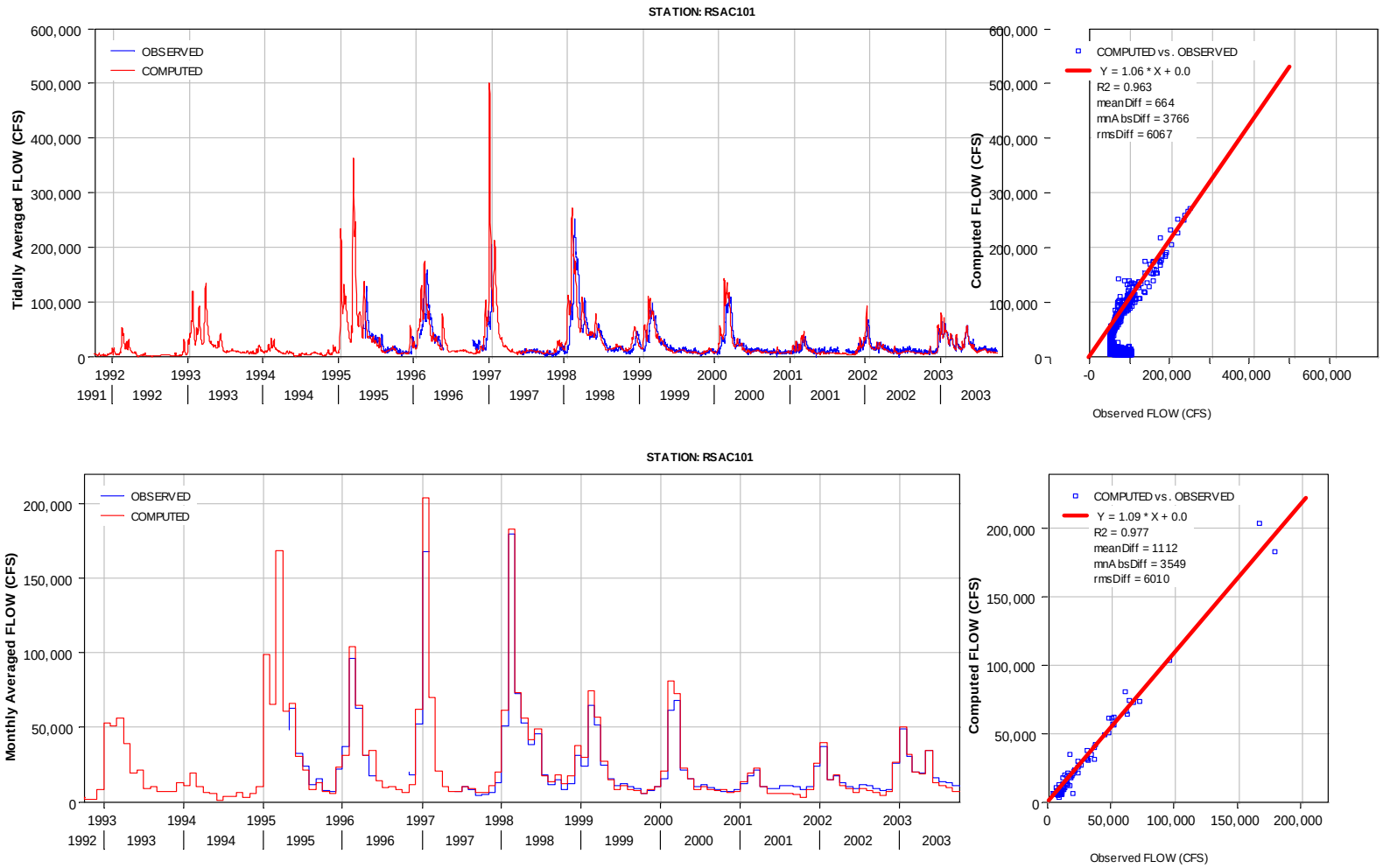

Figure E-4 Tidally Averaged and Monthly Averaged Flow at Station RSAC101 – Calibration to Dayflow Boundary Conditions

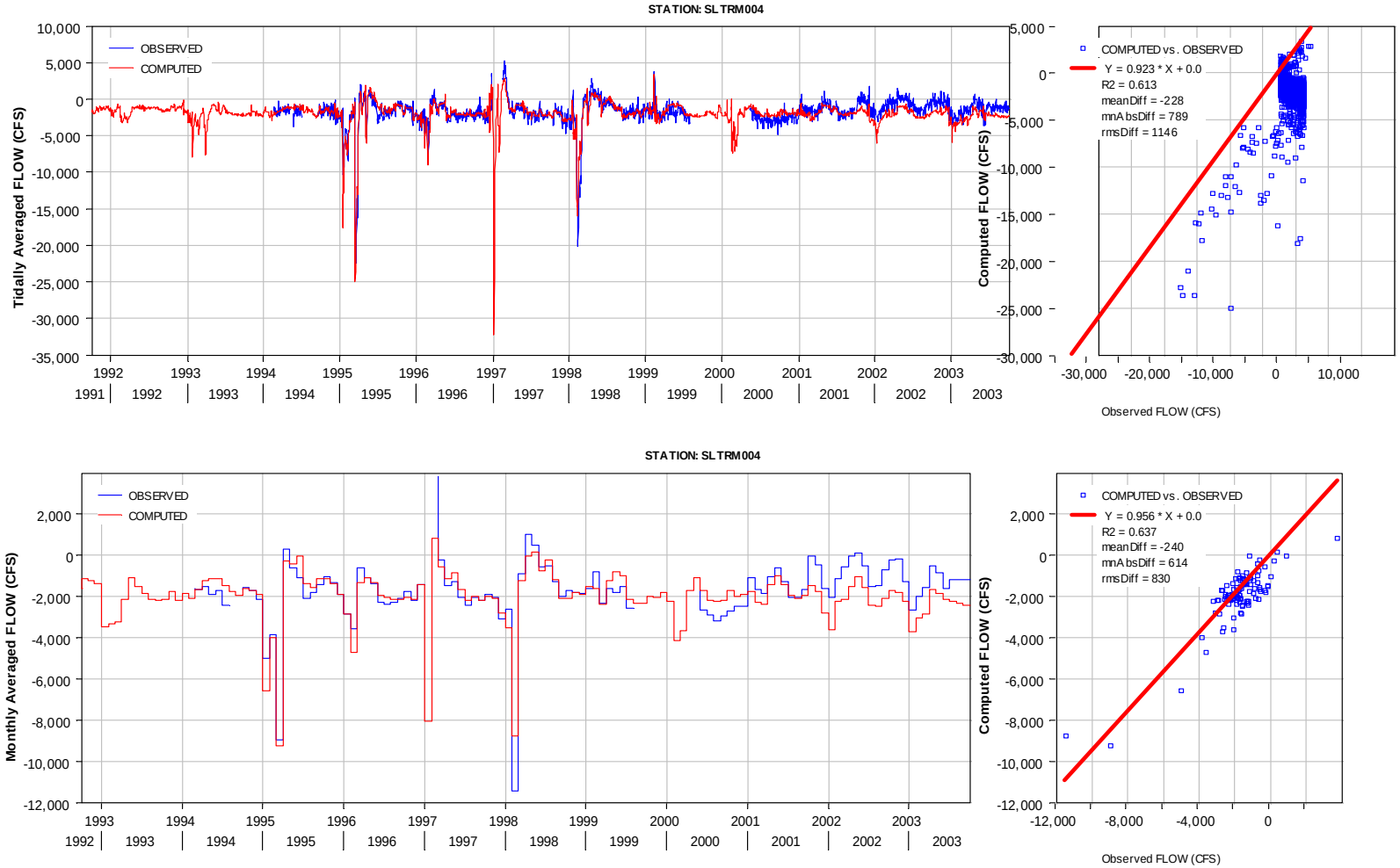

Figure E-5 Tidally Averaged and Monthly Averaged Flow at Station SLTRM004 – Calibration to Dayflow Boundary Conditions

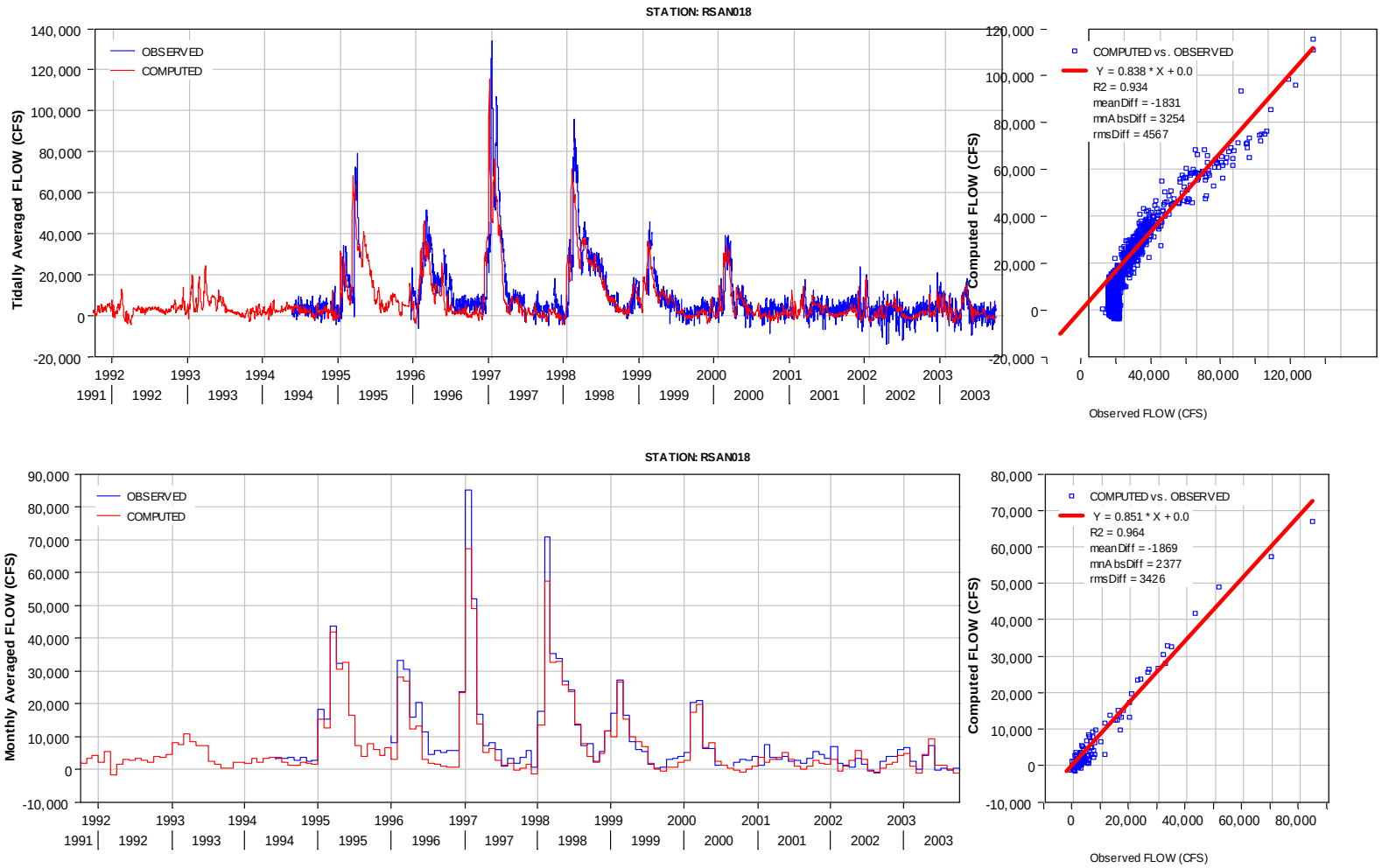

Figure E-6 Tidally Averaged and Monthly Averaged Flow at Station RSAN018 – Calibration to Dayflow Boundary Conditions

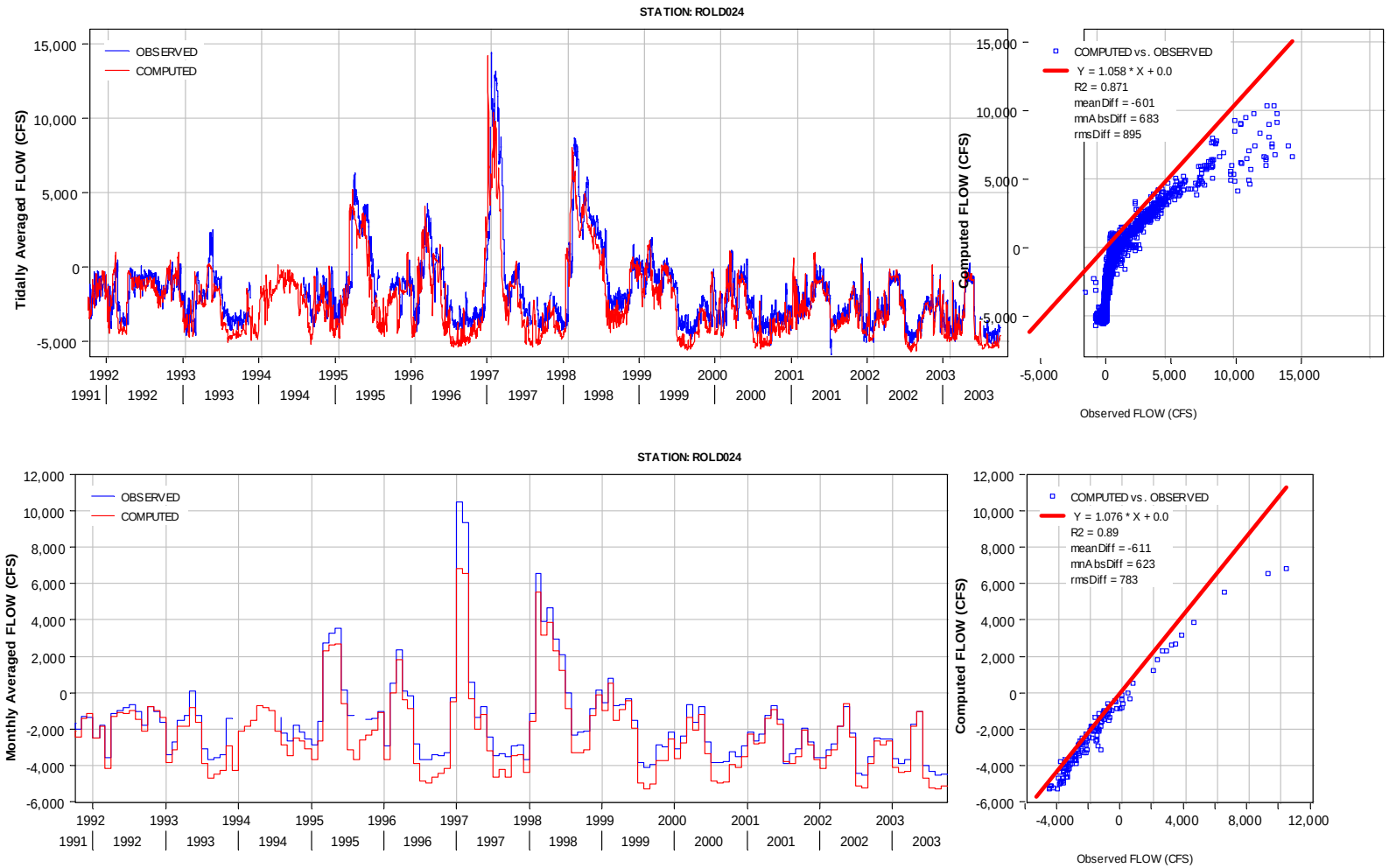

Figure E-7 Tidally Averaged and Monthly Averaged Flow at Station ROLD024 – Calibration to Dayflow Boundary Conditions

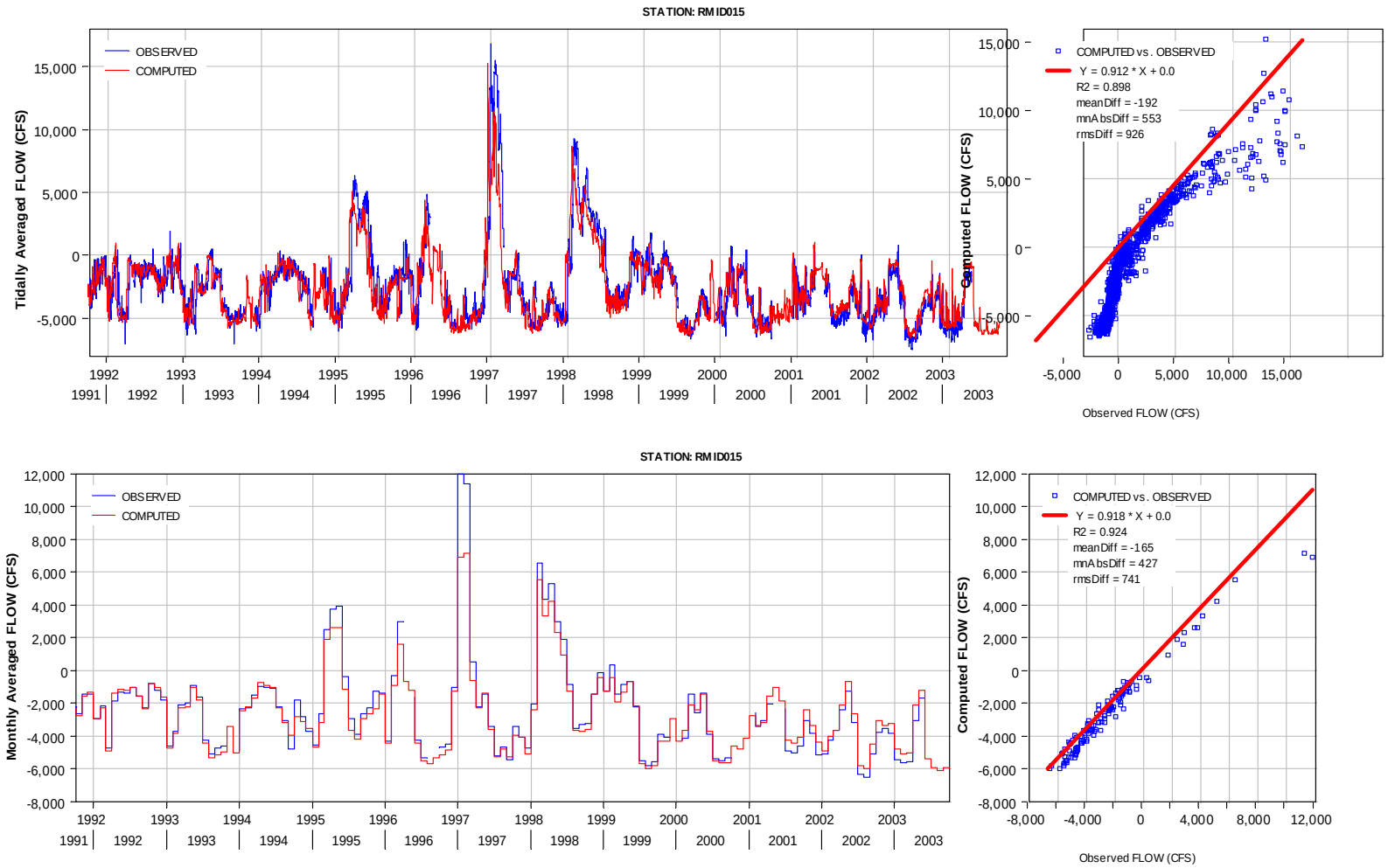

Figure E-8 Tidally Averaged and Monthly Averaged Flow at Station RMID015 – Calibration to Dayflow Boundary Conditions

river is not forced, rather it is a function of balance of flow resistance between the two channels. During periods of low NDO and high exports, the middle river station matches observed data closely but the old river station the computed results appears to have too much negative flow. This is due at least in part by the application of the southwest DICU group upstream of ROLD024. At both stations the WAM HD under predicts downstream flow during high runoff periods. This is most likely related to under predicting the flow from the San Joaquin through Old River at Head. Both the grouped DICU application and the flow balance between Old and Middle rivers should be revisited in future calibration efforts.

E.2.2 Salinity (EC) Comparisons

Comparisons of computed and observed EC are presented in figures E-10 to E-25. EC comparison locations are shown in Figure E-9. As with the flow comparisons, each EC comparison figure shows time series of tidally averaged and monthly averaged EC from October 1991 through September 2003. Scatter plots of computed verses observed are presented with each time series plot along and include the following error statistics.

- Linear regression with intercept forced to zero
- Coefficient of determination (r2)
- Mean difference - $\frac{1}{n}\sum_{i=1}^{n}\left(C_i - O_i\right)$
- Mean absolute difference - $\frac{1}{n}\sum_{i=1}^{n}\left|C_i - O_i\right|$
- RMS (root mean squared) difference - $\sqrt{\frac{1}{n}\sum_{i=1}^{n}\left(C_i - O_i\right)^2}$

where C_i and O_i are corresponding computed and observed values and n is the number of number of values in the observed time series.

EC at Martinez (RSAC054) is shown in Figure E-10. The match between computed and observed EC is very good with a linear slope of 0.966 and r2 of 0.944 for the daily values, particularly considering the simple one-dimension representation of the north San Francisco Bay and fixed EC boundary condition at the central Bay. The match at RSAC075 (Figure E-11) is also very good with a linear slope of 1.03 and r2 of 0.908, however, as shown in the monthly averaged time series, the model EC result tends to rise more quickly in the summer than observed data.

The observed data record at RSAC081 (Figure E-12) contains questionable data beginning in fall of 1998 and continuing through fall of 2001 where the EC during high flow periods does not drop much below 1500 μmhos/cm. Other stations upstream and downstream of RSAC081 have much lower EC during those periods. As a result the error statistics show a poorer match to observed data than should be the case.

EC for the Sacramento River at Emmaton (Rsac092) and Rio Vista (RSAC101) are shown in Figures E-13 and E-14. EC in the Sacramento River as it flows from the north Delta is typically on the order of 100-200 μmhos/cm. At Emmaton and Rio Vista the EC

increases during periods of low net flow when tidal mixing drives higher salt water up stream. At Rio Vista this happens infrequently. The computed reflects this behavior, however for the driest years the salinity increases too much during periods of highest consumptive use, which is again related to the grouped application of DICU. This is particularly true in 1992. Because Threemile Slough transfers some of the Sacramento flow upstream of Emmaton to the San Joaquin, EC at Emmaton has more frequent periods of salt intrusion. The model generally predicts the peak summer salinities, but as with the downstream stations, the salinity increases a little too quickly in the summer. In 1992 the peak summer salinity is overestimated as at Rio Vista.

EC for the San Joaquin River at stations RSAN007, RSAN008, and RSAN018 are shown in Figures E-15, E-16, and E-17, respectively. At Jersey Point (RSAN018) the model has peak summer salinity that is similar to observed; however, its simulated peak is too early and then the model results in the fall tend to be low. The early peak is primarily due to the net flow error described in section 2.1. The mean difference between computed and observed at this station is nearly zero (-2 μmhos/cm for daily average EC and 19 μmhos/cm for monthly averaged). Most of the year the model result is very close to the observed data and the resulting RMS difference is on the order of 300 μmhos/cm, or 15% of typical peak summer EC values.

Farther up stream on the San Joaquin At RSAN032 (Figure E-18) the daily average model result is on average 53 μmhos/cm too high and often has significantly higher salinity peaks. This is very likely related to the influence of the Mokelumne River flow, which enters the San Joaquin just upstream of RSAN032 and hugs the north bank where the sensor is placed. This behavior is shown in simulations using the RMA Bay-Delta model with represents this region in 2D.

Stations RSAN058, RSAN072, and RSAN087 (Figures E-19, E-20, E-21) are dominated by the San Joaquin River boundary EC at Vernalis. RSAN058, which is farthest downstream, is a sensitive indicator of the flow split between the San Joaquin and Old River at Head. If the model over predicts the flow from the San Joaquin into Old River at Head, then the net downstream flow at RSAN058 is too low mixing with Mokelumne River water will cause the EC to drop. Initial calibration simulations used the monthly averaged Vernalis EC from CALSIM as a boundary condition for the WAM HD. The quality of the calibration improved dramatically when the daily averaged observed EC at Vernalis was used instead. At all three stations the RMS difference is on the order of 100 μmhos/cm, or approximately 10% of peak summer EC values.

EC in Old River upstream of Franks Tract (ROLD014) is shown in Figure E-22. The fit at this station is similar to the fit at Jersey Point in that the model result tends to peak earlier than the observed data and then fall off in the fall, although the overall fit is good with a linear slope of 0.942, r2 of 0.788, and RMS difference of 108 μmhos/cm.

At RMID023 on Middle River (Figure E-23) the range of EC values is generally lower than other locations due (200-600 μmhos/cm) and is influence by mixing of Sacramento and Mokelumne water coming from the north with San Joaquin water coming through Turner Cut and occasionally Middle River from the south. While the r2 value comparing computed and observed is low at this location, the range of values predicted by the model

corresponds well with the observed data and the RMS difference is only 73 μmhos/cm for the daily averaged result.

EC at the SWP and CVP export locations (Figures E-24 and E-25) depends on the salinity of water drawn from the central Delta through Old and Middle Rivers as well as the salinity of the San Joaquin River. When pumping is high essentially all of the San Joaquin water is exported. The balance of salt that reaches the SWP and CVP pumps is dependent of the flow from the San Joaquin through Old River at Head verses Turner cut. The more San Joaquin water goes up to Turner Cut the more impacted the SWP is by San Joaquin salinity. Model prediction of EC at the export locations has RMS differences on the order of 100 μmhos/cm, or less than 15% of typical summer EC values.

E3. Comparison to RMA Bay-Delta Model 50 Breach Simulation

As part of the CALFED Bay Delta Program sponsored Preliminary Seismic Risk Analysis Associated with Levee Failures Sacramento-San Joaquin Delta the RMA Bay-Delta Model was used to simulate a 20 Island failure event with 50 individual levee breaches. Documentation for this simulation is provided in Appendix A of the Preliminary Seismic Risk Assessment documents, which can be found at http://calwater.ca.gov/Programs/LeveeSystemIntegrity/LeveeDeltaSeismic.shtml. The WAM HD was configured to replicate the 50 breach simulation.

For the Preliminary Seismic Risk Assessment, the RMA Bay-Delta model base geometry was modified to add 20 Delta islands with 50 explicit breach locations. Island topography was based on the best available data at the time and breach locations where determined base on the opinion of Delta levee engineers participating in the study. Islands and breaches were modeled using two dimensional flow elements. Most islands had one breach location, several islands had more than one breach, and Sherman Island, which was known to have extremely fragile levees, had 20 individual breaches. The breach event was simulated starting on July 1 2002. At the time of the breach exports were stopped. Because the RMA Bay-Delta Model did not interact with an operations decision making component, exports remained off for the duration of the simulation.

A WAM HD simulation was constructed to mimic the RMA Bay-Delta Model 50 breach simulation as closely as possible. The operations in the WAM were set to stop exports and not restart them. The island volumes provided by URS GIS team, which where based on an independent analysis using some updated topographic information, were adjusted to match the volumes estimated for the earlier RMA model geometry. Not all breach locations in the WAM HD configuration match exactly the breach locations in the RMA model although in most cases the locations are similar. One important exception is Bacon Island which is discussed below.

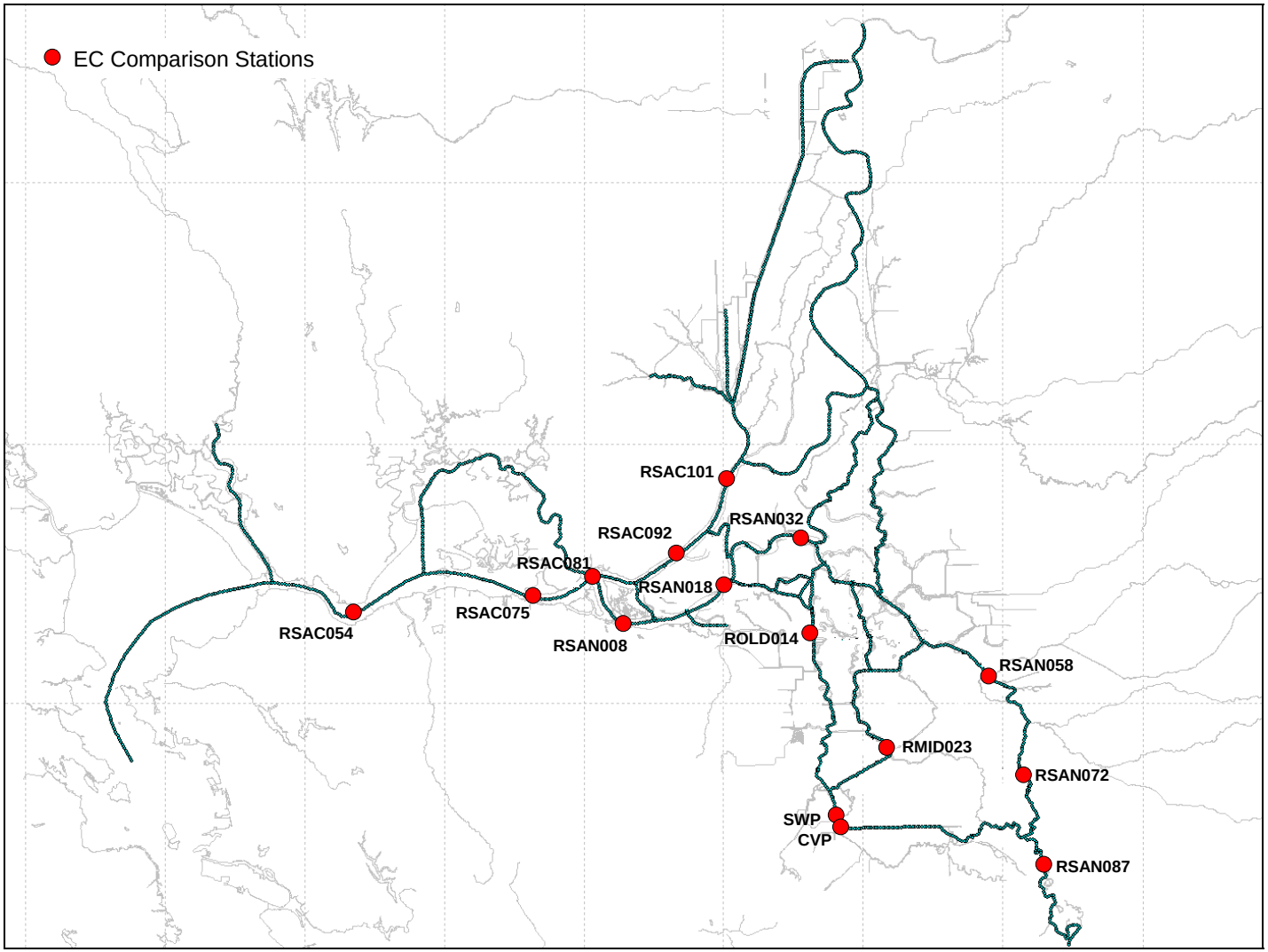

Figure E-9 EC Comparison Stations for 1991-2003 Calibration Period

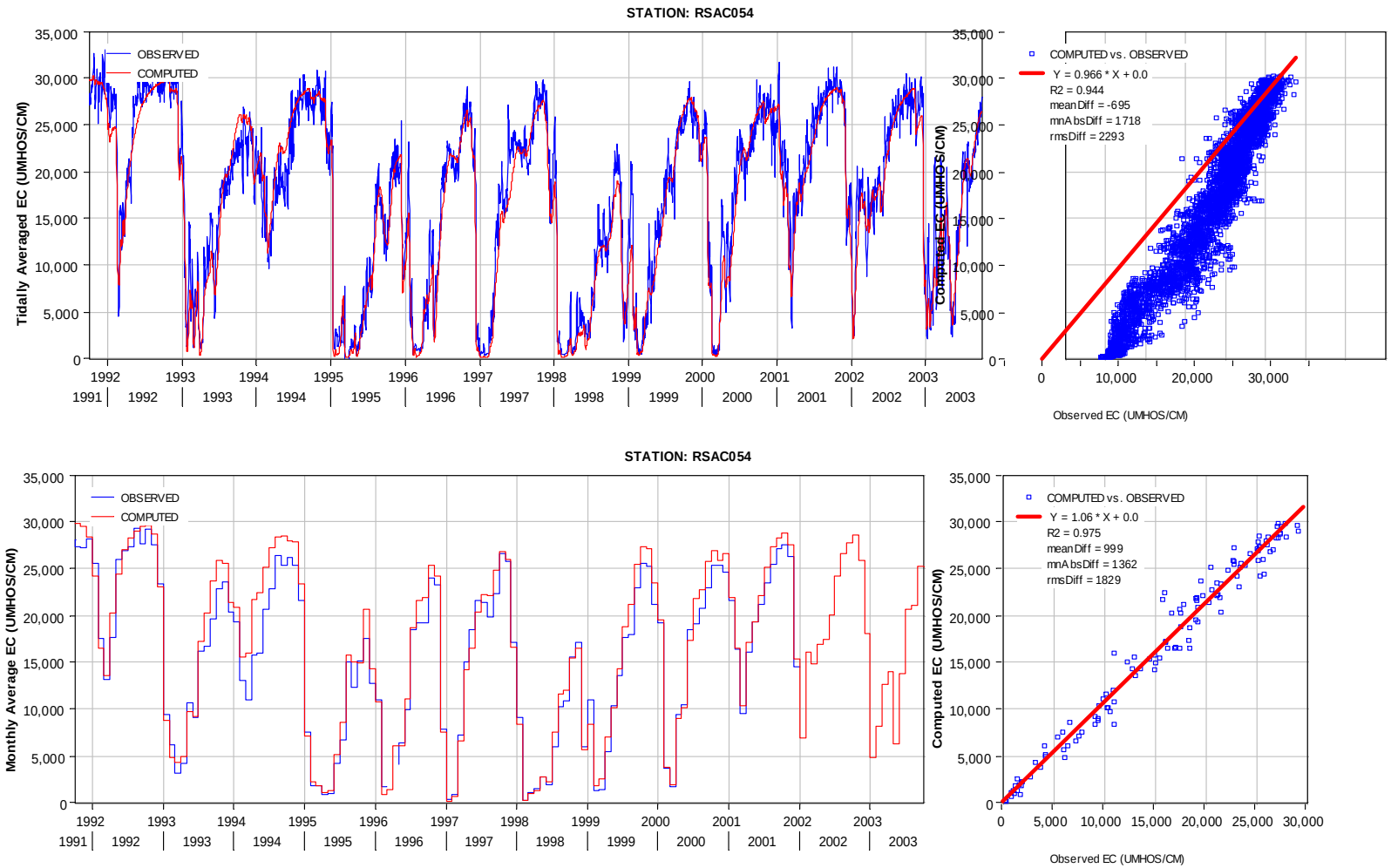

Figure E-10 Tidally Averaged and Monthly Averaged EC at Station RSAC054 – Calibration to Dayflow Boundary Conditions

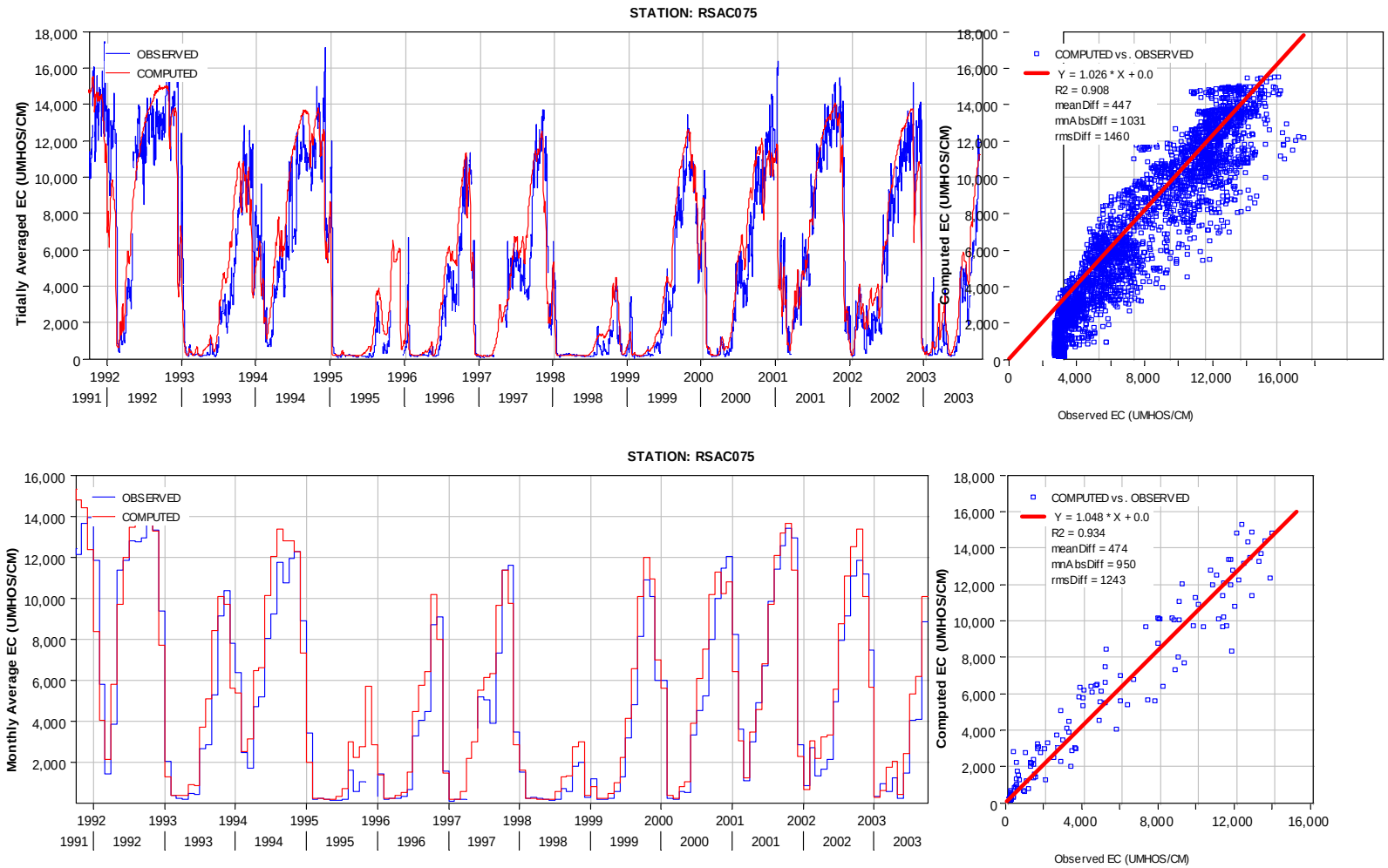

Figure E-11 Tidally Averaged and Monthly Averaged EC at Station RSAC075 – Calibration to Dayflow Boundary Conditions

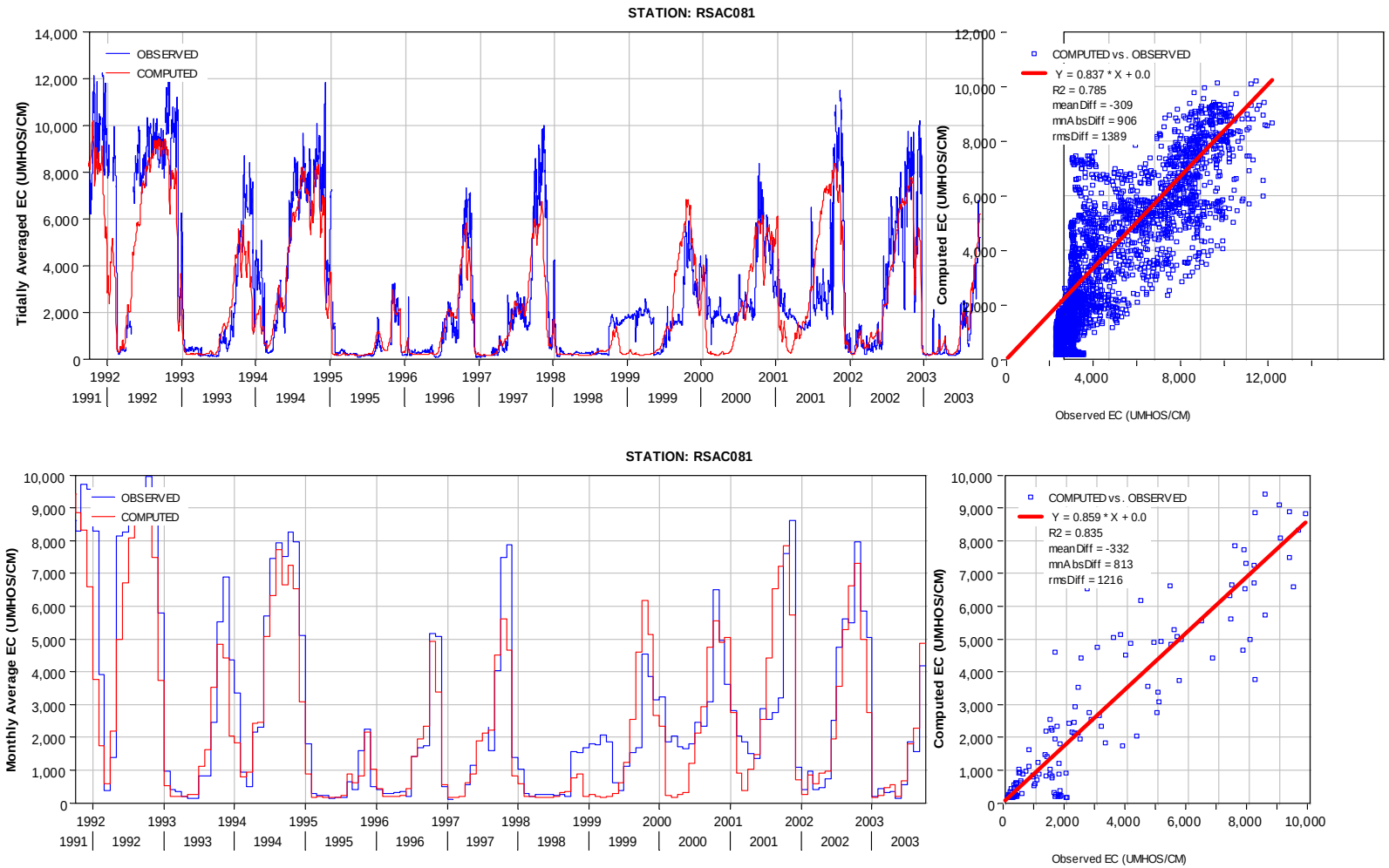

Figure E-12 Tidally Averaged and Monthly Averaged EC at Station RSAC081 – Calibration to Dayflow Boundary Conditions

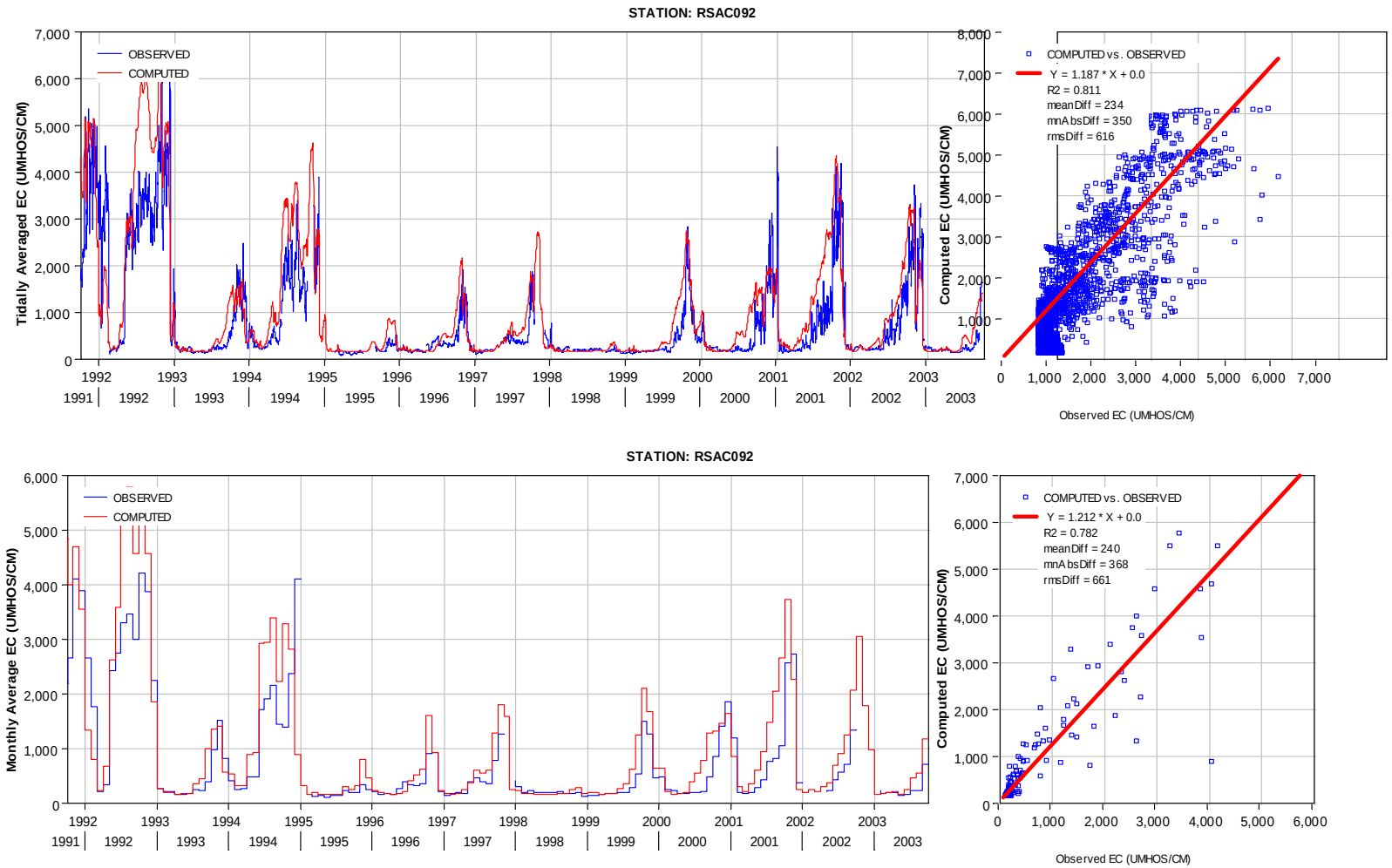

Figure E-13 Tidally Averaged and Monthly Averaged EC at Station RSAC092 – Calibration to Dayflow Boundary Conditions

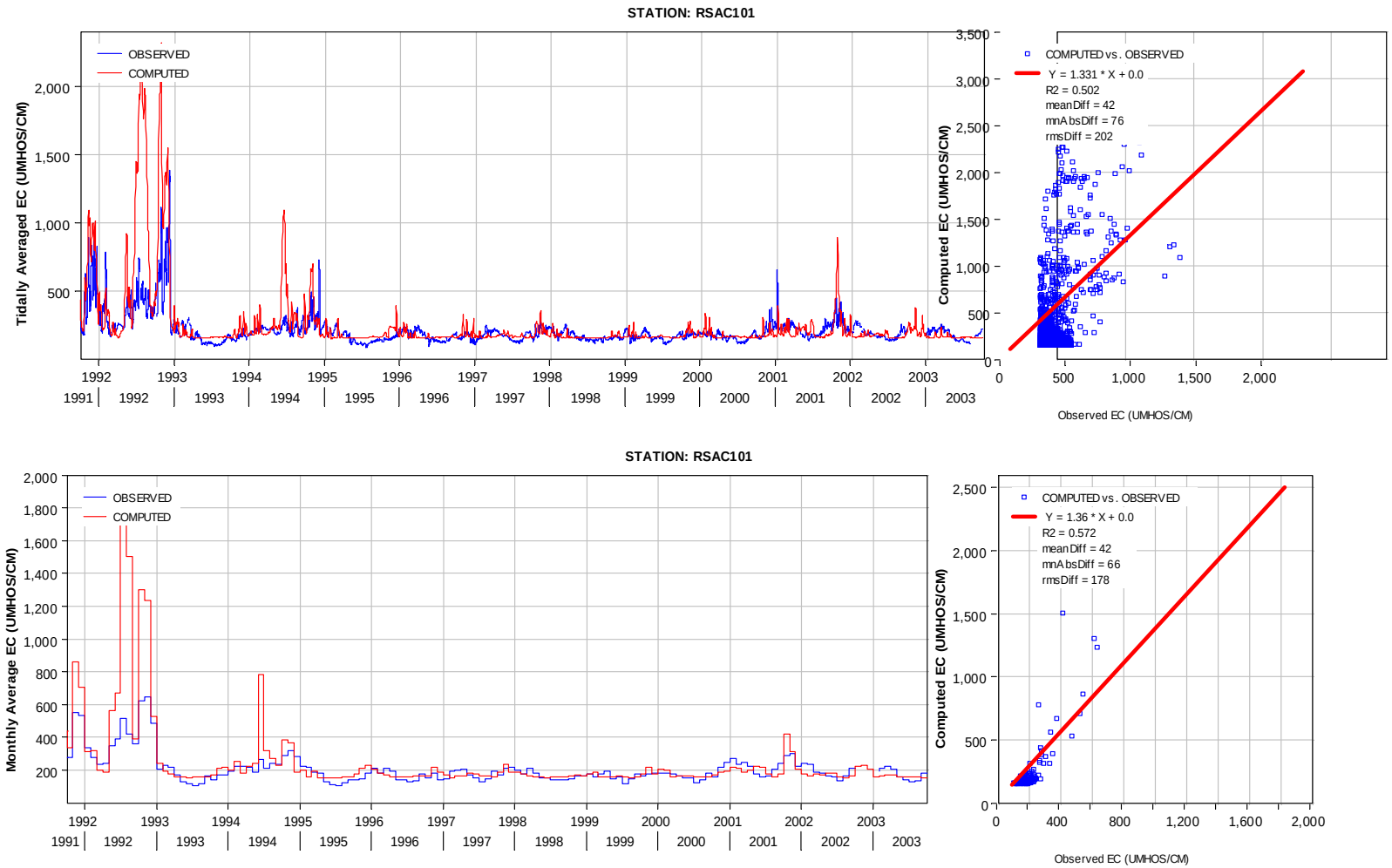

Figure E-14 Tidally Averaged and Monthly Averaged EC at Station RSAC101 – Calibration to Dayflow Boundary Conditions

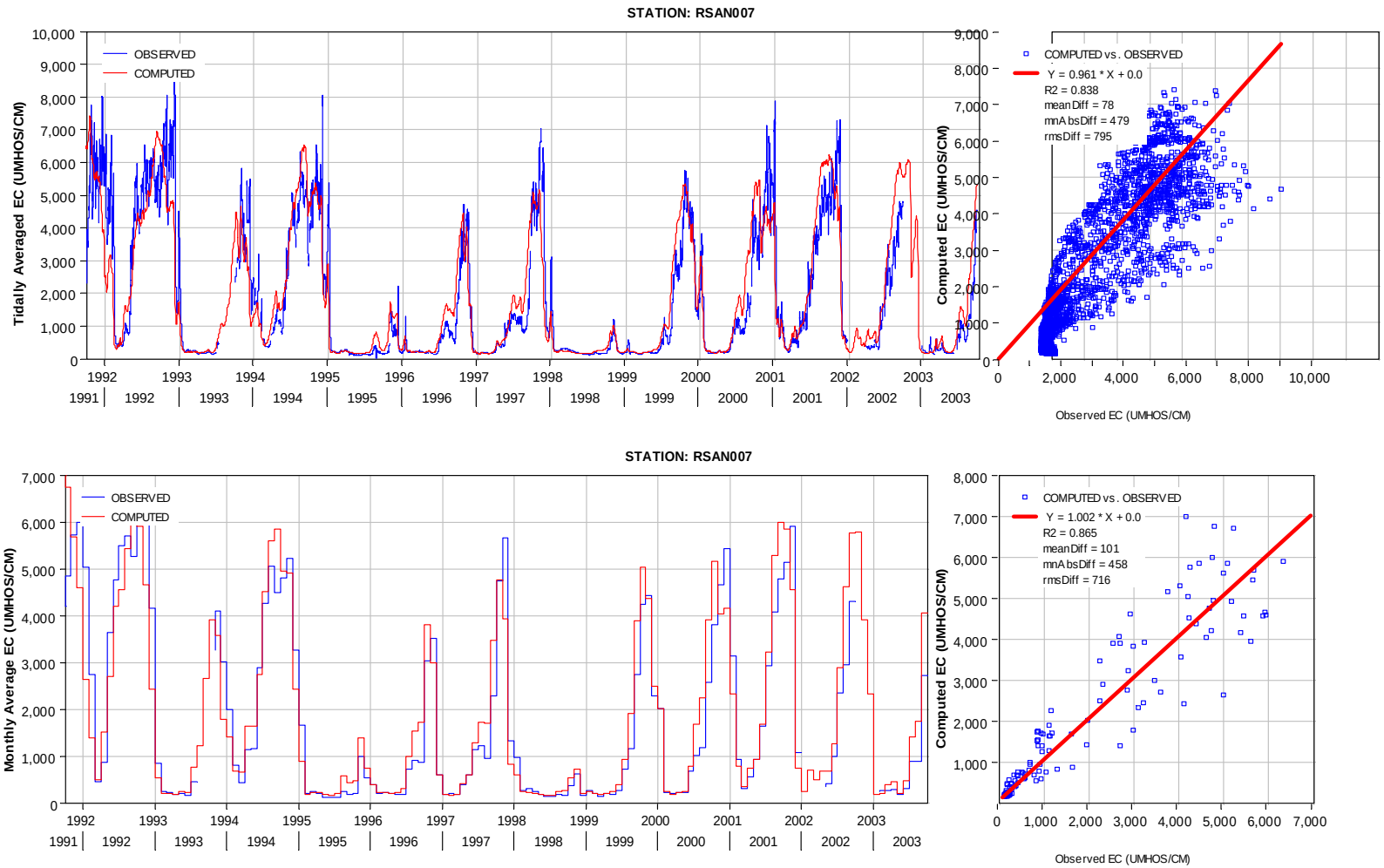

Figure E-15 Tidally Averaged and Monthly Averaged EC at Station RSAN007 – Calibration to Dayflow Boundary Conditions

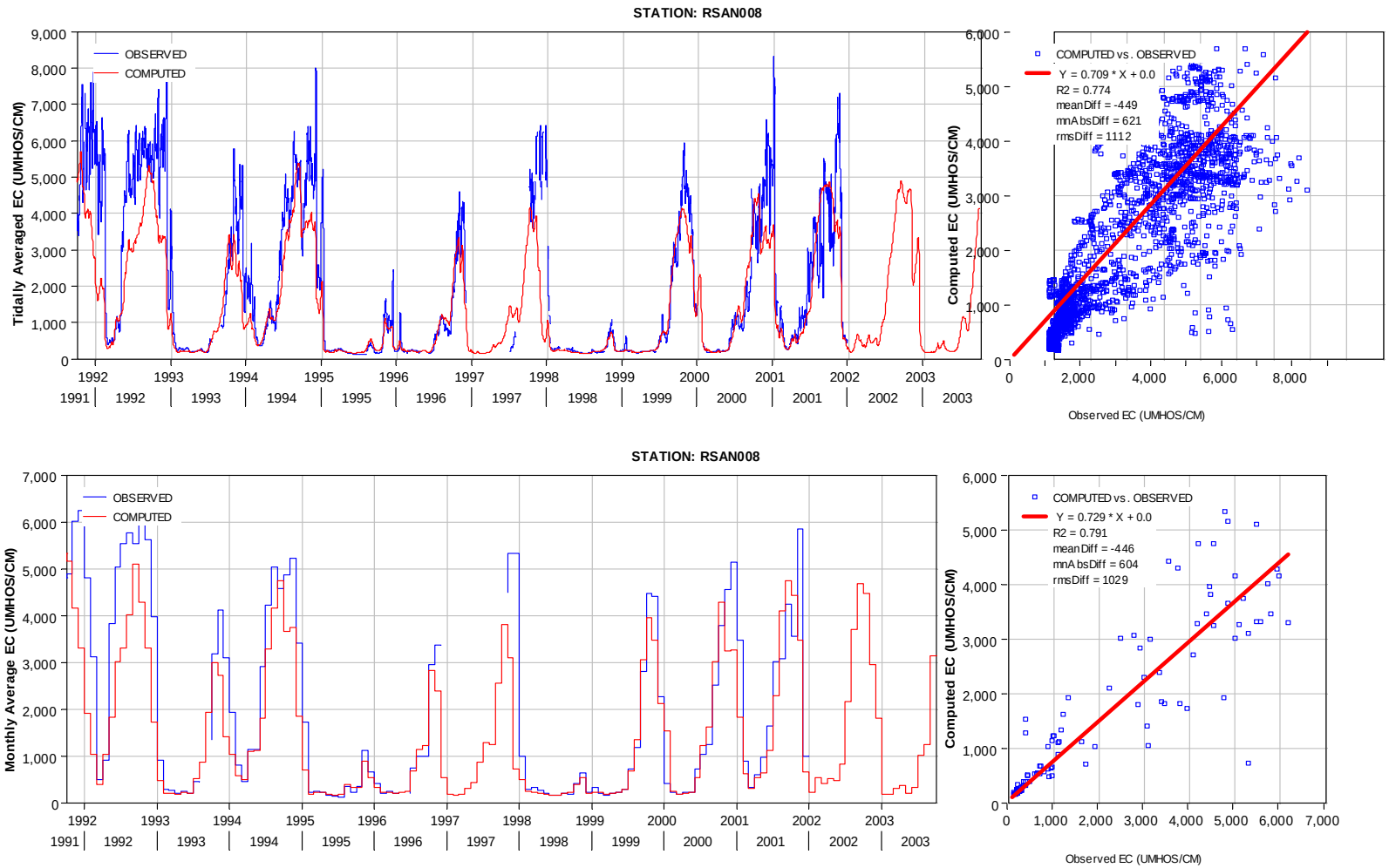

Figure E-16 Tidally Averaged and Monthly Averaged EC at Station RSAN008 – Calibration to Dayflow Boundary Conditions

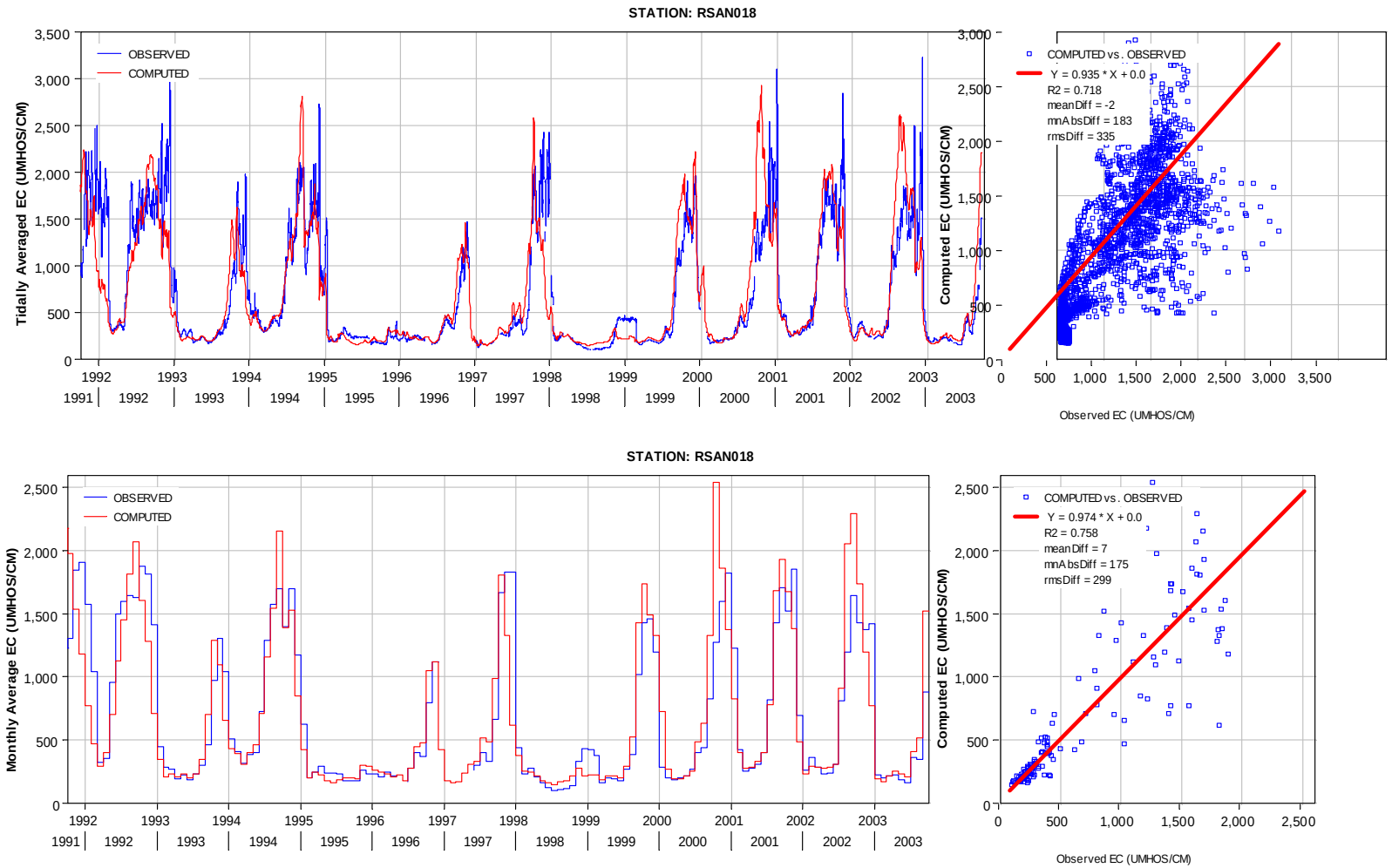

Figure E-17 Tidally Averaged and Monthly Averaged EC at Station RSAN018 – Calibration to Dayflow Boundary Conditions

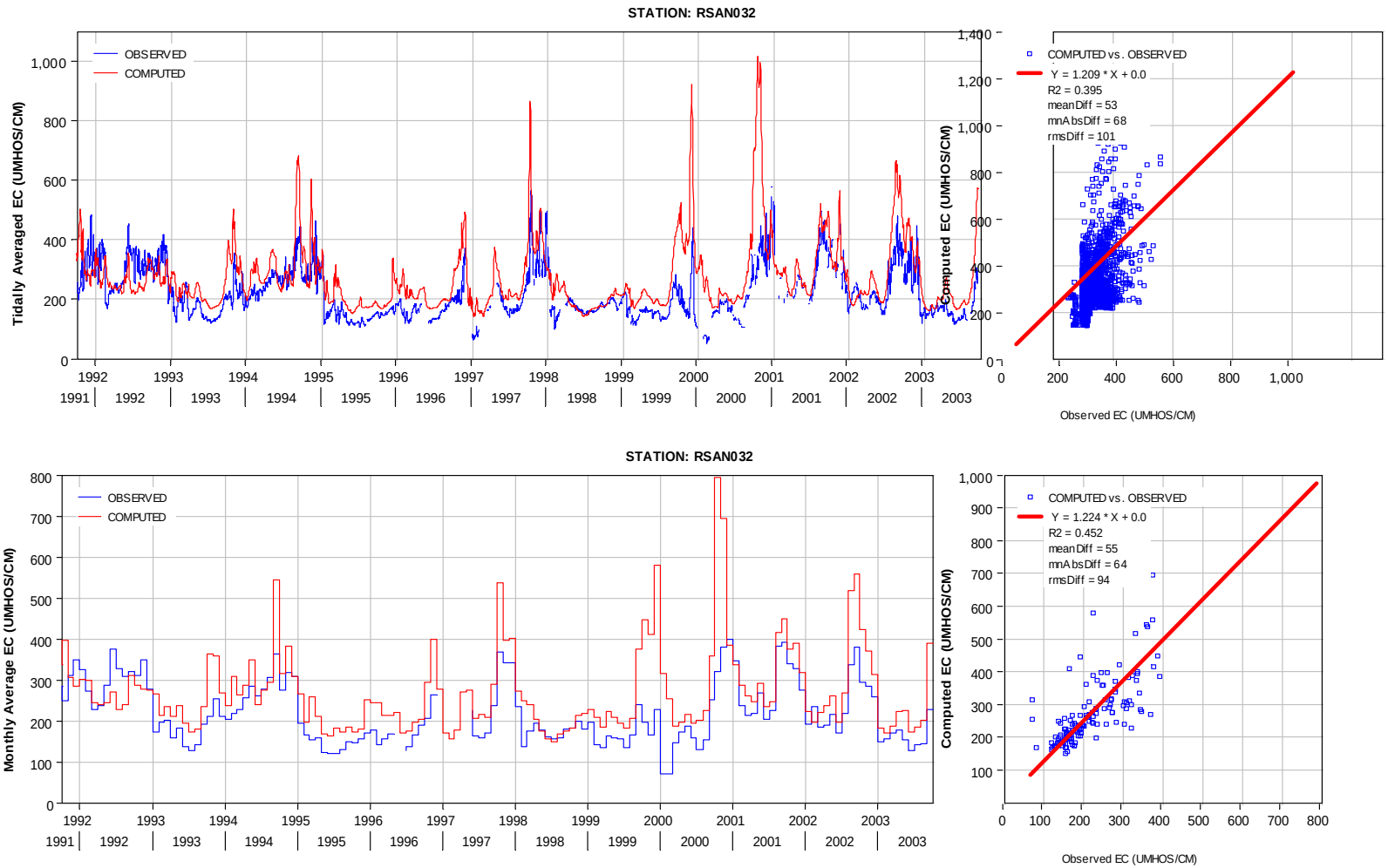

Figure E-18 Tidally Averaged and Monthly Averaged EC at Station RSAN032 – Calibration to Dayflow Boundary Conditions

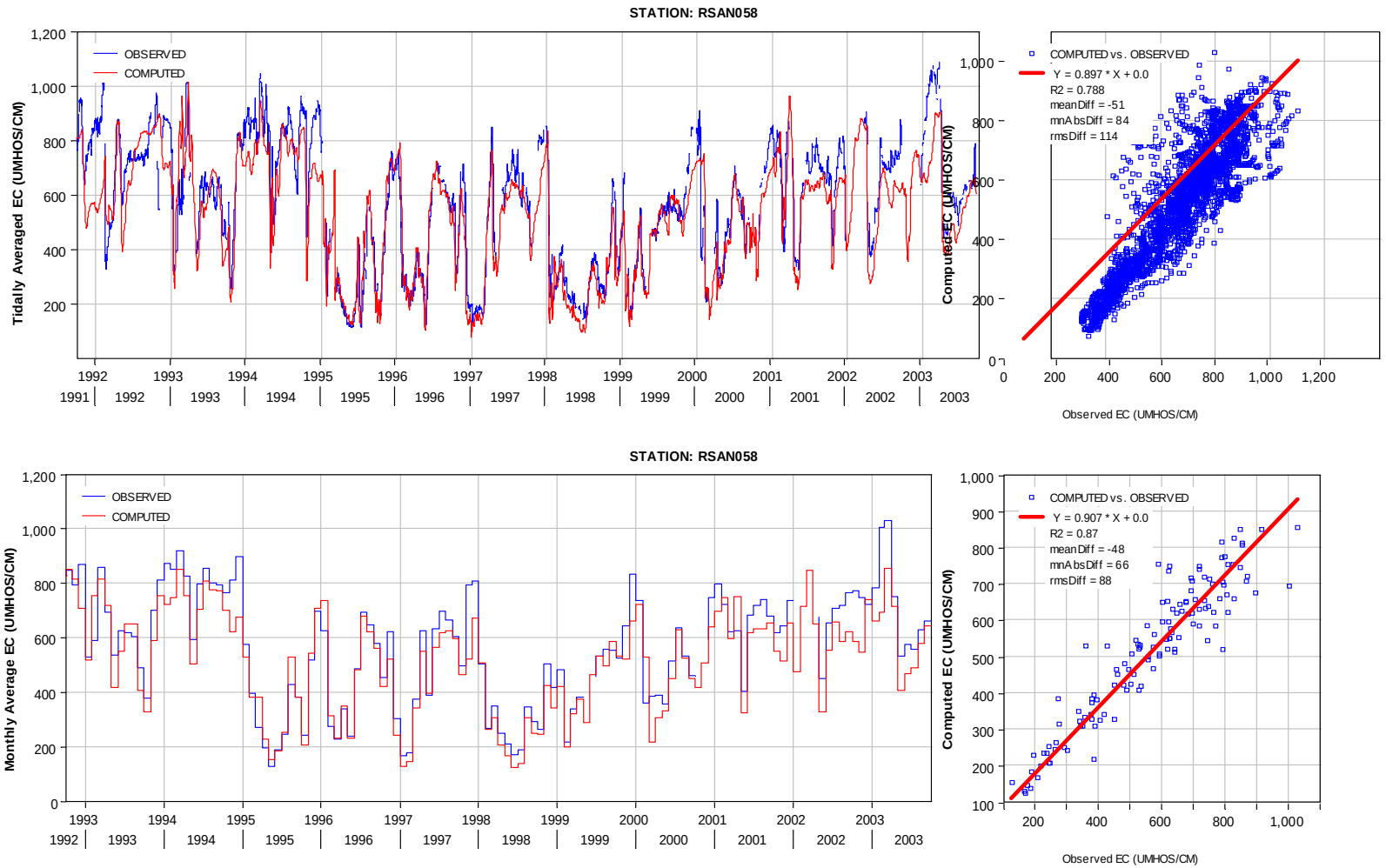

Figure E-19 Tidally Averaged and Monthly Averaged EC at Station RSAN058 – Calibration to Dayflow Boundary Conditions

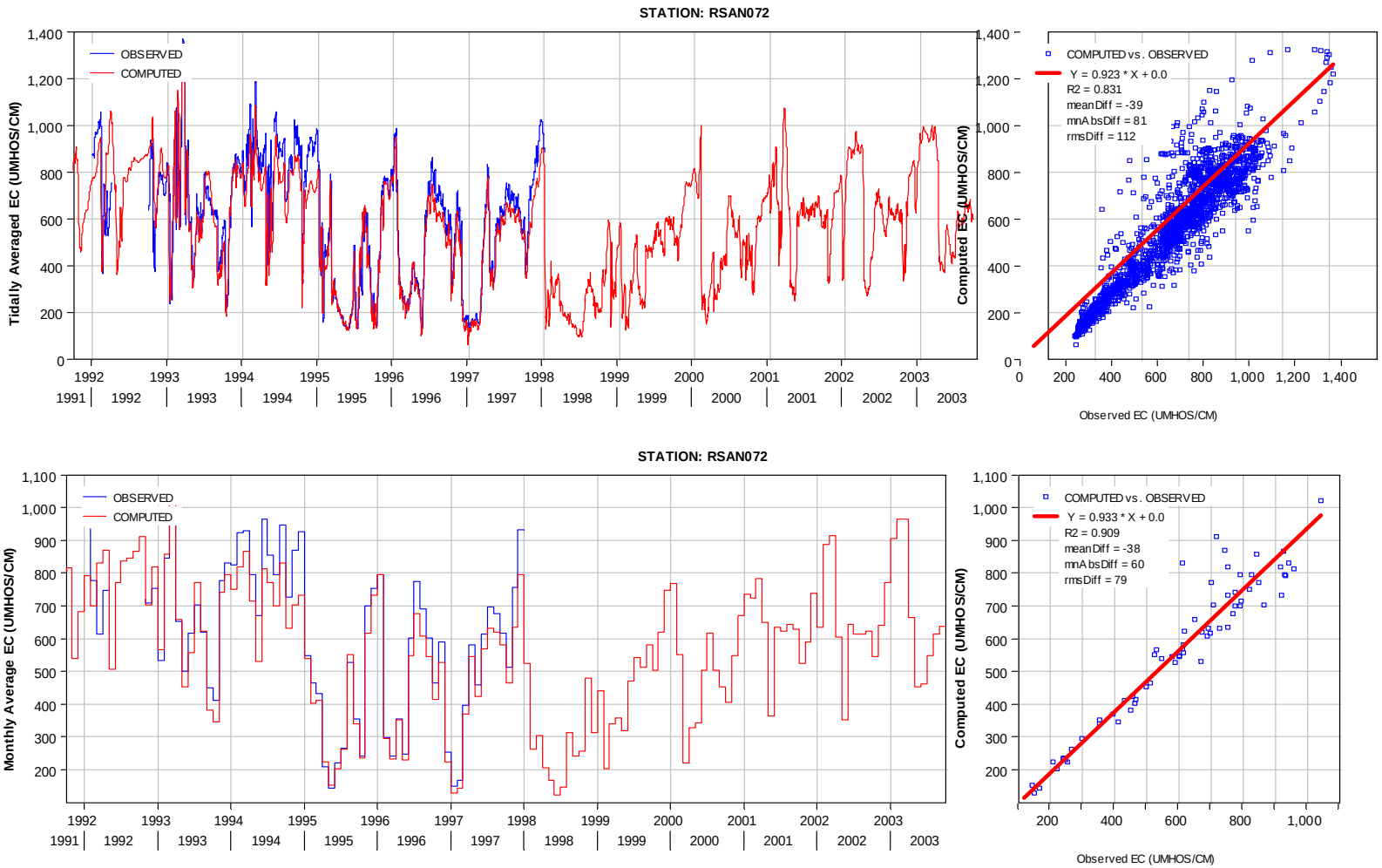

Figure E-20 Tidally Averaged and Monthly Averaged EC at Station RSAN072 – Calibration to Dayflow Boundary Conditions

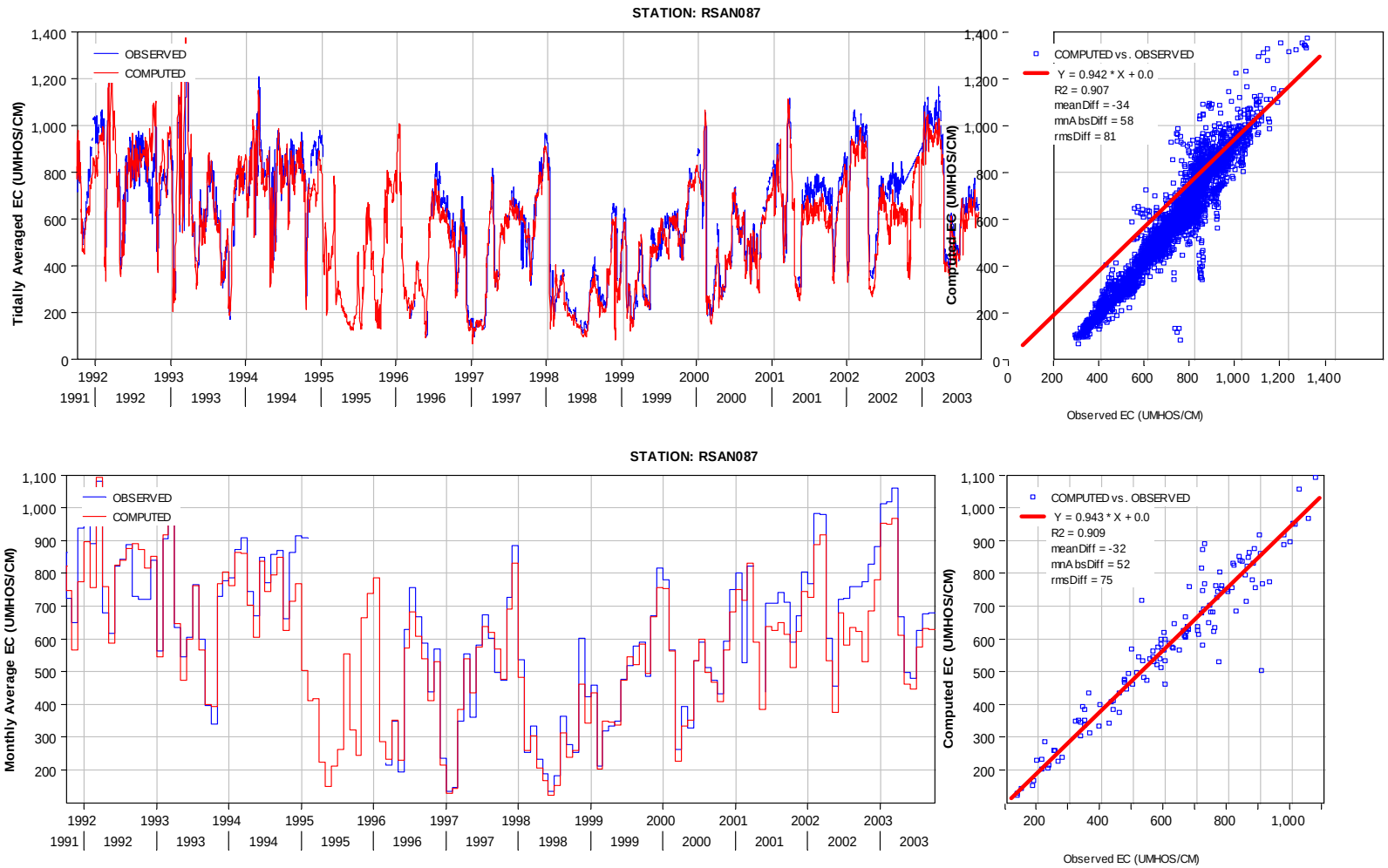

Figure E-21 Tidally Averaged and Monthly Averaged EC at Station RSAN087 – Calibration to Dayflow Boundary Conditions

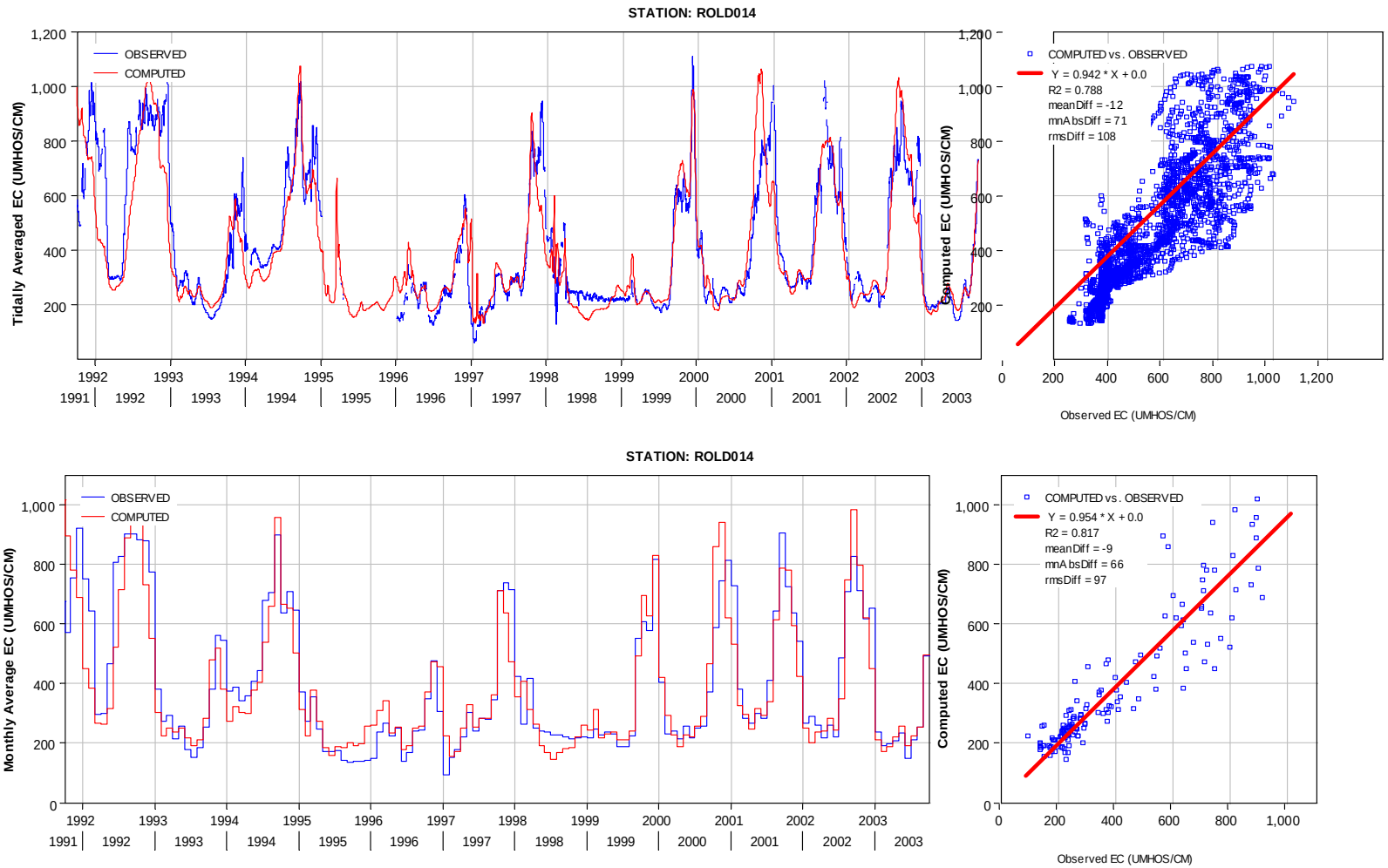

Figure E-22 Tidally Averaged and Monthly Averaged EC at Station ROLD014 – Calibration to Dayflow Boundary Conditions

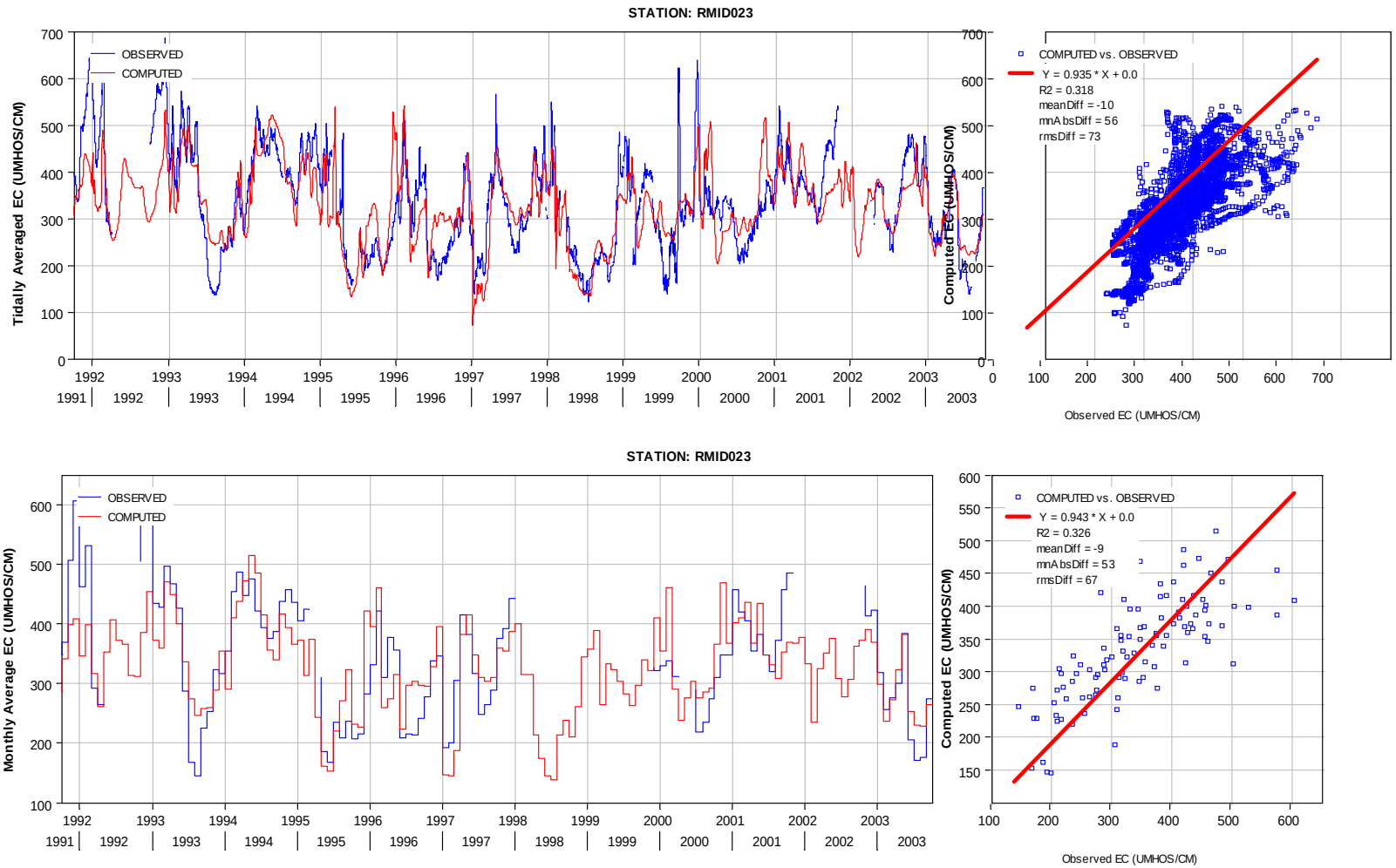

Figure E-23 Tidally Averaged and Monthly Averaged EC at Station RMID023 – Calibration to Dayflow Boundary Conditions

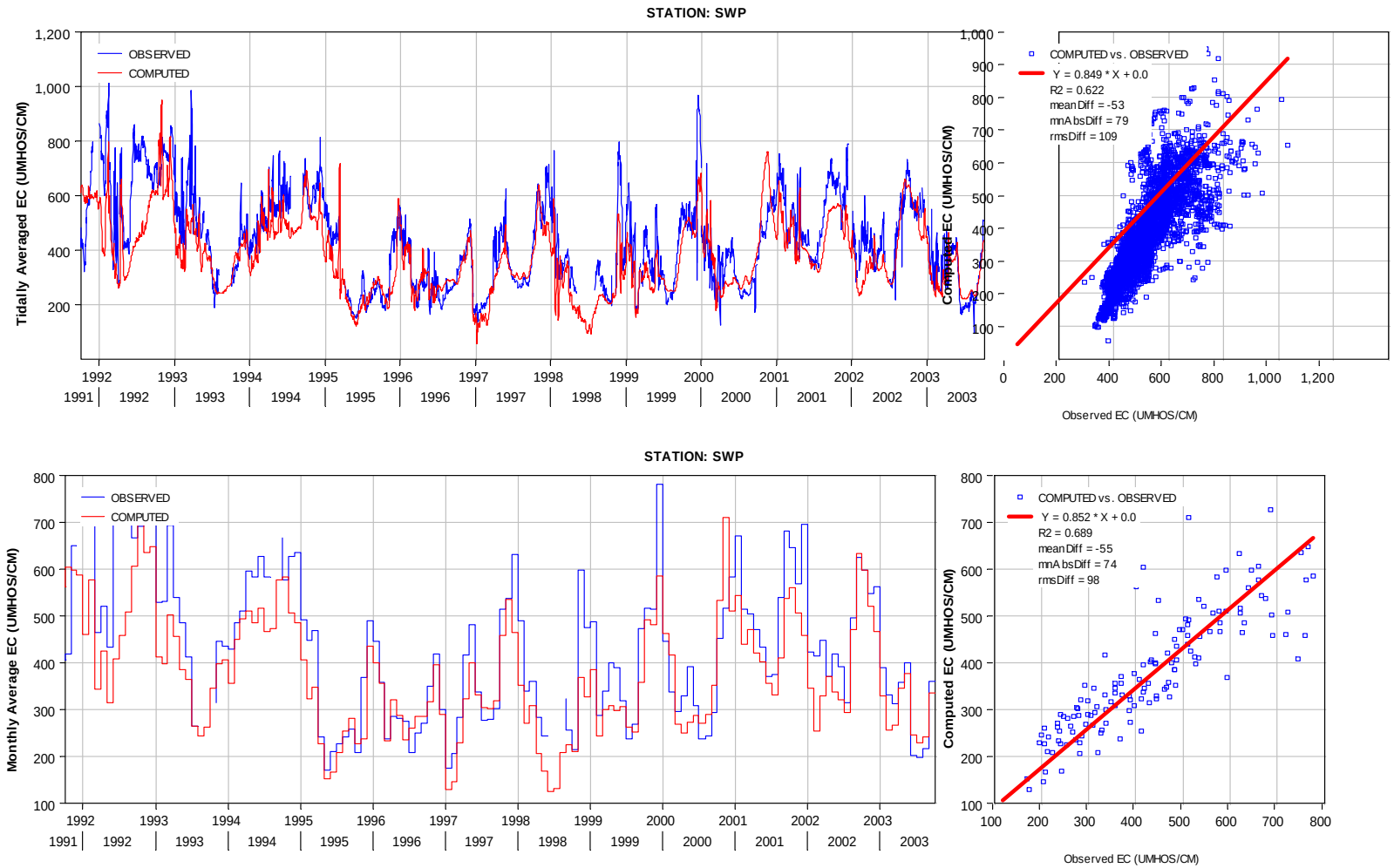

Figure E-24 Tidally Averaged and Monthly Averaged EC at Station SWP Export – Calibration to Dayflow Boundary Conditions

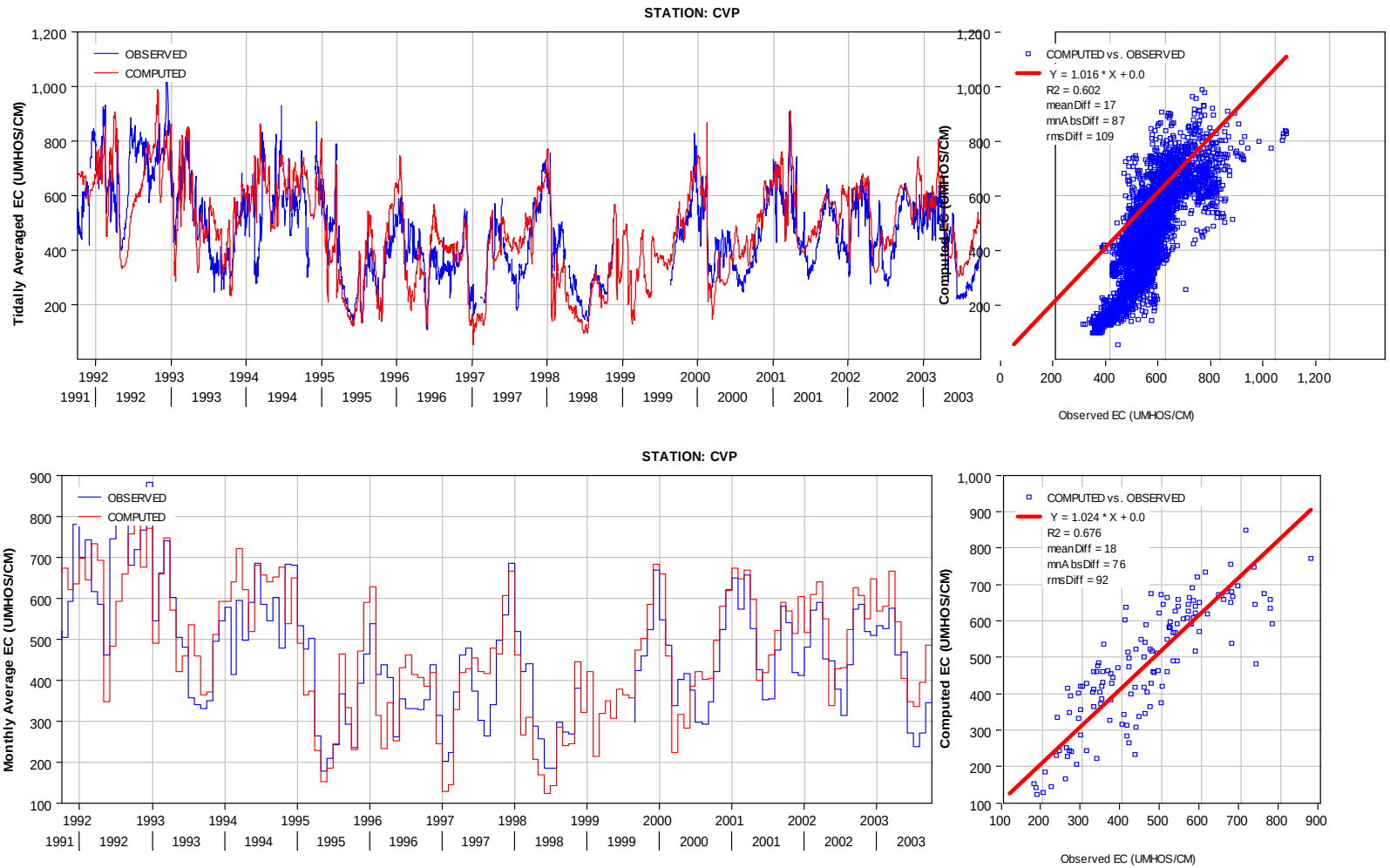

Figure E-25 Tidally Averaged and Monthly Averaged EC at Station CVP Export – Calibration to Dayflow Boundary Conditions

Comparison between the RMA Bay-Delta Model simulation result and WAM HD result was only used to tune the dispersion parameters representing net exchange between channels and flooded islands. As noted in section 2, because the WAM HD does not simulate tidal flows, the exchange between islands and channels that would result from filling and draining of islands with each tide must be parameterized.

Figure E-26 shows a spatial comparison of the EC contours for the two models at the time of peak salinity intrusion following the breach event. The representation of advective transport in the WAM HD provides a good approximation of the full Bay-Delta model as illustrated by the distribution of EC in the flooded islands.

Figure E-27 shows the spatial EC contours one month after the event. Recovery EC in the Delta occurs a little slower in the WAM HD result than in the full Bay-Delta Model. However the distribution of EC in both models is again very similar. Suisun Bay has nearly recovered to typical summer values, Sherman Island has been significantly freshened and relatively high salt water remains in many of the south Delta Islands.

EC time series at Antioch (RSAN008), Franks Tract, and ROLD034 are shown in Figure E-28. Given the very large range in EC values, a log scale is used so that the low salinity values can be more easily compared. Each plot contains simulation results from the WAM HD and RMA Bay-Delta Model for the breach case as well the RMA Bay-Delta model result for a base case simulation with out breaches. The base case simulation included normal export operations whereas in the breach case simulations exports stopped at the time of the event while reservoir releases where maintained at the base level. By turning off exports and maintaining reservoir releases the breach case EC at Antioch rapidly recover and become lower than the base condition.

At all three stations peak salinity following the flooding matches between the two models very closely. This indicates that channel and island volumes and the advective transport associated with island flooding are very similar in both models. After initial flooding, at Antioch and Franks Tract the WAM HD initially recovers more slowly than the RMA Bay-Delta Model. But before the salinity in the system has returned to normal Delta levels, the two models are in good agreement. In particular the time at which Frank Tract EC crosses the 1000 μmhos/cm level is similar. This is important because the central Delta EC of 1000 μmhos/cm is an important trigger point for WAM operations.

At ROLD034 the WAM HD shows rapid decline in salinity and then levels off and stays above the RMA Bay-Delta Model result until fall of 2003. The issue with the decline in EC immediately after reaching the peak EC appears to be related to flow through Bacon Island. Figure E-29 shows the breach configuration at Bacon for the two models. The Bay-Delta model has both breaches near each other on Old River, and flow though Bacon Island is in a limited region along the west side of the island. In the breach simulation this region is at a relatively high salinity so that water passing out of Old River, through Bacon, and back to Old River remains at a high salinity. In the WAM HD the two breaches are at the north and south ends of the island. As Bacon fills it draws freshwater into the southern part of the island. Because bacon has two breaches it fills faster than some of the other neighboring islands to the south. Once Bacon is partly full, water then flows through Bacon as the Victoria and other Islands continue to fill. In the WAM HD

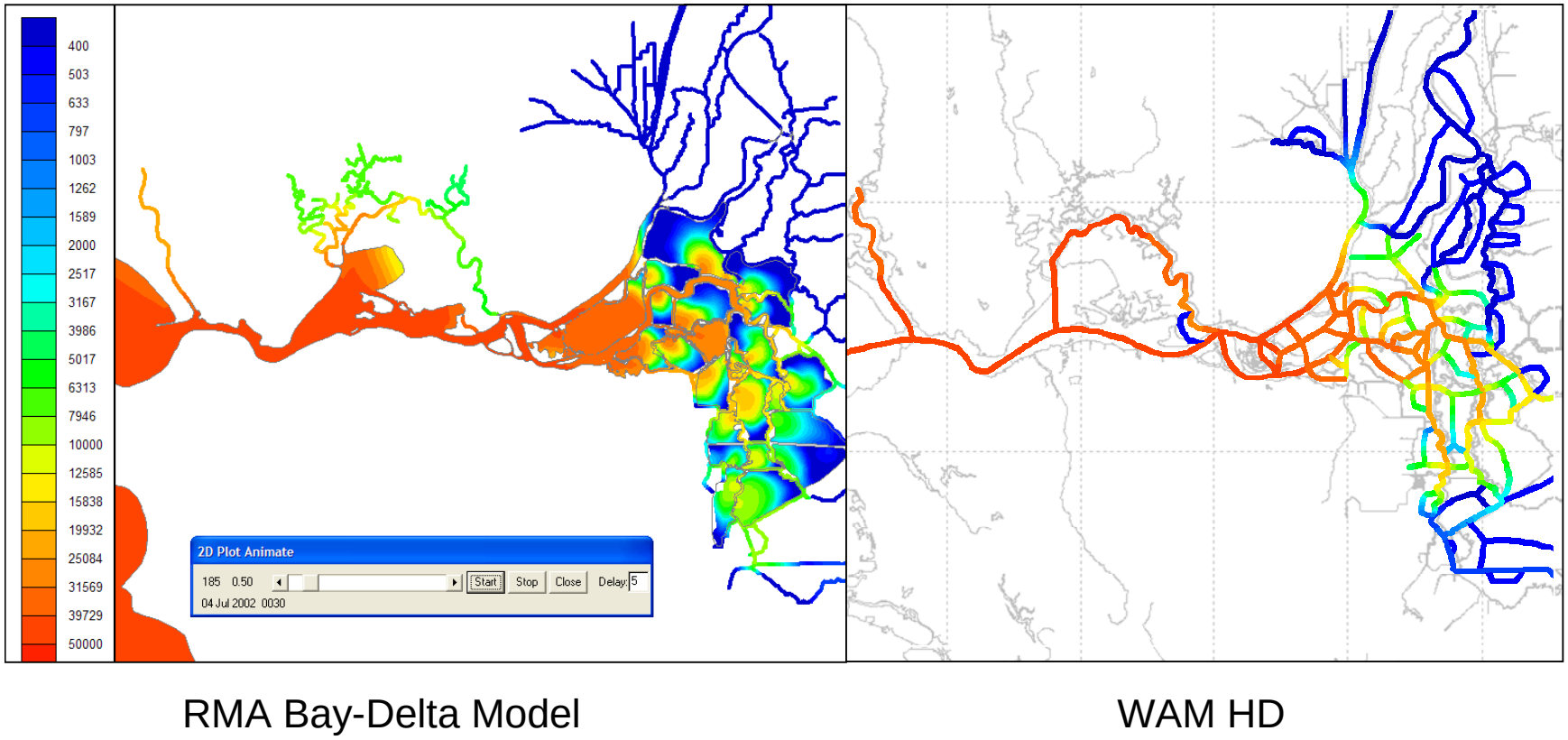

Figure E-26 Comparison of RMA Bay Delta Model and WAM HD Model for 20 Island Breach Case – Time of Peak Salinity Intrusion

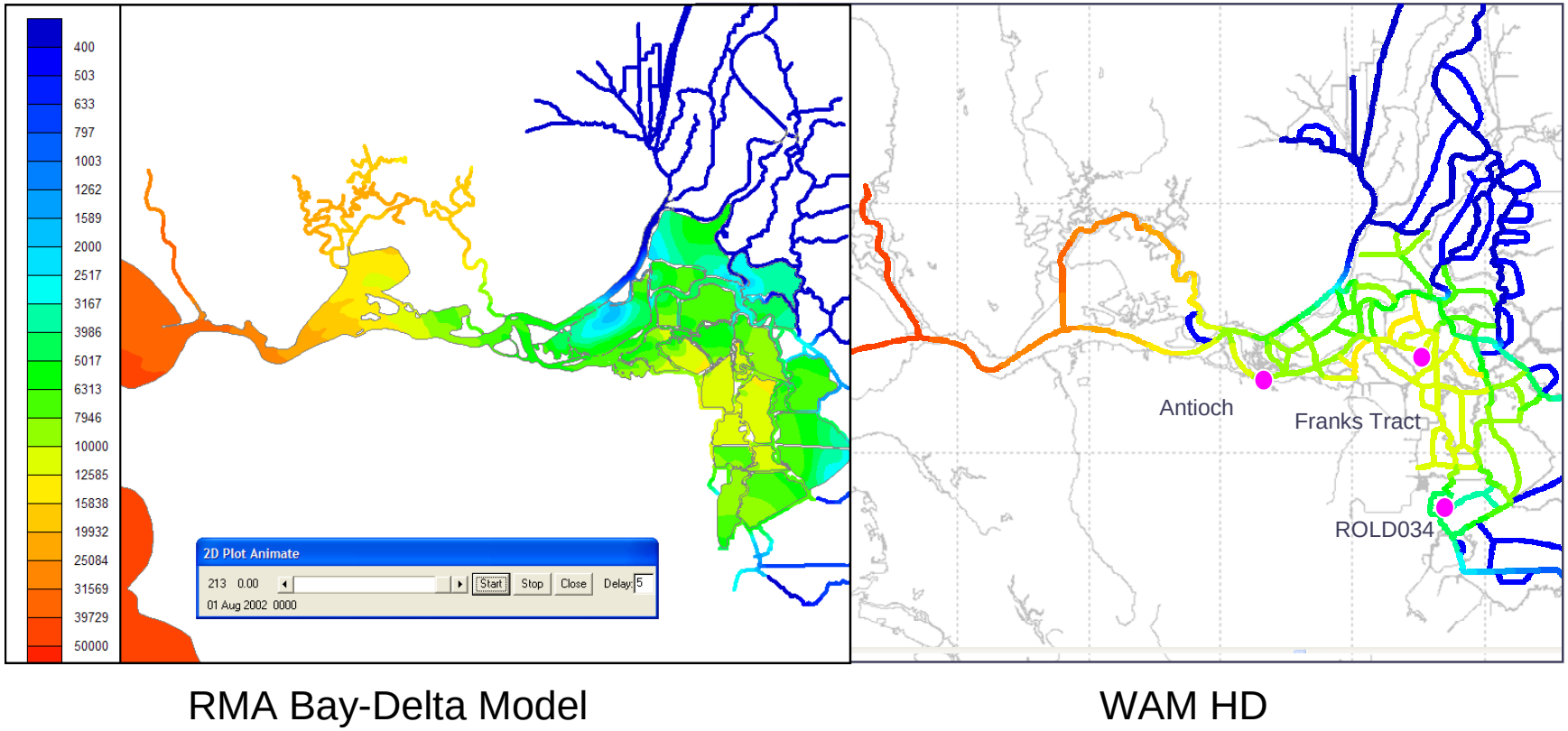

Figure E-27 Comparison of RMA Bay Delta Model and WAM HD Model for 20 Island Breach Case – One Month After Event

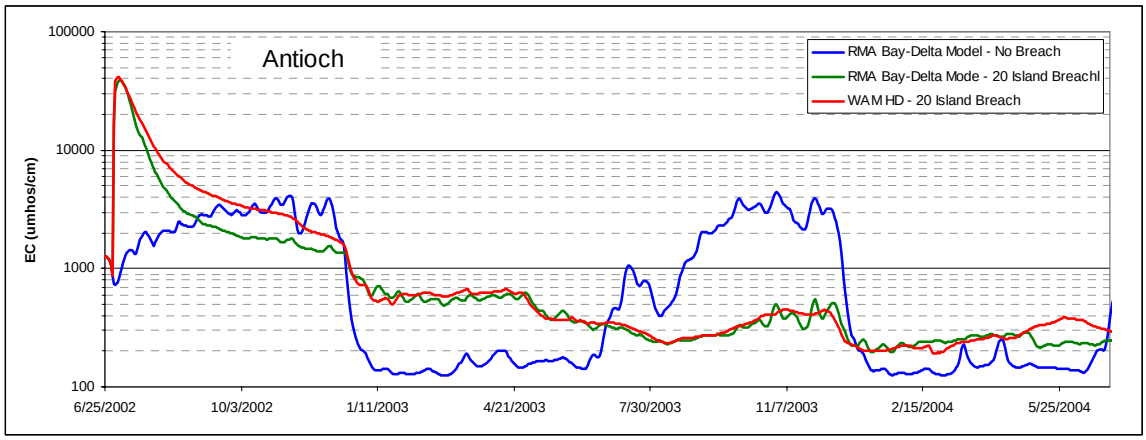

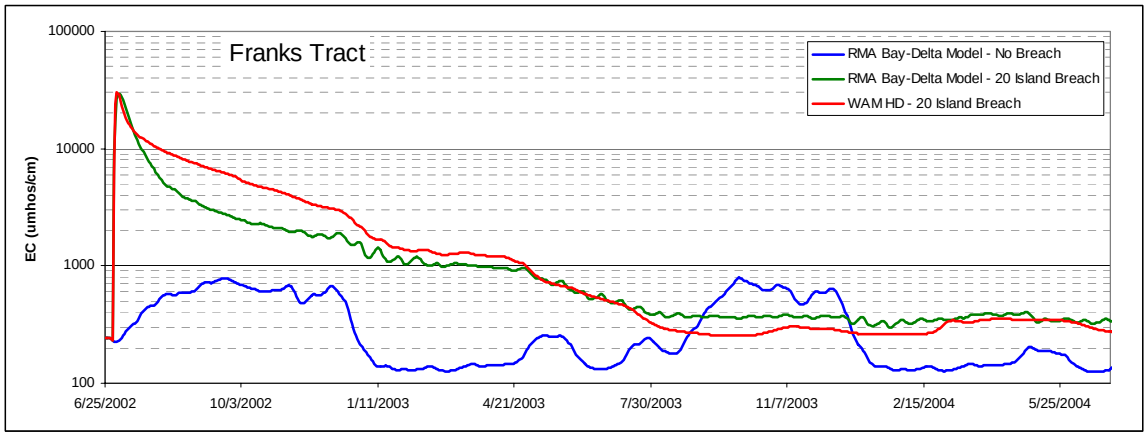

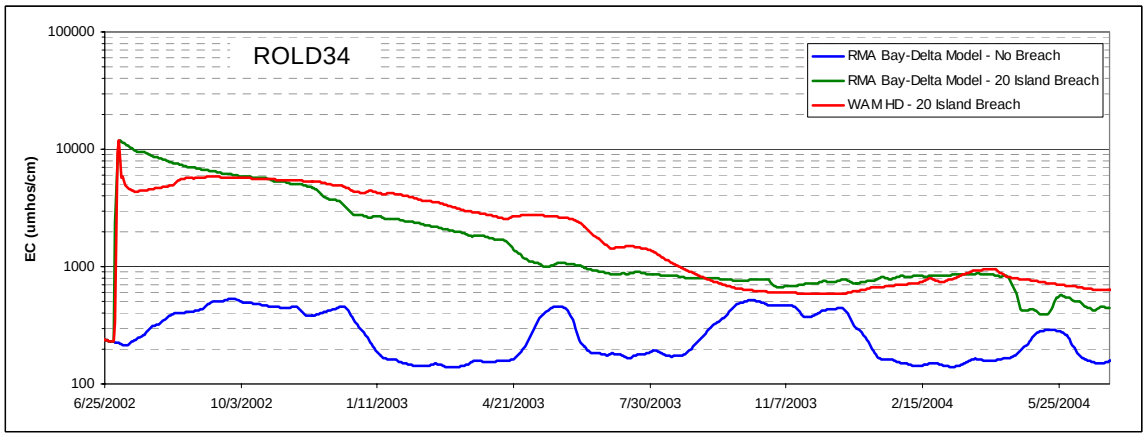

Figure E-28 Comparison of RMA Bay Delta Model and WAM HD Model for 20 Island Breach Case – EC Time Series At Antioch (Station RSAN008), Franks Tract, and Station ROLD034

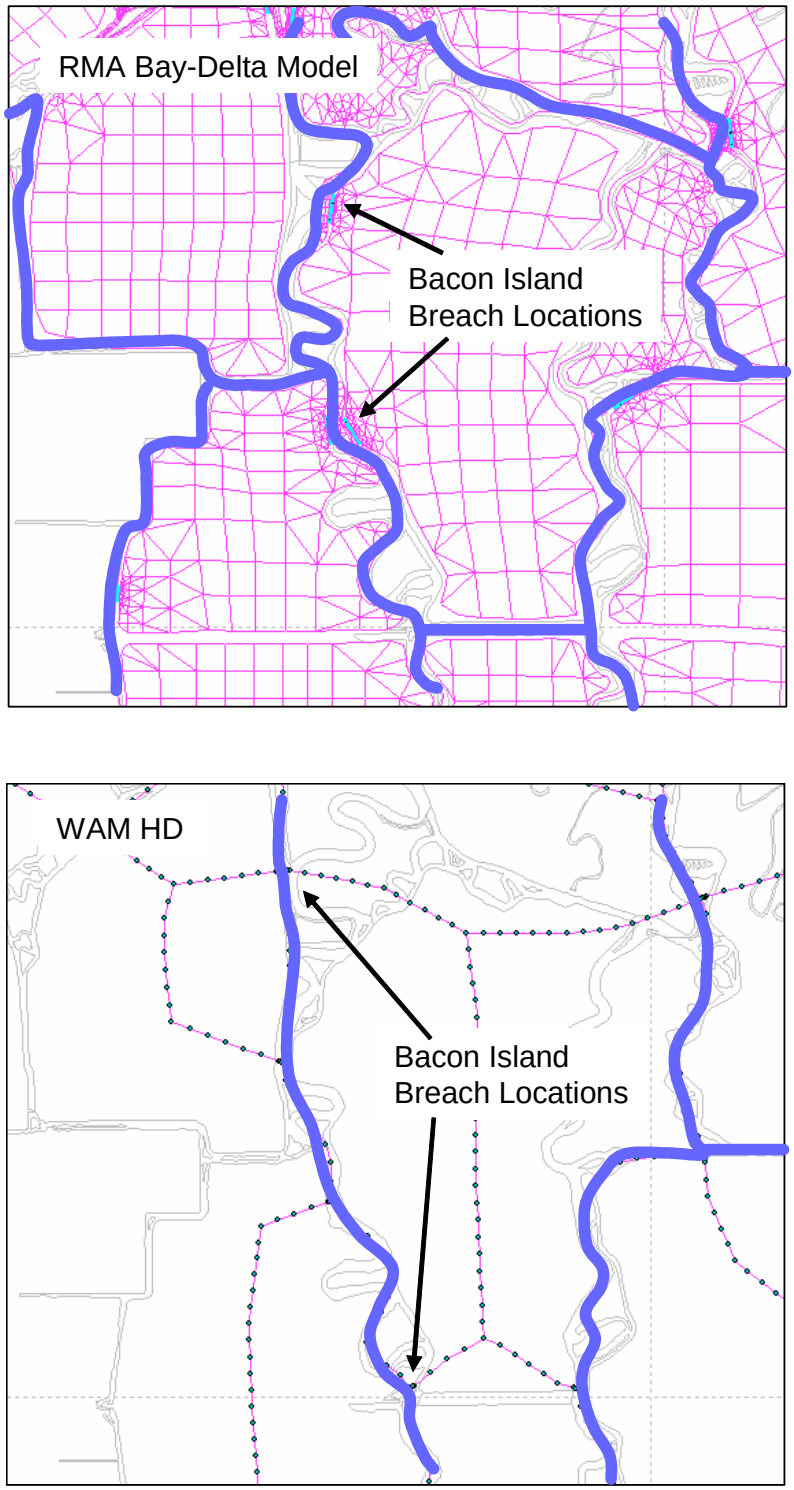

Figure E-29 Breach locations on Bacon Island in the RMA Bay-Delta Model and the WAM HD as used for the 20 Island Breach Case

the water that comes out of the south side of Bacon is fresher, reducing the channel salinity.

The slower rate of flushing from the WAM may in part be a function of the gravitational dispersion term included in the model, which would become more important in the Delta during a period of high salt intrusion. Because this term is not present in the RMA Bay-Delta Model no attempt was made to change dispersion in the channels to better fit the RMA Bay-Delta Model result. Further work comparing the WAM HD to multi-dimensional simulations would help to better determine whether the slower initial recovery is more or less correct. The most important point of comparison between the two models is that the central Delta returns to typical summer salinity range at the approximately the same time as that is a key criteria for the WAM reservoir and export operations.

E4. 2004 Jones Tract Event

In June of 2004 a breach occurred at Jones Tract on Middle River and the island filled with over 120,000 acre-ft of water. The event caused a small but measurable increase in salinity in the central Delta, but little impact at the CVP and SWP export locations. Export operations after a short reduction where continued while the Jones Tract breach was repaired and the island pumped out. This event has been modeled with the WAM HD utilizing Dayflow boundary conditions. The CU (consumptive use) record in Dayflow contains an estimate of the Jones Tract flooding impact. The CU record was used with the Jones Tract flooding component removed in establishing the total consumptive use for the WAM HD simulation. This was done to avoid double counting the flooding impact. The model was run with and without the breach event. The without breach event is considered the base case simulation. In both cases the WAM was not allowed to change release or export operations so the historic operations (as represented by the Dayflow boundary conditions) would be directly utilized. No adjustment of dispersion parameters were made for this simulation.

Comparison of computed and observed EC for the Jones Tract case is shown in figures E-31 to E-40. The stations presented are shown in Figure E-30. The salinity impact of Jones Tract flooding is evident at Martinez (Figure E-31) where EC increased over 7000 μmhos/cm or approximately 35%. At RSAC075 (Figure-32) and continuing up the Sacramento River to Emmaton and Threemile Slough as well as the San Joaquin River to Jersey Point (Figures E-33 to E-36) the rise in salinity following the breach event generally matches the observed data and then rapidly recovers to the base simulation. In the period following the breach through October, the model EC result for both base and breach conditions tends to rise ahead of the observed EC, although the ultimate peak EC is similar. In November to January the model under predicts EC. This behavior is consistent with the general trends observed in the calibration.

A slight increase in EC is observed in Old River at ROLD014 (Figure E-37). At Middle River at RMID023 (Figure E-38) the observed data shows a small immediate spike and then a reduction in EC. The model does not predict the small spike, but does match the reduction. At the SWP and CVP (Figures E-39 and E-40) there is a minor increase in EC

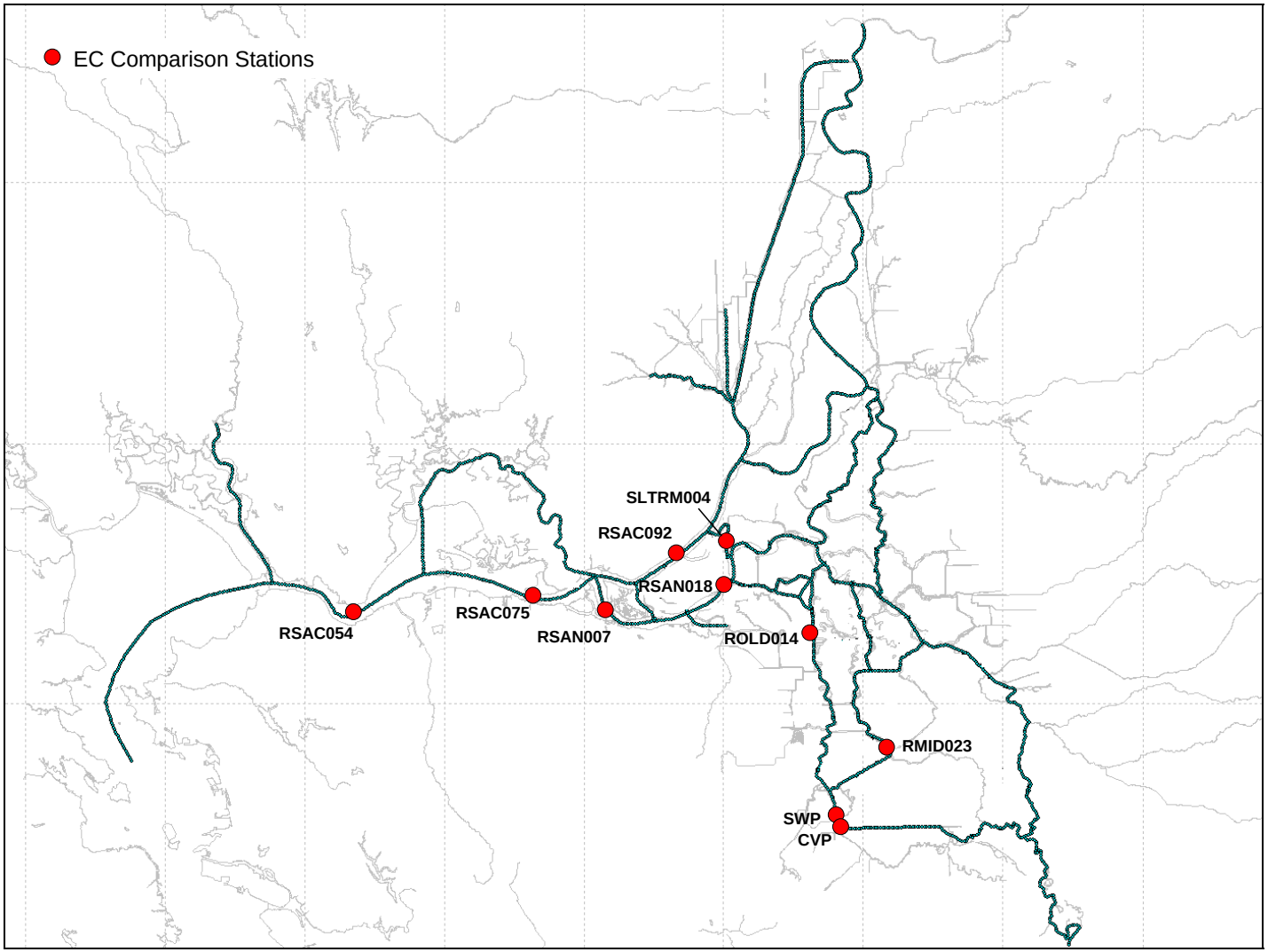

Figure E-30 EC Comparison Station for 2004 Jones Tract Breach Simulation

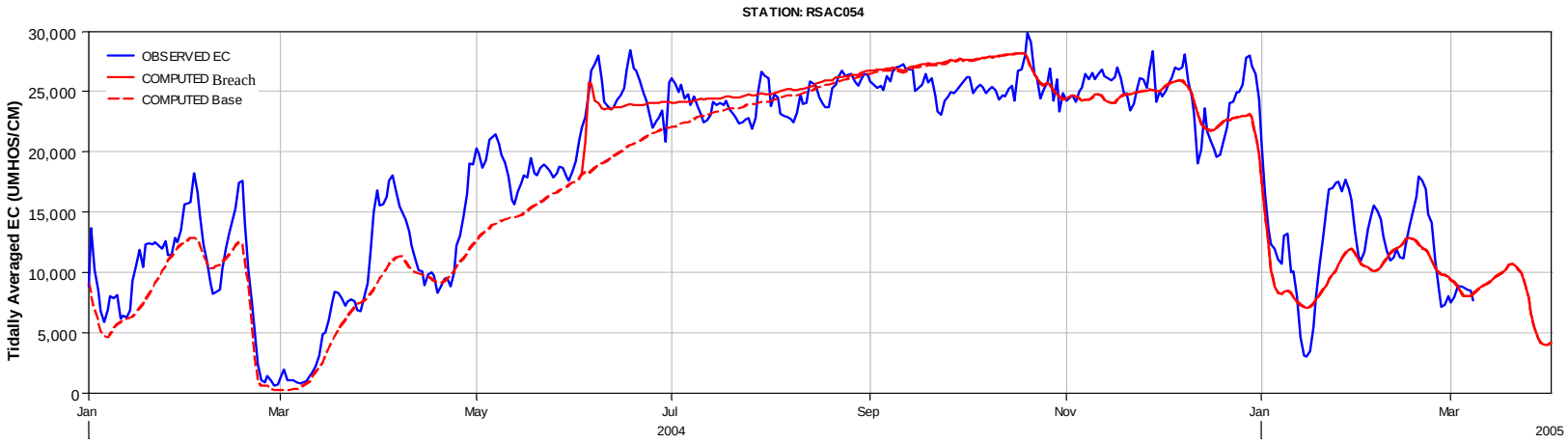

Figure E-31 Computed and Observed EC at Station RSAC054 – Jones Tract Event

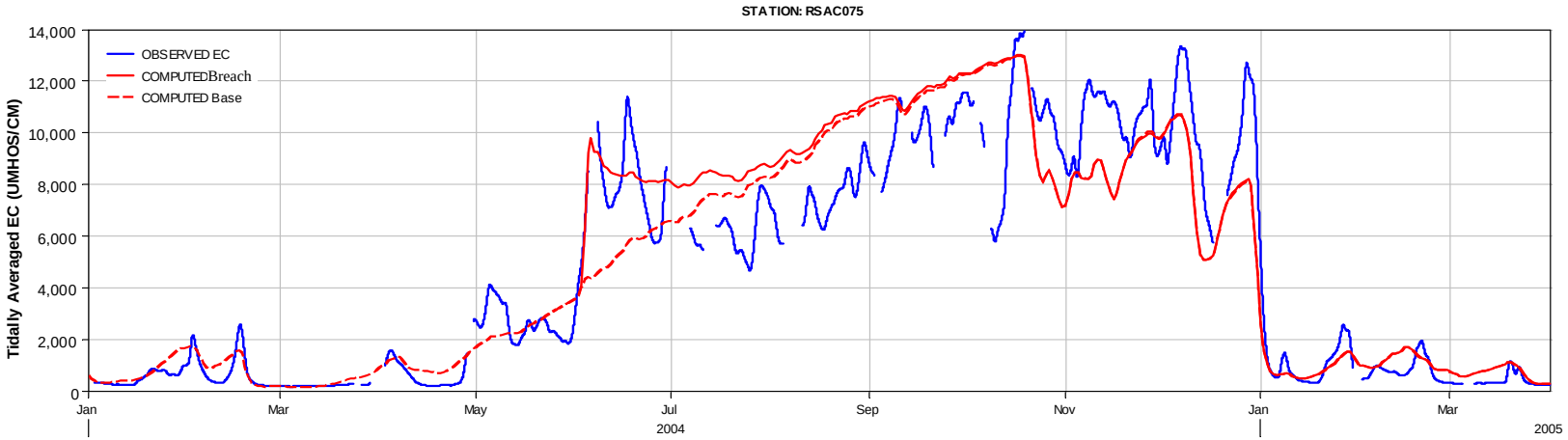

Figure E-32 Computed and Observed EC at Station RSAC075 – Jones Tract Event

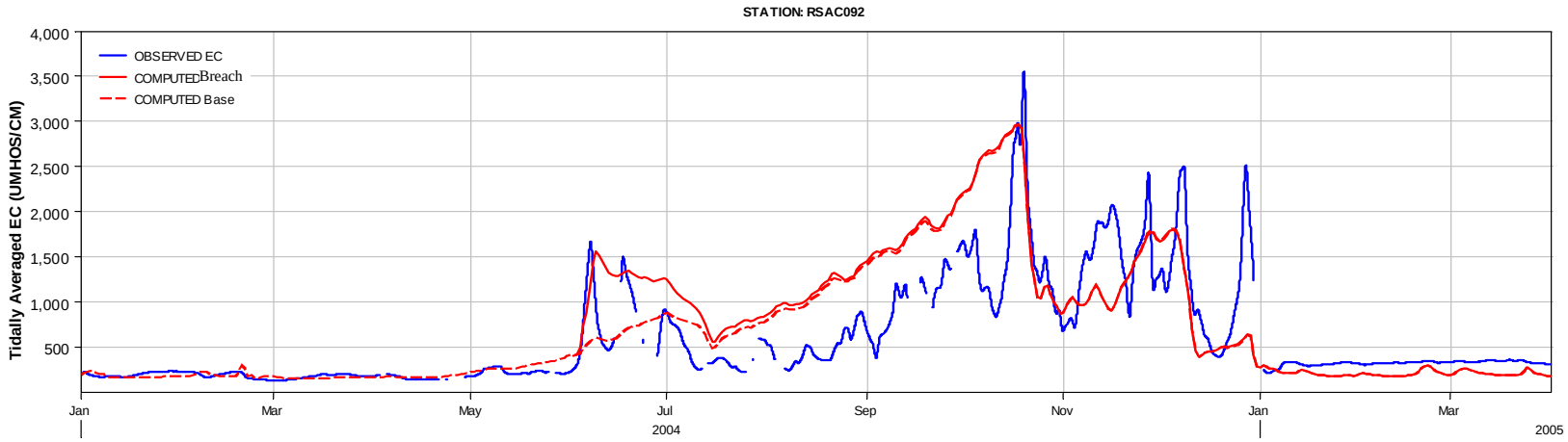

Figure E-33 Computed and Observed EC at Station RSAC092 – Jones Tract Event

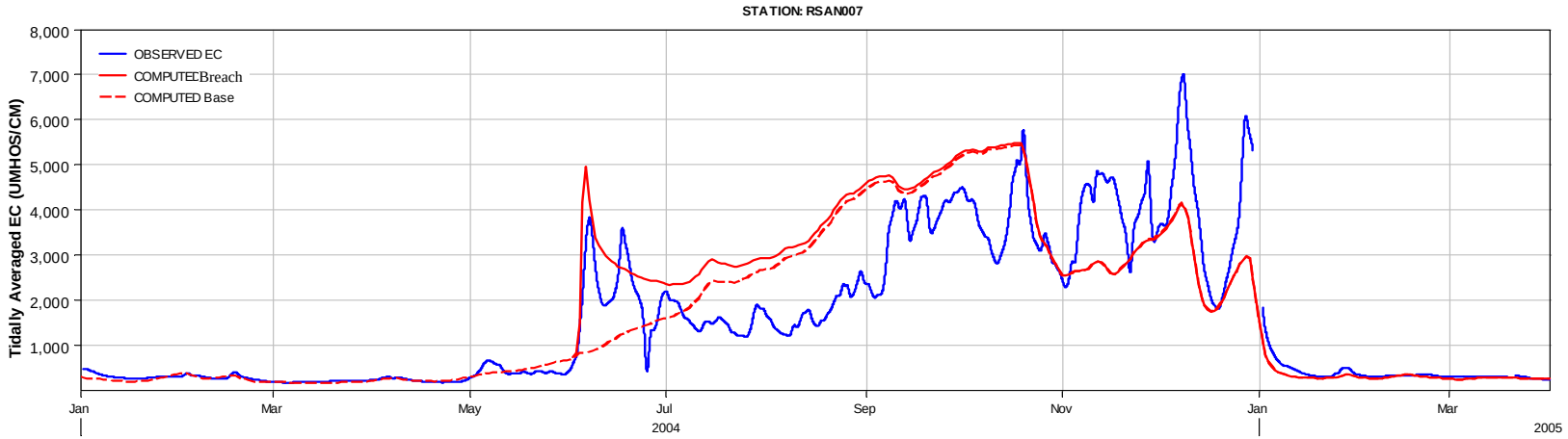

Figure E-34 Computed and Observed EC at Station RSAN007 – Jones Tract Event

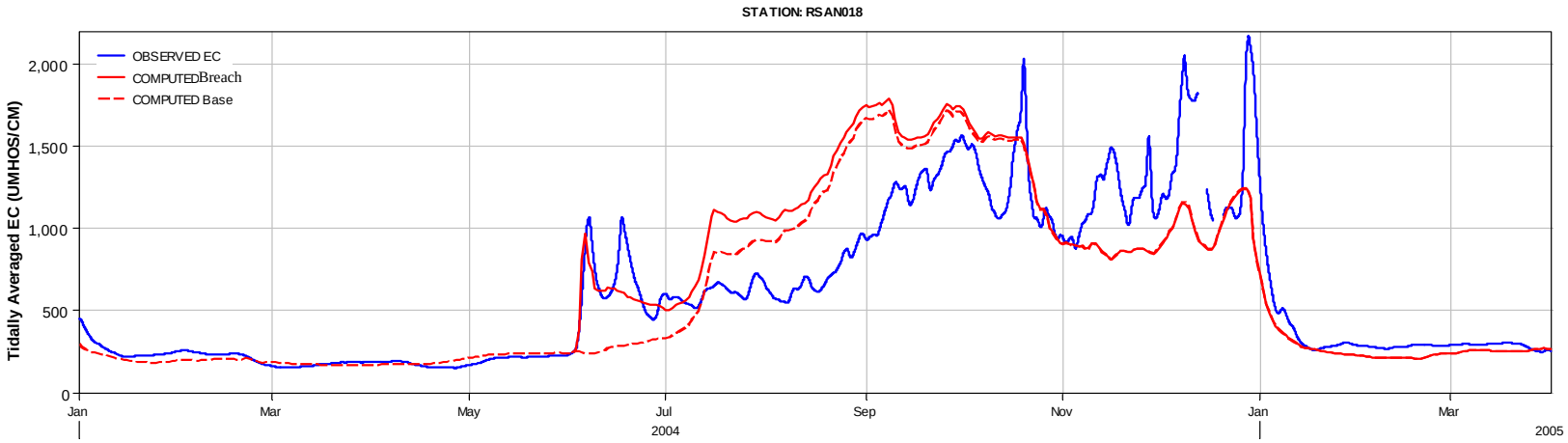

Figure E-35 Computed and Observed EC at Station RSAN018 – Jones Tract Event

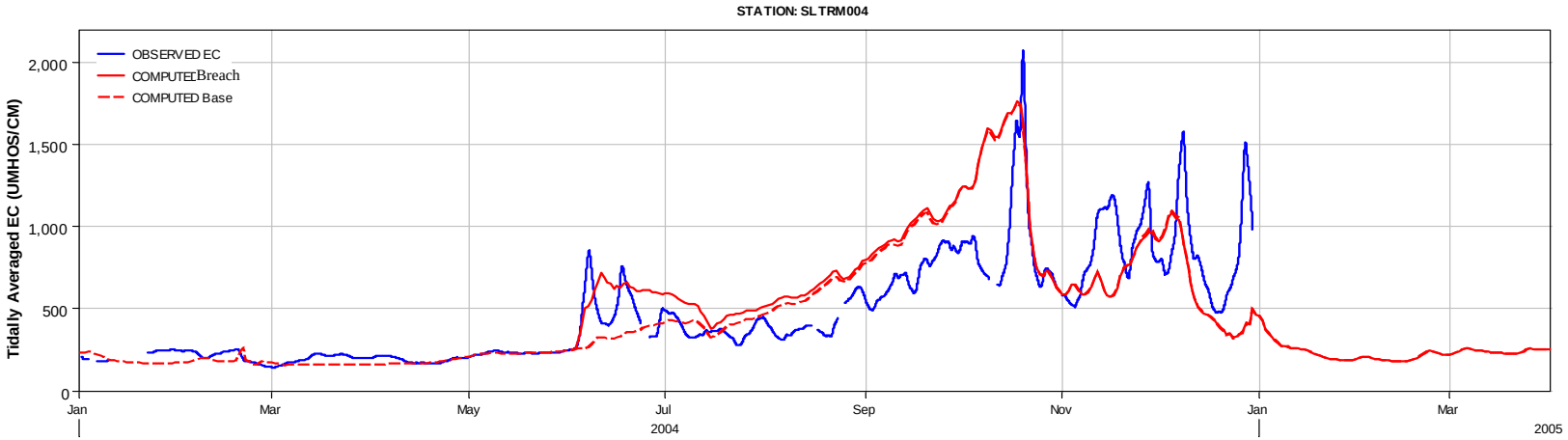

Figure E-36 Computed and Observed EC at Station SLTRM004 – Jones Tract Event

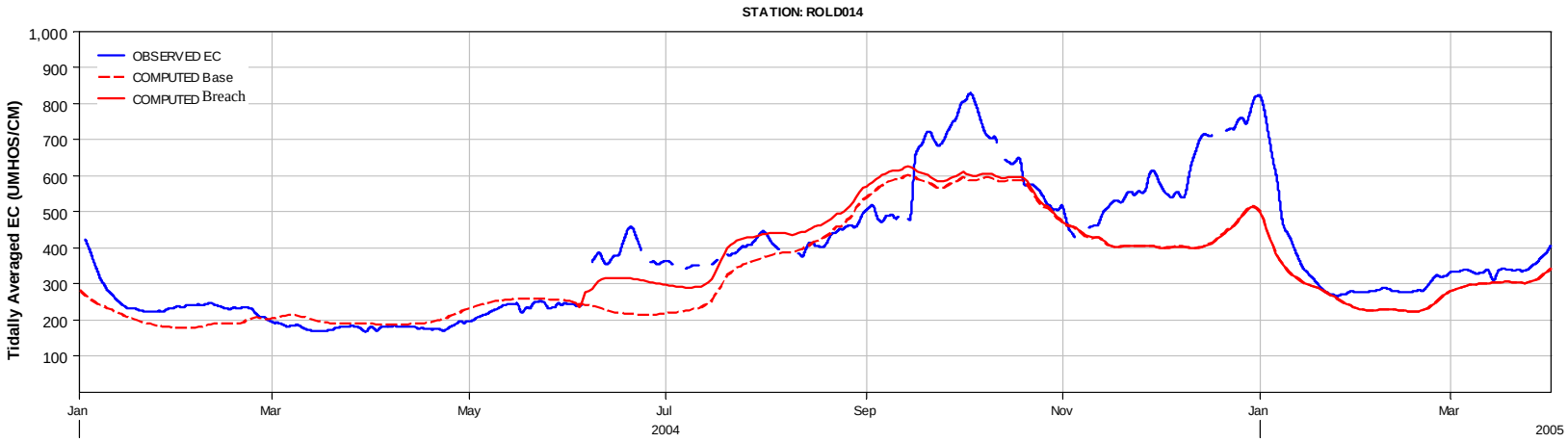

Figure E-37 Computed and Observed EC at Station ROLD014 – Jones Tract Event

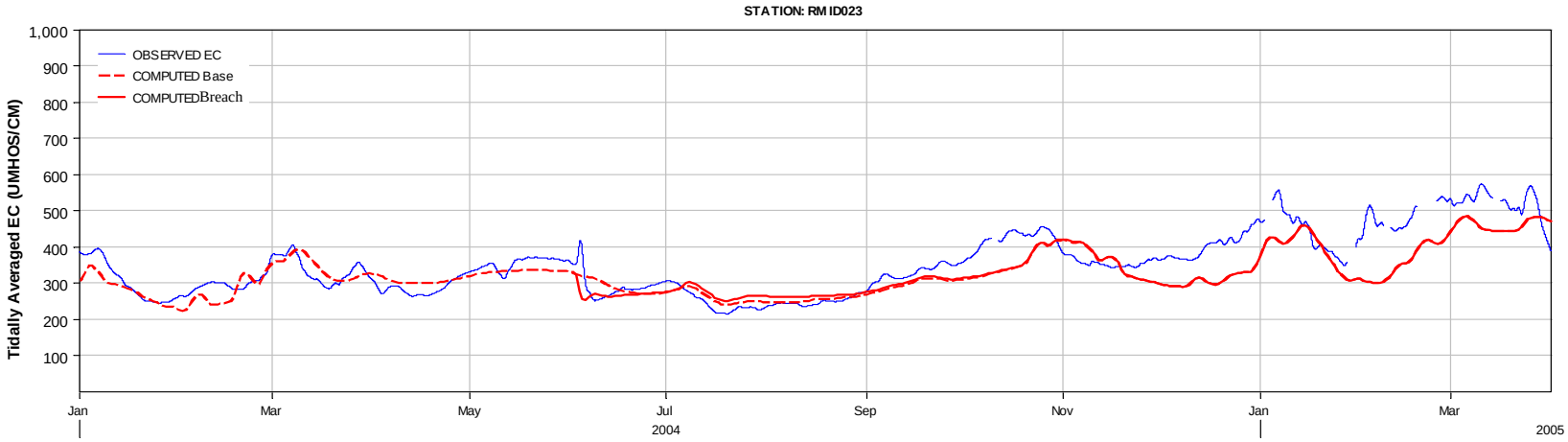

Figure E-38 Computed and Observed EC at Station RMID023 – Jones Tract Event

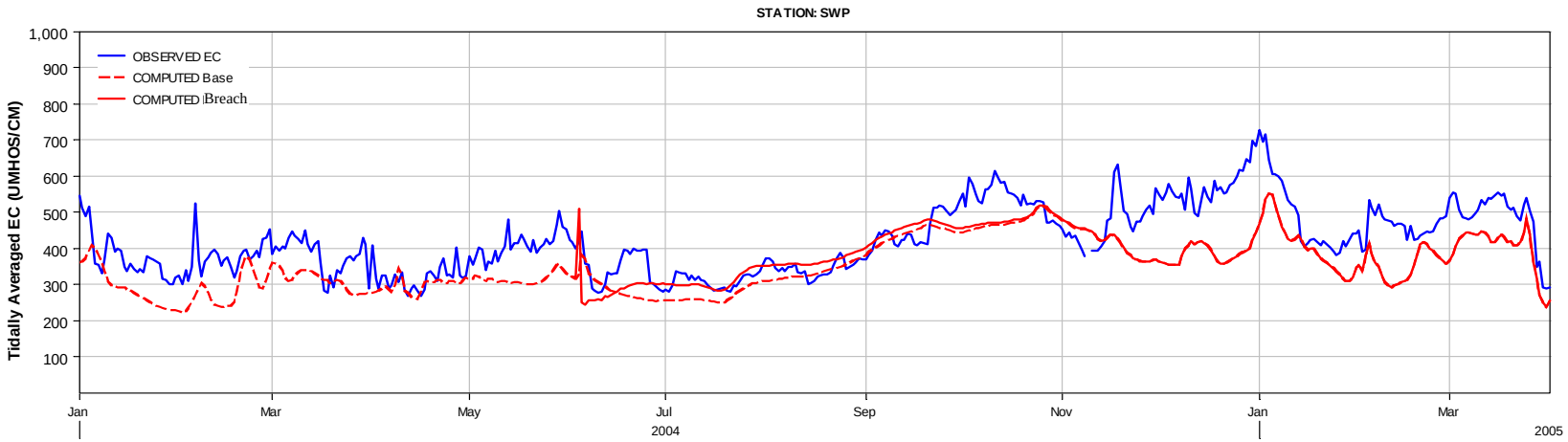

Figure E-39 Computed and Observed EC at Station SWP Export – Jones Tract Event

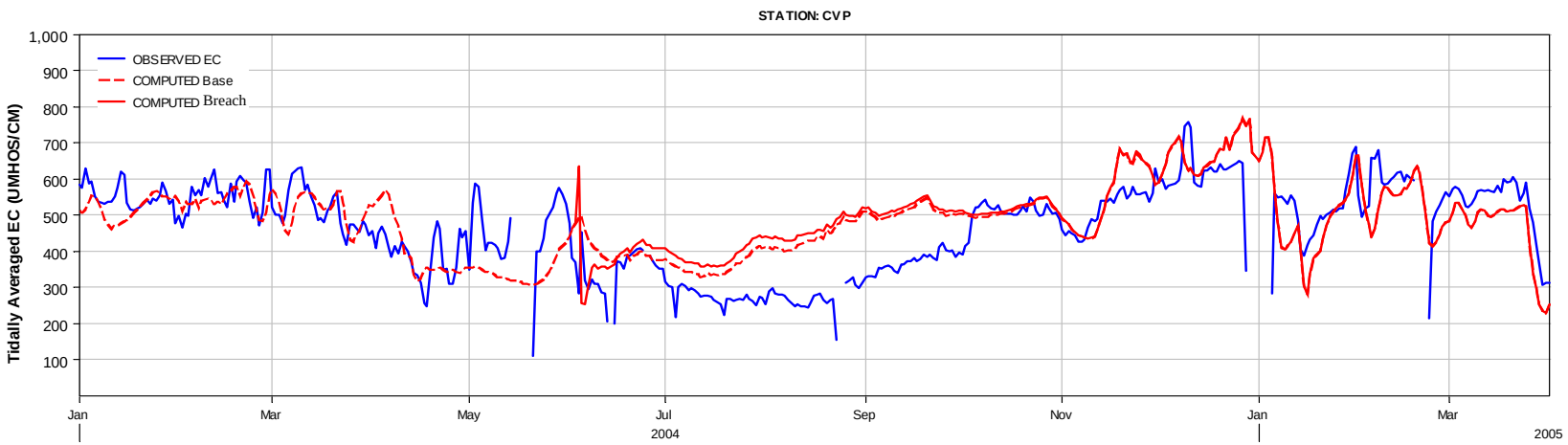

Figure E-40 Computed and Observed EC at Station CVP Export – Jones Tract Event

over the summer that is on the order of 50 μmhos, which is less than the RMS Difference estimate of 100 μmhos/cm for those locations.

E5. Discussion

The WAM HD was calibrated for the base, un-breached condition using observed data from October 1992 through September 2003. The salt flux between channels and flooded islands was calibrated by comparison of the WAM HD to the existing RMA Bay-Delta Model simulation of a 20 island, 50 levee breach event. A limited verification of the model was performed comparing model results to observed data for the Jones Tract breach event which occurred in 2002. The calibration to base conditions showed that in general the models ability to simulate salinity (as EC) was within approximately 15% of peak summer salinity values throughout the system. At the SWP and CVP export pumps RMS difference between computed and observed values was approximately 100 μmhos/cm where typical peak summer EC values are on the order of 800 μmhos/cm. The salinity impact of initial island flooding in the WAM HD simulation matches that of the RMA Bay-Delta Model closely, although salinity recovers more slowly in the WAM HD. Further validation would be useful for both the un-breached and breached cases.

The WAM HD was designed and implemented as within the aggressive schedule for the DRMS phase 1 risk assessment. As a risk assessment tool it has meet the requirements for computational speed and simulation capability. The WAM module including both Delta simulation and reservoir/export operations completes a five year simulation of multiple island breach events in approximately 90 seconds on readily available personal computers. Based on the calibration, the model predictions of EC at the SWP and CVP export locations are generally within approximately 15 % of peak summer observations. Sensitivity of the water operations should be explored to include plus or minus 15 % on the water quality operating criteria to establish bounds for environmental and economic consequences.

Simulating salt transport in the delta is a difficult task and there are certainly opportunities for improvements to the WAM HD. The approach to grouping DICU is probably more coarse than desirable. Whether the full distribution of DICU diversion and returns that are implemented in DSM2 and RMA Bay-Delta model is required is not clear, but five groups is too limiting. It may be also useful to explicitly represent more of the Delta channels in the model. While this would increase the complexity of establishing net flows and would incrementally increase run times, the added detail, particularly in the south Delta, may provide an important improvement in accuracy. Better gate operations should be included in internal flow multiple linear regressions, or, possible another technique could be used to more accurately impose internal boundaries.

The current calibration was accomplished by manual tuning of dispersion parameters. The model is fast enough that so that it may be desirable to implement an automated calibration algorithm. Any future calibration effort should include additional validation and sensitivity, both for the Delta transport simulation and the interaction with reservoir operations.

The level of calibration achieved to date suggests that the concept of developing a tidally averaged advection-dispersion model of the Delta utilizing a net flow simulations informed by historic data and detailed hydrodynamic modeling is valid. Such a model has important potential for rapid evaluation of levee breach scenarios as well as other of Delta issues.

Appendix F
Future Conditions – Hydrologic and Water Supply Impacts of Climate Change

Table of Contents

F.1. Introduction F-1
F.1.1 Available Simulations F-1
F.1.2 Trend Analysis F-3
F.1.3 Effects of Trends on Water Supply F-3
F.1.4 Effects of Levee Breach Incidents F-4
F.2 Previous Work F-4
F.2.1 Miller et al. (2001) F-4
F.2.2 Zhu et al. (2005) F-5
F.2.3 Lund et al. (2003) and Tanaka et al. (2006) F-5
F.2.4 Medellin et al. (2006) F-6
F.2.5 Joyce et al. (2006) F-6
F.2.6 DWR (2006) F-7
F.2.7 Vicuna (2006) F-8
F.2.8 Summary of Previous Work F-8
F.3 Approach Evolution from Previous Work F-9
F.3.1 Defining the Base Year F-14
F.3.2 Recognize the Limitations of the Data Sets F-16
F.3.3 Perform the Trend Analysis F-16
F.3.4 Adjust the CalSim Input Data Set Using the Trend-Indicated Change in Unimpaired Total Annual Flow for Each Gaging Site F-16
F.3.5 Perturb the Adjusted CalSim Monthly Unimpaired Flows for Each Gaging Site F-16
F.3.6 Normalize the Resulting Monthly Inflows to Meet the Adjusted Annual Inflow F-16
F.3.7 Perform CalSim Runs With the Modified Hydrologic Inputs F-17
F.4 Trend Analysis F-17
F.5 Effects on Water Supply F-18
F.6 Effects on Delta Levee Breach Water Conditions F-19
F.7 References F-19

Tables

F-1 DWR (2006) Percentage Decreases in Normal Deliveries for Four DRMS Climate Change Scenarios 2035-2064 (or 2050)

F-2 Vicuna (2006) Percentage Decreases in Normal Deliveries for Four DRMS Climate Change Scenarios 2070-2099 (or 2085)

F-3 Oroville Fractions and Ratios – with Climate Change Scenarios/Models

F-4 Shasta Fractions and Ratios – with Climate Change Scenarios/Model

Figures

F-1 Shasta Total Annual Inflow 1950 to 2100 Under Climate Change Scenario/Model SRESa2, gfdl

F-2 Shasta Monthly Inflow Percentages January-March, 1950 to 2100 Under Climate Change Scenario/Model SRESa2, gfdl

F-3 Shasta Total Annual Inflow Percentages April-June, 1950 to 2100 Under Climate Change Scenario/Model SRESa2,

F-4 Shasta Monthly Inflow Percentages Under Climate Change Scenario/Model SRESa2, gfdl

F-5 Oroville Monthly Inflow Percentages Including Historic, CalSim 2005, and Climate Change 2005 for Considering Base Year Selection

F-6 Oroville Monthly Inflow Percentages Including Climate Change

F-7 Oroville Annual Unimpaired Inflow – Historic and with Climate Change

F-8 Oroville Monthly Inflow Percentages – Historic and with Climate Change

F-9 Shasta Monthly Inflow Percentages Including Climate Change

F-10 Shasta Annual Unimpaired Inflow – Historic and with Climate Change

F-11 Shasta Monthly Inflow Percentages – Historic and with Climate Change

WAM Acronyms and Abbreviations

BAU	Business as Usual
CalSim	California Water System Simulation Model (DWR & USBR)
CALVIN	CALifornia Value Integrated Network
CEPA	California Environmental Protection Agency
CO_2	Carbon Dioxide
CVP	Central Valley Project
DRMS	Delta Risk Management Strategy
DWR	California Department of Water Resources
gfdl	Geophysical Fluid Dynamics Laboratory
IPCC	Intergovernmental Panel on Climate Change
ITF	Initial Technical Framework
JBA	Jack R. Benjamin & Associates, the DRMS risk analysis consultant
LINEST	A Microsoft Excel function for least squares line estimation
ncar	National Center for Atmospheric Research
NOAA	National Oceanographic and Atmospheric Administration
pcm	Parallel Climate Model
SRES	Special Report on Emissions Scenarios
SRESa2	SRES scenario a2
SRESb1	SRES scenario b1
SRESa1fi	SRES scenario a1 (fossil intensive variation)
SWP	State Water Project
TM	Technical Memorandum
URS	URS Corporation, the DRMS prime consultant
USBR	United States Bureau of Reclamation
WAM	Water Analysis Module or Model
WEAP	Water Evaluation And Planning model

F.1. Introduction

Climate change has caused changes in California's water resources and is expected to lead to further changes (DRMS, 2007). One expected alteration (due to increasing average temperatures) is less snowfall in the Sierra Nevada, with rain falling at higher elevations. And the snow that does accumulate is expected to melt earlier (DRMS, 2007, p1). This diminished snowpack is extremely important, since California depends on its snowpack for three to six months of storage – from winter until late spring and summer, when the water is needed. Additionally, there may be more or less precipitation and its temporal and/or geographic distribution may be altered. These changes are likely to result in a significantly changed availability of water supply. The State of California, through the Governor's initiative (CEPA Climate Action Team, 2006a and DWR, 2006), has recognized the possibility of future water resources impacts and performed initial analyses to incorporate climate change projections into management of California's water resources. The purpose of this portion of the Water Analysis Module (WAM) is to provide a tool for incorporating climate change projections into the DRMS analysis of risks from Delta levee failures.

The Climate Change Team (DRMS, 2007) obtained four (alternative) simulations of future Central Valley unimpaired runoff that were prepared for the Governor's State of California Climate Action Team. These simulations can be used to calculate inflows to the federal Central Valley Project (CVP) and State Water Project (SWP) facilities and then to provide estimates of future water supply available both for existing conditions in the Delta (no breaches) and during Delta levee breach incidents. The assessment of these simulations for inclusion into the WAM and Risk Analysis frameworks is outlined below.

F.1.1 Available Simulations

For the Climate Action Team Report (CEPA, 2006b) internationally and scientifically recognized global climate change simulations were analyzed and disaggregated to provide simulations at a finer spatial scale specific to California. The Climate Change Team (DRMS, 2007) obtained the four simulations, each resulting in a 151-year time series of monthly, unimpaired stream flows for 23 key Central Valley gaging sites. The four simulations are based on two of the global climate change scenarios developed by the Intergovernmental Panel on Climate Change (IPCC) and documented in the IPCC's Special Report on Emissions Scenarios (SRES). Each scenario is simulated by two widely respected global climate models – one model by the National Oceanic and Atmospheric Administration (NOAA) Geophysical Fluid Dynamics Laboratory (gfdl) and the other, the Parallel Climate Model (pcm), by the National Center for Atmospheric Research (ncar). The four scenario/model combinations are:

- Scenario SRESa2 with the gfdl model
- Scenario SRESa2 with the ncar/pcm model
- Scenario SRESb1 with the gfdl model
- Scenario SRESb1 with the ncar/pcm model

Note that the IPCC SRES (IPCC, 2000) presents six families of scenarios that have been judged to be credible. The findings also provide illustrative or "marker" scenarios for each family. The a2 marker scenario corresponds to a condition in which growth of global greenhouse gas emissions continues to accelerate. The b1 marker scenario corresponds to a condition where the rate of emissions growth moderates and the emission rates themselves eventually decrease. Both scenarios are hypothesized to potentially occur in the absence of new international initiatives to reduce greenhouse gas emissions. The SRES documentation states that "although no additional climate initiatives are included in the SRES scenarios, various changes have been assumed to occur that would require other interventions, such as those leading to reductions in sulfur emissions and significant penetration of new energy technologies" (IPCC, 2000). Note that the IPCC does not assess the comparative likelihoods of scenarios.

Two of approximately 22 global climate change simulation models (gfdl, and ncar/pcm) were used to develop the four time series. The rationale for their selection is described in the Climate Action Team Report (CEPA, 2006b). Note that the result is four time series, but each time series is a single realization of a particular scenario/model combination. That is, each is like a single role of the dice. If several other realizations for each scenario/model combination were available, a more reliable picture of scenario and model characteristics would be obtained. Of particular importance in this regard is the "mega drought" that occurs from 2085 to 2100 in the a2,gfdl time series (see Section 2.5 below and Joyce et al., 2006). It is not clear whether such severe droughts are an inherent common characteristic of this scenario/model or simply a chance occurrence of an improbable event that is no more likely in this scenario/model combination than others.

For each of the four simulations and 23 sites (see below), the time series of monthly, unimpaired flows begins with January 1950 and proceeds through December 2100, providing 151 years of simulated flows.

The 23 gaging sites are:

- Sacramento River at Shasta Dam
- Stanislaus River at New Melones Dam
- Merced River at Lake McClure
- American River at Folsom Dam
- Feather River at Oroville
- Tuolumne River at New Don Pedro
- Kings River at Pine Flat Dam
- San Joaquin River at Millerton Lake
- Yuba River at Smartville
- Mokelumne River at Pardee
- Consumnes River at McConnell

- Calaveras River at New Hogan
- Sacramento River at Delta
- Sacramento River at Bend Bridge
- NF American River at NF Dam
- Merced River at Pohono Bridge
- Bear Creek
- Paynes Creek
- Thomes Creek
- Stony Creek
- Butte Creek
- Fresno River
- Marsh Creek

F.1.2 Trend Analysis

Initially, representative simulation/site time series were analyzed for trends. Two types of trends that that may affect future water supplies and be particularly relevant to Delta levee risk analysis are trends in total annual unimpaired flow and trends of changing monthly proportions of total annual flow (i.e., the temporal distribution of annual runoff within the year). These analyses are described and examples of results are given in Section F4 below.

F.1.3 Effects of Trends on Water Supply

Trends in total annual unimpaired flow and modification to the annual distribution of flow (calculated for a given future year) can be used to provide potential future input conditions for CalSim simulation. CalSim is the water supply simulation model developed by DWR and USBR to represent the state's water supply system. Simulation of such future hydrology can thus be used to estimate a probability distribution for amounts of water supply expected to be available for delivery under climate change for that particular scenario during that particular future year. For example, for the year 2050, each of the 82 years of CalSim historic-record-based input data (for each of the 23 sites that is relevant) can be adjusted using the 2050 results of the trend analyses for a particular scenario/model. These adjusted inflows can be input to CalSim. The output will yield a probability of exceedance distribution for the amount of water supply deliverable in 2050 for that climate change scenario/model based on the 82 years of adjusted historical inputs. There are four years of interest for DRMS analysis:

- 2005 (the DRMS base case year and also a DWR planning and CalSim base case),
- 2030 (to use a future DWR planning and CalSim base year as a reference point),

- 2050, and
- 2100.

The climate change synthetic flows now available do not go beyond year 2100.

F.1.4 Effects of Levee Breach Incidents

Given climate change trends, future water supply available (e.g., in 2050) can be assessed with no levee breaches by adjusting CalSim inflows as described above. In other words, a new CalSim base case can be developed for 2050 by adjusting all 82 years of CalSim inflow hydrology for each relevant inflow stream to represent the inflow hydrology pertinent to 2050 with climate change. The new CalSim base case can then be input to the WAM calculator with expected sea level rise to indicate the impacts of the altered amounts of water available for Delta inflow in a new WAM base case (with no breaches).

Then, based on any given levee breach incident generated by other risk analysis modules and specified in WAM's input format, WAM is able to calculate the water quality and water export impacts of the levee breach incident as if it had occurred in the given future-year (e.g., 2050). WAM takes into account all of the major physical/environmental changes expected to influence future year conditions – altered water supply hydrology due to climate change, sea level rise, and (as another WAM input) the increases in Delta island flooding volumes due to subsidence.

F.2 Previous Work

The importance of climate change to California's water resources and future availability of water supply has been recognized previously and subjected to analysis.

F.2.1 Miller et al. (2001)

Miller et al. (2001) looked at six headwater basins in California and examined the streamflow implications of incremental temperature shifts and precipitation increase ratios by working with existing snow and soil moisture accounting models. Their base period was 30 years (1963 through 1992, i.e., centered on 1977-1978). After first looking at the effects of preset temperature shifts and precipitation increase ratios on the 30-year base period's record of 6-hour streamflows, they applied the same method to downscaled interpretations of the monthly shifts in temperature and precipitation outputs from global climate models. They found that, "for all cases, a larger proportion of the streamflow volume will occur earlier in the year. The amount and timing is dependent on the characteristics of each basin, particularly the elevation of the freezing line."

They used two quite different climate models (one somewhat warmer and drier and the other significantly warmer and wetter), but both were different from the scenario/models selected by the Governor's Climate Action Team. They analyzed impacts for three 20 or 30 year periods during the 21st century centered on 2024-2025, 2064-2065, and 2089-2190. Even for the results from the wetter model (with increases in annual precipitation of up to 62%), their calculated monthly streamflows for basins that have historically accumulated snow generally showed decreased flows compared with base period flows in

late spring and summer months (May – September). The exceptions were with increased precipitation in the higher headwater basins in the southern Sierra Nevada that have historically had temperatures several degrees below freezing – amounts at least similar to the degrees of the projected warming.

F.2.2 Zhu et al. (2005)

Zhu et al. (2005) extended the Miller et al. work to assess water supply availability for the Central Valley as a whole for use as subsequent input to the CALVIN (the CALifornia Value Integrated Network) model for water management. They considered ground water infiltration, reservoir evaporation, and local runoff in addition to major stream inflows (or rim flows) at the margins of the Central Valley. Their work substantially broadened the geographic and hydrologic scope of previous studies of climate change impacts on California hydrology. CALVIN requires 37 rim flows and includes 28 groundwater basins and 35 local runoff locations plus evaporation from 47 surface reservoirs. It was therefore necessary to use available climate change streamflow studies (primarily Miller et al) for indexing and to transfer the results from earlier work to these other locations. Other methods were used to address the other hydrologic variables. The result was a comprehensive representation of climate change impacts for the inter-tied state water system.

Without modeling system operations (i.e., assuming continuation of current policies and water allocations/uses), they estimated approximate changes in water availability over a 72-year hydrologic series (water years 1922 through 1993) for each of the twelve varied climate change states defined by Miller et al. They found that even most states with increased precipitation result in less availability of water because of the current storage systems' inability to catch increased winter streamflow in compensation for reduced summer runoff. For nine of twelve climate change states, they found two with no system-wide water supply change and seven with water supply decreases of up to 25%. For the three "wet scenario" states with precipitation increases of 26% to 62%, they found modest water supply increases of 7% to 12%.

F.2.3 Lund et al. (2003) and Tanaka et al. (2006)

Lund et al. (2003) and Tanaka et al. (2006) report on the results of using two of the twelve Zhu et al. inputs in CALVIN to simulate the water-related economic impacts of climate change. They project water demand (based on population and land use changes) for year 2100 and use the two Zhu et al. climate change states pertinent to 2100. Since CALVIN is an economic optimization model, it allocates scarce supplies to higher value uses thereby indicating a transfer of water from agricultural to urban users in addition to development of some higher cost supplies for urban uses.

The most severe impacts are for the warm and drier climate projection, with average annual water scarcity due to climate change of approximately 8 MAF and average annual climate change costs of about $1.8 billion. The wetter climate change state does not indicate water supply scarcity or cost impacts attributable to climate change. However, even without climate change, they estimate annual water scarcity and increased annual

costs of an additional 4.5 MAF and $4.1 billion. This, of course assumes optimal water management under the CALVIN objective function, not the continuation of present policies under "Business as Usual" (BAU).

F.2.4 Medellin et al. (2006)

Medellin et al. (2006) provided an updated application of CALVIN using the a2, gfdl climate change scenario/model, one that was chosen for use by the by the Governor's Climate Action Team and subsequently adopted for use by DRMS. They chose to use the current state/federal water infrastructure, the a2, gfdl streamflows representing 2085, and population and land development estimated for 2050. They calculate that, for 2085, the a2, gfdl scenario shows a 27.9% decrease in streamflow. Consistent with the studies described above, this compares two 30-year periods, in this case 1965-1994 as a base period versus 2170-2199 as the period representing 1985. It also relies heavily on the altered streamflow characteristics calculated for the six generally small headwater basins studied by Miller et al.

The results may be strongly impacted by the "mega drought" in the a2, gfdl scenario during the last 15 years of the century, a phenomenon recognized by Joyce et al. (see the more detailed discussion below in Section 2.5). As in the previous CALVIN work, they estimated both water scarcity and economic impacts from water scarcity with and without climate change. With the a2, gfdl 2085 state of conditions, they estimate approximately a 27% decrease in average annual water supply availability. Since CALVIN is a management (optimization) model, it shifts scarce water to uses of high economic value (i.e., urban uses). Thus, cutbacks are allocated to the uses of less economic value (agriculture), with agricultural deliveries decreasing approximately 24%. Urban scarcity (about 1%) is due to limited conveyance capacity for transferring water to southern California via the California Aqueduct and from the Colorado River. The model results indicate substantial adaptation of the water system, including significant increases in Delta exports during winter and reductions during summer and early fall. Overall economic impacts are estimated at several hundred million dollars per year. Given the severity of the water supply reduction, these impacts may seem optimistic. But they do reflect only 2050 population and demand rather than the more substantial numbers that would be associated with 2085 or 2100. The impacts also reflect optimized water use per the CALVIN objective function and other assumptions, not "Business as Usual."

F.2.5 Joyce et al. (2006)

Joyce et al. (2006) presented a case study of climate change impacts on agriculture in the Sacramento Valley. They applied the Water Evaluation and Planning (WEAP) model – an extension of the application by Yates et al. (2005). This model, which is relatively new to California, is physically based and driven by demand, priorities, and preferences (Yates et al, 2005). It also uses climate data (such as precipitation and temperature) as its direct input, avoiding the need to externally convert a climate time series into a perturbation of historic streamflows for use in other available models (CalSim and CALVIN). It was used to examine the impacts of the four climate change scenario/model combinations on Sacramento Valley agriculture both with current agricultural cropping

patterns and practices and with adaptive change of those approaches. Analyses were performed for a 40-year base period (1960-1999) and three different 30-year future periods – (2005-2034, 2035-2064, and 2070-2099). Their use of thirty-year periods for analysis, as was reported in other studies, is noted.

As was done for the studies described previously, these authors examined redistributions of the monthly flow fractions with time among scenarios. In addition they examined variations in total annual reservoir inflow and drought persistence, with interesting results. Their analysis revealed a "mega drought" in the last 15 years of the 2100's in the a2, gfdl time series. This may represent a unique and substantial risk of that particular scenario/model or may mean that the particular time series realization for a2, gfdl now available happens to be unusual. They also looked at drought persistence for the SRESa1fi, ncar/pcm scenario/model (this assumes a fossil fuel intensive future) and found a marked increase in drought frequency. This topic will require further inquiry and is likely to lead to generation of an ensemble of realizations (say 30 to 60 simulations) for each scenario/ model in order to better understand the likelihood of such events (in a probabilistic sense) within the context of each scenario/model's particular assumptions and parameters.

F.2.6 DWR (2006)

DWR (2006) has implemented an approach using CalSim to obtain preliminary results for climate change in about 2050. They used the four climate change scenarios selected for analysis by the Climate Action Team. DWR used climate change impact established by two 30-year year periods – 1961-1990 (centered on 1976 and serving as the base) and 2035-2064 (centered on 2050). This was the DWR implementation of perturbation ratios involving the calculation of the monthly ratio of "2050" average streamflow (e.g., May) divided by the same month's average flow for the base period (i.e., 1976). These ratios were used to transfer regional scale climate change behavior (represented by the four selected scenario/model simulations) to local historic data – i.e., the CalSim input. DWR established these ratios for ten streams. Their results are summarized in Table F-1.

Table F-1 DWR (2006) Percentage Decreases in Normal Deliveries for Four DRMS Climate Change Scenarios 2035-2064 (or 2050)

	Wettest		**Exceedance Probability**			**Driest**
	10	**25**	**50**	**75**	**85**	**95**
SWP (Table A)	Up to 4.2%	Up to 8.1%	3.5%-11.2%	19.4%-17.9%	7.8%-14.9%	Up to 14.2%
CVP (South of Delta)	Up to 2.9%	Up to 8.4%	7.2%-14.5%	7.6%-12.9%	Up to 13.9%	Up to 14.3%

F.2.7 Vicuna (2006)

Vicuna (2006) provided results and observations for a similar application of CalSim II to climate change analyses. He used a baseline version of CalSim II, called CalSim II Benchmark Studies (DWR/USBR, 2002) and altered the input streamflow hydrology based on each of seven different climate scenario/model time series of unimpaired flows, including the four selected for analysis by the Governor's Climate Action Team and DRMS. For each series he calculated monthly perturbation ratios for rim flow streams based on time series 30-year periods for 1961-1990 (base period) and 2070-2099 (centered on 2085). He then applied these ratios to each monthly CalSim streamflow input. Essentially all other CalSim inputs were unchanged. Results were compared to the "no climate change" base case. All climate change simulations except the b1, pcm/ncar series showed substantial negative impacts to state and federal water project deliveries. Table F-2 is a summary of results for the four DRMS scenarios including b1:

Table F-2 Vicuna (2006) Percentage Decreases in Normal Deliveries for Four DRMS Climate Change Scenarios 2070-2099 (or 2085)

	Wettest		**Exceedance Probability**			**Driest**
	10	**25**	**50**	**75**	**85**	**95**
SWP	Up to 1.7%	Up to 7.3%	3.5%-27.3%	19.4%-61.7%	7.8%-48.8%	Up to 40%
CVP (South of Delta)	Up to 16%	Up to 26.3%	7.2%-34.3%	7.6%-31.4%	Up to 27.0%	Up to 20.9%

Note that Vicuna's results for the other three scenario/model combinations he examined show reductions in normal deliveries that are generally more severe than the worst indications in the above table.

F.2.8 Summary of Previous Work

In summary, previous work has generally selected a 30-year base period centered approximately on 1976 as its reference point for measuring California climate change. Then a future 30-year period has been selected for analysis of climate change impacts. This has generally required use of global climate model temperature and precipitation outputs to calculate streamflows on reference streams. In some cases these reference streams had to then be used to make a reasonable transfer of the climate change stream flows to other streams that drive the water resources model to be used. Then perturbation ratios were calculated to alter the standard input to the base case water resources model. The notable exception is Joyce et al; their WEAP model is able to use the climatic outputs directly. The additional recent development has been the availability from Maurer (see DRMS, 2007, Vicuna, 2006, and DWR, 2006) of climate change scenario/model streamflow time series for many more of the relevant model-driving rivers in California.

F.3 Approach Evolution from Previous Work

In the DRMS analysis, it is necessary to consider somewhat different needs than existed in previous studies. The risk analysis is to address specific years – namely 2005, 2030, 2050, and 2100. Previous work has generally had the objective of estimating change over a time frame of 50 or 100 years and was able to be more approximate about the specific years being considered. Also, especially during the earliest work described above, the data available were limited and essentially dictated that approach. Thus, the comparison of 30-year averages for periods the requisite number of years apart was initiated and became routine practice. Also, previous studies tended to compare monthly quantities of streamflow. In the present analysis, there is an interest in seeing two features of the data – differences in total annual (water year) reservoir inflow and changes in monthly percentages of inflow, rather than just looking at monthly flows.

Initially, similar groupings of about 30 years were attempted in order to detect climate change impacts in the present analysis. Figures F-1a, F-2a, and F-3a are examples. But thirty years seemed to be inadequate to dampen random yearly variations in the climate simulations. The lumped data points from one target year to the next seemed to retain substantial random variability rather than all being a trend attributable to climate change. Then, when variations of monthly percentages of streamflow were plotted, a jumble of lines resulted as illustrated by Figure F-4a.

The objective was to eliminate this randomness and obtain a smooth trend of climate change progression and impacts on total annual inflow and monthly percentages of runoff. Then these trends could then be used to more precisely characterize climate change conditions at a specific future year by adjusting the hydrologic inputs for CalSim based on the trends. As an alternative to the “30-year period comparison” approach, fitting a linear trend line to the entire 151 years of data was attempted. As indicated in figures F-1b, F-2b, F-3b, and F-4b, the trend approach using the 151-year series provided more stable and insightful results. This approach has the additional advantage that the trend equation can be used to calculate a unique climate change progress point for any specific year of interest – in this case 2005, 2030, 2050, and 2100. A further advantage is the quality of fit of the linear trends; the trend lines with non-trivial slopes satisfy the 99 percentile test of statistical significance per the F distribution. The monthly percentages for 1975 are also shown on Figure F-4b for comparison.

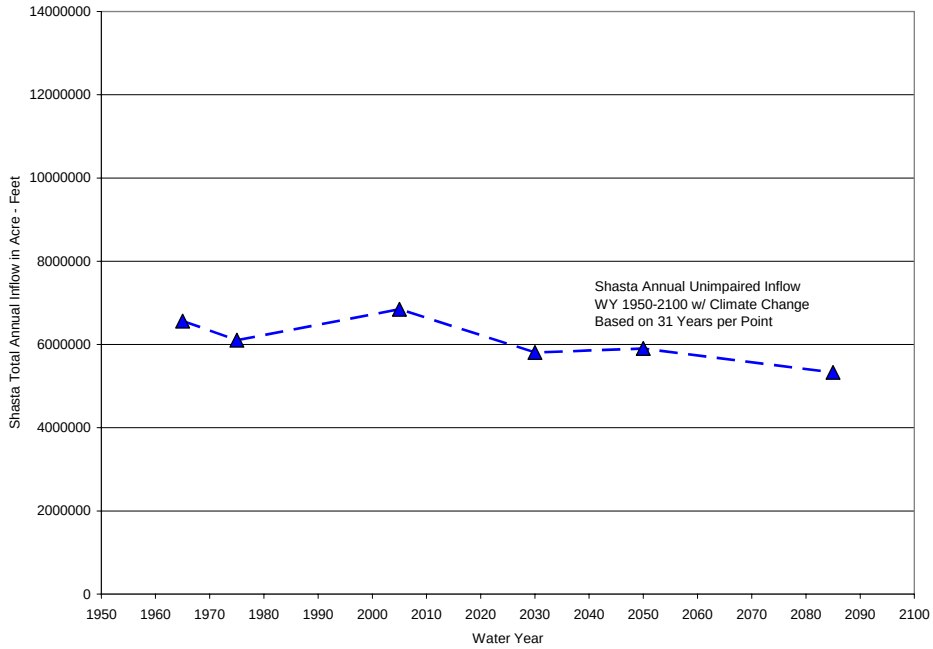

Figure F-1a Data Lumped Showing Points Based On 31-Year Averages

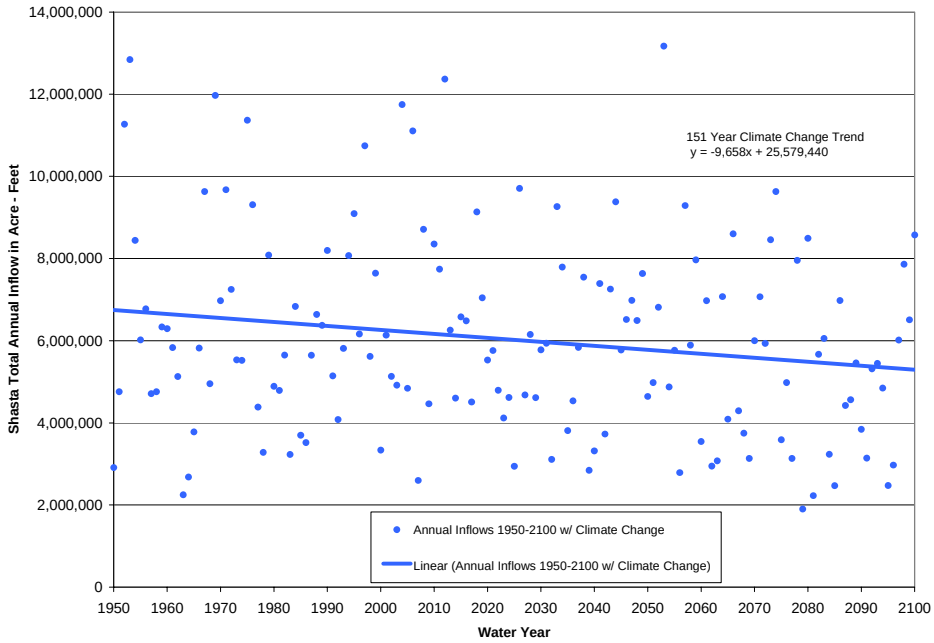

Figure F-1b Data Plotted as Annual Data Points and Fitted With a Least Squares Trend

Figure F-1 Shasta Total Annual Inflow 1950 to 2100 Under Climate Change Scenario/Model SRESa2, gfdl

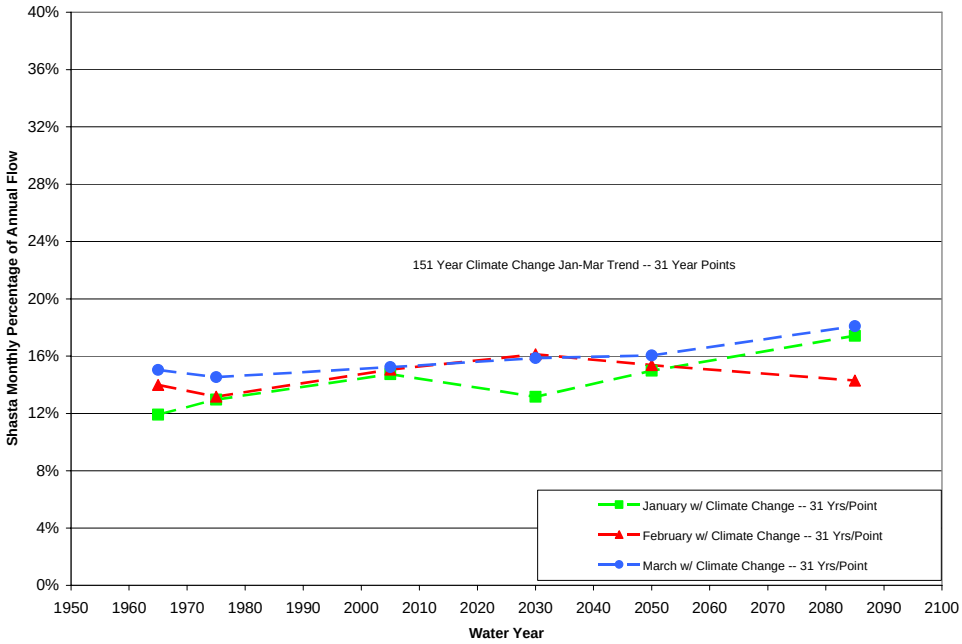

Figure F-2a Data Lumped Showing Points Based On 31-Year Averages

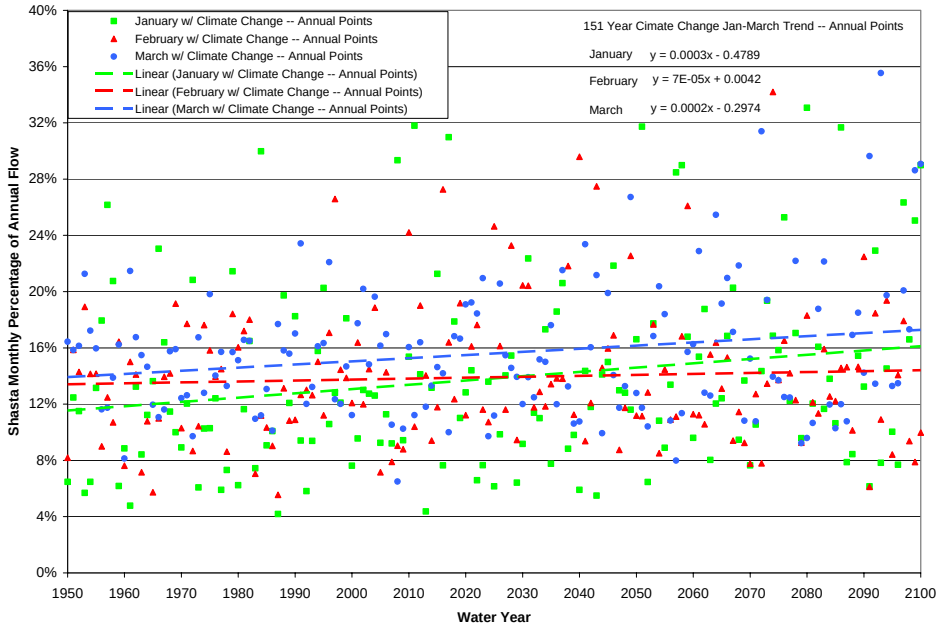

Figure F-2b Data Plotted as Annual Data Points and Fitted With a Least Squares Trend

Figure F-2 Shasta Monthly Inflow Percentages January-March, 1950 to 2100 Under Climate Change Scenario/Model SRESa2, gfdl

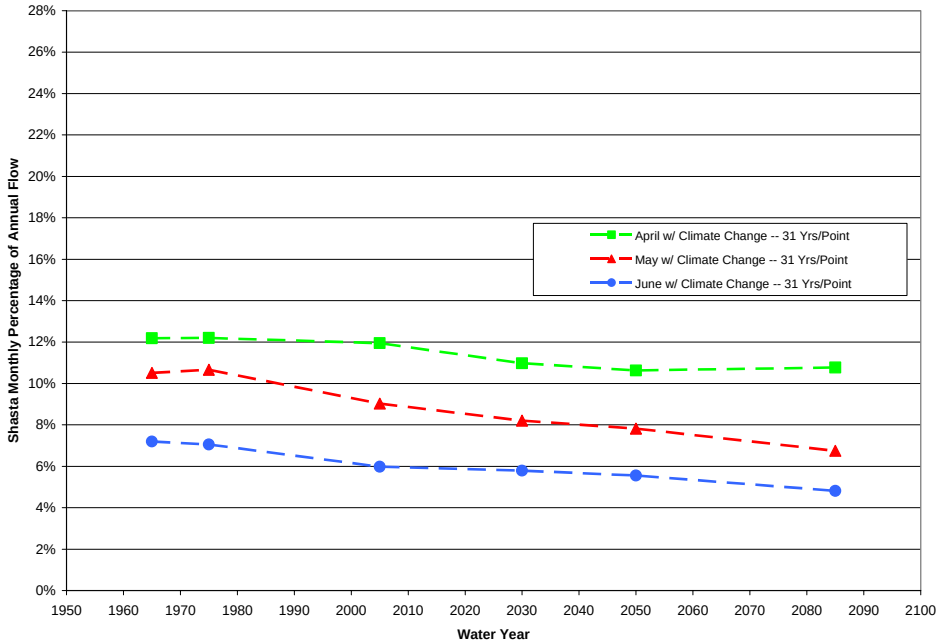

Figure F-3a Data Lumped Showing Points Based On 31-Year Averages

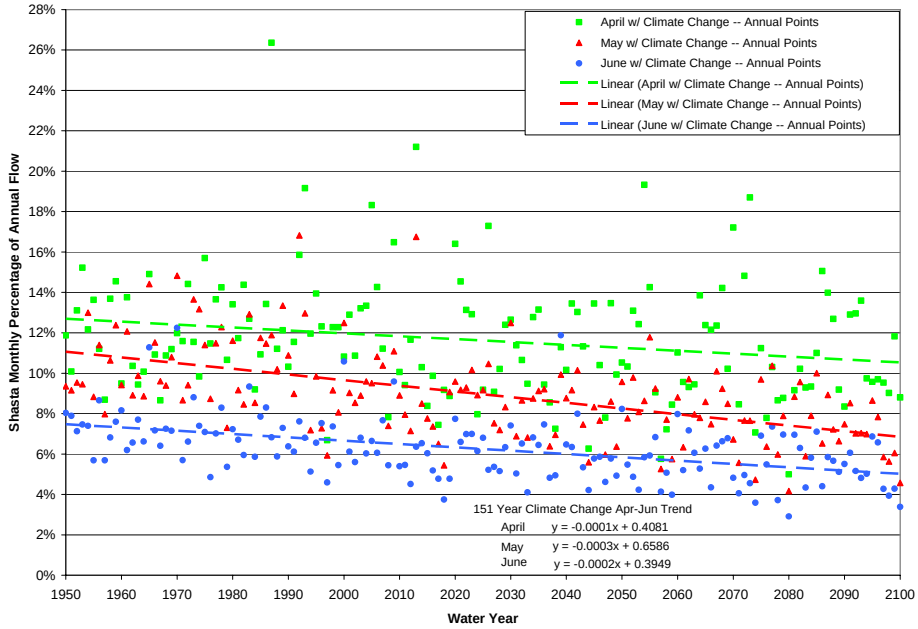

Figure F-3b Data Plotted as Annual Data Points and Fitted With a Least Squares Trend

Figure F-3 Shasta Total Annual Inflow Percentages April-June, 1950 to 2100 Under Climate Change Scenario/Model SRESa2, gfdl

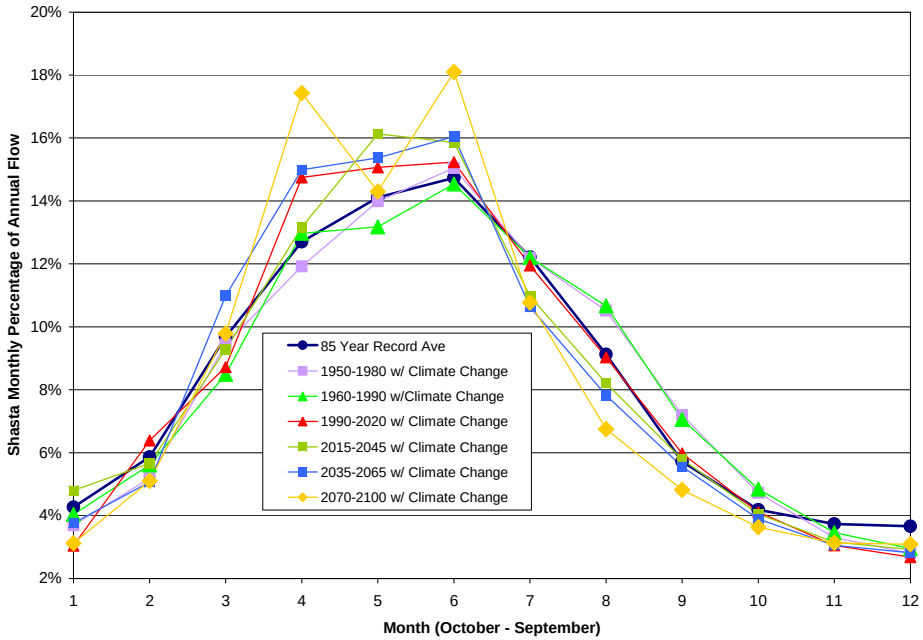

Figure F-4a Percentages from Lumped Points Based On 31-Year Averages

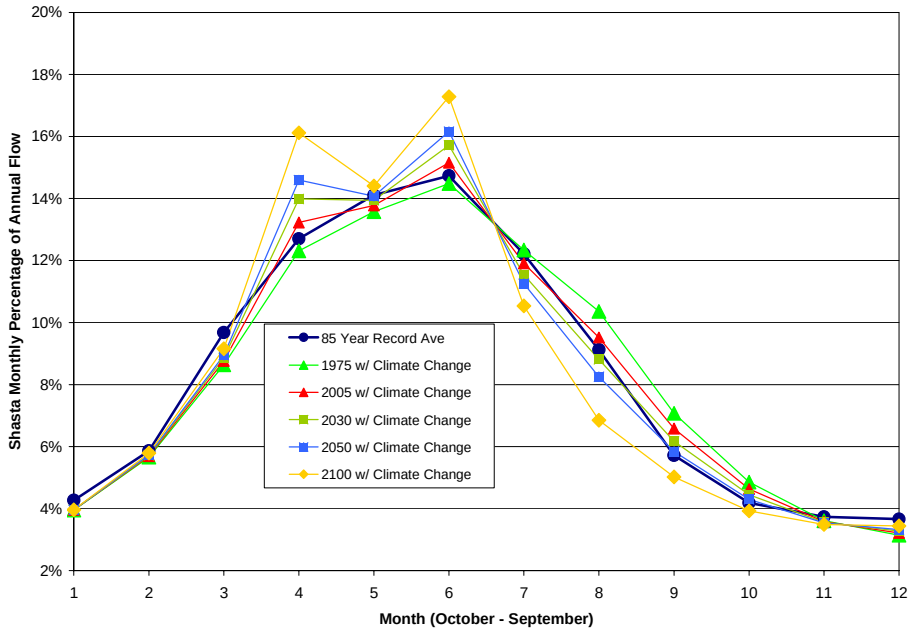

Figure F-4b Percentages Calculated from Trends Analysis of Annual Data Points

Figure F-4 Shasta Monthly Inflow Percentages Under Climate Change Scenario/Model SRESa2, gfdl

An additional important change is made possible by separating the annual flow and monthly percentages parts of the analysis and using "trend" approach. It is now possible to normalize the adjusted historic monthly data (e. g., in the CalSim input) to maintain the trend-indicated percentage of total annual flow for each year in the CalSim input series. For example, when setting up a CalSim Run for 2100, each of CalSim's 82 years of input data can be adjusted first by the appropriate total annual flow percentage for 2100 and then monthly percentage perturbation ratios can be applied. However, the perturbation ratios are likely to change the total annual flow. So it is now possible to readjust the twelve monthly flow values for each year so their sum comes back to the desired total annual flow. This avoids the possibility, when perturbing monthly flows directly, that uncontrolled changes in annual runoff may occur in the perturbation process.

The following steps were defined to implement the climate change trends approach, while preserving the yearly and monthly variations in the observed data used to drive the CalSim water resources model. The only use of the climate change 151-year time series is to detect the trends in total annual flow and monthly flow percentages.

F.3.1 Defining the Base Year

Definition of the base year is an important choice. Ideally, the base year would represent the year immediately prior to the onset of climate change. However, climate change appears to have started some time ago (perhaps slowly) and identification and agreement on a start year is unlikely.

A more practical approach is to focus on a year that is a representative reference year for the available 82 years of CalSim data. The midpoint of this record would be 1962 or 1963, which might be sufficiently far back in time to allow general agreement that climate change had not yet begun substantial acceleration. Another possibility would be to use 1976, since this is the base year previously used by DWR and others. Finally, 2005 might be used as the base year to be consistent with the DRMS anchor year.

Figures F-5a and F-5b provide illustrations for Oroville inflow that may be helpful in discussing which base year to choose. In particular, 1975 as shown in Figure F-5b appears to be quite close to the monthly percentages that are reflected in the 82-year CalSim data series being used for DWR's 2005 base case. This suggests that DWR's 2005 CalSim input data might be used as representative of the *"beginning of significant climate change in 1975."* It will be necessary to consider, in consultation with DWR, whether an adjusted 2005 base case should be developed to reflect climate change that has already occurred since the 1975 base year shown in Figure F-5b. That is attractive since 1976 has been used as a base year in several of the previous analyses. Figure F-5 shows data from only one gaging site – Oroville. Several other rivers need to be analyzed in a manner comparable to Oroville before proceeding with base year selection.

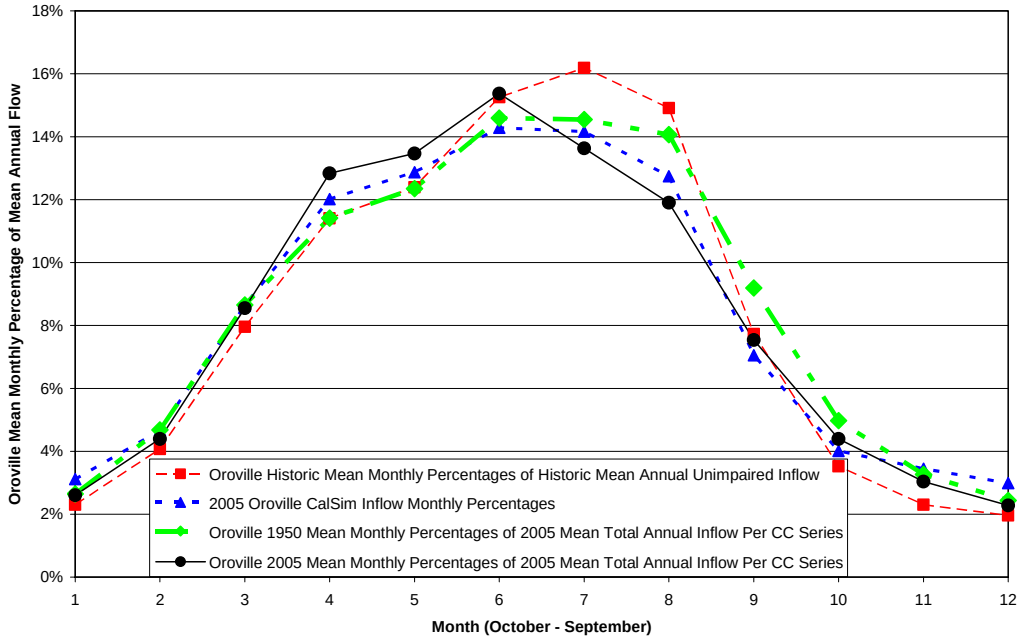

Figure F-5a Oroville Monthly Inflow Percentages Including Climate Change 1950

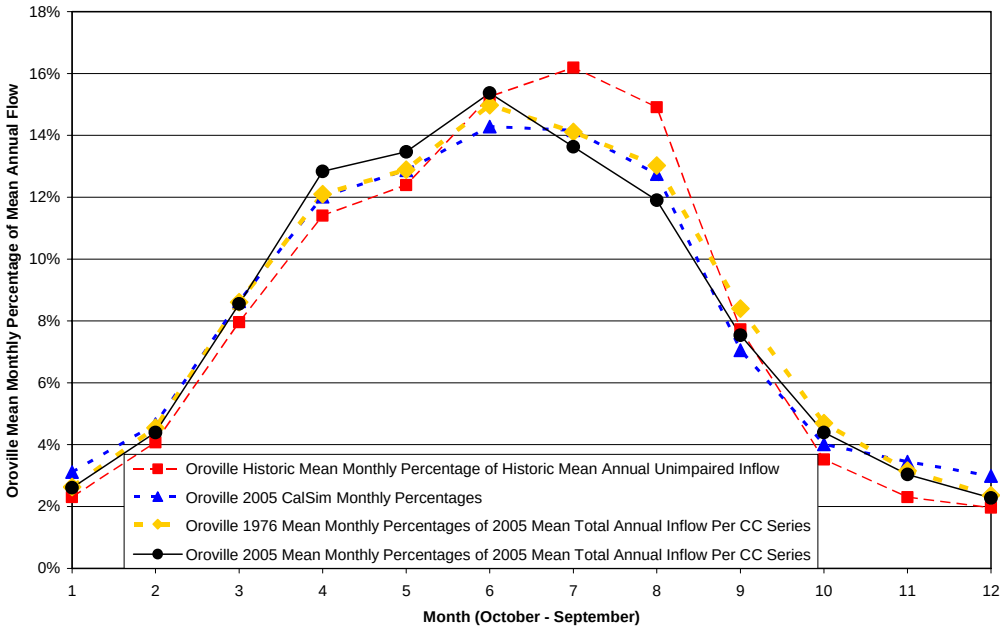

Figure F-5b Oroville Monthly Inflow Percentages Including Climate Change 1975

Figure F-5 Oroville Monthly Inflow Percentages Including Historic, CalSim 2005, and Climate Change 2005 for Considering Base Year Selection

F.3.2 Recognize the Limitations of the Data Sets

The 82 years of CalSim hydrologic data, especially the last 20 to 30 years or, potentially include some impacts of climate change. Ideally, any trend or non-stationary aspect of these data with respect to climate change would be removed. Unfortunately, there is no straightforward, accepted approach for removing these climate change impacts from the data, and such a procedure is not likely to be agreed upon soon. Use of the 1976 base year as a first approximation for "no substantial climate change yet" may be an agreeable first step. The data set also has other limitations – 82 years is not a large sample for a random process with the variability inherent in California hydrology. Furthermore, it is only one realization of the wide variety of sequences of water years that might occur.

The four climate change scenario/model time series have limitations as well. Although the 151 years is a longer record, each is synthetic, is downscaled from coarser results (with recognized uncertainties and opportunity for error), and represents only one of many scenario/model combinations. Each is also only one realization or sample of a random process. It is also a limited example of the variety of sequential arrangements in which water years might occur.

In both cases, these are the only data sets available. Thus, they are the ones that must be used for DRMS analyses.

F.3.3 Perform the Trend Analysis

The trend analysis procedure and example results are presented below in Section F4.

F.3.4 Adjust the CalSim Input Data Set Using the Trend-Indicated Change in Unimpaired Total Annual Flow for Each Gaging Site

For example, trend analysis of the a2/gfdl time series indicates that the year 2100 annual inflows to Oroville will be 85% of those realized for 2005 conditions. Therefore, for the 2100 CalSim a2/gfdl run, the 82 years of CalSim monthly inputs to Oroville would be reduced to 85% of their record values, assuming that the CalSim 2005 base case run properly represents the state of climate change in 2005.

F.3.5 Perturb the Adjusted CalSim Monthly Unimpaired Flows for Each Gaging Site

For example, for Oroville inflow, the trend analysis of the a2/gdfl time series indicates that the May inflow proportion for 2100 conditions will be 64% of that for 2005 conditions. Thus, each of the 82 years of adjusted May data for CalSim input would be further reduced to 64% (of the 85%), or to 54% of the CalSim 2005 May input values.

F.3.6 Normalize the Resulting Monthly Inflows to Meet the Adjusted Annual Inflow

In perturbing each of a year's monthly inflows and then summing them, a different yearly total than that indicated above for the adjusted total annual inflow may be obtained. That is (for the Oroville a2/gfdl 2100 analysis), when the 64% of the May 85% for 1972 is

summed with the results for the other eleven months of the 1972 water year, the total is likely to be different from 85% of the original CalSim annual inflow for that year. Thus, for each site and each water year of CalSim data, an annual sum of the perturbed monthly values is calculated. If the sum is larger or smaller than the initially adjusted annual flow, the monthly values are decreased or increased by the proportion necessary in order to conform with the initially adjusted total annual inflow. This prevents deviation from the adjusted annual estimates and, thus, the method will not be creating or loosing water within a year.

F.3.7 Perform CalSim Runs With the Modified Hydrologic Inputs

The available DWR CalSim model for 2030 level of development and modified hydrologic inflows described above would be used. Some other adjustments may be required to obtain meaningful CalSim outputs, but these would be minimized.

F.4 Trend Analysis

Initial examples of the trend analyses have been completed for all four simulations of Oroville inflow and Shasta inflow. The analytical procedure used for trend analysis of each simulation time series was the following:

- The time series was extended by three months (October through December 1949) so that the 1950 water year numbers could be used.
- The twelve monthly flow values for each water year were summed to get a water year total unimpaired flow.
- A linear trend was fitted for total annual unimpaired flow by least squares (using Microsoft Excel LINEST).
- The annual points and the trend line were plotted to obtain the annual trend diagram; available data for historic unimpaired flows were included on the diagram and a least squares historic trend line was also included for comparison to the simulation results.
- Each simulated monthly flow value was divided by the total annual flow to calculate the percentage of annual unimpaired flow occurring in that month.
- For each of the twelve months, the 151 respective monthly percentage values were fitted with a linear trend line by least squares (using Microsoft Excel LINEST) to obtain the trend for that month's percent of total annual unimpaired flow.
- The trend lines with non-trivial slopes satisfied the 99 percentile test of statistical significance per the F distribution.
- Each trend line (annual and 12 monthly) was used to calculate the trend value in 2005, 2030, 2050, and 2100. The trend lines were also extrapolated to calculate values for 2200, but the extrapolated results are speculative and uncertain. Thus, the 2200 results are not reported or used.

- The numbers calculated for the annual and monthly trend lines in future years are reported as ratios with the calculated 2005 values in a results table. These ratios can be used to adjust total annual flow and to perturb and then normalize the monthly proportions of flow for each year of the CalSim 82-year record in order to obtain CalSim inputs that reflect future climate change.

Figure F-6 presents a comparison of the four scenario/model results for Oroville for a) 2005, b) 2030, c) 2050, and d) 2100. The results are presented as fractions of the overall mean annual inflow for 2005, so that decreases and increases in future annual inflow are reflected in the curves. The mean 2005 curve and the historical record curve are provided for reference. Note the difference between the mean 2005 curve and the historical record curve. It appears that substantial climate change may have already impacted the Feather River Basin above Oroville by 2005.

Figure F-7 presents the annual inflow values and trend lines for Oroville for the four simulations and the historic record. There is overlap with the historic record in each scenario/model simulation for the water years 1950 through 2006, represented by the larger points. Although the overlap period for the simulations is not expected to coincide with historical points exactly because the two series have different random yearly variations, statistical properties of the annual inflows in the overlap period are expected to be and appear to be similar.

Figure F-8 presents the monthly percentage of inflows for Oroville for selected years in the four simulations and for the historic record. In each case there is a general increase in the inflow percentages in winter (especially January through March) and a decrease in the percentages during the spring snow melt period (April through June). Thus, the results suggest there will be less runoff to fill reservoirs after the winter flood control season.

Table F-3 presents the numeric ratios (annual and monthly) for the selected future years divided by 2005 values. They are presented for all four simulations for Oroville.

Figure F-9 presents the comparison of the four simulation results for Shasta in a) 2005, b) 2030, c) 2050, and d) 2100. Note that there is less difference between the mean 2005 curve and historical curve than there was for Oroville. Figure F-10 presents the annual inflows to Shasta and Figure F-11 presents the monthly percentages for Shasta. Table F-4 presents the future-year annual and monthly ratios to 2005 values for Shasta.

Further analyses for other sites and the CalSim analyses that would logically follow have not been performed. It is believed that at least eight and perhaps twelve of the other 21 sites must be analyzed to make meaningful adjustments to CalSim inputs.

F.5 Effects on Water Supply

CalSim must be run with altered inflow inputs to estimate the impacts of a particular scenario/model on water supply availability for any given future year. This is a challenging undertaking because CalSim does not use unimpaired flows as direct input. Appropriate supplemental assumptions and adjustments will likely be required within CalSim to obtain meaningful results. Even with these adjustments, some systematic error

due to essential approximations is anticipated. An additional need is to evaluate whether changes in precipitation, temperature, runoff and evapotranspiration downstream of the principal reservoirs (i.e., in the Sacramento Valley) are essential input modifications for purpose of knowing what stored water is available to address levee breach incidents (see WAM Appendix G).

CalSim should be run at least 12 times – for each combination of model/scenario and each future year of interest (2030, 2050, and 2100). Four additional runs may be needed (for 2005) if an earlier base year is selected. Because of the priority required to develop the WAM calculator, this work has not begun.

F.6 Effects on Delta Levee Breach Water Conditions

The WAM calculator is designed to use CalSim outputs to estimate the water management and Delta inflow consequences of levee breach incidents. When the climate-change-altered CalSim results and resulting Delta inflows are combined with the projected amounts of sea level rise (for the given scenario/model and target year) and their expected impacts on Delta hydrodynamics (see Appendix H), the WAM calculator will be able to calculate the consequences for any defined levee breach sequence on Delta water quality and exports.

F.7 References

CEPA, 2006a. California Environmental Protection Agency. Climate Action Team Report to Governor Schwarzenegger and the California Legislature. March, 2006.

CEPA, 2006b. California Environmental Protection Agency. Climate Action Team Report to Governor Schwarzenegger and the California Legislature. Appendix – Climate Scenarios for California. March, 2006. Also available as Cayan, D., E. Maurer, M. Dettinger, M. Tyree, K. Hayhoe, C. Bonfils, P. Duffy, and B. Santer, 2006b: Climate Change Scenarios for California; appendix to the California Energy Commission report # CEC-500-2005-203-SF, available at: http://www.energy.ca.gov/2005publications/CEC-500-2005-203/CEC-500-2005-203-SF.PDF

DRMS, 2007. Technical Memorandum: Delta Risk Management Strategy (DRMS) Phase 1, Topical Area: Climate Change. Prepared by URS Corporation/Jack R. Benjamin & Associates, Inc. Prepared for Department of Water Resources. January, 2007 (Draft)

DWR, 2006. California Department of Water Resources. Progress on Incorporating Climate Change into Management of California's Water Resources, Technical Memorandum Report. July, 2006.

DWR/USBR, 2002. California Department of Water Resources and U. S. Bureau of Reclamation. "CalSimII Benchmark Studies Assumptions." As cited by Vicuna (2006).

IPCC, 2000. Intergovernmental Panel on Climate Change. Special Report on Emissions Scenarios. Adopted March 2000. Available at: http://www.grida.no/climate/ipcc/emission/index.htm

Joyce et al, 2006. Brian Joyce, Sebastian Vicuna, Larry Dale, John Dracup, Michael Hanemann, David Purkey, and David Yates. "Climate Change Impacts on Water for Agriculture In California: A Case Study in the Sacramento Valley." A Report From: California Climate Change Center. CEC-500-2005-194-SF. Included as an appendix in the Climate Action Team Final Report, p737. March 2006.

Lund et al, 2003. Jay R. Lund, R. E. Howitt, M. W. Jenkins, T. Zhu, S. K. Tanaka, M. Pulido, M. Tauber, R. Ritzema, and I. Ferriera. "Climate Warming and California's Water Future." Report 03-1. Center for Environmental and Water Resources Engineering, University of California, Davis. March, 2003. Available: http://cee.engr.ucdavis.edu/faculty/lund/CALVIN/ReportCEC/CECReport2003.pdf

Miller et al, 2001. Norman L. Miller, Kathy E. Bashford & Eric Strem. "Climate Change Sensitivity Study of California Hydrology – A Report to the California Energy Commission." LBNL Technical Report No. 49110. November 2001.

Medellin et al, 2006. Josue Medellin, Julien Harou, Marcelo Olivares, Jay Lund, Richard Howitt, Stacy Tanaka, Marion Jenkins, Kaveh Madani, & TinjuZhu. "Climate Warming and Water Supply Management in California." A Report From: California Climate Change Center. CEC-500-2005-195-SF. Included as an appendix in the Climate Action Team Final Report, p822. March 2006.

Tanaka et al, 2006. Stacy K. Tanaka, T. Zhu, J. R. Lund, R.E. Howitt, M. W. Jenkins, M. A. Pulido, M. Tauber, R. S. Ritzema, and I. C. Ferreita. "Climatic Warming and Water Management Adaptation for California." *Climatic Change.*

Vicuna, 2006. Sebastian Vicuna. "Predictions of Climate Change Impacts on California Water Resources Using CalSim II: A Technical Note." A Report from: California Climate Change Center. CEC-500-2005-200-SF. Included as an appendix in the Climate Action Team Final Report, p1099. February 2006.

Yates et al, 2005. D. Yates, D. Purkey, A. Huber-Lee, H. Galbraith, J. West & S. Herrod-Julius. A Physically-Based, Water Resource Planning Model of the Sacramento Basin, California, USA. ASCE Journal of Water Resource Management. In Press.

Zhu et al, 2005. Tingju Zhu, Marion W. Jenkins & Jay R. Lund. "Estimated Impacts of Climate Warming on California Water Availability Under Twelve Future Climate Scenarios." Journal AWRA, p.1027, October 2005.

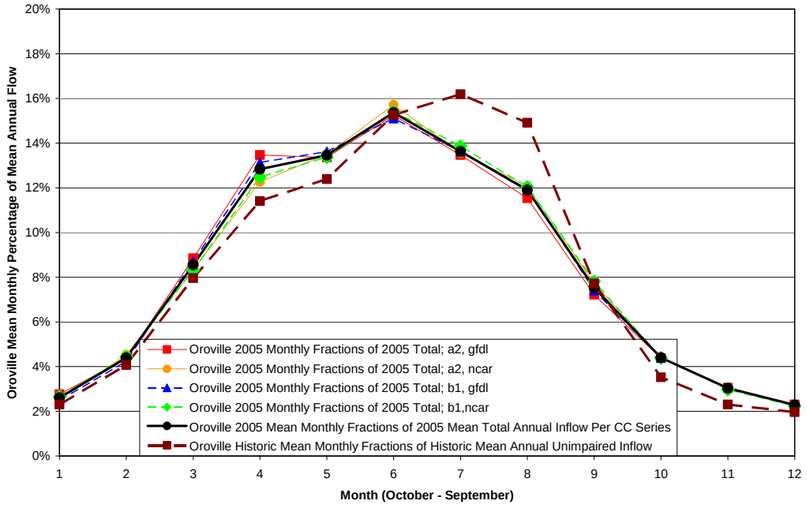

Figure F-6a Oroville 2005

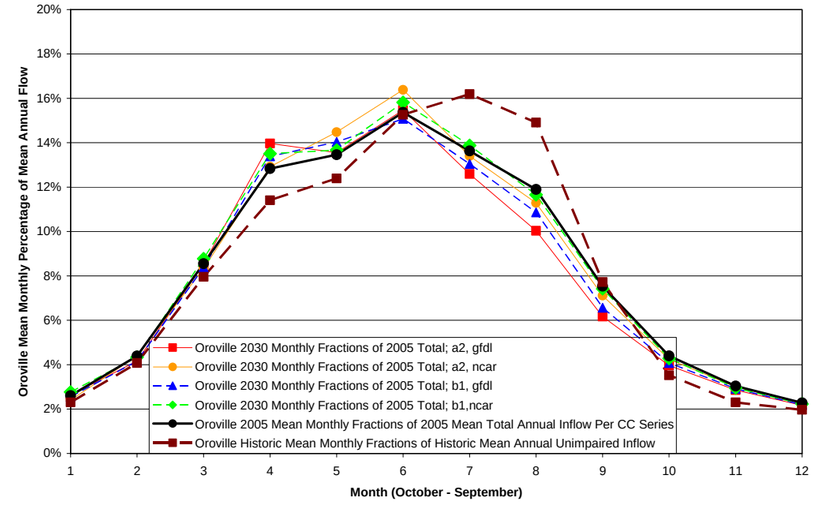

Figure F-6b Oroville 2030

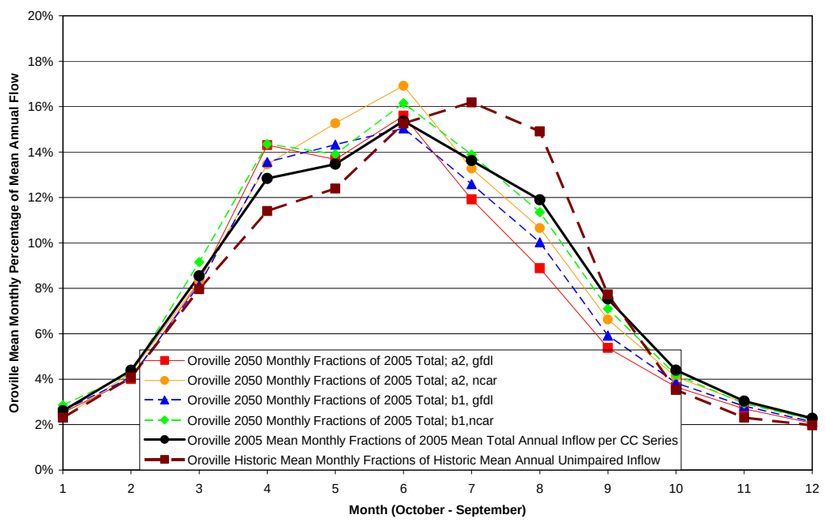

Figure F-6c Oroville 2050

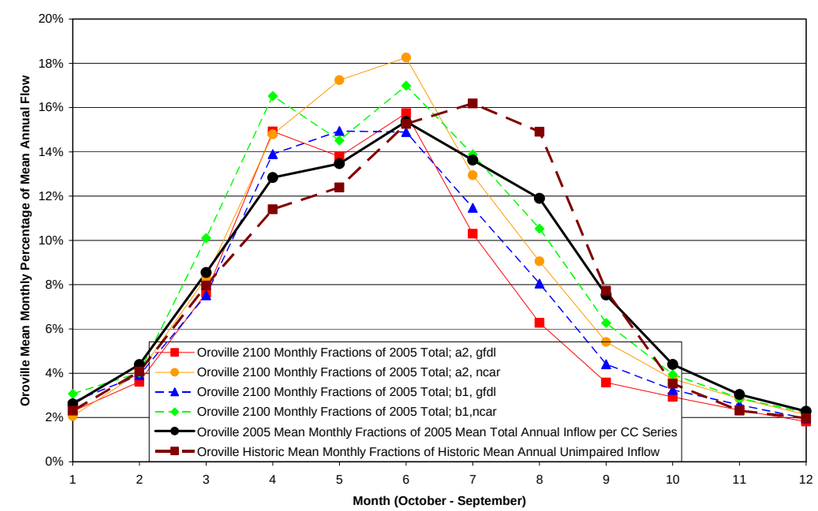

Figure F-6d Oroville 2100

Figure F-6 Oroville Monthly Inflow Percentages Including Climate Change

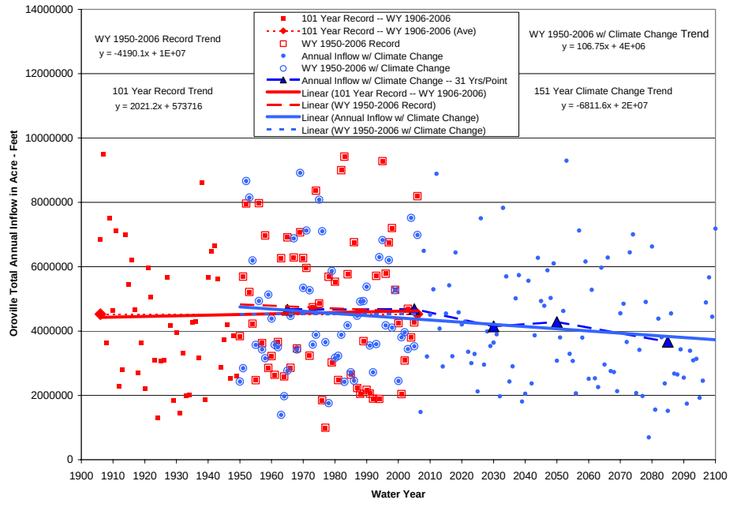

Figure F-7a Oroville SRES a2, gfdl

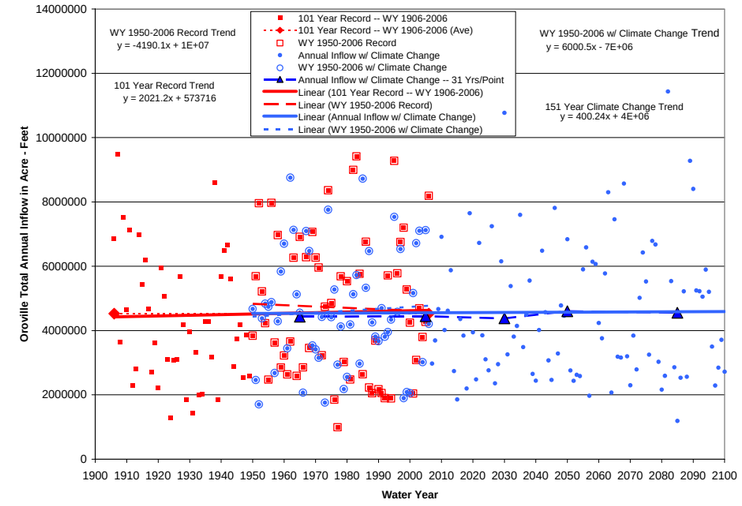

Figure F-7b Oroville SRES a2, ncar/pcm

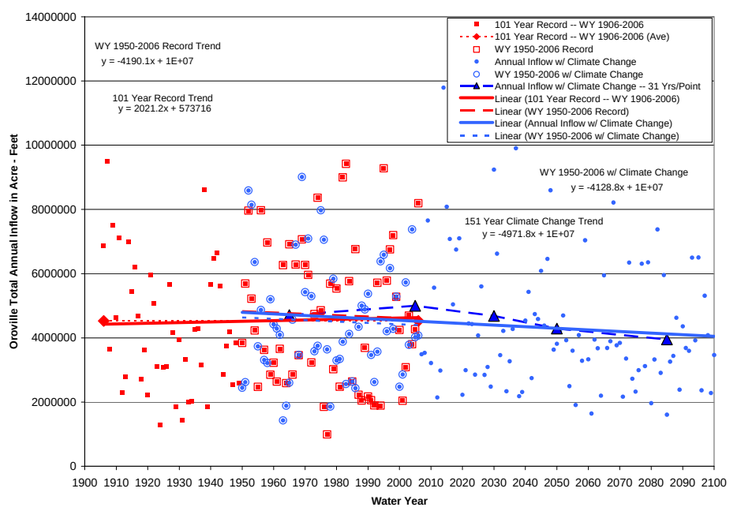

Figure F-7c Oroville SRES b1, gdfl

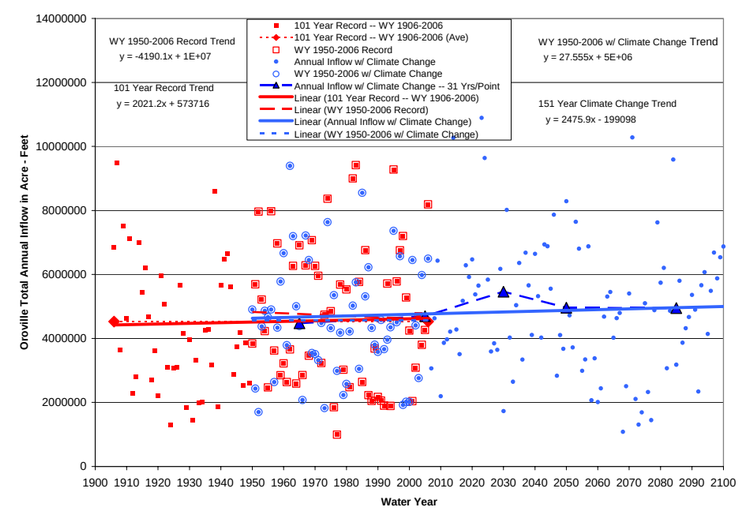

Figure F-7d Oroville SRES b1, ncar/pcm

Figure F-7 Oroville Annual Unimpaired Inflow – Historic and with Climate Change

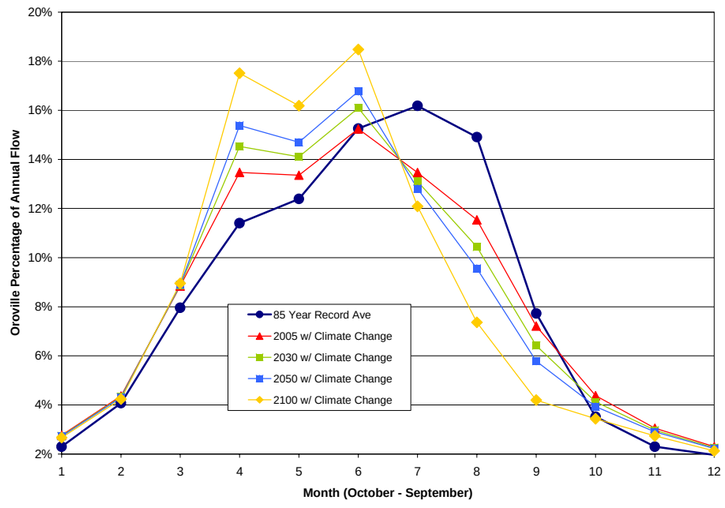

Figure F-8a Oroville SRES a2, gfdl

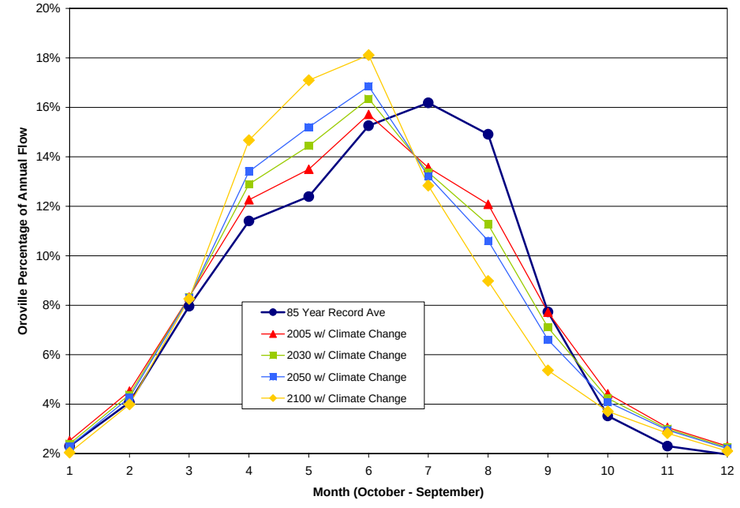

Figure F-8b Oroville SRES a2, ncar/pcm

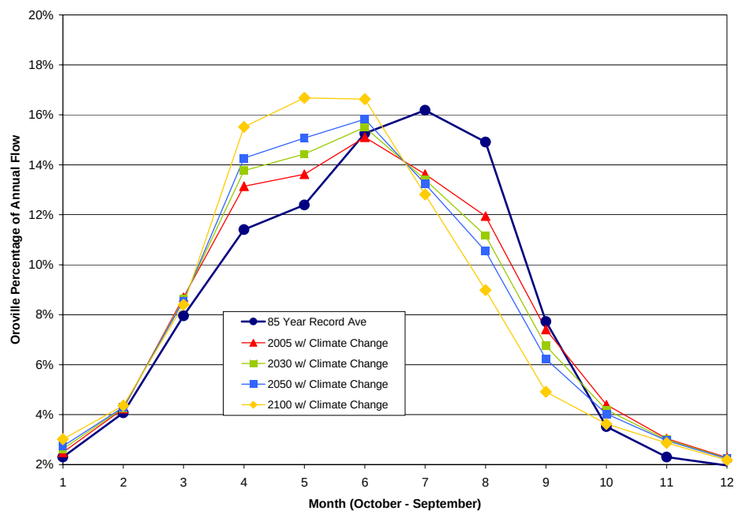

Figure F-8c Oroville SRES b1, gdfl

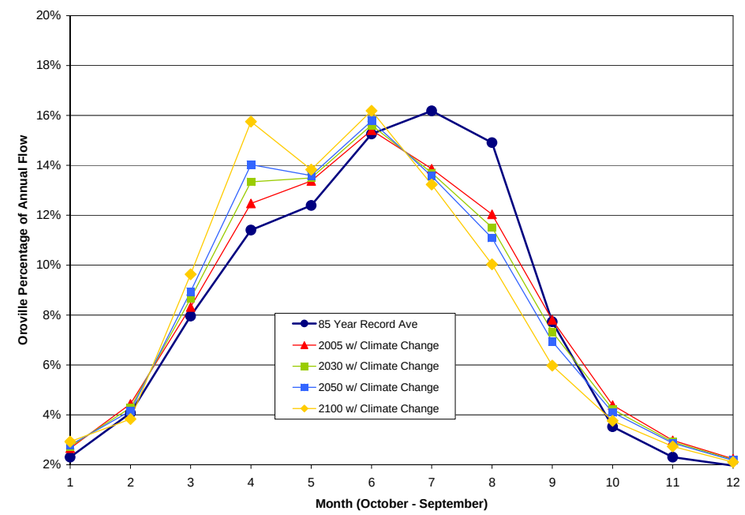

Figure F-8d Oroville SRES b1, ncar/pcm

Figure F-8 Oroville Monthly Inflow Percentages – Historic and with Climate Change

Table F-3 Oroville Fractions and Ratios – with Climate Change Scenarios/Models

Table F-3a. Oroville SRES a2, gfdl

Ratios to 2005 Value					Mean Fractions of Mean Annual 2005 Inflows				
Measusre	**2030**	**2050**	**2100**		**Month**	**2005**	**2030**	**2050**	**2100**
Annual Inflow	0.96	0.93	0.85		Annual Inflow	1.00	0.961	0.930	0.852
October %	0.99	0.98	0.97		October	0.028	0.026	0.025	0.023
November %	0.99	0.99	0.97		November	0.044	0.042	0.040	0.036
December %	1.00	1.01	1.01		December	0.088	0.085	0.083	0.076
January %	1.08	1.14	1.30		January	0.135	0.140	0.143	0.149
February %	1.06	1.10	1.21		February	0.134	0.136	0.137	0.138
March %	1.06	1.10	1.21		March	0.152	0.155	0.156	0.157
April %	0.97	0.95	0.90		April	0.135	0.126	0.119	0.103
May %	0.90	0.83	0.64		May	0.115	0.100	0.089	0.063
June %	0.89	0.80	0.58		June	0.072	0.062	0.054	0.036
July %	0.94	0.90	0.79		July	0.044	0.040	0.037	0.029
August %	0.97	0.95	0.90		August	0.031	0.029	0.027	0.023
September %	0.98	0.97	0.93		September	0.023	0.022	0.021	0.018
					Sum of Months	1.000	0.961	0.930	0.852

Table F-3b. Oroville SRES a2, ncar/pcm

Inflow Ratios to 2005					Mean Fractions of Mean Annual 2005 Inflows				
Measusre	**2030**	**2050**	**2100**		**Month**	**2005**	**2030**	**2050**	**2100**
Annual Inflow	1.00	1.00	1.01		Annual Inflow	1.00	1.002	1.004	1.008
October %	0.95	0.91	0.81		October	0.025	0.024	0.023	0.021
November %	0.97	0.94	0.88		November	0.045	0.044	0.043	0.040
December %	1.00	1.00	0.99		December	0.083	0.083	0.083	0.083
January %	1.05	1.09	1.20		January	0.123	0.129	0.135	0.148
February %	1.07	1.13	1.27		February	0.135	0.145	0.153	0.172
March %	1.04	1.07	1.15		March	0.157	0.164	0.169	0.183
April %	0.99	0.97	0.95		April	0.136	0.134	0.133	0.129
May %	0.93	0.88	0.74		May	0.121	0.113	0.107	0.091
June %	0.92	0.86	0.70		June	0.077	0.071	0.066	0.054
July %	0.96	0.92	0.84		July	0.044	0.042	0.041	0.037
August %	0.98	0.96	0.92		August	0.031	0.030	0.030	0.029
September %	0.98	0.96	0.91		September	0.023	0.023	0.022	0.021
					Sum of Months	1.000	1.002	1.004	1.008

Table F-3c. Oroville SRES b1, gfdl

Inflow Ratios to 2005					Mean Fractions of Mean Annual 2005 Inflows				
Measusre	**2030**	**2050**	**2100**		**Month**	**2005**	**2030**	**2050**	**2100**
Annual Inflow	0.97	0.95	0.90		Annual Inflow	1.00	0.973	0.951	0.896
October %	1.06	1.10	1.21		October	0.025	0.026	0.026	0.027
November %	1.01	1.01	1.03		November	0.042	0.042	0.041	0.039
December %	0.99	0.98	0.97		December	0.087	0.084	0.081	0.075
January %	1.05	1.09	1.18		January	0.131	0.134	0.136	0.139
February %	1.06	1.11	1.22		February	0.136	0.140	0.143	0.149
March %	1.03	1.05	1.10		March	0.151	0.151	0.150	0.149
April %	0.98	0.97	0.94		April	0.136	0.130	0.126	0.115
May %	0.93	0.88	0.75		May	0.119	0.109	0.100	0.080
June %	0.91	0.84	0.66		June	0.074	0.066	0.059	0.044
July %	0.95	0.92	0.83		July	0.044	0.041	0.038	0.032
August %	0.98	0.97	0.94		August	0.030	0.029	0.028	0.026
September %	0.99	0.98	0.96		September	0.023	0.022	0.021	0.020
					Sum of Months	1.000	0.973	0.951	0.896

Table F-3d. Oroville SRES b1, ncar/pcm

Inflow Ratios to 2005					Mean Fractions of Mean Annual 2005 Inflows				
Measusre	**2030**	**2050**	**2100**		**Month**	**2005**	**2030**	**2050**	**2100**
Annual Inflow	1.01	1.02	1.05		Annual Inflow	1.00	1.013	1.023	1.049
October %	1.03	1.05	1.10		October	0.027	0.028	0.029	0.031
November %	0.96	0.94	0.86		November	0.044	0.043	0.043	0.040
December %	1.04	1.07	1.16		December	0.083	0.088	0.091	0.101
January %	1.07	1.12	1.26		January	0.125	0.135	0.144	0.165
February %	1.01	1.02	1.03		February	0.134	0.137	0.139	0.145
March %	1.01	1.02	1.05		March	0.154	0.158	0.161	0.170
April %	0.99	0.98	0.95		April	0.139	0.139	0.139	0.139
May %	0.96	0.92	0.83		May	0.120	0.117	0.113	0.105
June %	0.94	0.89	0.77		June	0.078	0.074	0.071	0.063
July %	0.96	0.93	0.86		July	0.044	0.043	0.042	0.039
August %	0.98	0.96	0.92		August	0.030	0.030	0.029	0.029
September %	0.98	0.97	0.94		September	0.022	0.022	0.022	0.022
					Sum of Months	1.000	1.013	1.023	1.049

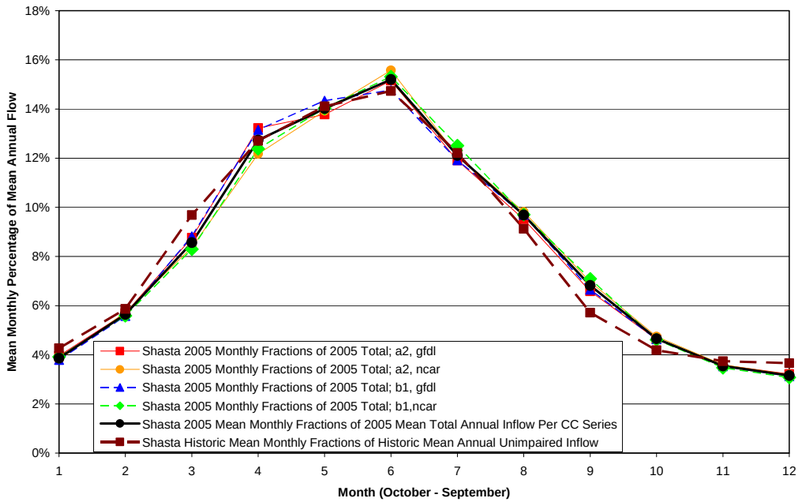

Figure F-9a Shasta 2005

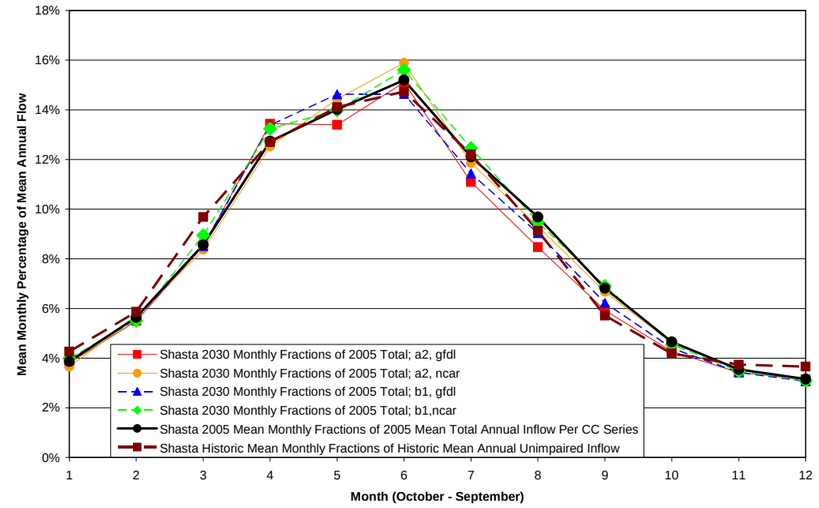

Figure F-9b Shasta 2030

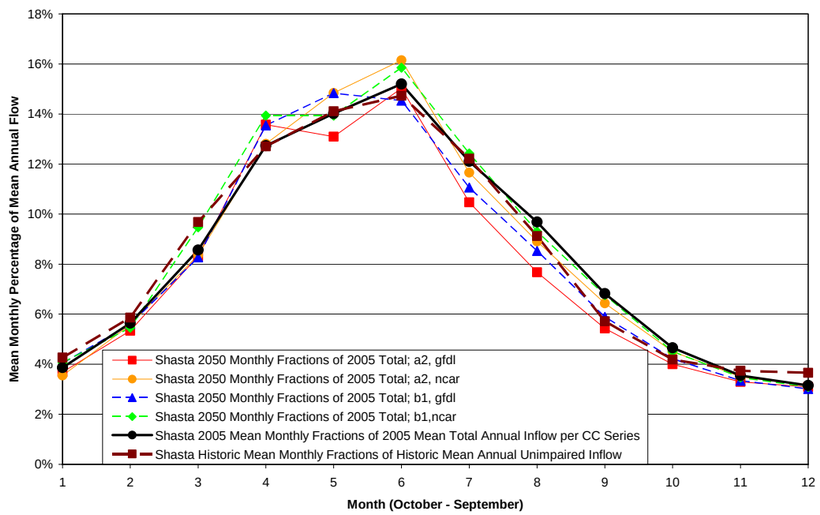

Figure F-9c Shasta 2050

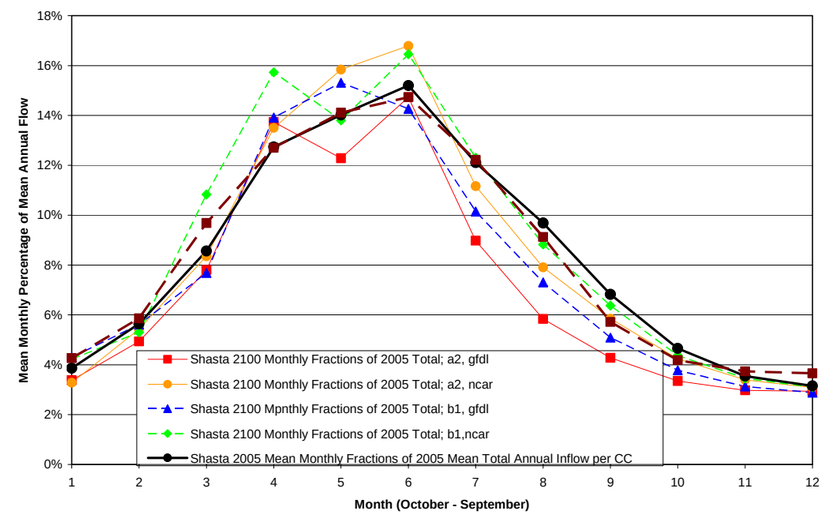

Figure F-9d Shasta 2100

Figure F-9 Shasta Monthly Inflow Percentages Including Climate Change

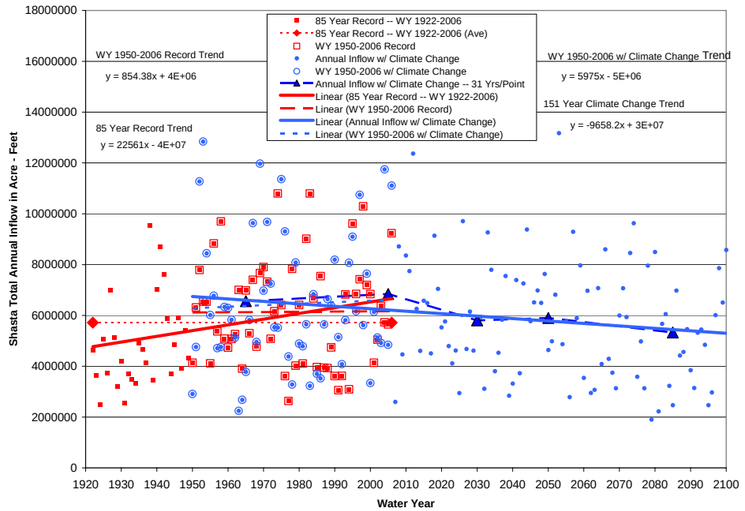

Figure F-10a Shasta SRES a2, gfdl

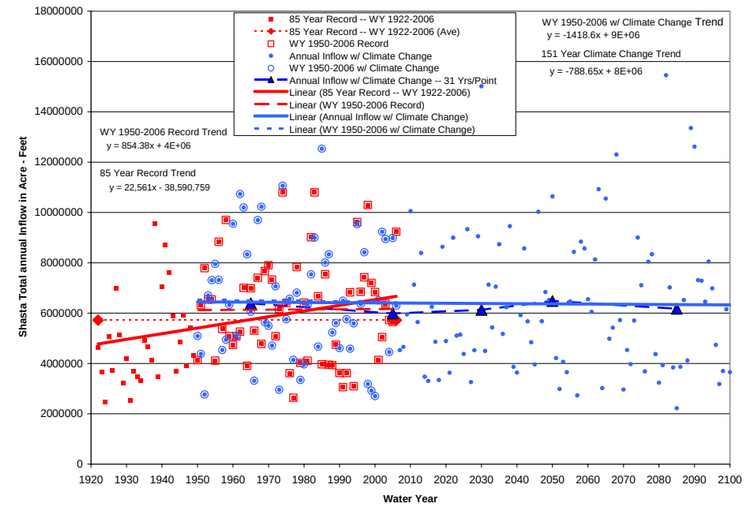

Figure F-10b Shasta SRES a2, ncar/pcm

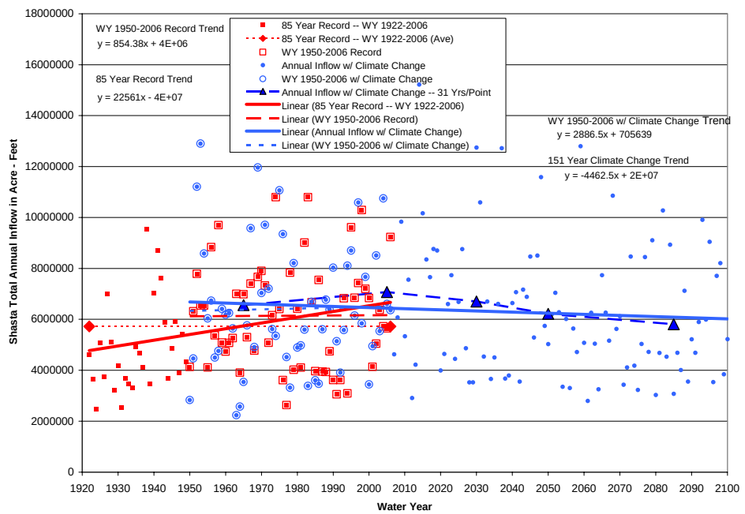

Figure F-10c Shasta SRES b1, gdfl

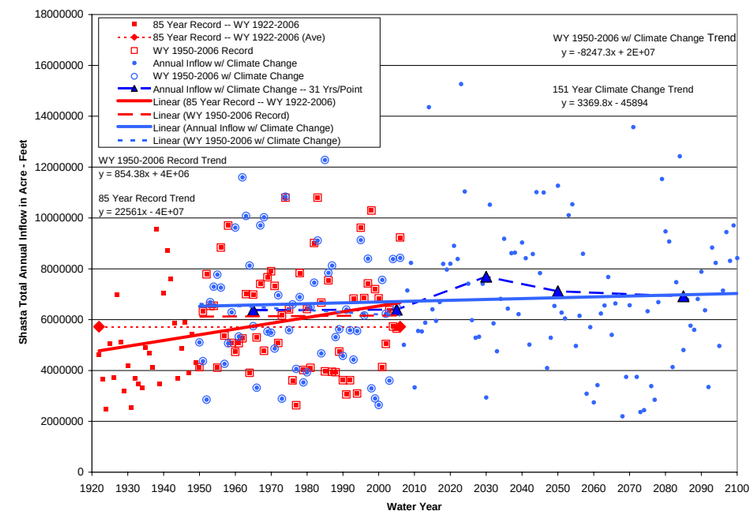

Figure F-10d Shasta SRES b1, ncar/pcm

Figure F-10 Shasta Annual Unimpaired Inflow – Historic and with Climate Change

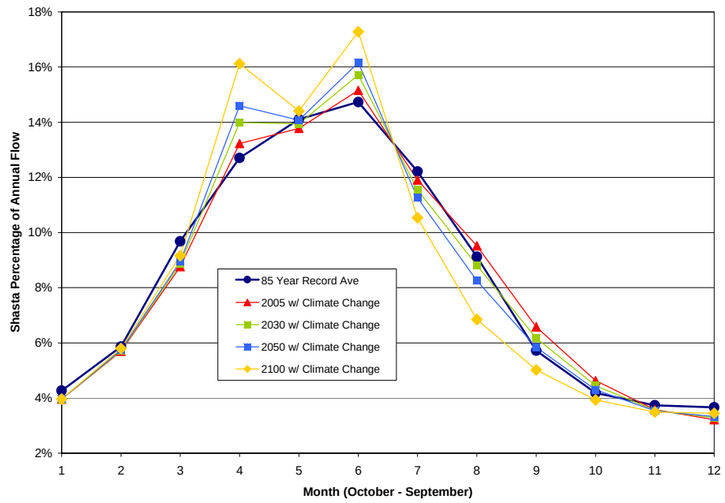

Figure F-11a Shasta SRES a2, gfdl

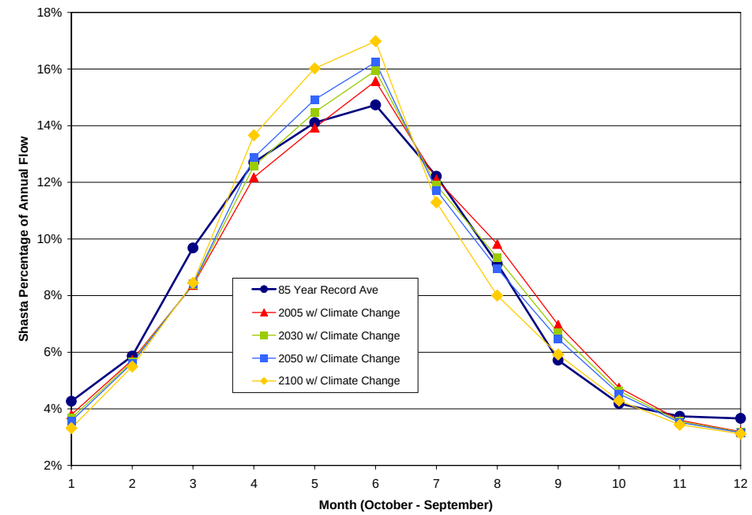

Figure F-11b Shasta SRES a2, ncar/pcm

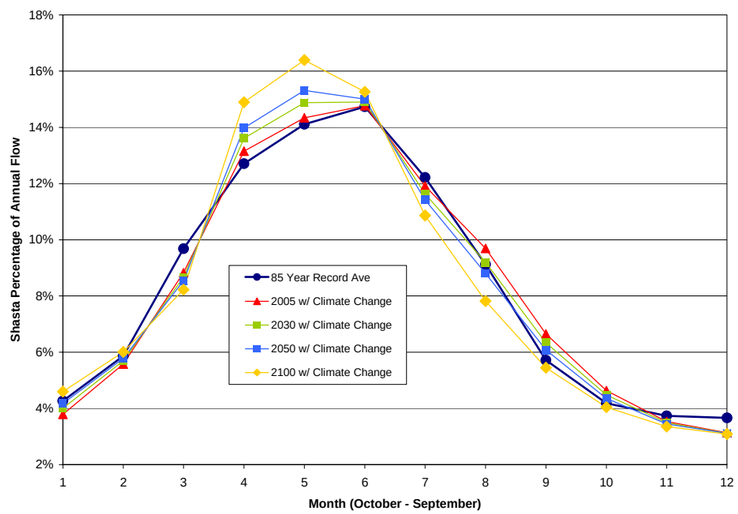

Figure F-11c Shasta SRES b1, gdfl

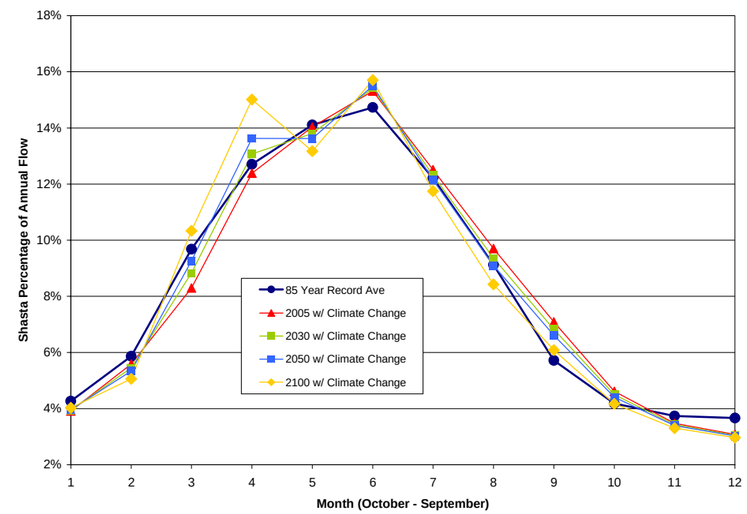

Figure F-11d Shasta SRES b1, ncar/pcm

Figure F-11 Shasta Monthly Inflow Percentages – Historic and with Climate Change

Table F-4 Shasta Fractions and Ratios – with Climate Change Scenarios/Model

Table F-4a. Shasta SRES a2, gfdl

Inflow Ratios to 2005					Mean Fractions of Mean Annual 2005 Inflows				
Measusre	**2030**	**2050**	**2100**		**Month**	**2005**	**2030**	**2050**	**2100**
Annual Inflow	0.96	0.93	0.85		Annual Inflow	1.00	0.961	0.930	0.852
October %	1.00	1.00	1.00		October	0.040	0.038	0.037	0.034
November %	1.00	1.01	1.02		November	0.057	0.055	0.053	0.049
December %	1.01	1.02	1.05		December	0.088	0.085	0.083	0.078
January %	1.06	1.10	1.22		January	0.132	0.134	0.136	0.137
February %	1.01	1.02	1.05		February	0.138	0.134	0.131	0.123
March %	1.04	1.07	1.14		March	0.152	0.151	0.150	0.147
April %	0.97	0.95	0.88		April	0.119	0.111	0.105	0.090
May %	0.93	0.87	0.72		May	0.095	0.085	0.077	0.058
June %	0.94	0.89	0.76		June	0.066	0.059	0.054	0.043
July %	0.96	0.93	0.85		July	0.046	0.043	0.040	0.033
August %	0.99	0.99	0.98		August	0.036	0.034	0.033	0.030
September %	1.02	1.03	1.07		September	0.032	0.031	0.031	0.029
					Sum of Months	1.000	0.961	0.930	0.852

Table F-4b. Shasta SRES a2, ncar/pcm

Inflow Ratios to 2005					Mean Fractions of Mean Annual 2005 Inflows				
Measusre	**2030**	**2050**	**2100**		**Month**	**2005**	**2030**	**2050**	**2100**
Annual Inflow	1.00	0.99	0.99		Annual Inflow	1.00	0.997	0.994	0.988
October %	0.97	0.94	0.87		October	0.038	0.037	0.036	0.033
November %	0.99	0.98	0.96		November	0.057	0.056	0.056	0.054
December %	1.00	1.00	1.01		December	0.084	0.084	0.084	0.084
January %	1.03	1.06	1.12		January	0.122	0.125	0.128	0.135
February %	1.04	1.07	1.15		February	0.139	0.144	0.148	0.158
March %	1.02	1.04	1.09		March	0.156	0.159	0.162	0.168
April %	0.98	0.97	0.93		April	0.121	0.119	0.117	0.112
May %	0.95	0.91	0.81		May	0.098	0.093	0.089	0.079
June %	0.96	0.93	0.85		June	0.070	0.067	0.064	0.059
July %	0.97	0.95	0.90		July	0.047	0.046	0.045	0.042
August %	0.99	0.98	0.96		August	0.036	0.035	0.035	0.034
September %	0.99	0.99	0.98		September	0.032	0.032	0.031	0.031
					Sum of Months	1.000	0.997	0.994	0.988

Table F-4c. Shasta SRES b1, gfdl

Inflow Ratios to 2005					Mean Fractions of Mean Annual 2005 Inflows				
Measusre	**2030**	**2050**	**2100**		**Month**	**2005**	**2030**	**2050**	**2100**
Annual Inflow	0.98	0.97	0.93		Annual Inflow	1.00	0.983	0.969	0.934
October %	1.06	1.10	1.21		October	0.038	0.039	0.040	0.043
November %	1.02	1.04	1.08		November	0.056	0.056	0.056	0.056
December %	0.98	0.97	0.93		December	0.088	0.085	0.083	0.077
January %	1.03	1.06	1.13		January	0.132	0.134	0.135	0.139
February %	1.04	1.07	1.14		February	0.143	0.146	0.148	0.153
March %	1.01	1.02	1.03		March	0.148	0.146	0.145	0.143
April %	0.98	0.96	0.91		April	0.119	0.114	0.111	0.101
May %	0.95	0.91	0.81		May	0.097	0.090	0.085	0.073
June %	0.95	0.91	0.82		June	0.066	0.062	0.059	0.051
July %	0.97	0.94	0.87		July	0.046	0.044	0.042	0.038
August %	0.99	0.98	0.95		August	0.035	0.034	0.033	0.031
September %	1.00	0.99	0.99		September	0.031	0.031	0.030	0.029
					Sum of Months	1.000	0.983	0.969	0.934

Table F-4d. Shasta SRES b1, ncar/pcm

Inflow Ratios to 2005					Mean Fractions of Mean Annual 2005 Inflows				
Measure	**2030**	**2050**	**2100**		**Month**	**2005**	**2030**	**2050**	**2100**
Annual Inflow	1.01	1.02	1.05		Annual Inflow	1.00	1.013	1.023	1.048
October %	1.01	1.01	1.03		October	0.039	0.040	0.041	0.042
November %	0.98	0.96	0.91		November	0.056	0.055	0.055	0.053
December %	1.06	1.12	1.25		December	0.083	0.089	0.095	0.108
January %	1.06	1.10	1.21		January	0.124	0.132	0.139	0.157
February %	0.98	0.97	0.94		February	0.140	0.140	0.139	0.138
March %	1.01	1.01	1.03		March	0.153	0.156	0.158	0.165
April %	0.98	0.97	0.94		April	0.125	0.125	0.124	0.123
May %	0.97	0.94	0.87		May	0.097	0.095	0.093	0.088
June %	0.96	0.93	0.86		June	0.071	0.069	0.068	0.064
July %	0.97	0.95	0.90		July	0.046	0.046	0.045	0.044
August %	0.99	0.98	0.95		August	0.035	0.035	0.035	0.035
September %	0.99	0.98	0.96		September	0.031	0.031	0.031	0.031
					Sum of Months	1.000	1.013	1.023	1.048

Appendix G
Future Conditions – Precipitation, Temperature and CO_2 Concentration Impacts on Water Supply and Use

Table of Contents

G1. Introduction G-1
G2. Climate Change Data Needs for WAM Input G-1
G3. Status of Climate Change Inputs G-2
G4. References G-2

Acronyms and Abbreviations

CalSim	California Water System Simulation Model (DWR & USBR)
CO_2	Carbon Dioxide
DRMS	Delta Risk Management Strategy
DWR	California Department of Water Resources
gfdl	Geophysical Fluid Dynamics Laboratory
ncar	National Center for Atmospheric Research
NDAL	Net Delta Area Losses (or Net Delta Consumptive Water Use)
pcm	Parallel Climate Model
SRES	Special Report on Emissions Scenarios
SRESa2	SRES Scenario a2
SRESb1	SRES Scenario b1
TM	Technical Memorandum
USBR	United States Bureau of Reclamation
WAM	Water Analysis Module or Model

G1. Introduction

Greenhouse gases, principally carbon dioxide (CO_2), are generally regarded as the main driver of climate change (DRMS, 2007). The general impacts of climate change relevant here are alterations of temperature (generally, region-wide warming) and changes in precipitation amounts, distribution, and timing. Also, CO_2 concentrations are thought to influence the amount of water consumed by plant transpiration (DWR, 2006). Higher CO_2 apparently reduces plant transpiration, thus compensating to some degree for the higher transpiration that would be expected with higher temperatures. These factors may result in changed availability of and demand for water supply going beyond the streamflow impacts discussed previously in Appendix F, although these additional changes are thought to be less dramatic. The purpose of this portion of the Water Analysis Module (WAM) Technical Memorandum is to recognize these factors and to provide for incorporating them into the DRMS/WAM analysis of water-supply related impacts that contribute to the risks from Delta levee failures in future years.

G2. Climate Change Data Needs for WAM Input

For each of the four (alternative) simulations of future Central Valley unimpaired runoff that are available, the Climate Change Team (DRMS, 2007) is expected to provide future year CO_2 concentrations, temperature increases and precipitation changes for the years to be addressed by the risk analysis (2005, 2030, 2050, and 2100). These can be used to calculate additional impacts pertaining to water supply availability as follows**:**

1. **Net Delta Area Losses –** One submodel in the WAM calculator estimates the Net Delta Area Losses (NDAL) from plant transpiration, plant and soil evaporation and water surface evaporation, net of precipitation. For each future-year risk calculation, the WAM calculator needs Delta-wide input information on atmospheric CO_2 concentration, ambient air temperature, and precipitation. Annual CO_2 concentrations are adequate, since seasonal variations are expected to be minor. Changes from 2005 ambient temperatures and precipitation on a seasonal (or preferably a monthly) basis are needed. These input data are needed in four unique sets keyed to the four scenario/model combinations that are being analyzed. As for streamflow, which was discussed in Appendix F, the four are:

   - Scenario SRESa2 with the gfdl model
   - Scenario SRESa2 with the ncar/pcm model
   - Scenario SRESb1 with the gfdl model
   - Scenario SRESb1 with the ncar/pcm model

Per the Climate Change TM (DRMS, 2007) these data may be available only on a statewide basis. The distinction between the four scenario/model combinations and the seasonal differences are more important than a finer spatial resolution.

2. **CalSim Analyses –** The CalSim analyses suggested in Appendix F require consideration of whether the water supply available for Delta inflow is also affected

by Sacramento-Valley-wide changes in CO_2, temperature, and precipitation. For the areas upstream of the valley floor, the impacts of these factors are addressed by the adjustments to inflows (or rim flows) that were discussed in Appendix F. So, if further adjustments are necessary, they represent reduced or increased inflow from valley floor watershed precipitation, groundwater recharge, local runoff, and evapotranspiration. It is not clear whether these adjustments to CalSim can be attempted within DRMS or not. If they are, the input information necessary would be the same as mentioned above for the Delta-wide area, but for the upstream Sacramento Valley floor instead. Again, statewide data may be all that are available and these can be used as an initial approximation. Distinction among the four scenario/model combinations and recognition of seasonal differences are more important than a finer spatial resolution.

3. **South of Delta Water Demand –** Even with climate change, the "demands" for State Water Project and Central Valley Project exports from the Delta are capped by the contractual amounts – which generally exceed the amounts of water available. Thus, climate change is not expected to change this measure of demand, at least under "Business as Usual." Climate change will, however, affect what can be accomplished with the water that is actually exported. If higher temperatures lead to higher crop evapotranspiration, fewer acres of crops can be supported. This type of climate change impact must be addressed within the economic water-use submodels, to the extent those models can respond to such changes. The Economics Team will address these impacts to the extent they can. They will need the same data (CO_2, temperature, precipitation) for water use regions (e.g., San Joaquin Valley, Tulare Basin, Bay Area, Central Coast, South Coast), recognizing seasonal differences and keyed to each of the four scenario/model combinations being analyzed. Again, it may be necessary to apply wider area climate change information (e.g., state-wide temperature increases or precipitation changes), if that is the best information available.

G3. Status of Climate Change Inputs

Per the Climate Change TM (DRMS, 2007), precipitation and temperature climate change data are available for future periods on a statewide basis. CO_2 concentrations are also available. It is not clear whether these data can be provided for each of the four scenario/model combinations or whether seasonal differences can be characterized.

G4. References

DRMS, 2007. Technical Memorandum: Delta Risk Management Strategy (DRMS) Phase 1, Topical Area: Climate Change. Prepared by URS Corporation/Jack R. Benjamin & Associates, Inc. Prepared for Department of Water Resources. January, 2007 (Draft)

DWR, 2006. "Progress on Incorporating Climate Change into Management of California's Water Resources." Technical Memorandum Report. California Department of Water Resources. July, 2006.

Appendix H
Three-Dimensional Modeling of Hydrodynamics and Water Quality for Existing Conditions and Sea Level Rise Scenarios

Table of Contents

H1. Introduction H-1
H2. Motivation of Three-Dimensional Modeling H-2
H3. Representation of Salt Intrusion in the WAM H-4
H4. A Three-Dimensional Bay-Delta Model H-4
H5. Sea Level Analysis Overview H-5
H6. Use of Sea Level Rise Analysis by WAM H-7
H7. References H-7

Subappendices

H1. Parameterization of Mixing using a Three-Dimensional Hydrodynamic Model

H2. UnTRIM San Francisco Bay-Delta Model Calibration Report

H3. Three-Dimensional Salinity Simulations of Sea Level Rise Scenarios

Acronyms and Abbreviations

3D	Three Dimensional
DRMS	Delta Risk Management Strategy
DWR	California Department of Water Resources
WAM HD	Hydrodynamics and Water Quality Submodel of the WAM
X2	The location in the Bay Delta Estuary where the salinity concentration is two parts per thousand, 2,000 parts per million, or 2,000 milligrams per liter, measured in kilometers from the Golden Gate

H1 Introduction

Three-dimensional simulations of flow and salt transport in San Francisco Bay and the Sacramento-San Joaquin Delta were performed to support the Delta Risk Management Strategy (DRMS) funded by the California Department of Water Resources. These simulations were performed with the three-dimensional TRIM and UnTRIM models in order to achieve several goals of the DRMS project, including:

- Develop parameters (dispersion coefficients) that allow the WAM to realistically predict salt intrusion in the Bay-Delta.
  - Quantify the strength of salt intrusion processes for a range of Net Delta Outflow
  - Quantify the relative contribution of "three-dimensional transport processes," including gravitational circulation, to salt intrusion
  - Quantify the strength of salt intrusion processes for different sea level rise scenarios
- Estimate salinity for sea level rise scenarios
- Inform uncertainty analysis of the WAM

These goals have been achieved and are documented here, with the exception of the uncertainty analysis of the WAM, which is in progress and will be documented in the future.

The specific products of the three-dimensional modeling are documented in three subappendices.

- Appendix H1 (Gross et al. 2007a) documents the application of the three-dimensional TRIM model to for a range of Delta outflows under the existing geometry and mean sea level in the Bay-Delta. From these simulations, parameters were estimated that represent salt intrusion processes in the WAM.
- Appendix H2 (MacWilliams and Gross, 2007) documents the development and calibration of the three-dimensional UnTRIM Bay-Delta model. This model was developed for the DRMS project to allow simulations further into the Sacramento-San Joaquin Delta and improve resolution of bathymetric features relative to the TRIM model, by using a flexible unstructured grid consisting of a mixture of triangles and quadrilaterals. The hydrodynamic calibration demonstrates accurate prediction of stage, flows, and salinity for a large range of conditions in the Bay-Delta.
- Appendix H3 (Gross et al, 2007b) documents the application of the UnTRIM model to simulate sea level rise scenarios. These simulations are used to estimate increased salinity associated with sea level rise and to estimate dispersion coefficients that quantify the strength of salt intrusion processes for a range of Mean Sea Level.

H2 Motivation of Three-Dimensional Modeling

Several models are currently applied to predict Delta hydrodynamic conditions and water quality. These models include one-dimensional tidally-averaged models (e.g., the Uncles-Peterson model), one-dimensional tidal models (e.g., DSM2), two-dimensional (depth-averaged) models (e.g., RMA2) and three-dimensional models (e.g., UnTRIM). Most of these models have been applied to both existing conditions and scenarios with altered Delta geometry, management, or altered environmental conditions such as sea level rise or climate change.

One-dimensional tidally-averaged models predict tidally-averaged longitudinal variability in salinity and velocity but do not resolve tidal, lateral, or vertical variability. When one-dimensional tidal models are applied to salinity simulations, the effects of all salt intrusion processes are parameterized by dispersion coefficients.

One-dimensional tidal models predict longitudinal variability in salinity and velocity but do not resolve the lateral or vertical variability. When one-dimensional tidal models are applied to salinity simulations, the effects of the unresolved lateral and vertical variability of velocity and salinity on salt transport are parameterized by dispersion coefficients.

Two-dimensional models predict longitudinal and lateral variability in salinity and velocity but do not resolve the vertical variability. When two-dimensional models are applied to salinity simulations, the effects of the unresolved vertical variability of velocity and salinity on salt transport are parameterized by dispersion coefficients. The dispersion coefficients used with a depth-averaged model will be smaller than the dispersion coefficients used with a comparable one-dimensional model, because more transport processes are resolved by the two-dimensional, depth-averaged model.

Three-dimensional models predict the full three-dimensional variability in salinity and velocity. The effects of turbulence and other motions that are smaller than the grid resolution of a three-dimensional model are represented by sub-grid scale mixing parameters that are one or more orders of magnitude smaller than dispersion coefficients typically used with one-dimensional and two-dimensional models. The small magnitude of the sub-grid scale mixing parameters indicates that nearly all important transport mechanisms are resolved by three-dimensional models.

The primary challenge in developing the WAM hydrodynamic/water quality submodel was representing enough of the physics to provide sufficient accuracy while maintaining the computational speed needed to simulate many thousands of levee breach events. The primary outputs of WAM are monthly average quantities including export volumes and salinity, and in-Delta salinity at selected locations. As such, it is not necessary for the simplified model to explicitly resolve tidal flow and transport. Therefore, a one-dimensional tidally-averaged transport model was developed, referred to as WAM HD. As mentioned above, the “dispersion coefficients” for a one-dimensional tidally-averaged model represent (parameterize) all salt intrusion processes. These salt intrusion processes can be resolved (explicitly calculated) by a three-dimensional model. In order to capture the large degree of spatial and temporal variability in dispersive mixing processes, three-dimensional models were applied to several scenario simulations yielding a dataset of

predictions from which dispersion coefficients were calculated. These dispersion coefficients represent the strength of salt intrusion at many locations in the estuary for a range of Net Delta Outflow, salinity and sea level rise conditions. Most crucially, the parameterization allows dispersion coefficient to vary in time, as relevant conditions change, to realistically represent salt intrusion processes.

In additional to calculating dispersion coefficients, the portion of these coefficients associated with three-dimensional processes was also estimated. The magnitude of these "three-dimensional dispersion coefficients" indicates where three-dimensional processes are important. It is in these locations that a depth-averaged modeling approach may not be adequate. For example, one key "three-dimensional process" is gravitational circulation. Gravitational circulation is a salt intrusion process that results from horizontal density gradients and is characterized by vertical variability in salinity and tidally-averaged velocity. The location and strength of gravitational circulation varies dramatically with Net Delta Outflow (Monismith et al. 2002). Strong density gradients and strong gravitational circulation are present in portions of San Pablo Bay and Central Bay at high Net Delta Outflow. At lower Net Delta Outflow, gravitational circulation is weaker in most of the estuary but has larger spatial extent, which can include the western Delta.

In depth-averaged models, dispersion coefficients represent (parameterize) the effect of gravitational circulation and other "three-dimensional processes" on salt transport. In most applications these coefficients are tuned during calibration so that models accurately predict salinity during an historic period. The resulting dispersion coefficients are typically variable in space but constant in time and, therefore, are likely to perform poorly for unusual salinity conditions, including the conditions following a levee failure. Inappropriate dispersion coefficients may cause an underestimate of the flow required from reservoirs to flush salt from Delta channels. Under any scenario with substantial salinity levels in the Delta, gravitational circulation and other "three-dimensional processes" are likely to be significant and to delay flushing of the Delta. Therefore the depth-averaged approximation associated with one-dimensional (e.g., DSM2) and two-dimensional (RMA2) models may create *biases* in model predictions that will not be reduced through increased numbers of model runs. The parameterization approach attempts to minimize the uncertainty and any biases associated with the WAM HD by adjusting dispersion coefficients as a function of salinity gradients, Net Delta Outflow, and Mean Sea Level.

In addition to the parameterization of transport processes, three-dimensional models were used in the DRMS project for several scenario simulations for which "three-dimensional processes" were expected to be important. These simulations include a set of sea level rise scenarios, discussed in Appendix H3, and flooded island scenario simulations, to be documented in a future report, which will inform uncertainty analysis of the WAM HD submodel.

The UnTRIM model was used for the majority of the three-dimensional simulations for the DRMS project. The UnTRIM model is an ideal three-dimensional model for Delta simulations due to the flexible grid structure allowed by the model, similar to the grid

structure of finite element models (e.g., RMA2), and the highly efficient and stable finite difference numerical method and matrix solver of UnTRIM. This combination of flexibility and efficiency allows the model to use high resolution where it is needed to accurately describe the geometry (bathymetry) of Delta channels junctions and other features. Every aspect of the method has been published in peer reviewed journals and the method is well established, and widely duplicated, in the scientific community. The TRIM and UnTRIM models have also been applied extensively in the San Francisco Estuary and are accepted both in scientific and regulatory applications.

H3 Representation of Salt Intrusion in the WAM

A critical component of the Water Analysis Module (WAM) used in the DRMS project is a set of dispersion coefficients that represent the mixing processes causing salt intrusion into the Delta. Appendix H1 (Gross et al., 2007a) discusses the dispersive transport mechanisms active in the San Francisco Estuary, scenarios designed to estimate the strength of dispersive transport, three-dimensional model results of these scenarios and the analysis of these results to estimate dispersion coefficients. The dispersion coefficients were determined at 28 locations in the estuary, for a range of Net Delta Outflow, and are now used in the hydrodynamics and water quality portion of the WAM. The dispersion coefficients were partitioned into components associated with different physical processes, and the variability of the component associated with gravitational circulation is specified as a function of a non-dimensional parameter called the horizontal Richardson number, that varies with horizontal salinity gradients such that the dispersion coefficients increase strongly as horizontal salinity gradients increase.

The accuracy of the WAM in predicting salinity for a wide range of Delta outflow conditions is evidence of the utility of the dispersion coefficients discussed in Appendix H1.

H4 A Three-Dimensional Bay-Delta Model

The three-dimensional TRIM model used in the work documented in Appendix H1 (Gross et al., 2007a) extends to the western Delta. In order to allow simulations further into the Sacramento-San Joaquin Delta and improve resolution of bathymetric features as compared with the TRIM model, the three-dimensional UnTRIM Bay-Delta model was developed for the DRMS project. This model allows improvements by using a flexible unstructured grid consisting of a mixture of triangles and quadrilaterals. Appendix H2 (MacWilliams and Gross, 2007) documents the calibration of the three-dimensional UnTRIM Bay-Delta model. The detailed analysis of flows in the Sacramento-San Joaquin Delta indicates that predicted tidal and tidally-averaged flows agree well with observations, which vary over several orders of magnitude between stations. The salinity calibration shows good agreement between predicted and observed salinities over a full year of time series comparisons. In addition, comparison of predicted and observed salinity profiles along the axis of the San Francisco Estuary demonstrate that the model is accurately predicting salinity distribution, stratification, and the extent of salinity intrusion into the western Delta through the full range of flow conditions experienced

during the simulation year. This model was applied to scenario simulations in Appendix H3 (Gross et al., 2007) and will also be used in uncertainty analysis for the WAM.

H5 Sea Level Analysis Overview

There are at least three important impacts of sea level rise related to flow and salinity in the Delta:

1. Increasing sea level may inundate additional land area where bay and channel boundaries are not constrained by levees or steep topography. This will lead to an increase in tidal prism and may increase Delta salinity.
2. Sea level rise may outpace the ability to raise and maintain levees leading to un-repairable flooding of some Delta islands. This flooding will lead to increases in tidal prism and Delta salinity.
3. Sea level rise is increasing water surface elevations leading to deeper channels in the San Francisco Estuary. These deeper channels will have larger cross-sectional areas than existing channels leading to proportionally lower net (tidally-averaged) velocities. These lower net velocities will be less effective in flushing salt from the Delta. Deeper channels are also more likely to become stratified because bottom friction is less effective in vertically mixing deeper water columns. Additional stratification may cause increased salt intrusion into the Delta from gravitational circulation.

The flooding of additional areas as sea level rises will have an impact on salinity in the Delta. However quantifying the impact requires more accurate topography than is currently available for areas that could potentially flood. This potential impact is not considered in this phase of the DRMS project.

The effect of sea level rise on levee failures is addressed in the DRMS project. Evaluating the impact of islands flooding due to sea level rise is one form of breach case to be analyzed by the Water Analysis Module (WAM) in Risk Analyses that address future conditions. The scenario simulations performed in this report will help in assessing the uncertainty related to WAM's calculations of these salinity impacts.

Increased water surface elevation from sea level rise will lead to deeper water in channels. Probably a larger source of deepening will be ongoing erosion in Suisun Bay (Cappiela et al., 2005) and other regions. Scour from restoration projects, levee failures, dredging, and larger and more frequent floods may also act to deepen channels. Therefore, it is likely that future channels in San Pablo Bay, Suisun Bay and the Delta will be deeper than the current channels. Analytical relationships (Hansen and Rattray 1965) and simulations of idealized geometries suggest that increases in water column depth can have a strong and non-linear effect on salt water intrusion as a result of increased gravitational circulation. This increased salt intrusion would increase the Net Delta Outflow (NDO) required to meet water quality standards. Channel deepening will also change the magnitude, distribution and phase of tidal currents, leading to altered tidal dispersion processes and altered turbulent mixing. A three-dimensional model is the most appropriate tool to address these issues.

The primary goals of the sea level rise scenario simulations are the following:

- Estimate salinity for idealized sea level rise scenarios
- Quantify the strength of salt intrusion processes for different sea level rise scenarios
- Quantify the relative contribution of "three-dimensional transport processes," including gravitational circulation, to salt intrusion
- Account for sea level rise in the parameterization of dispersive transport for the WAM

In Appendix H3 (Gross et al., 2007b) seven scenarios are considered to estimate the effects of sea level rise on salinity. In addition to the Baseline scenario without sea level rise, four increases in MSL are considered: 20 cm (0.66 ft), 50 cm (1.64 ft), 90 cm (2.95 ft) and 140 cm (4.59 ft). These levels of MSL increase were recommended by Phillip Duffy of the DRMS climate change group. Two additional simulations evaluate potential cumulative effects of 140 cm of sea level rise with other potential changes. The first cumulative effects scenario, the Amplified Tides scenario, assumes that tidal range is increased by 11 percent, based on the observed rates of amplification reported by Flick et al. (2003). Because the future trends in tidal amplitude are highly uncertain, the Amplified Tides scenario should be considered a sensitivity analysis. The second cumulative effects scenario, the Perforated Sherman Island scenario, assumes 20 breach locations in Sherman Island.

The scenarios simulated are designed to address the goals discussed previously and are limited in scope, given the short schedule and limited budget provided for the analysis. In addition, the model forcing is idealized in order to allow the estimation of dispersion coefficients. The assumptions and approximations employed include the following:

- No changes to the shoreline geometry of the estuary. This includes the assumption of current Delta geometry without any new levee breaches, except for one scenario that considers the effects of a flooded Sherman Island on salt intrusion. Also, it assumes no new flooding of lowlands around the Bay with sea level rise.
- No net accretion or erosion is assumed. The bed elevation of the estuary is specified based on existing bathymetry data. In contrast, the observed trend in Suisun Bay and is an average of 1.2 cm/year (0.47 in/year) of erosion (Cappiella et al. 2005).
- The tidal range applied at the ocean boundary is assumed to remain constant. Only the Mean Sea Level (MSL) is increased. One scenario examines the effect of increased tidal range.
- Other aspects of climate change, such as effects on hydrology, are not considered.
- The scenario simulations use specified hydrology. All scenarios use a constant Net Delta Outflow (NDO) of 260 m^3/s (9,182 cfs), corresponding to a typical summer flow rate.

The analysis of salt intrusion for the sea level rise led to the following products:

- Maps of salinity for different scenarios, maps of salinity differences
- Time series graph comparisons at specified locations
- Salinity transects along the axis of the estuary (showing longitudinal and vertical distribution of salinity).
- Estimated changes to X2 location for summer conditions as a function of sea level rise.
- A set of dispersion coefficients that represent the changes in the strength of salt intrusion mechanisms with sea level rise.

The simulation results indicate increased salt intrusion with increases in MSL, particularly for MSL rise of 90 cm (2.95 ft) or more. A simulation of 140 cm (4.59 ft) of MSL rise and flooded Sherman Island, suggests that the combination of substantial sea level rise and a small degree of Delta island flooding could lead to large impacts on Delta water quality and water supply reliability. The results of these idealized scenario simulations suggest that more realistic scenario simulations are warranted in order to better quantify cumulative effects of sea level rise, flooded islands, geomorphic change in the estuary, changes in Delta operations, hydrologic variability as a result of climate change and other expected changes. Many such scenarios will be addressed with the WAM, while others will not be addressed in this phase of the DRMS project. Given the substantial uncertainty associated with the WAM's simplified approach, a portion of these scenarios should be simulated with two-dimensional and three-dimensional models to better inform risk analysis and risk reduction measures.

H6 Use of Sea Level Rise Analysis by WAM

The approach used in Appendix H1 (Gross et al., 2007a) to analyze salt intrusion processes so that they can be parameterized in the WAM, was also used to analyze salt intrusion processes for the Sea Level Rise scenarios in Appendix H3 (Gross et al., 2007b). For the sea level rise analysis, the variability of dispersion with mean sea level was examined and parameterized. Therefore, the WAM accounts for both the effect of variable Net Delta Outflow and variable Mean Sea Level on salt intrusion processes through changes to dispersion coefficients.

Using the WAM module with these modified dispersion coefficients allows estimation of the change in water demand for Delta outflow (to maintain water quality standards) that results from the increased salt intrusion due to sea level rise.

H7 References

Cappiella, K., Malzone, C., Smith, R., and Jaffe, B., 2005. Sedimentation and bathymetry changes in Suisun Bay, 1867-1990, U.S. Geological Survey, Open-File Report 99-563.

Gross, E. S., Nidzieko, N., and MacWilliams, M. L., 2007a. Delta Risk Management Strategy – Parameterization of Mixing using a Three-Dimensional Hydrodynamic Model. Prepared for California Department of Water Resources. March, 2007.

Gross, E. S., MacWilliams, M. L., and Nidzieko, N., 2007b. Delta Risk Management Strategy – Three-Dimensional Salinity Simulations of Sea Level Rise Scenarios. Prepared for California Department of Water Resources. March, 2007.

Hansen, D.V., and Rattray, M., 1965. Gravitational circulation in straits and estuaries, *Journal of Marine Research*, 23, 104-122.

MacWilliams, M. L., and Gross, E. S., 2007. Delta Risk Management Strategy – UnTRIM San Francisco Bay-Delta Calibration Report. Prepared for California Department of Water Resources. March, 2007.

Monismith, S.G., Kimmerer, W., Burau, J.B., and Stacey, M.T., 2002. Structure and flow-induced variability of the subtidal salinity field in Northern San Francisco Bay, *Journal of Physical Oceanography*, 32, 3,003-3,019.

Appendix H1
Parameterization of Mixing Using a Three-Dimensional Hydrodynamic Model

Delta Risk Management Strategy

Parameterization of Mixing using a Three-Dimensional Hydrodynamic Model

Prepared For:

California Department of Water Resources

March 21, 2007

Prepared By:

Dr. Edward S. Gross

Environmental Consultant

Nicholas Nidzieko

Environmental Consultant

Dr. Michael L. MacWilliams

Environmental Consultant

Table of Contents

Executive Summary **1**
H1.1 Introduction **1**
H1.2 Overview of Key Dispersion Processes **2**
H1.3 Analysis of Dispersion Processes **4**
H1.3.1 Salt Flux Analysis 6
H1.3.2 Gravitational Circulation 8
H1.4 Model Description **9**
H1.5 Model Scenarios **11**
H1.6 Scenario Simulation Results **12**
H1.7 Analysis of Scenario Simulations **17**
H1.7.1 Central San Francisco Bay Cross-Sections 22
H1.7.2 San Pablo Bay Cross-Sections 29
H1.7.3 Suisun Bay Cross-Sections 41
H1.7.4 Western Delta Cross-Sections 50
H1.8 Discussion **57**
H1.9 Acknowledgements **60**
H1.10 References **60**

Tables

H1-1 Names and Net Delta Outflows of Each Simulation Scenario

H1-2 Results of parameterization analysis for use in WAM. The K_{2D} and K_{us} values listed are the average values for the flow scenarios, while a and b are the curve fit parameters for the equation $K_{gc}/u*H = a\ Ri_x^b$

Figures

H1.3-1 Cross-sections used in salt flux analysis.

H1.3-2 Centerline transect with labeled distance from Golden Gate.

H1.4-1 Bathymetry on the 200 meter resolution TRIM3D model grid.

H1.6-1 Tidally-averaged depth-averaged salinity (psu) at Martinez for all flow scenarios.

H1.6-2 Tidally-averaged salinity (psu) along the centerline transect from Golden Gate to Rio Vista for the scenario with Net Delta Outflow of 55 m3/s.

H1.6-3 Tidally-averaged salinity (psu) along the centerline transect from Golden Gate to Rio Vista for the scenario with Net Delta Outflow of 110 m3/s.

H1.6-4 Tidally-averaged salinity (psu) along the centerline transect from Golden Gate to Rio Vista for the scenario with Net Delta Outflow of 151 m3/s.

H1.6-5 Tidally-averaged salinity (psu) along the centerline transect from Golden Gate to Rio Vista for scenario with Net Delta Outflow of 260 m^3/s.

H1.6-6 Tidally-averaged salinity (psu) along the centerline transect from Golden Gate to Rio Vista for the scenario with Net Delta Outflow of 630 m^3/s.

H1.6-7 Tidally-averaged salinity (psu) along the centerline transect from Golden Gate to Rio Vista for the scenario with Net Delta Outflow of 2,810 m^3/s.

H1.7-1 Estimated depth-averaged salinity gradient for all flow scenarios. The horizontal scale is distance along the axis of the estuary from the Golden Gate.

H1.7-2 Estimated total dispersion coefficients (K) for all flow scenarios. The horizontal scale is distance along the axis of the estuary from the Golden Gate.

H1.7-3 Estimated dispersion coefficients associated with gravitational circulation (Kgc) for all flow scenarios. The horizontal scale is distance along the estuary from the Golden Gate.

H1.7-4 Estimated dispersion coefficients associated with “unsteady shear” (Kus) for all flow scenarios. The horizontal scale is distance along the estuary from the Golden Gate.

H1.7-5 Estimated dispersion coefficients associated with all tidal dispersion (K2D) for all flow scenarios. The horizontal scale is distance along the estuary from the Golden Gate.

H1.7-6 Estimated root mean square depth-averaged velocity for all flow scenarios. The horizontal scale is distance along the axis of the estuary from the Golden Gate.

H1.7-7 Estimated horizontal Richardson number for all flow scenarios. The horizontal scale is distance along the axis of the estuary from the Golden Gate.

H1.7.1-1 Estimated dispersion coefficients at section 1, located at the Golden Gate, as a function of Net Delta Outflow.

H1.7.1-2 Estimated dimensionless dispersion coefficients for gravitational circulation at section 1, located at the Golden Gate, as a function of horizontal Richardson number with corresponding best fit equation and r^2 value.

H1.7.1-3 Estimated dispersion coefficients at section 2, from San Francisco to Tiburon, as a function of Net Delta Outflow.

H1.7.1-4 Estimated dimensionless dispersion coefficients for gravitational circulation at section 2, extending from San Francisco to Tiburon, as a function of horizontal Richardson number with corresponding best fit equation and r^2 value.

H1.7.1-5 Estimated dispersion coefficients at section 3, extending from Albany to Tiburon, as a function of Net Delta Outflow.

H1.7.1-6 Estimated dimensionless dispersion coefficients for gravitational circulation at section 3, extending from Albany to Tiburon, as a function of horizontal Richardson number with corresponding best fit equation and r^2 value.

H1.7.1-7 Estimated dispersion coefficients at section 4, extending from Richmond to San Rafael, as a function of Net Delta Outflow.

H1.7.1-8 Estimated dimensionless dispersion coefficients for gravitational circulation at section 4, extending from Richmond to San Rafael, as a function of horizontal Richardson number with corresponding best fit equation and r^2 value.

H1.7.1-9 Estimated dispersion coefficients at section 5, extending from Point San Pablo to San Rafael, as a function of Net Delta Outflow.

H1.7.1-10 Estimated dimensionless dispersion coefficients for gravitational circulation at section 5, extending from Point San Pablo to San Rafael, as a function of horizontal Richardson number with corresponding best fit equation and r^2 value.

H1.7.2-1 Estimated dispersion coefficients at section 6, extending from Richmond to Point San Pedro, as a function of Net Delta Outflow.

H1.7.2-2 Estimated dimensionless dispersion coefficients for gravitational circulation at section 6, extending from Richmond to Point San Pedro, as a function of horizontal Richardson number with corresponding best fit equation and r^2 value.

H1.7.2-3 Estimated dispersion coefficients at section 7, extending from Pinole Point to Sonoma Creek, as a function of Net Delta Outflow.

H1.7.2-4 Estimated dimensionless dispersion coefficients for gravitational circulation at section 7, extending from Pinole Point to Sonoma Creek, as a function of horizontal Richardson number with corresponding best fit equation and r^2 value.

H1.7.2-5 Estimated dispersion coefficients at section 8, extending from Hercules to Mare Island, as a function of Net Delta Outflow.

H1.7.2-6 Estimated dimensionless dispersion coefficients for gravitational circulation at section 8, extending from Hercules to Mare Island, as a function of horizontal Richardson number with corresponding best fit equation and r^2 value.

H1.7.2-7 Estimated dispersion coefficients at section 9, extending from Rodeo to Mare Island, as a function of Net Delta Outflow.

H1.7.2-8 Estimated dimensionless dispersion coefficients for gravitational circulation at section 9, extending from Rodeo to Mare Island, as a function of horizontal Richardson number with corresponding best fit equation and r^2 value. Carquinez Strait Cross-Sections

H1.7.3-1 Estimated dispersion coefficients at section 10, extending from Davis Point to Mare Island, as a function of Net Delta Outflow.

H1.7.3-2 Estimated dimensionless dispersion coefficients for gravitational circulation at section 10, extending from Davis Point to Mare Island, as a function of horizontal Richardson number with corresponding best fit equation and r^2 value.

H1.7.3-3 Estimated dispersion coefficients at section 11, at the Carquinez Bridge, as a function of Net Delta Outflow.

H1.7.3-4 Estimated dimensionless dispersion coefficients for gravitational circulation at section 11, at the Carquinez Bridge, as a function of horizontal Richardson number with corresponding best fit equation and r^2 value.

H1.7.3-5 Estimated dispersion coefficients at section 12, extending from Crockett to Glen Cove, as a function of Net Delta Outflow.

H1.7.3-6 Estimated dimensionless dispersion coefficients for gravitational circulation at section 12, extending from Crockett to Glen Cove, as a function of horizontal Richardson number with corresponding best fit equation and r^2 value.

H1.7.3-7 Estimated dispersion coefficients at section 13, extending from Ozol to Benicia Point, as a function of Net Delta Outflow.

H1.7.3-8 Estimated dimensionless dispersion coefficients for gravitational circulation at section 13, extending from Ozol to Benicia Point, as a function of horizontal Richardson number with corresponding best fit equation and r^2 value.

H1.7.3-9 Estimated dispersion coefficients at section 14, extending from Martinez to Benicia, as a function of Net Delta Outflow.

H1.7.3-10 Estimated dimensionless dispersion coefficients for gravitational circulation at section 14, extending from Martinez to Benicia, as a function of horizontal Richardson number with corresponding best fit equation and r^2 value.

H1.7.3-11 Estimated dispersion coefficients at section 15, at the Benicia Bridge, as a function of Net Delta Outflow.

H1.7.3-12 Estimated dimensionless dispersion coefficients for gravitational circulation at section 15, at the Benicia Bridge, as a function of horizontal Richardson number with corresponding best fit equation and r^2 value.

H1.7.4-1 Estimated dispersion coefficients at section 16, from Pacheco Creek to the Mothball Fleet, as a function of Net Delta Outflow.

H1.7.4-2 Estimated dimensionless dispersion coefficients for gravitational circulation at section 16, from Pacheco Creek to the Mothball Fleet, as a function of horizontal Richardson number with corresponding best fit equation and r^2 value.

H1.7.4-3 Estimated dispersion coefficients at section 17, east of the Mothball Fleet, as a function of Net Delta Outflow.

H1.7.4-4 Estimated dimensionless dispersion coefficients for gravitational circulation at section 17, east of the Mothball Fleet, as a function of horizontal Richardson number with corresponding best fit equation and r^2 value.

H1.7.4-5 Estimated dispersion coefficients at section 18, from Point Edith to Suisun Slough, as a function of Net Delta Outflow.

H1.7.4-6 Estimated dimensionless dispersion coefficients for gravitational circulation at section 18, from Point Edith to Suisun Slough, as a function of horizontal Richardson number with corresponding best fit equation and r^2 value.

H1.7.4-7 Estimated dispersion coefficients at section 19, from Port Chicago to Grizzly Bay, as a function of Net Delta Outflow.

H1.7.4-8 Estimated dimensionless dispersion coefficients for gravitational circulation at section 19, from Port Chicago to Grizzly Bay, as a function of horizontal Richardson number with corresponding best fit equation and r^2 value.

H1.7.4-9 Estimated dispersion coefficients at section 20, from Middle Point to Simmons Island, as a function of Net Delta Outflow.

H1.7.4-10 Estimated dimensionless dispersion coefficients for gravitational circulation at section 20, from Middle Point to Simmons Island, as a function of horizontal Richardson number with corresponding best fit equation and r^2 value.

H1.7.4-11 Estimated dispersion coefficients at section 21, from Concord to Dutton Island, as a function of Net Delta Outflow.

H1.7.4-12 Estimated dimensionless dispersion coefficients for gravitational circulation at section 21, from Concord to Dutton Island, as a function of horizontal Richardson number with corresponding best fit equation and r^2 value.

H1.7.4-13 Estimated dispersion coefficients at section 22, from Stake Point to Wheeler Island, as a function of Net Delta Outflow.

H1.7.4-14 Estimated dimensionless dispersion coefficients for gravitational circulation at section 22, from Stake Point to Wheeler Island, as a function of horizontal Richardson number with corresponding best fit equation and r2 value.

H1.7.4-15 Estimated dispersion coefficients at section 23, extending south from Simmons Point, as a function of Net Delta Outflow.

H1.7.4-16 Estimated dimensionless dispersion coefficients for gravitational circulation at section 23, extending south from Simmons Point, as a function of horizontal Richardson number with corresponding best fit equation and r^2 value.

H1.7.5-1 Estimated dispersion coefficients at section 24, extending from Mallard Island to Chipps Island, as a function of Net Delta Outflow.

H1.7.5-2 Estimated dimensionless dispersion coefficients for gravitational circulation at section 24, extending from Mallard Island to Chipps Island, as a function of horizontal Richardson number with corresponding best fit equation and r^2 value.

H1.7.5-3 Estimated dispersion coefficients at section 25, extending from Pittsburg to Mallard Island, as a function of Net Delta Outflow.

H1.7.5-4 Estimated dimensionless dispersion coefficients for gravitational circulation at section 25, extending from Pittsburg to Mallard Island, as a function of horizontal Richardson number with corresponding best fit equation and r^2 value.

H1.7.5-5 Estimated dispersion coefficients at section 26, extending from Brown Island to Van Sickle Island, as a function of Net Delta Outflow.

H1.7.5-6 Estimated dimensionless dispersion coefficients for gravitational circulation at section 26, extending from Brown Island to Van Sickle Island, as a function of horizontal Richardson number with corresponding best fit equation and r^2 value.

H1.7.5-7 Estimated dispersion coefficients at section 27, extending north from Sherman Island, as a function of Net Delta Outflow.

H1.7.5-8 Estimated dimensionless dispersion coefficients for gravitational circulation at section 27, extending north from Sherman Island, as a function of horizontal Richardson number with corresponding best fit equation and r2 value.

H1.7.5-9 Estimated dispersion coefficients at section 28, on Sacramento River near Emmaton, as a function of Net Delta Outflow.

H1.7.5-10 Estimated dimensionless dispersion coefficients for gravitational circulation at section 28, on Sacramento River near Emmaton, as a function of horizontal Richardson number with corresponding best fit equation and r2 value.

Abbreviations

3D	Three-dimensional
ADCP	Acoustic Doppler Current Profiler
DEM	Digital Elevation Model
DRMS	Delta Risk Management Study
DWR	Department of Water Resources
MLLW	Mean Lower Low Water
NAD27	North American Datum of 1927
NGVD 29	National Geodetic Vertical Datum of 1929
NOAA	National Oceanic & Atmospheric Administration
NOS	National Ocean Service (NOAA)
RMA	Resource Management Associates
SIPS	Strain Induced Periodic Stratification
TRIM	Tidal, Residual, Intertidal Mudflat Model
UnTRIM	Unstructured Tidal, Residual, Intertidal & Mudflat Model
USGS	United States Geological Survey
UTM	Universal Transverse Mercator
WAM	Water Analysis Module
K_{gc}	Dispersion associated with gravitational circulation
K_{us}	Dispersion associated with unsteady vertical shear
K_{2D}	Dispersion associated with tidal dispersion

Executive Summary

A critical component of the Water Analysis Module (WAM) used in the DRMS project is a set of dispersion coefficients which represent dispersive mixing processes. This report presents a discussion of dispersive transport mechanisms active in the San Francisco Estuary, simulation scenarios designed to estimate the strength of dispersive transport, model results of these scenarios and the analysis of these results to estimate dispersion coefficients. These dispersion coefficients were determined at many locations in the estuary and are now used in the water quality portion of the WAM. The limitations, approximations and uncertainties of the simulations and analysis approach are discussed. Ongoing work that should improve accuracy of the parameterization of dispersive mixing and other potential improvements are also discussed.

In order to parameterize dispersion, three-dimensional simulations of hydrodynamics and salt transport in the San Francisco Estuary were performed with the TRIM3D model. The model was originally developed to support the "Fish-X2" research project funded by CALFED (Gross et al. 2006). The model applications discussed here build on the detailed calibration and salt transport analysis work performed as part of the Fish-X2 study.

Scenarios with simplified forcing were simulated in which tidally-averaged steady state salinity conditions are approximately reached. The predicted tidally-averaged salinity distribution and salt fluxes at steady state were then analyzed in order to estimate the magnitude of dispersive transport and the physical mechanisms responsible for this dispersive transport. Much of the dispersive transport is associated with gravitational circulation which has highly variable magnitude but is expected to vary in a consistent and predictable manner with a parameter termed "horizontal Richardson number" (e.g., Monismith et al. 2002). Therefore, the variability of this portion of the dispersion coefficient is fit with an equation similar to the curve fit equation of Monismith et al. (2002) to capture some of the variability of dispersion with variable Delta outflow.

The results of the dispersion analysis are qualitatively consistent with the existing understanding of transport in the San Francisco Estuary. The curve fit approach also appears successful in most sections in the sense that the assumed equation generally describes the variability of the dispersion associated with gravitational circulation. Preliminary results using the dispersion coefficients in the WAM are also encouraging.

H1.1 Introduction

The work documented in this report was performed as part of the development of the Water Analysis Module (WAM) for the Delta Risk Management Strategy (DRMS). The WAM is the primary product of the Water Quality component of the DRMS study. This model calculates the direct water-quality-related consequences of levee breach events. The module fits in the center of the risk analysis framework receiving the sequence description of a breach event from the seismic or flood hazard, levee fragility, and emergency response and repair modules. It provides water supply, hydrodynamic, and water quality consequences to the economic and environmental modules.

The hydrodynamics/water quality submodel of the WAM is responsible for calculating the water quality distribution in the Delta over time. Because the full risk analysis requires evaluation of hundreds if not thousands of discrete levee breach sequences, the WAM provides very rapid calculation of consequences related to any given breach sequence. The Water Analysis Module contains a tidally-averaged transport model that parameterizes the effect of all dispersive transport processes with dispersion coefficients. The methodology of the WAM is described in detail in the Hydrodynamics/Water Quality White Paper. The primary goal of the analysis documented here is to estimate dispersion coefficients for the Water Analysis Module.

The parameterization of transport outlined here is one of several components required in the development of the WAM. Because the WAM is applied for the current geometry of the estuary and for a large number of levee failure sequences, the net flows and dispersion coefficients used in the WAM should be appropriate both for the current geometry and the altered geometries experienced during levee failure scenarios. The main effects on transport processes in the Bay are expected to be caused by shifts in the location and strength of salinity gradients and changes in tidal currents. These changed salinity gradients will lead to changes in the location and strength of gravitational circulation and, possibly, other transport mechanisms. Tidal currents may increase in portions of the Estuary as a result of increased tidal prism in the Delta. Therefore, the parameterization of dispersive transport documented here accounts for the variability of the strength of gravitational circulation with salinity gradients and tidal current speed. The parameterization method outlined here does not address changes to tidal dispersion that may result from altered Delta geometry resulting from levee failures. Ongoing particle tracking work with the RMA2 model may address these changes in tidal dispersion.

The three-dimensional TRIM model has been extensively calibrated for a range of historic conditions in the San Francisco Estuary. This model involves a minimal amount of empirical information because key transport processes are explicitly resolved, not parameterized by dispersion coefficients. Therefore the strength of individual transport processes can be estimated by analysis of model results.

H1.2 Overview of Key Dispersion Processes

Salinity in the San Francisco Estuary depends on:

- salinity in the coastal ocean and exchange between the ocean and the estuary,
- freshwater input to the Delta,
- pumping, consumptive use and operations in the Delta,
- salt input from agricultural drainage and other sources,
- evaporation and precipitation.

The properties of water in the estuary vary seasonally. The San Francisco Estuary reaches its highest salinity values during the summer and fall, when the river flows are at their

minimum. Seasonal and yearly variations in salinity are driven primarily by variability in freshwater flow.

Mixing of ocean water and salt into an estuary results "from a combination of small-scale turbulent diffusion and larger scale variation of … velocities" (Fischer et al. 1979) which are primarily forced by astronomical tides in the San Francisco Estuary (Walters et al. 1985). The combination of differential advection and turbulent mixing is typically referred to as dispersive transport. Dispersive transport in estuaries is a complex topic due to the large range of spatial and temporal scales associated with different forcing processes driving flows.

Transport mechanisms are driven by the tides, winds, freshwater inflows and density gradients in the Estuary. Therefore salinity varies over many time scales. Over the tidal time scale salinity gradients are advected several kilometers by tidal currents and vertical stratification can be created (or reduced) as a result of tidal straining and reduced by vertical turbulent mixing (Simpson et al. 1990). Over the spring-neap cycle the strength of the tides varies substantially and during neap tides the largest stratification is noted due to reduced vertical mixing (Cloern et al. 1985). Wind driven circulation also results in differential advection of salt. River inflows cause a net seaward advection of salt as the estuary water is displaced seaward by the incoming freshwater. Therefore, freshwater input results in longitudinal density gradients and may cause gravitational circulation and stratification. Monismith et al. (2002) predicted that dispersion from gravitational circulation can increase by several orders of magnitude from low Delta outflow to high Delta outflow, assuming uniform bathymetry.

Another inherently three-dimensional "exchange flow" process is Strain Induced Periodic Stratification (SIPS), which results from ebb-flood asymmetries in velocity profiles (Simpson et al. 1990). These tidal-asymmetries are a result of different stratification and vertical shear during ebb and flood. Asymmetries occur because stratification decreases turbulent mixing leading to more vertical shear in velocity and stratification. Due to tidal straining, stratification is typically stronger on ebb tides than flood tides, and, therefore, the velocity profile is more strongly sheared during ebb tide than flood tide. The resulting tidally-averaged velocity profile is an exchange flow, similar to that caused by gravitational circulation. Stacey et al. (2001) found the SIPS mechanism to be active in a Suisun Bay field study.

An important dispersive transport mechanism in the Estuary is tidal dispersion, including the processes of "tidal trapping" and "tidal pumping." Tidal trapping is a term used by Fischer et al. (1979) to describe one simple process by which tidal dispersion can cause landward transport of salt. The classic case of tidal trapping occurs in an estuary with side embayments when some of the salt mass that enters the side embayments on the flood tide and remains "trapped" in the subembayment for a large portion of all of the ebb tide. More generally, tidal dispersion occurs as the result of tidal flows over bathymetric features including side embayments, junctions, mudflats and marshes. Tidal dispersion is typically effective when substantial variability in bathymetry and geometry is experienced over the distance of a tidal excursion.

The goal of the parameterization analysis is to estimate dispersion parameters that represent the effect of the three-dimensional and time varying tidal hydrodynamics on tidally-averaged salt transport along the axis of the estuary. The parameterization is tailored to the one-dimensional tidally-averaged salt transport that comprises the hydrodynamics/water quality submodel of the WAM. More specifically, the parameterization varies only with quantities (tidally-averaged salinity, cross-sectional area, etc.) represented by the simplified hydrodynamics/water quality submodel.

H1.3 Analysis of Dispersion Processes

The "salt balance" equation (Fischer et al. 1979) is a simplified but useful description of salt transport that applies to estuaries with an unambiguous longitudinal axis:

$$QS = - KA\ dS/dx, \qquad (3\text{-}1)$$

where Q is the tidally-averaged flow, S is tidally and cross-sectionally averaged salinity, K is the dispersion coefficient, A is the cross-sectional area, and x is the longitudinal position. The salt balance equation applies to the longitudinal salinity distribution and tidally-averaged steady state conditions. This equation states that the seaward advection of salinity due to net seaward velocity resulting from steady freshwater inflows is balanced by landward dispersion of salt by all dispersive transport mechanisms (Fischer et al. 1979). Dispersion coefficients (K) quantify the strength of dispersive salt transport.

The salt balance equation will be used directly to estimate dispersion coefficients as follows

$$K = -QS/(A\ dS/dx). \qquad (3\text{-}2)$$

As will be described in Section 5, scenario simulations with simplified forcing have been used to eliminate difficulties in tidal averaging and to reach a tidally-averaged steady state salinity field. Once these conditions are reached, Equation 3-2 is used to estimate dispersion coefficients.

The strength of dispersion mechanisms varies in space and time. In order to accurately parameterize dispersive transport in the WAM, the analysis technique is designed to capture much of this variability. The spatial variability is accounted for by performing analysis of fluxes at the 28 cross-sections shown in Figure H1.3-1. At each cross-section and for each flow scenario, Q, S and A are calculated for tidally-averaged steady state conditions. The salinity gradient (dS/dx) is estimated along the centerline of the estuary shown in Figure H1.3-2. Because the WAM is intended to predict monthly time scale variability, it is not necessary to estimate how dispersion coefficients vary with tidal amplitude in the spring-neap or other tidal cycles. However, it is important to capture some of the variability of dispersion coefficients with Delta outflow.

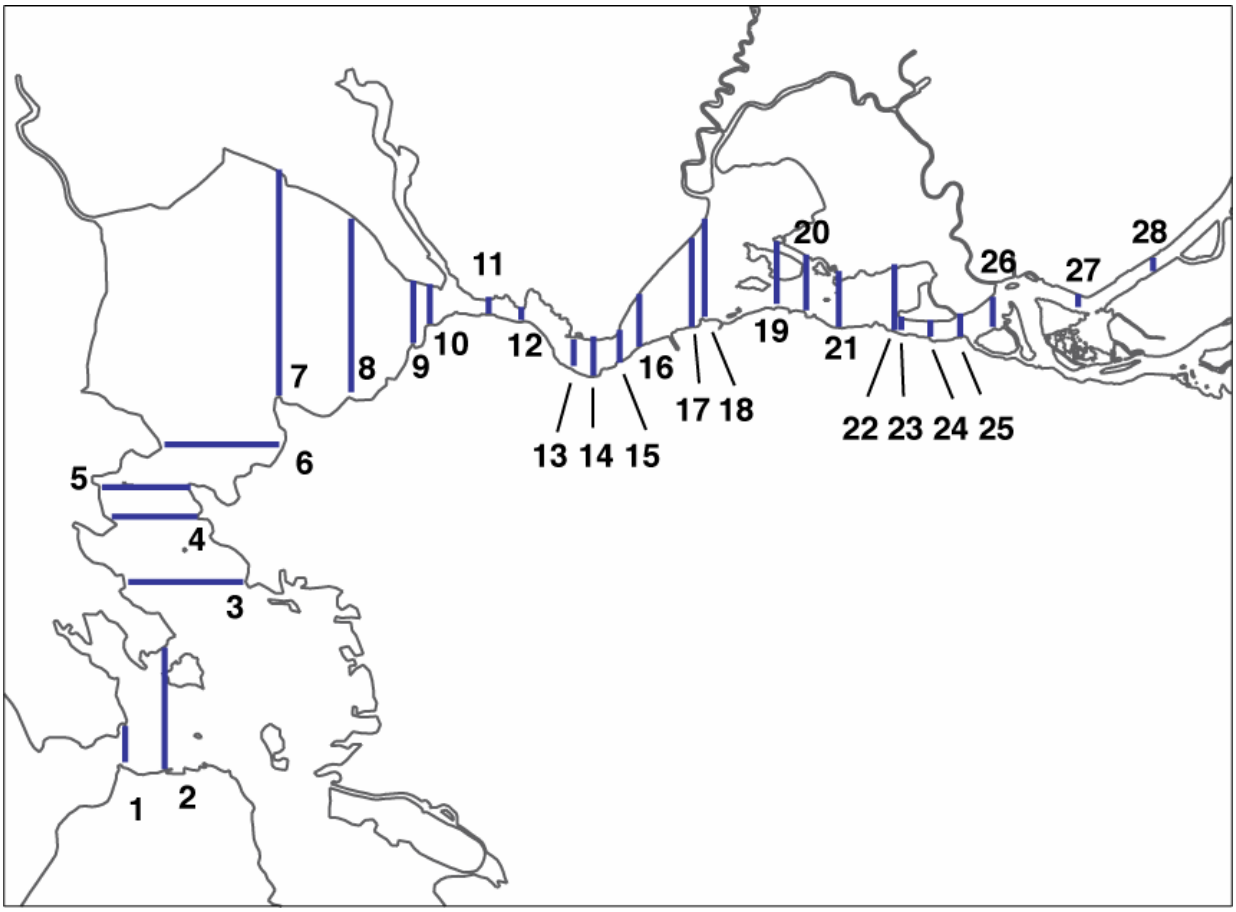

Figure H1.3-1 Cross-sections used in salt flux analysis.

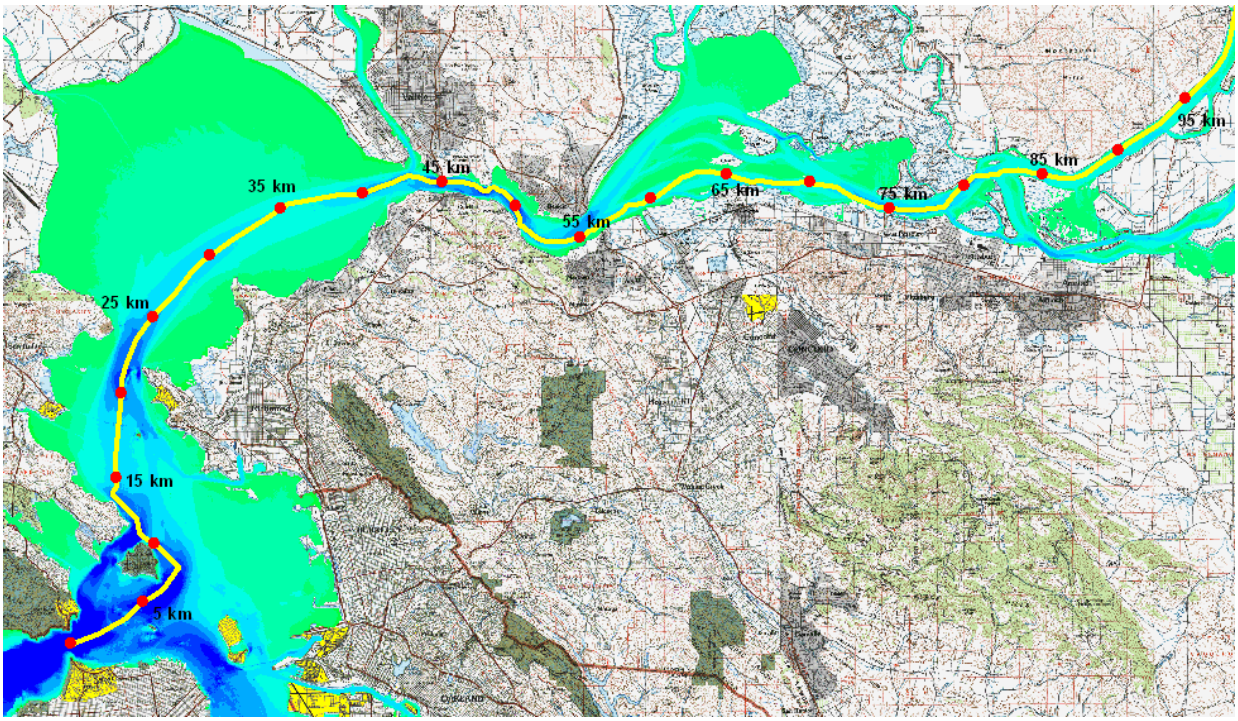

Figure H1.3-2 Centerline transect with labeled distance from Golden Gate.

H1.3.1 Salt Flux Analysis

Estimating the portion of the total dispersion coefficient associated with gravitational circulation and other individual processes requires detailed analysis of simulation results. The salt flux associated with individual physical processes can be estimated at any cross-section by an analysis method outlined in Fischer et al. (1979) and several other sources. First the velocity, u, and salinity, s, are decomposed into several components as

$$u(x,y,z,t) = U_a(x) + U_c(x,t) + u_s(x,y,z) + u'(x,y,z,t) \quad (3.1\text{-}1)$$

$$s(x,y,z,t) = S_a(x) + S_c(x,t) + s_s(x,y,z) + s'(x,y,z,t) \quad (3.1\text{-}2)$$

where x is the longitudinal position of a cross-section, y is the lateral distance within a cross-section, z is the vertical location and t is time. The velocity components are the cross-sectional and tidally-averaged velocity (U_a), the deviation of the cross-sectional average from the cross-sectional and tidally-averaged velocity (U_c), the deviation of the tidally-averaged velocity from the cross-sectional and tidally-averaged velocity (u_s) and the remaining variability (u'). The salinity terms are analogous to the velocity terms and the capital letters refer to depth-averaged quantities. The last two terms of each decomposition are further decomposed into lateral and vertical variability:

$$u_s(x,y,z) = U_t(x,y) + u_v(x,y,z) \quad (3.1\text{-}3)$$

$$u'(x,y,z,t) = U_t'(x,y,t) + u_v'(x,y,z,t) \quad (3.1\text{-}4)$$

$$s_s(x,y,z) = S_t(x,y) + s_v(x,y,z) \quad (3.1\text{-}5)$$

$$s'(x,y,z,t) = S_t'(x,y,t) + s_v'(x,y,z,t). \quad (3.1\text{-}6)$$

In this notation the cross-sectional averaged velocity at any time is $U_a + U_c$, the residual velocity at a point in space is $U_a + u_s$, and the term u_v is associated with exchange flows.

The cross-sectional area is decomposed into tidal cycle average and variation from this average,

$$A(x,t) = A_a(x) + A_c(x,t). \quad (3.1\text{-}7)$$

Therefore the salt flux through a cross-section at any moment in time is

$$\text{Flux}(x,t) = [u(x,y,z,t)\ s(x,y,z,t)]A(x,t), \quad (3.1\text{-}8)$$

where A is the cross-sectional area and the square brackets represent a cross-sectional average. This compact notation implies integration over the cross-sectional area. The average salt flux during a tidal cycle is determined by averaging over the tidal cycle:

$$\text{Flux}(x) = \langle[u(x,y,z,t)\ s(x,y,z,t)]A(x,t)\rangle, \quad (3.1\text{-}9)$$

where the angle brackets represent a tidal cycle average. This notation follows Fischer et al. (1979) closely except that square brackets are used instead of an overbar to represent cross-sectional averages. Next the decomposed velocity, salinity and area are substituted into Equation 3.1-9. Many product terms are zero or negligible (Dyer 1974). Keeping all terms that are expected to be significant in any part of the San Francisco Estuary results in the equation

$$\begin{aligned}\text{Flux}(x) \quad &= A_a U_a S_a + S_a \langle A_c U_c\rangle + A_a \langle U_c S_c\rangle + U_a\langle A_c S_c\rangle + \langle A_c U_c S_c\rangle \\ &+ A_a [U_t S_t] + A_a [u_v s_v] + \langle[U'_t S'_t](A_a + A_c)\rangle + \langle[u'_v s'_v](A_a + A_c)\rangle \\ &+ \langle[U_t S'_t](A_a + A_c)\rangle + \langle[u_v s'_v](A_a + A_c)\rangle \\ &+ \langle[U'_t S_t](A_a + A_c)\rangle + \langle[u'_v s_v](A_a + A_c)\rangle \quad (3.1\text{-}10)\end{aligned}$$

Many terms in this equation are associated with one or more physical processes while others have less clear physical interpretations. Several terms not included in equation 3.1-10 have been neglected in the flux analysis presented here and the notation used and degree of decomposition varies in previous applications of this methodology. For example, several terms above could be decomposed into a term associated with constant area and a term associated with tidally variable area, but this is not of interest in the context of the WAM. The largest difference between this analysis and previous analyses of this type available in the literature are that many terms are retained here that are usually neglected. Particularly when field data are employed, many of these terms can not be estimated meaningfully due to inadequate spatial resolution. The most important terms for the analysis of transport in the San Francisco Estuary are:

- $A_a U_a S_a + S_a \langle A_c U_c\rangle$ – Advective salt flux (QS in the salt balance equation)
- $A_a [u_v s_v]$ – gravitational circulation
- $\langle[u'_v s'_v] (A_a + A_c)\rangle$ - the primary term associated with unsteady vertical shear

- A_a <U_c S_c> - the primary term associated with tidal dispersion

Most other terms are also associated with some form of tidal dispersion. The reasons that the gravitational circulation and unsteady vertical shear terms are given special attention are that these terms are substantial in most of the estuary and they involve vertical variability in velocity and salinity and, therefore, are not represented in a depth-averaged approach. The SIPS mechanism discussed in Section 2 may contribute both to $A_a[u_v\, s_v]$ and $<[u'_v s'_v](A_a + A_c)>$ as well as other terms.

The salt flux at each cross-sectional location shown in Figure H1.3-1 is analyzed for several flow scenarios. The salt flux associated with each mechanism is calculated for each cross-section and each scenario. The overall dispersion coefficient for each section and flow scenario is then portioned into 3 components:

- 1) K_{gc} – the dispersion coefficient associated with gravitational circulation
- 2) K_{us} – the dispersion coefficient associated with unsteady vertical shear
- 3) K_{2D} – the dispersion coefficient represented with all other processes

Though K_{2D} can reasonably be referred to as a dispersion coefficient for "two-dimensional" tidal dispersion processes it should be emphasized that a three-dimensional model should predict a different K_{2D} than an otherwise equivalent depth-averaged model. More generally, the interpretation of Equation 3.1-10, and definition of dispersion components does NOT imply that these physical processes are independent and that their effects are additive. In reality, the circulation in the San Francisco Estuary is three-dimensional and physical processes interact in a complex and nonlinear manner. In other words, while the salt flux analysis is mathematically precise, the interpretation of the analysis is not precise. Some terms in the salt flux analysis are associated with one or more physical process while other terms are less directly associated with any distinct physical processes. Furthermore, while these physical processes are conceptually distinct, in a complex setting such as the San Francisco Estuary, they are all simplified conceptual representations that are a useful but limited attempt to understand or "untangle" the complex physics that result in dispersive transport.

H1.3.2 Gravitational Circulation

Previous studies have indicated that the strength of gravitational circulation increases with a non-dimensional parameter termed the horizontal Richardson number, Ri_x (Stacey et al. 2001):

$$Ri_x = g\,(d\rho/dx)\,H^2/u_*^2, \qquad (3.2\text{-}1)$$

where g is gravity, ρ is density, x is longitudinal position, H is water column depth and u_* is friction velocity. Dispersion resulting from gravitational circulation is found to increase strongly with increased Ri_x (Monismith, 2002). When the "critical Richardson number" is reached conditions of periodic stratification transition to conditions of persistent stratification, leading to dramatically increased salt transport (Monismith et al. 2002). Monismith et al. (2002) used a "water column" model to estimate that the dispersion

coefficient associated with gravitational circulation varied according to the relationship $K/u*H = a\ Ri_x^2$.This finding was consistent with a previous analytical relationship derived by Hansen & Rattray (1965) though the constant "a" determined by Monismith et al. (2002) was 4 orders of magnitude larger.

The salt flux analysis results in one value of calculated K_{gc} and Ri_x at each cross-section and flow scenario that can be used to develop a relationship between Ri_x and K_{gc}. Previous modeling and analytical efforts assumed uniform bathymetry in both the longitudinal and lateral directions to derive the relationship $K_{gc}/u*H = a\ Ri_x^2$. In the San Francisco Estuary depth, velocity and salinity vary both in the lateral and longitudinal directions. This complicates the analysis in two ways. First, it is not clear if cross-sectional average values or channel centerline ("thalweg") values are more appropriate to use in calculating Ri_x. This analysis uses u*, H and $d\rho/dx$ predicted along the channel centerline because gravitational circulation occurs primarily in the deepest part of cross-sections. The second issue is longitudinal variability of bathymetry. Some distance is required to allow development of strong gravitational circulation, so sills along the axis of the estuary can limit the development of gravitational circulation. Because longitudinal bathymetric variability is substantial, the relationship used by Monismith et al. (2002) has been generalized to the form $K_{gc}/U*H = a\ Ri_x^b$ and the coefficients "a" and "b" are determined by a best fit approach. This generalization is somewhat arbitrary but appears to be useful because, as will be shown in Section 6, this form of equation describes the variability of the estimated K_{gc} well at most cross-sections.

H1.4 Model Description

The TRIM3D model was used in the simulations described in this report. The TRIM3D model is a state-of-the-art three-dimensional model and, unlike most models, all details and properties of the numerical method are well-documented in peer reviewed literature (Casulli 1990; Cheng et al. 1993; Casulli & Cattani 1994). The TRIM model has been applied extensively to simulate San Francisco Estuary hydrodynamics both as a depth-averaged model (TRIM2D) and a three-dimensional model (TRIM3D). Cheng et al. (1993) performed depth-averaged simulations of hydrodynamics and showed excellent tidal calibration against an extensive set of harmonic constants derived from observations of tidal elevation and tidal currents. Three-dimensional simulations of salinity in SSFB were performed with the TRIM3D model (Gross et al. 1999b). The model was later applied to all of San Francisco Bay as part of the SFO Proposed Runway Reconfiguration Studies (URS, 2003). Calibration for this study involved using harmonic constants from tidal observations and mechanical current meter and validation included comparison against ADCP data. Salinity was simulated during 3 water years, 1993, 1994, and 1998, spanning a large range of flow conditions (URS, 2003). The exact version of TRIM3D used in the DRMS project was developed as part of a CALFED funded study focused on transport processes in the "northern reach" of the San Francisco Estuary (Gross et al. 2006). This version of the model incorporated a recently developed generalized length scale turbulence closure model (Umlauf and Burchard 2003).

The TRIM3D model domain for the San Francisco Estuary simulations includes South San Francisco Bay, Central San Francisco Bay, San Pablo Bay, Suisun Bay, a portion of the Sacramento-San Joaquin River Delta, and a portion of the coastal ocean extending to approximately 22 km west of the Golden Gate. The primary data source for the bathymetric grid of South San Francisco Bay, Central Bay, and San Pablo Bay was NOAA DEM (Digital Elevation Model) data. Several additional bathymetric data sources were used to develop a 200 meter resolution Cartesian model grid, as described by Gross et al. (2006).

As seen in Figure H1.4-1, geometric approximations were made to represent the coastal ocean and Sacramento-San Joaquin River Delta portions of the model grid. The model domain in the coastal ocean uses an idealized geometry which excludes a portion of the coastal ocean along the coastline south of the Golden Gate. The reason for this simplification is to reduce computational time associated with the inclusion of many additional computational cells that would be required to represent the open ocean region. The Sacramento River seaward of Rio Vista is included in the bathymetric grid and the San Joaquin River seaward of Dutch Slough and Jersey Point is included in the bathymetric grid. These locations were chosen as the upstream boundaries of the resolved grid because tidal flows are observed at these locations by the USGS using UVM instruments (Oltmann 1998). Two polygons are used to roughly represent the remaining portion of the Delta and a simplified geometry is used to represent Threemile Slough. The size of the polygons was adjusted to reproduce the tidal prism observed at the UVM stations. These approximations were made because the actual Delta geometry can not be adequately resolved using a 200 m bathymetric grid, and representation of this geometry on a coarse grid would not result in an accurate resolved area or tidal prism in the Delta. The final bathymetric grid consists of 42,424 active water columns and is shown in Figure H1.4-1. The three-dimensional model uses 1 meter vertical resolution and consists of 569,602 active grid cells.

The TRIM3D model was applied to study circulation and salt transport in the San Francisco Estuary during a range of weather conditions. The model was calibrated to match tidal elevation, tidal current, flow and salinity data during a period in 1997 and then compared with data collected in 1994 which indicates the vertical distribution of velocity and salinity. The model realistically predicts tidal currents and variability in salinity at both the seasonal and tidal time scale, as described by Gross et al. (2006).

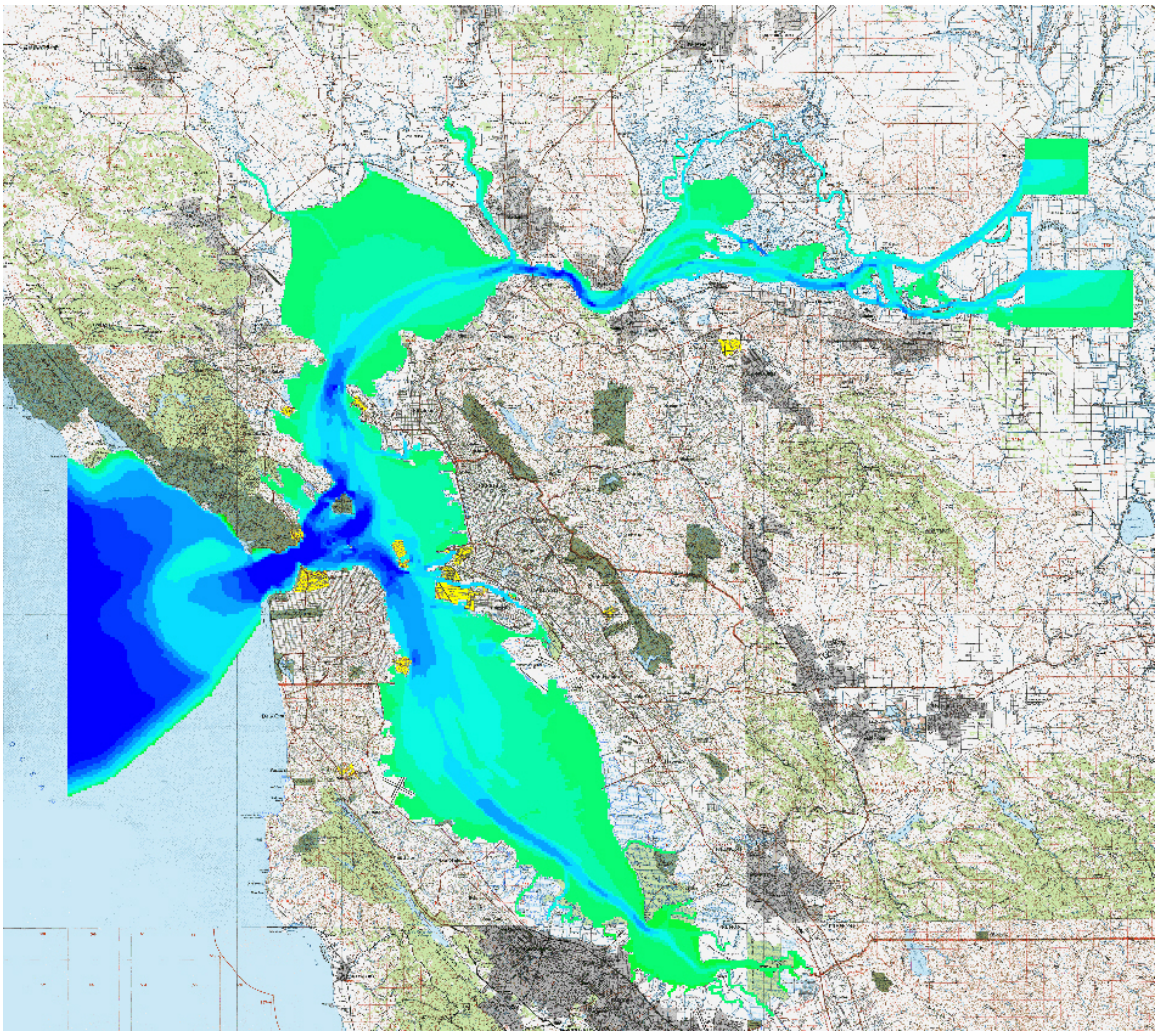

Figure H1.4-1Bathymetry on the 200 meter resolution TRIM3D model grid.

H1.5 Model Scenarios

The dispersion analysis method described in Section 3 requires that the tidally-averaged salinity field reaches steady state conditions. If model scenarios used realistic tidal forcing, variable Net Delta Outflow (NDO) and incorporated wind and other forcing, tidally-averaged steady state conditions would not be reached because the model would be continuously responding to variations in forcing. Therefore simplified forcing is used in the scenario simulations to allow the predicted salinity to reach tidally-averaged steady state conditions. As described in Section 3, the WAM, which will incorporate the dispersion coefficients determined by this analysis, predicts monthly-averaged salinity. Therefore estimating variability of dispersion coefficients with tidal amplitude (e.g., during the spring-neap cycle) is beyond the scope of the analysis. The desired product of the dispersion analysis is a set of dispersion coefficients that vary with the salinity field (NDO) and apply to average tidal conditions.

Six scenarios were simulated with TRIM3D. All scenarios used an idealized tide based on the M2 and K1 harmonic constituents reported by NOAA at the Point Reyes station (station 9415020). The M2 period was modified to 12.0 hours so that exactly 2 M2 cycles occur per K1 cycle (day). All other harmonic constituents and non-tidal forcing at the seaward boundary were neglected. The only difference between the scenarios is the Net Delta Outflow used. The Net Delta Outflows used and the names of these scenarios are given in Table H1-1.

The simplified forcing is premised on several approximations, including 1) that tidal forcing is dominant relative to wind forcing and other environmental forcing, 2) that a repeating M2 and K1 tide, with M2 period modified to 12 hours closely approximate "typical" tidal conditions, 3) that the average dispersion over a spring-neap tidal cycle is similar to the dispersion for average tidal amplitude, and 4) that local tributary inflows do not affect tidal dispersion.

Table H1-1 Names and Net Delta Outflows of Each Simulation Scenario

Scenario	Net Delta Outflow (m^3/s)
Critical	55
Drought	110
Drought Low	151
Low	260
Medium	630
High	2810

H1.6 Scenario Simulation Results

Each scenario simulation was run for several weeks until tidally-averaged steady state salinity conditions were achieved. Figure H1.6-1 shows that tidally-averaged salinity conditions have approximately reached steady state by the end of each scenario simulation and that the simulations are longer for the lower flow scenarios than the higher flow scenarios. When the tidally-averaged salinity is constant in time the tidally-averaged salt flux past all cross-sections is approximately zero. Under these conditions the net advective flux (from Net Delta Outflow) of salt in the seaward direction balances the dispersive flux of salt in the landward. The net flux is less than one percent of the advective flux at nearly all sections and scenarios used in this analysis. The tidally-averaged salinity profile along the transect shown in Figure H1.6-1 is shown for each scenario in Figures H1.6-2 to H1.6-7.

As expected the degree of salt intrusion increases with decreased Net Delta Outflow. Salinity gradients move seaward and stratification increases with increased Net Delta Outflow. The results of the medium and high flow scenarios show strong stratification in San Pablo Bay and Carquinez Strait and limited "flushing" of salt from these regions. These results suggest strong gravitational circulation in these regions and are consistent with the findings of Burau et al (1998) and Monismith et al. (2002). More evidence of the

locations of active gravitational circulation and variability with Delta outflow will be presented in the following section.

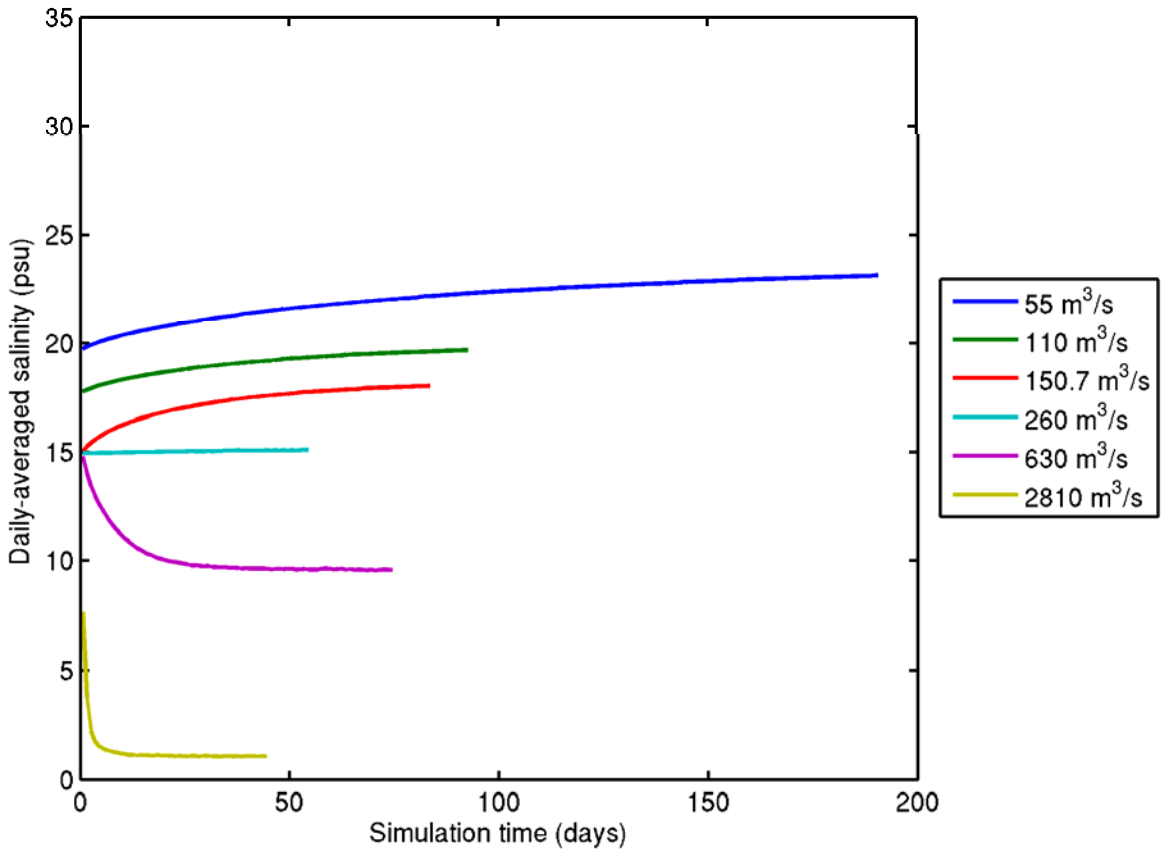

Figure H1.6-1Tidally-averaged depth-averaged salinity (psu) at Martinez for all flow scenarios.

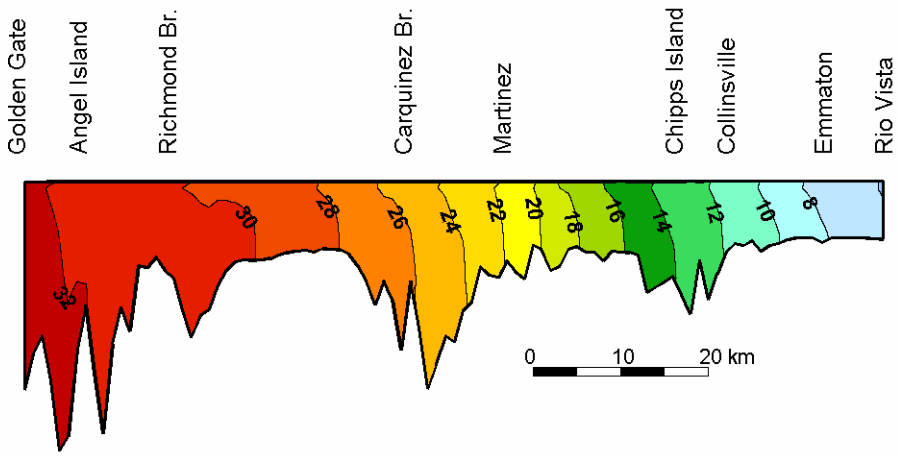

Figure H1.6-2Tidally-averaged salinity (psu) along the centerline transect from Golden Gate to Rio Vista for the scenario with Net Delta Outflow of 55 m3/s.

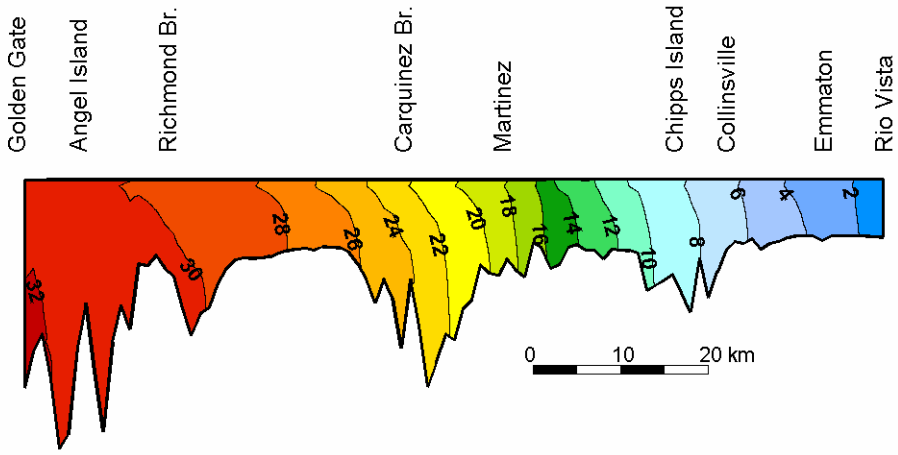

Figure H1.6-3Tidally-averaged salinity (psu) along the centerline transect from Golden Gate to Rio Vista for the scenario with Net Delta Outflow of 110 m3/s.

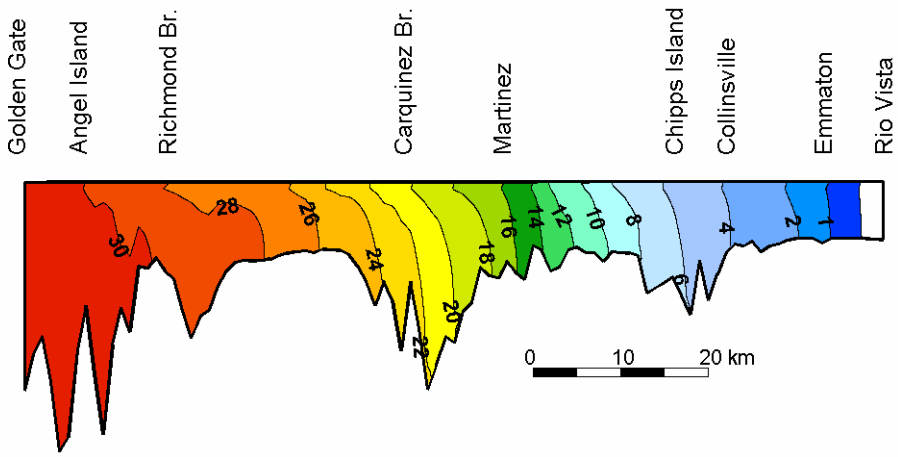

Figure H1.6-4Tidally-averaged salinity (psu) along the centerline transect from Golden Gate to Rio Vista for the scenario with Net Delta Outflow of 151 m3/s.

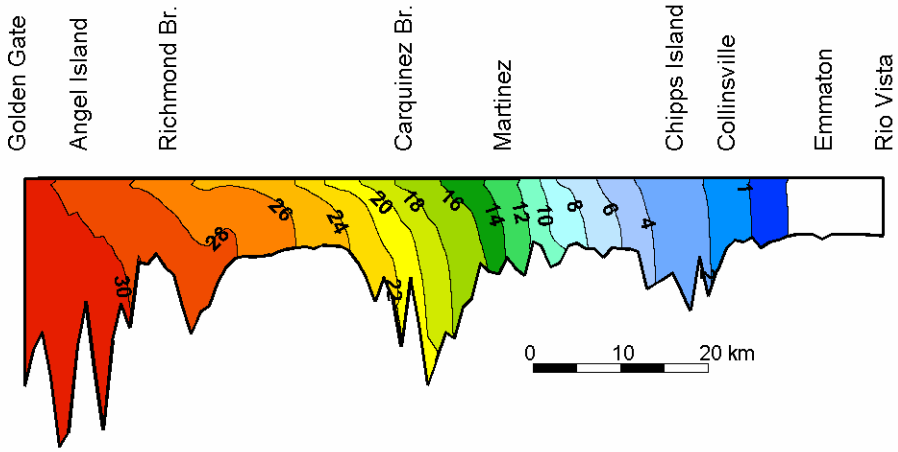

Figure H1.6-5Tidally-averaged salinity (psu) along the centerline transect from Golden Gate to Rio Vista for scenario with Net Delta Outflow of 260 m^3/s.

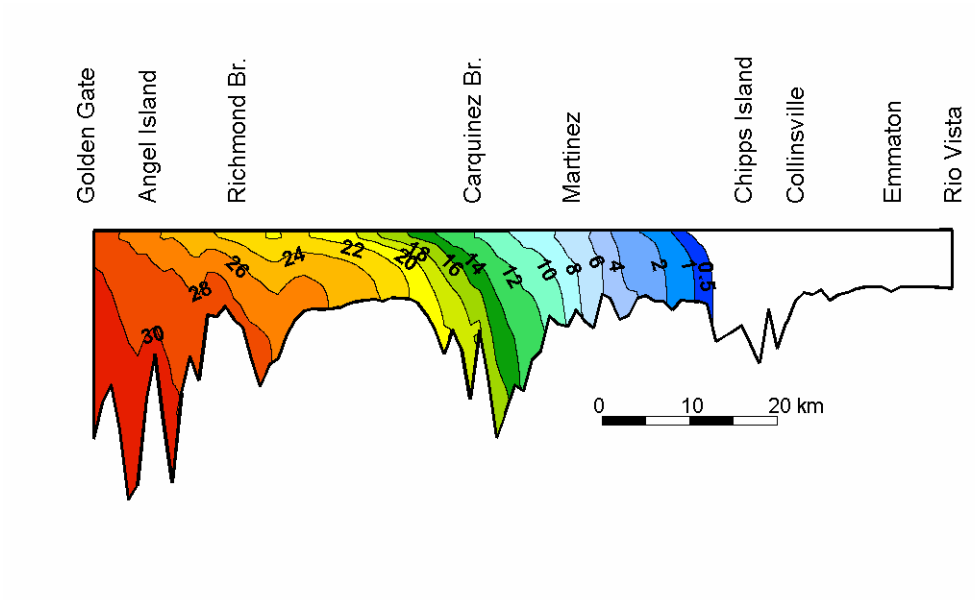

Figure H1.6-6Tidally-averaged salinity (psu) along the centerline transect from Golden Gate to Rio Vista for the scenario with Net Delta Outflow of 630 m3/s.

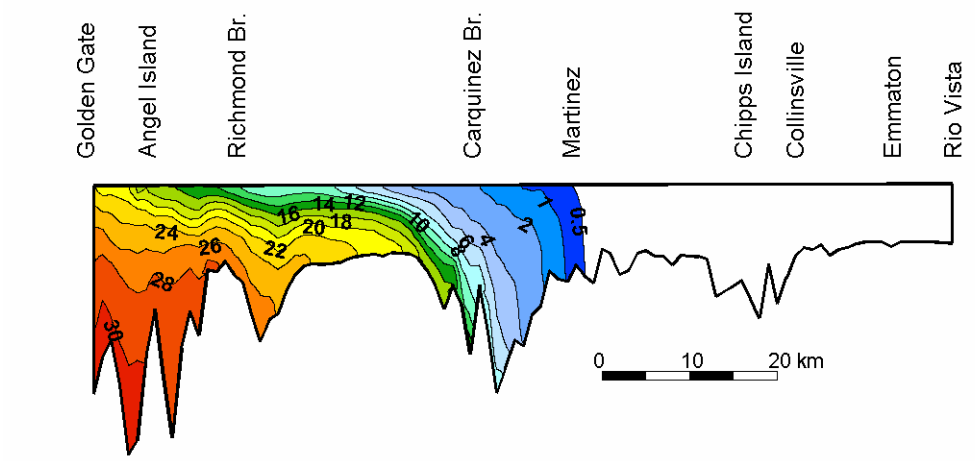

Figure H1.6-7Tidally-averaged salinity (psu) along the centerline transect from Golden Gate to Rio Vista for the scenario with Net Delta Outflow of 2,810 m3/s.

H1.7 Analysis of Scenario Simulations

The predicted salinity along the centerline transect shown in Figure H1.7-1 is depth-averaged for each scenario at tidally-averaged steady state conditions. The longitudinal salinity gradient at each point is determined by a linear fit to the depth-averaged salinity over roughly one tidal excursion (12 km) to determine the longitudinal salinity gradients shown in Figure H1.7-1. Note that the salinity gradient necessarily approaches zero when salinity approaches zero in the landward reaches of the domain. This information was used along with the estimated tidally-averaged cross-sectional area, salinity and flow at each cross section and scenario to determine the dispersion coefficients shown in Figure H1.7-2. Dispersion coefficients were not calculated in regions with tidally-averaged salinity gradients of less than 0.05 psu per km, horizontal Richardson number of less than 0.1, or minimum instantaneous salinity less than 0.4 psu during any portion of the tidal cycle. Different symbol colors and sizes are used for different flow scenarios in Figure H1.7-2. The dispersion coefficients show large spatial variability and variability with Delta outflow. A logarithmic vertical scale was used to show the large variability of estimated dispersion coefficients.

The flux analysis described in Section 3 was used to divide this dispersion coefficient into the three components discussed in Section 3. The estimated dispersion coefficients associated with gravitational circulation (K_{gc}) are shown in Figure H1.7-3. These dispersion coefficient components are even more variable with both flow and location than the overall dispersion coefficients. The dispersion coefficients associated with gravitational circulation drop substantially in Suisun Bay, starting at 55 km from the Golden Gate, and account for most of the drop in the overall dispersion coefficients in this region. These results are consistent with the findings of Burau et al. (1998) in the Entrapment Zone Study. The interpretation in that study is that the reduced depth at the Benicia shoal reduced the strength of gravitational circulation. Also note that dispersion coefficients associated with gravitational circulation increase with flow in Central San Francisco Bay and San Pablo Bay but decrease with increased flow in Suisun Bay and the western Delta. This is consistent with Figure H1.7-1, which shows that longitudinal salinity gradients increase with flow in Central San Francisco Bay and San Pablo Bay but decrease with increased flow in Suisun Bay and the western Delta as salt is flushed from those regions by the increased flow.

The dispersion coefficients associated with unsteady vertical shear (K_{us}) are shown in Figure H1.7-4. Many of the spatial trends and variability with flow are similar for the unsteady vertical shear component and the gravitational circulation component. This is not surprising because both components are expected to increase with increased stratification. While the unsteady vertical shear component is smaller than the gravitational circulation component in Central San Francisco Bay and San Pablo Bay, it is of similar magnitude as the gravitational circulation component in Suisun Bay and the western Delta. Some of the dispersion associated with unsteady vertical shear component is associated with the SIPS mechanism which is known to be active in portions of Suisun Bay (Stacey et al. 2001).

The dispersion coefficients associated with all other processes, termed K_{2D}, are shown in Figure H1.7-5. This dispersion is primarily associated with tidal dispersion. The tidal dispersion coefficient shows less spatial variability and variability with flow than the other components of dispersion. Since this component of the dispersion coefficient is not expected to have strong variation with stratification, the less pronounced variability with flow was expected.

Next each cross-section is examined individually and a curve fit is used to describe the variability of the gravitational circulation component with horizontal Richardson number. The horizontal Richardson estimates were calculated along the centerline transect shown in Figure H1.3-2. The root mean square (rms) depth-averaged velocity is shown in Figure H1.7-6. The root mean square velocity varies from roughly 0.3 m/s to 1 m/s along the transect. This velocity is used in the estimate of friction velocity for calculation of horizontal Richardson number. The assumed coefficient of drag was 0.0025. The WAM will use rms depth-averaged velocity to calculate horizontal Richardson number. For this reason the same approach was followed here, instead of saving the friction velocity used internally in the TRIM3D model. The tidally-averaged and depth-averaged salinity gradients shown in Figure H1.7-1 and the channel invert (“thalweg”) depth along the centerline transect were also used to calculate the horizontal Richardson numbers shown in Figure H1.7-7. In the following sections, the analysis of each sub-embayment will be discussed in turn.

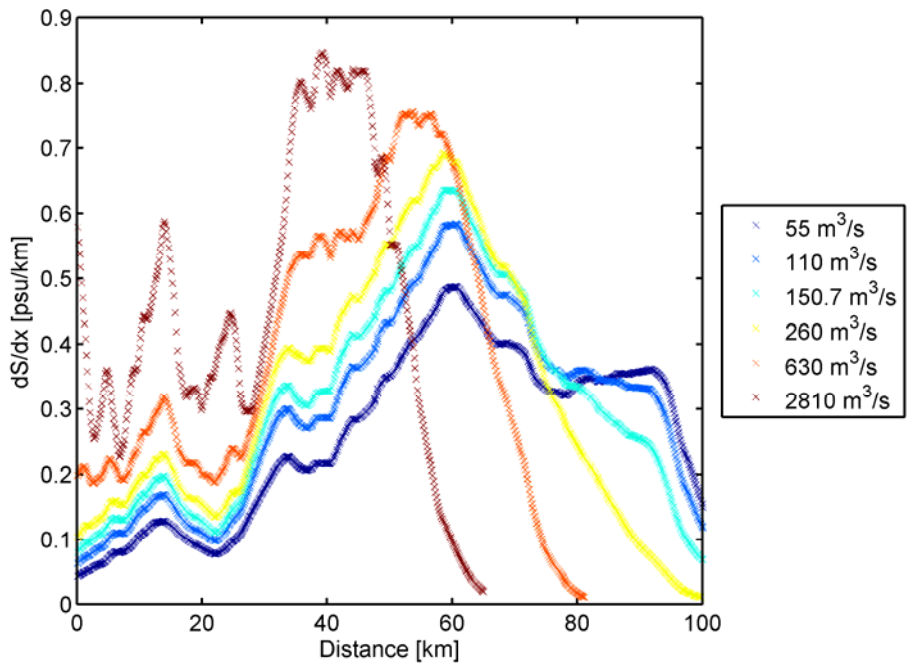

Figure H1.7-1Estimated depth-averaged salinity gradient for all flow scenarios. The horizontal scale is distance along the axis of the estuary from the Golden Gate.

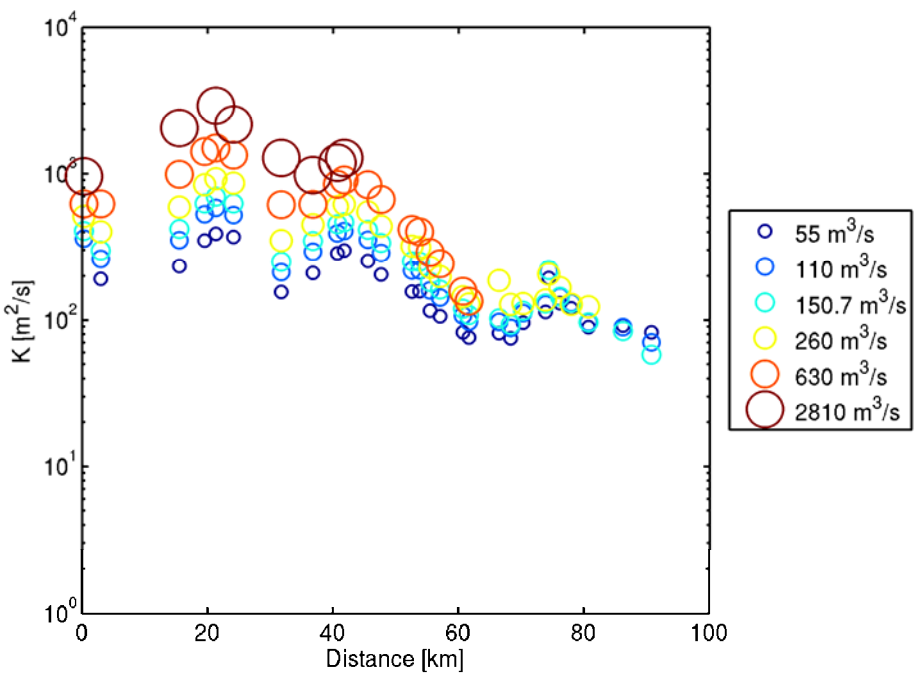

Figure H1.7-2Estimated total dispersion coefficients (K) for all flow scenarios. The horizontal scale is distance along the axis of the estuary from the Golden Gate.

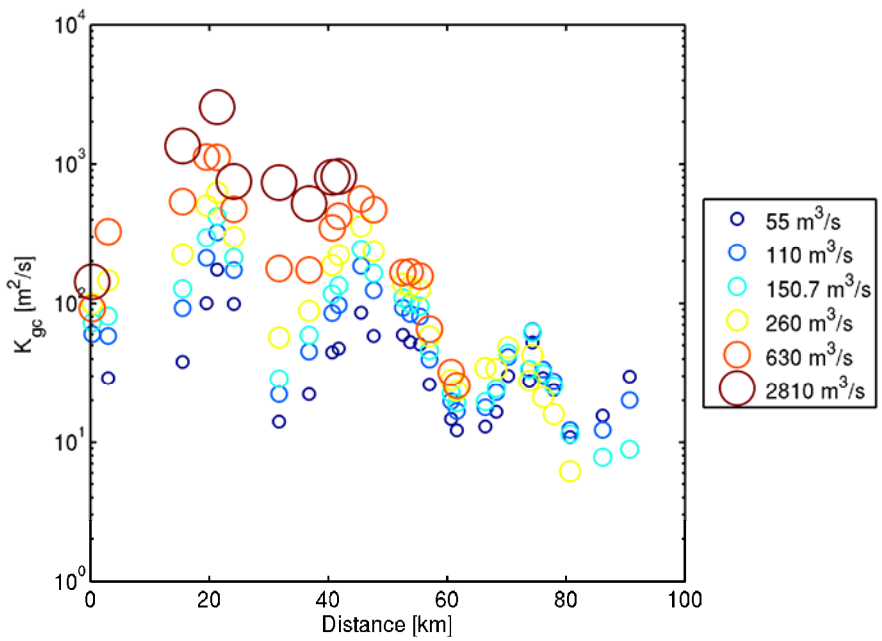

Figure H1.7-3Estimated dispersion coefficients associated with gravitational circulation (Kgc) for all flow scenarios. The horizontal scale is distance along the estuary from the Golden Gate.

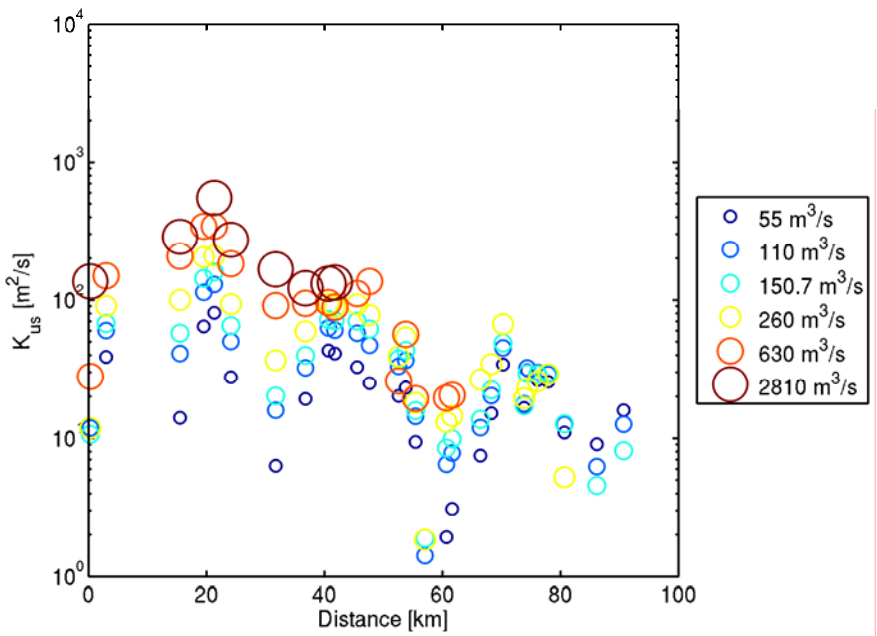

Figure H1.7-4Estimated dispersion coefficients associated with "unsteady shear" (Kus) for all flow scenarios. The horizontal scale is distance along the estuary from the Golden Gate.

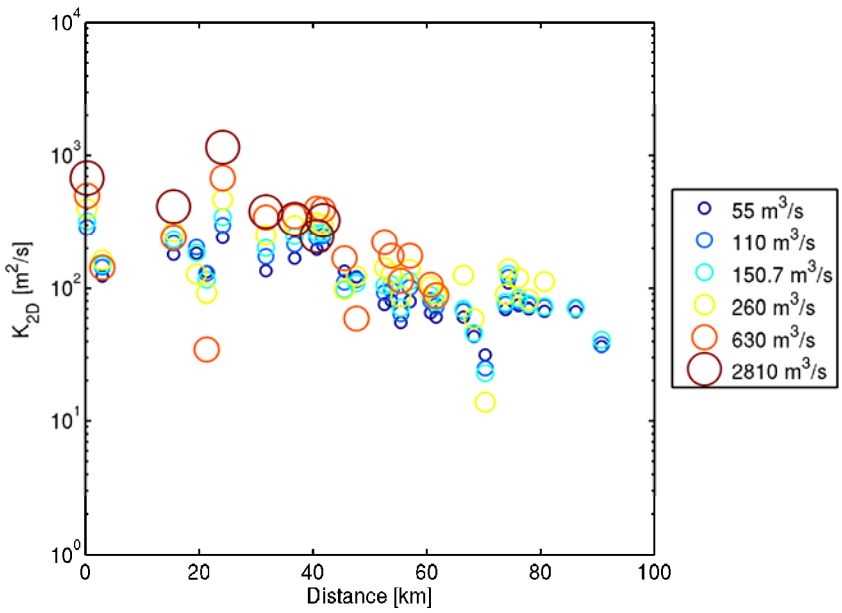

Figure H1.7-5Estimated dispersion coefficients associated with all tidal dispersion (K2D) for all flow scenarios. The horizontal scale is distance along the estuary from the Golden Gate.

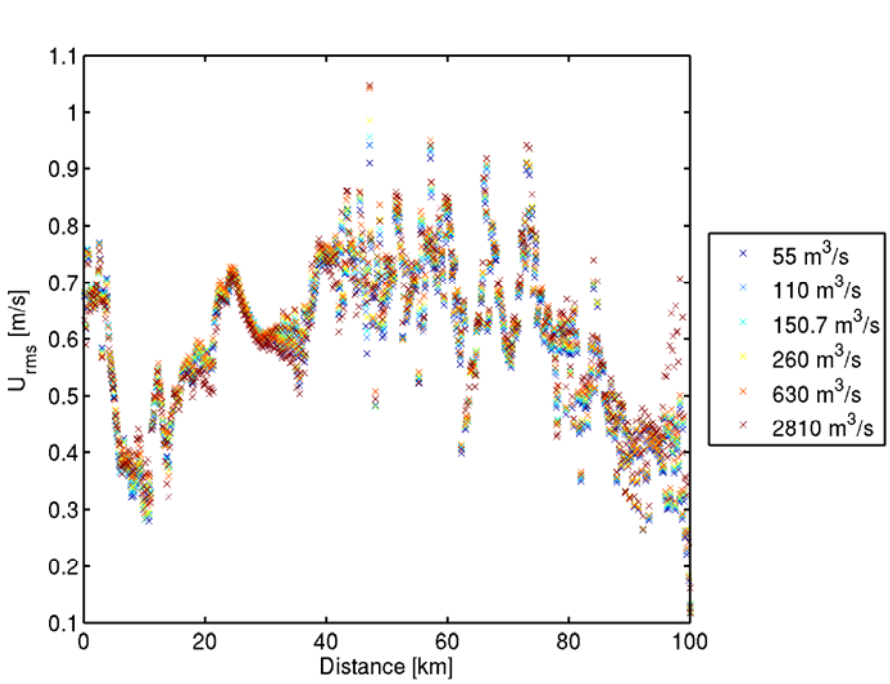

Figure H1.7-6Estimated root mean square depth-averaged velocity for all flow scenarios. The horizontal scale is distance along the axis of the estuary from the Golden Gate.

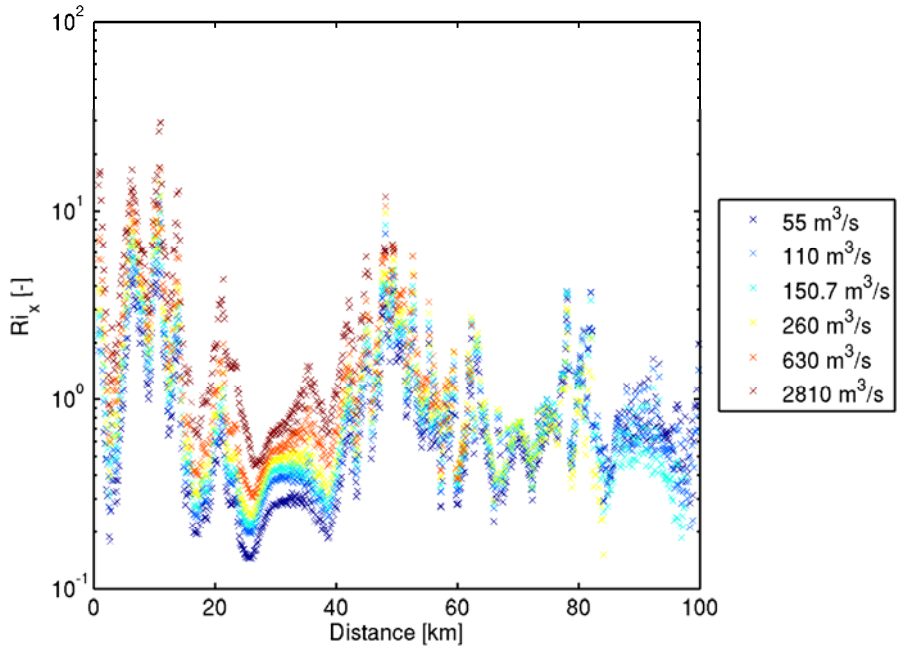

Figure H1.7-7Estimated horizontal Richardson number for all flow scenarios. The horizontal scale is distance along the axis of the estuary from the Golden Gate.

H1.7.1 Central San Francisco Bay Cross-Sections

Dispersion coefficients and fluxes were estimated at five cross-sections in Central Bay (sections 1 through 5), shown in Figure H1.3-1. The analysis method requires that all sections are aligned with the x or y coordinate axis which limits the locations where cross-sections can be analyzed. This limitation has been eliminated in more recent unstructured grid modeling which allows analysis of arbitrary cross-section transects. The unstructured grid model was used in several scenarios for the DRMS project, discussed in other appendices.

Figures H1.7.1-1 through H1.7.1-10 show each dispersion coefficient and the individual components of each dispersion coefficient as well as the curve fit of the gravitational circulation component at each cross-section in Central Bay. Note that the curve fit minimizes the error in $K_{gc}/U*H$, not the logarithm of $K_{gc}/U*H$. Therefore, because the values are plotted on a logarithmic scale, the best fit line may appear biased to better fit the larger values of $K_{gc}/U*H$.

The dispersion coefficients are generally quite large in Central Bay. Dispersion in the Golden Gate cross-section is dominated by tidal dispersion processes, while gravitational circulation is dominant at other cross-sections in Central Bay. The strength of gravitational circulation and unsteady shear increases strongly with flow at all cross-sections with the exception of the Golden Gate cross-section where the variability is not as strong. This is expected because horizontal salinity gradients and stratification increase with increased NDO, as shown in Figures H1.6-2 through H1.6-7.

The fit of K_{gc}/U^*H with Ri_x yields a range of exponents in the Central Bay cross-sections. The exponent of the curve fit is expected to be near 2 in regions with minimal lateral and longitudinal variability in depth, but the depth varies greatly both longitudinally and laterally in Central Bay. For example, at section 5, extending west from Point San Pablo, the thalweg depth is large locally, reaching 32 meters at MSL at the deepest point. This depth is used in the Richardson number calculation although it is only present in less then 500 meters of longitudinal distance. This longitudinal distance is too small for strong gravitational circulation to develop. Instead the actual gravitational circulation will be limited by shallower regions both landward and seaward of Point San Pablo.

As noted previously, K_{2D} becomes negative at sections 4 and 5 for the medium and high flow scenarios in which gravitational circulation dominates. The physical explanation for these negative values is not clear, but these unintuitive results emphasize that the actual transport processes are always three-dimensional. The physical mechanisms associated with different flux terms are conceptually distinct, but are all simplified conceptual representations that are useful to attempt to “untangle” the complex physics that result in dispersive transport.

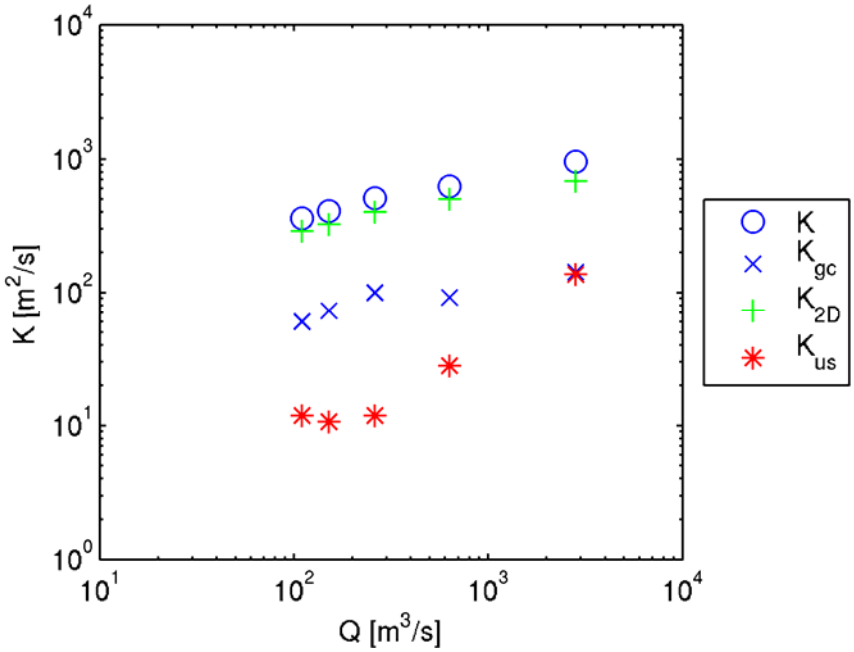

Figure H1.7.1-1 Estimated dispersion coefficients at section 1, located at the Golden Gate, as a function of Net Delta Outflow.

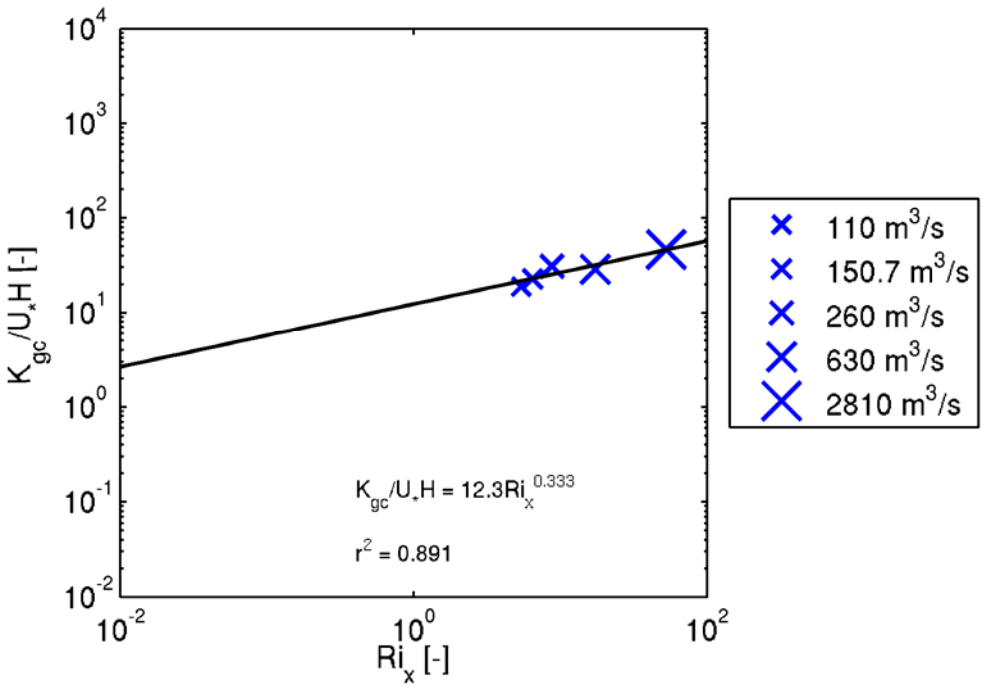

Figure H1.7.1-2 Estimated dimensionless dispersion coefficients for gravitational circulation at section 1, located at the Golden Gate, as a function of horizontal Richardson number with corresponding best fit equation and r^2 value.

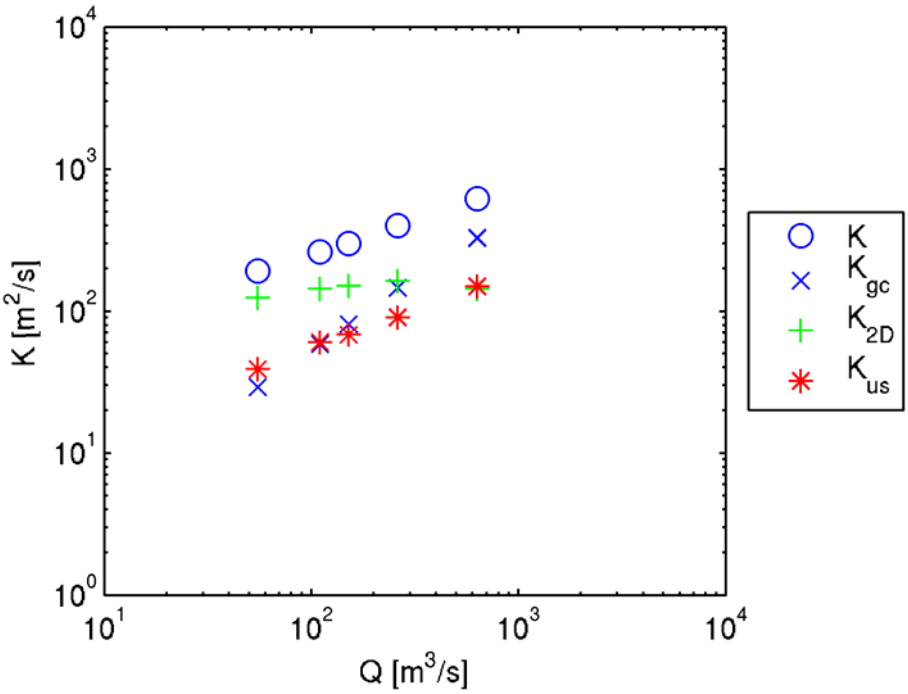

Figure H1.7.1-3 Estimated dispersion coefficients at section 2, from San Francisco to Tiburon, as a function of Net Delta Outflow.

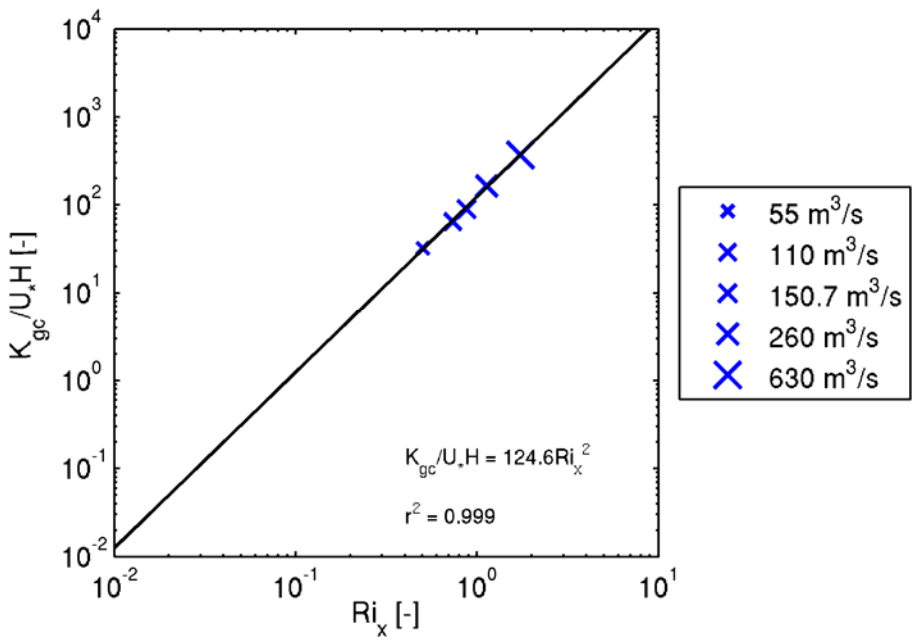

Figure H1.7.1-4 Estimated dimensionless dispersion coefficients for gravitational circulation at section 2, extending from San Francisco to Tiburon, as a function of horizontal Richardson number with corresponding best fit equation and r^2 value.

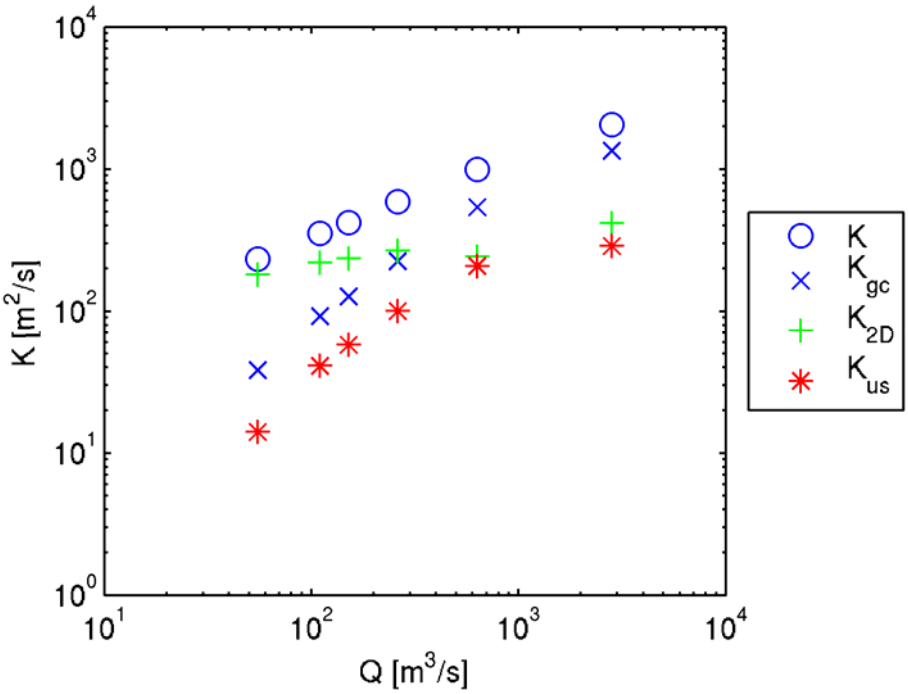

Figure H1.7.1-5 Estimated dispersion coefficients at section 3, extending from Albany to Tiburon, as a function of Net Delta Outflow.

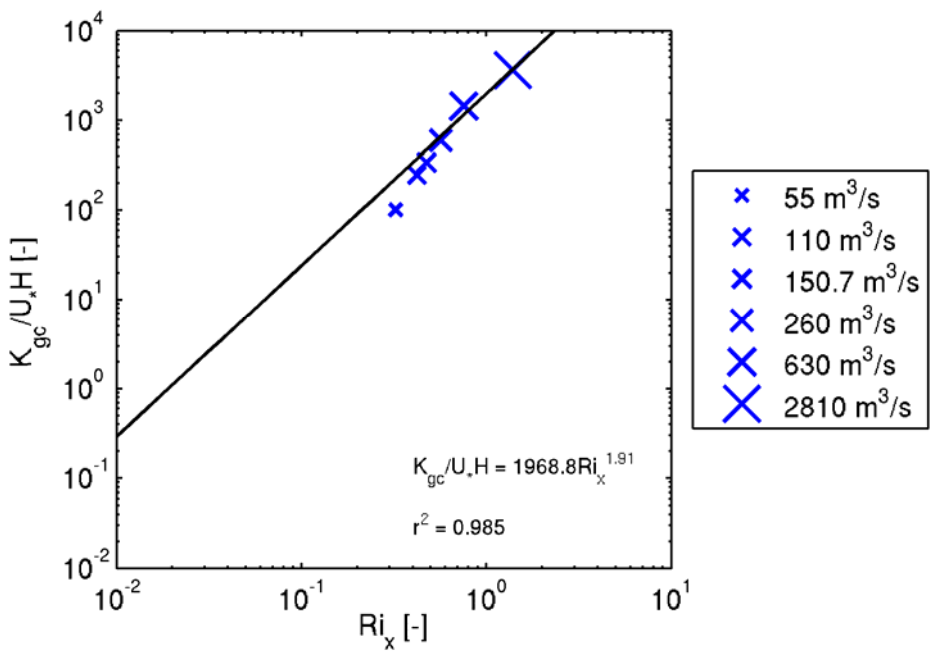

Figure H1.7.1-6 Estimated dimensionless dispersion coefficients for gravitational circulation at section 3, extending from Albany to Tiburon, as a function of horizontal Richardson number with corresponding best fit equation and r^2 value.

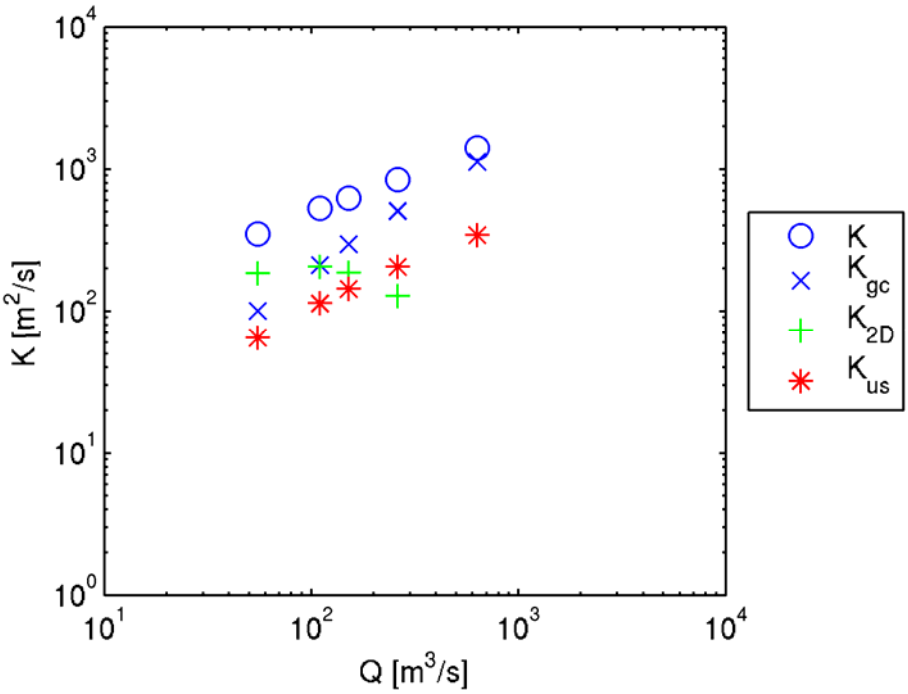

Figure H1.7.1-7 Estimated dispersion coefficients at section 4, extending from Richmond to San Rafael, as a function of Net Delta Outflow.

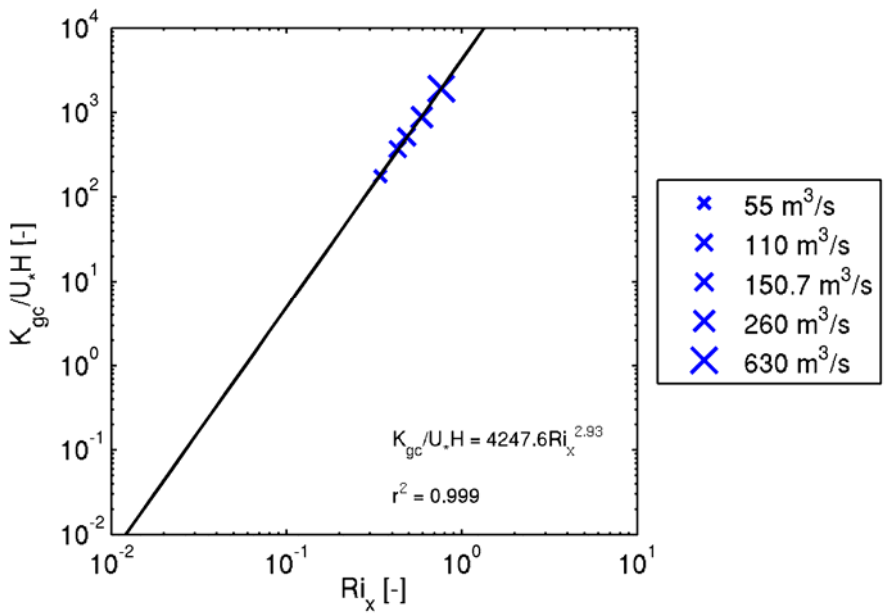

Figure H1.7.1-8 Estimated dimensionless dispersion coefficients for gravitational circulation at section 4, extending from Richmond to San Rafael, as a function of horizontal Richardson number with corresponding best fit equation and r^2 value.

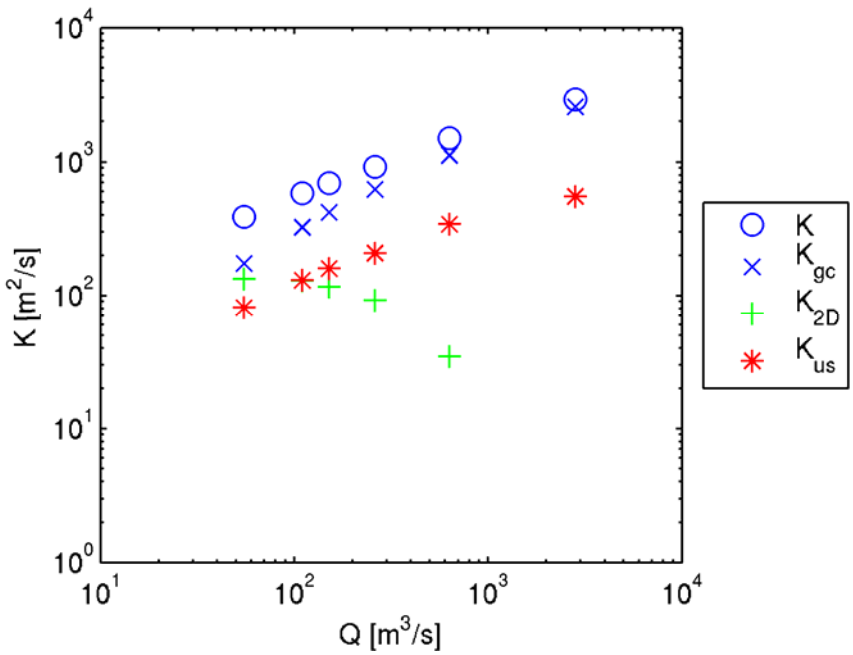

Figure H1.7.1-9 Estimated dispersion coefficients at section 5, extending from Point San Pablo to San Rafael, as a function of Net Delta Outflow.

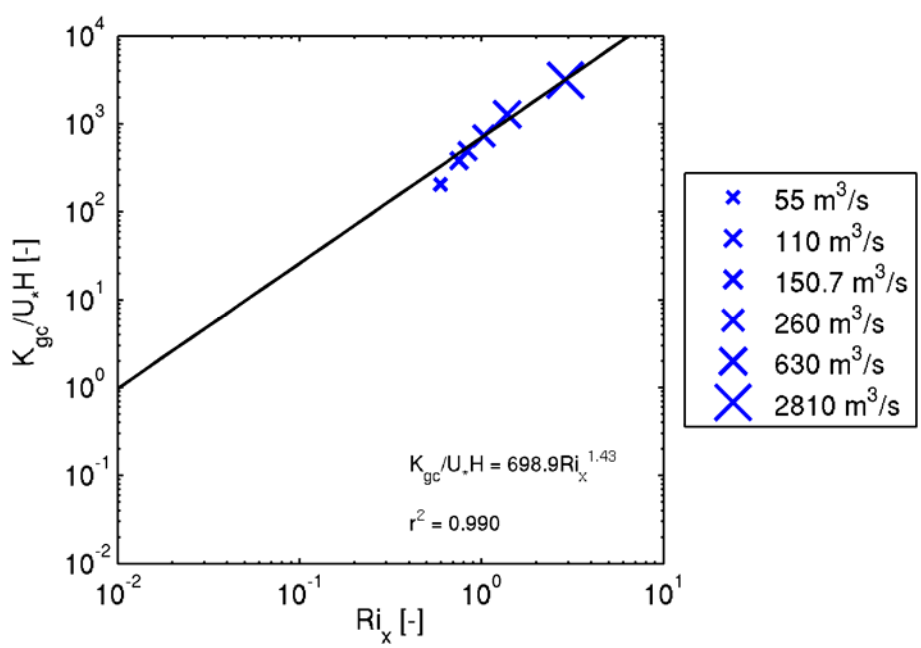

Figure H1.7.1-10 Estimated dimensionless dispersion coefficients for gravitational circulation at section 5, extending from Point San Pablo to San Rafael, as a function of horizontal Richardson number with corresponding best fit equation and r^2 value.

H1.7.2 San Pablo Bay Cross-Sections

Dispersion coefficients and fluxes were estimated at four cross-sections in San Pablo Bay (sections 6 through 9), shown in Figure H1.3-1. Figures H1.7.2-1 through H1.7.2-8 show each dispersion coefficient and the individual components of dispersion as well as the curve fit of the gravitational circulation component at each cross-section in San Pablo Bay. Note that the curve fit minimizes the error in $K_{gc}/U*H$, not the logarithm of $K_{gc}/U*H$. Therefore, because the values are plotted on a logarithmic scale, the best fit line may appear biased to better fit the larger values of $K_{gc}/U*H$.

The dispersion coefficients are large in San Pablo Bay. Dispersion in all cross-sections is dominated by tidal dispersion processes for the critical flow to low flow scenarios, while gravitational circulation is important at medium and high flow. As in Central Bay, the strength of gravitational circulation increases strongly with flow at all cross-sections. The dispersion component associated with unsteady shear also increases with NDO. The increase in the strength of three-dimensional transport processes with NDO is expected because horizontal salinity gradients and stratification increase with increased NDO, as shown in Figures H1.6-2 through H1.6-7. Tidal dispersion varies less strongly with NDO at all sections.

The fit of $K_{gc}/U*H$ with Ri_x yields a large range of exponents in the San Pablo Bay cross-sections. One likely reason for this variability is large longitudinal and lateral bathymetric variability, as discussed for the Central Bay sections. In addition, the width of shoals relative to the channel width in San Pablo Bay also varies greatly. In these regions using the thalweg depth of the channel in the Richardson number calculation might not be ideal. As shown in Figure H1.6-6 and Figure H1.6-7, strong stratification is present in San Pablo Bay for the medium and high flow scenarios. The large increase in $K_{gc}/U*H$ with Ri_x at section 7 may indicate a large increase in salt transport corresponding to the transition from periodic stratification for the lower flow scenarios to persistent stratification for the higher flow scenarios (Monismith et al., 2002).

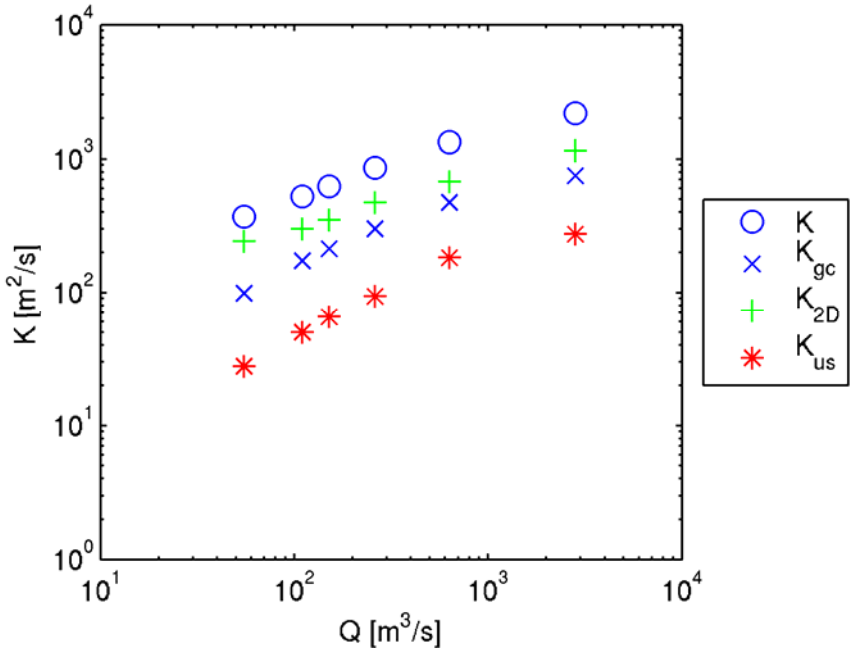

Figure H1.7.2-1 Estimated dispersion coefficients at section 6, extending from Richmond to Point San Pedro, as a function of Net Delta Outflow.

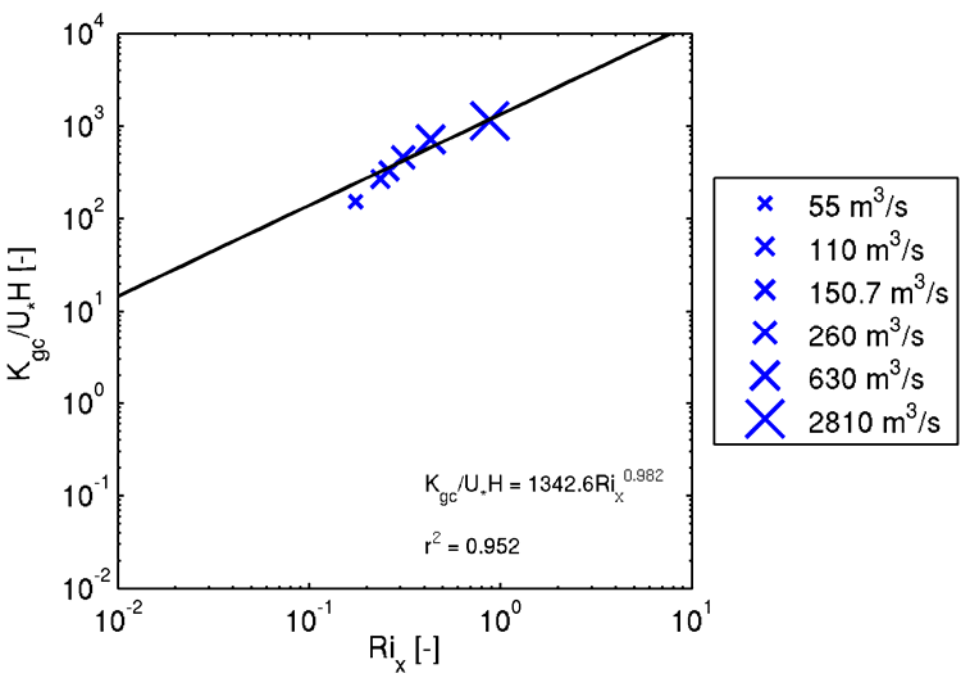

Figure H1.7.2-2 Estimated dimensionless dispersion coefficients for gravitational circulation at section 6, extending from Richmond to Point San Pedro, as a function of horizontal Richardson number with corresponding best fit equation and r^2 value.

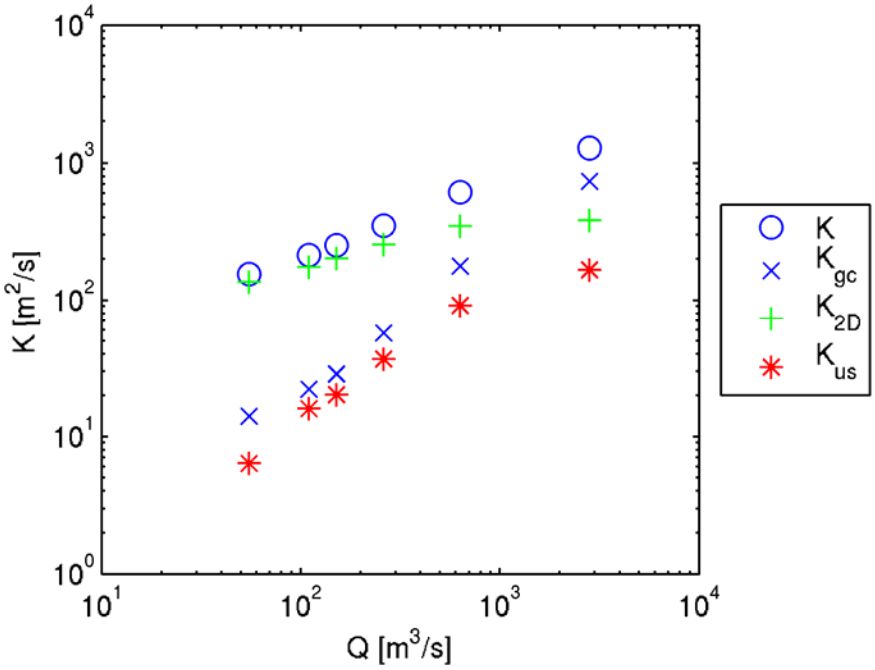

Figure H1.7.2-3 Estimated dispersion coefficients at section 7, extending from Pinole Point to Sonoma Creek, as a function of Net Delta Outflow.

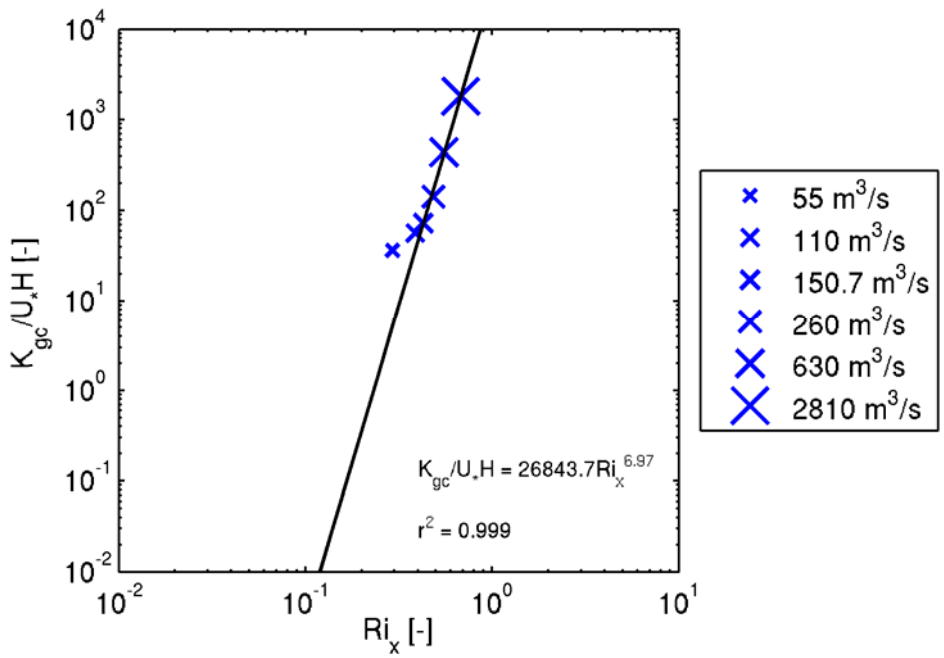

Figure H1.7.2-4 Estimated dimensionless dispersion coefficients for gravitational circulation at section 7, extending from Pinole Point to Sonoma Creek, as a function of horizontal Richardson number with corresponding best fit equation and r^2 value.

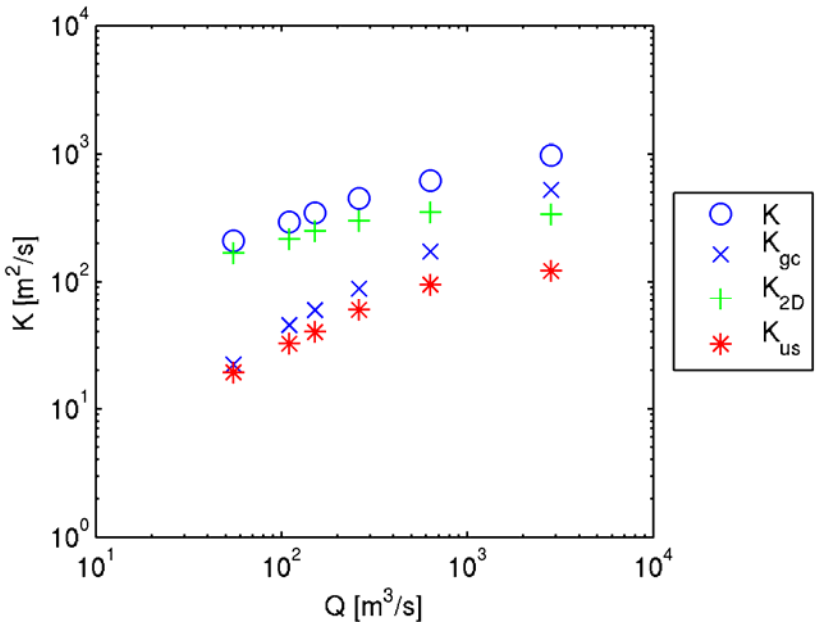

Figure H1.7.2-5 Estimated dispersion coefficients at section 8, extending from Hercules to Mare Island, as a function of Net Delta Outflow.

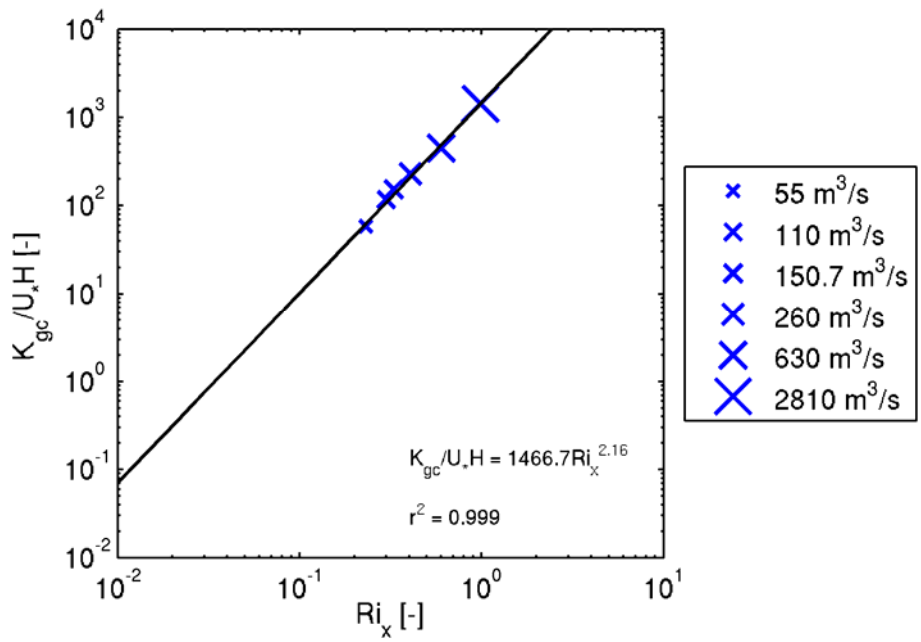

Figure H1.7.2-6 Estimated dimensionless dispersion coefficients for gravitational circulation at section 8, extending from Hercules to Mare Island, as a function of horizontal Richardson number with corresponding best fit equation and r^2 value.

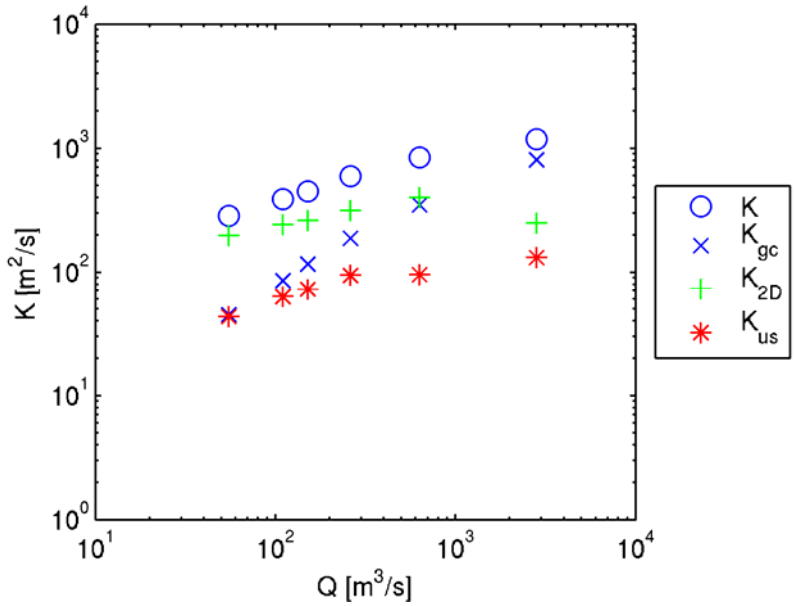

Figure H1.7.2-7 Estimated dispersion coefficients at section 9, extending from Rodeo to Mare Island, as a function of Net Delta Outflow.

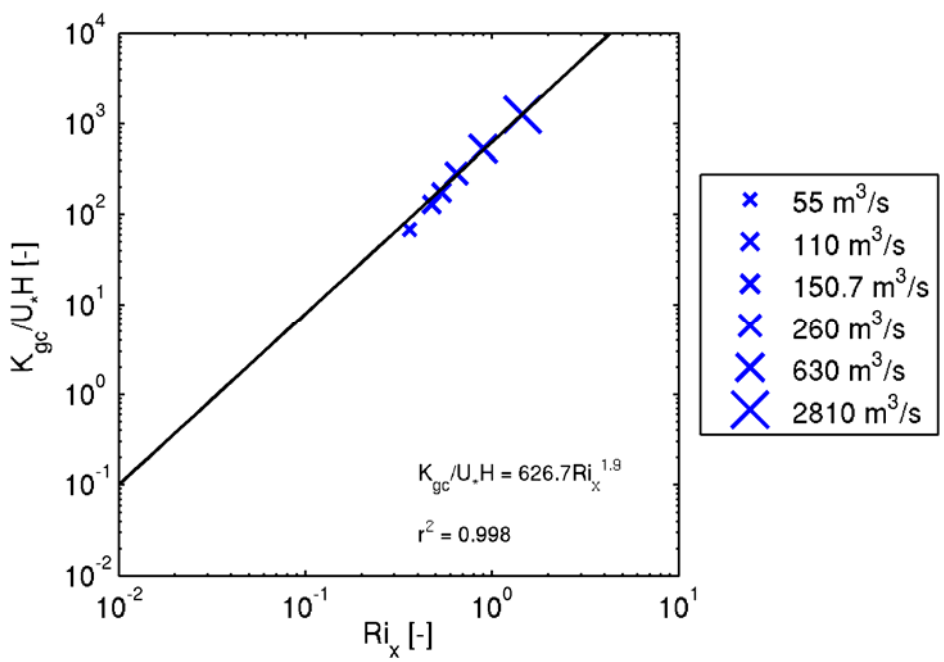

Figure H1.7.2-8 Estimated dimensionless dispersion coefficients for gravitational circulation at section 9, extending from Rodeo to Mare Island, as a function of horizontal Richardson number with corresponding best fit equation and r^2 value. Carquinez Strait Cross-Sections

H1.7.3 Carquinez Strait Cross-Sections

Dispersion coefficients and fluxes were estimated at six cross-sections in Carquinez Strait (sections 10 through 15), shown in Figure H1.3-1. Figures H1.7.3-1 through H1.7.3-12 show each dispersion coefficient and the individual components of each dispersion coefficient as well as the curve fit of the gravitational circulation component at each cross-section in Carquinez Strait. Note that the curve fit minimizes the error in $K_{gc}/U*H$, not the logarithm of $K_{gc}/U*H$. Therefore, because the values are plotted on a logarithmic scale, the best fit line may appear biased to better fit the larger values of $K_{gc}/U*H$.

The dispersion coefficients are large at the seaward end of Carquinez Strait and decrease with distance landward. Both tidal dispersion and gravitational circulation are important at all cross-sections, while unsteady shear is smaller. The strength of gravitational circulation increases strongly with flow at all cross-sections while the magnitude of unsteady shear is more constant. Note that the strength of gravitational circulation decreases for the high flow scenario, relative to the medium flow scenario at all Carquinez Strait sections, except section 10. The reason is clear in Figure H1.6-7, which indicates that salt is almost entirely flushed from Carquinez Strait for the high flow scenario, resulting in reduced salinity gradients, relative to medium flow scenario, as indicated in Figure H1.7-1. The curve fit of $K_{gc}/u*H = a\ Ri_x^b$ yields a value of b close to 2, as found by Monismith at al. (2002). The reason for this agreement may be the absence of broad shoals in this region, which reduces ambiguity in the specification of u* and H. All sections also show high correlation coefficients indicating that the curve fit equation describes the variability in observed K_{gc} accurately.

The strength of tidal dispersion (K_{2D}) increases substantially with flow scenarios at sections 13, 14 and 15. The exact reason for this increase is not clear but the increase may be associated with large differences in salinity and salinity gradients between flood tides and ebb tides for the medium and high flow scenarios.

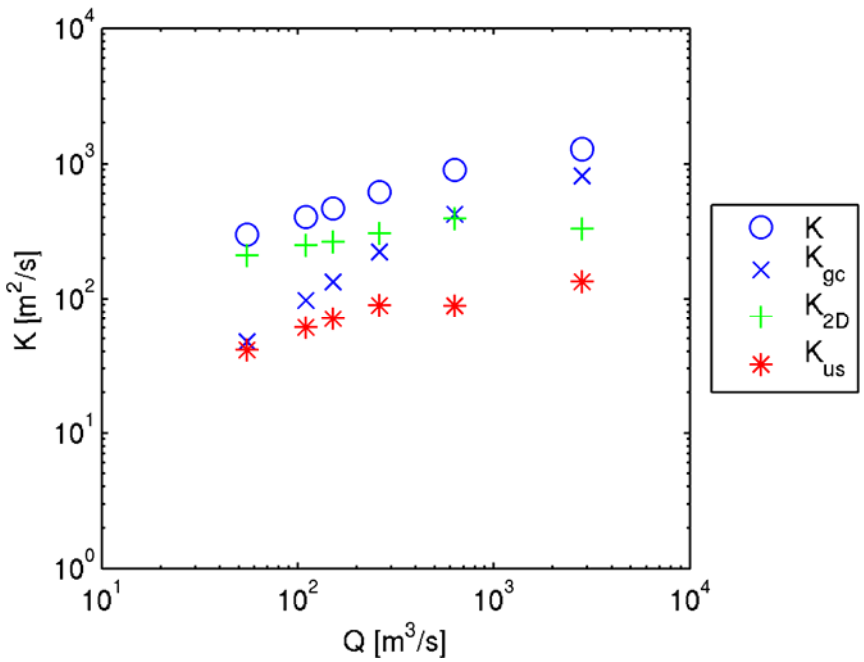

Figure H1.7.3-1 Estimated dispersion coefficients at section 10, extending from Davis Point to Mare Island, as a function of Net Delta Outflow.

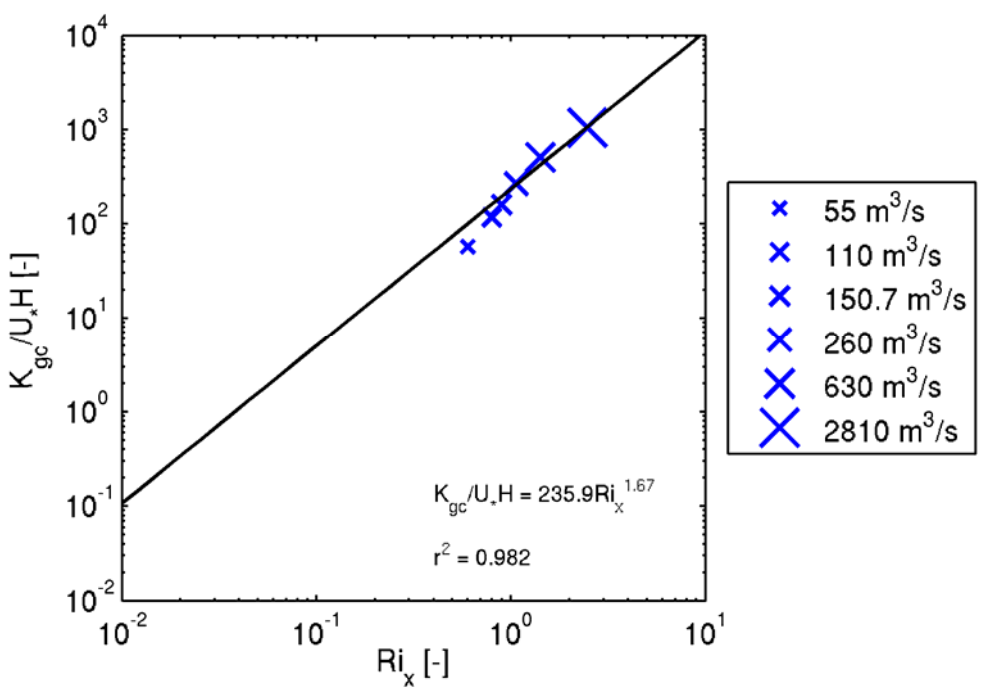

Figure H1.7.3-2 Estimated dimensionless dispersion coefficients for gravitational circulation at section 10, extending from Davis Point to Mare Island, as a function of horizontal Richardson number with corresponding best fit equation and r^2 value.

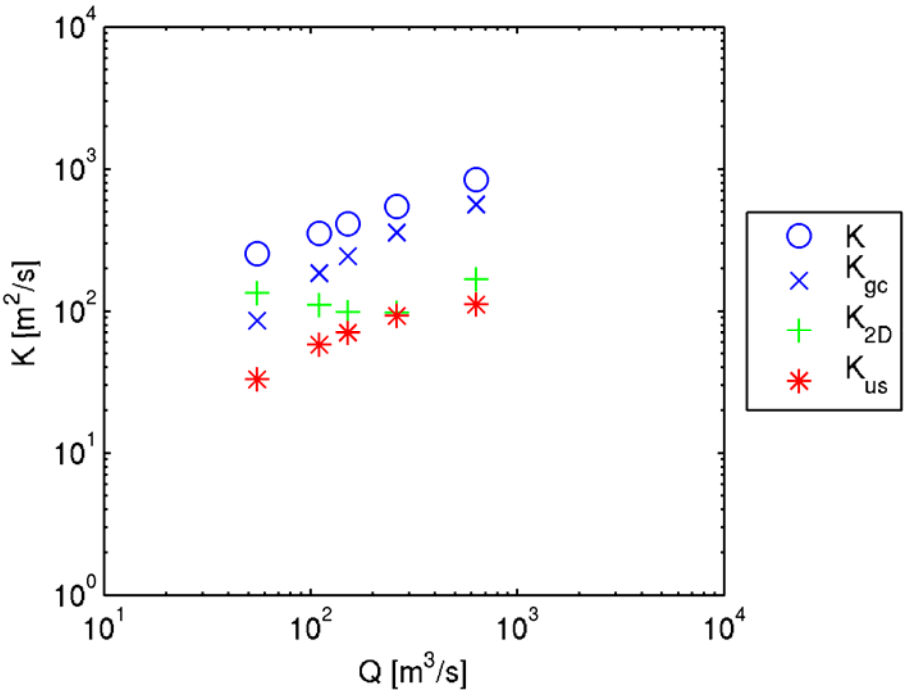

Figure H1.7.3-3 Estimated dispersion coefficients at section 11, at the Carquinez Bridge, as a function of Net Delta Outflow.

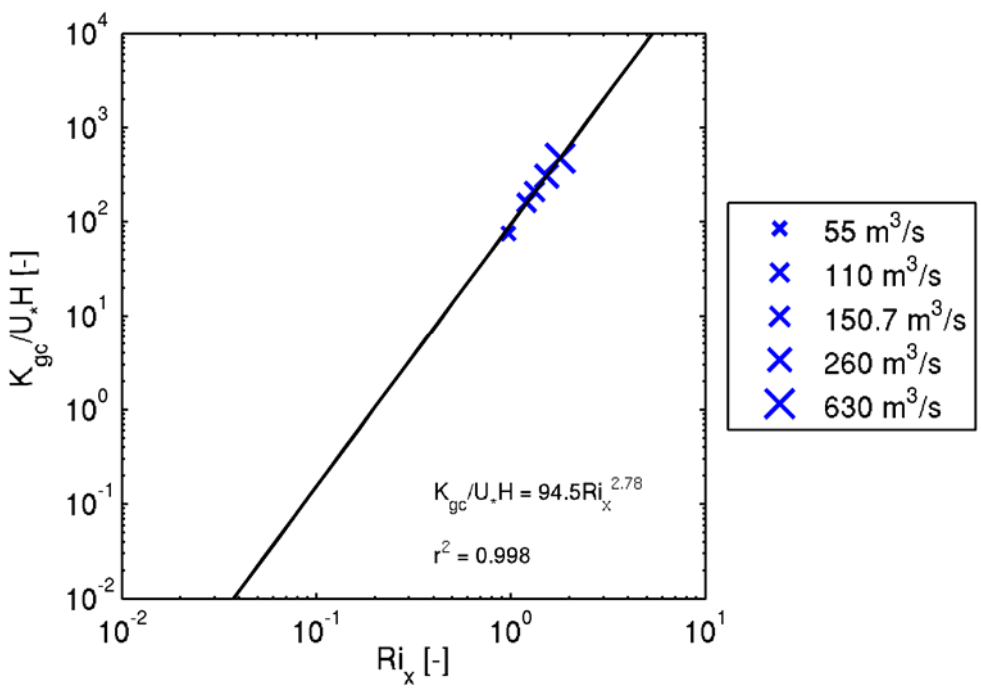

Figure H1.7.3-4 Estimated dimensionless dispersion coefficients for gravitational circulation at section 11, at the Carquinez Bridge, as a function of horizontal Richardson number with corresponding best fit equation and r^2 value.

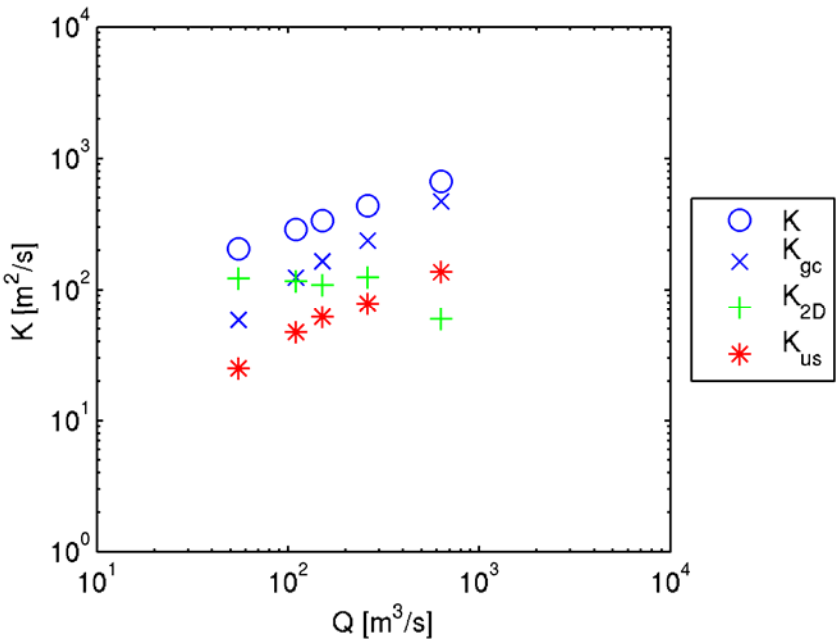

Figure H1.7.3-5 Estimated dispersion coefficients at section 12, extending from Crockett to Glen Cove, as a function of Net Delta Outflow.

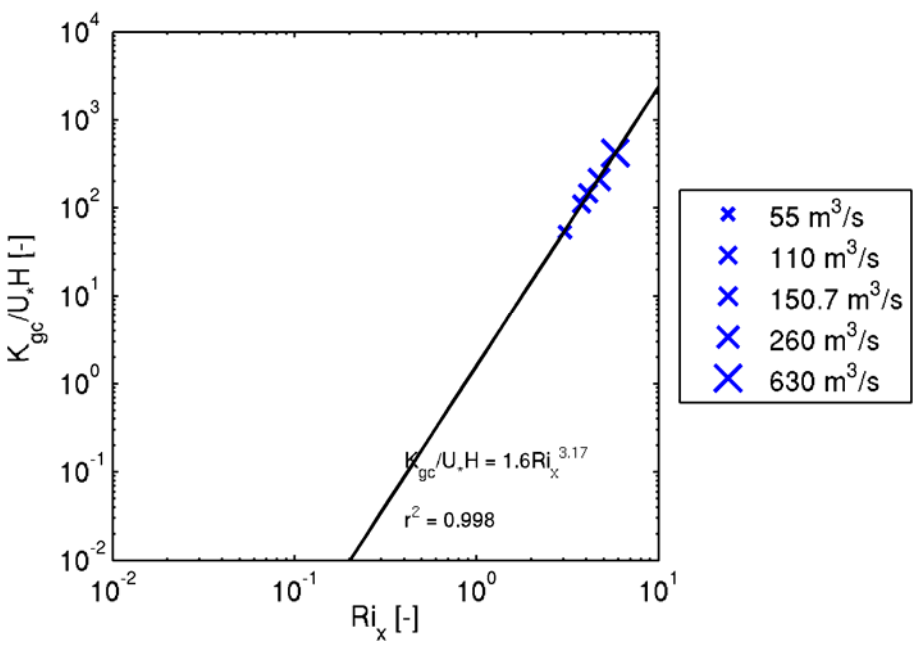

Figure H1.7.3-6 Estimated dimensionless dispersion coefficients for gravitational circulation at section 12, extending from Crockett to Glen Cove, as a function of horizontal Richardson number with corresponding best fit equation and r^2 value.

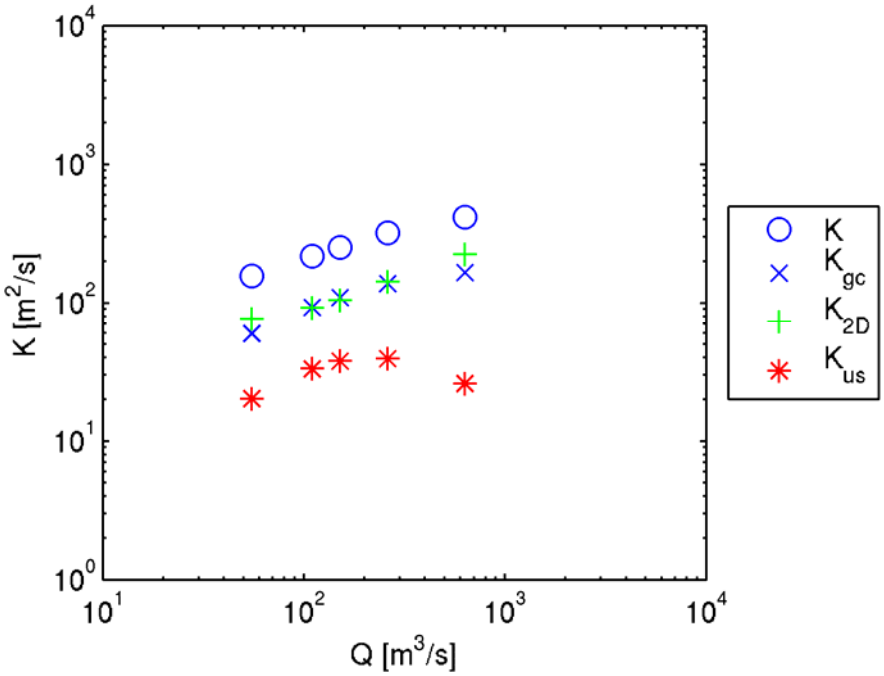

Figure H1.7.3-7 Estimated dispersion coefficients at section 13, extending from Ozol to Benicia Point, as a function of Net Delta Outflow.

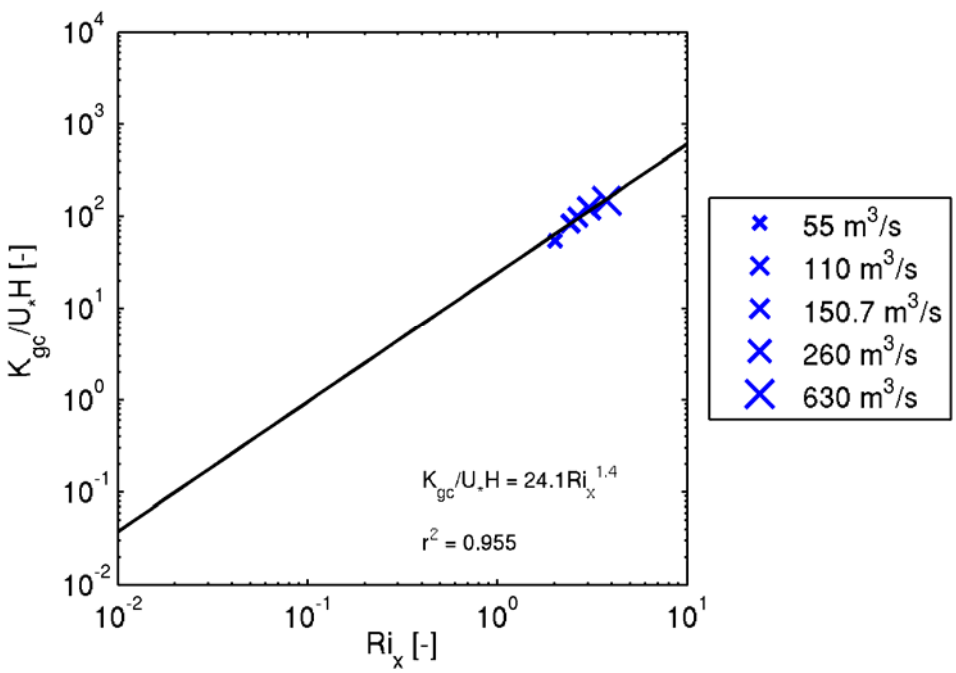

Figure H1.7.3-8 Estimated dimensionless dispersion coefficients for gravitational circulation at section 13, extending from Ozol to Benicia Point, as a function of horizontal Richardson number with corresponding best fit equation and r^2 value.

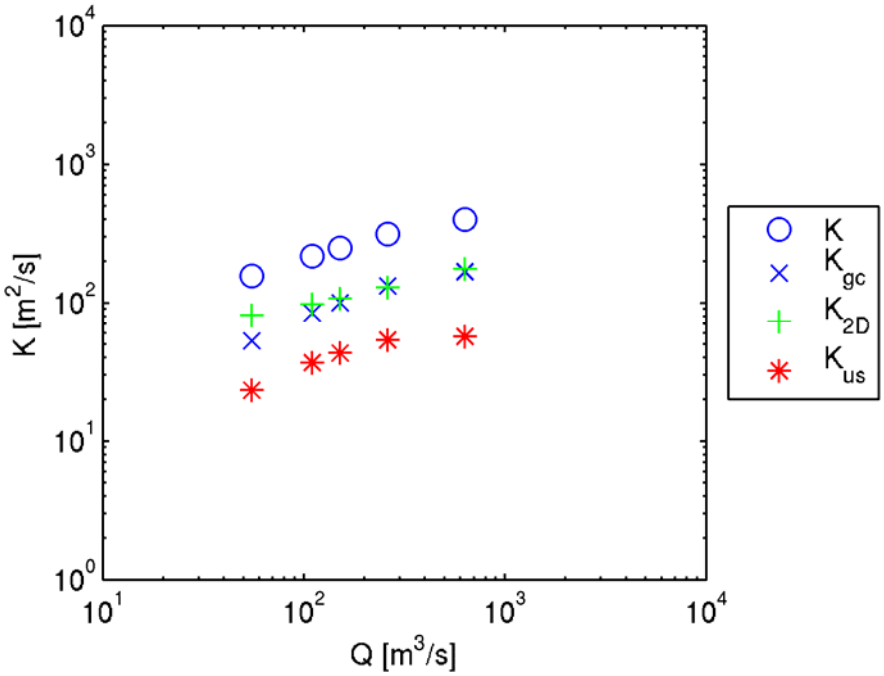

Figure H1.7.3-9 Estimated dispersion coefficients at section 14, extending from Martinez to Benicia, as a function of Net Delta Outflow.

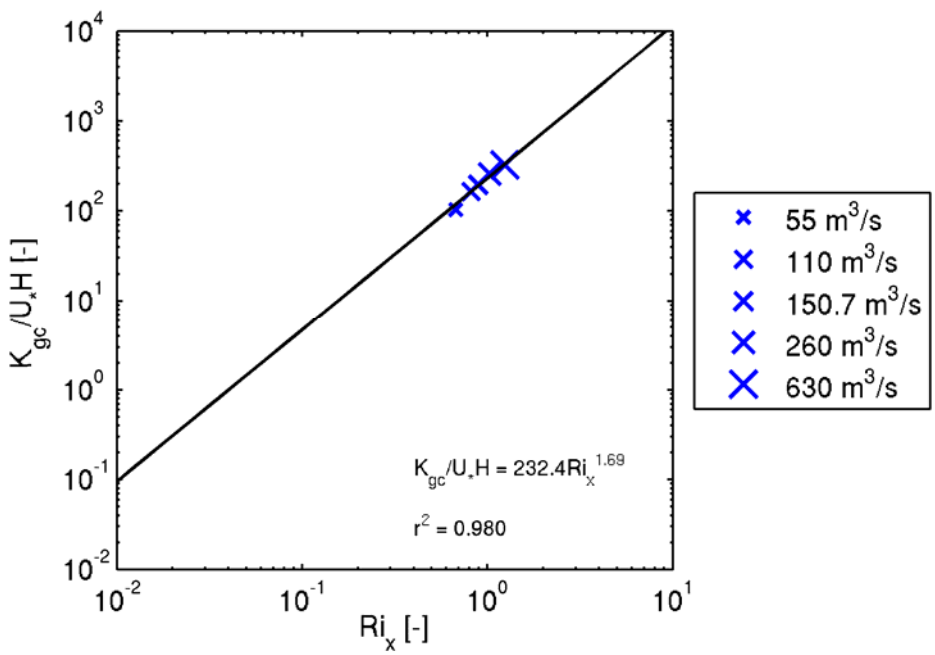

Figure H1.7.3-10 Estimated dimensionless dispersion coefficients for gravitational circulation at section 14, extending from Martinez to Benicia, as a function of horizontal Richardson number with corresponding best fit equation and r^2 value.

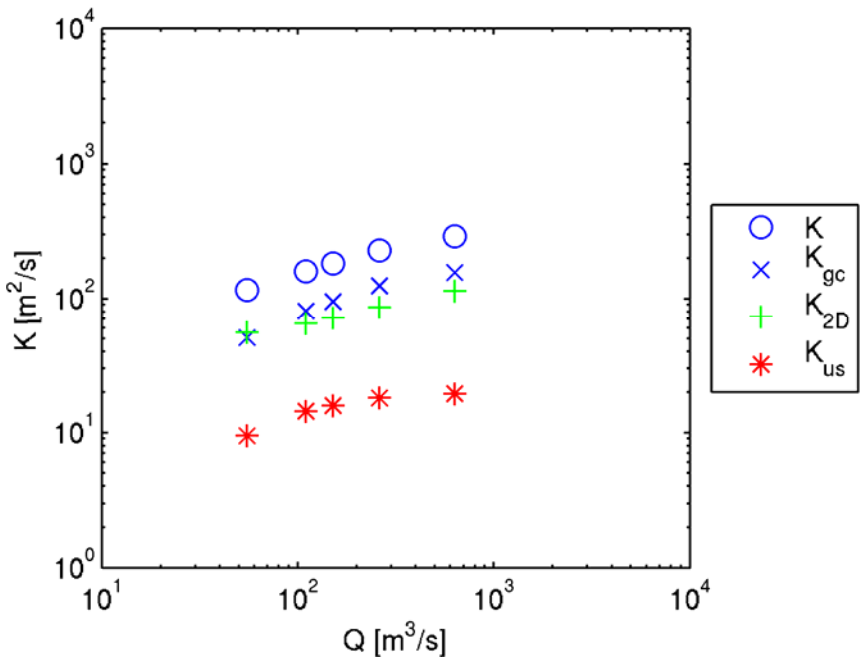

Figure H1.7.3-11 Estimated dispersion coefficients at section 15, at the Benicia Bridge, as a function of Net Delta Outflow.

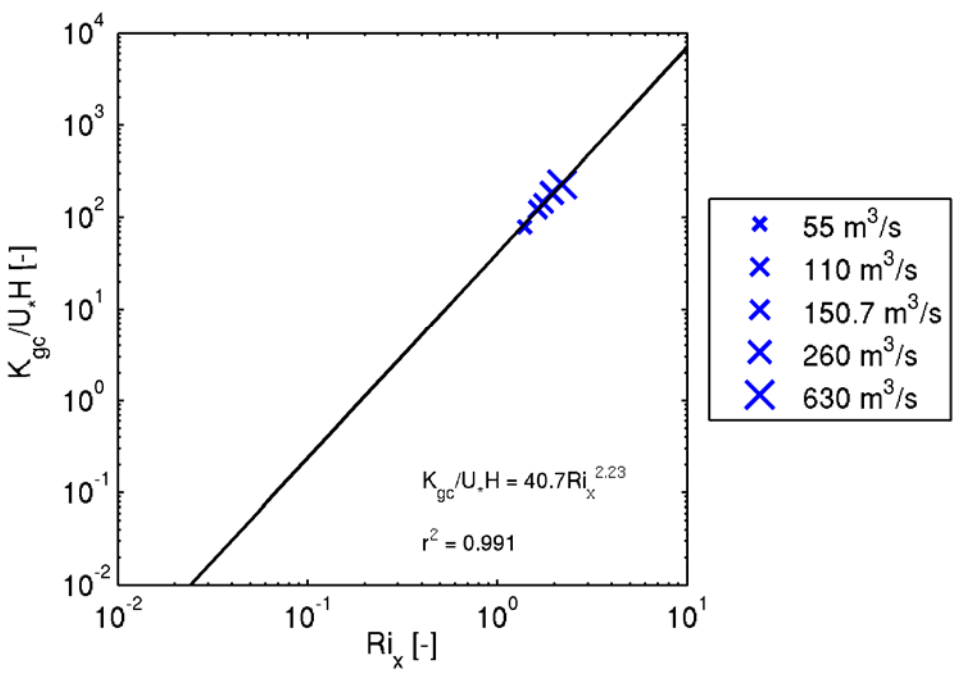

Figure H1.7.3-12 Estimated dimensionless dispersion coefficients for gravitational circulation at section 15, at the Benicia Bridge, as a function of horizontal Richardson number with corresponding best fit equation and r^2 value.

H1.7.4 Suisun Bay Cross-Sections

Dispersion coefficients and fluxes were estimated at eight cross-sections in Suisun Bay (sections 16 through 23), shown in Figure H1.3-1. Figures H1.7.4-1 through H1.7.4-16 show each dispersion coefficient and the individual components of each dispersion coefficient as well as the curve fit of the gravitational circulation component at each cross-section in Suisun Bay. Note that the curve fit minimizes the error in K_{gc}/U*H, not the logarithm of K_{gc}/U*H. Therefore, because the values are plotted on a logarithmic scale, the best fit line may appear biased to better fit the larger values of K_{gc}/U*H.

The dispersion coefficients are relatively small in Suisun Bay relative to those estimated in Central San Francisco Bay and San Pablo Bay. Dispersion in all cross-sections except section 21 is dominated by tidal dispersion processes. The analysis results at section 21 are suspect because they suggest much lower tidal dispersion than present at neighboring stations. The physical reason for this is not clear.

The strength of gravitational circulation and unsteady shear varies within a relatively narrow range at all cross-sections. The fit of K_{gc} as a function of Ri_x is questionable at section 19 through section 23 due to the limited range of estimated K_{gc} values. However, this will NOT affect the performance of the WAM because the K_{gc} values applied in the WAM are limited to the maximum and minimum values estimated. Therefore, the K_{gc} values applied in the WAM for section 19 through section 23 will essentially be constant.

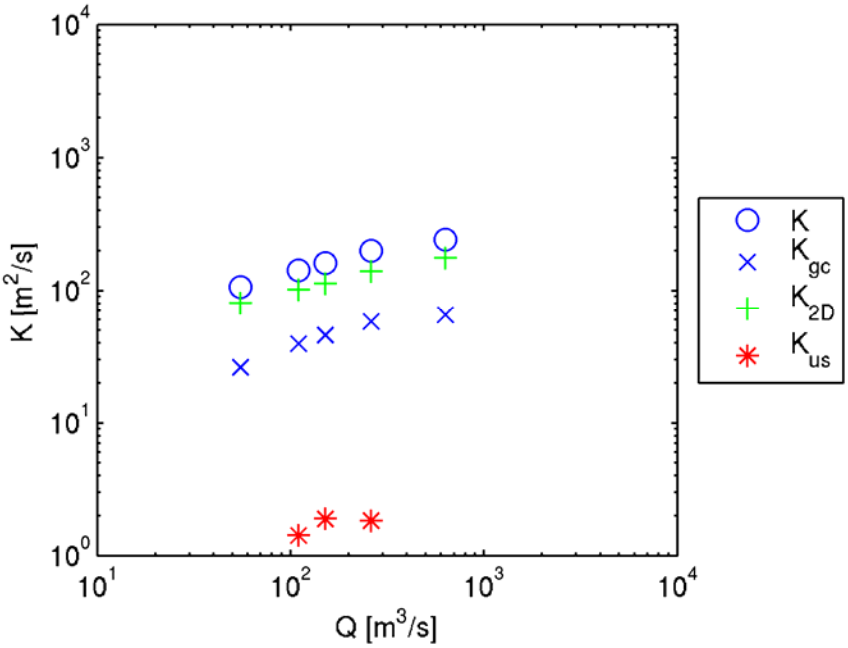

Figure H1.7.4-1 Estimated dispersion coefficients at section 16, from Pacheco Creek to the Mothball Fleet, as a function of Net Delta Outflow.

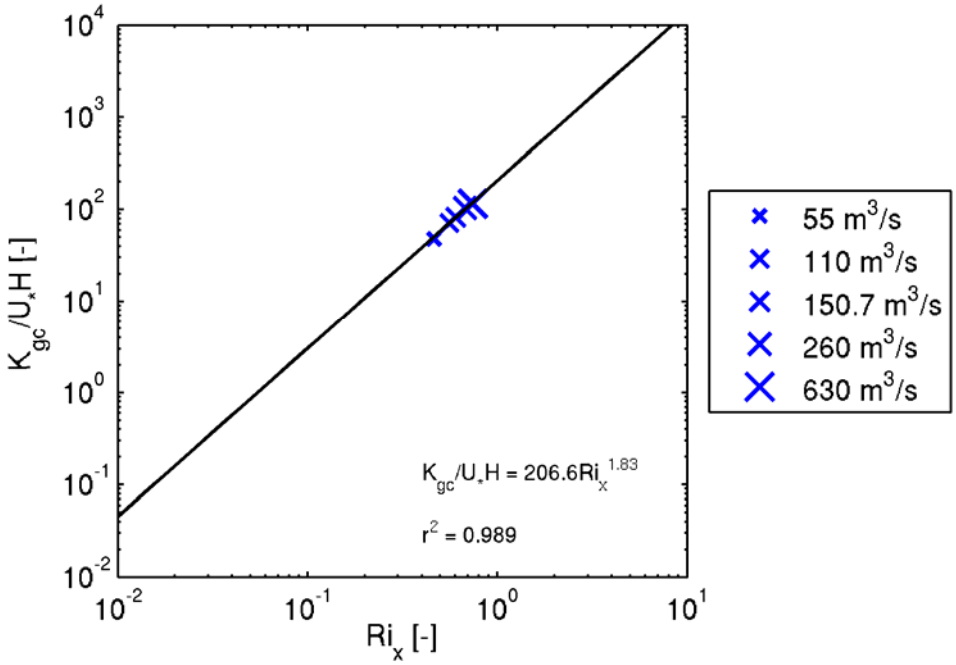

Figure H1.7.4-2 Estimated dimensionless dispersion coefficients for gravitational circulation at section 16, from Pacheco Creek to the Mothball Fleet, as a function of horizontal Richardson number with corresponding best fit equation and r^2 value.

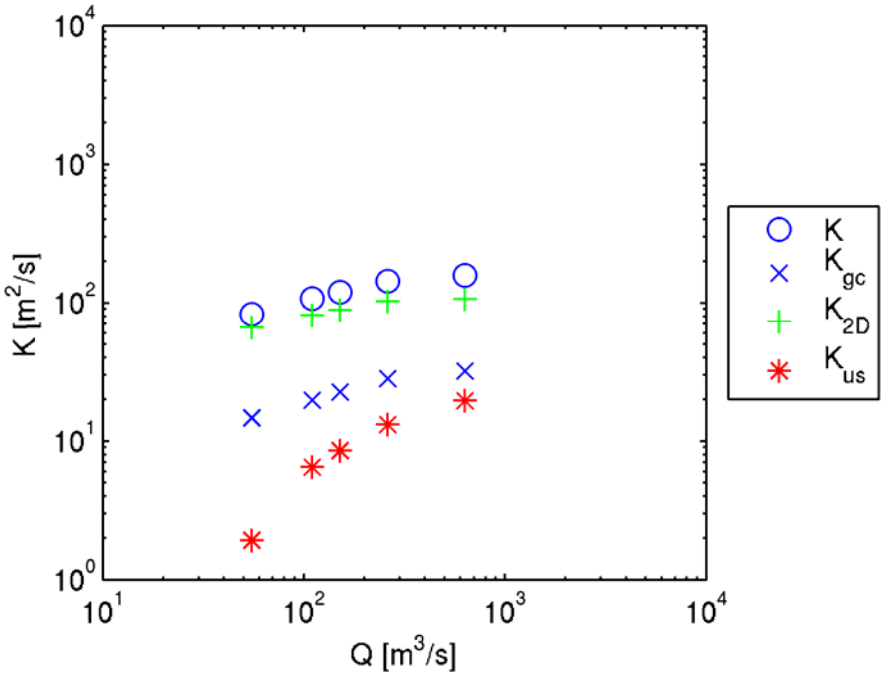

Figure H1.7.4-3 Estimated dispersion coefficients at section 17, east of the Mothball Fleet, as a function of Net Delta Outflow.

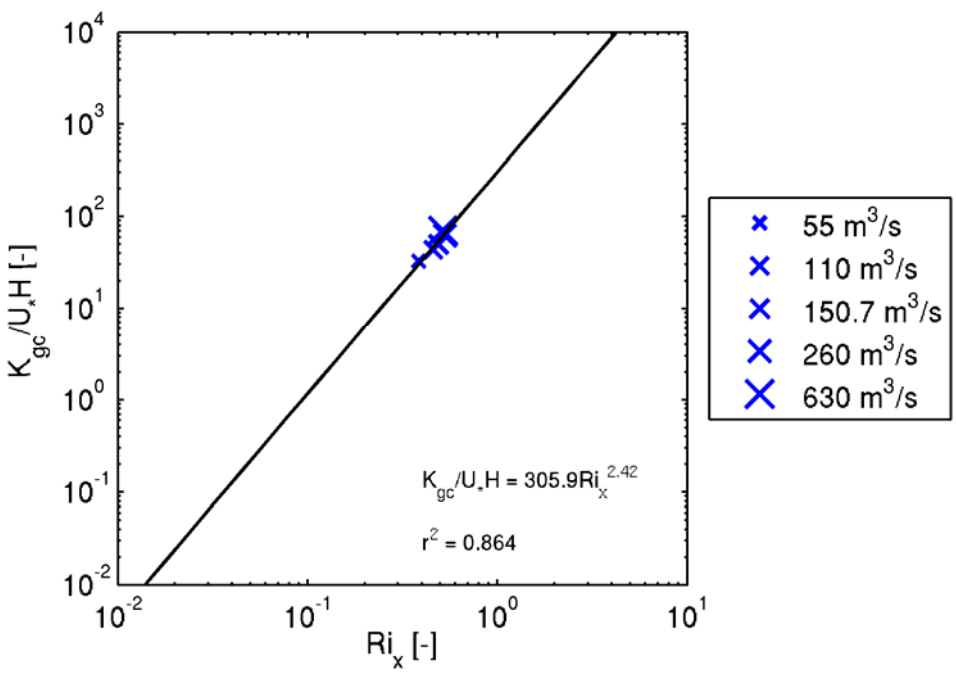

Figure H1.7.4-4 Estimated dimensionless dispersion coefficients for gravitational circulation at section 17, east of the Mothball Fleet, as a function of horizontal Richardson number with corresponding best fit equation and r^2 value.

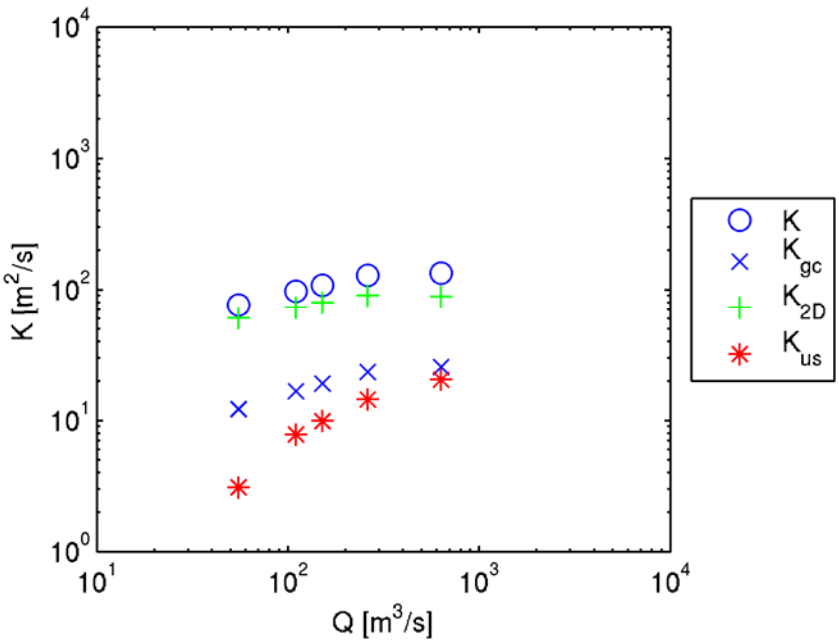

Figure H1.7.4-5 Estimated dispersion coefficients at section 18, from Point Edith to Suisun Slough, as a function of Net Delta Outflow.

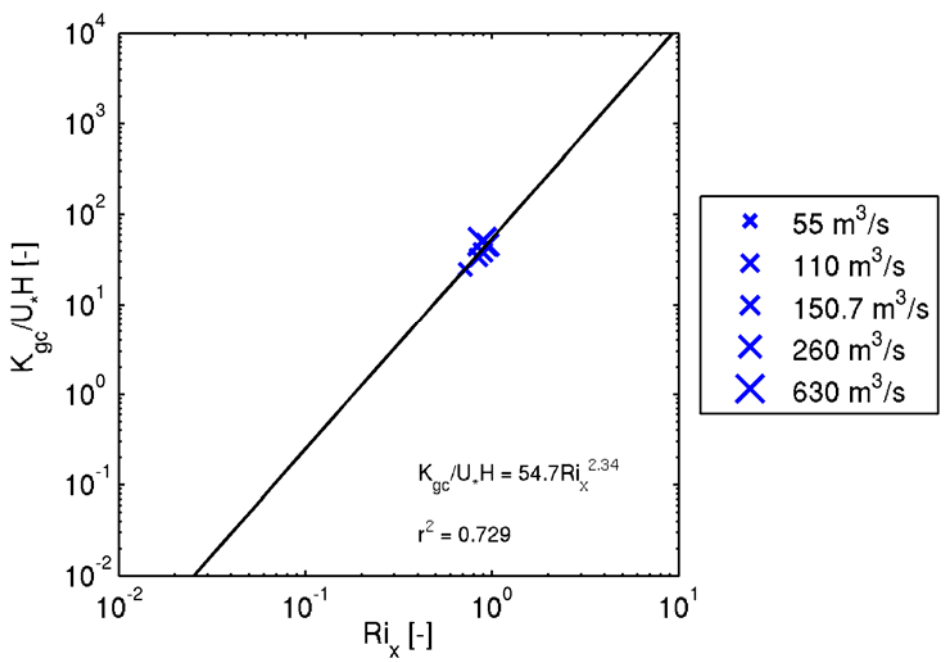

Figure H1.7.4-6 Estimated dimensionless dispersion coefficients for gravitational circulation at section 18, from Point Edith to Suisun Slough, as a function of horizontal Richardson number with corresponding best fit equation and r^2 value.

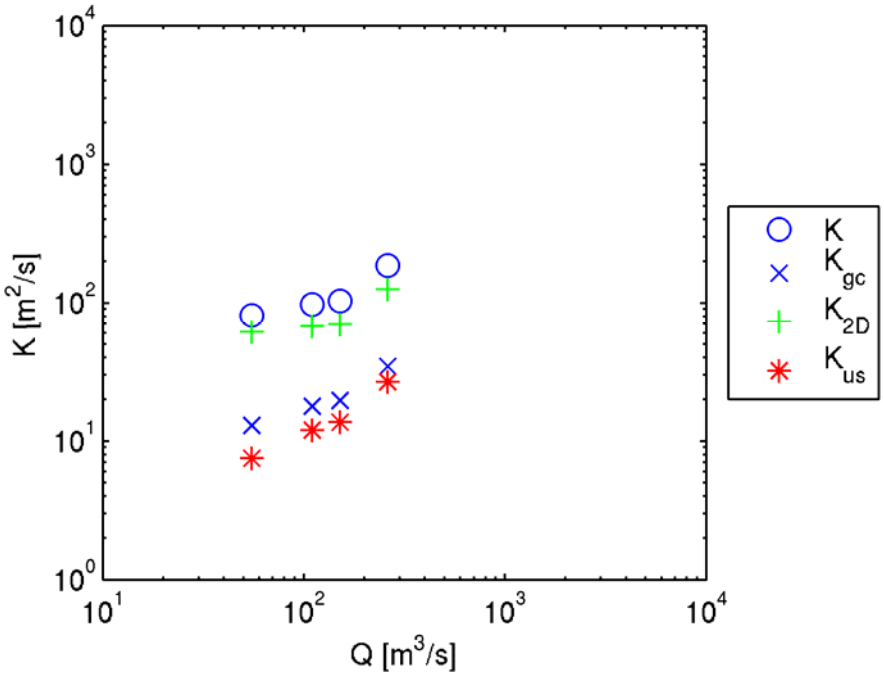

Figure H1.7.4-7 Estimated dispersion coefficients at section 19, from Port Chicago to Grizzly Bay, as a function of Net Delta Outflow.

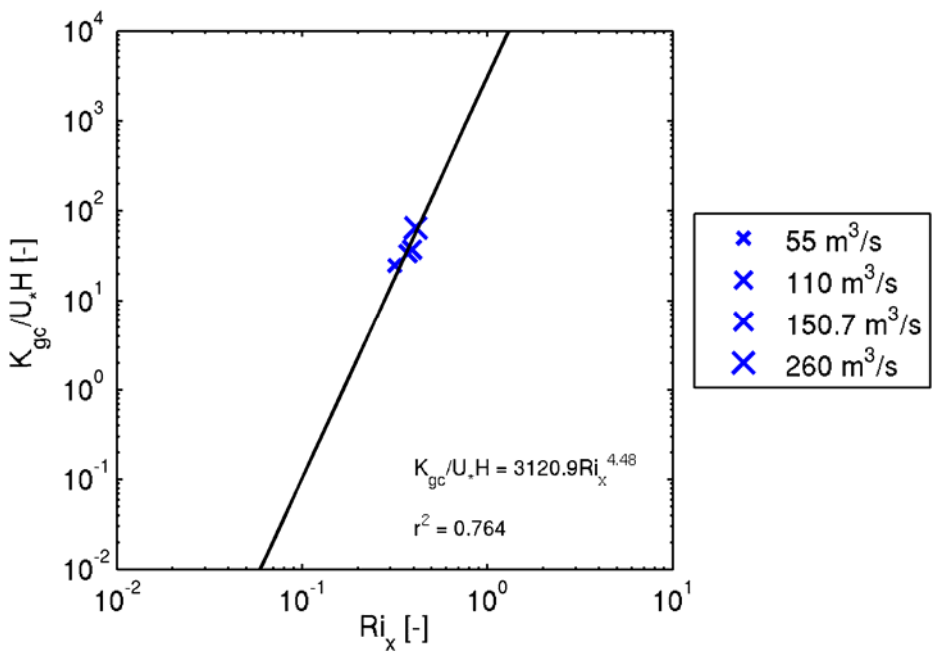

Figure H1.7.4-8 Estimated dimensionless dispersion coefficients for gravitational circulation at section 19, from Port Chicago to Grizzly Bay, as a function of horizontal Richardson number with corresponding best fit equation and r^2 value.

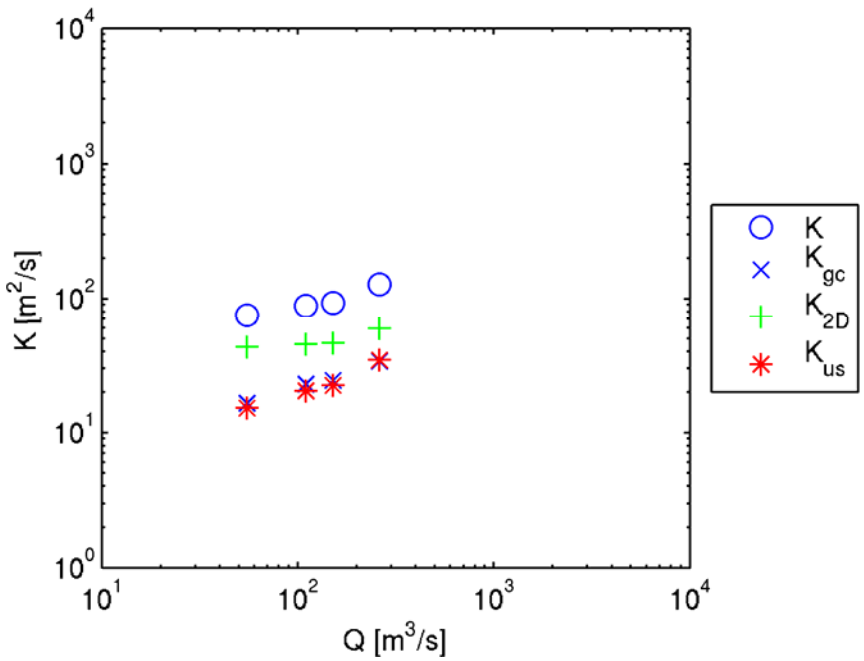

Figure H1.7.4-9 Estimated dispersion coefficients at section 20, from Middle Point to Simmons Island, as a function of Net Delta Outflow.

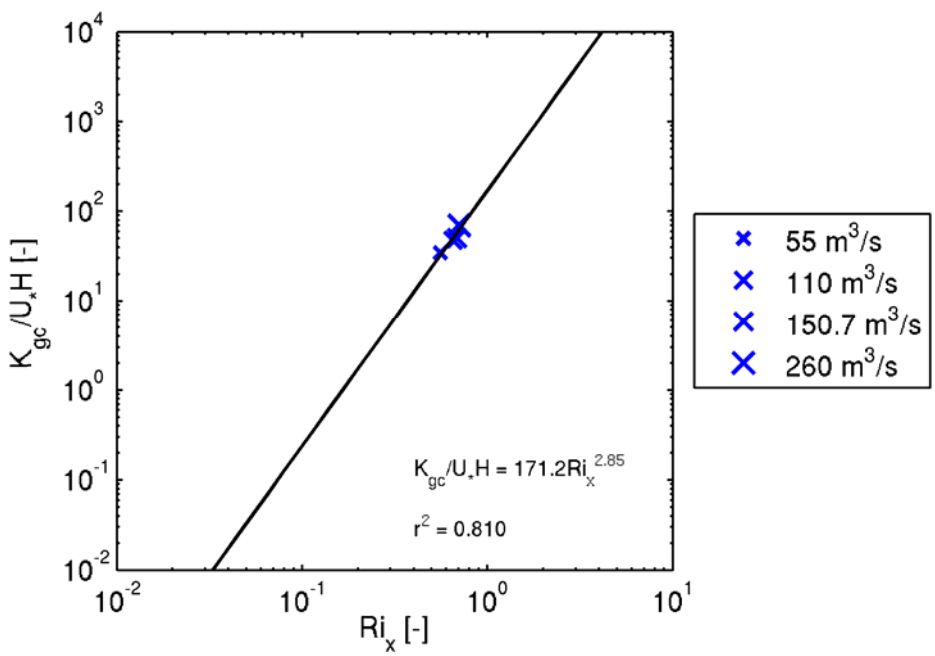

Figure H1.7.4-10 Estimated dimensionless dispersion coefficients for gravitational circulation at section 20, from Middle Point to Simmons Island, as a function of horizontal Richardson number with corresponding best fit equation and r^2 value.

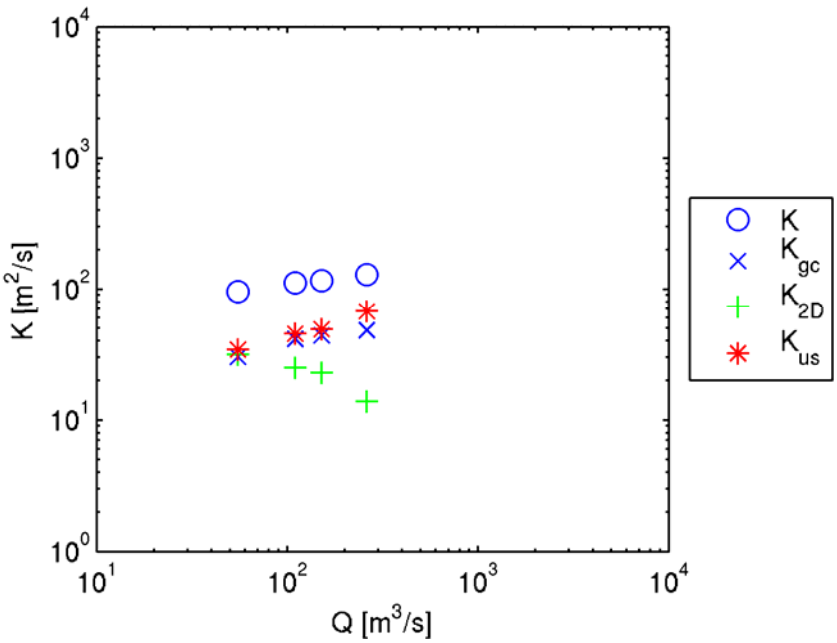

Figure H1.7.4-11 Estimated dispersion coefficients at section 21, from Concord to Dutton Island, as a function of Net Delta Outflow.

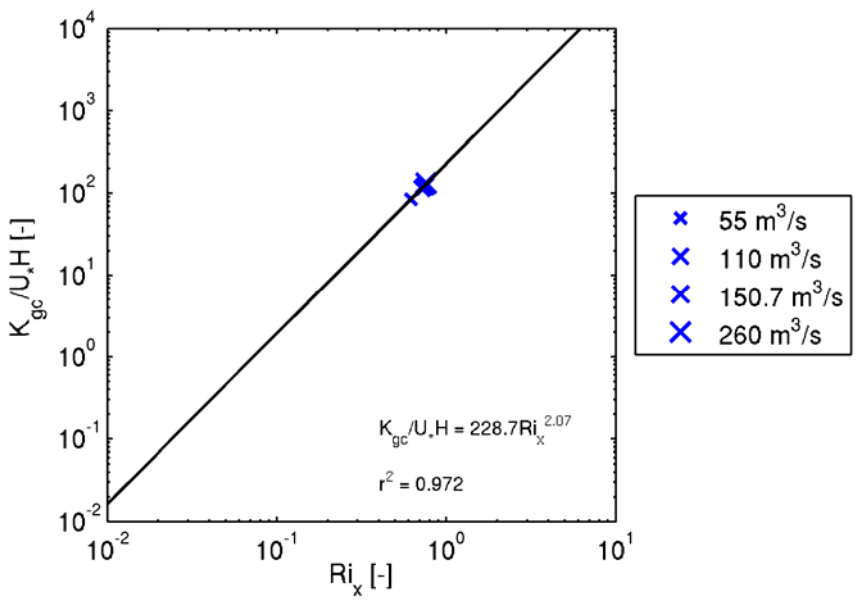

Figure H1.7.4-12 Estimated dimensionless dispersion coefficients for gravitational circulation at section 21, from Concord to Dutton Island, as a function of horizontal Richardson number with corresponding best fit equation and r^2 value.

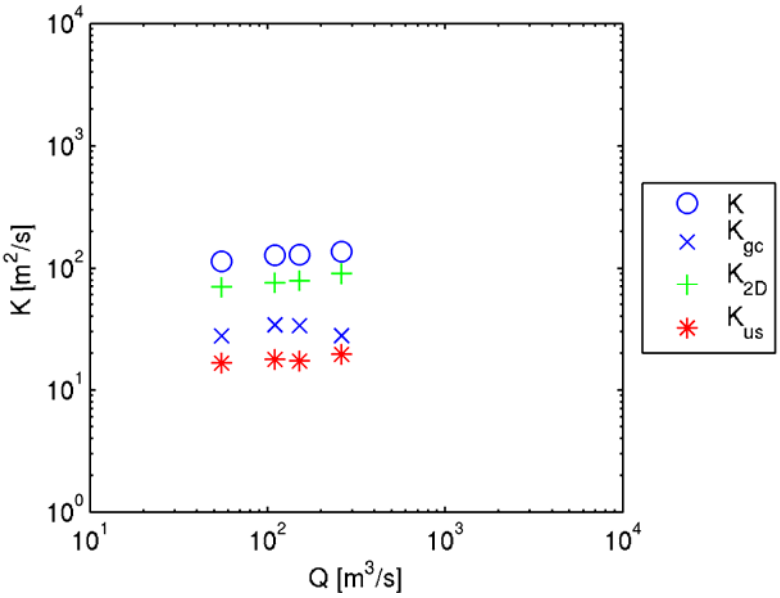

Figure H1.7.4-13 Estimated dispersion coefficients at section 22, from Stake Point to Wheeler Island, as a function of Net Delta Outflow.

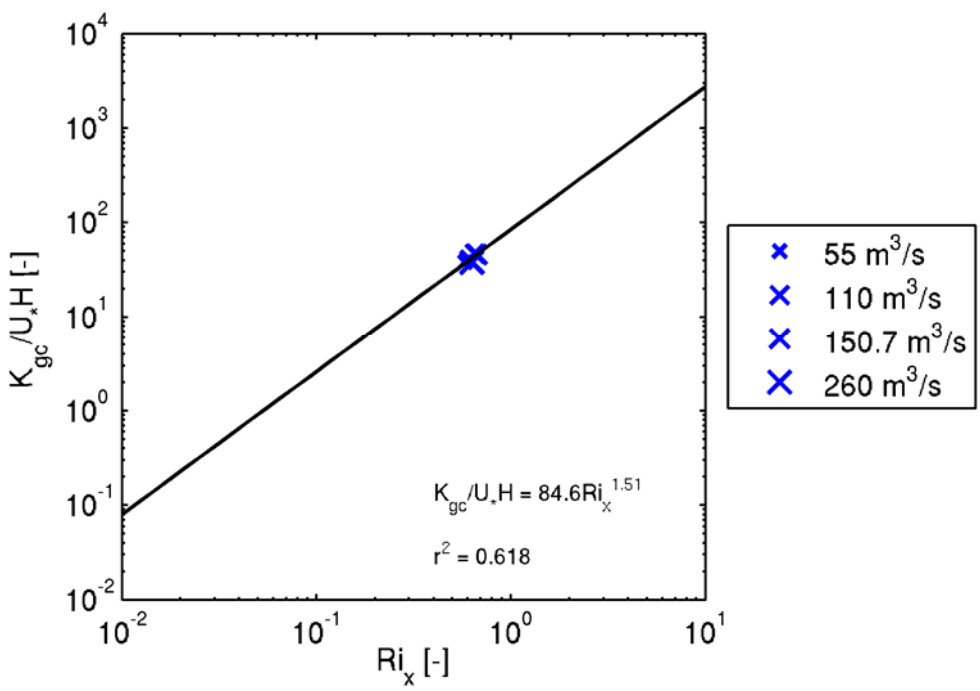

Figure H1.7.4-14 Estimated dimensionless dispersion coefficients for gravitational circulation at section 22, from Stake Point to Wheeler Island, as a function of horizontal Richardson number with corresponding best fit equation and r2 value.

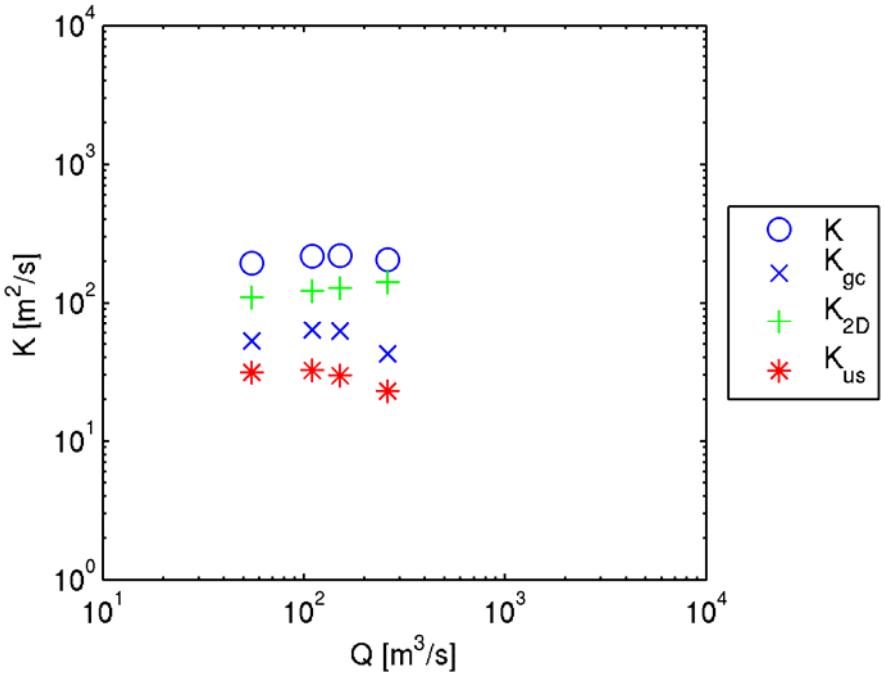

Figure H1.7.4-15 Estimated dispersion coefficients at section 23, extending south from Simmons Point, as a function of Net Delta Outflow.

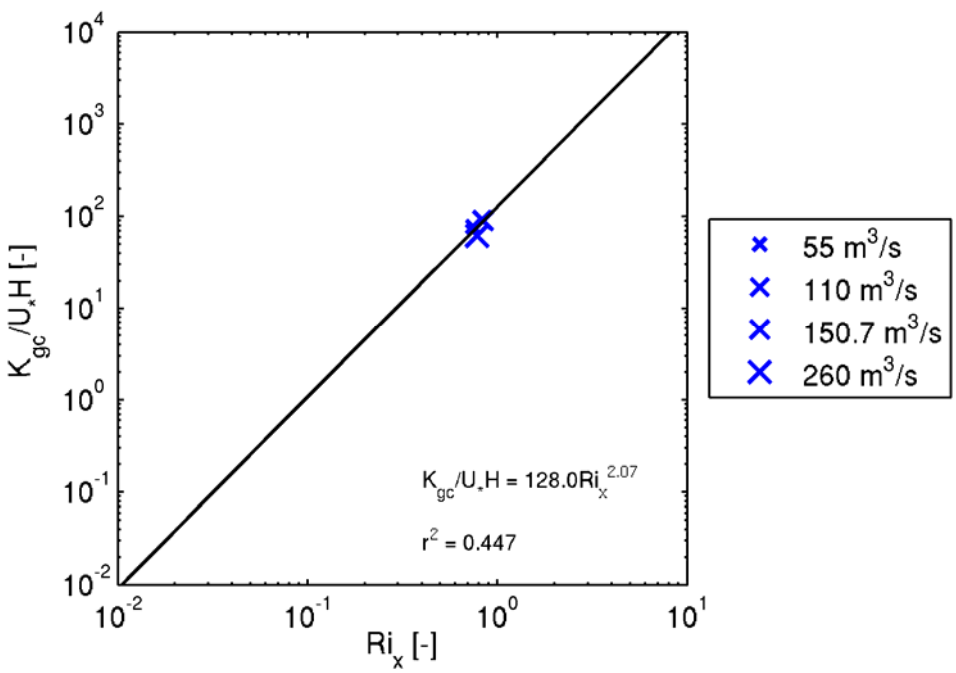

Figure H1.7.4-16 Estimated dimensionless dispersion coefficients for gravitational circulation at section 23, extending south from Simmons Point, as a function of horizontal Richardson number with corresponding best fit equation and r^2 value.

H1.7.5 Western Delta Cross-Sections

Dispersion coefficients and fluxes were estimated at five cross-sections in the western Delta (sections 24 through 28), shown in Figure H1.3-1. Figures H1.7.5-1 through H1.7.5-10 show each dispersion coefficient and the individual components of each dispersion coefficient as well as the curve fit of the gravitational circulation component at each cross-section in San Pablo Bay. Note that the curve fit minimizes the error in K_{gc}/u*H, not the logarithm of K_{gc}/u*H. Therefore, because the values are plotted on a logarithmic scale, the best fit line may appear biased to better fit the larger values of K_{gc}/u*H.

The estimated dispersion coefficients are relatively small in the Western Delta. Dispersion is generally dominated by tidal dispersion processes. Both gravitational circulation and unsteady shear components are important at medium and high flow. As in Suisun Bay, the strength of gravitational circulation and unsteady shear decrease with flow. This is expected because horizontal salinity gradients and stratification decrease with increased NDO as salt is flushed from the Delta leaving only freshwater, as shown in Figures H1.6-2 through H1.6-7. The reliability of the curve fits of K_{gc}/u*H with Ri_x is questionable because the range of the gravitational circulation component is small. However, this will NOT affect the performance of the WAM because the K_{gc} values applied in the WAM are limited to the maximum and minimum values estimated. Therefore, the K_{gc} values applied in the WAM for the Western Delta cross-sections will essentially be constant.

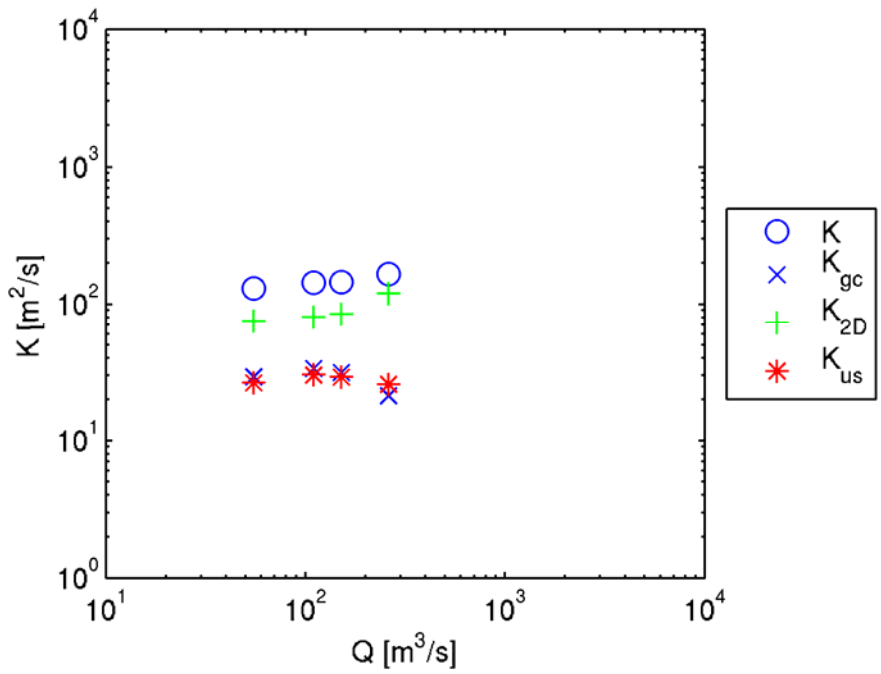

Figure H1.7.5-1 Estimated dispersion coefficients at section 24, extending from Mallard Island to Chipps Island, as a function of Net Delta Outflow.

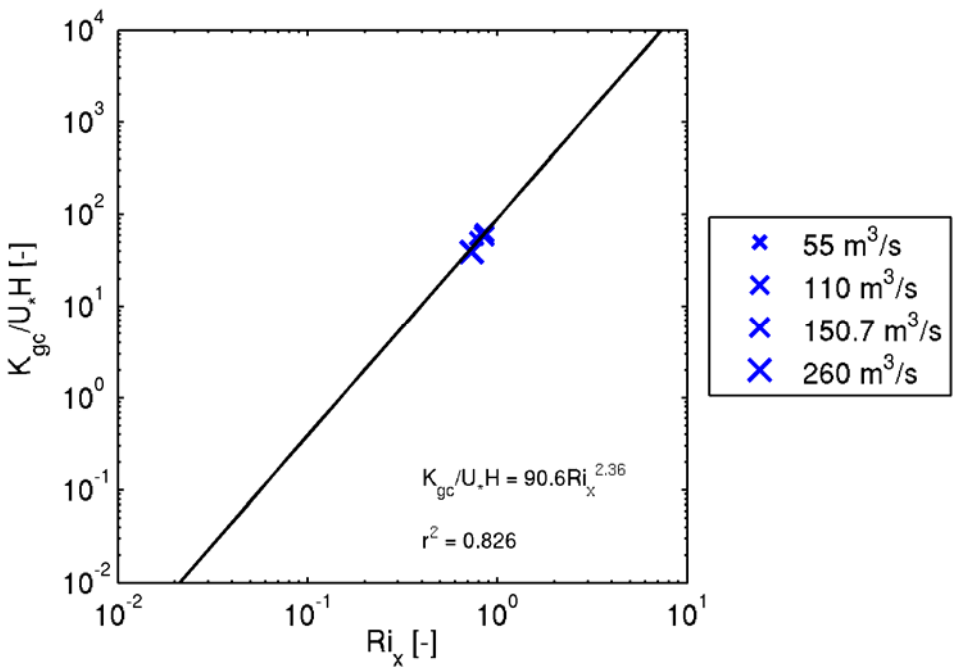

Figure H1.7.5-2 Estimated dimensionless dispersion coefficients for gravitational circulation at section 24, extending from Mallard Island to Chipps Island, as a function of horizontal Richardson number with corresponding best fit equation and r^2 value.

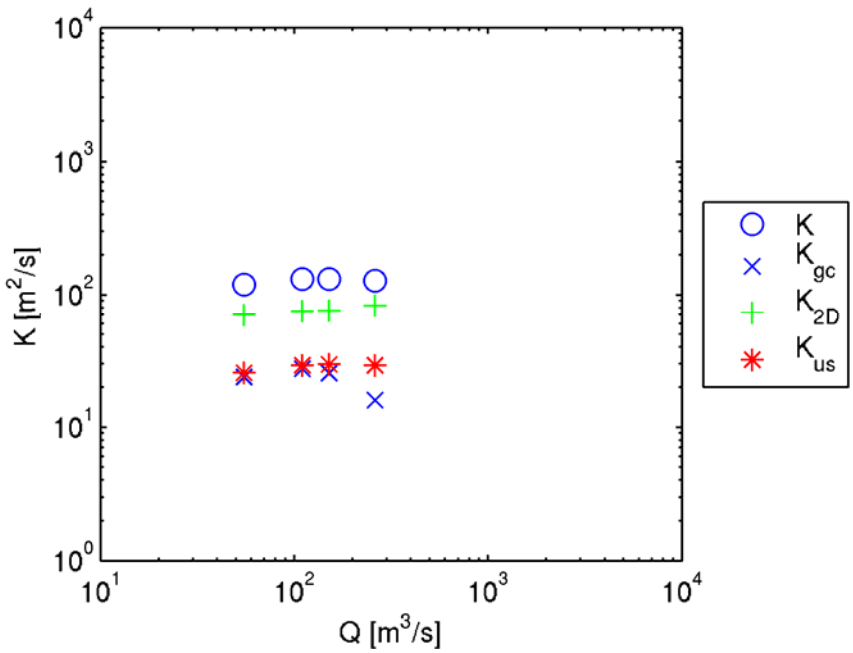

Figure H1.7.5-3 Estimated dispersion coefficients at section 25, extending from Pittsburg to Mallard Island, as a function of Net Delta Outflow.

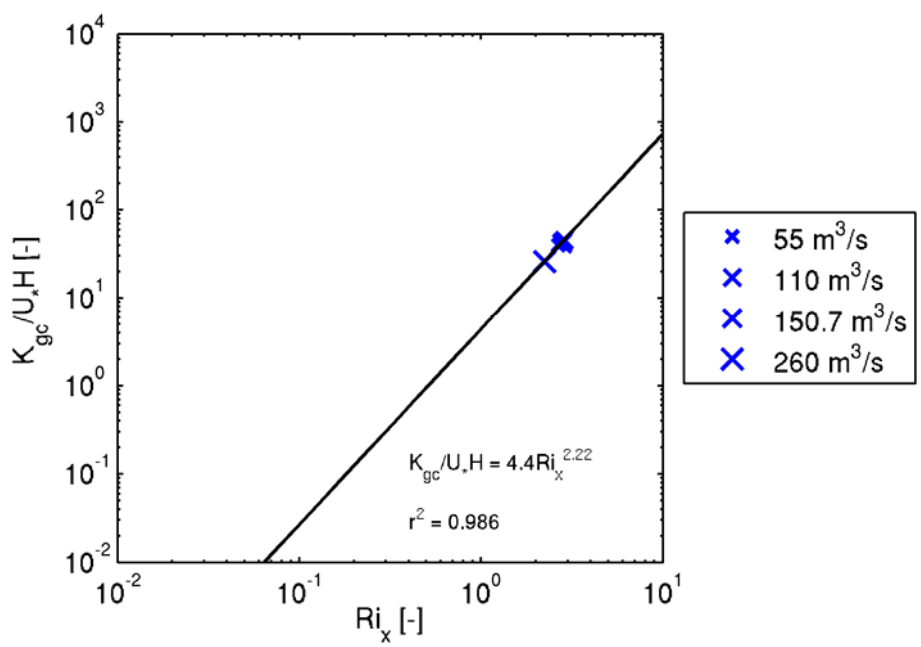

Figure H1.7.5-4 Estimated dimensionless dispersion coefficients for gravitational circulation at section 25, extending from Pittsburg to Mallard Island, as a function of horizontal Richardson number with corresponding best fit equation and r^2 value.

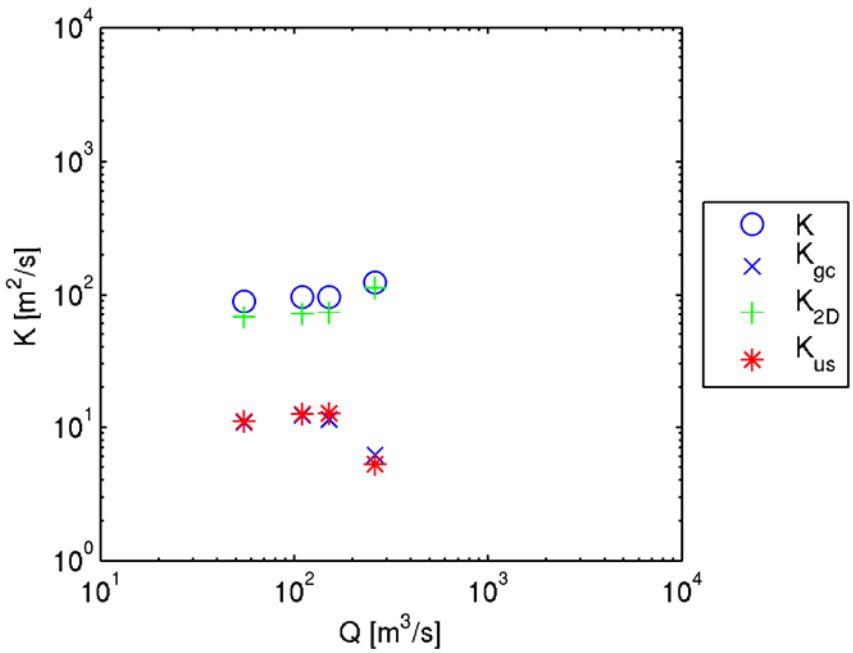

Figure H1.7.5-5 Estimated dispersion coefficients at section 26, extending from Brown Island to Van Sickle Island, as a function of Net Delta Outflow.

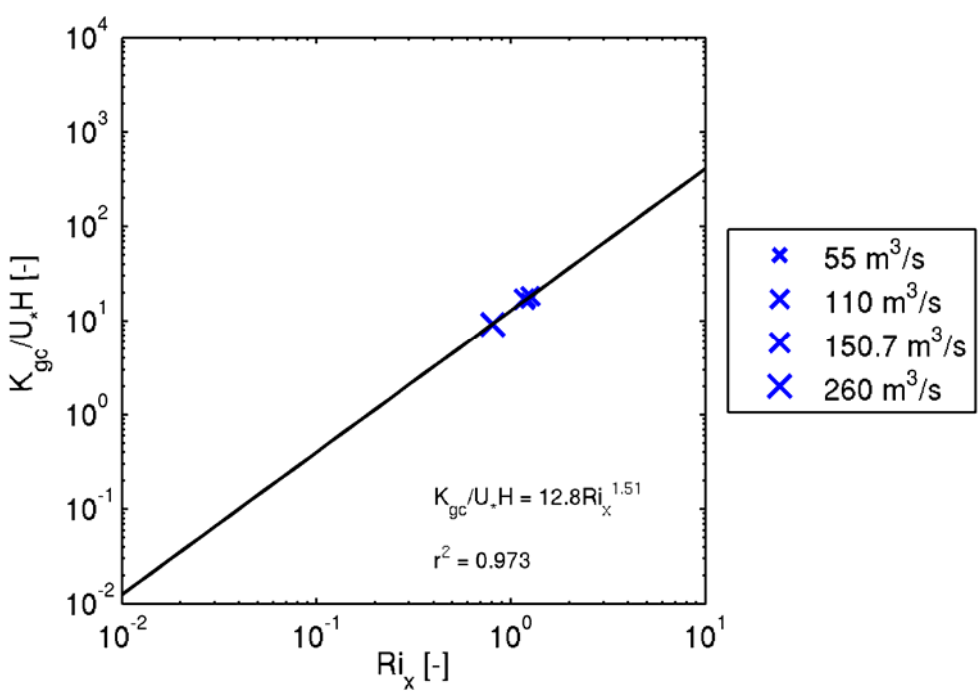

Figure H1.7.5-6 Estimated dimensionless dispersion coefficients for gravitational circulation at section 26, extending from Brown Island to Van Sickle Island, as a function of horizontal Richardson number with corresponding best fit equation and r^2 value.

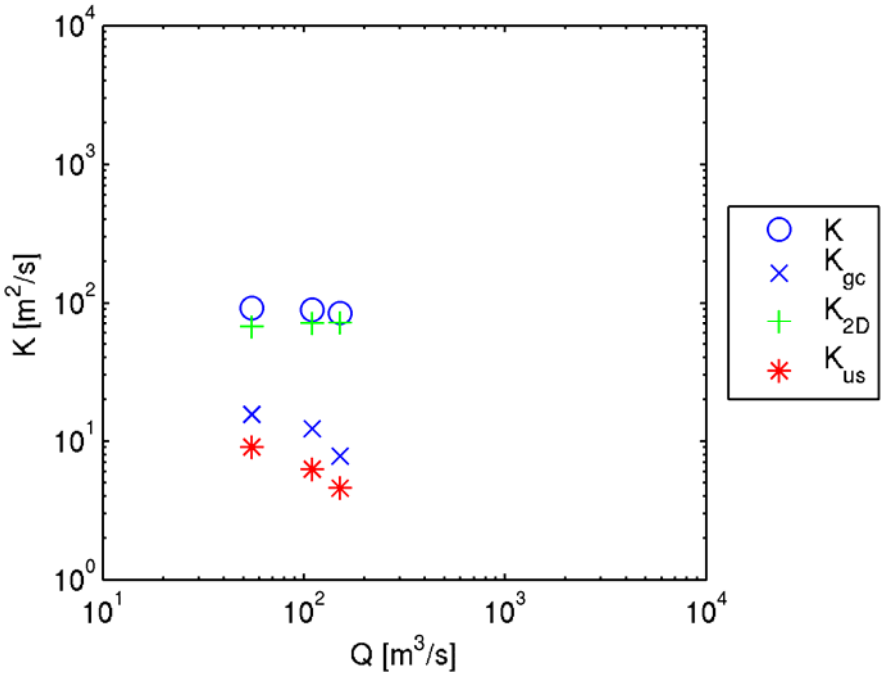

Figure H1.7.5-7 Estimated dispersion coefficients at section 27, extending north from Sherman Island, as a function of Net Delta Outflow.

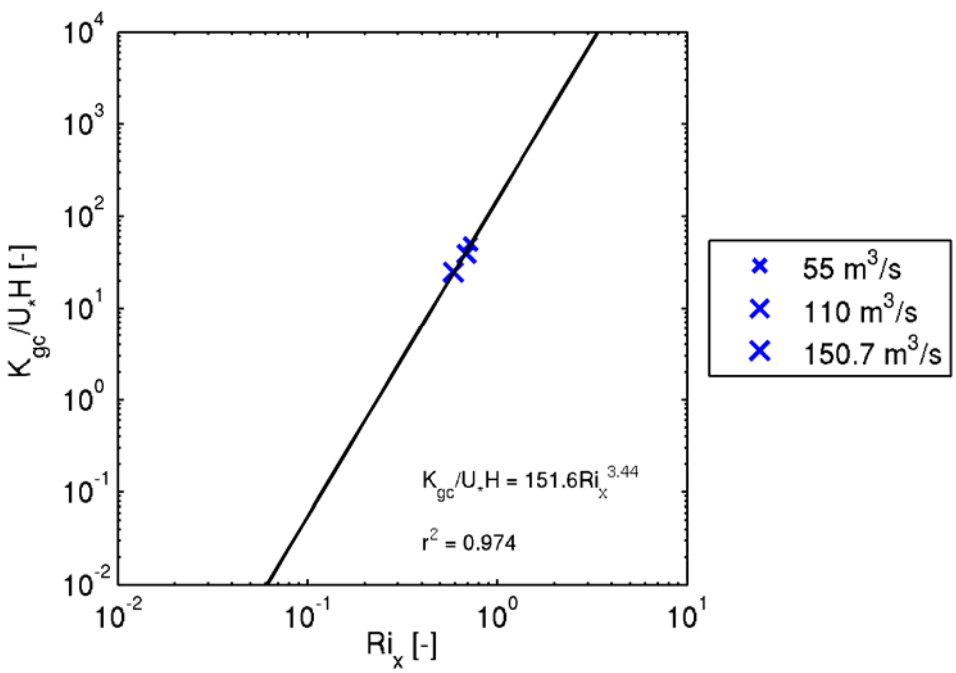

Figure H1.7.5-8 Estimated dimensionless dispersion coefficients for gravitational circulation at section 27, extending north from Sherman Island, as a function of horizontal Richardson number with corresponding best fit equation and r^2 value.

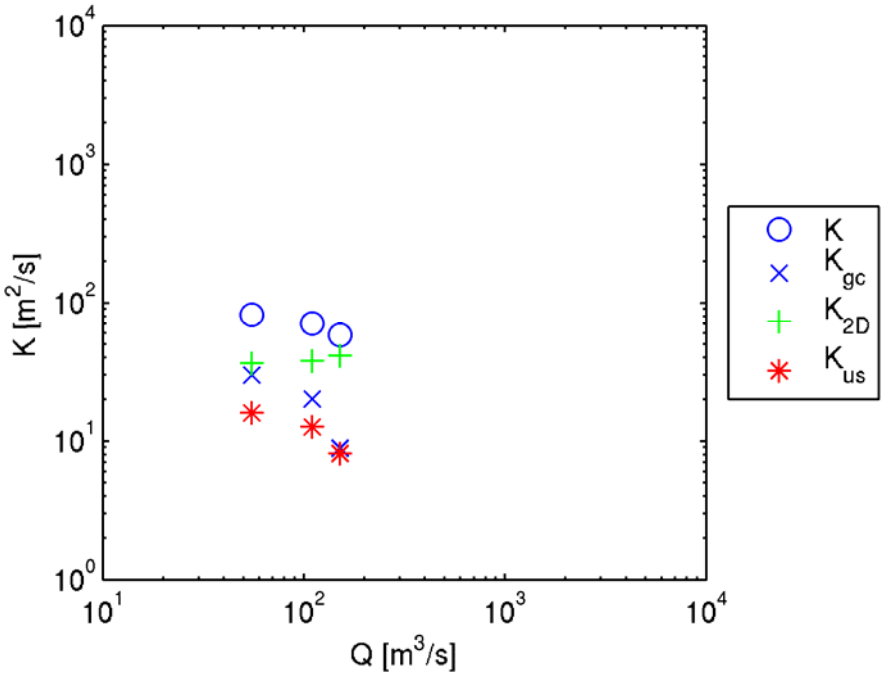

Figure H1.7.5-9 Estimated dispersion coefficients at section 28, on Sacramento River near Emmaton, as a function of Net Delta Outflow.

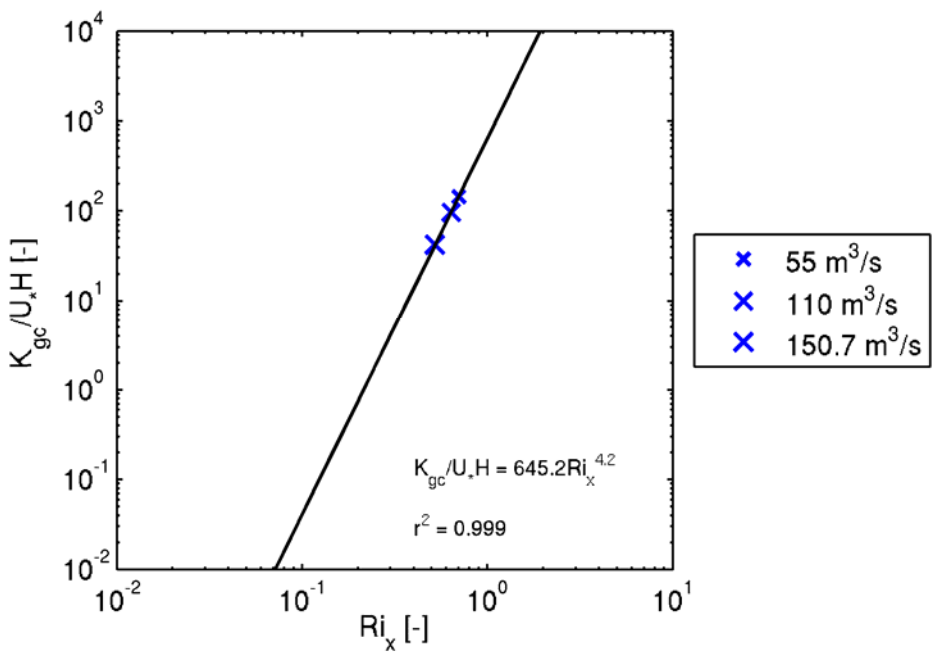

Figure H1.7.5-10 Estimated dimensionless dispersion coefficients for gravitational circulation at section 28, on Sacramento River near Emmaton, as a function of horizontal Richardson number with corresponding best fit equation and r^2 value.

H1.7.6 Summary of Dispersion Coefficient Estimates

Dispersion coefficients have been estimated at 28 cross-sections in the San Francisco Estuary. Dispersion coefficients at each cross-section were estimated for 6 flow scenarios ranging from flow corresponding to fall flows during a "critical" year to flow corresponding to peak winter flows of an average or wet year. These results are shown in Section 7.1 through Section 7.5. At each section the variability of K_{gc}/u^*H with Ri_x is described by a curve fit using an equation of the form $K_{gc}/U^*H = a\ Ri_x^b$. Because there is some analytical motivation for an equation of this form (Hansen & Rattray 1965), and the equation fits data at most cross-sections reasonably well, it is expected that this approach will apply for levee breach scenarios as well as historic scenarios, at least in regions not near levees. K_{2D} and K_{us} also vary among scenarios at each cross-section but it is not clear if this variability can be described in a way that would apply both for historic/current conditions and levee failure scenarios. For existing conditions, these components could be varied according to an interpolation ("look up table") between the values determined from analysis of the scenario simulations. However, this approach may be a rough approximation for scenario simulations with dramatically changed Delta geometry (levee breaches).

The values in Table H1-2 are used in the WAM to specify dispersion coefficients. At each element and time step in the WAM, a value of Ri_x is calculated and used to calculate K_{gc}. Because the WAM is a tidally-averaged model, u* and H are constant in time at each section, and, therefore, only dS/dx varies in time. However, u* and H can vary among scenarios, with u* increasing proportional to increases in tidal currents that can occur from increased tidal prism and H increasing in sea level rise scenarios. The computed K_{gc} is then compared against the maximum and minimum K_{gc} values estimated the parameterization analysis and listed in Table H1-2. If the calculated K_{gc} is greater than the maximum K_{gc} listed in Table H1-2, the maximum K_{gc} is used. Similarly, if the calculated K_{gc} is less than the minimum K_{gc} listed in Table H1-2, the minimum K_{gc} is used. To obtain the total dispersion coefficient at each time step, the calculated K_{gc} is added to K_{2D} and K_{us}.

Minimal budget was provided for the parameterization analysis outlined here. The apparent success of the simplified model in reproducing historic salinity conditions in the Estuary suggests that the parameterization approach is useful. However, it could be improved substantially both by more detailed analysis of existing model results and by performing additional simulations. A first level of improvement would be more careful evaluation of the validity of each dispersion coefficient shown in the figures in this section, which are also the data used to generate Table H1-2. Currently only global screening criteria have been applied to eliminate dispersion coefficient values that may be invalid, primarily due to low salinity gradient. This coarse screening allowed some suspect dispersion estimates to remain in the dataset used to generate Table H1-2. Additional improvement could be made with more substantial improvements in the three-dimensional model and the analysis technique used to estimate dispersion coefficients. Several uncertainties and proposed improvements are discussed in the following section.

Table H1-2 Results of parameterization analysis for use in WAM. The K_{2D} and K_{us} values listed are the average values for the flow scenarios, while a and b are the curve fit parameters for the equation $K_{gc}/u*H = a\ Ri_x^b$

Section	a	b	r^2	K_{2D}	K_{us}	Max K_{gc}	Min K_{gc}
1	12	0.33	0.89	439	40	142	60
2	125	2.00	1.00	145	81	328	29
3	1969	1.91	0.99	260	118	1346	38
4	4248	2.93	1.00	130	174	1126	100
5	699	1.43	0.99	49	246	2564	174
6	1343	0.98	0.95	532	116	750	99
7	26844	6.97	1.00	249	56	736	14
8	1467	2.16	1.00	270	61	523	22
9	627	1.90	1.00	278	83	807	45
10	236	1.67	0.98	292	81	815	47
11	94	2.78	1.00	122	73	564	86
12	2	3.17	1.00	106	70	471	59
13	24	1.40	0.96	128	31	166	60
14	232	1.69	0.98	118	43	168	53
15	41	2.23	0.99	78	15	157	51
16	207	1.83	0.99	122	1	66	26
17	306	2.42	0.86	89	10	32	15
18	55	2.34	0.73	79	11	26	12
19	3121	4.48	0.76	81	15	35	13
20	171	2.85	0.81	49	23	34	17
21	229	2.07	0.97	23	49	48	30
22	85	1.51	0.62	78	18	34	28
23	128	2.07	0.45	125	29	63	43
24	91	2.36	0.83	90	28	34	21
25	4	2.22	0.99	76	28	27	16
26	13	1.51	0.97	81	10	12	6
27	152	3.44	0.97	70	7	16	8
28	645	4.20	1.00	39	12	30	9

H1.8 Discussion

The dispersion analysis presented in this report was tailored to the needs of the DRMS project. An existing calibrated TRIM3D model was used so that scenario simulations could start immediately. The large range of conditions simulated accurately with the TRIM3D model provides a good deal of confidence that physical processes responsible for salt transport are represented adequately. The method used for the calculation of dispersion coefficients is well established in many previous applications employing observed salinity (e.g., Fischer et al. 1979). The method to distinguish fluxes from different physical processes is also well-established. The novel aspects of the analysis include using simplified forcing to reach a precise tidally-averaged steady state salinity field and the generalized equation used to curve fit the dispersion coefficient associated with gravitational circulation. The final results of the analysis are consistent with the

conceptual model of transport developed through many field studies (e.g., Burau et al. 1998). The conceptual model is that gravitational circulation is the most important transport mechanism in San Pablo Bay and Carquinez Strait and that the importance of gravitational circulation decreases sharply at the Benicia shoal due to limited depth. In Suisun Bay, due to complex bathymetry as well as less pronounced gravitational circulation, tidal dispersion processes are the dominant transport processes. In addition, the strong increase in the dispersion resulting from gravitational circulation with increased horizontal Richardson number noted by Monismith et al. (2002) was also found in this analysis.

Though the approach is likely to be adequate for the DRMS project, several limitations and uncertainty limit confidence in the dispersion estimates. Some of this uncertainty is associated with the three-dimensional model predictions while additional uncertainty is associated with the analysis method. The three-dimensional model applied in this analysis provides a more detailed description of fluid motion in the San Francisco Estuary than depth-averaged or one-dimensional models. However, there are several sources of uncertainty inherent in the application of this model:

Spatial resolution – the spatial resolution of the bathymetry of the model domain, and velocity and salinity distributions, is limited by the large computational expense associated with high-resolution models.

Bathymetry data – limited spatial coverage and accuracy of bathymetry data can be a substantial source of error. Converting all data to a uniform vertical datum and horizontal datum can lead to some error. In particular, LiDAR data may have substantial errors in vertical datum and removing vegetation from the dataset can be difficult.

Site-specific parameters – the TRIM model requires bottom friction coefficients to parameterize the resistance to flow at solid boundaries. These parameters are specified in model calibration by tuning to improve the calibration.

Turbulence closure – the effect of turbulent motions on the tidal time scale motions is estimated by a turbulence closure. While many turbulence closures are available, this is an ongoing area of research and, particularly in stratified settings, the effect of turbulence on tidal flows and salinity is not easy to estimate accurately and different turbulence closures may give significantly different results (e.g., Celebioglu and Piasecki 2006).

- Numerical errors –a numerical method approximates the governing equations to some level of accuracy. The mathematical properties of the numerical method of the TRIM model are well understood due to detailed mathematical analysis presented in several peer reviewed publications. While the stability and conservation properties of the method are ideal, a source of error in the numerical method is some degree of numerical diffusion of momentum and potential for damping of tidal propagation.

Though additional sources of uncertainty can be identified, the largest sources of uncertainty for hydrodynamic predictions are the accuracy and resolution of available bathymetry and the grid resolution available to represent this bathymetry in the model. This study made use of the best available bathymetric data, and the bathymetry applied to

the model grid is based on a high resolution master grid which was developed and used as part of a large TRIM calibration effort in the San Francisco Estuary (Gross et al. 2006). Ongoing work in the DRMS project includes the development and application of a three-dimensional unstructured grid model (UnTRIM). This flexible grid structure of this model allows better resolution of bathymetric features. Therefore this model should provide improved accuracy for estimation of dispersion coefficients in the future.

Additional uncertainty is associated with the simplified forcing used in the scenario simulations. As noted in Section 5, these approximations include:

- That tidal forcing is dominant relative to wind forcing and other environmental forcing.
- That a repeating M2 and K1 tide, with M2 period modified to 12 hours closely approximate "typical" tidal conditions
- That local tributary inflows do not affect tidal dispersion.
- That the average dispersion over a spring-neap tidal cycle is similar to the dispersion for average tidal amplitude.

The second and fourth approximation were examined in section 8 and found to be reasonable approximations.

Substantial uncertainty is also associated with the analysis technique. Sources of uncertainty include the following:

- The model cross-sections are not perfectly aligned normal to flow.
- Precise tidally-averaged steady state conditions are approached asymptotically. Advective and dispersive fluxes typically balance to within a 2% difference indicating steady-state conditions are nearly, but not precisely, achieved.
- The salinity gradient is estimated based on centerline ("thalweg") salinity, not cross-sectionally averaged salinity. The salt balance equation strictly applies only to cross-sectionally averaged salinity.
- Similarly, the depth value used to calculate horizontal Richardson number is the channel invert ("thalweg") elevation and the friction velocity is also estimated at this location. Most previous uses of horizontal Richardson number assumed uniform depth.
- The depth and shear velocity in the Richardson number estimate are from a single point longitudinally while gravitational circulation must occur over a substantial distance to be substantial. This is expected to be a primary reason for differences in the curve fit between different cross-sections.
- Some suspect dispersion coefficients were included in the analysis. These estimated dispersion coefficients generally correspond to regions with weak salinity gradients. The tidally-averaged salinity gradients are estimated by a linear best fit algorithm and then dispersion coefficients estimates involve dividing by these salinity gradients.

This suggests several potential sources of error: 1) use of tidally-averaged salinity gradients in regions with minimal salinity gradient for part of the tidal cycle, 2) the distance over which the salinity gradient is determined is fixed (12 km).

Additional uncertainty is related to the use of the dispersion coefficient information in the WAM. Sources of uncertainty include:

- Only the dispersion coefficient component associated with gravitational circulation is expected to apply precisely to WAM scenario simulations with dramatically different Delta geometry (breached islands). The effect of changed Delta geometry on the tidal dispersion component may be large. This variability may be addressed in the future by a particle tracking approach with the RMA2 Bay-Delta model.
- The limited number of sections provided by the dispersion analysis requires some spatial interpolation and extrapolation of dispersion coefficients. Most notably dispersion coefficients were not determined landward of the western Delta.

Overall the WAM predicts salinity fairly accurately for historic conditions suggesting that the parameterization approach is adequately accurate despite a large number of approximations and other sources of uncertainty. However errors for DRMS scenarios could be substantially larger than errors for historic conditions because the approach here only captures a portion of the variability of transport processes with different conditions (e.g., salinity gradients and tidal current amplitude). Ongoing work with the UnTRIM model is likely to improve accuracy due to advantages of this model including a domain extending through the central Delta and improved representation of bathymetric features.

H1.9 Acknowledgements

The Department of Water Resources funded this work. John DeGeorge and Richard Rachiele of RMA collaborated on all hydrodynamic modeling for the DRMS project. Professor Mark Stacey provided technical guidance.

H1.10 References

Burau, J.R., Gartner, J.W., and Stacey, M., 1998. Results for the hydrodynamic element of the 1994 Entrapment Zone Study in Suisun Bay. In Report of the 1994 Entrapment Zone Study, edited by Wim Kimmerer, 13-53. Interagency Ecological Program for the San Francisco Bay/Delta Estuary.

Casulli, V. 1990. Semi-implicit finite difference methods for the two-dimensional shallow water equations. *Journal of Computational Physics*. 86, 56-74.

Casulli, V., and Cattani, E. 1994. Stability, accuracy and efficiency of a semi-implicit method for three-dimensional shallow water flow, *Computers and Mathematics with Applications*, 27(4), 99-112.

Celebioglu, K., and Piasecki, M., 2006. Comparison of turbulence models with use of UnTRIM in the Delaware Bay, Proceedings of the Estuarine and Coastal Modeling Conference, ASCE, 2006.

Cheng, R.T., Casulli, V., and Gartner, J.W., 1993. Tidal residual intertidal mudflat (TRIM) model and its applications to San Francisco Bay, California. *Estuarine, Coastal and Shelf Science*, 369, 235-280.

Cloern, J.E., and Nichols, F.H., 1985. Time scales and mechanisms of estuarine variability, a synthesis from studies of San Francisco Bay: *Hydrobiologia*, v. 129, p. 229-237.

Fischer, H.B., List, E.J., Koh, R.C.Y., Imberger, J., and Brooks, N.H., 1979. *Mixing in Inland and Coastal Waters*. New York: Academic Press

Gross, E.S., Koseff, J.R., and Monismith, S.G., 1999. Three-dimensional salinity simulations of South San Francisco Bay. *Journal of Hydraulic Engineering*, 125 (11), 1199-1209.

Gross, E.S., Schaaf and Wheeler, 2003. South Bay Salt Ponds Initial Stewardship Plan: South San Francisco Bay Hydrodynamic Model Results Report. Prepared for Cargill Salt.

Gross, E. S., M. L. MacWilliams and W. Kimmerer, 2006. Simulating Periodic Stratification in San Francisco Bay, Proceedings of the Estuarine and Coastal Modeling Conference, ASCE.

Hansen, D.V., and Rattray, M., 1965. Gravitational circulation in straits and estuaries, *Journal of Marine Research*, 23, 104-122.

Kantha, L.H., Clayson, C.A., 1994. An improved mixed layer model for geophysical applications, *Journal of Geophysical Research*, 99, 25,235–25,266.

Monismith, S.G., Kimmerer, W., Burau, J.B., and Stacey, M.T., 2002. Structure and flow-induced variability of the subtidal salinity field in Northern San Francisco Bay, *Journal of Physical Oceanography*, 32, 3,003-3,019.

Oltmann, R.N., 1998. Indirect measurement of Delta outflow using ultrasonic velocity meters and comparison with mass-balance calculated outflow. Interagency Ecological Program for the Sacramento-San Joaquin Estuary, 11(1).

Simpson, J.H., Brown, J., Matthews, J. and Allen, G., 1990. Tidal straining, density currents and stirring in the control of estuarine stratification, *Estuaries*, **13**, 125-131.

Stacey, M.T., Burau, J.R, and Monismith, S.G., 2001. The creation of residual flows in a patially stratified estuary, *Journal of Geophysical Research*, 106(C8), 17,013-17,038.

Umlauf, L., Burchard, H., 2003. A generic length-scale equation for geophysical turbulence models. *Journal of Marine Research*, 61, 235–265.

URS, 2003. Proposed SFO Runway Reconfiguration Project, Final Technical Report: Predicted Changes in Hydrodynamics, Sediment Transport, Water Quality, and

Aquatic Biotic Communities Associated with SFO Runway Reconfiguration, Alternatives BX-6, A3 and BX-R.

Walters, R.A., Cheng, R.T. and Conomos, T.J., 1985. Time scales of circulation and mixing processes of San Francisco Bay waters, *Hydrobiologia*, 129, 13-36.

Warner, J.C., Schoellhamer, D.H., Ruhl, C.A. and Burau, J.B., 2004. Floodtide pulses after low tides in shallow subembayments adjacent to deep channels, *Estuarine, Coastal and Shelf Science*, 60, 213-228.

Appendix H2
UnTRIM San Francisco Bay-Delta Model Calibration Report

Delta Risk Management Strategy
UnTRIM San Francisco Bay-Delta Model Calibration Report

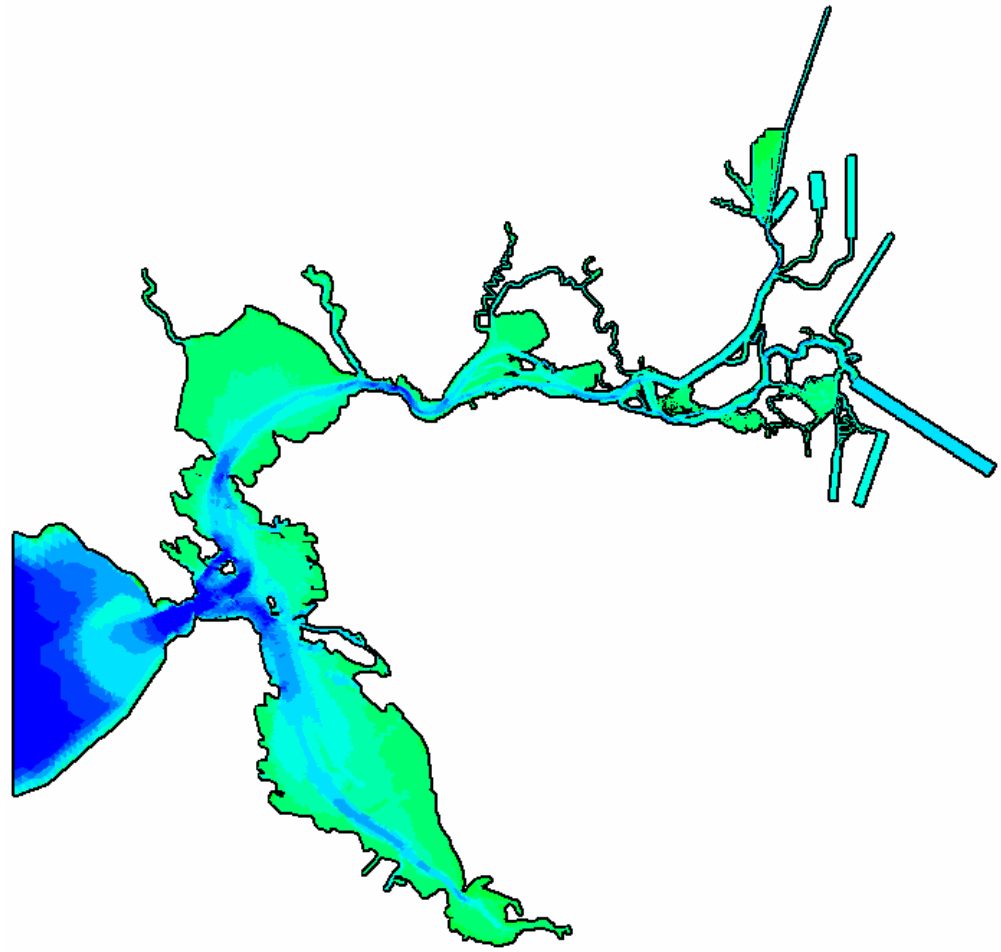

Prepared For:

California Department of Water Resources

March 21, 2007

Prepared By:

Dr. Michael L. MacWilliams

Environmental Consultant

Dr. Edward S. Gross

Environmental Consultant

Table of Contents

Executive Summary **H2-1**
H2.1 Introduction **H2-1**
H2.2 Project Approach and Objectives **H2-2**
H2.3 UnTRIM Model Description **H2-3**
H2.3.1 Governing Equations H2-3
H2.3.2 Turbulence Model H2-5
H2.3.3 Previous Applications H2-5
H2.3.4 Model Uncertainty H2-6
H2.4 The UnTRIM San Francisco Bay-Delta Model **H2-8**
H2.4.1 Model Domain and Grid H2-8
H2.4.2 Model Bathymetry H2-10
H2.4.3 Boundary Conditions H2-10
H2.4.3.1 Water Level H2-10
H2.4.3.2 Flow H2-10
H2.4.3.3 Salinity H2-12
H2.4.3.4 Wind H2-12
H2.4.3.5 Evaporation H2-12
H2.4.3.6 Bottom Friction H2-12
H2.4.4 Initial Conditions H2-13
H2.4.5 Simulation Periods H2-13
H2.5 Hydrodynamic Calibration **H2-11**
H2.5.1 Overview H2-13
H2.5.2 Method H2-14
H2.5.3 Stage Calibration H2-15
H2.5.3.1 San Francisco Bay H2-15
H2.5.3.2 Sacramento-San Joaquin Delta H2-16
H2.5.4 Delta Flow Calibration H2-18
H2.5.5 Discussion H2-20
H2.6 Salinity Calibration **H2-51**
H2.6.1 Overview H2-51
H2.6.2 USGS Synoptic Salinity Observations H2-51

H2.6.3 Time Series H2-53
H2.6.4 Suisun Bay Salinity Transects H2-55
H2.6.5 Discussion H2-58
H2.7 Summary and Conclusions H2-80
H2.8 Acknowledgments H2-80
H2.9 References H2-80

Tables

H2.5-1 Predicted and observed stage and cross-correlation statistics for San Francisco Bay water level monitoring stations.
H2.5-2 Predicted and observed stage and cross-correlation statistics for Sacramento-San Joaquin Delta water level monitoring stations
H2.5-3 Predicted and observed flow and cross-correlation statistics for Sacramento-San Joaquin Delta flow monitoring stations
H2.6-1 Average error and correlation coefficient for each synoptic sampling cruise covering the axis of the San Francisco Estuary
H2.6-2 Predicted and observed salinity and cross-correlation statistics for continuous salinity monitoring stations
H2.6-3 Mean salinity error (bias) and correlation for Entrapment Zone synoptic salinity dataset

Figures

H2.4.1-1 UnTRIM San Francisco Bay-Delta Model domain (top left), showing selected portions of the model grid in the Central Bay (top right), Carquinez Strait (middle right), and Sacramento-San Joaquin Delta (bottom left and bottom right).
H2.4.2-1 UnTRIM San Francisco Bay-Delta Model bathymetry.
H2.5.3-1 San Francisco Bay water level observation stations.
H2.5.3-2 Observed and predicted stage at Fort Point NOAA station (9414290).
H2.5.3-3 Observed and predicted stage at Alameda NOAA station (9414750).
H2.5.3-4 Observed and predicted stage at Richmond NOAA station (9414863).
H2.5.3-5 Observed and predicted stage at Port Chicago NOAA station (9415144).
H2.5.3-6 Observed and predicted stage at DWR Antioch station (ANH).
H2.5.3-7 Sacramento-San Joaquin Delta water level observation stations.
H2.5.3-8 Observed and predicted stage at Rio Vista.
H2.5.3-9 Observed and predicted stage at Three Mile Slough.
H2.5.3-10 Observed and predicted stage at Jersey Point.

H2.5.3-11 Observed and predicted stage at Dutch Slough.

H2.5.3-12 Observed and predicted stage at False River.

H2.5.3-13 Observed and predicted stage at Taylor Slough.

H2.5.3-14 Observed and predicted stage in the Mokelumne River.

H2.5.3-15 Observed and predicted stage in Old River, near the San Joaquin River.

H2.5.3-16 Observed and predicted stage in Old River, near Mandeville Island.

H2.5.3-17 Observed and predicted stage in Holland Cut.

H2.5.4-1 Flow observation stations in the Sacramento-San Joaquin Delta.

H2.5.4-2 Observed and predicted flow at Rio Vista.

H2.5.4-3 Observed and predicted flow at Three Mile Slough.

H2.5.4-4 Observed and predicted flow at Jersey Point.

H2.5.4-5 Observed and predicted flow at Dutch Slough.

H2.5.4-6 Observed and predicted flow at False River.

H2.5.4-7 Observed and predicted flow at Fishermans Cut.

H2.5.4-8 Observed and predicted flow at Taylor Slough.

H2.5.4-9 Observed and predicted flow at Old River, near the San Joaquin River.

H2.5.4-10 Observed and predicted flow at Mokelumne River.

H2.5.4-11 Observed and predicted flow at Old River, near Mandeville Island.

H2.5.4-12 Observed and predicted flow at Holland Cut.

H2.6.1-1 San Francisco Bay continuous and synoptic salinity stations.

H2.6.2-1 Observed and predicted salinity profiles at synoptic sampling station locations, interpolated along the axis of the San Francisco Estuary on March 16, 1994.

H2.6.2-2 Observed and predicted salinity profiles at synoptic sampling station locations, interpolated along the axis of the San Francisco Estuary on April 19, 1994.

H2.6.2-3 Observed and predicted salinity profiles at synoptic sampling station locations, interpolated along the axis of the San Francisco Estuary on May 17, 1994.

H2.6.2-4 Observed and predicted salinity profiles at synoptic sampling station locations, interpolated along the axis of the San Francisco Estuary on June 15, 1994.

H2.6.2-5 Observed and predicted salinity profiles at synoptic sampling station locations, interpolated along the axis of the San Francisco Estuary July 28, 1994.

H2.6.2-6 Observed and predicted salinity profiles at synoptic sampling station locations, interpolated along the axis of the San Francisco Estuary on August 30, 1994.

H2.6.2-7 Observed and predicted salinity profiles at synoptic sampling station locations, interpolated along the axis of the San Francisco Estuary on September 27, 1994.

H2.6.2-8 Observed and predicted salinity profiles at synoptic sampling station locations, interpolated along the axis of the San Francisco Estuary on October 26, 1994.

H2.6.2-9 Observed and predicted salinity profiles at synoptic sampling station locations, interpolated along the axis of the San Francisco Estuary on November 29, 1994.

H2.6.2-10 Observed and predicted salinity profiles at synoptic sampling station locations, interpolated along the axis of the San Francisco Estuary on January 18, 1995.

H2.6.2-11 Observed and predicted salinity profiles at synoptic sampling station locations, interpolated along the axis of the San Francisco Estuary on February 7, 1995.

H2.6.3-1 Observed and predicted salinity at the San Mateo Bridge bottom sensor.

H2.6.3-2 Observed and predicted salinity at the San Mateo Bridge top sensor.

H2.6.3-3 Observed and predicted salinity at the Oakland Bay Bridge bottom sensor.

H2.6.3-4 Observed and predicted salinity at the Oakland Bay Bridge top sensor.

H2.6.3-5 Observed and predicted salinity at the Presidio station.

H2.6.3-6 Observed and predicted salinity at the Point San Pablo bottom sensor.

H2.6.3-7 Observed and predicted salinity at the Point San Pablo top sensor.

H2.6.3-8 Observed and predicted salinity at the Martinez top sensor.

H2.6.3-9 Observed and predicted salinity at the Mallard bottom sensor.

H2.6.3-10 Observed and predicted salinity at the Mallard top sensor.

H2.6.4-1 Entrapment Zone synoptic salinity sampling stations.

H2.6.4-2 Observed and predicted salinity profiles at synoptic sampling stations for the Entrapment Zone Study, interpolated through Suisun Bay and the western Delta on April 27, 1994 at 6:18 am.

H2.6.4-3 Observed and predicted salinity profiles at synoptic sampling stations for the Entrapment Zone Study, interpolated through Suisun Bay and the western Delta on April 27, 1994 at 9:44 am.

H2.6.4-4 Observed and predicted salinity profiles at synoptic sampling stations for the Entrapment Zone Study, interpolated through Suisun Bay and the western Delta on April 27, 1994 at 2:03 pm.

H2.6.4-5 Observed and predicted salinity profiles at synoptic sampling stations for the Entrapment Zone Study, interpolated through Suisun Bay and the western Delta on April 27, 1994 at 5:28 pm.

H2.6.4-6 Observed and predicted salinity profiles at synoptic sampling stations for the Entrapment Zone Study, interpolated through Suisun Bay and the western Delta on April 27, 1994 at 10:47 pm.

H2.6.4-7 Observed and predicted salinity profiles at synoptic sampling stations for the Entrapment Zone Study, interpolated through Suisun Bay and the western Delta on April 28, 1994 at 3:46 am.

H2.6.4-8 Observed and predicted salinity profiles at synoptic sampling stations for the Entrapment Zone Study, interpolated through Suisun Bay and the western Delta on April 28, 1994 at 8:26 am.

H2.6.4-9 Observed and predicted salinity profiles at synoptic sampling stations for the Entrapment Zone Study, interpolated through Suisun Bay and the western Delta on April 28, 1994 at 12:44 pm.

H2.6.4-10 Observed and predicted salinity profiles at synoptic sampling stations for the Entrapment Zone Study, interpolated through Suisun Bay and the western Delta on May 17, 1994 at 6:46 am.

H2.6.4-11 Observed and predicted salinity profiles at synoptic sampling stations for the Entrapment Zone Study, interpolated through Suisun Bay and the western Delta on May 17, 1994 at 9:41 am.

H2.6.4-12 Observed and predicted salinity profiles at synoptic sampling stations for the Entrapment Zone Study, interpolated through Suisun Bay and the western Delta on May 17, 1994 at 12:30 pm.

H2.6.4-13 Observed and predicted salinity profiles at synoptic sampling stations for the Entrapment Zone Study, interpolated through Suisun Bay and the western Delta on May 17, 1994 at 5:53 pm.

H2.6.4-14 Observed and predicted salinity profiles at synoptic sampling stations for the Entrapment Zone Study, interpolated through Suisun Bay and the western Delta on May 17, 1994 at 7:24 pm.

H2.6.4-15 Observed and predicted salinity profiles at synoptic sampling stations for the Entrapment Zone Study, interpolated through Suisun Bay and the western Delta on May 17, 1994 at 11:44 pm.

H2.6.4-16 Observed and predicted salinity profiles at synoptic sampling stations for the Entrapment Zone Study, interpolated through Suisun Bay and the western Delta on May 17, 1994 at 3:27 am.

H2.6.4-17 Observed and predicted salinity profiles at synoptic sampling stations for the Entrapment Zone Study, interpolated through Suisun Bay and the western Delta on May 18, 1994 at 8:05 am.

H2.6.4-18 Observed and predicted salinity profiles at synoptic sampling stations for the Entrapment Zone Study, interpolated through Suisun Bay and the western Delta on May 18, 1994 at 11:14 am.

Abbreviations

3D	Three-dimensional
ADCP	Acoustic Doppler Current Profiler
CVP	Central Valley Project
DEM	Digital Elevation Model
DICU	Delta Island Consumptive Use
DRMS	Delta Risk Management Study
DWR	Department of Water Resources
MLLW	Mean Lower Low Water
NAD27	North American Datum of 1927
NDO	Net Delta Outflow
NGVD 29	National Geodetic Vertical Datum of 1929
NOAA	National Oceanic & Atmospheric Administration
NOS	National Ocean Service (NOAA)
QCD	Delta Net Channel Depletion in DAYFLOW
QGCD	Delta Gross Channel Depletion in DAYFLOW
QMISDIV	Flooded Island and Island Storage Diversion in DAYFLOW
QOUT	Net Delta outflow at Chipps Island in DAYFLOW
QPREC	Delta precipitation and runoff estimate in DAYFLOW
QRIO	Sacramento River Flow Estimate past Rio Vista in DAYFLOW
SWP	State Water Project
RMA	Resource Management Associates
SFPORTS	San Francisco Physical Oceanographic Real-Time System
TRIM	Tidal, Residual, Intertidal & Mudflat Model
UnTRIM	Unstructured Tidal, Residual, Intertidal & Mudflat Model
USGS	United States Geological Survey
UTM	Universal Transverse Mercator

Executive Summary

Three-dimensional simulations of flow and transport in San Francisco Bay and the Sacramento-San Joaquin Delta were performed using the three-dimensional unstructured grid hydrodynamic model UnTRIM. The model was developed to support the Delta Risk Management Study (DRMS) funded by the California Department of Water Resources. The model applications build on previous TRIM and UnTRIM applications. A model grid consisting of quadrilaterals and triangles was developed that extends from the Pacific Ocean through San Francisco Bay and further into the Sacramento-San Joaquin Delta than previous TRIM and UnTRIM applications. In addition, a state-of-the-art turbulence closure was incorporated into the UnTRIM model from the TRIM model. This report presents the hydrodynamic and salinity calibration of the resulting UnTRIM San Francisco Bay-Delta Model.

The hydrodynamic calibration demonstrates that the model is accurately predicting water levels from the Golden Gate into the Sacramento-San Joaquin Delta. The detailed analysis of flows in the Sacramento-San Joaquin Delta indicates that predicted tidal and tidally-averaged flows agree well with observations, which vary over several orders of magnitude between stations. The salinity calibration shows good agreement between predicted and observed salinities over a full year of time series comparisons. In addition, comparison of predicted and observed salinity profiles along the axis of the San Francisco Estuary demonstrate that the model is accurately predicting salinity distribution, stratification, and the extent of salinity intrusion into the western Delta through the full range of flow conditions experienced during the simulation year. Comparisons to observations in Suisun Bay collected during the Entrapment Zone Study suggest that the model predicts tidal time scale variability in salinity accurately.

The calibrated model was used for simulating DRMS scenarios for evaluating the three-dimensional effects resulting from channel-island exchange following levee failure, evaluating the three-dimensional effects which impact the effectiveness of flushing flows, and investigating salt intrusion into the Delta resulting from sea level rise. The results and conclusions of these scenarios are included in separate reports. Understanding the importance of three-dimensional effects for each of these scenarios is important in order to quantify the uncertainties associated with one- and two-dimensional models which are used in other components of the DRMS project. The calibration outlined in this document provides confidence that the three-dimensional UnTRIM model is performing adequately to assess the importance of three-dimensional effects on hydrodynamics and salt transport.

H2.1 Introduction

This report presents the results of the hydrodynamic and salinity calibration component of three-dimensional UnTRIM model of the San Francisco Bay, San Pablo Bay, Suisun Bay and the Sacramento-San Joaquin Delta used in the DRMS project.

This report is organized into seven major sections:

- **Section 1. Introduction.** This section presents the scope and organization of the report.
- **Section 2. Project Approach and Objectives.** This section presents approach used and describes how the UnTRIM model fits into overall the DRMS project.
- **Section 3. UnTRIM Model Description.** This section provides a description of the UnTRIM hydrodynamic model, with a discussion of the governing equations and model uncertainty.
- **Section 4. UnTRIM San Francisco Bay-Delta Model.** This section presents the model domain, and boundary conditions, and initial conditions used in the UnTRIM Bay-Delta Model.
- **Section 5. Hydrodynamic Calibration.** This section presents the water level and flow calibration results for the UnTRIM Bay-Delta Model.
- **Section 6. Salinity Calibration.** This section presents the salinity calibration results of the UnTRIM Bay-Delta Model.
- **Section 7. Summary and Conclusions.** This section presents a brief summary of the hydrodynamic modeling results and the conclusions drawn from the model setup and calibration.

H2.2 Project Approach and Objectives

The Sacramento-San Joaquin Delta is a critical resource to the state of California because the Delta is a source of drinking water for roughly 2 out of 3 Californians. However, the 2,800 km^2 of islands in the Delta region are at risk of inundation from levee failures. These deeply subsided islands are protected by levees typically 4 to 5 meters high which are, in most cases, not engineered levees and are constructed partially with peat and other weak and compressible soils. The Delta Risk Management Study has been funded by the California Department of Water Resources to “look at sustainability of the Delta, and … assess major risks to the Delta resources from floods, seepage, subsidence, and earthquakes” (DWR). Part of this effort involves the application of hydrodynamic models to estimate the effect of levee failures on salinity in the Delta. Levee failures in the Delta generally result in increased salinity as islands flood and brackish water from Suisun Bay is entrained into the Delta. Increased salinity can result in exceedence of water quality objectives for drinking water causing interruption of water exports, resulting in a large economic impact.

Several hydrodynamic and water quality simulation tools are applied in the DRMS project, ranging from a tidally-averaged advection-dispersion model, which can perform a decade of salinity projections in approximately 5 minutes of computational time, to the sophisticated and computationally intensive three-dimensional model described here. The first phase of the DRMS work involves quantification of risk and consequences of Delta levee failures while the second phase will study risk reduction actions that can be taken to reduce risks of levee failures and the impacts of levee failures.

The UnTRIM model discussed in this report will be applied to several scenarios in the DRMS project with the following goals:

1) Quantify epistemic uncertainties associated with depth-averaged simulations of DRMS scenarios.
    a. Flushing scenarios of the period following initial flooding of islands.
    b. Sherman Island breach scenarios.
2) Estimate and analyze salt intrusion resulting from sea level rise scenarios

The details and results of all these scenario simulations will be documented in the scenario reports. In order to confidently meet the goals of the three-dimensional simulations, the calibration should indicate that the model accurately represents hydrodynamic and salt transport processes in the estuary. The calibration emphasizes Suisun Bay and the Delta which are the geographical focus of the DRMS project.

H2.3 UnTRIM Model Description

The primary tool used in this technical study was the three-dimensional hydrodynamic model UnTRIM (Casulli and Zanolli, 2002). A complete description of the governing equations, numerical discretization, and numerical properties of UnTRIM are described in Casulli and Zanolli (2002, 2005), Casulli (1999), and Casulli and Walters (2000). This section presents a brief overview of the governing equations, numerical method, turbulence model used in UnTRIM for the DRMS project. Additionally, previous applications of the UnTRIM model in San Francisco Bay, and the primary sources of model uncertainty are discussed.

The UnTRIM model solves the three-dimensional Navier-Stokes equations (3.1-3.3) on an unstructured grid in the horizontal plane. The boundaries between vertical layers are at fixed elevations, and cell heights can be varied vertically to provide increased resolution near the surface or other vertical locations. Volume conservation is satisfied by a volume integration of the incompressible continuity equation (3.4), and the free-surface is calculated by integrating the continuity equation over the depth (3.5), and using a kinematic condition at the free-surface as described in Casulli (1990). The numerical method allows full wetting and drying of cells in the vertical and horizontal directions. The governing equations are discretized using a finite difference – finite volume algorithm. Discretization of the governing equations and model boundary conditions are presented in detail by Casulli and Zanolli (2002) and is not reproduced here. All details and numerical properties of this state-of-the-art three-dimensional model are well-documented in peer reviewed literature (Casulli and Zanolli, 2002; 2005).

H2.3.1 Governing Equations

Three-dimensional simulations were made using the three-dimensional non-hydrostatic hydrodynamic model for free-surface flows on unstructured grids, UnTRIM, described in Casulli and Zanolli (2002). The UnTRIM model solves the full three-dimensional momentum equations for an incompressible fluid under a free-surface given by

$$\frac{\partial u}{\partial t}+u\frac{\partial u}{\partial x}+v\frac{\partial u}{\partial y}+w\frac{\partial u}{\partial z}-fv=-\frac{\partial p}{\partial x}+\nu^h\left(\frac{\partial^2 u}{\partial x^2}+\frac{\partial^2 u}{\partial y^2}\right)+\frac{\partial}{\partial z}\left(\nu^v\frac{\partial u}{\partial z}\right)$$
(3.1)

$$\frac{\partial v}{\partial t}+u\frac{\partial v}{\partial x}+v\frac{\partial v}{\partial y}+w\frac{\partial v}{\partial z}+fu=-\frac{\partial p}{\partial y}+\nu^h\left(\frac{\partial^2 v}{\partial x^2}+\frac{\partial^2 v}{\partial y^2}\right)+\frac{\partial}{\partial z}\left(\nu^v\frac{\partial v}{\partial z}\right)$$
(3.2)

$$\frac{\partial w}{\partial t}+u\frac{\partial w}{\partial x}+v\frac{\partial w}{\partial y}+w\frac{\partial w}{\partial z}=-\frac{\partial p}{\partial z}+\nu^h\left(\frac{\partial^2 w}{\partial x^2}+\frac{\partial^2 w}{\partial y^2}\right)+\frac{\partial}{\partial z}\left(\nu^v\frac{\partial w}{\partial z}\right)-g$$
(3.3)

where $u(x,y,z,t)$ and $v(x,y,z,t)$ are the velocity components in the horizontal x - and y - directions, respectively; $w(x,y,z,t)$ is the velocity component in the vertical z - direction; t is the time; $p(x,y,z,t)$ is the normalized pressure defined as the pressure divided by a constant reference density; f is the Coriolis parameter; g is the gravitational acceleration; and ν^h and ν^v are the coefficients of horizontal and vertical eddy viscosity, respectively (Casulli and Zanolli, 2002). Conservation of mass is expressed by the continuity equation for incompressible fluids

$$\frac{\partial u}{\partial x}+\frac{\partial v}{\partial y}+\frac{\partial w}{\partial z}=0.$$
(3.4)

The free-surface equation is obtained by integrating the continuity equation over depth and using a kinematic condition at the free-surface (Casulli and Zanolli, 2002)

$$\frac{\partial \zeta}{\partial t}+\frac{\partial}{\partial x}\left[\int_{-H^0}^{\zeta} u dz\right]+\frac{\partial}{\partial y}\left[\int_{-H^0}^{\zeta} v dz\right]=0,$$
(3.5)

where $h(x,y)$ is the prescribed bathymetry measured downward from the reference elevation and $\eta(x,y,t)$ is the free-surface elevation measured upward from the reference elevation. Thus, the total water depth is given by $H(x,y,t)=h(x,y)+\eta(x,y,t)$.

The boundary conditions at the free-surface are specified by the prescribed wind stresses as (Casulli and Zanolli, 2002)

$$\nu^v\frac{\partial u}{\partial z}=\tau_x{}^w,\quad \nu^v\frac{\partial v}{\partial z}=\tau_y{}^w,\quad \text{at } z=\eta$$
(3.6)

where $\tau_x{}^w$ and $\tau_y{}^w$ are the wind stress components in the x and y direction, respectively. Similarly, at the sediment-water interface the bottom friction is specified by

$$\nu^{v}\frac{\partial u}{\partial z}=\tau_{x},\qquad \nu^{v}\frac{\partial v}{\partial z}=\tau_{y},\qquad \text{at } z=\eta \tag{3.7}$$

where τ_x and τ_y are the bottom stress components in the *x* and *y* direction, respectively. A quadratic stress formula is applied at each boundary. At the free-surface the coefficient of drag is specified as a function of wind speed using the formulation of Large and Pond (1981). At the bottom boundary the coefficient of drag is estimated using a specified roughness coefficient (z_0).

The governing equation for salt transport (Casulli and Zanolli, 2002) is

$$\frac{\partial s}{\partial t}+\frac{\partial(us)}{\partial x}+\frac{\partial(vs)}{\partial y}+\frac{\partial(ws)}{\partial z}=\frac{\partial}{\partial x}\left(\varepsilon_h\frac{\partial s}{\partial x}\right)+\frac{\partial}{\partial y}\left(\varepsilon_h\frac{\partial s}{\partial y}\right)+\frac{\partial}{\partial z}\left(\varepsilon_v\frac{\partial s}{\partial z}\right) \tag{3.8}$$

where *s* is the scalar concentration; ε_h is the horizontal diffusion coefficient; and ε_v is the vertical diffusion coefficient. A linear equation of state was used to relate salinity to density. This approximation allows a substantial reduction in computational time relative to the use of the nonlinear relationships. The estimation of eddy viscosity and eddy diffusivity is discussed below.

H2.3.2 Turbulence Model

The turbulence closure model used in the present study is a two-equation model comprised of a turbulent kinetic energy equation and a generic length-scale equation. The parameters of the generic length-scale (GLS) equation are chosen to yield the “gen” closure proposed by Umlauf and Burchard (2003). The Kantha and Clayson quasi-equilibrium stability functions (Kantha and Clayson, 1994) are used. This closure has been shown by Warner et al. (2005) to have several advantages relative to the commonly used Mellor-Yamada level 2.5 closure (MY) and to generally perform similarly to the GLS versions of k-ε and k-ω. All parameter values used in the “gen” closure are identical to those used by Warner et al. (2005), except for the minimum eddy diffusivity and eddy viscosity values which were $5\text{x}10^{-5}$ m^2/s.

The numerical method used to solve the equations of the turbulence closure is a semi-implicit method that results in tridiagonal positive-definite matrices in each water column and ensures that the turbulent variables remain positive (Deleersnijder et al., 1997).

H2.3.3 Previous Applications

The TRIM3D model (Casulli and Cheng, 1992) and UnTRIM model have been applied previously to San Francisco Bay (Cheng and Casulli, 2002; MacWilliams and Cheng, 2007). The TRIM3D model (Casulli and Cattani, 1994), which follows a similar numerical approach on structured horizontal grids, has been widely applied in San Francisco Bay (e.g., Cheng et al. 1993; Cheng and Casulli, 1996; Gross et al., 1999; Gross et al., 2006), and a 2D version, TRIM2D, is used in San Francisco Bay Physical Oceanographic Real-Time System, SFPORTS (http://sfports.wr.usgs.gov/sfports) (Cheng

and Smith, 1998). Thus, the UnTRIM numerical approach has been well-tested in the San Francisco Estuary.

H2.3.4 Model Uncertainty

As discussed above, the TRIM and UnTRIM models have been widely used in San Francisco Bay, and numerous detailed model calibrations have been performed (e.g., Cheng et al., 1993; Gross and Schaaf & Wheeler, 2003; Gross et al., 2006; MacWilliams and Cheng, 2007). Due to this extensive history of application, these models are the best established three-dimensional models of San Francisco Bay.

The equations governing fluid motion and salt transport, representing conservation of water volume, momentum and salt mass, are well established, but can not be solved analytically for complex geometry and boundary conditions. Therefore models are used to give approximate solutions to these governing equations. Many decisions are made in constructing and applying numerical models. The governing equations are first chosen to represent the appropriate physical processes in one, two or three-dimensions and at the appropriate time scale. Then these governing equations that describe fluid motion and salt transport in a continuum are discretized to apply over distinct volumes. The resulting discretized equations must be solved, often requiring the use of an iterative matrix solver. The discretization and matrix solution must be developed carefully to yield a numerical approach that is consistent with the governing equations, stable and efficient. To apply the models, the bathymetric grid, boundary conditions, initial conditions and several model parameters must be chosen. The accuracy of the model application will depend on the accuracy of this input, including site-specific parameters and reduction of numerical error by choosing appropriate time step and grid size.

The three-dimensional models applied in this project provide a more detailed description of fluid motion in the San Francisco Estuary than depth-averaged or one-dimensional models. The UnTRIM model, like almost all large scale hydrodynamic models, average over the turbulent time scale to describe tidal time scale motions. The resulting three-dimensional hydrodynamic models represent the effect of turbulent motions as small scale mixing of momentum and salt, parameterized by eddy viscosity and eddy diffusivity coefficients, respectively. These turbulent mixing coefficients are estimated from the tidal flow properties (velocity and density) by “turbulence closure” models embedded within the three-dimensional models. Three-dimensional models estimate the variability in velocity and salinity in all dimensions and through the tidal cycle, therefore provide a detailed description of hydrodynamics and salinity. However, several sources of uncertainty are inherent in the application of these three-dimensional models:

- Spatial resolution/computational cost – the spatial resolution of the bathymetry of the model domain, and velocity and salinity distributions, is limited by the large computational expense associated with high-resolution models. The description of the Bay bathymetry is improved by the use of a flexible unstructured grid.
- Bathymetry data – limited spatial coverage and accuracy of bathymetry data can be a substantial source of error. Converting all data to a uniform vertical datum and horizontal datum can lead to some error. In particular, LiDAR data may have

substantial errors in vertical datum and removing vegetation from the dataset can be difficult.

- Site-specific parameters – the TRIM and UnTRIM models require bottom friction coefficients to parameterize the resistance to flow at solid boundaries. These parameters are specified in model calibration by tuning to improve the calibration.
- Turbulence closure – the effect of turbulent motions on the tidal time scale motions is estimated by a turbulence closure. While many turbulence closures are available, this is an ongoing area of research and, particularly in stratified settings, the effect of turbulence on tidal flows and salinity is not easy to estimate accurately and different turbulence closures may give significantly different results (e.g., Celebioglu and Piasecki 2006).
- Numerical errors – a numerical method approximates the governing equations to some level of accuracy. The mathematical properties of the numerical method of the TRIM and UnTRIM models are well understood due to detailed mathematical analysis presented in several peer reviewed publications. While the stability and conservation properties of the method are ideal, a source of error in the numerical method is some degree of numerical diffusion of momentum and potential for damping of tidal propagation.
- Boundary conditions and initial conditions – The salinity in South San Francisco Bay varies laterally (e.g., Huzzey et al., 1990) but this lateral variability can not be described by existing observations. In addition, limited observations are available to describe the vertical distribution of salinity. Therefore, lateral and vertical distributions must be assumed to interpolate and extrapolate from the limited observations to obtain initial salinity fields. Inflows to the estuary are also quite uncertain in several regions due to ungauged portions of watersheds and uncertainty in estimates of Delta Island Consumptive Use (DICU) and net channel depletions (QCD).

Though additional potential sources of uncertainty can be identified, the largest sources of uncertainty for hydrodynamic predictions are the accuracy and resolution of available bathymetry and the grid resolution used to represent this bathymetry in the model. This study made use of the best available bathymetric data, and the bathymetry applied to the model grid is based on a high resolution master grid which was developed and used as part of a large TRIM calibration effort in San Francisco Bay (Gross et al., 2006). However, many of the available data sets are fairly old and have required vertical and or horizontal coordinate transformations for the grid used in this project.

The uncertainty in Delta outflows can also be a substantial uncertainty in summer conditions, particularly when consumptive use within the Delta (which is only known approximately) is typically the same order of magnitude as Delta tributary flows. The current application makes use of Delta gross channel depletion estimates (QGCD) from DAYFLOW. However, because these estimates do not vary annually, they may not be representative of actual consumptive use in a particular year. This uncertainty would impact the accuracy of net Delta outflows predicted at the flow monitoring stations in the

western Delta, when compared to observed flows. In addition, uncertainty in net Delta outflows has a significant impact on salinity predictions.

H2.4 The UnTRIM San Francisco Bay-Delta Model

The UnTRIM San Francisco Bay-Delta Model was developed for the DRMS project, and is designed to take full advantage of the unstructured grid capabilities of UnTRIM. The model uses relatively coarse resolution in the Pacific Ocean, Central Bay, and South Bay, with gradually increasing grid resolution along the Northern axis of the Estuary to provide relatively high resolution in the Sacramento-San Joaquin Delta. The model domain extends through Franks
Tract to the East and includes Liberty Island in the North. Because development of a full Delta model was not possible under the time and budgetary constraints of this phase of the DRMS project, “False Delta Region” geometries were used to represent the area and tidal prism of unresolved portions of the Delta. In future applications of the UnTRIM San Francisco Bay-Delta Model, the model domain can be extended to include additional regions of the Delta, and these False Delta Regions can be reduced or eliminated.

This section presents the model domain and model grid, bathymetry, boundary and initial conditions used in the development of the UnTRIM Bay-Delta Model. The model was applied to two independent calibration periods, to take advantage of extensive availability of flow and water level data collected in the Delta during 2002, and salinity data collected in Suisun Bay during 1994.

H2.4.1 Model Domain and Grid

The model domain for the San Francisco Estuary simulations includes San Francisco Bay, San Pablo Bay, Suisun Bay, the western and central portions of the Sacramento-San Joaquin Delta, and a portion of the Pacific Ocean extending to approximately 22 km west of the Golden Gate (Figure H2.4.1-1). The ocean portion of the model domain uses a simplified geometry, and unresolved portions of the Sacramento-San Joaquin Delta are approximated using rectangular “False Delta Regions” areas sized to produce the appropriate tidal prism of the unresolved areas following the approach of Gross et al. (2006). The purpose of the “False Delta Regions” is to represent the tidal prism of the unresolved portions of the Delta, such that the tidal fluxes at the upstream extent of the resolved portions of the Delta are accurately represented in the model.

An unstructured grid for the model domain was developed using the grid generator JANET (Lippert and Sellerhoff, 2007). The grid was developed such that the main channels of the estuary are discretized using “orthogonal curvilinear” quadrilaterals which are aligned with the principal flow directions, while the remainder of the mesh is constructed using a mix of triangles and quadrilaterals (Figure H2.4.1-1). The grid resolution along the axis of the estuary varies as necessary to resolve bathymetric variability. Grid cell side lengths are approximately 400 m at the Golden Gate and in the Central Bay and become gradually smaller eastward, with resolution of 50 to 75 m in the Western and central Delta (Figure H2.4.1-1). This approach takes advantage of the full flexibility of unstructured grids, and offers significant advantages both in terms of numerical efficiency and accuracy.

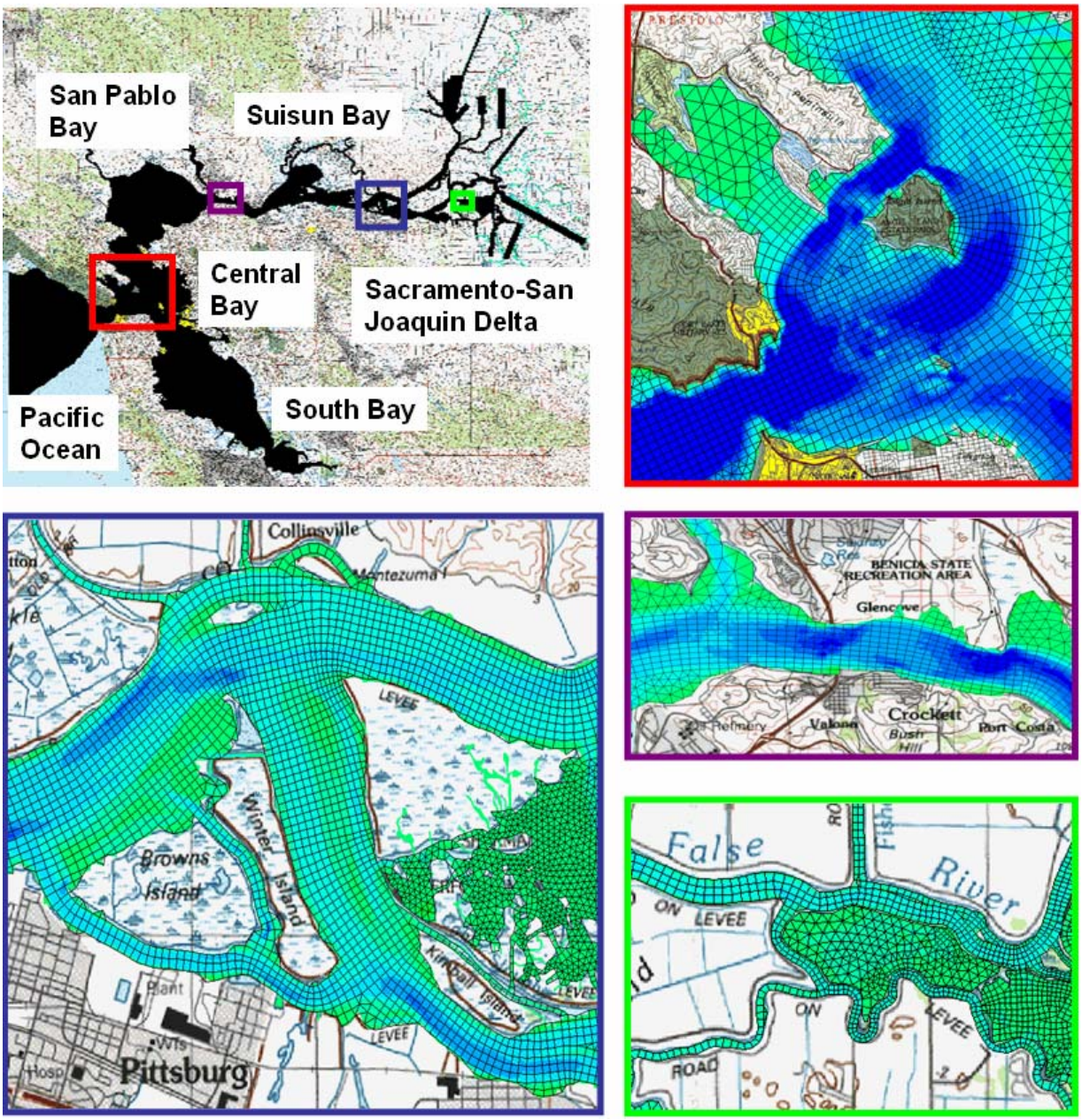

Figure H2.4.1-1 UnTRIM San Francisco Bay-Delta Model domain (top left), showing selected portions of the model grid in the Central Bay (top right), Carquinez Strait (middle right), and Sacramento-San Joaquin Delta (bottom left and bottom right).

H2.4.2 Model Bathymetry

The primary bathymetry data source for the model grid of South San Francisco Bay, Central Bay, and San Pablo Bay was NOAA DEM (Digital Elevation Model) data. The DEM data were created by NOAA using NOS soundings and other bathymetry data collected in San Francisco Bay from 1979 to 1985. Coastal ocean bathymetry was also based on NOAA NOS sounding data. In Suisun Bay and the Sacramento-San Joaquin Delta the model bathymetry was developed using the USGS 10 m horizontal resolution bathymetric grid based on nearly one million depth soundings augmented by contours and recent aerial photography (Smith et al., 2003). Additional bathymetric data were used to represent bathymetry in Liberty Island and Sherman Island. The resulting model bathymetry is shown on Figure H2.4.2-1.

H2.4.3 Boundary Conditions

H2.4.3.1 Water Level

Observations of water surface elevation at Fort Point, near the southern end of the Golden Gate, were used to drive the tidal (ocean) boundary of the model domain. These observations were multiplied by an amplification factor of 0.9544 to account for the difference in tidal range between observed Fort Point tides and tides along the model boundary, and a phase lead of 30 minutes was applied to account for the phase difference between Fort Point and the model boundary, following the approach of Gross et al. (2006).

H2.4.3.2 Flow

At most of the landward boundaries of the Delta in the UnTRIM model, flow boundary conditions were applied to account for the primary freshwater inflows to the San Francisco Estuary. Daily averaged flows are estimated at several locations in the Delta by the “DAYFLOW” program (CDWR, 1986). The flows are estimated using a volume balance approach incorporating the principal Delta stream inflows, Delta precipitation, Delta exports, and Delta gross channel depletions (CDWR, 1986). During the period simulated in 2002, typical summer inflows into the northern portion of the Delta are on the order of 400 to 500 m^3/s while there is a net export on the order of 100 to 300 m^3/s from the southern portion of the Delta. The estimates of flows produced by the “DAYFLOW” program contain substantial uncertainty, particularly during low Delta flow conditions, because several terms in the volume balance are quite uncertain. Flow monitoring data collected since 1997 (Oltmann, 1998) suggests that the actual daily-averaged Delta outflows can be very different from the “DAYFLOW” values. In particular the Delta gross channel depletion estimates (QGCD), which do not vary annually may not be representative of actual channel depletion for all water years. In addition to the Delta flows, freshwater inflow from several rivers, creeks and water pollution control plants (WPCPs) are included in the simulations. The additional flows considered in the simulations are Napa River, Petaluma River, Alameda Creek, Guadalupe River, Coyote Creek, and flows from the San Jose/Santa Clara WPCP.

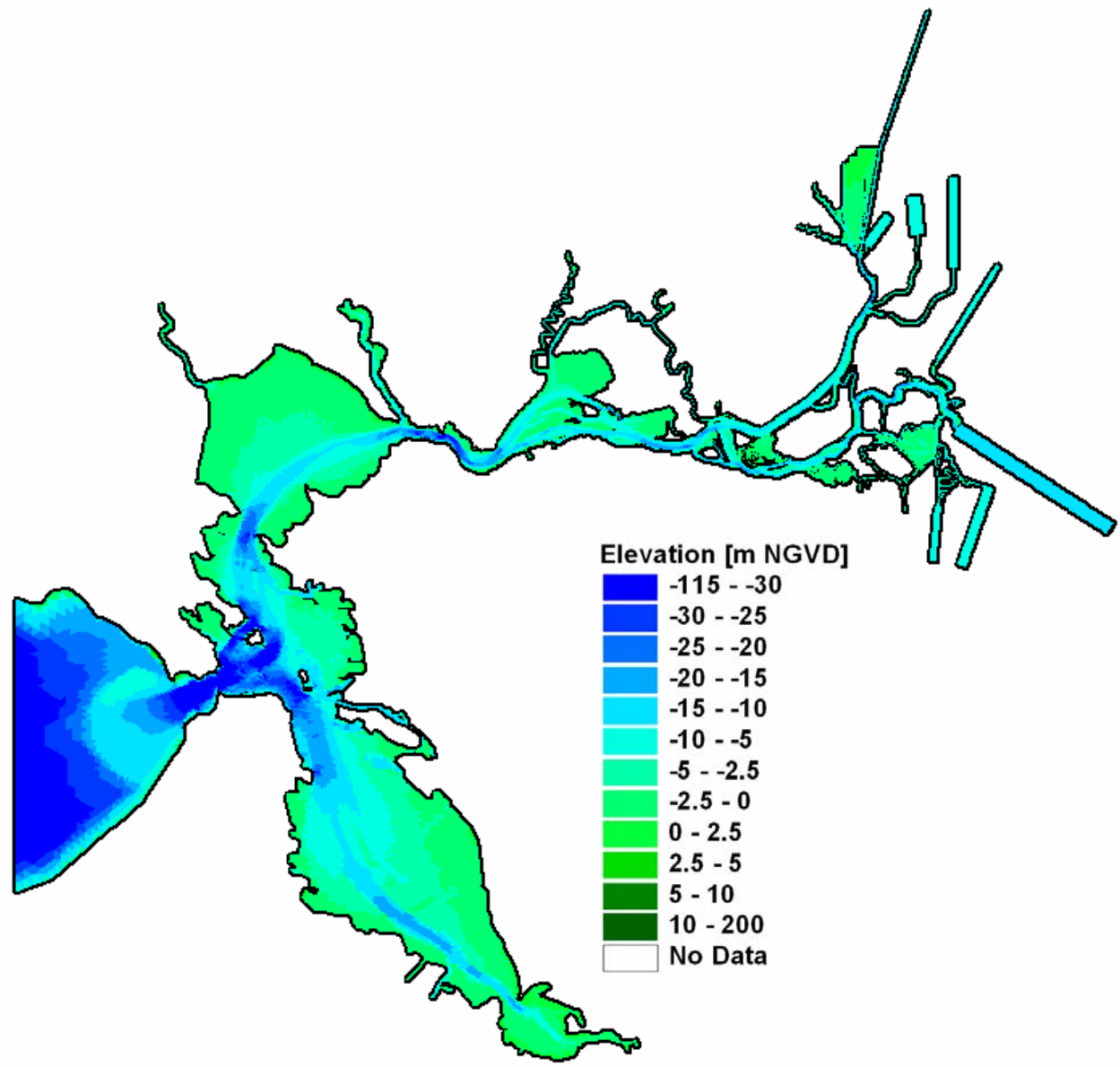

Figure H2.4.2-1 UnTRIM San Francisco Bay-Delta Model bathymetry.

Since the current model does not resolve all portions of the Delta, some approximations are made as to the appropriate location for each of the net inflows and outflows obtained from DAYFLOW. This is particularly true for the net Delta channel depletions (QCD), which include the Delta gross channel depletion estimates (QGCD), precipitation (QPREC), and QMISDIV. Since much of this consumptive use falls outside of the model domain. For this reason the net channel depletion is subtracted from the net inflows following a ratio based on a very approximate estimate of contribution of different portions of the unresolved Delta net channel depletion. The net Delta channel depletion fraction applied to the Sacramento River is estimated as 28% based on the calculation of QRIO within DAYFLOW. The remainder of the net Delta channel depletion is divided between the other major inflow boundaries. This approach ensures the net Delta outflow (QOUT) is represented accurately. Delta exports are divided between the Holland Cut,

Old River, and San Joaquin boundaries of the model, since the actual export locations and all of the net flow pathways to the exports are not included in the model domain. Based on the net flows calculated at Holland Cut and at Old River near Mandeville Island, this distribution of inflows produces reasonable net flows into the south Delta, and through Franks Tract at the Old River station near the San Joaquin. Future expansion of the model into more regions of the Delta will allow for more accurate representation of these flow conditions in the model.

H2.4.3.3 Salinity

The salinity at the ocean boundary is assumed to be 33.5 psu, which is a typical of observed salinity in the coastal ocean near San Francisco Bay (Dever and Lentz, 1994). For the purposes of calibration, the salinity of all freshwater inflows is considered to be 0 psu. For some scenario simulations, non-zero inflow concentrations are applied to facilitate comparison with equivalent RMA simulations.

H2.4.3.4 Wind

Wind forcing was applied at the water surface as a wind stress. Hourly wind speed and direction observations from the Bay Area Air Quality Control District were used from three locations, San Carlos, Pittsburg and Point San Pablo, to account for spatial variability in wind velocities. The San Carlos wind is used in South San Francisco Bay, the Point San Pablo wind is used in Central San Francisco Bay and San Pablo Bay and the Pittsburg wind is used in Carquinez Strait, Suisun Bay and the Delta. In transition regions, speed and direction are linearly interpolated between neighboring stations. The wind drag coefficient is varied based on local wind speed according to the formulation of Large and Pond (1981).

H2.4.3.5 Evaporation

Daily evaporation and precipitation data collected by the California Irrigation Management Information System at 2 stations bordering the San Francisco Estuary were used to specify spatially variable evaporation and precipitation at the water surface of the estuary. In the 1994 simulations, the Fremont and Novato stations were used to specify evaporation and precipitation. Fremont was used in South Bay and Novato was used in Central San Francisco Bay, San Pablo Bay, Carquinez Strait and Suisun Bay. In the 2002 simulation the Union City station was used for South San Francisco Bay and the Carneros station was used for Central San Francisco Bay, San Pablo Bay, Carquinez Strait and Suisun Bay. Evaporation and precipitation were not specified inside the Legal Delta because evaporation and precipitation are accounted for in the QCD components of DAYFLOW.

H2.4.3.6 Bottom Friction

The bottom roughness coefficient, z_o, is used to characterize the bottom friction. In San Francisco Bay, the values of z_o used varied as a function of water column depth and ranged from 0.1 mm to 2 mm, with the highest values in intertidal regions and the lowest values in the deep channel following the approach used by Gross et al. (2006). In the Sacramento-San Joaquin Delta portion of the grid, a uniform bottom roughness

coefficient of 0.1 mm was used. This value is equal to the value typically applied to channels in the San Francisco Bay portion of the model domain.

H2.4.4 Initial Conditions

The initial water surface elevation was assumed to be uniform at 0 m NGVD and quiescent conditions (no velocities) were assumed. The initial salinity field is specified based on synoptic salinity data collected by the USGS in the main channel of San Francisco Bay (e.g., Edmonds et al., 1995), and assuming that salinity is laterally uniform in the Estuary and equal to 33.5 psu in the coastal ocean. Therefore the initial salinity field varies longitudinally and vertically but is laterally uniform. The synoptic salinity data is typically collected over a period of 10 to 12 hours, as the USGS research vessel travels along the channel of the San Francisco Estuary from the South Bay to the western Delta. For each simulation period, the simulation start date is approximately two days prior to a USGS synoptic salinity collection period to allow for hydrodynamic spin-up. The observed salinity field is specified at the beginning of the simulation as an initial condition and then reset to the observed values again at approximately the mid-point of the cruise, when realistic tidal velocities were present in the simulation. Applying the initial condition in the entire domain simultaneously and assuming laterally uniform salinity, results in some error in salinity predictions. Therefore over 6 weeks of model "spin-up" is allowed before model salinity predictions are compared with observations.

H2.4.5 Simulation Periods

The UnTRIM Bay-Delta Model described above was applied to two independent calibration periods, to take advantage of specific calibration data sets which provide the best data coverage for the regions of interest to the DRMS project. The model was first applied to a hydrodynamic calibration period in 2002 when a large number of flow observations were available in the Delta (Section 5). Then the model was applied during a period in 1994 (Section 6) when a large salinity and hydrodynamic dataset was available in Suisun Bay and the western Delta (Burau et al., 1998).

H2.5 Hydrodynamic Calibration

The hydrodynamic calibration indicates the ability of the UnTRIM Bay-Delta Model to accurately predict water levels (stage) and flows in the San Francisco Bay and Sacramento-San Joaquin Delta. Accurate prediction of water levels in San Francisco Bay demonstrate that tides are accurately propagating through the Bay and into the Delta. Comparison of predicted flows to observations in the Delta demonstrate the degree that the model captures the instantaneous, tidally-averaged, and net flows in specific channels within the Delta.

H2.5.1 Overview

The hydrodynamic calibration period spans from May 8, 2002 through August 24, 2002. This period was selected due to the availability of a large number of flow and stage observations in the Sacramento-San Joaquin Delta. Salinity initial conditions for the 2002 simulation were specified based upon a dataset collected by the USGS at the synoptic

monitoring stations on May 7, 2002. Because salinity calibration was not performed for this period, only a short hydrodynamic spin-up period was required.

H2.5.2 Method

The quality of fit between predicted model results and observed stage, flow, and salinity is assessed following a cross-correlation procedure similar to that used by RMA (2005). Statistics are derived to quantify the differences between predicted and observed data records. Four types of statistics are presented in this report, following the approach used by RMA (2005):

- Mean – Comparison of simple mean values of the predicted and observed time series.
- Phase Shift – The average shift in time between the predicted and observed time series.
- Amplitude Ratio – Comparison of the time series range, which ideally would equal 1. This value is estimated after removing the phase shift between predicted and observed time series.
- Scatter – The remaining difference between predicted and observed time series after phase and amplitude errors are removed. One measure of the scatter is the goodness of fit parameter, R^2, from a linear regression performed on the observed and predicted time series with phase error removed. Note that this R^2 is a measure of the scatter around a best-fit line, not a 1:1 line, on the scatter plots.

For each stage, flow, and time series comparison, a total of three different types of plots are shown. The top figure shows the tidal time scale variability for a 29-day period. For flow (Section 5.4), two separate tidal time scale periods are shown to represent a periods of low and high Delta exports. For stage (Section 5.3) and salinity time series (Section 6.3) only a single tidal time-scale period is shown. On the lower left, a tidally-averaged plot is shown for the full analysis period to evaluate spring-neap and longer time scale variability. Tidal averages are computed by filtering twice using a 24.75 hour running average filter. On the lower right, the scatter plot shows a comparison between the observed and predicted data over the analysis period. The scatter plot is produced by first running a cross-correlation between the observed data and model predictions to find the average phase lag over the entire record. The cross correlation was completed following the procedure outlined by RMA (2005). The process entails repeatedly shifting the predicted time series record at one minute increments relative to the observed time series while computing the correlation coefficient at each time shift. The correlation has a maximum value when the shifted model time series best aligns with the observed time series. The time shift when the maximum correlation occurs represents the phase difference in minutes between the predicted and observed data, with positive values indicating that the predicted time series lags the observed time series. The linear regression is then performed between the time shifted model results and observed data record to yield the amplitude ratio, best-fit line, and correlation coefficient. The statistics reported on each scatter plot follow the approach used by RMA (2005) and include the following:

- Mean Obs – Average value of observed time series for analysis period

- Mean Pred – Average value of predicted time series for analysis period
- Lag – Phase difference in minutes between observed and predicted; a positive value indicates that the predicted time series lags behind the observed time series.
- Y = slope*X + offset – Best linear fit, where Y is predicted, X is observed. The slope value is used as the amplitude ratio.
- R^2 – Linear regression goodness of fit parameter.

The observed and predicted means, phase lag, amplitude ratio, and R^2 value are also summarized in tables for each data type.

H2.5.3 Stage Calibration

The analysis of stage in the UnTRIM Bay-Delta Model entails comparing observed and predicted water levels over the analysis period following the approach outlined in Section 5.2. In San Francisco Bay, the datum of each water level observation station is well-defined and there are typically only small variations between observed and predicted mean water levels. However, the Sacramento-San Joaquin Delta dataset collected in 2002 made use of many temporary stations, and the vertical datum of each station is not well established. Subsequent surveying of some stations under the NAVD 88 datum has been conducted, but may not apply to previously collected data. Because it is not possible to definitively reference the observed stage to NGVD at some these Delta stations for the data set used, significant differences between observed and predicted mean water levels are assumed to result from differences in stage datum, and the stage datum is not specified on the plots (predicted stages are in ft above 0 NGVD). However, the cross-correlation analysis is not affected by this potential difference and the amplitude ratio, phase lag, and R^2 values all provide useful measures of model performance.

H2.5.3.1 San Francisco Bay

Water level calibration was conducted at continuous observation stations throughout the San Francisco Estuary at the locations shown in Figure H2.5.3-1. Water level data at Antioch were collected by DWR, while water level data at the remaining 4 stations were collected by NOAA. For each station, the observed and predicted stage is plotted over a twenty-nine day period between July 6, 2002 and August 4, 2002. In addition, the observed and predicted stage are tidally-averaged over the full calibration period, to assess the accuracy of the model in predicting water level variability on spring-neap time scales. Lastly, the cross-correlation (as described in Section 5.2) is used to determine the mean observed and predicted water level, the amplitude ratio, the phase lag, and the correlation coefficient, R^2. Each of these values is compiled in Table H2.5-1.

At Fort Point (NOAA station 9414290), the observed and predicted water levels show nearly identical agreement, indicating that the applied offset and amplification at the simplified ocean boundary is accurately propagating tides into the estuary (Figure H2.5.3-2). The cross-correlation analysis shows a phase lag of 0 minutes indicating the model is exactly in phase with observed tides, an amplitude ratio of 0.999 indicating that observed and predicted tidal range is nearly identical, and an R^2 of 0.999. The observed and predicted water levels show a slight deviation of 0.07 ft (0.84 inches) in the mean

water level, however the tidally-averaged stage demonstrates that the model is accurately capturing spring-neap and longer time scale filling and draining of the Bay. At Alameda (NOAA station 9414750), the observed and predicted water levels show a similar level of agreement (Figure H2.5.3-3), with a phase lag of 15 minutes, an amplitude ratio of 1.016 and an R^2 of 0.999. The observed and predicted water levels show a slight difference of 0.06 ft in the mean water level, and the model accurately predicts trends in the tidally-averaged stage. A similar level of agreement is achieved at Richmond (NOAA station 9414863) and at Port Chicago (NOAA station 9415144), as seen in Figure H2.5.3-4 and 5.3-5, respectively. At Antioch (Figure H2.5.3-6), the observed and predicted water levels show very good agreement, with a phase lag of 9 minutes, an amplitude ratio of 1.005 and an R^2 of 0.990. The mean observed and predicted stage at Antioch agree to within 0.007 feet, and the observed and predicted tidally-averaged stage are nearly identical. Since Antioch is near the seaward boundary of the Delta, this indicates that the model accurately predicts spring-neap filling and draining of the Delta.

Table H2.5-1 Predicted and observed stage and cross-correlation statistics for San Francisco Bay water level monitoring stations.

Location	Dates	Mean Water Level (ft)		Cross Correlation		R^2
		Observed	Predicted	Amp Ratio	Lag (min)	
San Francisco	5/8/02 – 8/24/02	0.363	0.436	0.999	0	0.999
Alameda	5/8/02 – 8/24/02	0.403	0.542	1.016	15	0.999
Richmond	5/8/02 – 8/24/02	0.506	0.570	1.011	12	0.998
Port Chicago	5/8/02 – 8/24/02	1.174	1.065	1.010	9	0.996
Antioch	5/8/02 – 8/24/02	1.234	1.227	1.005	9	0.990

H2.5.3.2 Sacramento-San Joaquin Delta

During the calibration period, observed stage is available from four permanent DWR water level observation stations (Rio Vista, Three Mile Slough, Jersey Point, and Dutch Slough), as well as an additional six temporary stations within the resolved portion of the Sacramento-San Joaquin Delta where data were collected (Figure H2.5.3-7). Since 2002, many of these station have become permanent monitoring stations.

As discussed above, it was not possible to definitively determine the vertical datum for all of the Delta water level stations, leading to significant variations between observed and predicted mean water level (Table H2.5-2). Because the cross-correlation method removes this bias, the following discussion focuses on the amplitude ratio, lag, R^2 and tidally-averaged trends which provide a quantitative assessment of model performance which does not depend on the water level datum.

At Rio Vista (Figure H2.5.3-8), predicted water levels show good agreement with observed water levels, with a phase lag of 16 minutes, an amplitude ratio of 0.988 and an R^2 of 0.989. The predicted tidally-averaged stage shows similar trends to the observed tidally-averaged stage indicating that the spring-neap filling and draining of the Sacramento portions of the Delta, which include Liberty Island, the Sacramento Deep Water Ship Channel, and Steamboat Slough. In Three Mile Slough (Figure H2.5.3-9),

predicted water levels show a larger tidal range than observed water levels, with a phase lag of 1 minute, an amplitude ratio of 1.145 and an R^2 of 0.990. At Jersey Point (Figure H2.5.3-10), predicted and observed water levels show very good agreement, with a phase lag of 10 minutes, an amplitude ratio of 1.104 and an R^2 of 0.988. Similar agreement is achieved at Dutch Slough (Figure H2.5.3-11), with a phase lag of 10 minutes, an amplitude ratio of 1.082 and an R^2 of 0.987. Overall, the predicted stage shows very good agreement with observed stage at these four stations in the western Delta, in terms of amplitude, phase, and spring-neap variations in tidally-averaged stage.

Table H2.5-2 Predicted and observed stage and cross-correlation statistics for Sacramento-San Joaquin Delta water level monitoring stations

Location	Dates	Mean Water Level (ft)		Cross Correlation		R^2
		Observed	Predicted	Amp Ratio	Lag (min)	
Rio Vista	5/8/02 – 8/24/02	1.038	1.351	0.988	16	0.989
Three Mile Sl.	5/8/02 – 8/24/02	0.985	1.264	1.145	1	0.990
Jersey Point	5/8/02 – 8/24/02	1.240	1.265	1.104	10	0.988
Dutch Slough	5/8/02 – 8/24/02	0.734	1.262	1.082	10	0.987
False River	5/8/02 – 8/24/02	1.487	1.280	1.159	19	0.990
Taylor Slough	5/8/02 – 8/24/02	1.518	1.278	1.186	18	0.990
Mokelumne Riv.	5/8/02 – 8/10/02	1.700	1.362	1.166	1	0.984
Old River, SJR	5/8/02 – 8/24/02	1.550	1.315	1.210	14	0.991
Old River, Man.	5/8/02 – 8/24/02	1.536	1.300	1.215	16	0.991
Holland Cut	5/8/02 – 8/24/02	1.641	1.286	1.162	13	0.976

Observed and predicted stage at the six central Delta stations are shown in Figures H2.5.3-12 through 5.3-17. At False River (Figure H2.5.3-12), observed and predicted water levels show very good agreement, with a phase lag of 19 minutes, an amplitude ratio of 1.159 and an R^2 of 0.990. A similar level of agreement is achieved at Taylor Slough (Figure H2.5.3-13), with a phase lag of 18 minutes, an amplitude ratio of 1.186 and an R^2 of 0.990. At the mouth of the Mokelumne River (Figure H2.5.3-14) near the San Joaquin River, predicted and observed stage show good agreement with a phase lag of 1 minute, an amplitude ratio of 1.166 and an R^2 of 0.984. At Old River, between Franks Tract and the San Joaquin River (Figure H2.5.3-15), observed water levels show good agreement with predicted water levels, with a phase lag of 14 minutes, an amplitude ratio of 1.210 and an R^2 of 0.991. In Old River near Mandeville Island (Figure H2.5.3-16), observed and predicted water levels show good agreement, with a phase lag of 16 minutes, an amplitude ratio of 1.215 and an R^2 of 0.991. A similar level of agreement is achieved at Holland Cut (Figure H2.5.3-17), with a phase lag of 13 minutes, an amplitude ratio of 1.162 and an R^2 of 0.976. Overall, the predicted water levels central Delta stations show good agreement with observed water levels in terms of phase lag and spring-neap trends in tidally-averaged stage. However, the predicted water levels at the central Delta stations show a larger tidal range than observed water levels, with

increasing amplitude ratios moving landward. The potential reasons for this are discussed in Section 5.5.

H2.5.4 Delta Flow Calibration

During the calibration period, flow measurements are available at a total of eleven stations in the resolved portion of the UnTRIM Bay-Delta Model (Figure H2.5.4-1). Some of these flow data were collected as part of an extensive USGS monitoring program using a large number of temporary stations in the Sacramento-San Joaquin Delta. Additional data were available at a smaller number of permanent DWR stations. The predicted flow at each of these locations was compared with the observed flow to fine-tune the model calibration in the Delta portion of the domain. This calibration involved adjusting the size of the "False Delta Region" geometries to accurately represent the prism of unresolved portions of the Delta, and adjusting the distribution of net flow export between the southern arms of the Delta. In addition, it was found that applying daily average flow exports did not produce satisfactory agreement with the phase of observed flows and, subsequently, time varying exports were used to account for operation of gates and pumps and produced noticeably better agreement with the phase of observed flows in the Delta.

For each station, the mean observed and predicted net flow was calculated, and the same cross-correlation procedure used in the water level analysis was applied to flow. Table H2.5-3 gives the predicted and observed mean flow at each station as well as the corresponding amplitude ratio, phase lag, and R^2 for each station.

Table H2.5-3 Predicted and observed flow and cross-correlation statistics for Sacramento-San Joaquin Delta flow monitoring stations

Location	Dates	Mean Flow (cfs)		Cross Correlation		R^2
		Observed	Predicted	Amp Ratio	Lag (min)	
Rio Vista	5/8/02 – 8/24/02	10547.	9542.	1.022	7.000	0.992
Three Mile Sl.	5/8/02 – 8/24/02	-844.6	-2229.	1.197	-18.000	0.993
Jersey Point	5/8/02 – 8/24/02	663.0	1014.	0.945	-19.000	0.992
Dutch Slough	5/8/02 – 8/24/02	-93.97	-443.9	1.082	-12.000	0.993
False River	5/8/02 – 8/24/02	-439.0	-302.6	0.954	-2.000	0.980
Fishermans Cut	5/8/02 – 8/08/02	-764.4	1559.	0.747	15.000	0.614
Taylor Slough	5/8/02 – 8/24/02	-12.60	-139.9	0.221	-14.000	0.376
Old River, SJR	5/8/02 – 8/24/02	-1361.	-1267.	1.263	-25.000	0.945
Mokelumne Riv.	5/8/02 – 8/24/02	3178.	6344.	0.942	-12.000	0.962
Old River, Man.	5/8/02 – 8/24/02	-1889.	-1819.	0.951	-3.000	0.977
Holland Cut	5/8/02 – 8/24/02	-1666.	-2180.	1.112	4.000	0.974

At Rio Vista on the Sacramento River (Figure H2.5.4-2), the observed and predicted flows show good agreement, with typical peak flood tide flows ranging from 100,000 to

120,000 cfs and typical peak ebb tide flows ranging from 80,000 to 100,000 cfs. The cross-correlation analysis yields an amplitude ratio of 1.022, indicating that the model is accurately predicting the flow amplitude, a phase lag of 7 minutes. Overall the model shows similar tidally-averaged net flows over the analysis period, and the predicted and observed mean flows are similar in magnitude. At Three Mile Slough (Figure H2.5.4-3), observed and predicted peak flows are typically 20,000 to 25,000 cfs with the model predicting larger negative (south) net flows. The predicted flows show a slightly larger amplitude than observed flows, with an amplitude ratio of 1.197, and a phase lag of -18 minutes. At Jersey Point (Figure H2.5.4-4), peak flows are typically 100,000 to 150,000 cfs; predicted flows show a slightly smaller amplitude than observed flows, with an amplitude ratio of 0.945, and a phase lag of -19 minutes. The predicted tidally-averaged flows show good agreement with observed tidally-averaged flows, with a somewhat larger predicted mean predicted flow than mean observed flow. At Dutch Slough (Figure H2.5.4-5), predicted and observed flows show good agreement, with peak flows of about 10,000 cfs, and an amplitude ratio of 1.082. Overall, the predicted and observed flows at the four western Delta stations show very good agreement, with the largest discrepancy being a somewhat larger southward net flow in Three Mile Slough than observed. A similar result in Three Mile Slough has been obtained in other studies, using different models (e.g., RMA, 2005).

Observed and predicted flows at False River (Figure H2.5.4-6) show good agreement, with typical peak flows of 50,000 cfs. Predicted flows show a slightly smaller amplitude than observed flows, with an amplitude ratio of 0.954, and a phase lag of -2 minutes. The predicted tidally-averaged flow shows very good agreement with observed tidally-averaged flow, and similarly the predicted and observed mean net flows show good agreement. At Fishermans Cut (Figure H2.5.4-7) predicted flows tend to be significantly larger than observed flows, with a positive net predicted flow and a negative net observed flow. A similar result was achieved at this station by RMA (2005). At Taylor Slough (Figure H2.5.4-8) the observed and predicted flows show similar magnitudes, with typical peak flows around 1,000 cfs. However, both the predicted and observed flows show high frequency variability and the cross-correlation yields relatively poor statistical agreement. At Old River between Franks Tract and the San Joaquin River (Figure H2.5.4-9), the predicted and observed flows show better agreement with typical peak flows of 15,000 cfs. The predicted tidally-averaged and net flows into Franks Tract through Old River are predicted accurately. At the central Delta stations, the model shows good agreement at False River and Old River near the San Joaquin, and relatively poor agreement at Fishermans Cut and Taylor Slough. The magnitude of flows through Fishermans Cut and Taylor Slough are relatively small, and therefore these channels are less critical to Delta circulation. The good agreement at False River and Old River demonstrate that the primary flows through the central Delta are predicted accurately.

Three additional flow stations are available near three of the False Delta Regions in the model. At the Mokelumne River (Figure H2.5.4-10), the predicted and observed flows show relatively good agreement with peak flows typically around 20,000 cfs, and an amplitude ratio of 0.942. The good agreement with flow amplitude at this station demonstrates that the False Delta Region associated with the Mokelumne River boundary is adequately representing the tidal prism of the unresolved regions in this part of the

Delta. However, the predicted tidally-averaged and net mean flows are significantly larger than observed net flows. This may result because all the Delta Cross Channel, Georgiana Slough, and Mokelumne River flows are all applied at the False Delta Region attached to the Mokelumne River, and other potential pathways for these flows to reach the San Joaquin River (such as Potato Slough, White Slough, and Honker Cut) are not resolved in the model. At Old River near Mandeville Island (Figure H2.5.4-11), the predicted and observed flows show very good agreement with am amplitude ratio of 0.951. The predicted tidally-averaged and net mean flows show very good agreement with tidally-averaged and net observed flows indicating that the False Delta Region near this station accurately represents the tidal prism of unresolved portions of the south Delta, and the flow exports applied to this boundary are appropriate. Similarly at Holland Cut (Figure H2.5.4-12), observed and predicted flows show very good agreement, both in terms of tidal flows and tidally-averaged flows. The good agreement between observed and predicted net flows at the Holland Cut and Old River near Mandeville stations demonstrate that the model is accurately predicting net flows into the south Delta.

H2.5.5 Discussion

The hydrodynamic calibration demonstrates that the model is accurately predicting water levels from the Golden Gate into the Sacramento-San Joaquin Delta. At the five San Francisco Bay stations, the amplitude ratio ranged from 0.999 to 1.016 demonstrating that predicted tidal range was within 1.6% of observed tidal range at all of the water level stations from Golden Gate through Antioch in the western Delta. Within the Delta, amplitude ratios ranged from 0.988 at Rio Vista to 1.36 in the Mokelumne River. The high level of agreement between predicted and observed water levels at the four western Delta stations (Rio Vista, Three Mile Slough, Jersey Point, and Dutch Slough) demonstrate that the model is accurately predicting tides in the western Delta. This represents a significant advance from previous TRIM3D applications (e.g., Gross et al., 2006), where the Delta was largely unresolved past Jersey Point and Rio Vista and significant water level amplification occurred near the large False Delta used to represent the Delta in the TRIM3D model. Predicted tidal range at all stations in the central Delta is larger than observed tidal range. This overestimate of tidal range is believed to result from reflection of tides at the landward end of False Delta Regions. The amplitude ratios in the central Delta show somewhat larger predicted tidal range relative to observed water levels, resulting either from less damping of tidal range in the model relative to observations moving landward, or alternatively amplification resulting from reflection of water levels from the upstream end of the False Delta Regions. Because this effect is most pronounced at the stations closest to the False Delta Regions, it is believed that the latter is the case. This conclusion is supported by the good agreement with observed tidal range at Rio Vista since large upstream portions such as Liberty Island and the Sacramento Deep Water Ship Channel are resolved, whereas on the Mokelumne River the predicted tidal range is significantly larger than the observed tidal range, which could result from not adequately representing the prism or tidal propagation distance of significant portions of the Delta including Georgiana Slough, the Delta Cross Channel, and upstream tidal reaches of the Mokelumne River and its tributaries. When the model

grid is extended to resolve additional portions of the Delta, this artifact can be significantly reduced.

The detailed analysis of flows in the Sacramento-San Joaquin Delta shows good agreement between predicted flows and observed flows, both of which vary over several orders of magnitude between stations. The predicted and observed flows at the four western Delta stations show very good agreement, with the largest discrepancy being a somewhat larger southward net flow in Three Mile Slough than observed. The good agreement between predicted and observed flows at False River and Old River near the San Joaquin demonstrate that the primary flows through the central Delta are predicted accurately, although substantial differences between predicted and observed flows in Taylor Slough and Fishermans Cut are noted. In the south Delta, the predicted tidally-averaged and net flows show very good agreement with tidally-averaged and net observed flows at Holland Cut and Old River near Mandeville Island, indicating that the False Delta Regions are reasonably representing the tidal prism of unresolved portions of the south Delta, and that the CVP and SWP flow exports applied to these boundary are producing accurate net flows into the south Delta.

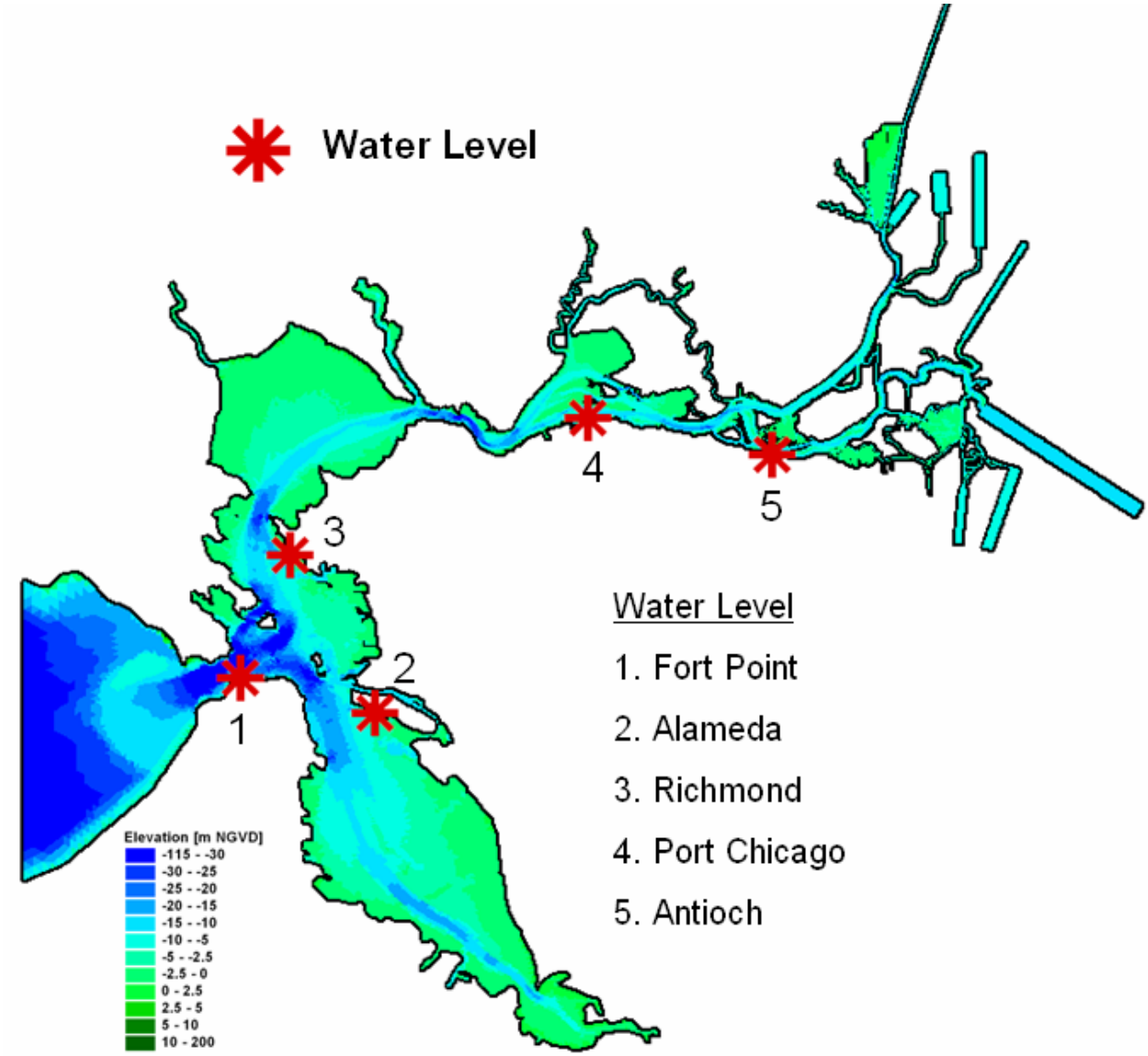

Figure H2.5.3-1 San Francisco Bay water level observation stations.

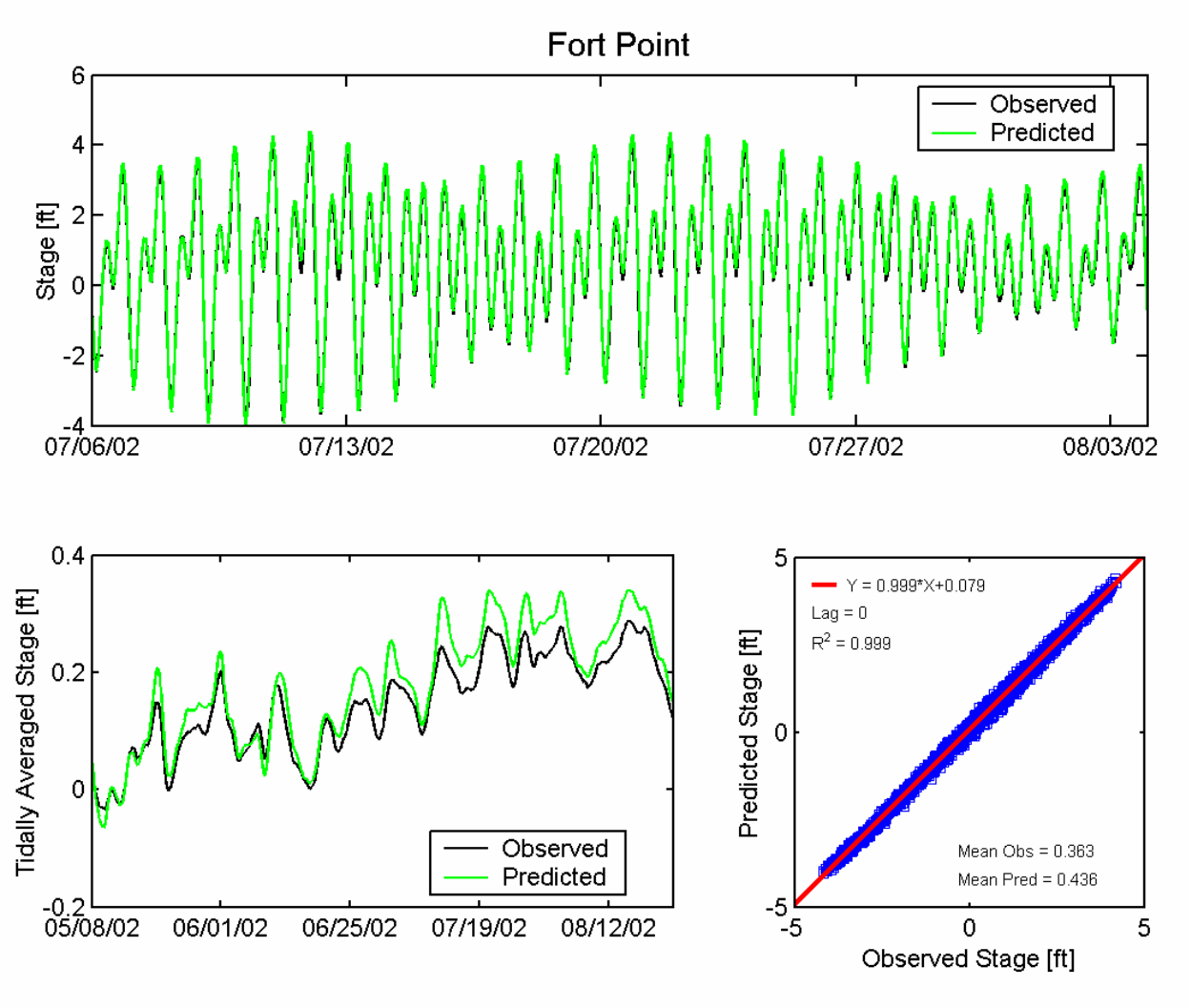

Figure H2.5.3-2 Observed and predicted stage at Fort Point NOAA station (9414290).

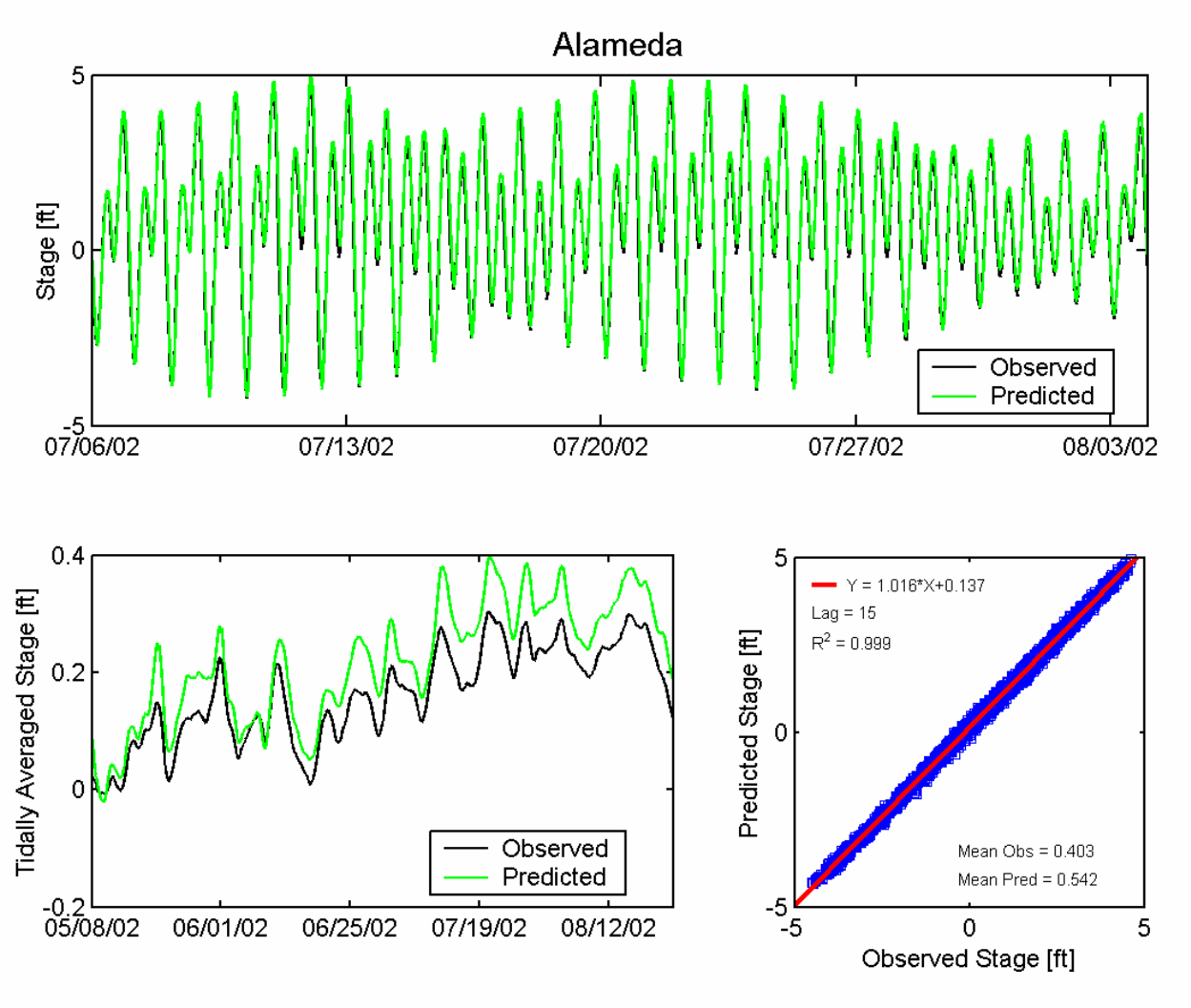

Figure H2.5.3-3 Observed and predicted stage at Alameda NOAA station (9414750).

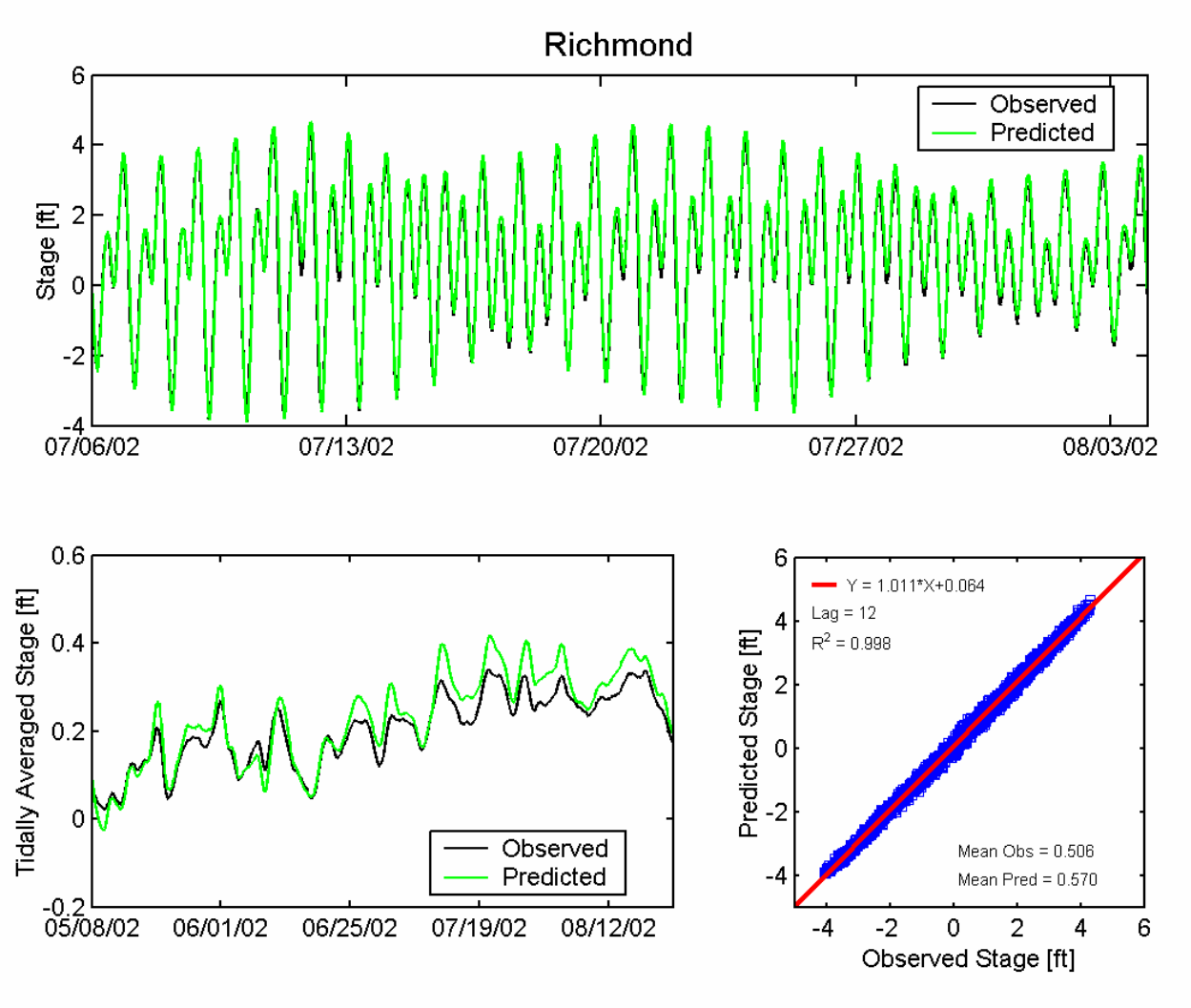

Figure H2.5.3-4 Observed and predicted stage at Richmond NOAA station (9414863).

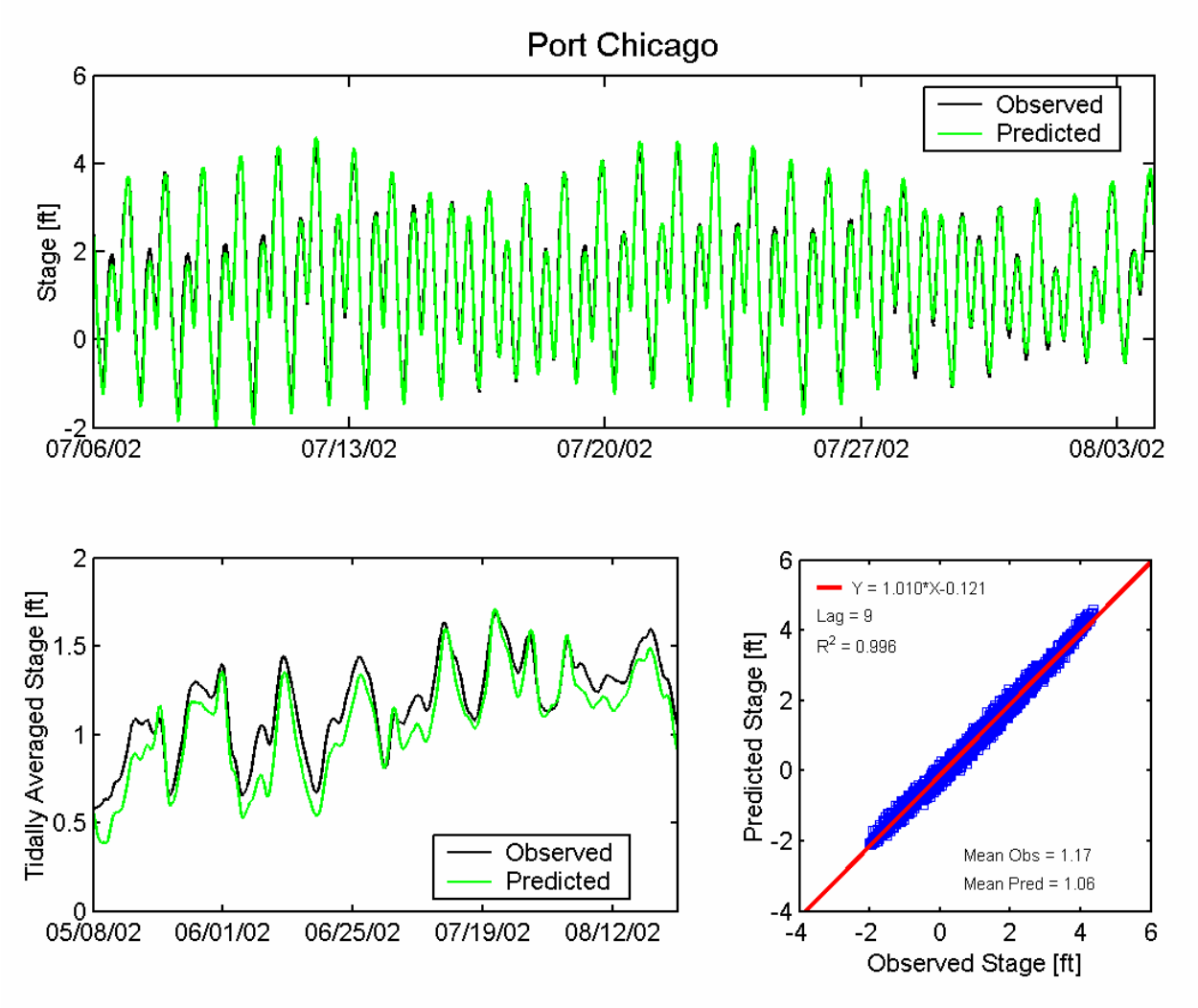

Figure H2.5.3-5 Observed and predicted stage at Port Chicago NOAA station (9415144).

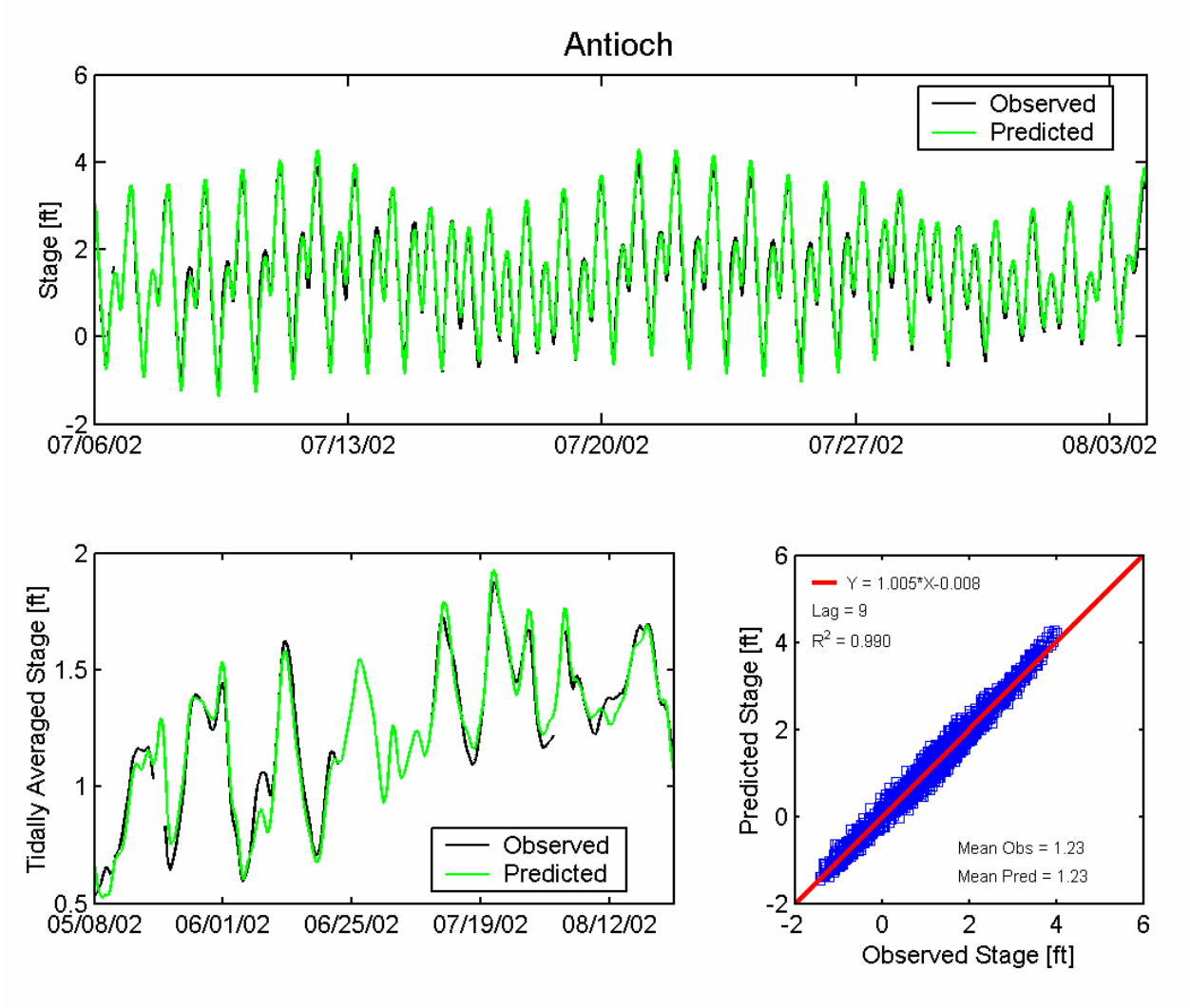

Figure H2.5.3-6 Observed and predicted stage at DWR Antioch station (ANH).

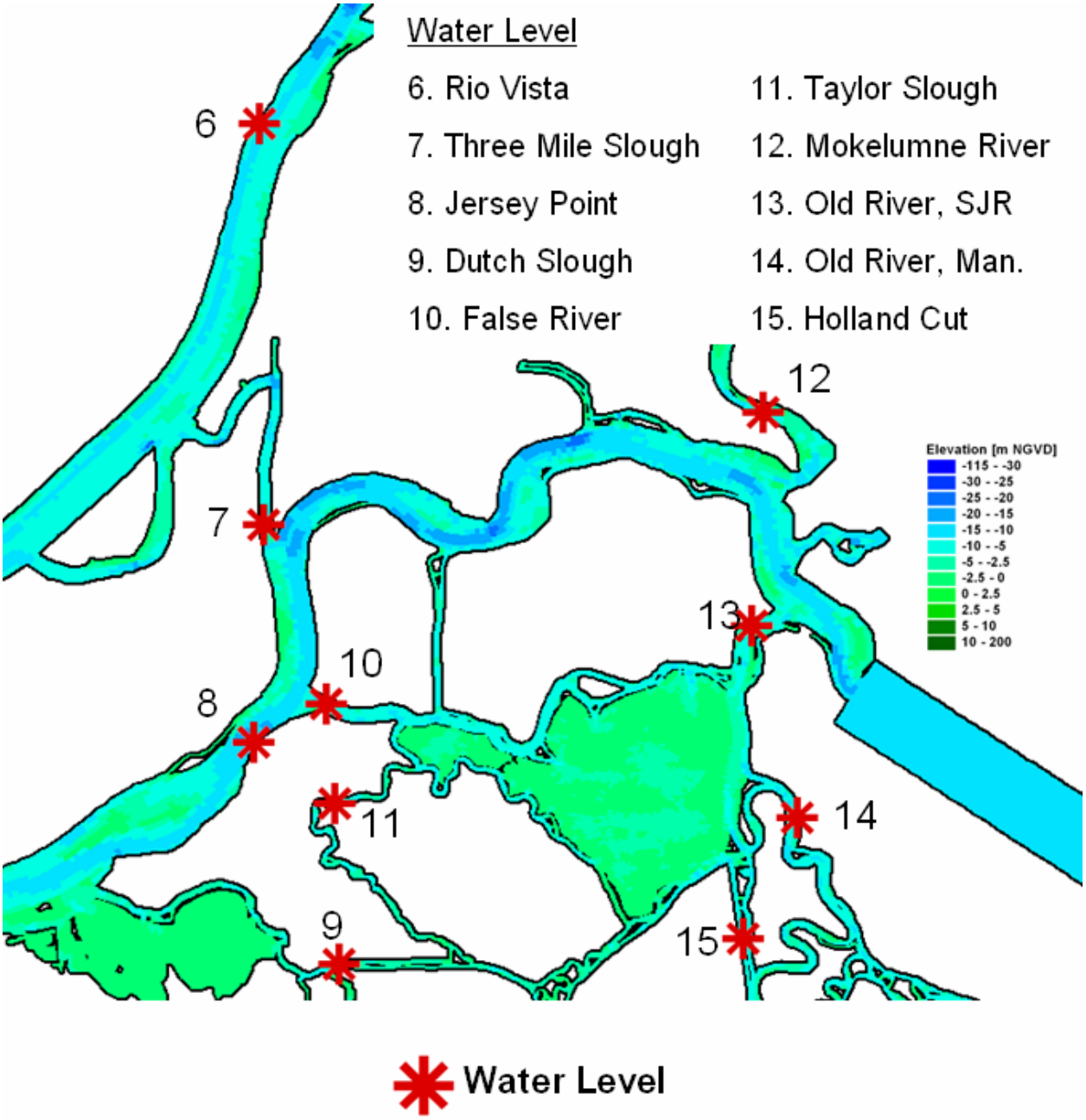

Figure H2.5.3-7 Sacramento-San Joaquin Delta water level observation stations.

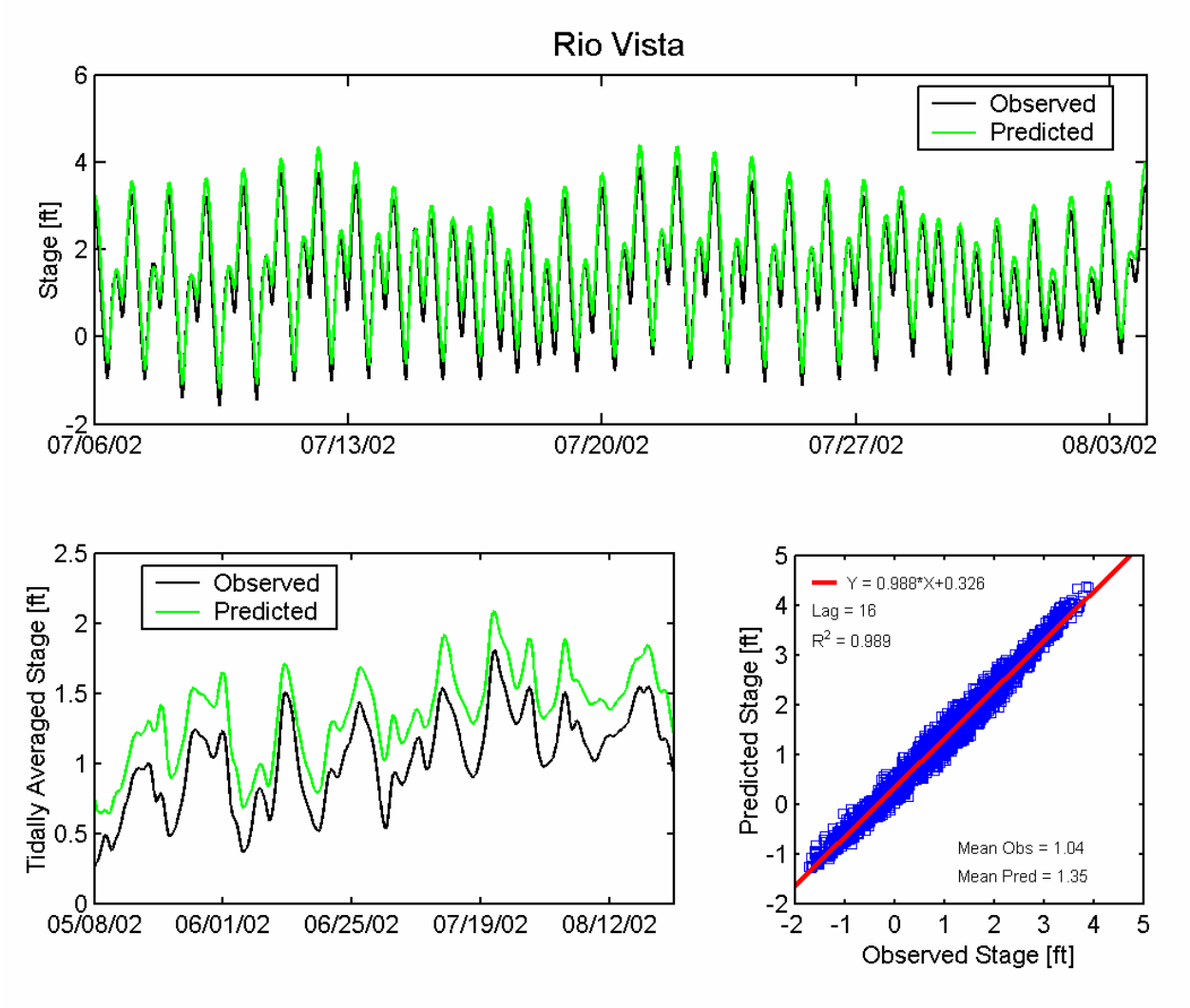

Figure H2.5.3-8 Observed and predicted stage at Rio Vista.

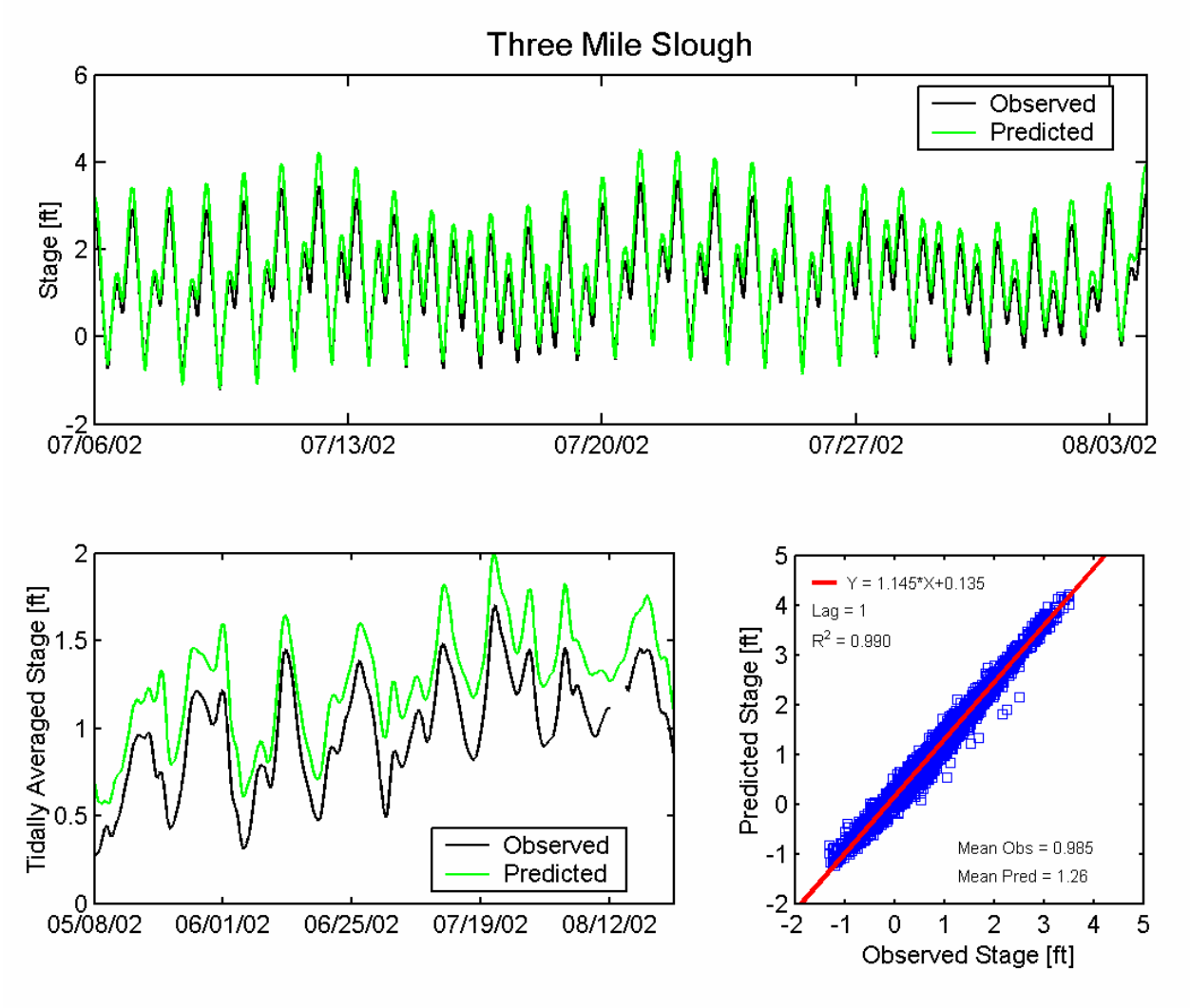

Figure H2.5.3-9 Observed and predicted stage at Three Mile Slough.

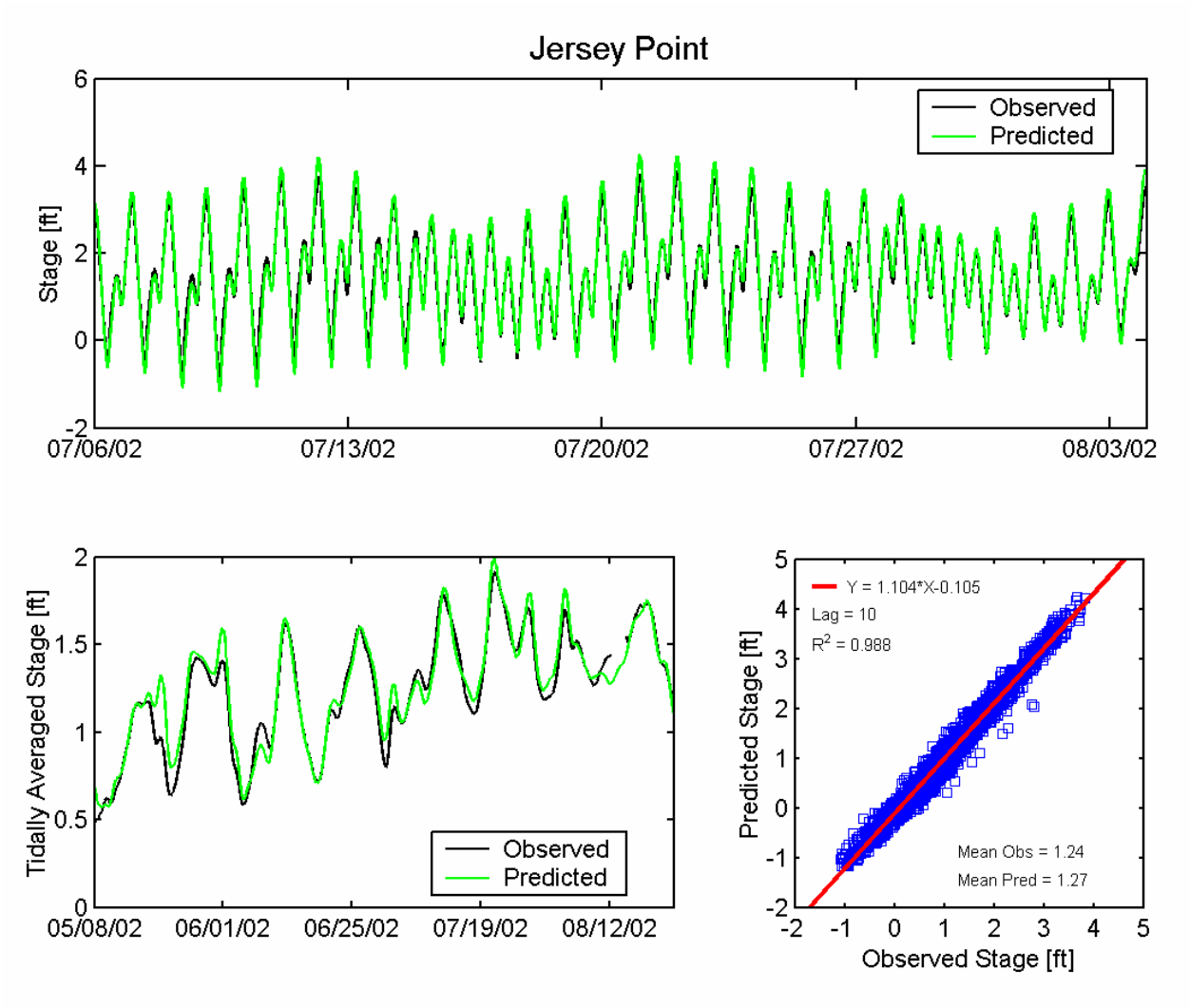

Figure H2.5.3-10 Observed and predicted stage at Jersey Point.

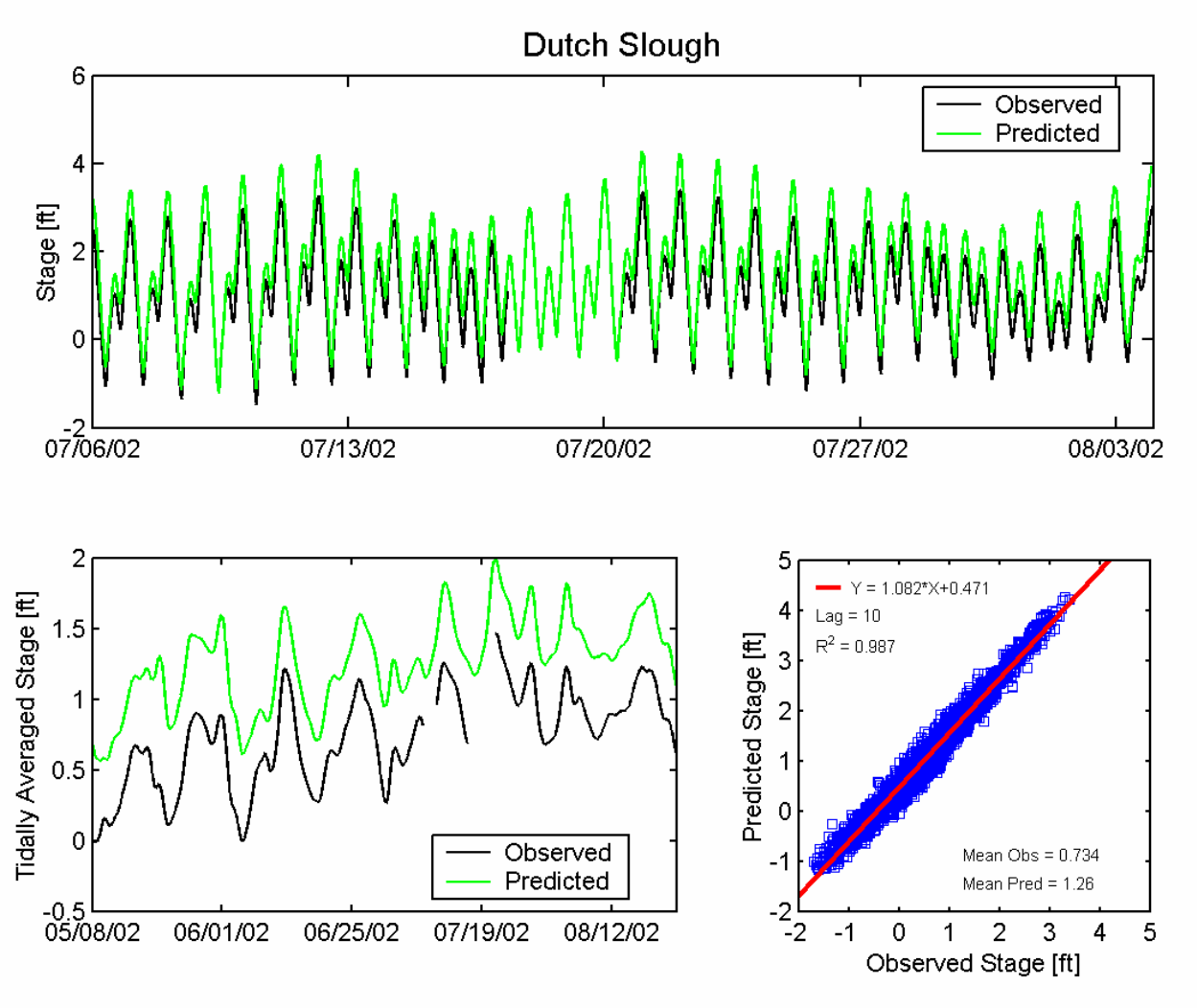

Figure H2.5.3-11 Observed and predicted stage at Dutch Slough.

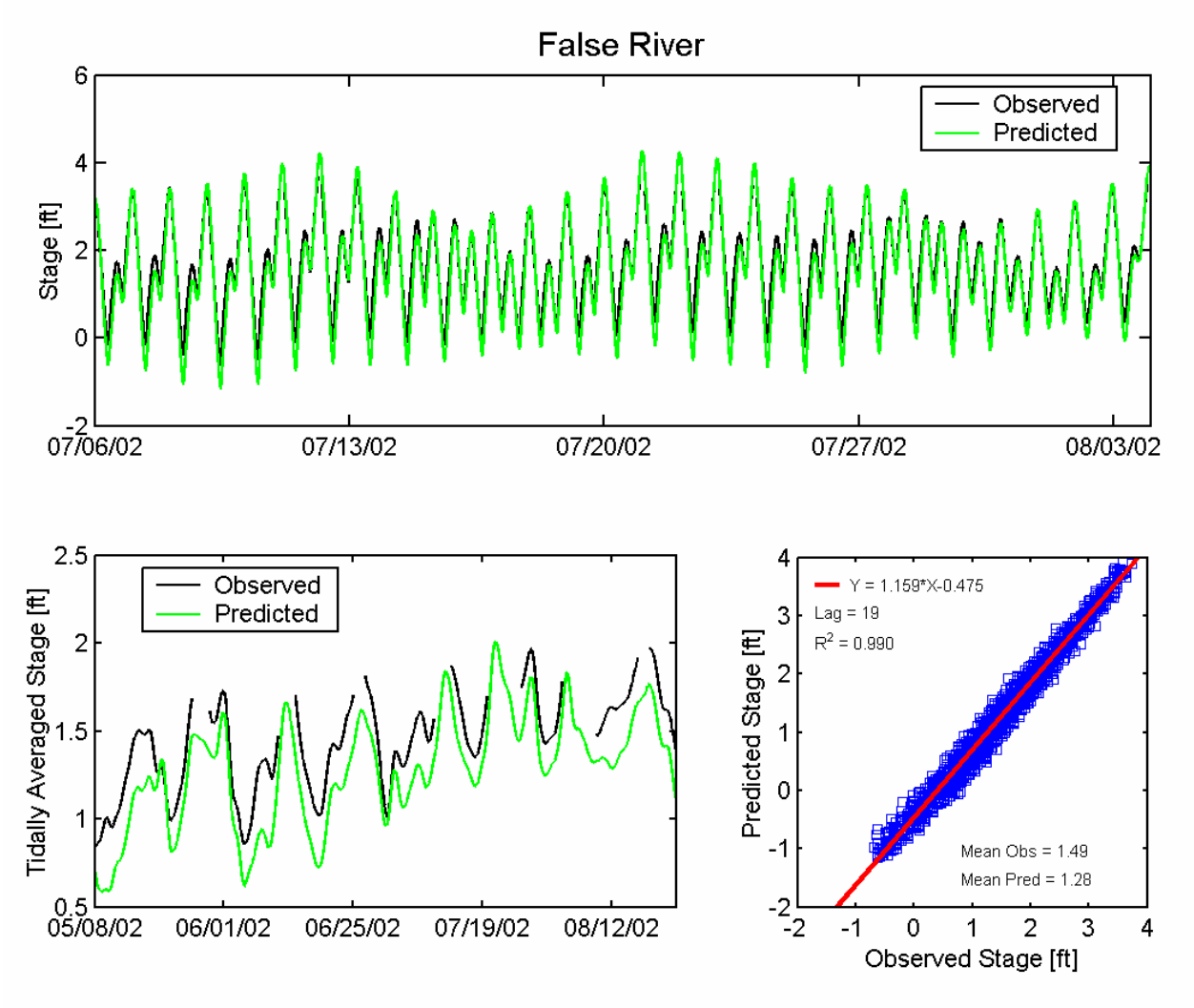

Figure H2.5.3-12 Observed and predicted stage at False River.

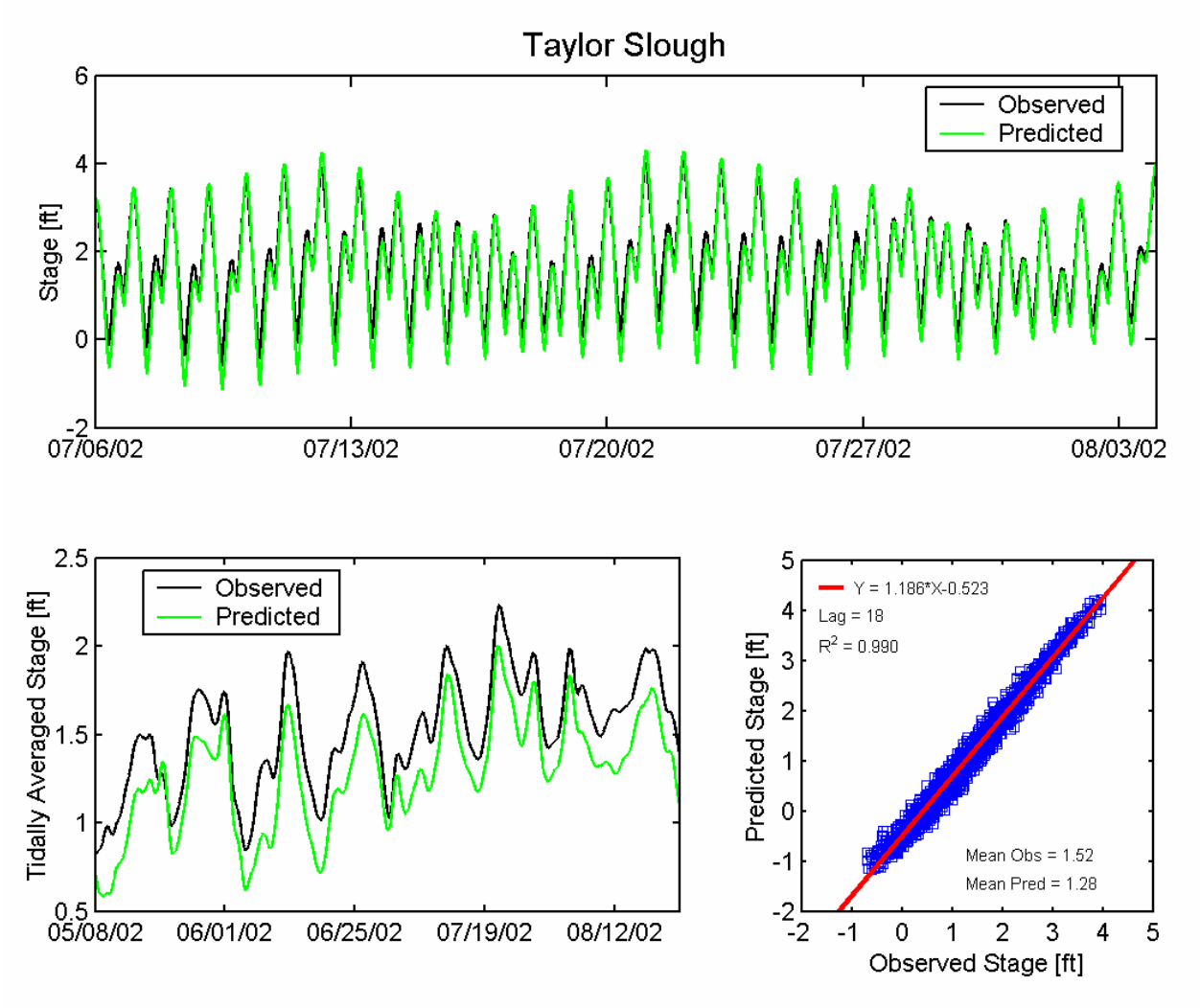

Figure H2.5.3-13 Observed and predicted stage at Taylor Slough.

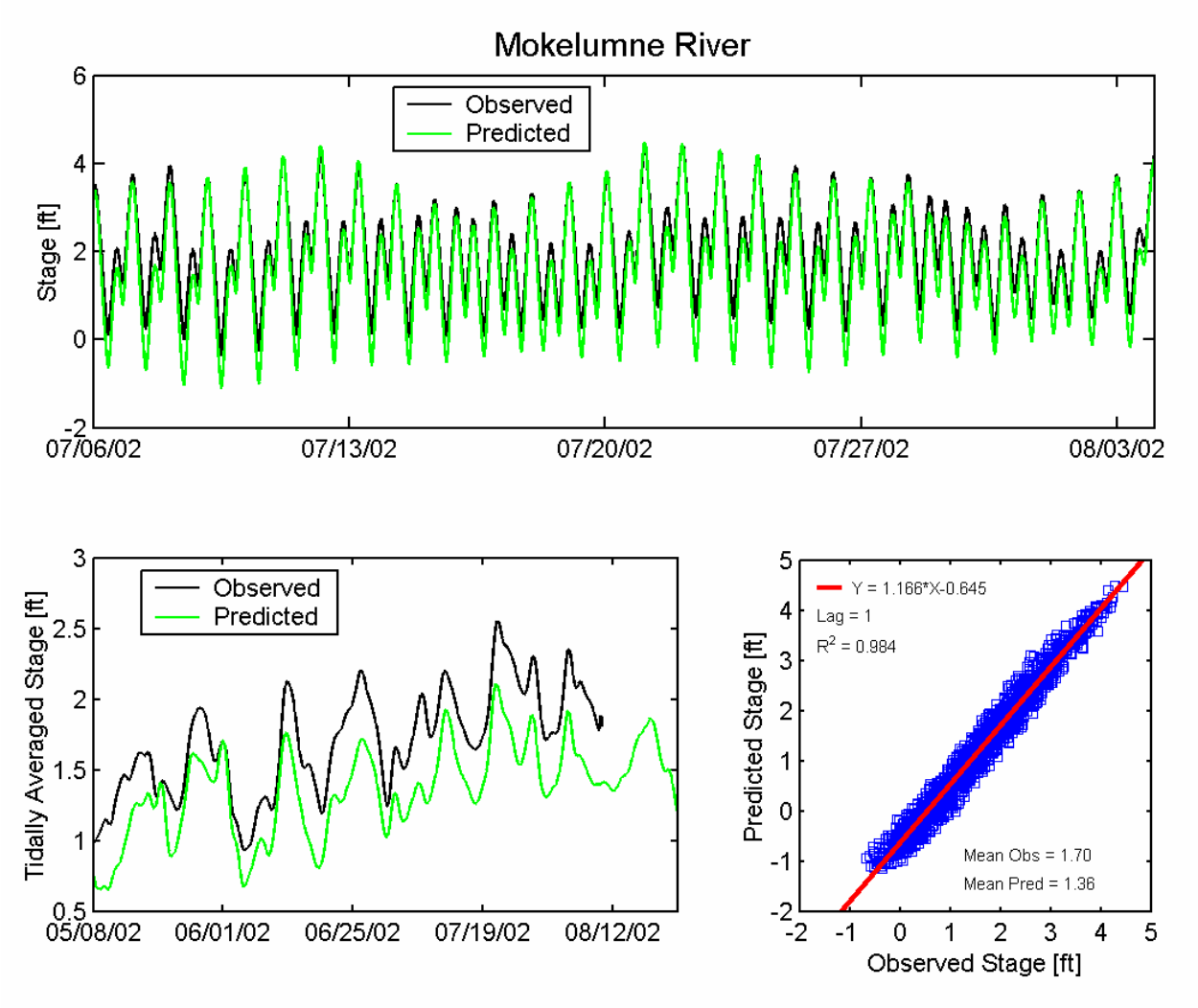

Figure H2.5.3-14 Observed and predicted stage in the Mokelumne River.

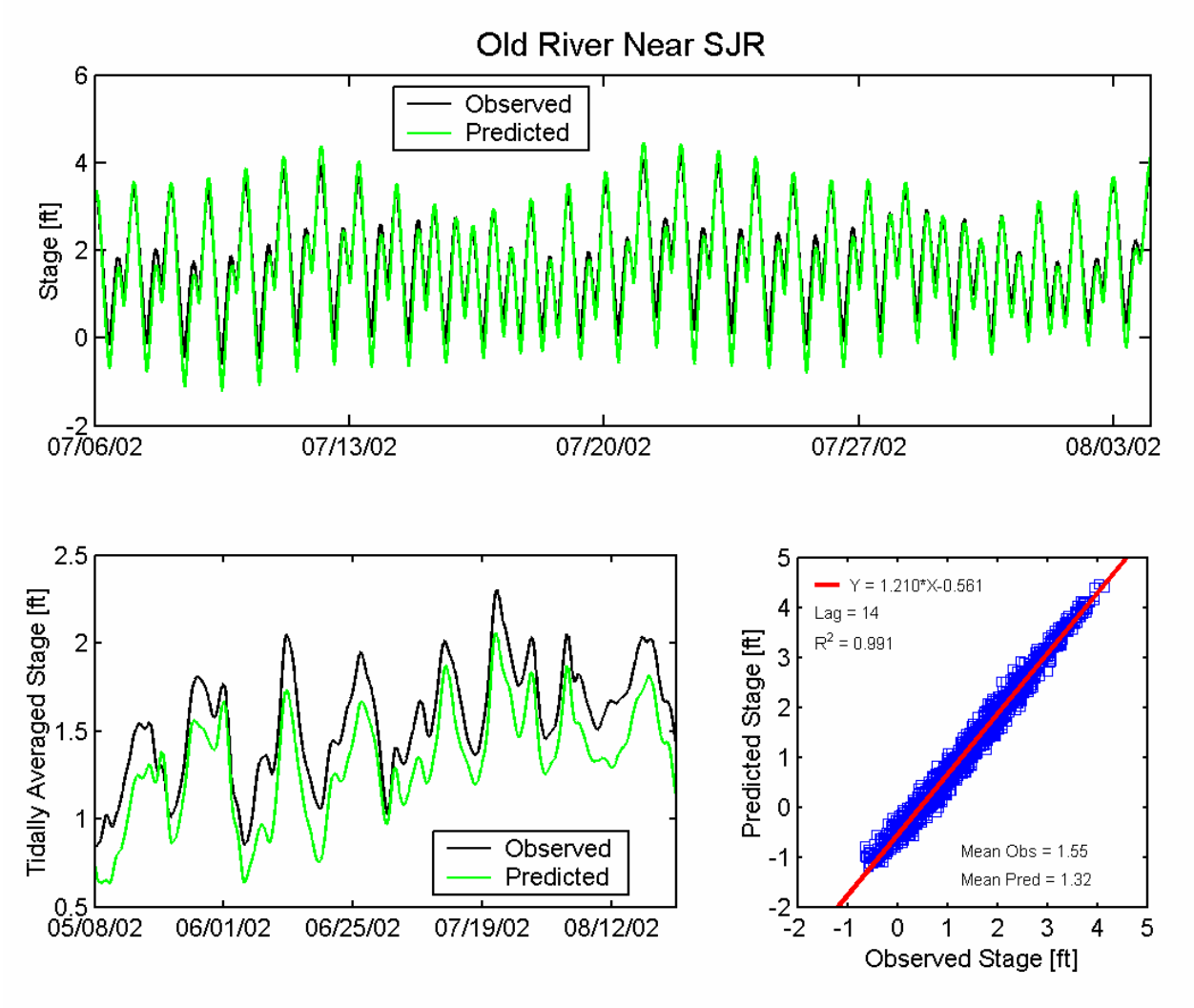

Figure H2.5.3-15 Observed and predicted stage in Old River, near the San Joaquin River.

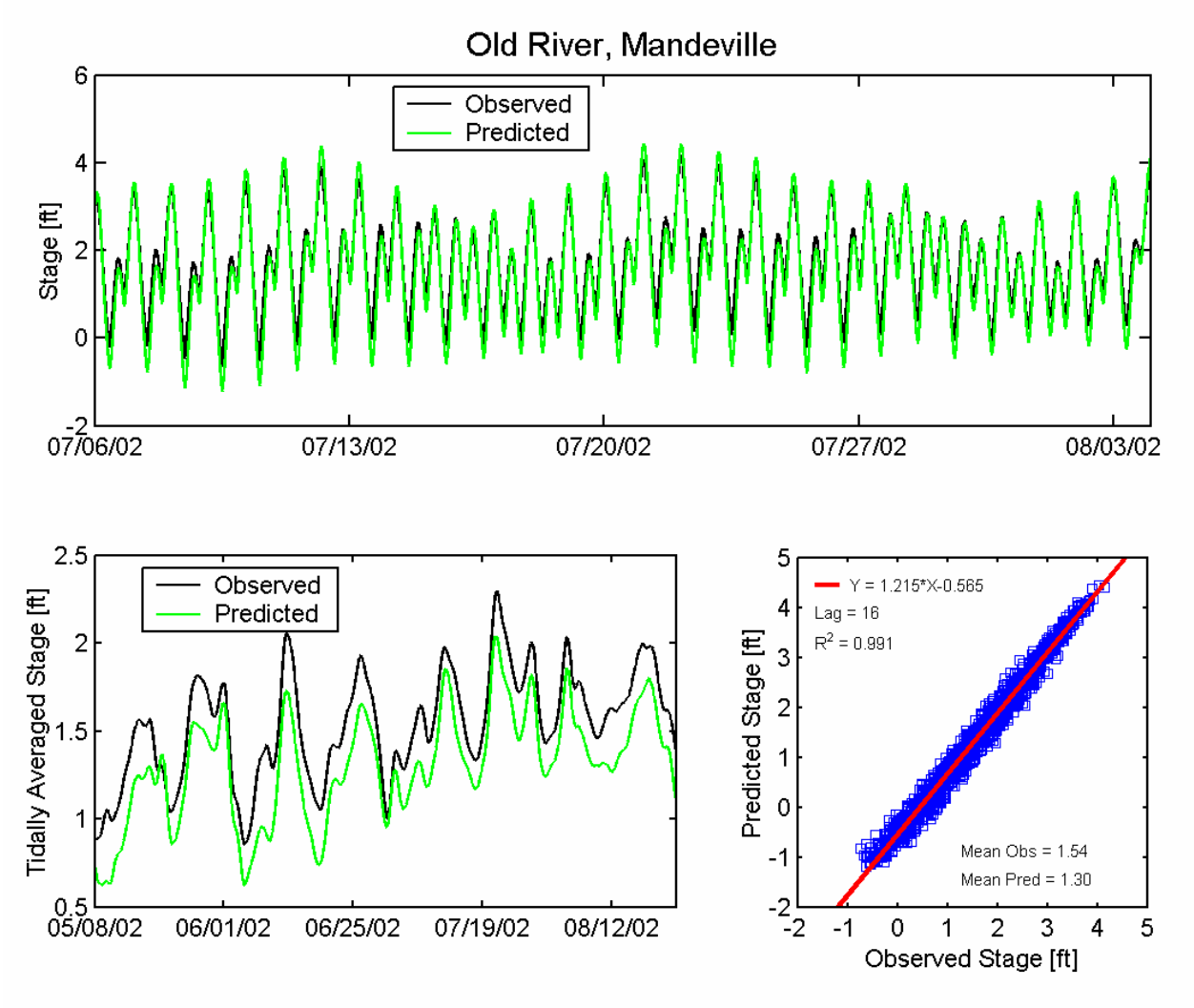

Figure H2.5.3-16 Observed and predicted stage in Old River, near Mandeville Island.

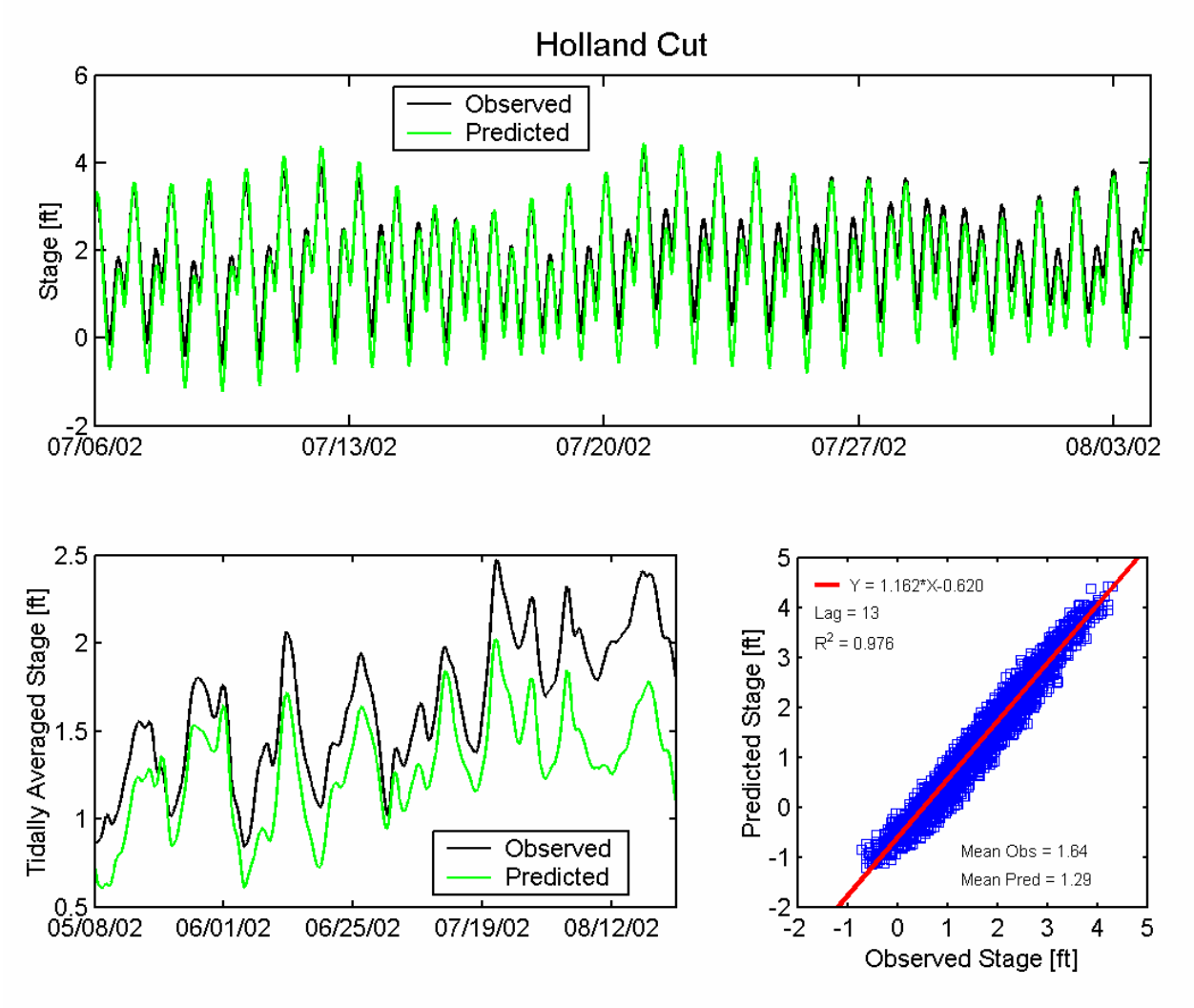

Figure H2.5.3-17 Observed and predicted stage in Holland Cut.

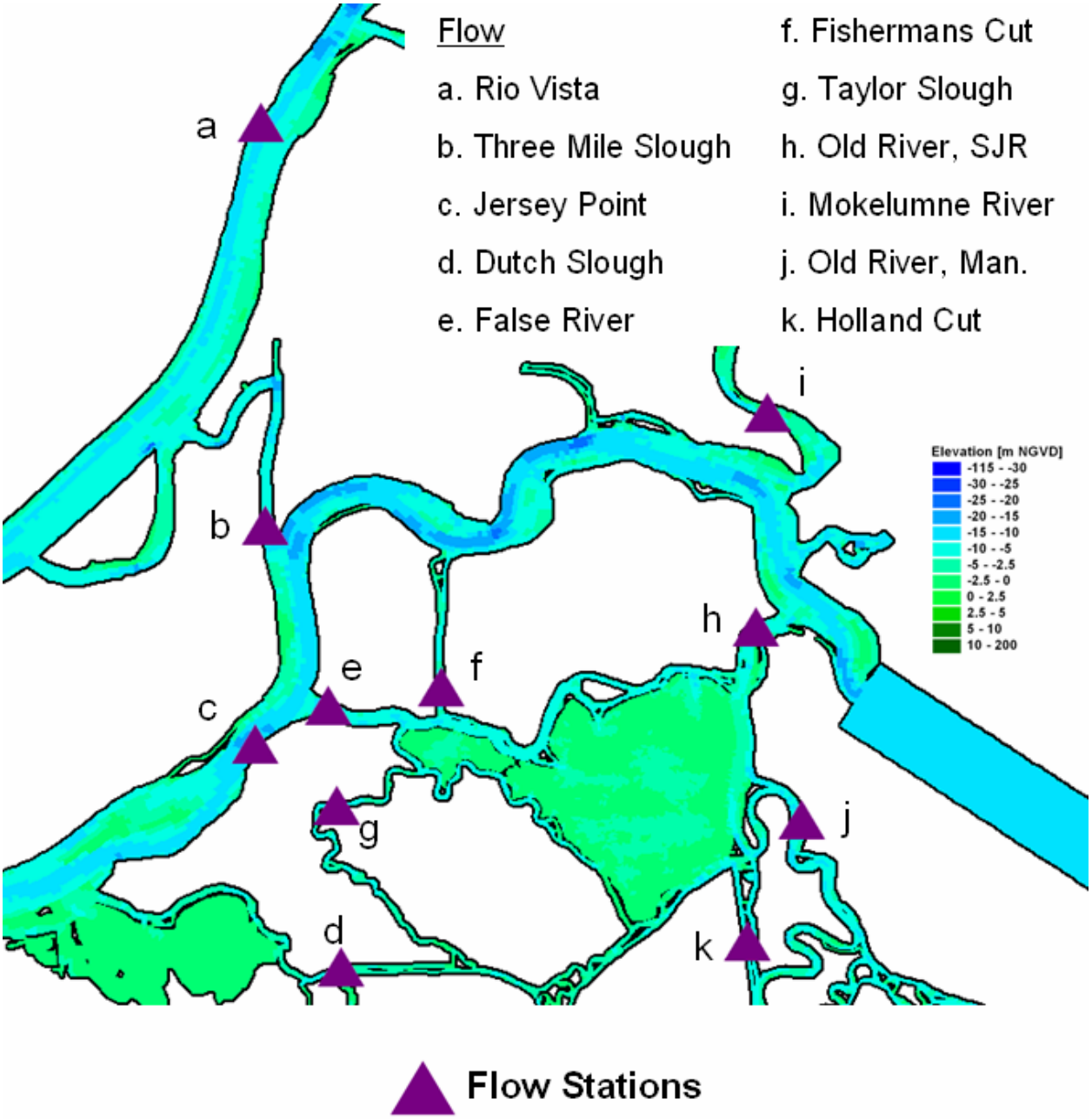

Figure H2.5.4-1 Flow observation stations in the Sacramento-San Joaquin Delta.

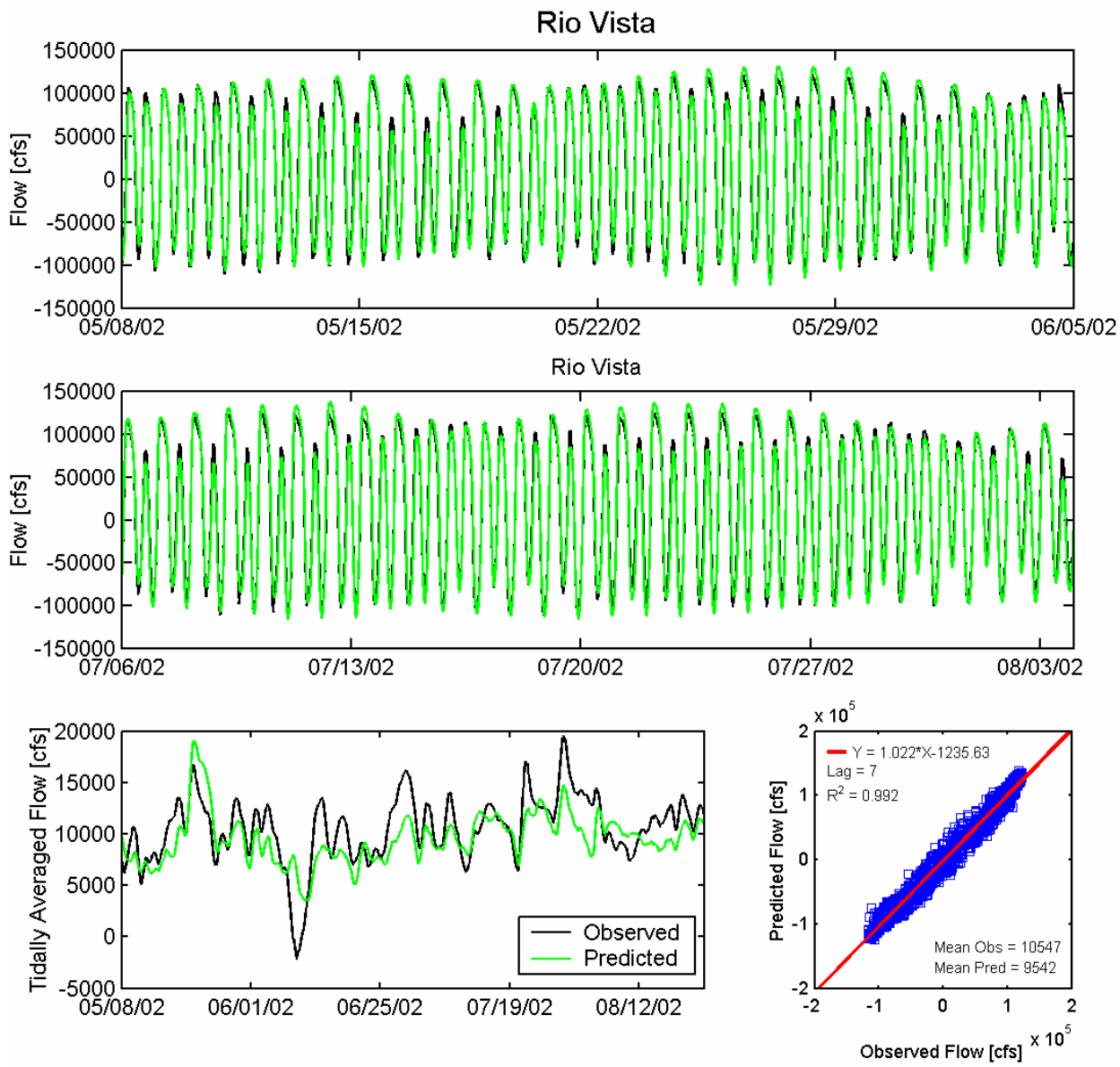

Figure H2.5.4-2 Observed and predicted flow at Rio Vista.

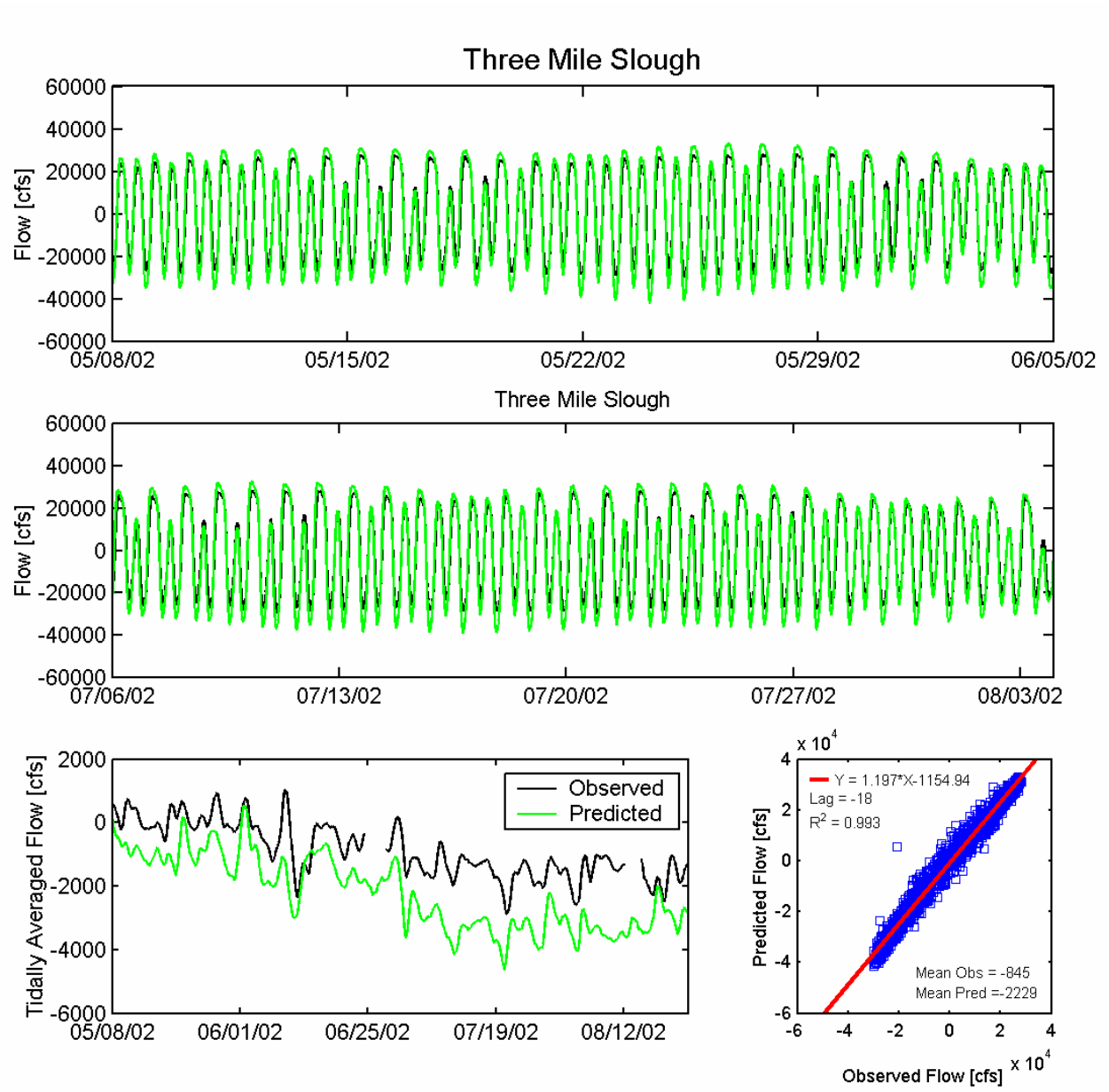

Figure H2.5.4-3 Observed and predicted flow at Three Mile Slough.

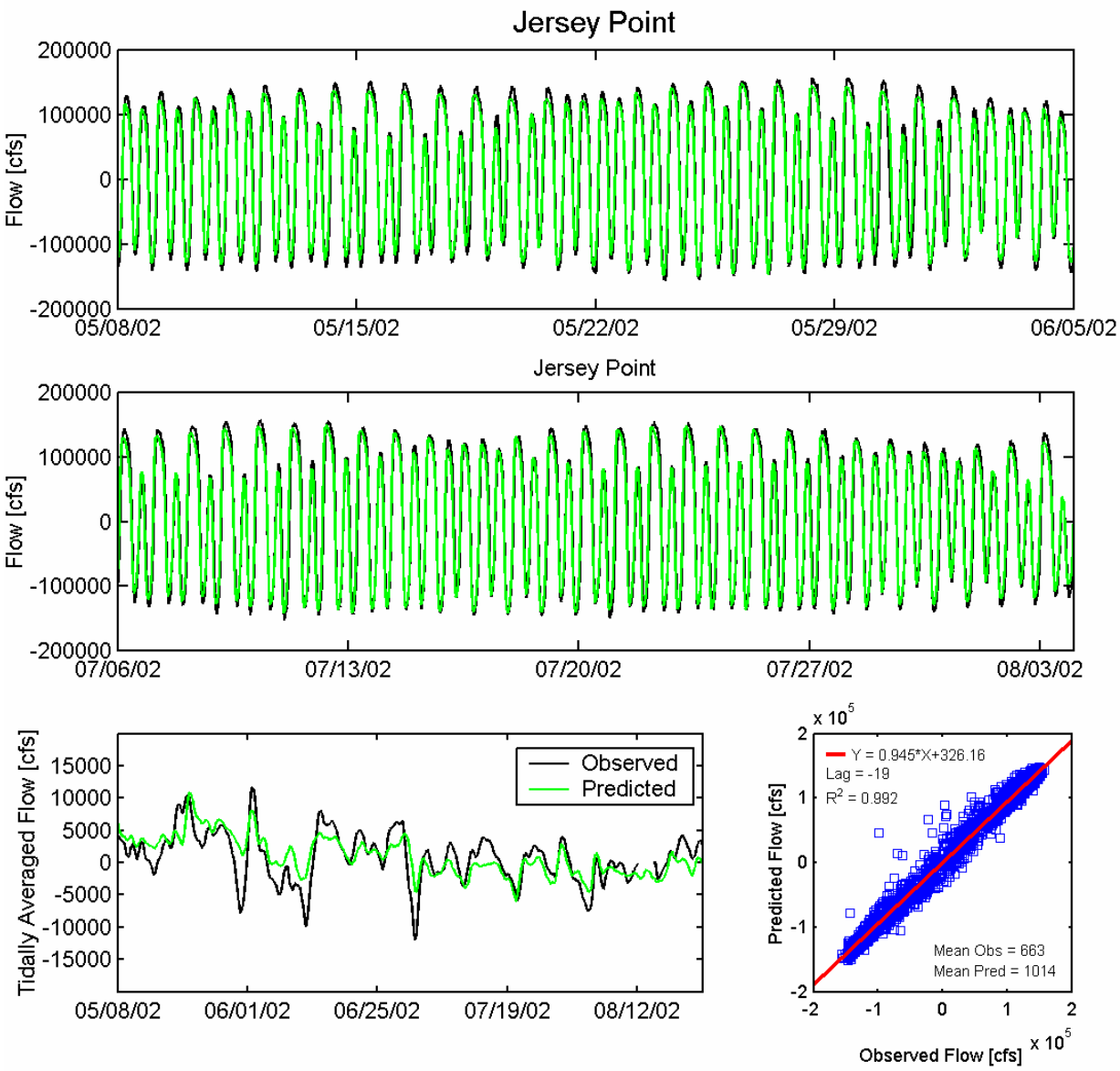

Figure H2.5.4-4 Observed and predicted flow at Jersey Point.

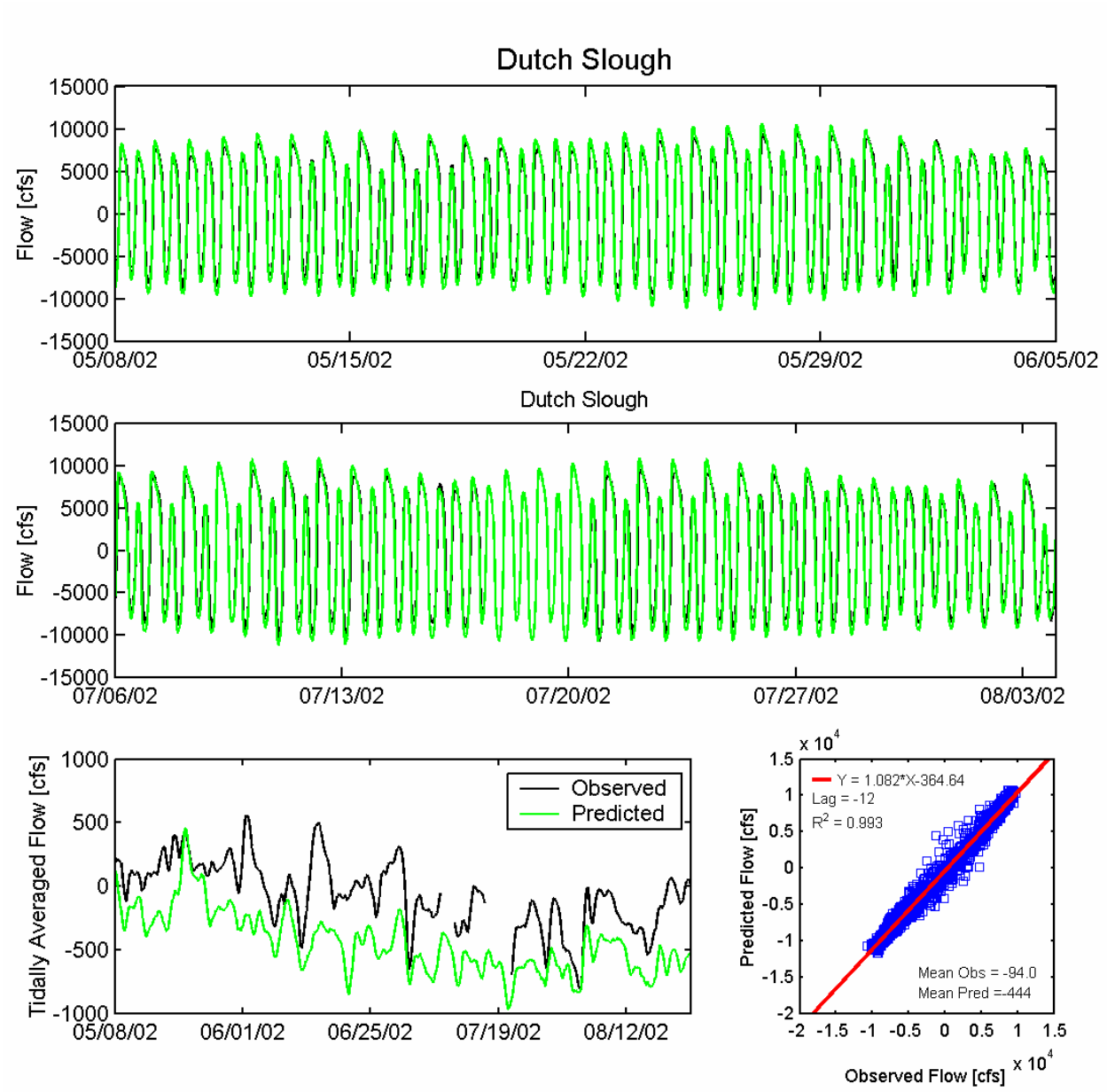

Figure H2.5.4-5 Observed and predicted flow at Dutch Slough.

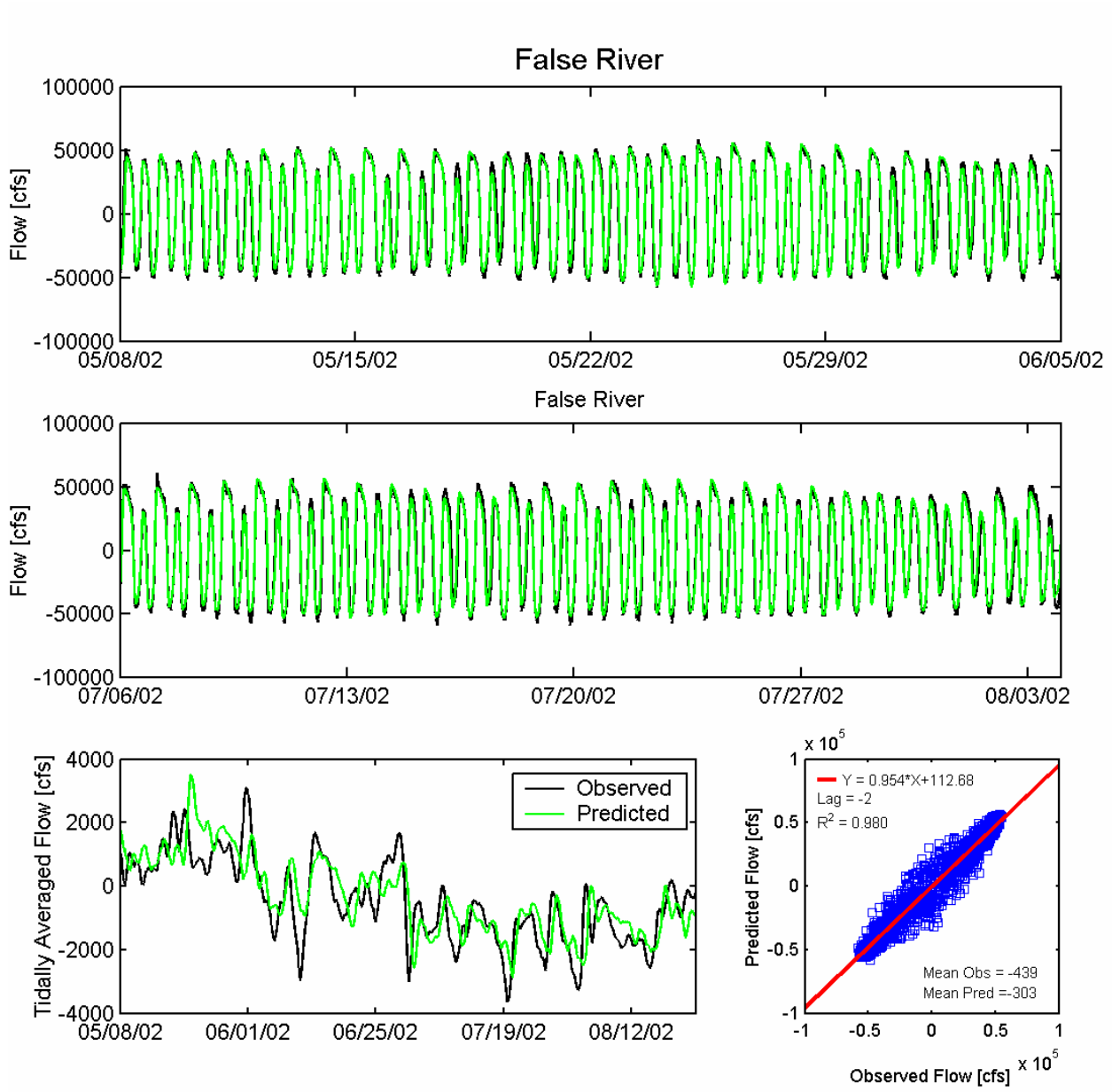

Figure H2.5.4-6 Observed and predicted flow at False River.

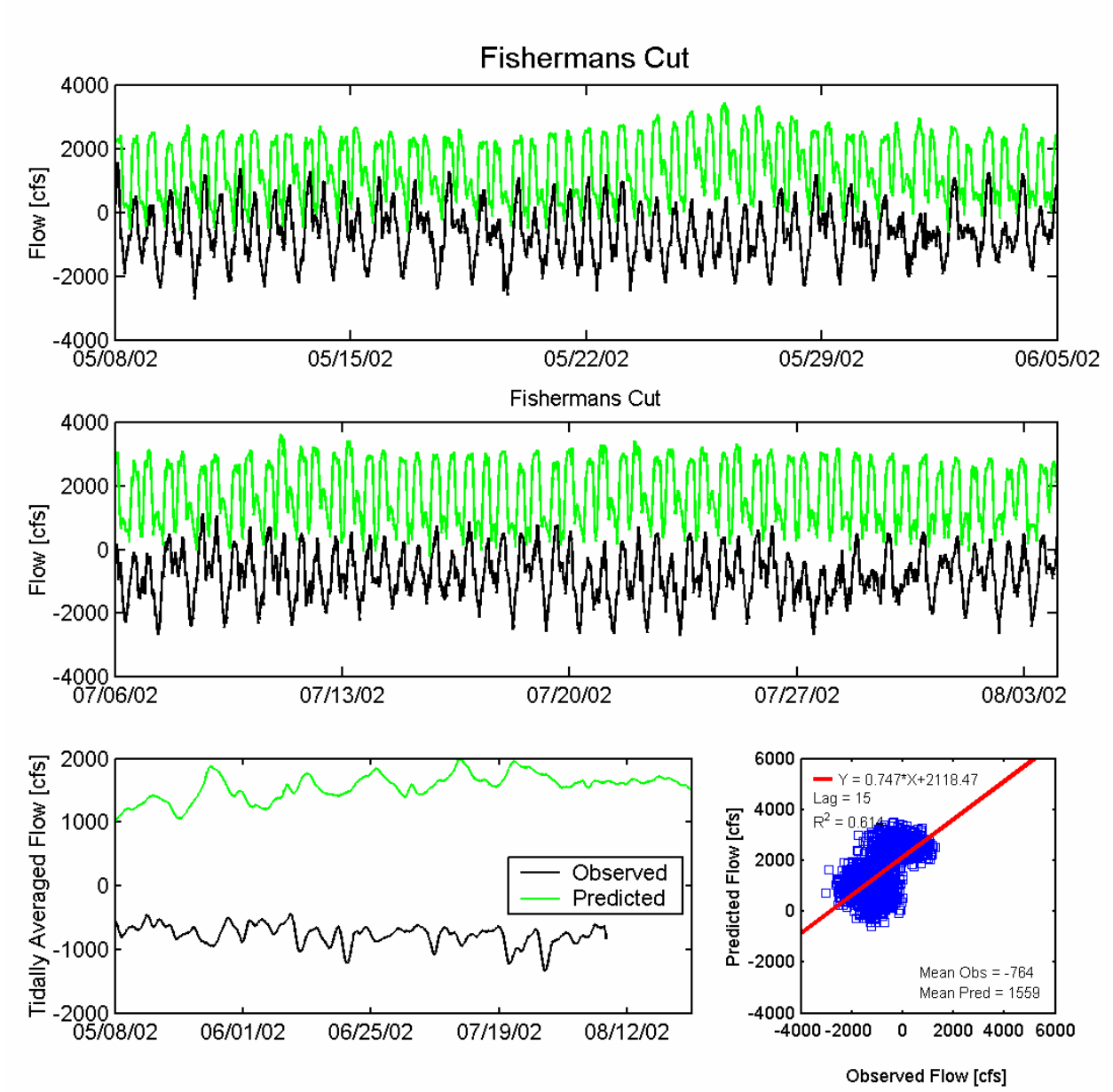

Figure H2.5.4-7 Observed and predicted flow at Fishermans Cut.

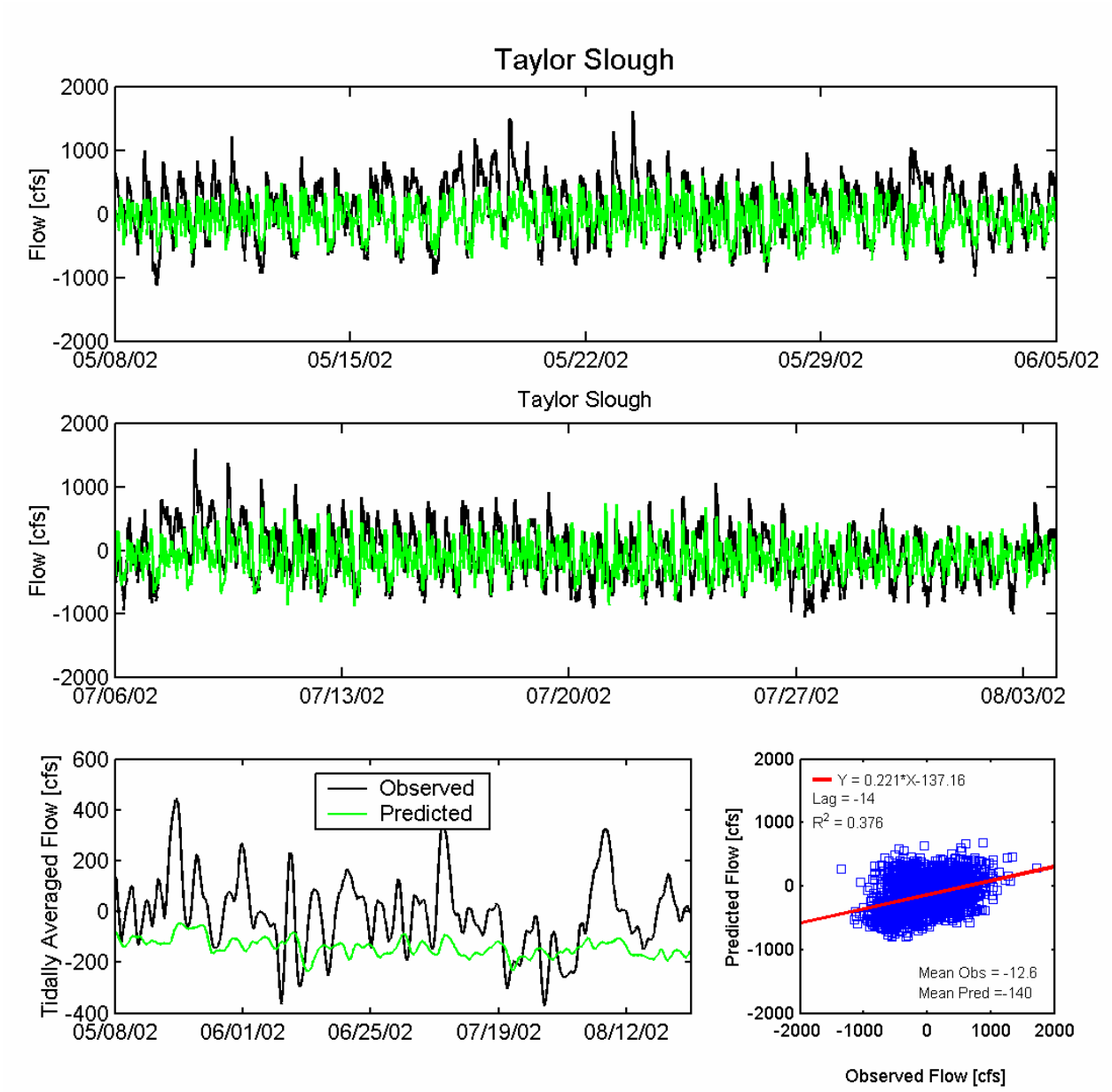

Figure H2.5.4-8 Observed and predicted flow at Taylor Slough.

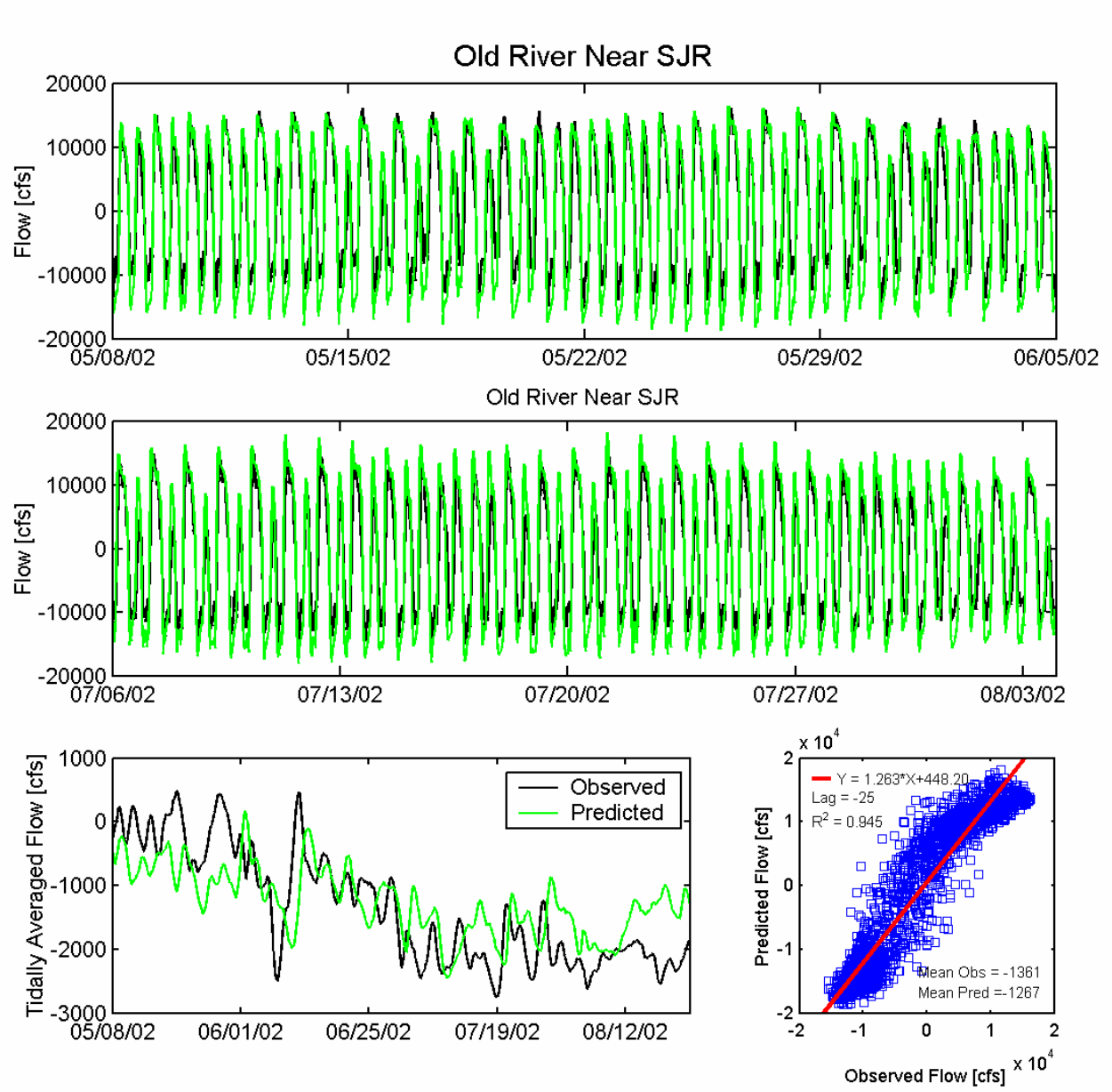

Figure H2.5.4-9 Observed and predicted flow at Old River, near the San Joaquin River.

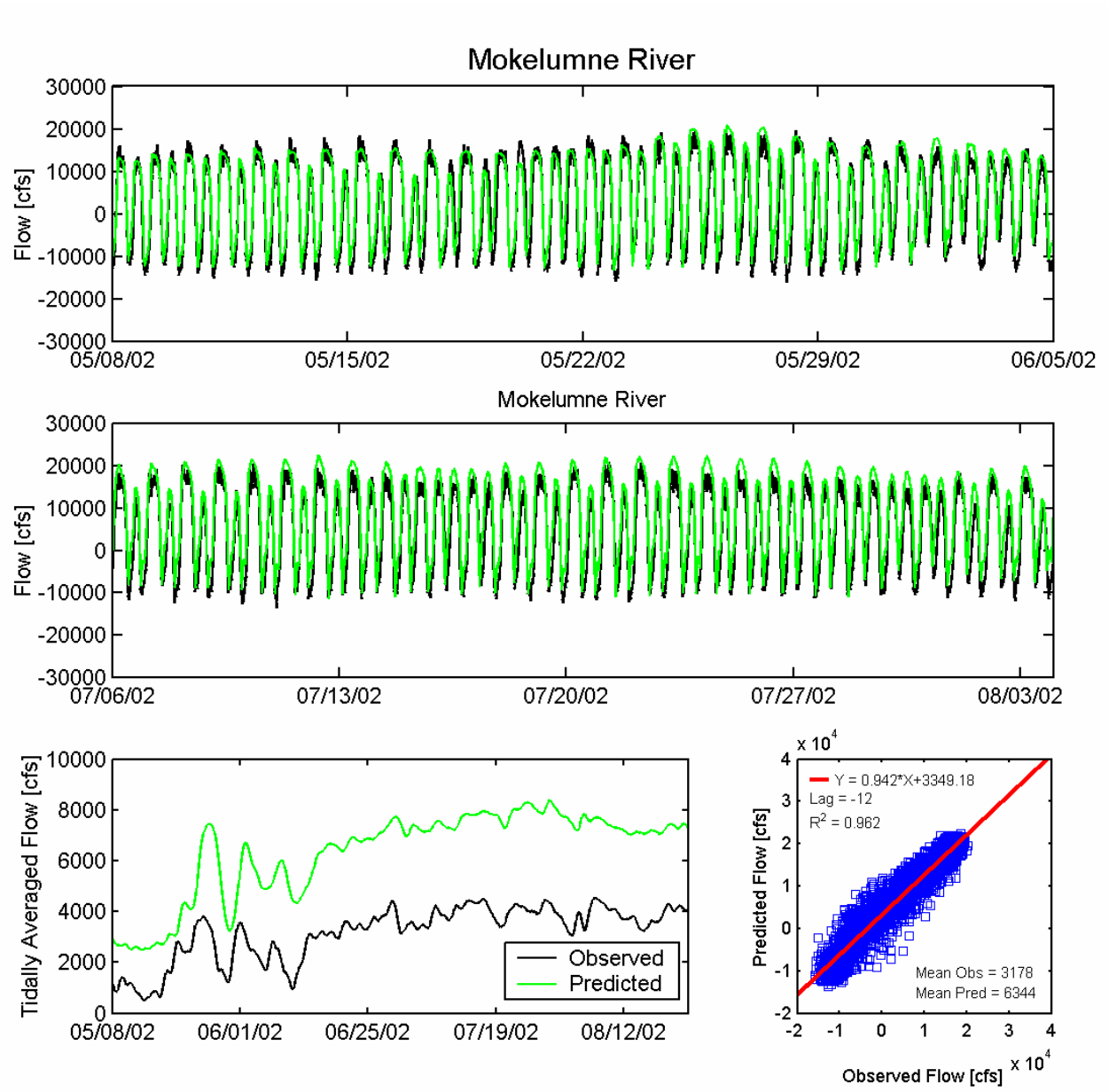

Figure H2.5.4-10 Observed and predicted flow at Mokelumne River.

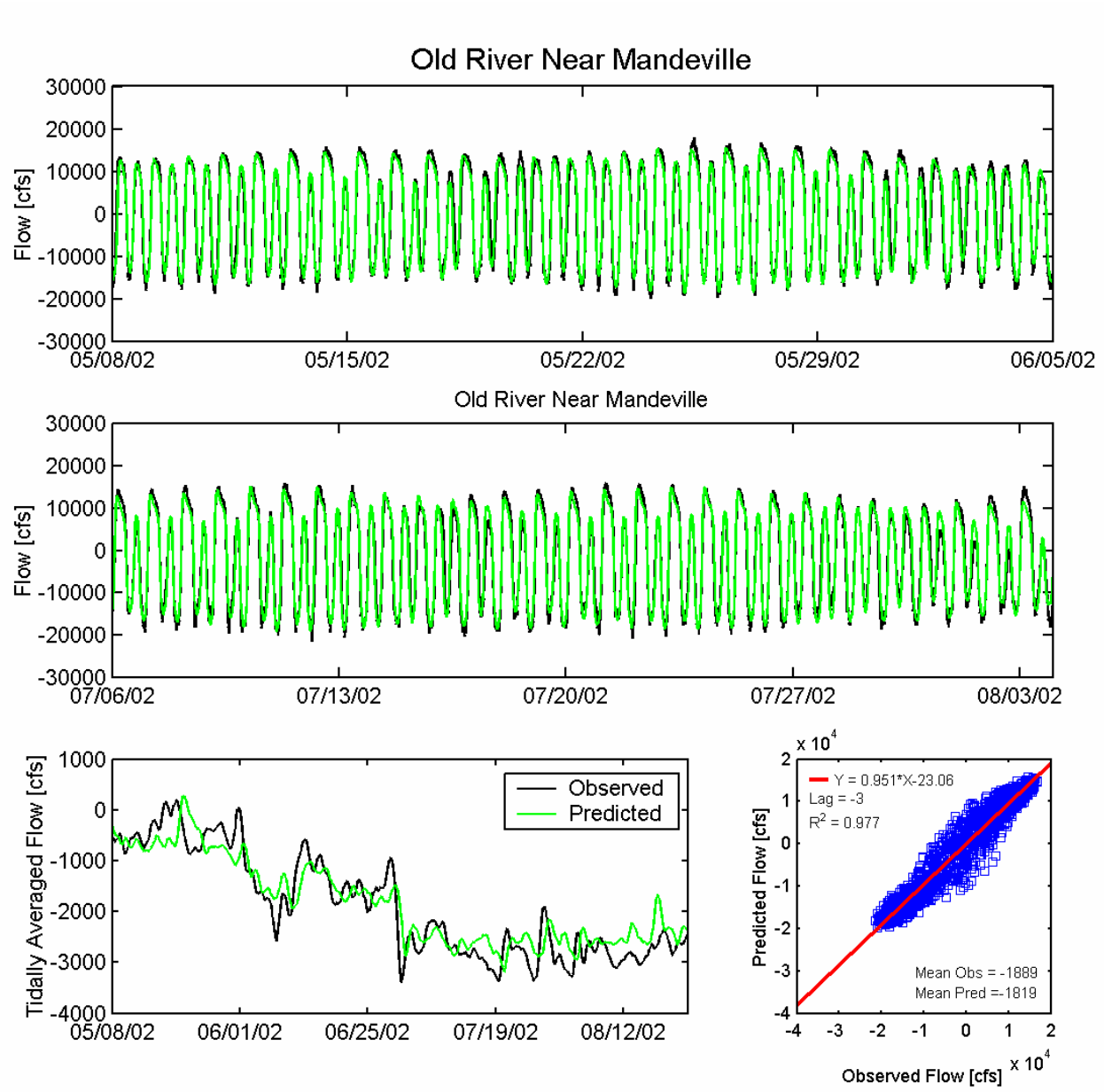

Figure H2.5.4-11 Observed and predicted flow at Old River, near Mandeville Island.

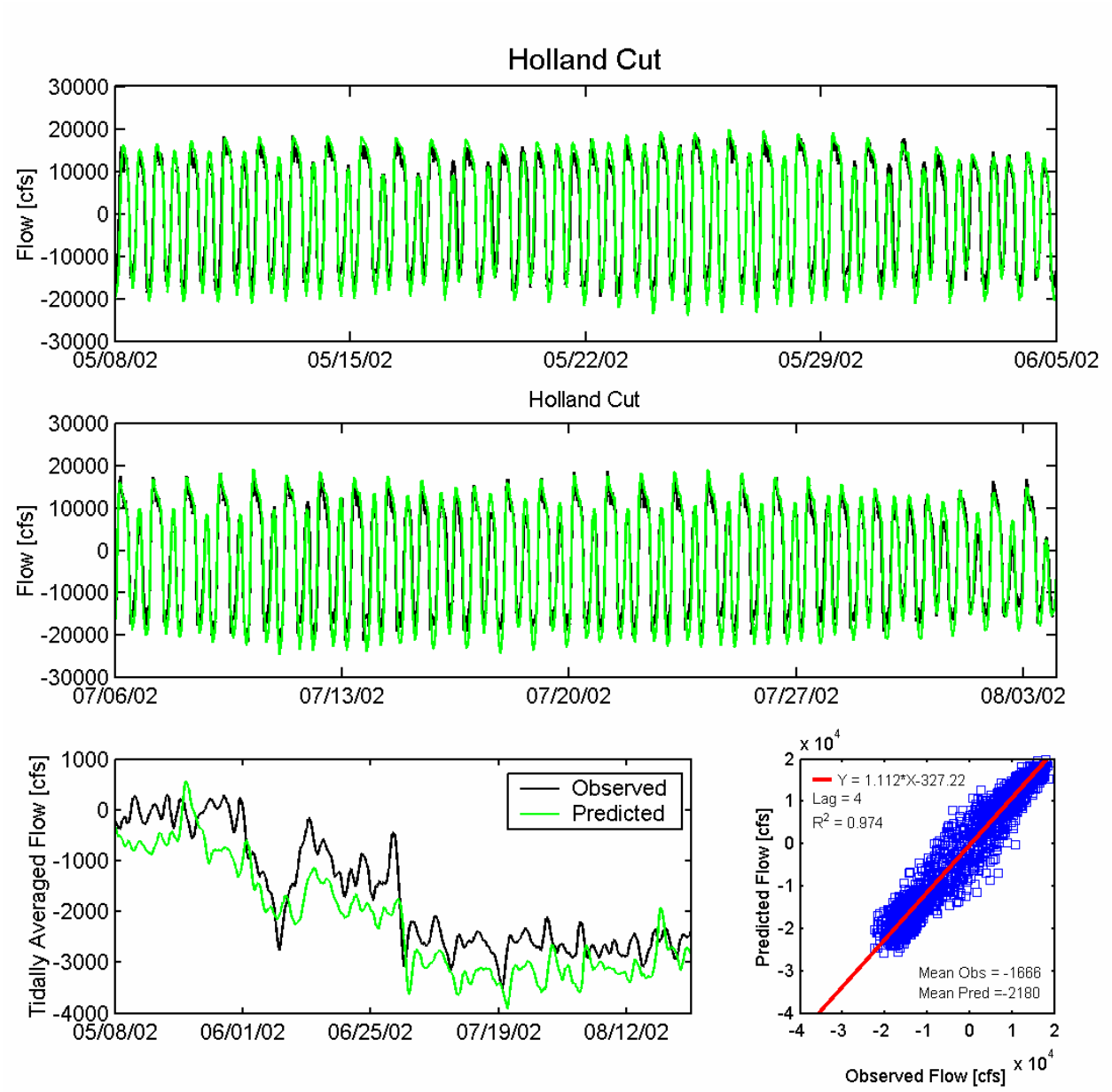

Figure H2.5.4-12 Observed and predicted flow at Holland Cut.

H2.6 Salinity Calibration

The salinity calibration documented here indicates the ability of the UnTRIM Bay-Delta Model to predict salinity. Because the three-dimensional model represents all major transport mechanisms it can be expected to have similar accuracy for levee breach scenarios, to the extent that levee breach geometry, island topography and other model inputs are represented realistically. In contrast, most one-dimensional models and two-dimensional models rely heavily on dispersion coefficients determined by for existing conditions and, therefore, may perform poorly for levee breach scenarios.

H2.6.1 Overview

Salinity initial conditions for the 1994 simulation period were specified based on United States Geological Survey (USGS) synoptic salinity observations collected on January 18, 1994 (Edmunds et al., 1995). The synoptic salinity data available for this date consists of vertical profiles of salinity at 1 meter vertical resolution at 38 sampling locations along the axis of San Francisco Bay, shown on Figure H2.6.1-1. Because the data does not provide information on lateral distribution of salinity, the initial salinity is assumed to be laterally uniform.

The salinity simulation used the same model grid, bathymetry and model parameters as the hydrodynamic calibration. The simulation extended from January 17,1994 to March 1, 1995, and the first six weeks was considered the salinity spin-up period to minimize the effect of errors in specification of the salinity initial conditions, such as the assumption of laterally uniform salinity. This simulation period was chosen because the Entrapment Zone Study dataset was collected in 1994 and because 1994 was a dry year. It is particularly important for the DRMS project that the model is able to simulate salinity during this period of relatively high Delta salinity. The simulation was continued into 1995 to test the ability of the model to simulate salinity during high Net Delta Outflow conditions.

The simulation tests the model's ability to simulate increasing salt intrusion into Suisun Bay and the Delta during the transition from winter to summer conditions and flushing of salt from these regions in the transition from summer/fall conditions to winter conditions.

H2.6.2 USGS Synoptic Salinity Observations

The predicted salinity was compared to synoptic salinity observations made by the USGS along the axis of the estuary (Edmunds et al., 1995), at station locations shown in Figure H2.6.1-1, at roughly a monthly interval. Observations and predictions for each cruise covering the entire estuary during the simulation period are shown in Figures H2.6.2-1 to H2.6.2-11.

Figure H2.6.2-1 shows the predicted observed and predicted salinity profile along the axis of the estuary on March 16, 1994, roughly 2 months after the salinity initial conditions were applied. During this period the salinity field is "recovering" from a small flow event in February. Figures H2.6.2-2 through H2.6.2-9 show observed and predicted salinity from April to November 1994. No substantial flow events occur during this period and Net Delta Outflow (NDO) ranges from 14 m^3/s to 424 m^3/s. Both observed

and predicted salinity slowly increase during this period and both observed and predicted stratification is minimal to moderate. The trends in salinity and stratification are predicted quite well during this period. In January 1995, a flow event with peak NDO of 7,020 m^3/s occurred which causes nearly complete flushing of salt from the Delta and Suisun Bay by the USGS cruise on January 18, 1995. Figure H2.6.2-10 shows that both observed and predicted salinity are below 0.5 psu in the western Delta and Suisun Bay on January 18, 1995 and sharp horizontal salinity gradients have formed in Carquinez Straight and San Pablo Bay. All portions of the estuary with significant salinity are strongly stratified in both observations and predictions. Generally the salinity field is predicted well during this dramatic transition with the exception of South San Francisco Bay, in which salinity is substantially overestimated. This is likely due to neglect of a large number of tributaries, representing a substantial portion of inflows to South San Francisco Bay. The salinity field observed during the following USGS cruise covering the entire estuary on February 7, 1995, is fairly similar to the salinity field observed on January 18, 1995, with strong stratification noted in both. The strong horizontal salinity gradients in Carquinez Strait and strong stratification through San Pablo Bay and Central San Francisco Bay are predicted well by the model.

As indicated in Table H2.6-1, the synoptic salinity dataset is predicted well by the model, with average error (bias) ranging from -0.76 to 2.49 psu and standard error ranging from 0.33 to 2.54 psu. Standard error is the standard deviation of the error and, therefore, measures the degree of scatter in the error. The largest errors are present during the high flow period in January and February of 1995. During the simulation period both the predictions and observations show a trend of slowly increasing salinity, with increased salt intrusion into the Delta and decreased stratification.

Table H2.6-1 Average error and correlation coefficient for each synoptic sampling cruise covering the axis of the San Francisco Estuary

Date	Average Error (psu)	Standard Error (psu)
3/16/1994	-0.24	0.49
4/19/1994	0.18	0.33
5/17/1994	-0.37	0.37
6/15/1994	-0.76	0.80
7/28/1994	-0.26	0.73
8/30/1994	-0.74	0.93
9/27/1994	-0.54	0.75
10/26/1994	-0.45	0.98
11/29/1994	-0.35	0.35
1/18/1995	1.03	1.68
2/07/1995	2.49	2.54

H2.6.3 Time Series

Figure H2.6.1-1 shows the locations and names of six continuous monitoring salinity stations used in the model calibration. The salinity data were collected by USGS (Buchanan et al., 1996) and DWR at top and bottom sensors at all stations except Fort Point, which is in shallow water, and Martinez, where little valid data is available during the calibration period.

Figures H2.6.3-1 through H2.6.3-10 indicate the predicted and observed tidal variability in salinity during a portion of the calibration period corresponding to the Entrapment Zone Study, during which synoptic salinity data are available and will be discussed in the following section. Each figure also shows tidally-averaged salinity for the entire simulation period and a scatter plot shows a comparison between the observed and predicted salinity over the analysis period. The scatter plot is produced by first running a cross-correlation between the observed data and model predictions to find the average phase lag over the entire record. The cross correlation was completed following the procedure outlined by RMA (2005). The process entails repeatedly shifting the predicted time series record at one minute increments relative to the observed time series while computing the correlation coefficient at each time shift. The correlation has a maximum value when the shifted predicted time series best aligns with the observed time series. The reported lag is the phase shift in the predicted time series, with positive values indicating that the predicted time series lags the observed time series. A linear regression is then performed between the time shifted model results and observed data record to yield the amplitude ratio, best-fit line, and correlation coefficient. The statistics reported on each scatter plot follow the approach used by RMA (2005) and include the following:

- Mean Obs – Average value of observed time series for analysis period
- Mean Pred – Average value of predicted time series for analysis period
- Lag – Phase difference in minutes between observed and predicted; a positive value indicates that the predicted time series lags behind the observed time series.
- Y = slope*X + offset – Best linear fit, where Y is predicted, X is observed. The slope value is used as the amplitude ratio. In the case of salinity this amplitude ratio roughly indicates the degree of variability with tides and freshwater flows.
- R^2 – Linear regression goodness of fit parameter.

Figures H2.6.3-1 and H2.6.3-2 show the predicted and observed salinity at the San Mateo Bridge station. Salinity is predicted well at this station until the large flow event in January 1995 when salinity is overpredicted by the model by roughly 5 psu. The salinity error in South San Francisco Bay during this period, which was also apparent in the synoptic salinity comparisons during 1995, is probably due to neglecting inflows from many tributaries in South San Francisco Bay. The salinity at the Oakland Bay Bridge is predicted fairly accurately at both sensors but varies over a narrow range during the period in which data were available. Valid data were not available after September 1994.

Figures H2.6.3-3 and H2.6.3-4 show the predicted and observed salinity at the Oakland Bay Bridge station. Valid data are available only up to October 1, 1994. For this reason the observed and predicted salinity can only be compared over a narrow range of salinity

corresponding to low inflow conditions. The model predicts salinity well during these conditions.

Figure H2.6.3-5 shows the predicted and observed salinity at the Presidio station. The model predicts salinity well during the entire simulation period. The tidally-averaged salinity drops below 14 psu during February 1995. This suggests the importance of applying the salinity boundary condition in the coastal ocean where salinity is relatively constant in time, instead of at the Golden Gate where substantial salinity variability is observed. However, treating the coastal ocean salinity as a constant 33.5 psu may lead to some degree of error in the very wet conditions experienced during January and February 1995 and may account for overprediction of salinity at the Presidio station during February 1995.

Figures H2.6.3-6 and H2.6.3-7 show the predicted and observed salinity at the Point San Pablo station. A long data gap is present at both sensors from October 27, 1994 to January 19, 1995. Overall, the model predicts salinity accurately at this location but the tidal variability of salinity is significantly underpredicted. In addition the observations indicate high frequency variability that is largely absent in the predictions. This variability may be related to very small scale bathymetric features near the Pier in the Richmond Terminal where the Point San Pablo station is located. This steep geometry and bathymetry associated with the Terminal area are not well resolved by the model grid. The seasonal variability of tidally-averaged salinity is represented quite well at this location though, again, the observed range of variability is larger than predicted.

Figure H2.6.3-8 shows the predicted and observed salinity at the surface sensor of the Martinez station. Few valid data were available from the bottom sensor during the calibration period. Both the tidal and seasonal variability of salinity are predicted accurately during the calibration period though salinity is typically slightly overestimated by the model.

Figures H2.6.3-9 and H2.6.3-10 show predicted and observed salinity at the Mallard Island station. The bottom sensor data used are associated with the Entrapment Zone Study and extends only to August 19, 1994. The surface sensor is from a permanent station and data are available for the entire simulation period. Both the tidal and seasonal variability of salinity are predicted well at this station, particularly during the high flow events in 1995.

As indicated in Table H2.6-2, salinity is predicted reasonably well at the continuous observation stations. Likely sources of error associated with the model predictions at these locations include:

- Limited number of tributaries used in South San Francisco Bay
- Assumption of constant coastal ocean boundary salinity of 33.5 psu
- Limited resolution of small scale bathymetric features, including piers, near stations
- Errors in Net Delta Outflow values, particularly during low flow periods

Though substantial room for improvement remains, the comparison of predicted salinity and continuously monitored salinity suggests that the model is adequately representing most of the key physical processes responsible for salt transport.

Table H2.6-2 Predicted and observed salinity and cross-correlation statistics for continuous salinity monitoring stations

Location	Dates	Mean Salinity (psu)		Cross Correlation		R^2
		Observed	Predicted	Amp Ratio	Lag (min)	
San Mateo Bottom	3/1/94-3/1/95	28.0	28.4	0.652	36	0.989
San Mateo Top	3/1/94-3/1/95	26.9	28.4	0.642	83	0.992
Bay Bridge Bot	3/1/94-10/1/94	30.8	29.3	0.798	-8	0.899
Bay Bridge Top	3/1/94-10/1/94	30.6	29.3	0.702	-35	0.914
Presidio	3/1/94-3/1/95	29.8	29.8	0.786	-4	0.97
Pt. San Pablo Bot	3/1/94-3/1/95	26.0	25.7	0.795	32	0.969
Pt. San Pablo Top	3/1/94-3/1/95	25.2	24.8	0.772	9	0.974
Martinez Surface	3/1/94-3/1/95	11.3	12.2	0.993	-36	0.962
Mallard Bottom	4/16/94-8/19/94	5.10	4.01	0.913	14	0.976
Mallard Surface	3/1/94-1/20/95	4.24	4.01	1.013	-2	0.971

H2.6.4 Suisun Bay Salinity Transects

The Entrapment Zone Study (Burau et al. 1998) collected transects of salinity consisting of vertical profiles of salinity at each of the 10 synoptic sampling stations, numbered 0 through 9 on Figure H2.6.4-1. Salinity transects were collected for both spring and neap conditions. This dataset allows a detailed comparison of tidal time scale variability in salinity in Suisun Bay. Because the spatial and temporal resolution of these observations is higher than the resolution of the USGS synoptic salinity data, this comparison provides additional insight into model performance.

In a spring tide period on April 27th and April 28th, eight salinity transects were collected. The salinity transects were collected at 3 to 5 hour increments with 90 to 150 minutes typically required for the research vessel to travel from station 0 to station 9 on a single transect. Note that the observed channel bathymetry varies slightly among transects due to small differences in location of data collection among transects. The salinity predictions are always shown at the reported station locations.

The first transect during this period, shown on Figure H2.6.4-2, collected during an ebb tide from 6:18 am to 8:26 am Pacific Standard Time on April 27th, shows salinity ranging from below 2 psu to over 18 psu in the observations and predicted salinity is typically underestimated by 2 psu. The second transect, shown on Figure H2.6.4-3, collected near low water, shows vertically well-mixed conditions. Predicted salinity also shows well-mixed conditions but is typically 1 to 2 psu low. The third transect, shown on Figure H2.6.4-4, collected during a flood tide, shows vertically well-mixed conditions. The

predicted salinity indicates well-mixed conditions but underestimates salinity by 1 psu to 2 psu. The fourth transect, Figure H2.6.4-5, collected during an ebb tide, shows fairly strong longitudinal salinity gradients at the seaward end of Suisun Bay and a small degree of stratification in Suisun Bay. The predicted salinity underpredicts salinity and stratification significantly. The fifth transect, shown on Figure H2.6.4-6, collected during a flood tide, shows roughly 2 psu stratification at the seaward end of Suisun Bay. The predicted salinity is fairly accurate but the stratification is somewhat underestimated and salinity is underestimated by between 1 and 2 psu. The sixth transect, shown on Figure H2.6.4-7, collected following high water, shows fairly compressed longitudinal salinity gradients and substantial stratification. The predicted salinity transect shows similar longitudinal salinity gradients but less stratification and lower salinity. The seventh transect, shown on Figure H2.6.4-8, collected during an ebb tide, shows salinity ranging from below 2 psu to over 12 psu and vertically well-mixed conditions. The predicted salinity transect shows the same range of salinity. The eighth transect, shown on Figure H2.6.4-9, collected during a flood tide, shows mild longitudinal salinity gradients and vertically well-mixed conditions. The predictions underestimate salinity by 1 to 2 psu. The mean error and R^2 coefficient for each salinity transect is listed in Table H2.6-3.

The model predicts salinity realistically during spring tide conditions on April 27th and April 28th. Most notably, the temporal trends are captured accurately. In both the observations and predictions, the isohalines are advected 5 to 10 km during a flood or ebb tide and salinity remains vertically uniform during much of this period. The strongest stratification is noted in the sixth transect, near high water. This stratification appears to be the result of the relatively strong longitudinal salinity gradients that develop during flood tide and reduced vertical mixing experienced near slack water. The timing and location of stratification are predicted quite accurately while the magnitude of stratification is often underestimated.

Salinity transect data were collected on May 17th and May 18th during neap tides. The first neap tide transect, shown on Figure H2.6.4-10, collected on May 17th from 6:46 am to 8:40 am, shortly following high water, shows salinity ranging up to 18 psu and strong stratification at the seaward end of Suisun Bay. The predicted salinity ranges up to 16 psu and underestimates the degree of stratification. The second transect, shown on Figure H2.6.4-11, collected during an ebb tide, shows strong stratification. The predicted salinity is also strongly stratified, though again the predicted stratification is weaker than the observed stratification and salinity is underestimated by 1 to 3 psu. The third transect, shown on Figure H2.6.4-12, collected near low water, shows fairly well-mixed conditions with salinity ranging up to 8 psu. The predicted salinity is similar to the observed salinity. The fourth transect, shown on Figure H2.6.4-13, collected during a flood tide, shows mild stratification and fairly weak longitudinal salinity gradients. The predicted salinity is underestimated by 1 psu to 4 psu. The fifth transect, shown on Figure H2.6.4-14, collected near high water, shows nearly well-mixed conditions with salinity ranging up to 14 psu. The predicted salinity during this period is similar but 1 psu to 3 psu lower than observed salinity. The sixth transect, shown on Figure H2.6.4-15, collected during an ebb tide, shows strong longitudinal salinity gradients and stratified conditions with stratification up to 6 psu. The predicted salinity transect shows significantly less stratification and 1 psu to 3 psu lower salinity. The seventh transect, shown on Figure

H2.6.4-16, collected during a weak flood tide, shows strongly stratified conditions and strong longitudinal salinity gradients. The predicted salinity transect shows less stratification and weaker longitudinal gradients. The eighth salinity transect, shown on Figure H2.6.4-17, collected near high water, shows strong longitudinal salinity gradients and strong stratification. The predicted salinity transect shows slightly lower salinity and weaker stratification. The ninth salinity transect, shown on Figure H2.6.4-18, collected during ebb tides, shows strong longitudinal salinity gradients and strong stratification. The predicted salinity transect shows the same range of salinity but weaker stratification. The mean error and standard error for each salinity transect is listed in Table H2.6-3.

Stronger and more persistent stratification is observed during neap tide conditions on May 17th and 18th than was observed during spring tide conditions on April 27th and April 28th. This trend was also evident in the salinity predictions. Stratification was observed and predicted to persist through ebb tides during this period. During the second flood tide on May 17th nearly well-mixed conditions were observed and predicted, while substantial stratification was observed and predicted to persist through the weaker subsequent flood tide on May 18th. The general trends are predicted by the model but the predicted stratification in several transects was weaker than the observed stratification and the predicted salinity was typically lower than the observed salinity.

The mean error in predicted salinity was -1.4 psu during the spring tide cruise and –0.8 psu during the neap tide cruise indicating a bias toward underestimation of salinity during the Entrapment Zone Study period. Standard error is the standard deviation of the error and, therefore, measures the degree of scatter in the error. The standard error values computed for each salinity transect ranged from 0.59 to 1.2 psu for the spring tide cruise 0.61 to 1.44 psu for the neap tide cruise. Overall the salinity comparison to the Entrapment Zone Study salinity transects provides additional confidence in the ability of the model to predict salinity.

Table H2.6-3 Mean salinity error (bias) and correlation for Entrapment Zone synoptic salinity dataset

Date	Time	Average Error (psu)	Standard Error (psu)
4/27/1994	6:18	-1.3	0.76
4/27/1994	9:44	-0.96	0.59
4/27/1994	14:03	-1.88	0.97
4/27/1994	17:28	-1.87	1.03
4/27/1994	22:47	-1.15	0.68
4/28/1994	3:46	-2.34	1.2
4/28/1994	8:26	-1.28	0.67
4/28/1994	12:44	-1.2	0.74
5/17/1994	6:46	-1.17	1.25
5/17/1994	9:41	-1.09	1.16
5/17/1994	12:30	-0.56	0.61

5/17/1994	17:53	-1.14	1.08
5/17/1994	19:24	-1.8	1.32
5/17/1994	23:44	-1.21	1.22
5/18/1994	3:27	-1.22	1.27
5/18/1994	8:05	-1.61	1.44
5/18/1994	11:04	-1.13	1.05

H2.6.5 Discussion

This section showed the comparison between predicted and observed salinity for two synoptic salinity datasets and at ten continuous monitoring sensors during a one year period that spans a large range of Net Delta Outflow conditions. Both tidal and seasonal variability in salinity are predicted well at most locations. The calibration provides confidence that the model is adequately representing most of the key physical processes responsible for salt transport. This good comparison with observations was achieved without resorting to excessive tuning. The only tuning parameters available are a minimum vertical mixing parameter in the turbulence closure, set to a relatively low value of $5x10^{-5}$ m^2/s and a constant horizontal "subgrid scale mixing" parameter of 5 m^2/s. These values are physically realistic for the San Francisco Estuary and the model results are not sensitive to changes in these parameters over an order of magnitude. Due to this minimal use of empirical information in the three-dimensional model, we expect that the model is valid for dramatically different Delta geometries.

Though the simulation results indicate good accuracy, substantial room for improvement remains. Potential improvements include:

- Representing flows in additional South San Francisco Bay tributaries
- Accounting for variability in coastal ocean boundary salinity
- Extension of model grid further into the Delta
- Improved grid resolution to better represent small scale bathymetric features
- Accounting for operations, including operation of the Suisun Marsh Salinity Control Structure
- Improvements in net Delta flow estimates and consumptive use, particularly during low flow periods when the uncertain terms representing consumptive use are substantial relative to NDO
- Additional site-specific tuning of bottom friction parameters

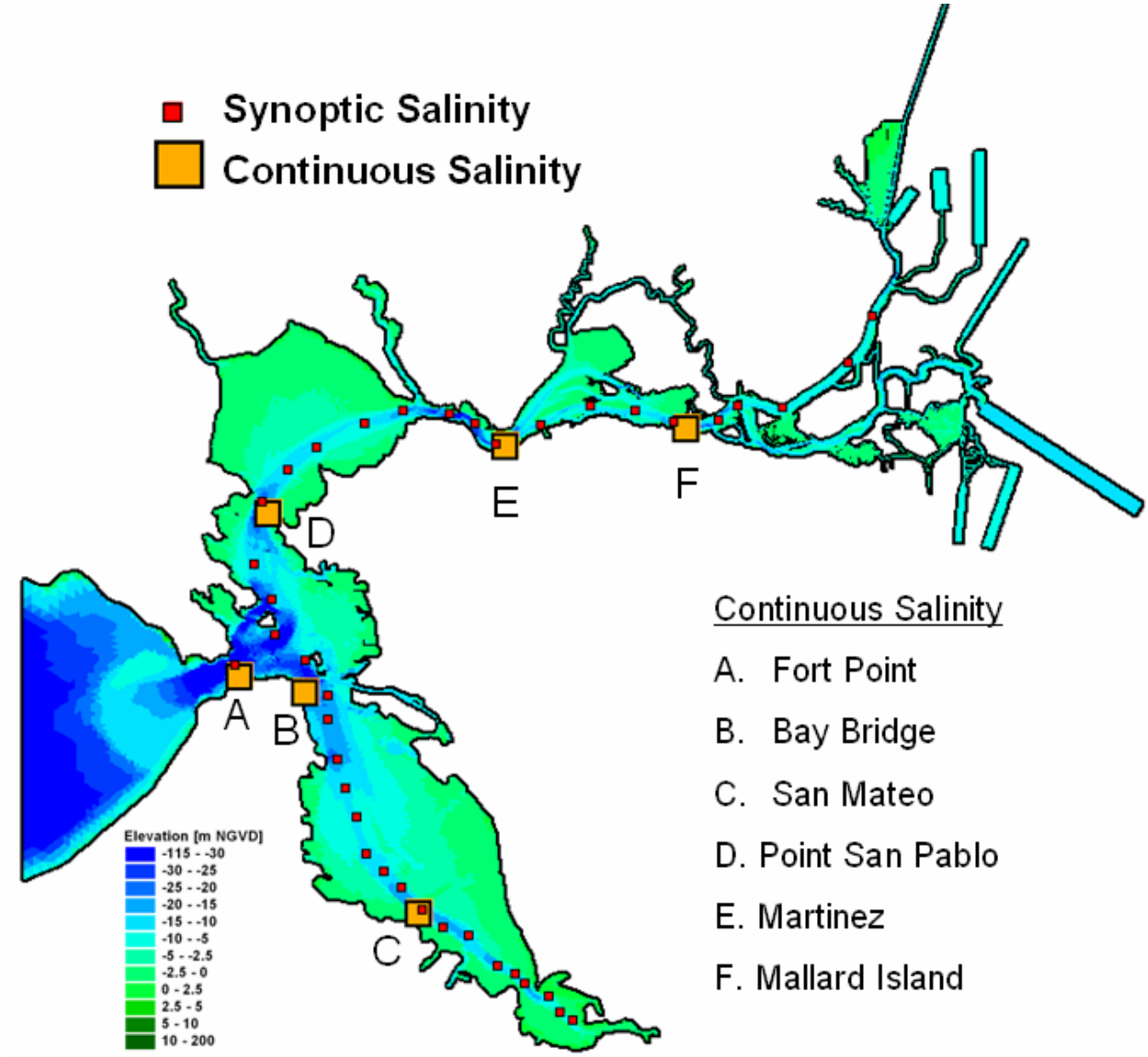

Figure H2.6.1-1 **San Francisco Bay continuous and synoptic salinity stations.**

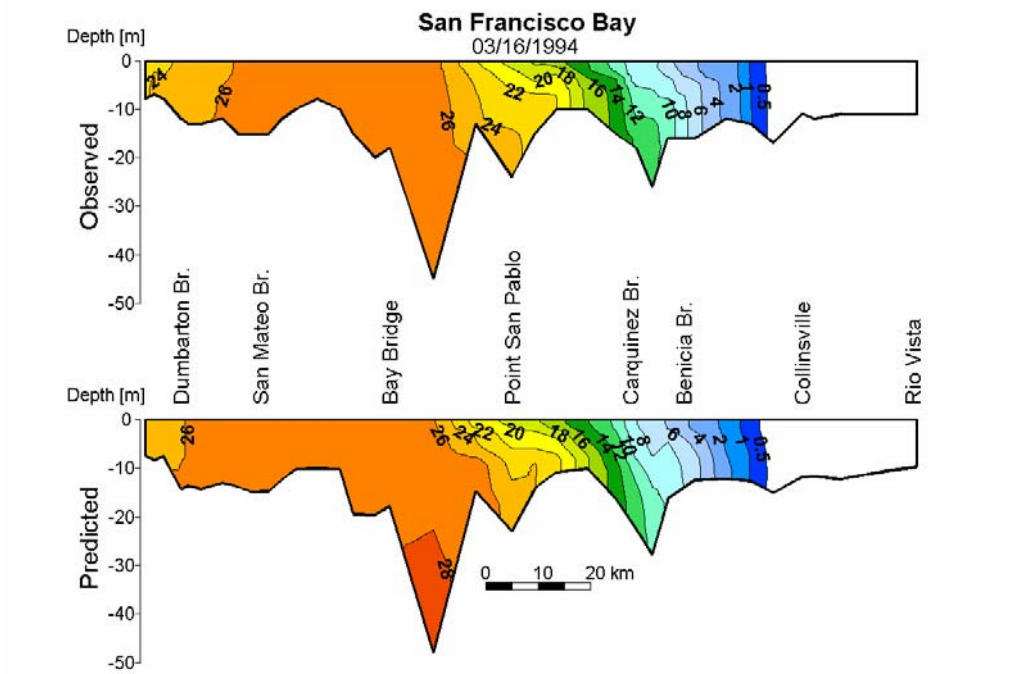

Figure H2.6.2-1 Observed and predicted salinity profiles at synoptic sampling station locations, interpolated along the axis of the San Francisco Estuary on March 16, 1994.

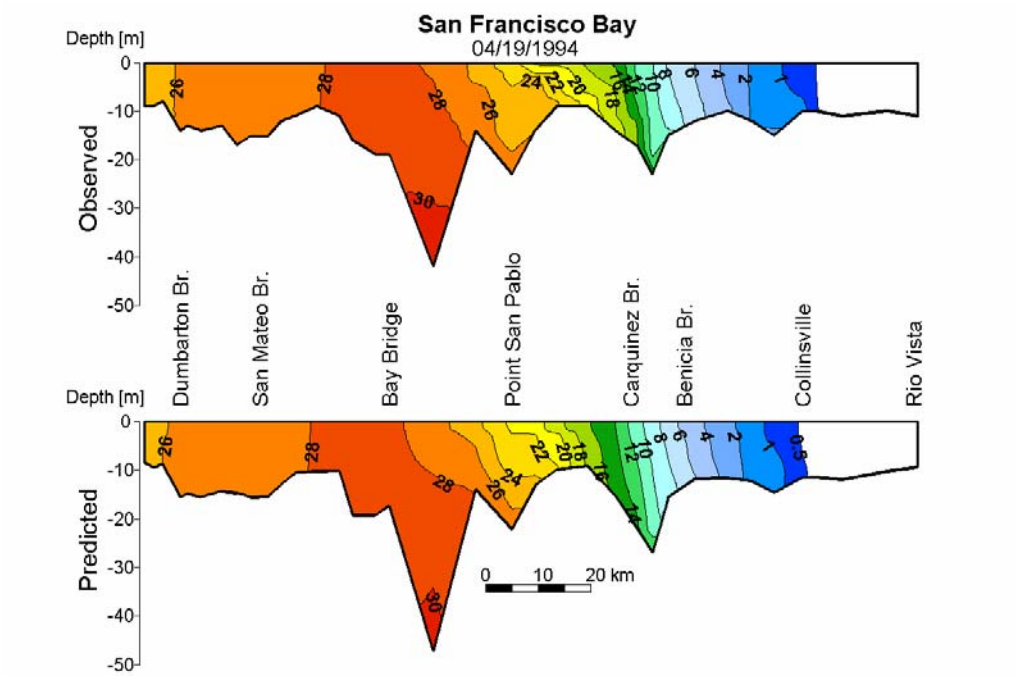

Figure H2.6.2-2 Observed and predicted salinity profiles at synoptic sampling station locations, interpolated along the axis of the San Francisco Estuary on April 19, 1994.

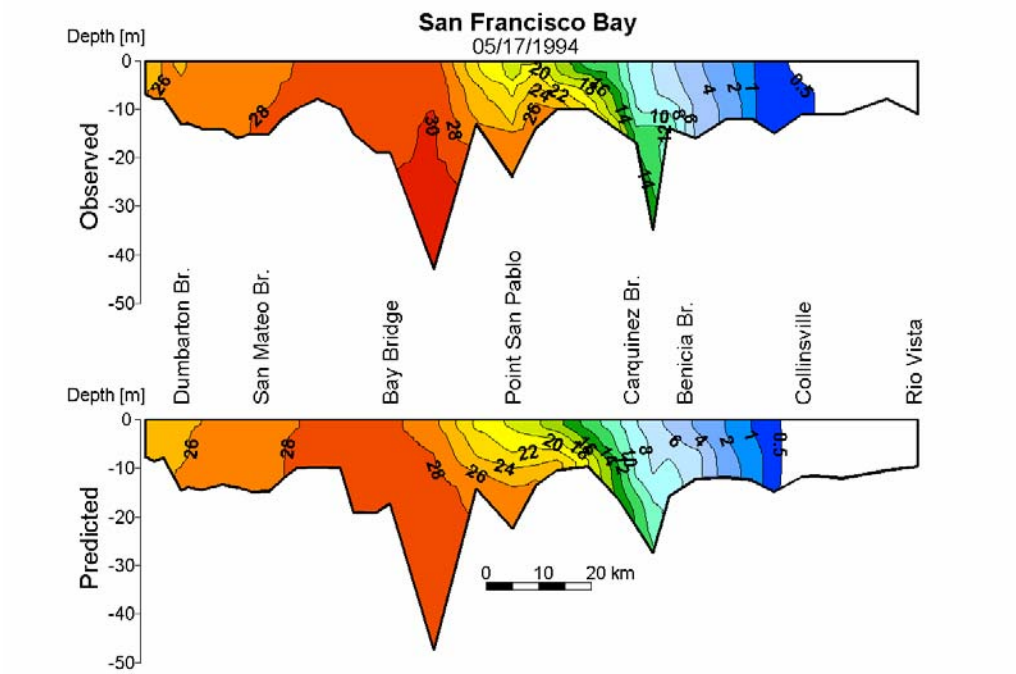

Figure H2.6.2-3 Observed and predicted salinity profiles at synoptic sampling station locations, interpolated along the axis of the San Francisco Estuary on May 17, 1994.

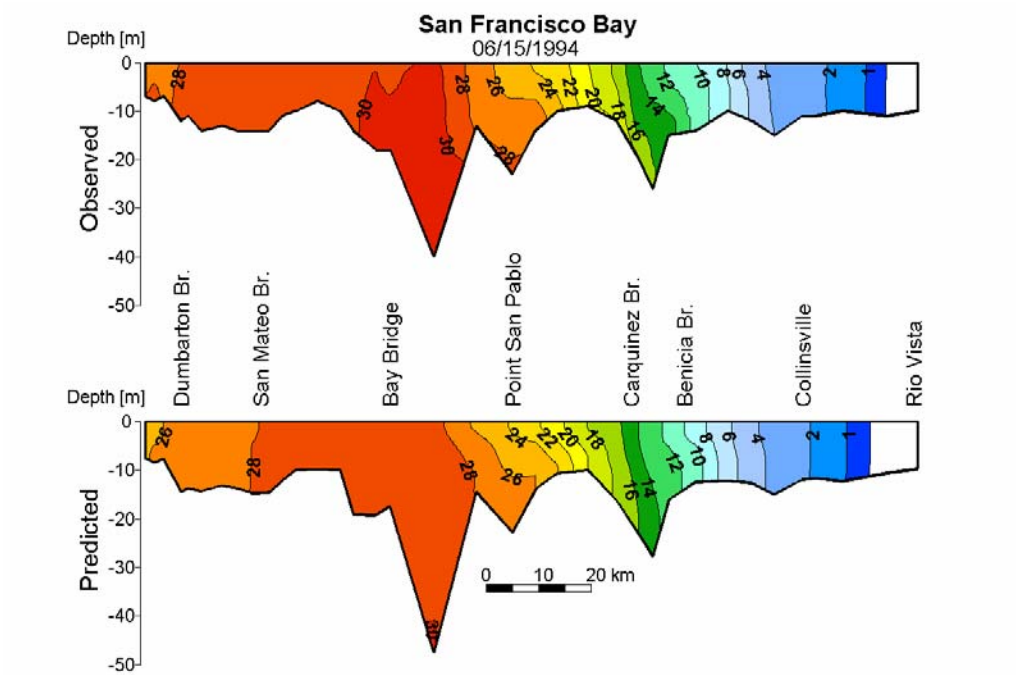

Figure H2.6.2-4 Observed and predicted salinity profiles at synoptic sampling station locations, interpolated along the axis of the San Francisco Estuary on June 15, 1994.

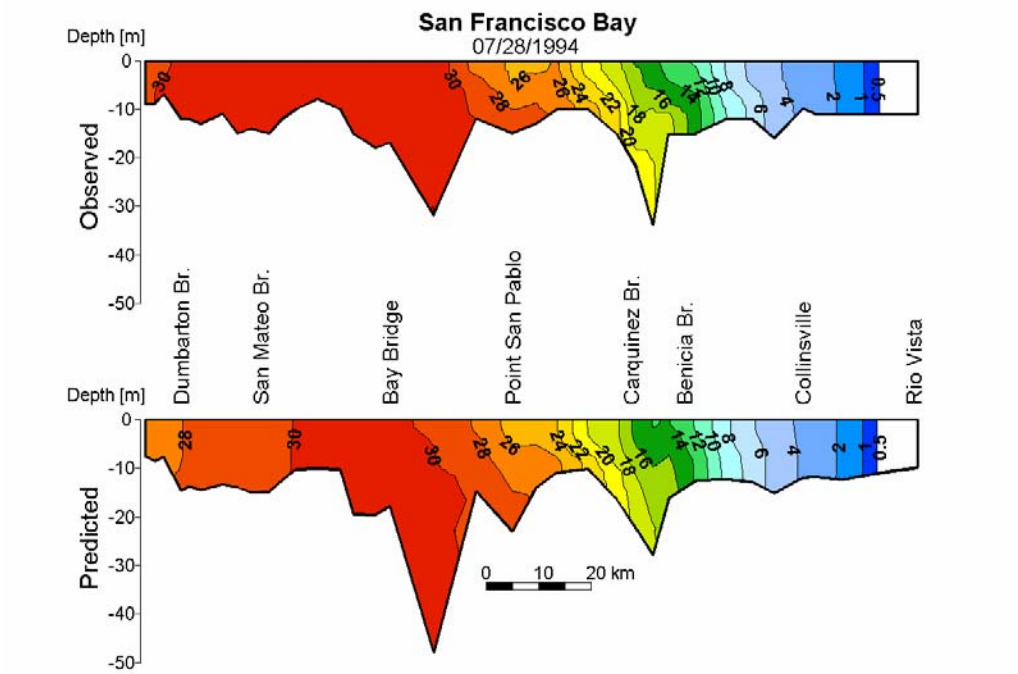

Figure H2.6.2-5 Observed and predicted salinity profiles at synoptic sampling station locations, interpolated along the axis of the San Francisco Estuary July 28, 1994.

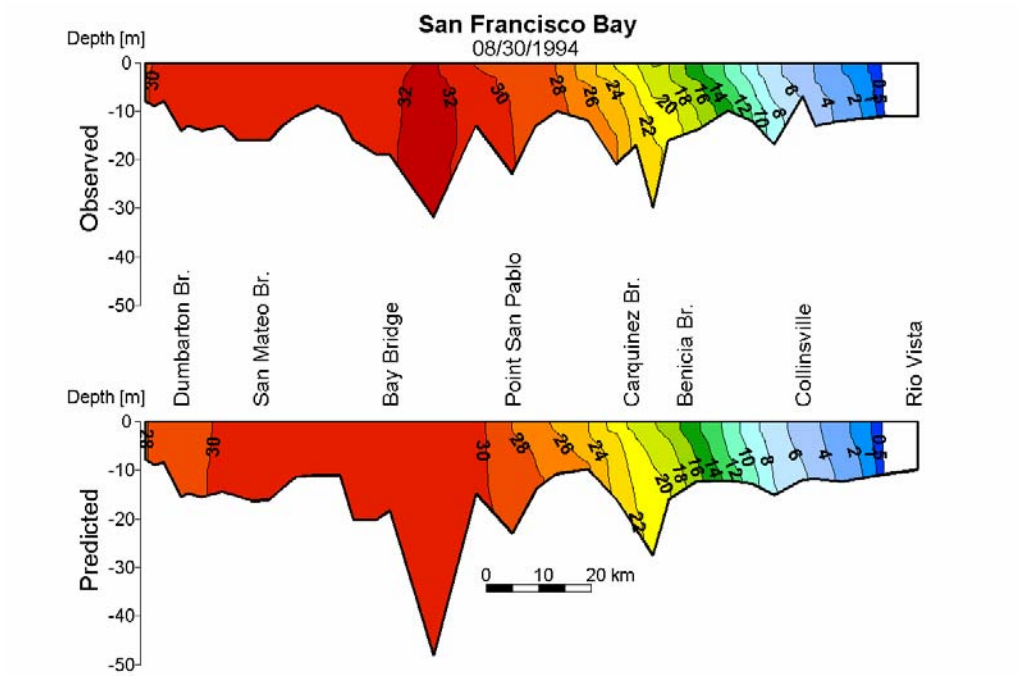

Figure H2.6.2-6 Observed and predicted salinity profiles at synoptic sampling station locations, interpolated along the axis of the San Francisco Estuary on August 30, 1994.

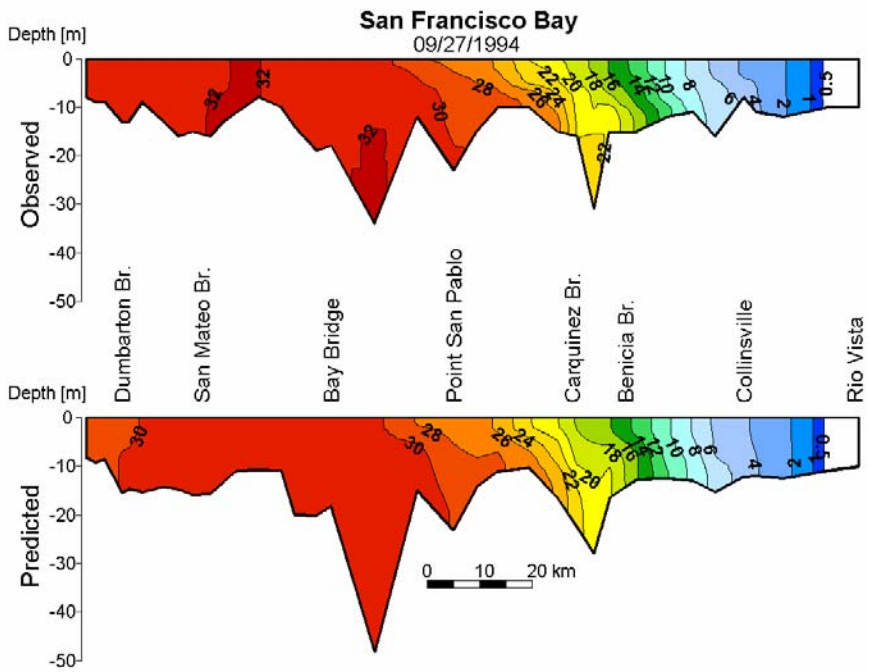

Figure H2.6.2-7 Observed and predicted salinity profiles at synoptic sampling station locations, interpolated along the axis of the San Francisco Estuary on September 27, 1994.

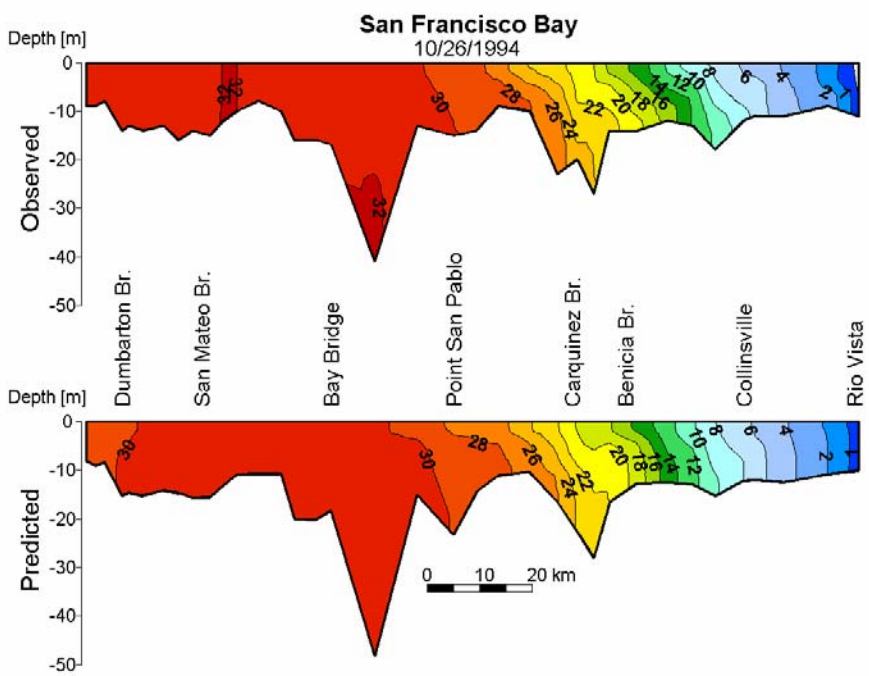

Figure H2.6.2-8 Observed and predicted salinity profiles at synoptic sampling station locations, interpolated along the axis of the San Francisco Estuary on October 26, 1994.

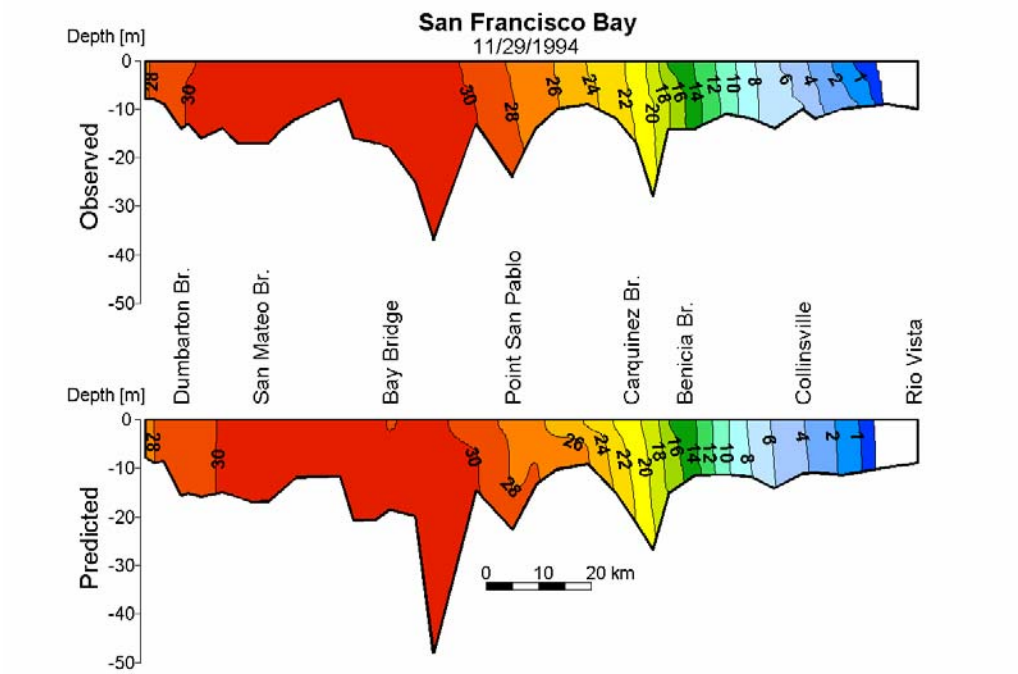

Figure H2.6.2-9 Observed and predicted salinity profiles at synoptic sampling station locations, interpolated along the axis of the San Francisco Estuary on November 29, 1994.

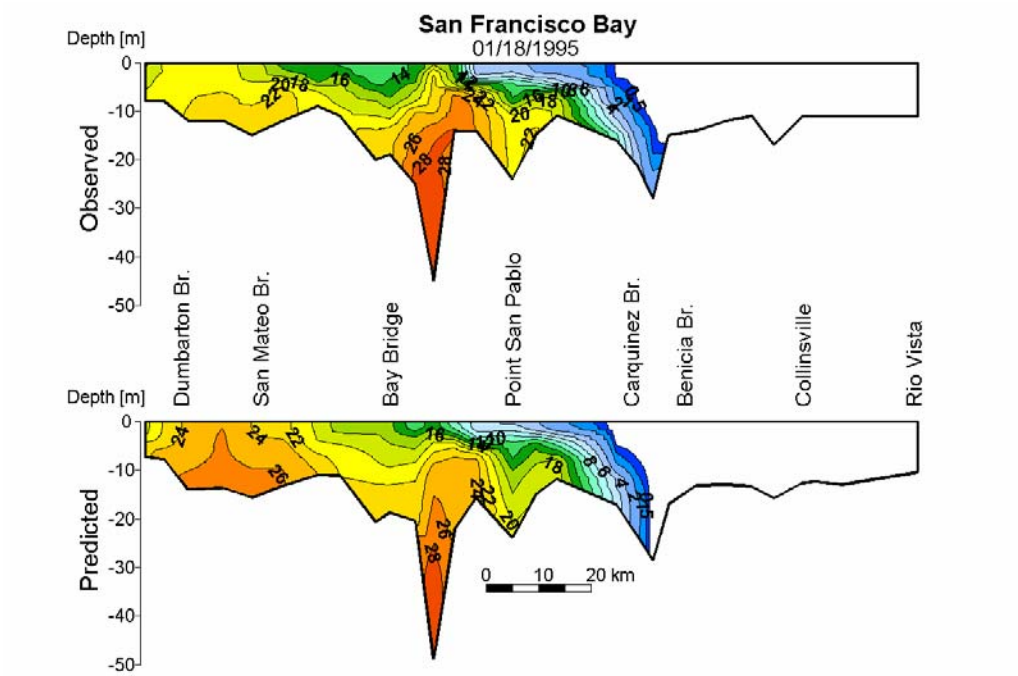

Figure H2.6.2-10 Observed and predicted salinity profiles at synoptic sampling station locations, interpolated along the axis of the San Francisco Estuary on January 18, 1995.

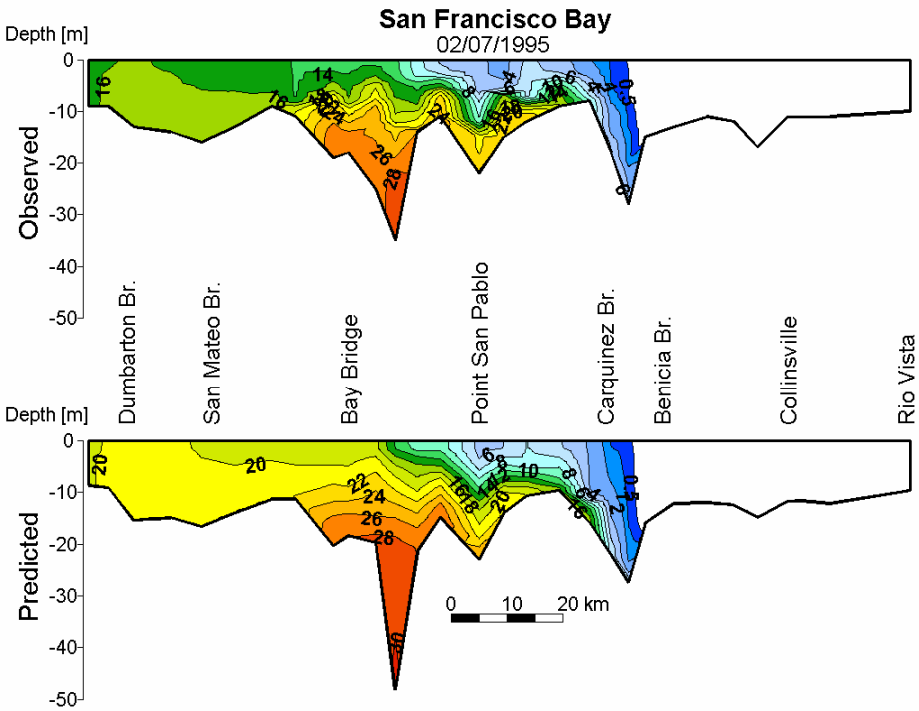

Figure H2.6.2-11 Observed and predicted salinity profiles at synoptic sampling station locations, interpolated along the axis of the San Francisco Estuary on February 7, 1995.

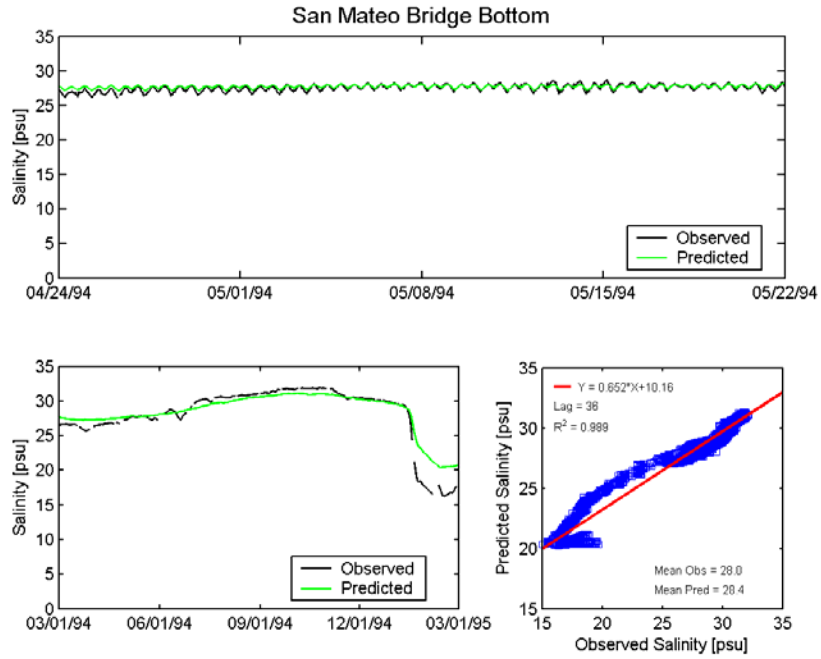

Figure H2.6.3-1 Observed and predicted salinity at the San Mateo Bridge bottom sensor.

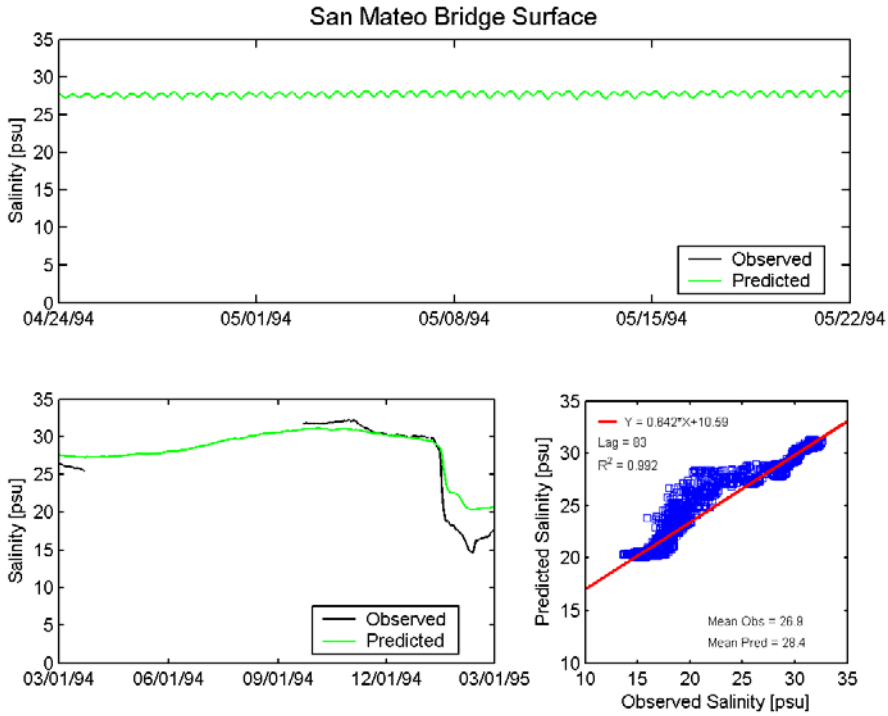

Figure H2.6.3-2 Observed and predicted salinity at the San Mateo Bridge top sensor.

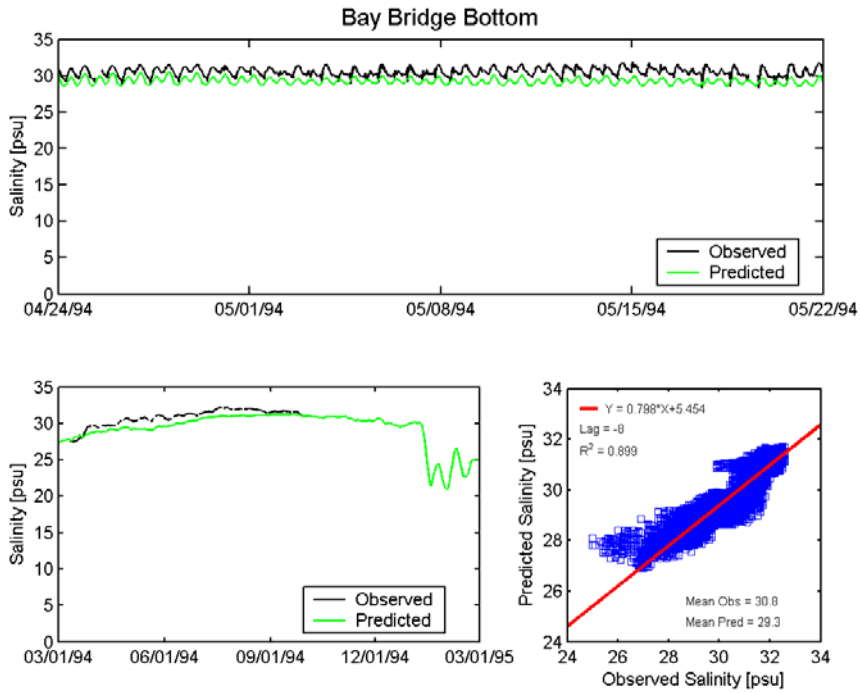

Figure H2.6.3-3 Observed and predicted salinity at the Oakland Bay Bridge bottom sensor.

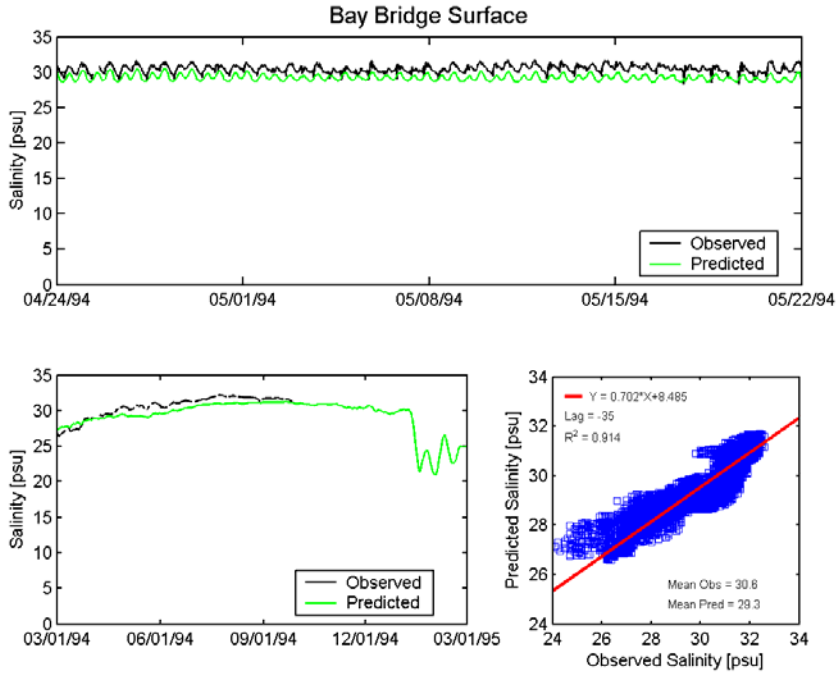

Figure H2.6.3-4 Observed and predicted salinity at the Oakland Bay Bridge top sensor.

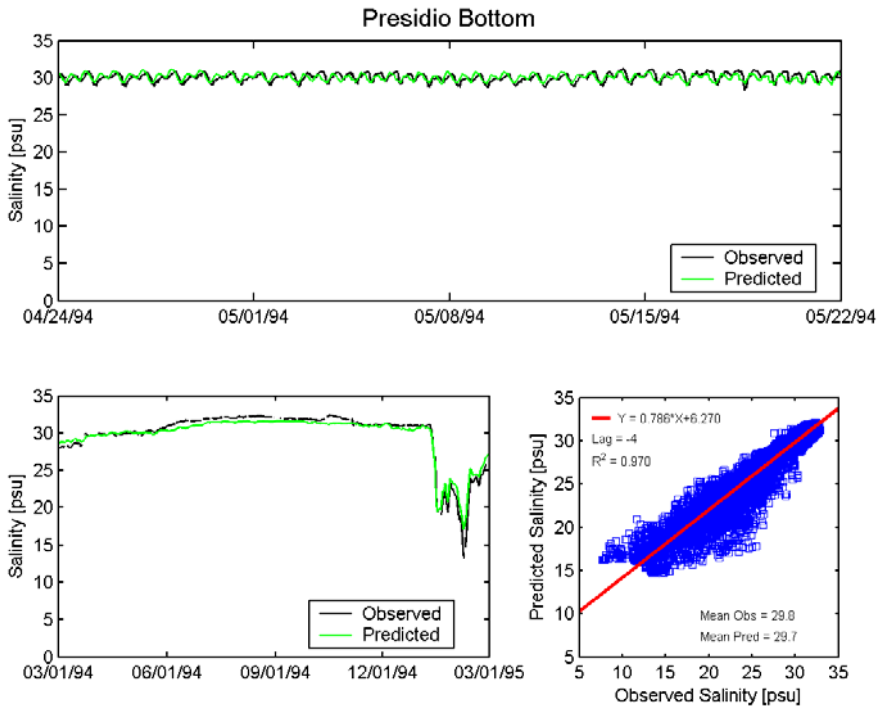

Figure H2.6.3-5 Observed and predicted salinity at the Presidio station.

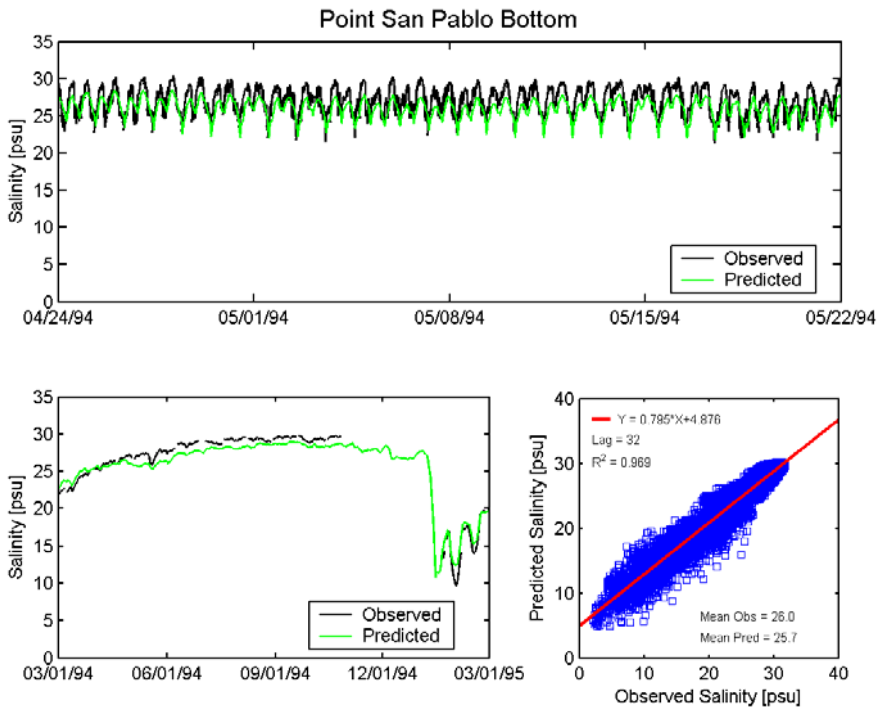

Figure H2.6.3-6 Observed and predicted salinity at the Point San Pablo bottom sensor.

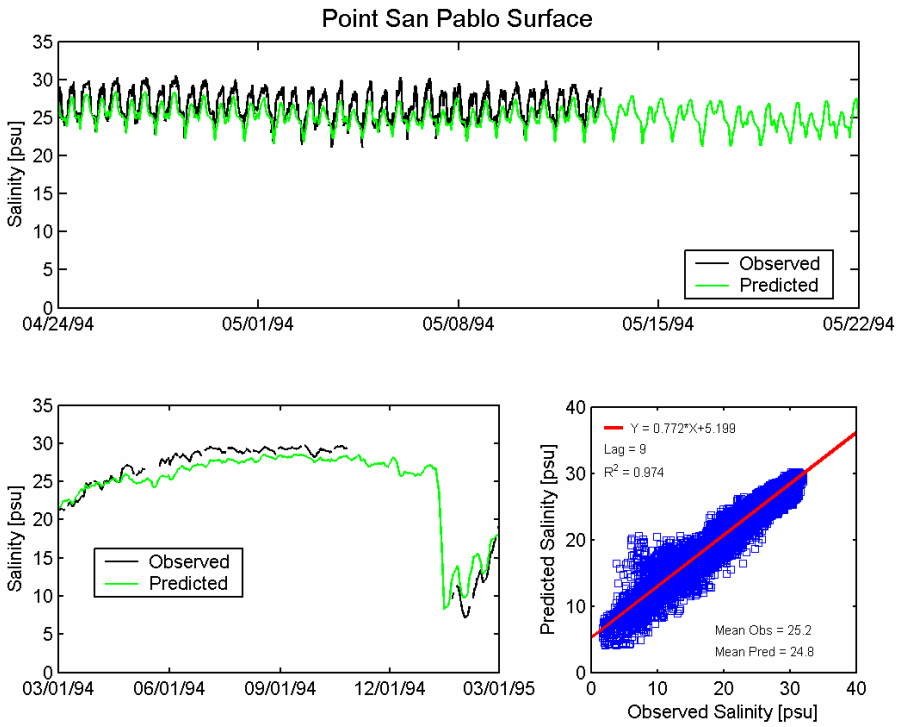

Figure H2.6.3-7 Observed and predicted salinity at the Point San Pablo top sensor.

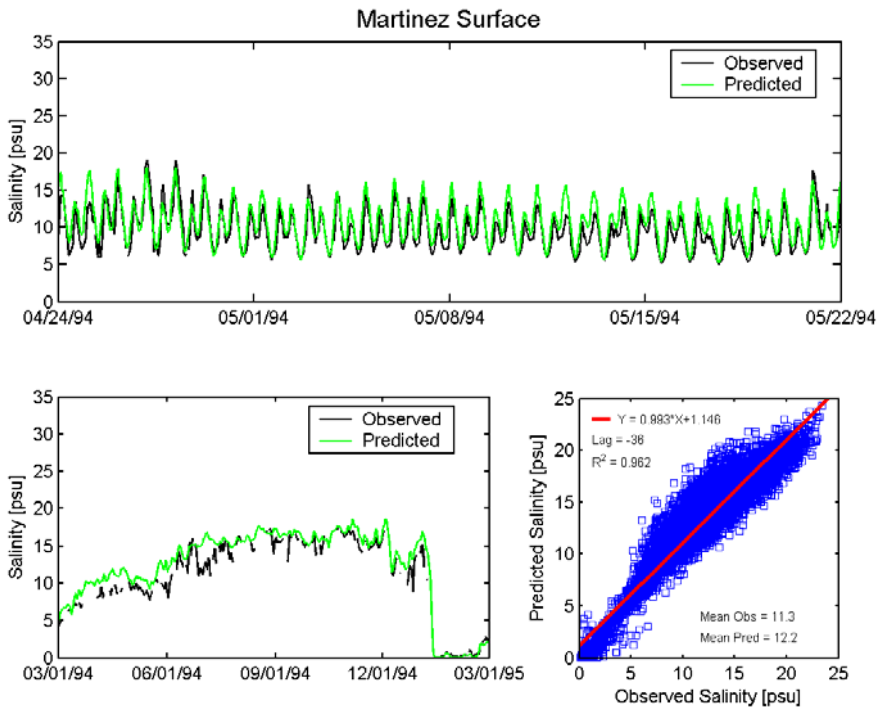

Figure H2.6.3-8 Observed and predicted salinity at the Martinez top sensor.

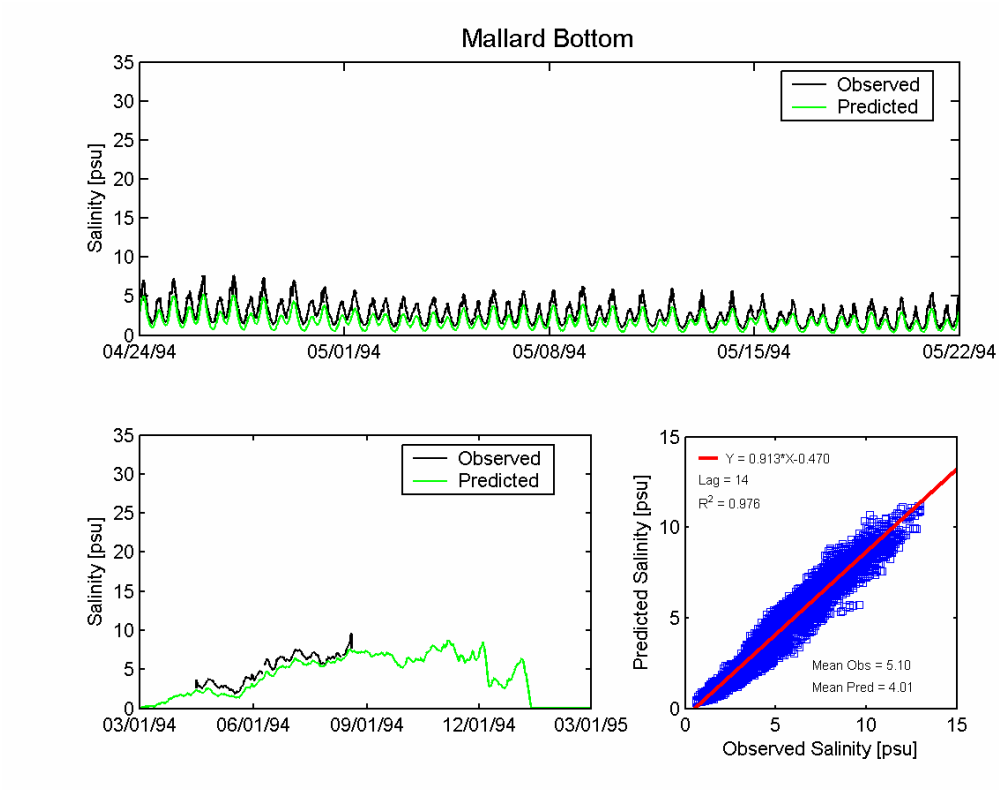

Figure H2.6.3-9 Observed and predicted salinity at the Mallard bottom sensor.

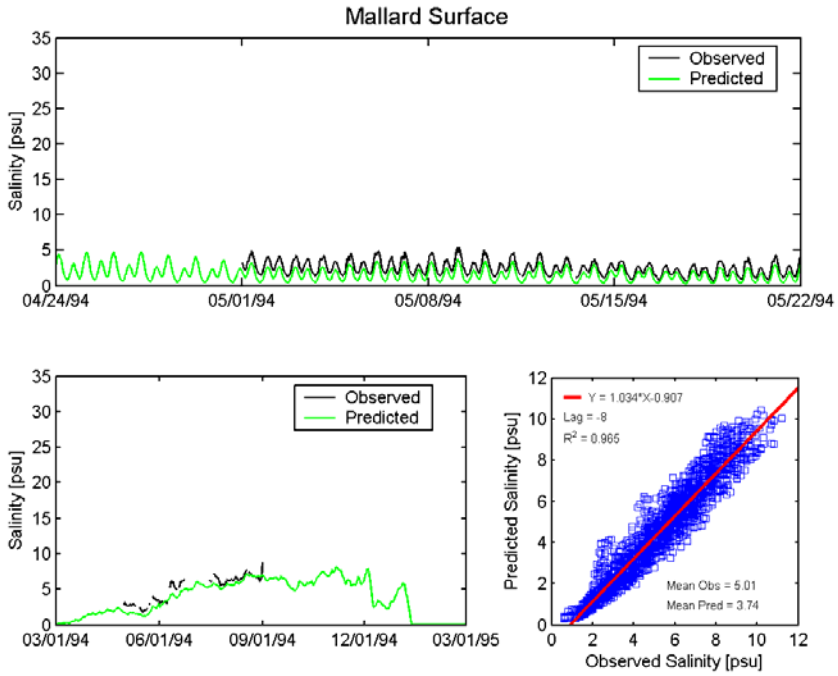

Figure H2.6.3-10 Observed and predicted salinity at the Mallard top sensor.

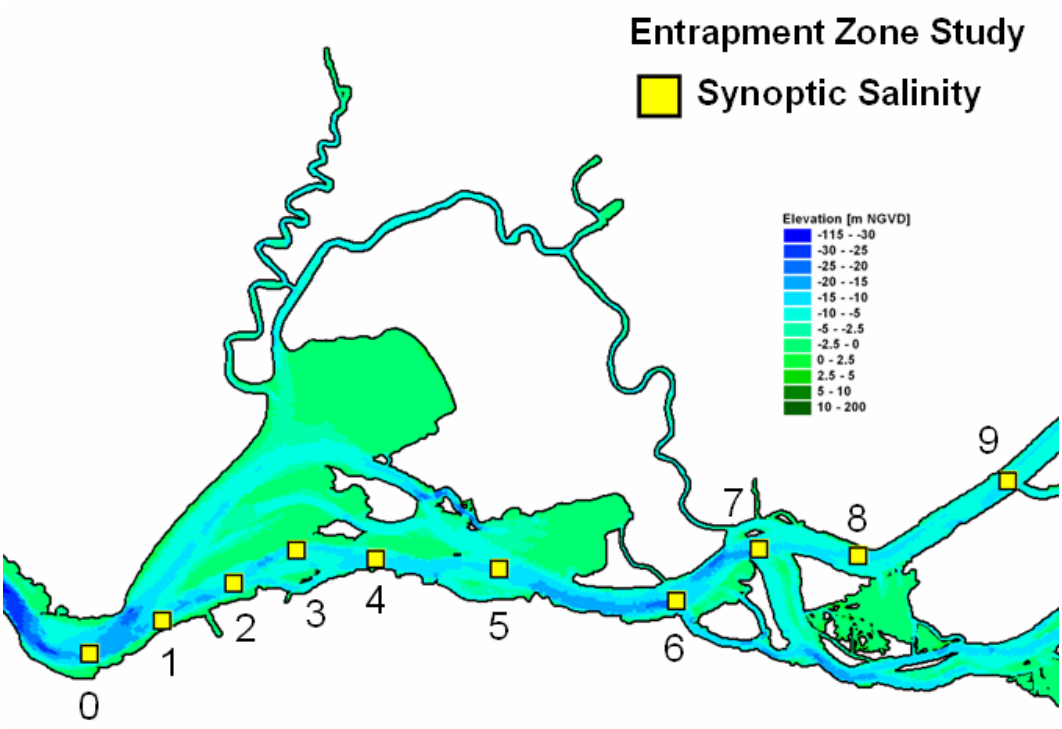

Figure H2.6.4-1 Entrapment Zone synoptic salinity sampling stations.

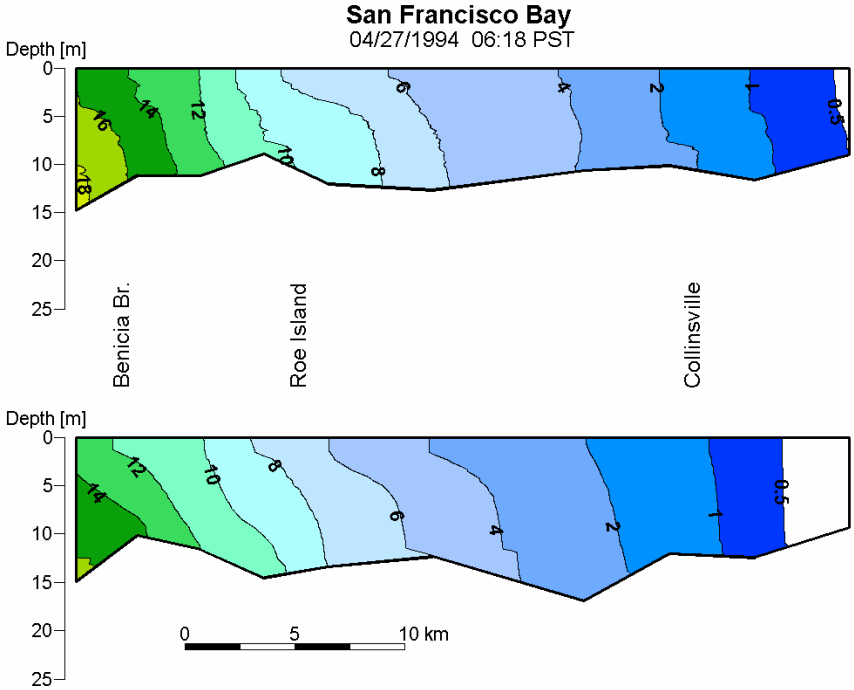

Figure H2.6.4-2 Observed and predicted salinity profiles at synoptic sampling stations for the Entrapment Zone Study, interpolated through Suisun Bay and the western Delta on April 27, 1994 at 6:18 am.

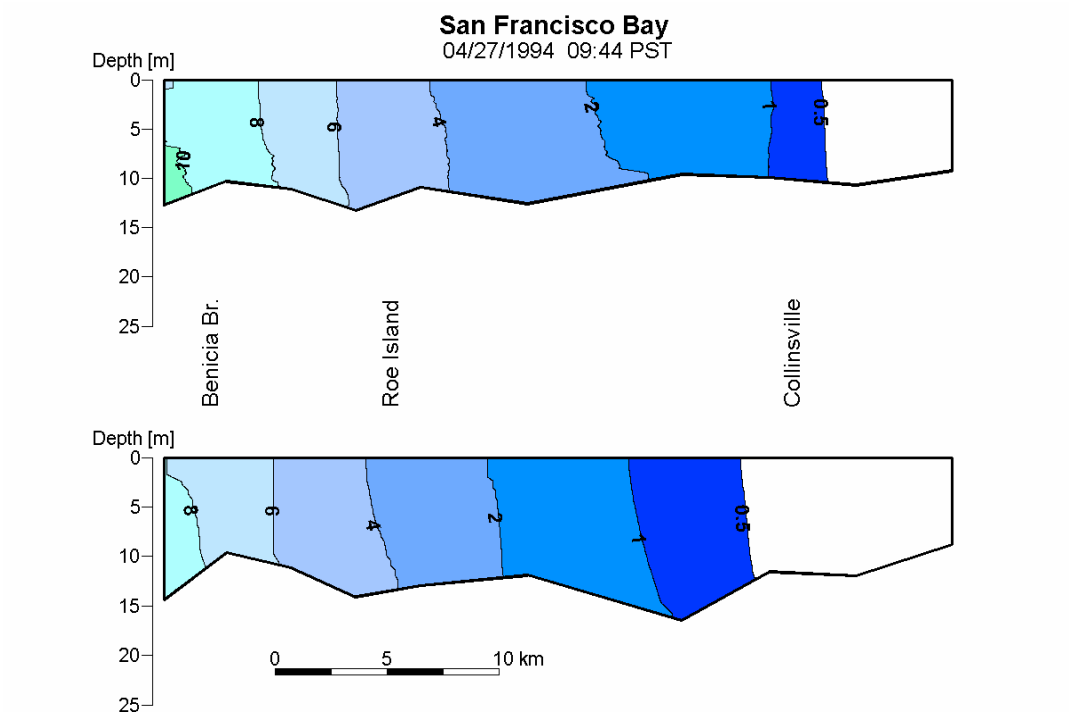

Figure H2.6.4-3 Observed and predicted salinity profiles at synoptic sampling stations for the Entrapment Zone Study, interpolated through Suisun Bay and the western Delta on April 27, 1994 at 9:44 am.

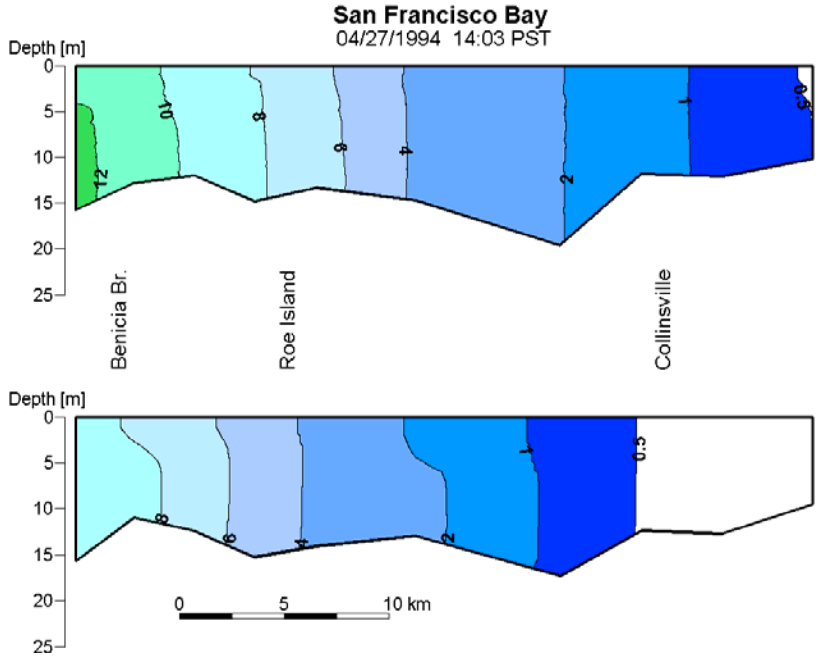

Figure H2.6.4-4 Observed and predicted salinity profiles at synoptic sampling stations for the Entrapment Zone Study, interpolated through Suisun Bay and the western Delta on April 27, 1994 at 2:03 pm.

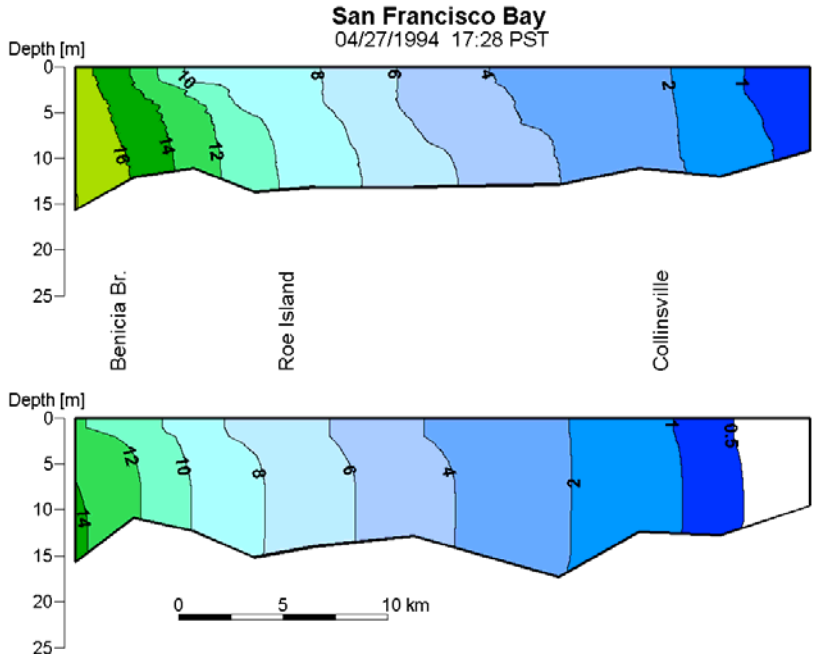

Figure H2.6.4-5 Observed and predicted salinity profiles at synoptic sampling stations for the Entrapment Zone Study, interpolated through Suisun Bay and the western Delta on April 27, 1994 at 5:28 pm.

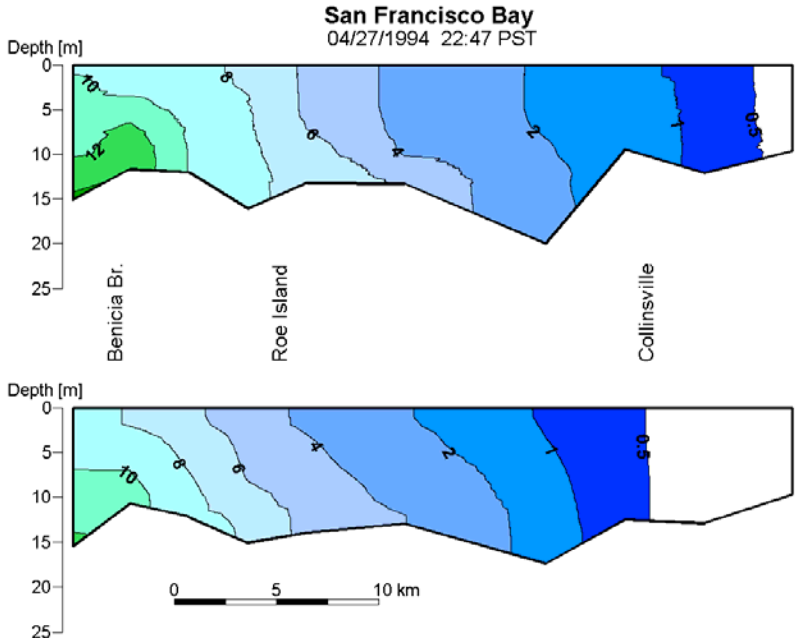

Figure H2.6.4-6 Observed and predicted salinity profiles at synoptic sampling stations for the Entrapment Zone Study, interpolated through Suisun Bay and the western Delta on April 27, 1994 at 10:47 pm.

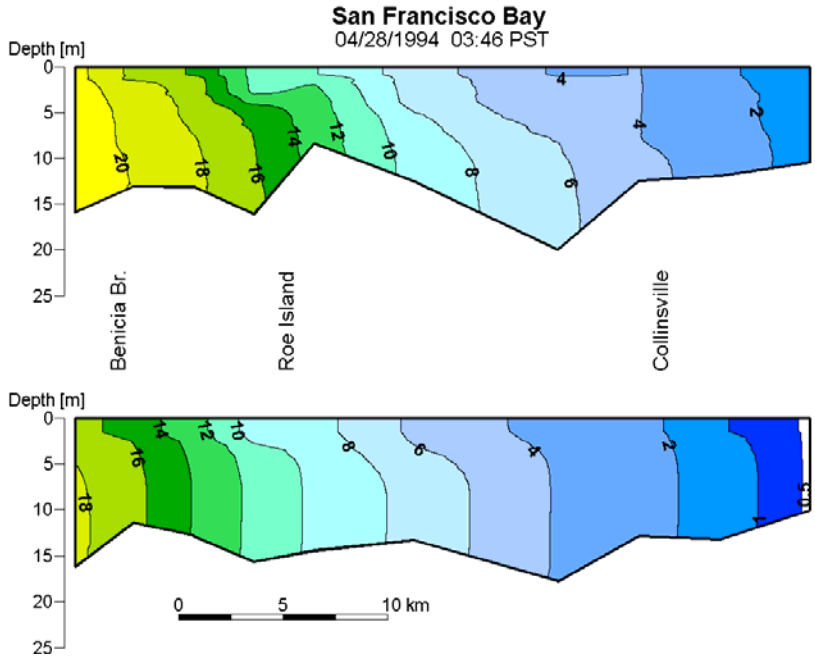

Figure H2.6.4-7 Observed and predicted salinity profiles at synoptic sampling stations for the Entrapment Zone Study, interpolated through Suisun Bay and the western Delta on April 28, 1994 at 3:46 am.

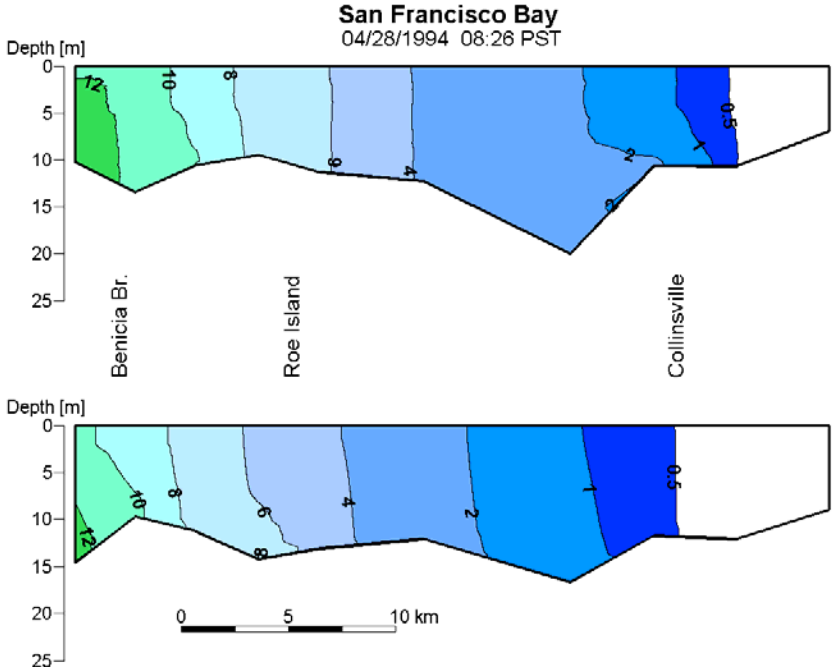

Figure H2.6.4-8 Observed and predicted salinity profiles at synoptic sampling stations for the Entrapment Zone Study, interpolated through Suisun Bay and the western Delta on April 28, 1994 at 8:26 am.

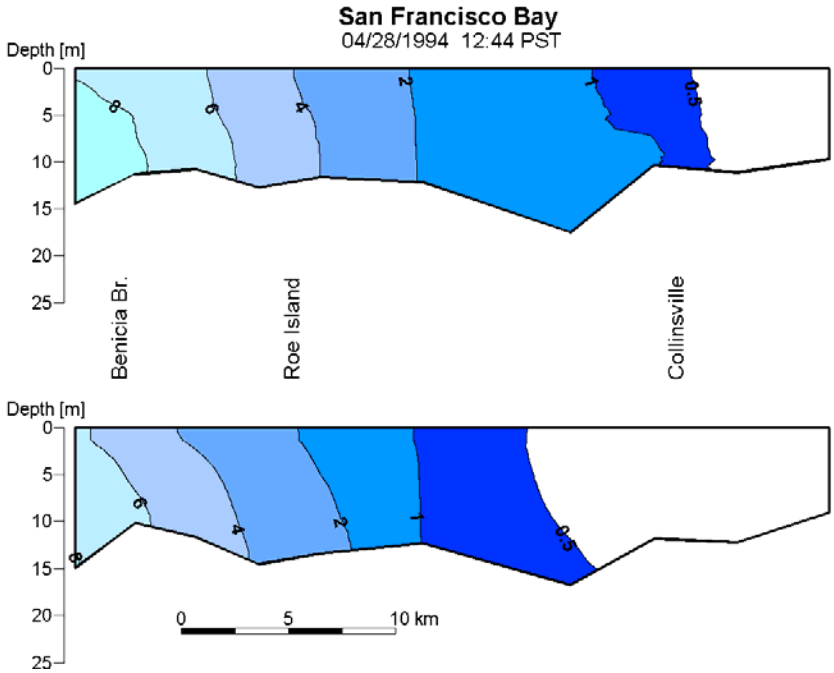

Figure H2.6.4-9 Observed and predicted salinity profiles at synoptic sampling stations for the Entrapment Zone Study, interpolated through Suisun Bay and the western Delta on April 28, 1994 at 12:44 pm.

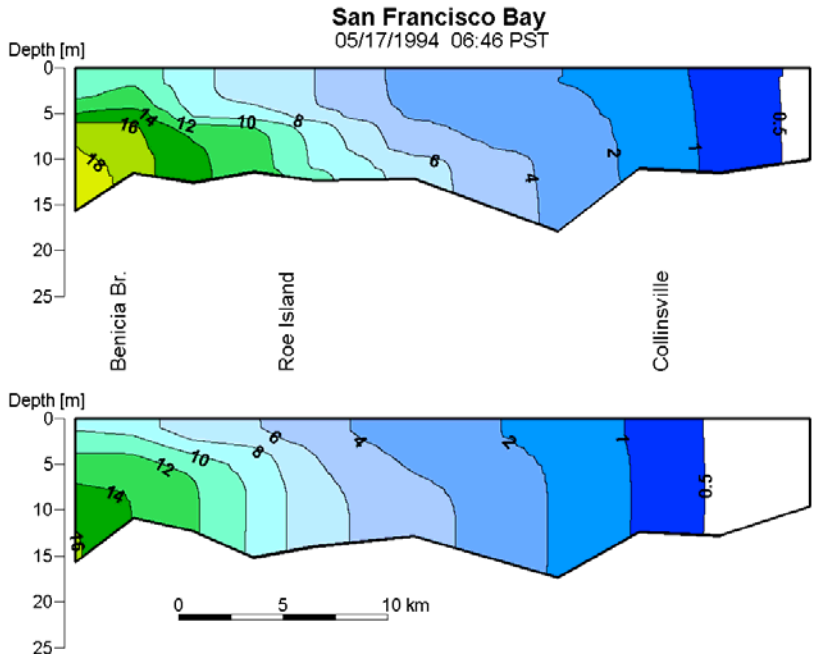

Figure H2.6.4-10 Observed and predicted salinity profiles at synoptic sampling stations for the Entrapment Zone Study, interpolated through Suisun Bay and the western Delta on May 17, 1994 at 6:46 am.

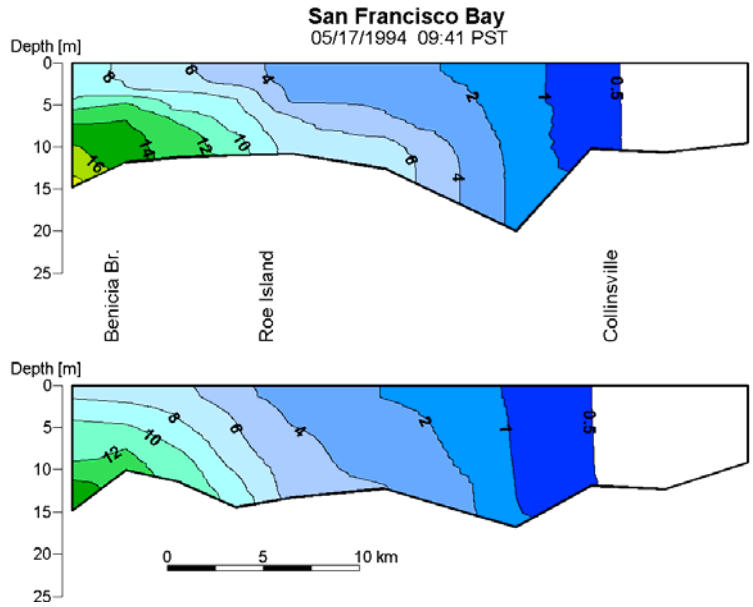

Figure H2.6.4-11 Observed and predicted salinity profiles at synoptic sampling stations for the Entrapment Zone Study, interpolated through Suisun Bay and the western Delta on May 17, 1994 at 9:41 am.

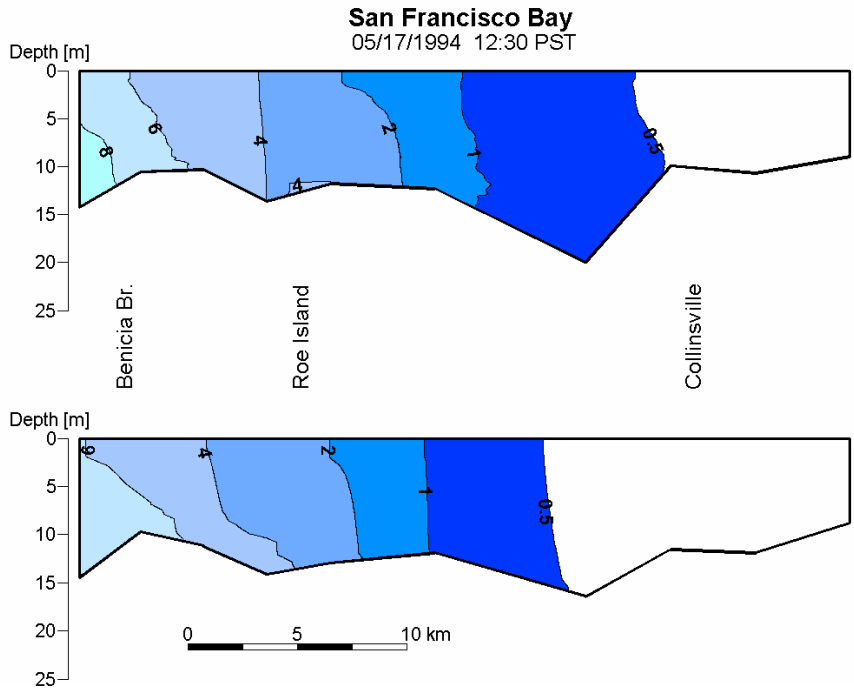

Figure H2.6.4-12 Observed and predicted salinity profiles at synoptic sampling stations for the Entrapment Zone Study, interpolated through Suisun Bay and the western Delta on May 17, 1994 at 12:30 pm.

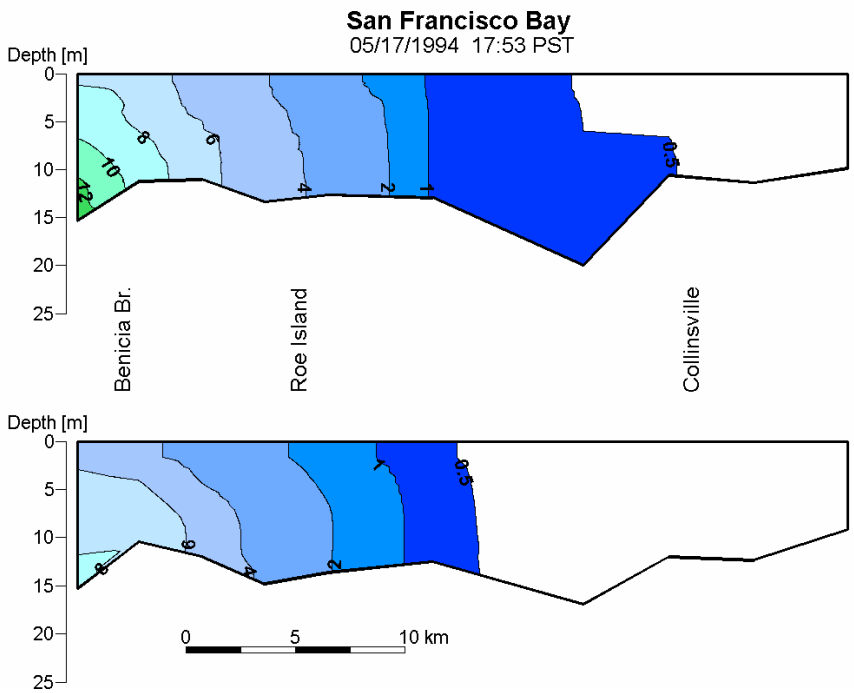

Figure H2.6.4-13 Observed and predicted salinity profiles at synoptic sampling stations for the Entrapment Zone Study, interpolated through Suisun Bay and the western Delta on May 17, 1994 at 5:53 pm.

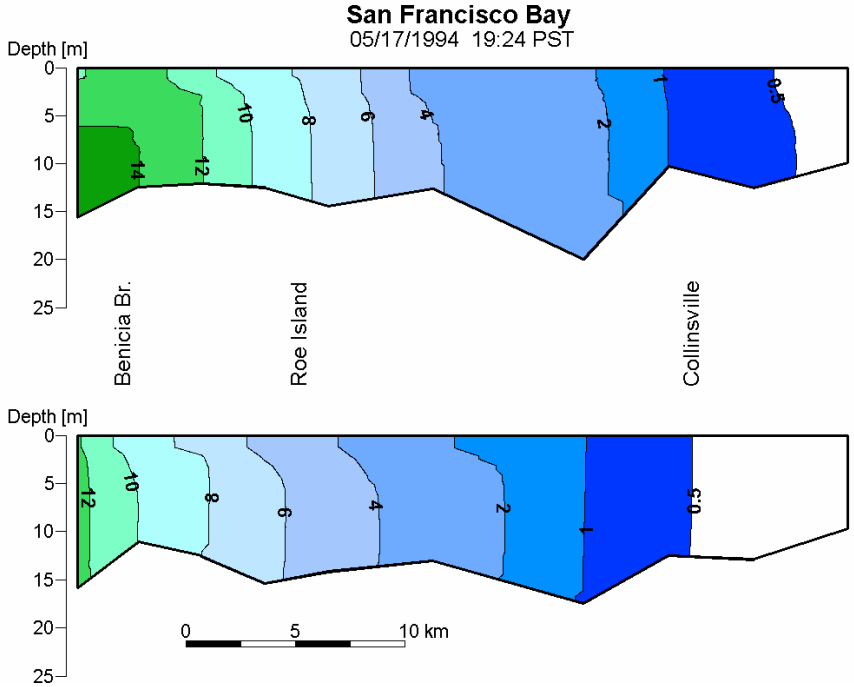

Figure H2.6.4-14 Observed and predicted salinity profiles at synoptic sampling stations for the Entrapment Zone Study, interpolated through Suisun Bay and the western Delta on May 17, 1994 at 7:24 pm.

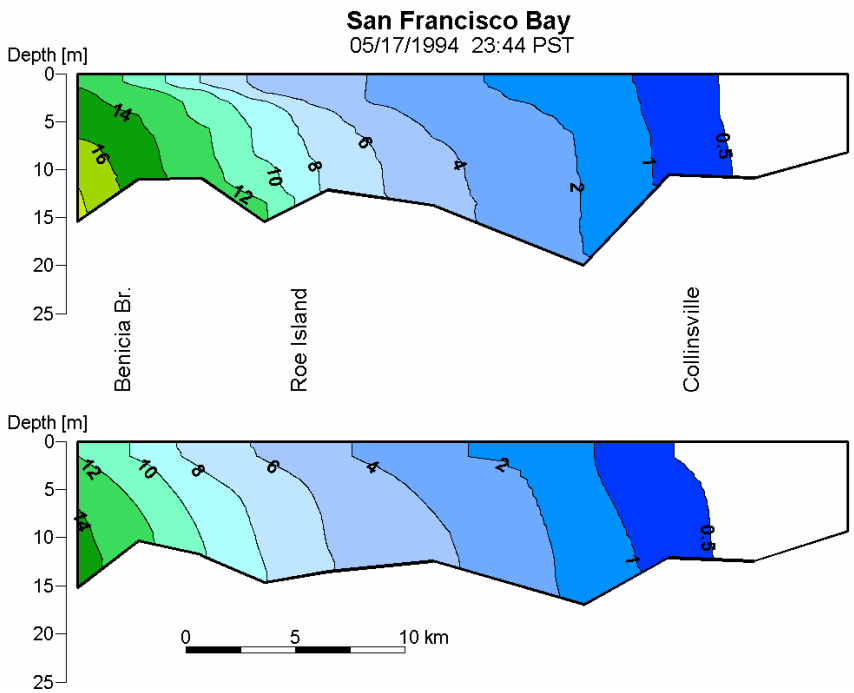

Figure H2.6.4-15 Observed and predicted salinity profiles at synoptic sampling stations for the Entrapment Zone Study, interpolated through Suisun Bay and the western Delta on May 17, 1994 at 11:44 pm.

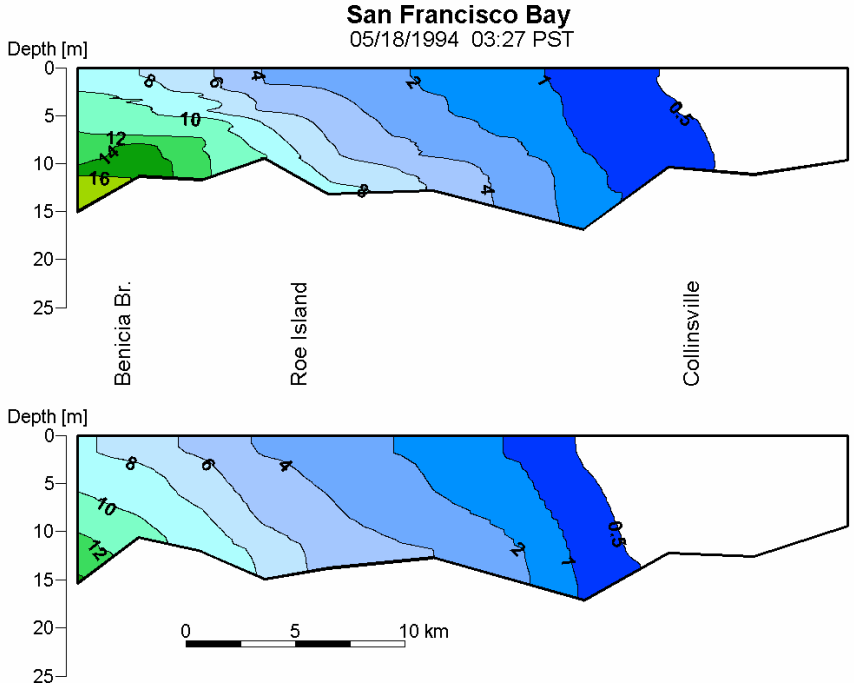

Figure H2.6.4-16 Observed and predicted salinity profiles at synoptic sampling stations for the Entrapment Zone Study, interpolated through Suisun Bay and the western Delta on May 17, 1994 at 3:27 am.

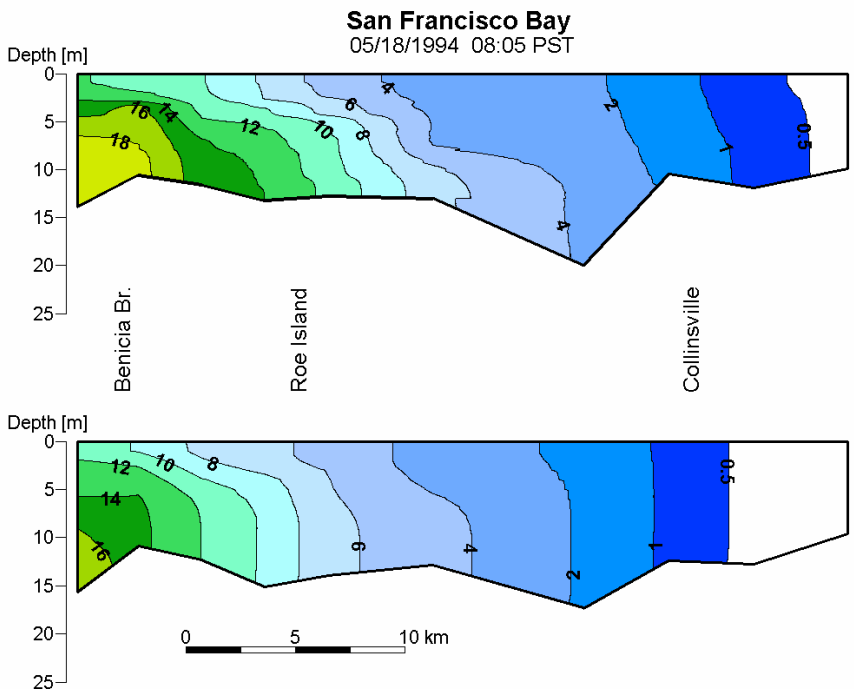

Figure H2.6.4-17 Observed and predicted salinity profiles at synoptic sampling stations for the Entrapment Zone Study, interpolated through Suisun Bay and the western Delta on May 18, 1994 at 8:05 am.

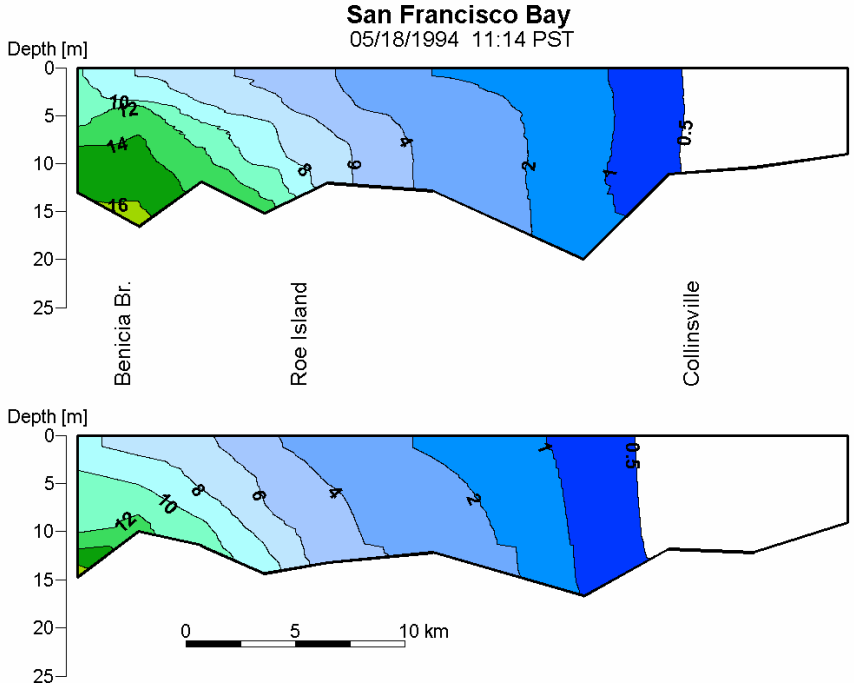

Figure H2.6.4-18 Observed and predicted salinity profiles at synoptic sampling stations for the Entrapment Zone Study, interpolated through Suisun Bay and the western Delta on May 18, 1994 at 11:14 am.

H2.7 Summary and Conclusions

The UnTRIM Bay-Delta Model has been successfully calibrated to reproduce observed tides, flows and salinity in the San Francisco Estuary. This three-dimensional unstructured grid model with over 600,000 active grid cells runs on a standard PC at roughly 10 times faster than real time. The good quality of the calibration depended largely on the development of an adequately resolved unstructured grid that meets orthogonality criteria and other numerical constraints, the incorporation of a sophisticated turbulence model, and proper representation of Delta inflows and exports.

The hydrodynamic calibration demonstrates that the model is accurately predicting water levels from the Golden Gate into the Sacramento-San Joaquin Delta. The detailed analysis of predicted flows in the Sacramento-San Joaquin Delta indicates very good agreement with the magnitude of observed flows over several orders of magnitude between stations and good agreement with flows in the western Delta and through Franks Tract.

The salinity calibration shows good agreement between predicted and observed salinities over a full year of time series comparisons. In addition, comparison of predicted and observed salinity profiles along the axis of San Francisco Bay and in Suisun Bay during the Entrapment Zone Study period demonstrates that the model is accurately predicting salinity distribution, stratification, and the extent of salinity intrusion into the western Delta through the full range of flow conditions experienced during the simulation year.

The UnTRIM model applications have already proven useful in understanding the role of stratification and baroclinic circulation in salt transport for historic conditions, levee failure scenarios and sea level rise scenarios. In addition, results from both TRIM and UnTRIM applications have been analyzed to develop parameterizations of dispersion that are used in a one-dimensional tidally-averaged model which can simulate a year of salinity conditions in roughly 1 minute of computational time. The simplified model is being applied in the risk-based framework to evaluate the consequences of thousands of Delta levee failure scenarios. In the next phase of the DRMS work the UnTRIM model and other hydrodynamic models will be applied to additional scenarios to evaluate measures to reduce the risks and impacts of levee failures.

H2.8 Acknowledgments

We wish to thank the Department of Water Resources for funding this work, John DeGeorge and Richard Rachiele of RMA for general collaboration on the DRMS project, Jon Burau and Greg Shellenbarger of the USGS for providing data, and Nicholas Nidzieko for contributions to manuscript preparation.

H2.9 References

Buchanan, P.A., Schoellhamer, D.H., and Sheipline, R.C., 1996. Summary of suspended-solids concentration data, Central and South San Francisco Bays, California, water year 1994: U.S. Geological Survey Open-File Report 95-776, 48 p.

Burau, J.R., Gartner, J.W., and Stacey, M., 1998. Results for the hydrodynamic element of the 1994 Entrapment Zone Study in Suisun Bay. In Report of the 1994 Entrapment Zone Study, edited by Wim Kimmerer, 13-53. Interagency Ecological Program for the San Francisco Bay/Delta Estuary.

[CDWR] California Department of Water Resources, 1986. DAYFLOW program documentation and data summary user's guide. California Department of Water Resources, Sacramento.

Casulli, V., 1990. Semi-implicit finite difference methods for the two-dimensional shallow water equations. *Journal of Computational Physics*. 86, 56-74.

Casulli, V. and Cheng, R.T., 1992. Semi-implicit finite difference methods for three-dimensional shallow water flow, *International Journal for Numerical Methods in Fluids*, 15, p. 629-648.

Casulli, V., and Cattani, E., 1994. Stability, accuracy and efficiency of a semi-implicit method for three-dimensional shallow water flow, *Computers and Mathematics with Applications*, 27(4), 99-112.

Casulli, V., 1999. A semi-implicit numerical method for non-hydrostatic free-surface flows on unstructured grid, in Numerical Modelling of Hydrodynamic Systems, ESF Workshop, pp. 175-193, Zaragoza, Spain.

Casulli, V. and R.A. Walters, 2000. An unstructured, three-dimensional model based on the shallow water equations, *International Journal for Numerical Methods in Fluids*, 32, 331-348.

Casulli, V. and Zanolli, P., 2002. Semi-Implicit Numerical Modelling of Non-Hydrostatic Free-Surface Flows for Environmental Problems, *Mathematical and Computer Modelling*, 36, 1,131-1,149.

Casulli, V. and Zanolli, P., 2005. High Resolution Methods for Multidimensional Advection- Diffusion Problems in Free-Surface Hydrodynamics, *Ocean Modelling*, 2005, 10, p.137-151.

Celebioglu, K., and Piasecki, M., 2006. Comparison of turbulence models with use of UnTRIM in the Delaware Bay, Proceedings of the Estuarine and Coastal Modeling Conference, ASCE, 2006.

Cheng, R.T., Casulli, V., and Gartner, J.W., 1993. Tidal residual intertidal mudflat (TRIM) model and its applications to San Francisco Bay, California. *Estuarine, Coastal and Shelf Science*, 369, 235-280.

Cheng, R. T. and Casulli, V., 1996. Modeling the Periodic Stratification and Gravitational

Circulation in San Francisco Bay, in Proceedings of 4th Inter. Conf. on Estuarine and Coastal Modeling, Spaulding and Cheng (Eds.), ASCE, San Diego, CA, October 1995, p.240-254.

Cheng, R T. and Smith, R.E., 1998. A Nowcast Model for Tides and Tidal Currents in San Francisco Bay, California, Ocean Community Conf. '98, Marine Technology Society, Baltimore, Nov. 15-19, p. 537-543.

Cheng, R. T., and Casulli, V., 2002. Evaluation of the UnTRIM model for 3-D Tidal Circulation, Proceedings of the 7th International Conference on Estuarine and Coastal Modeling, St. Petersburg, FL, November 2001, 628-642.

Dever, E.P., and Lentz, S.J., 1994. Heat and salt balances over the northern California shelf in winter and spring, Journal of Geophysical Research, 99(C8), 16,001-16,017. Edmunds, J.L., Cole, B.E., Cloern, J.E., Caffrey, J.M., and Jassby, A.D. (1995). Studies of the San Francisco Bay, California, Estuarine Ecosystem. Pilot Regional Monitoring Program Results, 1994: U.S. Geological Survey Open-File Report 95-378, 436 p.

Edmunds, J.L., Cole, B.E., Cloern, J.E., Caffrey, J.M., and Jassby, A.D., 1995. Studies of the San Francisco Bay, California, Estuarine Ecosystem. Pilot Regional Monitoring Program Results, 1994: U.S. Geological Survey Open-File Report 95-378, 436p.

Gross, E.S., Koseff, J.R., and Monismith, S.G., 1999. Three-dimensional salinity simulations of South San Francisco Bay. *Journal of Hydraulic Engineering*, 125 (11), 1199-1209.

Gross E.S., Schaaf and Wheeler, 2003. South Bay Salt Ponds Initial Stewardship Plan: South San Francisco Bay Hydrodynamic Model Results Report. Prepared for Cargill Salt.

Gross, E. S., M. L. MacWilliams and Kimmerer, W., 2006. Simulating Periodic Stratification in San Francisco Bay, Proceedings of the Estuarine and Coastal Modeling Conference, ASCE.

Kantha, L.H., Clayson, C.A., 1994. An *improved mixed layer model for geophysical applications, Journal* of Geophysical Research, 99, 25235–25266.

Lippert, C. and Sellerhoff, F., 2007. Efficient Generation of Unstructured Orthogonal Grids, The 7th Int. Conf. on Hydroscience and Engineering (ICHE-2006), Sep. 10 – Sep. 13, Philadelphia, USA.

Large, W., and Pond, S., 1981. Open ocean momentum flux measurements in moderate to strong winds. *Journal of Physical Oceanography*, 11, 324-336.

MacWilliams, M. L., and Cheng, R.T., 2007. Three-dimensional hydrodynamic modeling of San Pablo Bay on an unstructured grid, The 7th Int. Conf. on Hydroscience and Engineering (ICHE-2006), Sep. 10 – Sep. 13, Philadelphia, USA.

Oltmann, R.N., 1998. Indirect measurement of Delta outflow using ultrasonic velocity meters and comparison with mass-balance calculated outflow. Interagency Ecological Program for the Sacramento-San Joaquin Estuary, 11(1).

[RMA] Resource Management Associates, 2005. Flooded Islands Pre-Feasibility Study: RMA Delta Model Calibration Report, prepared for CA Department of Water Resources for submittal to California Bay-Delta Authority, June 30.

Smith, R. E., Foxgrover, A., and Smith, P.E., 2003. Suisun Bay & Delta Bathymetry: Production of a 10-meter Grid, http://sfbay.wr.usgs.gov/access/Bathy/Delta, Second Biennial CALFED Science Conference: Advances in Science and Restoration in the Bay, Delta and Watershed, Sacramento, California, January 14-16.

Umlauf, L., Burchard, H., 2003. A generic length-scale equation for geophysical turbulence models. *Journal of Marine Research*, 61, 235–265.

Appendix H3
Three-Dimensional Salinity Simulations of Sea Level Rise Scenarios

Delta Risk Management Strategy
Three-Dimensional Salinity Simulations of Sea Level Rise Scenarios

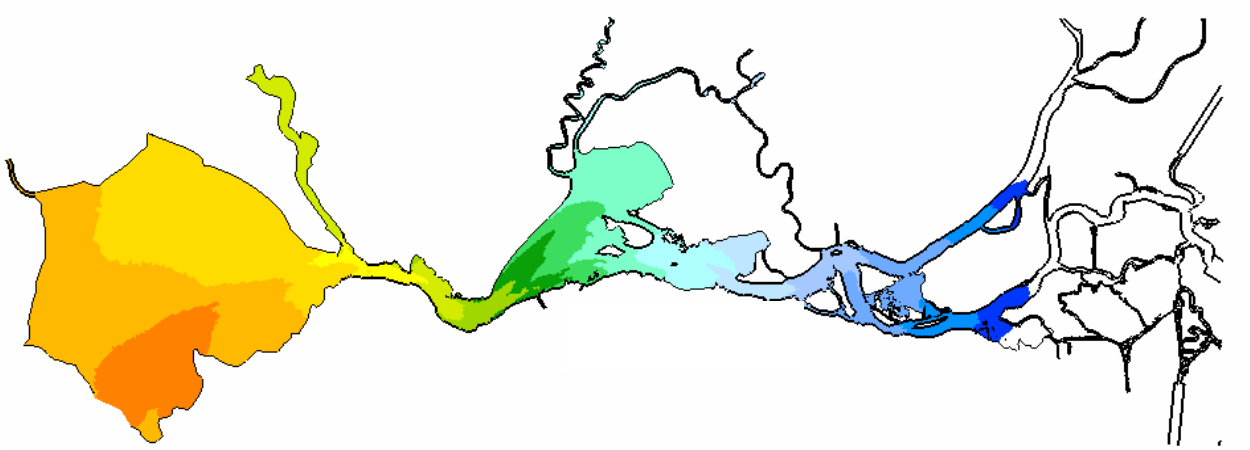

Prepared For:

California Department of Water Resources

March 31, 2007

Prepared By:

Dr. Edward S. Gross

Environmental Consultant

Dr. Michael L. MacWilliams

Environmental Consultant

Nicholas Nidzieko

Environmental Consultant

Table of Contents

Executive Summary **H3-1**
H3.1 Introduction **H3-3**
H3.2 UnTRIM Model Description **H3-5**
H3.3 Analysis of Dispersion Processes **H3-5**
H3.4 Sea Level Rise Scenario Descriptions **H3-8**
H3.5 Sea Level Rise Scenario Simulation Results **H3-11**
H3.6 Cumulative Effects of Sea Level Rise **H3-30**
H3.7 Effect of Sea Level Rise on Dispersive Transport **H3-49**
H3.7.1 Central San Francisco Bay Cross-Sections H3-54
H3.7.2 San Pablo Bay Cross-Sections H3-60
H3.7.3 Carquinez Strait Cross-Sections H3-65
H3.7.4 Suisun Bay Cross-Sections H3-72
H3.7.5 Western Delta Cross-Sections H3-81
H3.7.6 Summary of Dispersion Coefficient Estimates H3-87
H3.7.7 Uncertainty of Dispersion Coefficient Estimates H3-88
H3.8 Discussion **H3-91**
H3.9 Acknowledgements **H3-93**
H3.10 References **H3-93**

Tables

H3-1 Names and Mean Sea Level Increase ror Each Simulation Scenario

H3-2 X2 location for MSL rise scenarios and estimates of additional Net Delta Outflow that would be required to return X2 to the value calculated for the Baseline scenario, based upon published regression equations for the estimation of X2

H3-3 X2 Location for Baseline Scenario, 140 cm MSL Rise Scenario and the Two Cumulative Effects Scenarios

H3-4 Results of parameterization of the effects of sea level rise on dispersive transport for use in WAM. The values listed are the slopes and intercepts of best fit lines for the variability of dispersion coefficients with Mean Sea Level rise

Figures

H3.3-1 Cross-sections used in salt flux analysis

H3.3-2 Centerline transect with labeled distance from Golden Gate

H3.4-1 The 20 breach locations for the Perforated Sherman Island scenario

H3.5-1 Predicted advective, dispersive and net (tidally-averaged) salt fluxes during the last day of the baseline scenario

H3.5-2 Depth-averaged and tidally-averaged salinity at tidally-averaged steady state conditions for the Baseline scenario

H3.5-3 Depth-averaged and tidally-averaged salinity at tidally-averaged steady state conditions for the 20 cm MSL Rise scenario and increase in salinity relative to the Baseline scenario

H3.5-4 Depth-averaged and tidally-averaged salinity at tidally-averaged steady state conditions for the 50 cm MSL Rise scenario and increase in salinity relative to the Baseline scenario

H3.5-5 Depth-averaged and tidally-averaged salinity at tidally-averaged steady state conditions for the 90 cm MSL Rise and increase in salinity relative to the Baseline scenario

H3.5-6 Depth-averaged and tidally-averaged salinity at tidally-averaged steady state conditions for the 140 cm MSL Rise scenario and increase in salinity relative to the Baseline scenario

H3.5-7 The two channel centerline transects used for output of salinity data

H3.5-8 Tidally-averaged salinity along the centerline transect from the Golden Gate to Rio Vista at tidally-averaged steady state conditions for the Baseline scenario

H3.5-9 Tidally-averaged salinity along the centerline transect from Martinez to Prisoners Point at tidally-averaged steady state conditions for the Baseline scenario

H3.5-10 Tidally-averaged salinity along the centerline transect from Golden Gate to Rio Vista at tidally-averaged steady state conditions for the 20 cm MSL Rise scenario

H3.5-11 Tidally-averaged salinity along the centerline transect from Martinez to Prisoners Point at tidally-averaged steady state conditions for the 20 cm MSL Rise scenario

H3.5-12 Tidally-averaged salinity along the centerline transect from Golden Gate to Rio Vista at tidally-averaged steady state conditions for the 50 cm MSL Rise scenario

H3.5-13 Tidally-averaged salinity along the centerline transect from Martinez to Prisoners Point at tidally-averaged steady state conditions for the 50 cm MSL Rise scenario

H3.5-14 Tidally-averaged salinity along the centerline transect from Golden Gate to Rio Vista at tidally-averaged steady state conditions for the 90 cm MSL Rise scenario

H3.5-15 Tidally-averaged salinity along the centerline transect from Martinez to Prisoners Point at tidally-averaged steady state conditions for the 90 cm MSL Rise scenario

H3.5-16 Tidally-averaged salinity along the centerline transect from Golden Gate to Rio Vista at tidally-averaged steady state conditions for the 140 cm MSL Rise scenario

H3.5-17 Tidally-averaged salinity along the centerline transect from Martinez to Prisoners Point at tidally-averaged steady state conditions for the 140 cm MSL Rise scenario

H3.5-18 Locations used to compare tidal variability of salinity among scenarios

H3.5-19 Depth-averaged salinity at Martinez during the last day of each MSL rise scenario simulation

H3.5-20 Depth-averaged salinity at Antioch during the last day of each MSL rise scenario simulation

H3.5-21 Depth-averaged salinity at Jersey Point during the last day of each MSL rise scenario simulation

H3.5-22 Depth-averaged salinity at Emmaton during the last day of each MSL rise scenario simulation

H3.6-1 Predicted advective, dispersive and net (tidally-averaged) salt fluxes during the last day of the Baseline scenario

H3.6-2 Depth-averaged and tidally-averaged salinity at tidally-averaged steady state conditions for the Baseline scenario

H3.6-3 Depth-averaged and tidally-averaged salinity at tidally-averaged steady state conditions for the 140 cm MSL Rise scenario and increase in salinity relative to the Baseline scenario

H3.6-4 Depth-averaged and tidally-averaged salinity at tidally-averaged steady state conditions for the Perforated Sherman Island scenario and increase in salinity relative to the Baseline scenario

H3.6-5 Difference in depth-averaged and tidally-averaged salinity at tidally-averaged steady state conditions between the Perforated Sherman Island scenario and the 140 cm MSL Rise scenario

H3.6-6 Depth-averaged and tidally-averaged salinity at tidally-averaged steady state conditions for the Amplified Tides scenario and increase in salinity relative to the Baseline scenario

H3.6-7 Difference in depth-averaged and tidally-averaged salinity at tidally-averaged steady state conditions between the Amplified Tides scenario and the 140 cm MSL Rise scenario

H3.6-8 The two channel centerline transects used for output of salinity data

H3.6-9 Tidally-averaged salinity along the centerline transect from Golden Gate to Rio Vista at tidally-averaged steady state conditions for the Baseline scenario

H3.6-10 Tidally-averaged salinity along the centerline transect from Martinez to Prisoners Point at tidally-averaged steady state conditions for the Baseline scenario

H3.6-11 Tidally-averaged salinity along the centerline transect from Golden Gate to Rio Vista at tidally-averaged steady state conditions for the 140 cm MSL Rise scenario

H3.6-12 Tidally-averaged salinity along the centerline transect from Martinez to Prisoners Point at tidally-averaged steady state conditions for the 140 cm MSL Rise scenario

H3.6-13 Tidally-averaged salinity along the centerline transect from Golden Gate to Rio Vista at tidally-averaged steady state conditions for the Perforated Sherman Island scenario

H3.6-14 Tidally-averaged salinity along the centerline transect from Martinez to Prisoners Point at tidally-averaged steady state conditions for the Perforated Sherman Island scenario

H3.6-15 Tidally-averaged salinity along the centerline transect from Golden Gate to Rio Vista at tidally-averaged steady state conditions for the Amplified Tides scenario

H3.6-16 Tidally-averaged salinity along the centerline transect from Martinez to Prisoners Point at tidally-averaged steady state conditions for the Amplified Tides scenario

H3.6-17 Locations used to compare tidal variability of salinity among scenarios

H3.6-18 Depth-averaged salinity at Martinez during the last day of each cumulative effects scenario simulation

H3.6-19 Depth-averaged salinity at Antioch during the last day of each cumulative effects scenario simulation

H3.6-20 Depth-averaged salinity at Jersey Point during the last day of each cumulative effects scenario simulation

H3.6-21 Depth-averaged salinity at Emmaton during the last day of each cumulative effects scenario simulation

H3.7-1 Estimated root mean square depth-averaged velocity for all MSL rise scenarios. The horizontal scale is distance along the axis of the estuary from the Golden Gate

H3.7-2 Estimated depth-averaged salinity gradient for all MSL rise scenarios. The horizontal scale is distance along the axis of the estuary from the Golden Gate

H3.7-3 Estimated dispersion coefficients for all MSL rise scenarios. The horizontal scale is distance along the axis of the estuary from the Golden Gate

H3.7-4 Estimated dispersion coefficients associated with gravitational circulation for all MSL rise scenarios. The horizontal scale is distance along the axis of the estuary from the Golden Gate

H3.7-5 Estimated dispersion coefficients associated with “unsteady vertical shear” for all MSL rise scenarios. The horizontal scale is distance along the axis of the estuary from the Golden Gate

H3.7-6 Estimated dispersion coefficients associated with tidal dispersion for all MSL rise scenarios. The horizontal scale is distance along the axis of the estuary from the Golden Gate

H3.7.1-1 Dispersion coefficients and dispersion coefficient components calculated for each MSL rise scenario at cross-section 1, located at the Golden Gate

H3.7.1-2 Total and three-dimensional dispersion coefficients calculated for each MSL rise scenario at cross-section 1, located at the Golden Gate. A best fit equation and r^2 value is shown for each set of coefficients

H3.7.1-3 Dispersion coefficients and dispersion coefficient components calculated for each MSL rise scenario at cross-section 2, extending from San Francisco to Tiburon

H3.7.1-4 Total and three-dimensional dispersion coefficients calculated for each MSL rise scenario at cross-section 2, extending from San Francisco to Tiburon. A best fit equation and r^2 value is shown for each set of coefficients

H3.7.1-5 Dispersion coefficients and dispersion coefficient components calculated for each MSL rise scenario cross-section 3, extending from Point Richmond to Bluff Point

H3.7.1-6 Total and three-dimensional dispersion coefficients calculated for each MSL rise scenario at cross-section 3, extending from Point Richmond to Bluff Point. A best fit equation and r^2 value is shown for each set of coefficients

H3.7.1-7 Dispersion coefficients and dispersion coefficient components calculated for each MSL rise scenario at cross-section 4, at the Richmond-San Rafael Bridge

H3.7.1-8 Total and three-dimensional dispersion coefficients calculated for each MSL rise scenario at cross-section 4, at the Richmond-San Rafael Bridge. A best fit equation and r^2 value is shown for each set of coefficients

H3.7.1-9 Dispersion coefficients and dispersion coefficient components calculated for each MSL rise scenario at cross-section 5, extending from Point San Pablo to Point San Pedro

H3.7.1-10 Total and three-dimensional dispersion coefficients calculated for each MSL rise scenario at cross-section 5, extending from Point San Pablo to Point San Pedro. A best fit equation and r^2 value is shown for each set of coefficients

H3.7.2-1 Dispersion coefficients and dispersion coefficient components calculated for each MSL rise scenario at section 6, extending from San Pablo to Point San Pedro

H3.7.2-2 Total and three-dimensional dispersion coefficients calculated for each MSL rise scenario at cross-section 6, extending from San Pablo to Point San Pedro. A best fit equation and r^2 value is shown for each set of coefficients

H3.7.2-3. Dispersion coefficients and dispersion coefficient components calculated for each MSL rise scenario at cross-section 7, extending from Pinole Point to Sonoma Creek

H3.7.2-4 Total and three-dimensional dispersion coefficients calculated for each MSL rise scenario at cross-section 7, extending from Pinole Point to Sonoma Creek. A best fit equation and r^2 value is shown for each set of coefficients

H3.7.2-5 Dispersion coefficients and dispersion coefficient components calculated for each MSL rise scenario at cross-section 8, extending from Wilson Point to Mare Island

H3.7.2-6 Total and three-dimensional dispersion coefficients calculated for each MSL rise scenario at cross-section 8, extending from Wilson Point to Mare Island. A best fit equation and r^2 value is shown for each set of coefficients.

H3.7.2-7 Dispersion coefficients and dispersion coefficient components calculated for each MSL rise scenario at cross-section 9, extending from Davis Point to Mare Island

H3.7.2-8 Total and three-dimensional dispersion coefficients calculated for each MSL rise scenario at cross-section 9, extending from Davis Point to Mare Island. A best fit equation and r^2 value is shown for each set of coefficients.

H3.7.3-1 Dispersion coefficients and dispersion coefficient components calculated for each MSL rise scenario at cross-section 10, extending from Davis Point to Mare Island Straight

H3.7.3-2 Total and three-dimensional dispersion coefficients calculated for each MSL rise scenario at cross-section 10, extending from Davis Point to Mare Island Straight. A best fit equation and r^2 value is shown for each set of coefficients

H3.7.3-3 Dispersion coefficients and dispersion coefficient components calculated for each MSL rise scenario at cross-section 11, at the Carquinez Bridge

H3.7.3-4 Total and three-dimensional dispersion coefficients calculated for each MSL rise scenario at cross-section 11, at the Carquinez Bridge. A best fit equation and r^2 value is shown for each set of coefficients

H3.7.3-5 Estimated dispersion coefficients at cross-section 12, extending from Crockett to Dillon Point, as a function of MSL rise

H3.7.3-6 Total and three-dimensional dispersion coefficients calculated for each MSL rise scenario at cross-section 12, extending from Crockett to Dillon Point. A best fit equation and r^2 value is shown for each set of coefficients

H3.7.3-7 Dispersion coefficients and dispersion coefficient components calculated for each MSL rise scenario at cross-section 13, extending from Ozol to Benicia Point

H3.7.3-8 Total and three-dimensional dispersion coefficients calculated for each MSL rise scenario at cross-section 13, extending from Ozol to Benicia Point. A best fit equation and r^2 value is shown for each set of coefficients

H3.7.3-9 Dispersion coefficients and dispersion coefficient components calculated for each MSL rise scenario at cross-section 14, extending from Martinez to Benicia

H3.7.3-10 Total and three-dimensional dispersion coefficients calculated for each MSL rise scenario at cross-section 14, extending from Martinez to Benicia. A best fit equation and r^2 value is shown for each set of coefficients

H3.7.3-11 Dispersion coefficients and dispersion coefficient components calculated for each MSL rise scenario at cross-section 15, at the Benicia Bridge, as a function of MSL rise

H3.7.3-12 Total and three-dimensional dispersion coefficients calculated for each MSL rise scenario at cross-section 15, at the Benicia Bridge. A best fit equation and r^2 value is shown for each set of coefficients

H3.7.4-1 Dispersion coefficients and dispersion coefficient components calculated for each MSL rise scenario at cross-section 16, from Pacheco Creek to the Mothball Fleet

H3.7.4-2 Total and three-dimensional dispersion coefficients calculated for each MSL rise scenario at cross-section 16, from Pacheco Creek to the Mothball Fleet. A best fit equation and r^2 value is shown for each set of coefficients

H3.7.4-3 Dispersion coefficients and dispersion coefficient components calculated for each MSL rise scenario at cross-section 17, east of the Mothball Fleet

H3.7.4-4 Total and three-dimensional dispersion coefficients calculated for each MSL rise scenario at cross-section 17, east of the Mothball Fleet. A best fit equation and r^2 value is shown for each set of coefficients

H3.7.4-5 Dispersion coefficients and dispersion coefficient components calculated for each MSL rise scenario at cross-section 18, from Point Edith to Bahia

H3.7.4-6 Total and three-dimensional dispersion coefficients calculated for each MSL rise scenario at cross-section 18, from Point Edith to Bahia. A best fit equation and r^2 value is shown for each set of coefficients

H3.7.4-7 Dispersion coefficients and dispersion coefficient components calculated for each MSL rise scenario at cross-section 19, from Port Chicago to Grizzly Bay

H3.7.4-8 Total and three-dimensional dispersion coefficients calculated for each MSL rise scenario at cross-section 19, from Port Chicago to Grizzly Bay. A best fit equation and r^2 value is shown for each set of coefficients

H3.7.4-9 Dispersion coefficients and dispersion coefficient components calculated for each MSL rise scenario at cross-section 20, from Middle Point to Simmons Island

H3.7.4-10 Total and three-dimensional dispersion coefficients calculated for each MSL rise scenario at cross-section 20, from Middle Point to Simmons Island. A best fit equation and r^2 value is shown for each set of coefficients

H3.7.4-11 Dispersion coefficients and dispersion coefficient components calculated for each MSL rise scenario at cross-section 21, from Concord to Dutton Island

H3.7.4-12 Total and three-dimensional dispersion coefficients calculated for each MSL rise scenario at cross-section 21, from Concord to Dutton Island. A best fit equation and r^2 value is shown for each set of coefficients

H3.7.4-13 Dispersion coefficients and dispersion coefficient components calculated for each MSL rise scenario at cross-section 22, from Stake Point to Wheeler Island

H3.7.4-14 Total and three-dimensional dispersion coefficients calculated for each MSL rise scenario at cross-section 22, from Stake Point to Wheeler Island. A best fit equation and r^2 value is shown for each set of coefficients

H3.7.4-15 Dispersion coefficients and dispersion coefficient components calculated for each MSL rise scenario at cross-section 23, extending south from Simmons Point

H3.7.4-16 Total and three-dimensional dispersion coefficients calculated for each MSL rise scenario at cross-section 23, extending south from Simmons Point. A best fit equation and r^2 value is shown for each set of coefficients

H3.7.5-1 Dispersion coefficients and dispersion coefficient components calculated for each MSL rise scenario at cross-section 24, extending from Mallard Island to Chipps Island

H3.7.5-2 Total and three-dimensional dispersion coefficients calculated for each MSL rise scenario at cross-section 24, extending from Mallard Island to Chipps Island. A best fit equation and r^2 value is shown for each set of coefficients

H3.7.5-3 Dispersion coefficients and dispersion coefficient components calculated for each MSL rise scenario at cross-section 25, extending from Pittsburg to Chipps Island

H3.7.5-4 Total and three-dimensional dispersion coefficients calculated for each MSL rise scenario at cross-section 25, extending from Pittsburg to Chipps Island. A best fit equation and r^2 value is shown for each set of coefficients.

H3.7.5-5 Dispersion coefficients and dispersion coefficient components calculated for each MSL rise scenario at cross-section 26, extending from Winter Island to Van Sickle Island

H3.7.5-6 Total and three-dimensional dispersion coefficients calculated for each MSL rise scenario at cross-section 26, extending from Winter Island to Van Sickle Island. A best fit equation and r^2 value is shown for each set of coefficients

H3.7.5-7 Dispersion coefficients and dispersion coefficient components calculated for each MSL rise scenario at cross-section 27, extending north from Sherman Island

H3.7.5-8 Total and three-dimensional dispersion coefficients calculated for each MSL rise scenario at cross-section 27, extending north from Sherman

	Island. A best fit equation and r^2 value is shown for each set of coefficients
H3.7.5-9	Dispersion coefficients and dispersion coefficient components calculated for each MSL rise scenario at cross-section 28, on Sacramento River near Emmaton
H3.7.5-10	Total and three-dimensional dispersion coefficients calculated for each MSL rise scenario at cross-section 28, on Sacramento River near Emmaton. A best fit equation and r^2 value is shown for each set of coefficients

Abbreviations

3D	Three-dimensional
DRMS	Delta Risk Management Strategy
DWR	Department of Water Resources
MSL	Mean Sea Level
NDO	Net Delta Outflow
NOAA	National Oceanic & Atmospheric Administration
RMA	Resource Management Associates
SIPS	Strain Induced Periodic Stratification
TRIM	Tidal, Residual, Intertidal Mudflat Model
UnTRIM	Unstructured Tidal, Residual, Intertidal & Mudflat Model
USGS	United States Geological Survey
WAM	Water Analysis Module
K_{gc}	Dispersion associated with gravitational circulation
K_{us}	Dispersion associated with unsteady vertical shear
K_{2D}	Dispersion associated with tidal dispersion
K_{3D}	Dispersion associated with three-dimensional processes

Units and Conversion Factors

ft	Length unit, foot
m	Length unit, meter. 1 m = 3.281 feet
in	Length unit, inches
cm	Length unit, centimeter. 1 cm = 0.3937 inches
cfs	Flow unit, cubic feet per second
cms	Flow unit, cubic meters per second (m^3/s). 1 cms = 35.3147 cfs
psu	Practical salinity unit, equivalent to parts per thousand (ppt)

Executive Summary

This report documents the application of the three-dimensional UnTRIM model to simulate salinity for several sea level rise scenarios. These scenario simulations supplement and support the large number of simulations performed with the one-dimensional Water Analysis Module (WAM) as part of the DRMS project. The specific goals of the three-dimensional simulations are:

- Estimate salinity for idealized sea level rise scenarios
- Quantify the strength of salt intrusion processes for different sea level rise scenarios
- Quantify the relative contribution of "three-dimensional transport processes," including gravitational circulation, to salt intrusion
- Account for sea level rise in the parameterization of dispersive transport for the WAM
- Inform uncertainty analysis of the WAM

The goals of the sea level rise scenario simulations were achieved, as is documented in this report. The only goal not explicitly addressed here is the uncertainty analysis of the WAM which is discussed in a separate DRMS report.

The work outlined in this report builds upon other DRMS three-dimensional modeling studies. The key physical processes that result in salt intrusion are reviewed in the DRMS report "Parameterization of Mixing using a Three-Dimensional Hydrodynamic Model." The technical term for these salt intrusion processes is "dispersive transport processes" and the strength of these processes is quantified by "dispersion coefficients." That report documents the analysis approach used to parameterize dispersive transport using dispersion coefficients. The UnTRIM model formulation, configuration and calibration are described in the DRMS report "UnTRIM San Francisco Bay-Delta Model Calibration."

Seven scenarios are considered to estimate the effects of sea level rise on salinity. In addition to the Baseline scenario without sea level rise, four increases in MSL are considered: 20 cm (0.66 ft), 50 cm (1.64 ft), 90 cm (2.95 ft) and 140 cm (4.59 ft). These levels of MSL increase were recommended by Phillip Duffy of the DRMS climate change group. Two additional simulations evaluate potential cumulative effects of 140 cm of sea level rise with other potential changes. The first cumulative effects scenario, the Amplified Tides scenario, assumes that tidal range is increased by 11 percent, based on the observed rates of amplification reported by Flick et al. (2003). Because the future trends in tidal amplitude are highly uncertain, the Amplified Tides scenario should be considered a sensitivity analysis. The second cumulative effects scenario, the Perforated Sherman Island scenario, assumes 20 breach locations in Sherman Island. Only Sherman Island was used for the flooded island scenario because a flooded Sherman Island scenario was simulated by UnTRIM without sea level rise, as described in the DRMS report "Three-Dimensional Simulations of Salt Transport for Flooded Island Scenarios."

The scenarios simulated are designed to address the goals discussed previously and are limited in scope given the short schedule and limited budget provided for the analysis. In addition, the model forcing is idealized in order to allow the estimation of dispersion coefficients. The assumptions and approximations employed include the following:

- No changes to the shoreline geometry of the estuary. This includes the assumption of current Delta geometry without any new levee breaches, except for one scenario that considers the effects of a flooded Sherman Island on salt intrusion. Also, it assumes no new flooding of lowlands around the Bay with sea level rise.
- No net accretion or erosion is assumed. The bed elevation of the estuary is specified based on existing bathymetry data. In contrast, the observed trend in Suisun Bay and is an average of 1.2 cm/year (0.47 in/year) of erosion (Cappiella et al. 2005).
- The tidal range applied at the ocean boundary is assumed to remain constant. Only the Mean Sea Level (MSL) is increased. One scenario examines the effect of increased tidal range.
- Other aspects of climate change, such as effects on hydrology, are not considered.
- The scenario simulations use specified hydrology. All scenarios use a constant Net Delta Outflow (NDO) of 260 m^3/s (9,182 cfs), corresponding to a typical summer flow rate.

The spatial and temporal variability of salinity for each sea level rise scenario are explored with several types of figures. The model predictions indicate increased salt intrusion with increases in MSL, particularly for MSL increases of 90 cm (2.95 ft) or more. Increased salt intrusion also results in increased stratification in Suisun Bay and the western Delta, which allows the strength of gravitational circulation and other “three-dimensional processes” to increase. Estimating additional water required to meet relevant water quality standards under realistic sea level rise scenarios is beyond the scope of the current analysis. However, rough estimates of additional Net Delta Outflow that may be required to meet a specific water quality standard for the idealized scenarios are provided. These estimates suggest that the additional flow required may be substantial, but the actual flow requirements will depend on many additional factors not considered in the idealized scenarios.

Simulation results for the cumulative effects scenarios indicate increased Delta salinity with tidal amplification and greatly increased Delta salinity as a result of tidal exchange with Sherman Island. These predicted increases are consistent with the understanding that mixing in Franks Tract causes substantial mixing of salt into the central Delta (RMA 2005). Because Sherman Island is both much larger than Franks Tract and closer to the large salinity gradients present in Suisun Bay during summer conditions, the effects of Sherman Island on salt intrusion should be much larger than those of Franks Tract. The simulation results suggest that the combination of substantial sea level rise and a small degree of Delta island flooding could lead to large impacts on Delta water quality and water supply reliability.

In order to quantify the strength of salt intrusion processes for a range of MSL rise scenarios, a detailed analysis of dispersive transport is performed following the method

described in the DRMS report "Parameterization of Mixing using a Three-Dimensional Hydrodynamic Model." This analysis supplements the previous analysis that characterized the variability of dispersive transport with changes in Net Delta Outflow. The strength of predicted salt intrusion processes are represented by dispersion coefficients. The calculated dispersion coefficients are nearly constant with increasing MSL in Central Bay and most of San Pablo Bay, increase slightly to moderately with increasing MSL in Carquinez Strait and western Suisun Bay, and increase substantially with increasing MSL in the eastern portion of Suisun Bay and in the western Delta. Three-dimensional processes are found to be significant throughout the estuary and dominant in some regions. The strength of three-dimensional salt intrusion processes increases with sea level rise in most of the Estuary, with large increases in the western Delta. The computed variability of dispersion coefficients with sea level rise will be used in the WAM to represent the effects of sea level rise on salt intrusion processes.

The scenarios simulated are quite idealized, consistent with the limited scope and goals of the sea level rise analysis documented here. The results of these idealized scenario simulations suggest that more realistic scenario simulations are warranted in order to better quantify cumulative effects of sea level rise, flooded islands, geomorphic change in the estuary, changes in Delta operations, hydrologic variability as a result of climate change and other expected changes. Many such scenarios are underway with the WAM, while others will not be addressed in this phase of the DRMS project. Given the substantial uncertainty associated with the WAM's simplified structure, a portion of these scenarios should be simulated with two-dimensional and three-dimensional models to better inform risk analysis and risk reduction measures.

H3.1 Introduction

There are at least three important impacts of sea level rise related to flow and salinity in the Delta:

1. Increasing sea level may inundate additional land area where bay and channel boundaries are not constrained by levees or steep topography. This will lead to an increase in tidal prism and may increase Delta salinity.
2. Sea level rise may outpace the ability to raise and maintain levees leading to un-repairable flooding of some Delta islands. This flooding will lead to increases in tidal prism and Delta salinity.
3. Sea level rise is increasing water surface elevations leading to deeper channels in the San Francisco Estuary. These deeper channels will have larger cross-sectional areas than existing channels leading to proportionally lower net (tidally-averaged) velocities. These lower net velocities will be less effective in flushing salt from the Delta. Deeper channels are also more likely to become stratified because bottom friction is less effective in vertically mixing deeper water columns. Additional stratification may cause increased salt intrusion into the Delta from gravitational circulation.

The flooding of additional areas as sea level rises will have an impact on salinity in the Delta. However quantifying the impact requires more accurate topography than is

currently available of areas which could potentially flood. This potential impact will not be considered in this phase of the DRMS project.

The effect of sea level rise on levee failures is addressed in the DRMS project. Evaluating the impact of islands flooding due to sea level rise is one form of breach case to be analyzed by the Water Analysis Module (WAM) in Risk Analyses that address future conditions. The scenario simulations performed in this report will inform the uncertainty analysis related to the WAM.

To our knowledge, the effect of channel deepening on salt intrusion in the San Francisco Estuary has not been previously addressed with a three-dimensional model. Increased water surface elevation from sea level rise will lead to deeper water in channels. Probably a larger source of deepening will be ongoing erosion in Suisun Bay (Cappiela et al., 2005) and other regions. Scour from restoration projects, levee failures and dredging may also act to deepen channels. Therefore it is likely that future channels in San Pablo Bay, Suisun Bay and the Delta will be deeper than the current channels. Analytical relationships (Hansen and Rattray 1965) and simulations of idealized geometries suggest that increases in water column depth can have a strong and non-linear effect on salt water intrusion as a result of increased gravitational circulation. This increased salt intrusion would increase the Net Delta Outflow (NDO) required to meet water quality standards. Channel deepening will also change the magnitude, distribution, and phase of tidal currents, leading to altered tidal dispersion processes and altered turbulent mixing. A three-dimensional model is the most appropriate tool to address these issues. Ideally, the three-dimensional model should be coupled with a water management model, following an approach similar to the WAM, to estimate increased reservoir discharges required to meet water quality standards under sea level rise scenarios. However, due to schedule and budget constraints, these coupled simulations are beyond the scope of the current analysis.

The primary goals of the sea level rise scenario simulations that are addressed in this document the following:

- Estimate salinity for idealized sea level rise scenarios
- Quantify the strength of salt intrusion processes for different sea level rise scenarios
- Quantify the relative contribution of “three-dimensional transport processes,” including gravitational circulation, to salt intrusion
- Account for sea level rise in the parameterization of dispersive transport for the WAM

In Section 5, the increased salt intrusion under sea level rise scenarios will be discussed. These salt intrusion estimates should be considered a lower bound of the potential effects of sea level rise on salt intrusion because the scenarios assumes no levee failures, no additional inundation of low lying coastal regions, no channel erosion, and no changes to hydrology from climate change. In Section 6, the cumulative effects of sea level rise with additional changes to the estuary are considered. In Section 7, increases in the strength of salt dispersion processes resulting from sea level rise are discussed. The dispersive transport processes which result in salt intrusion are parameterized with dispersion

coefficients. The estimates of variation in dispersion coefficients with sea level rise should improve the accuracy of the WAM for sea level rise scenarios. In Section 8, the results of the sea level rise scenario simulations are discussed and some conclusions are presented.

The work outlined in this report builds upon other DRMS three-dimensional modeling studies. The key physical processes that result in dispersion of salt are reviewed in the DRMS report "Parameterization of Mixing using a Three-Dimensional Hydrodynamic Model." That report also documents the analysis approach used to parameterize dispersive transport. The UnTRIM model formulation, configuration, and calibration are described in the DRMS report "UnTRIM San Francisco Bay-Delta Model Calibration." The details of the Sherman Island breach geometry are described in the DRMS report "Three-Dimensional Simulations of Salt Transport for Flooded Island Scenarios."

H3.2 UnTRIM Model Description

The primary tool used in this technical study was the three-dimensional hydrodynamic model UnTRIM (Casulli and Zanolli, 2002). A complete description of the governing equations, numerical discretization, and numerical properties of UnTRIM are described in Casulli and Zanolli (2002, 2005), Casulli (1999), and Casulli and Walters (2000).

The UnTRIM model solves the three-dimensional Navier-Stokes equations on an unstructured grid in the horizontal plane. The boundaries between vertical layers are at fixed elevations, and cell heights can be varied vertically to provide increased resolution near the surface or other vertical locations. The numerical method allows full wetting and drying of cells in the vertical and horizontal directions. The governing equations are discretized using a finite difference – finite volume algorithm. Discretization of the governing equations and model boundary conditions are presented in detail by Casulli and Zanolli (2002). The governing equations, turbulence closure model, previous applications and model uncertainty associated with UnTRIM are discussed in more detail in the DRMS report "UnTRIM San Francisco Bay-Delta Model Calibration."

H3.3 Analysis of Dispersion Processes

The method used to analyze dispersion processes is documented in the DRMS report "Parameterization of Mixing using a Three-Dimensional Hydrodynamic Model." The method applies the salt balance equation (Fischer et al. 1979) to estimate dispersion coefficients as follows

$$K = -QS/(A\ dS/dx) \qquad (3\text{-}1)$$

where Q is the tidally-averaged flow, S is tidally and cross-sectionally averaged salinity, K is the dispersion coefficient, A is the cross-sectional area, and x is the longitudinal position. The salt balance equation applies to the longitudinal salinity distribution at tidally-averaged steady state conditions. This equation states that the seaward advection of salinity due to net seaward velocity resulting from steady freshwater inflows is balanced by landward transport of salt by all dispersive transport mechanisms (Fischer et al. 1979). Dispersion coefficients (K) quantify the strength of dispersive salt transport processes, which are responsible for salt intrusion.

The strength of dispersion mechanisms varies in space and time. In order to accurately parameterize dispersive transport in the WAM, the analysis technique is designed to capture much of this variability. The spatial variability is accounted for by analysis of fluxes at each of the cross-sections shown in Figure H3.3-1. At each cross-section and for each MSL rise scenario, Q, S and A are calculated for tidally-averaged steady state conditions. The salinity gradient (dS/dx) is estimated along the centerline of the estuary shown in Figure H3.3-2. The results of this dispersion analysis are presented in Section 7.

After dispersion coefficients are estimated, the contributions of different physical processes to salt transport are estimated by a detailed salt flux analysis documented in "Parameterization of Mixing using a Three-Dimensional Hydrodynamic Model." The overall dispersion coefficient for each section and flow scenario is then partitioned into 3 components:

1) K_{gc} – the dispersion coefficient associated with gravitational circulation

2) K_{us} – the dispersion coefficient associated with unsteady vertical shear

3) K_{2D} – the dispersion coefficient represented with all other processes

Though K_{2D} can reasonably be referred to as a dispersion coefficient for "two-dimensional" tidal dispersion processes, it should be emphasized that a three-dimensional model should predict a different K_{2D} than an otherwise equivalent depth-averaged model. More generally, the definition of dispersion components does NOT imply that these physical processes are independent and that their effects are additive. In reality, the circulation in the San Francisco Estuary is three-dimensional and physical processes interact in a complex and nonlinear manner. In other words, while the salt flux analysis is mathematically precise, the interpretation of the analysis is not precise. Furthermore, while these physical processes are conceptually distinct, in a complex setting such as the San Francisco Estuary, they are all simplified conceptual representations that are a useful but limited attempt to understand or "untangle" the complex physics that result in dispersive transport.

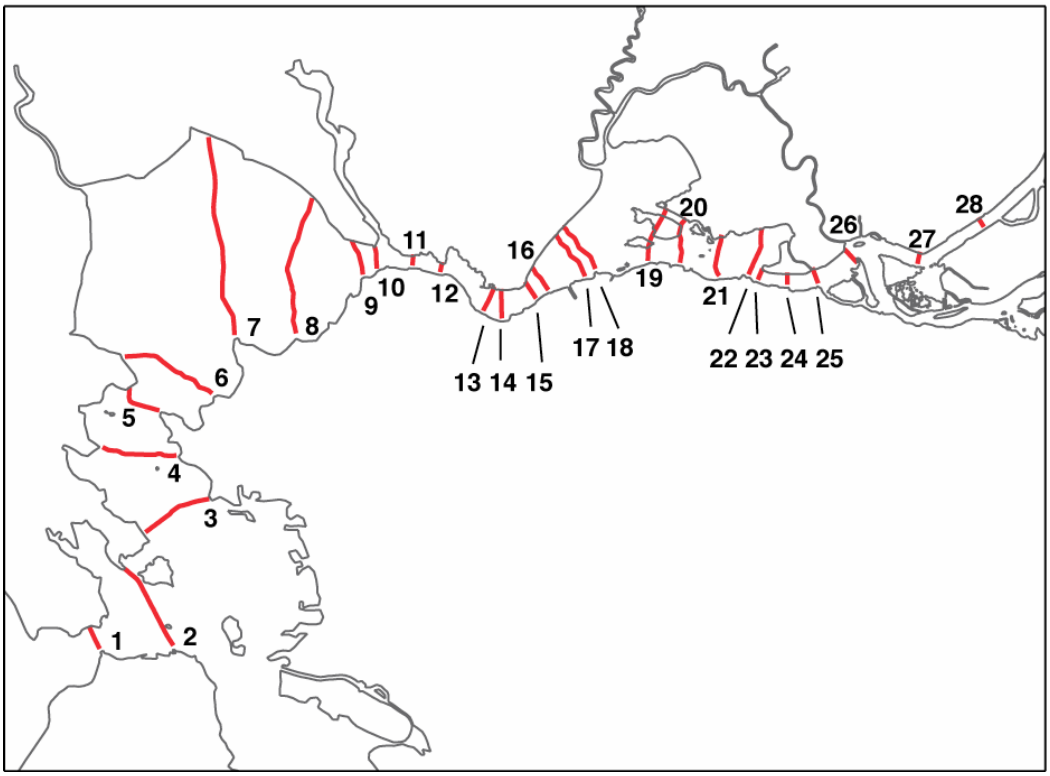

Figure H3.3-1 Cross-sections used in salt flux analysis

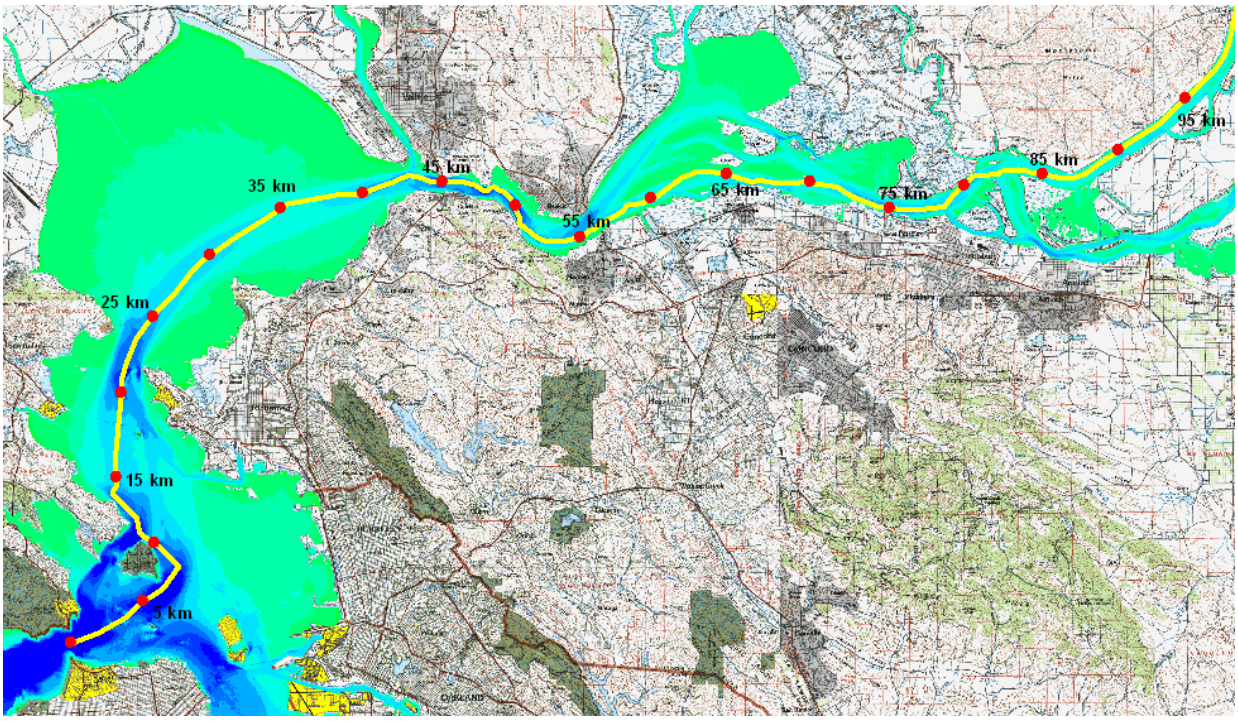

Figure H3.3-2 Centerline transect with labeled distance from Golden Gate

H3.4 Sea Level Rise Scenario Descriptions

The sea level rise scenarios are intended to explore changes to salt transport resulting from deeper water in the estuary. Therefore, the scenarios involve several assumptions. All shorelines were considered fixed, except in one scenario where a breached Sherman Island was included. No net accretion (or erosion) was assumed. The bed elevation of the estuary is specified based on existing bathymetry data. This may underestimate potential future salt intrusion because a trend of erosion has been observed in Suisun Bay (e.g., Cappiela et al. 2005). Changes to hydrology from climate change are not considered; instead specified constant flows are used for all scenarios. The scenarios all use specified constant inflows, as required for the analysis of dispersive transport processes. In contrast, the WAM will use a water management model to adjust inflows based on predicted salinity. Using the dispersion coefficients presented in this report and the previous DRMS report "Parameterization of Mixing using a Three-Dimensional Hydrodynamic Model," the water management model and other model components, the WAM will estimate the water supply and water quality impacts of all scenarios including sea level rise scenarios.

In addition to constant freshwater inflows, an idealized tide was used with the M2 and K1 amplitude reported by NOAA at Point Reyes (station 9415020). The M2 period was modified to 12.0 hours so that exactly 2 M2 cycles occur per K1 cycle (day) and all other harmonic constituents and non-tidal forcing at the seaward boundary were neglected. For this reason, the terms "tidally-averaged" and "daily-averaged" are interchangeable in the context of this report. The idealized tide and constant flows are applied to simplify the analysis of dispersion mechanisms. The dispersion analysis method described in the DRMS report "Parameterization of Mixing using a Three-Dimensional Hydrodynamic Model" requires that the tidally-averaged salinity field reaches steady state conditions. If the scenario simulations used realistic tidal forcing, variable Net Delta Outflow (NDO) and incorporated wind and other forcing, the model would be continuously responding to variations in forcing and tidally-averaged steady state conditions would never be reached. The simplified forcing allows the simulations to reach a close approximation of tidally-averaged steady state conditions. The WAM uses dispersion coefficients to predict monthly-averaged salinity. Therefore, estimating variability of dispersion coefficients with tidal amplitude (e.g., during the spring-neap cycle) is beyond the scope of the analysis. The desired product of the dispersion analysis is a set of dispersion coefficients that vary both with the salinity field and with MSL, that apply to average tidal conditions.

The simplified forcing is premised on several approximations, including 1) that tidal forcing is dominant relative to wind forcing and other environmental forcing, 2) that a repeating M2 and K1 tide, with M2 period modified to 12 hours closely approximate "typical" tidal conditions, 3) that the average dispersion over a spring-neap tidal cycle is similar to the dispersion for average tidal amplitude, and 4) that local tributary inflows do not affect tidal dispersion.

The validity of approximations 2 & 3 was examined by a simulation using real tides and constant Net Delta Outflow. The dispersion coefficients calculated over the spring-neap cycle were typically within 25 percent of the dispersion coefficients calculated for the idealized tides. However, it should be noted that each spring-neap cycle is different and,

therefore, the dispersion coefficient estimates for real tides would vary depending on the exact period during which they are computed. The use of idealized tides avoids that ambiguity and simplifies the dispersion analysis. The apparent success of the WAM in calculating salinity for historic conditions also suggests that the assumptions and approach used are appropriate.

The first five scenarios consist of a baseline scenario of no sea level rise, and four scenarios with increased MSL, as described in Table H3-1. The last two scenarios both use sea level rise of 140 cm and consider the cumulative effects of additional changes. The Perforated Sherman Island scenario assumes 20 breach locations in Sherman Island, as shown on Figure H3.4-1. These breach locations were selected to be consistent with the geometry used by RMA in previous simulations and are discussed in more detail in the DRMS report "Three-Dimensional Simulations of Salt Transport for Flooded Island Scenarios." The Amplified Tides scenario assumes that tides are amplified by 11 percent relative to existing tides. The currently observed trend at NOAA station 9414290 at Fort Point is an increase in tidal range of 5.9 cm per century (Flick et al. 2003) with an existing tidal range of 122 cm, leading to an observed trend of 5% amplification per century. However larger amplification was observed by Flick et al (2003) in stations inside San Francisco Bay. At station 9414750, at Alameda, the observed trend is 9% amplification per century. At station 9415144 at Port Chicago, the observed trend is 26% amplification per century. The authors "discount" this station due to short record length. Therefore, the average of the two stations inside San Francisco Bay is 17.5% amplification. The assumed 11% amplification used in the scenario is the average of the Fort Point station and the average of the two stations inside San Francisco Bay. The actual amplification that will be experienced during the next century is uncertain, so the Amplified Tides scenario should be considered a sensitivity analysis. The actual rate of tidal amplitude increase may accelerate in the future as MSL rise is expected to accelerate. On the other hand, it is not clear that the trend of tidal amplification is related to sea level rise or that it will continue in the future, so the chosen scenario seems appropriate given this large uncertainty.

Table H3-1 Names and Mean Sea Level Increase ror Each Simulation Scenario

Scenario	Mean Sea Level Increase (cm)	Cumulative Effects
Baseline	0	none
20 cm MSL Rise	20	none
50 cm MSL Rise	50	none
90 cm MSL Rise	90	none
140 cm MSL Rise	140	none
Perforated Sherman Is.	140	breached Sherman Island
Amplified Tides	140	tides amplified by 11%

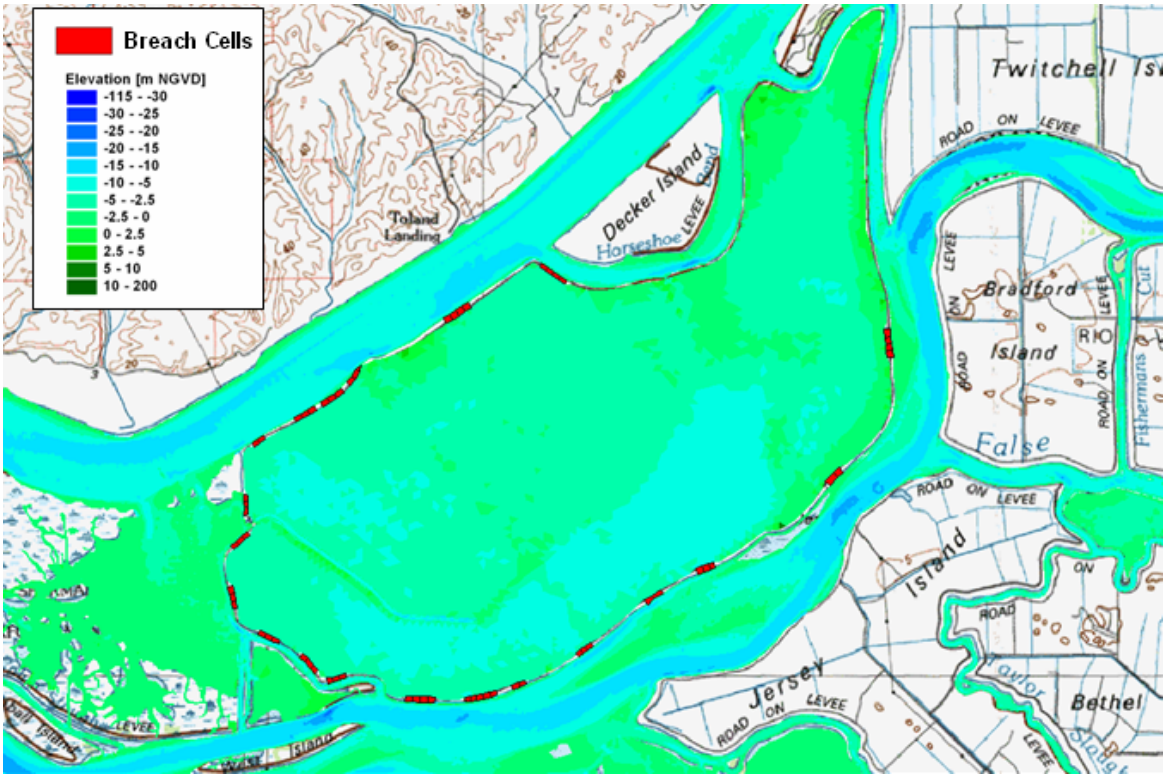

Figure H3.4-1The 20 breach locations for the Perforated Sherman Island scenario

H3.5 Sea Level Rise Scenario Simulation Results

Each scenario simulation was run until tidally-averaged steady state salinity conditions were achieved. Under these conditions, the daily-averaged salinity field no longer changes. It was determined that tidally-averaged steady state conditions were achieved when tidally-averaged salt flux past each cross-section was approximately zero. Figure H3.5-1 shows the predicted fluxes at the cross-sections indicated on Figure H3.3-1 at steady state conditions for the Baseline scenario. Note that the net salt flux over a tidal cycle is small because the advective and dispersive fluxes approximately balance. The analysis of salt fluxes and transport will be discussed in more detail in Section 7.

All predicted salinity values are presented in “practical salinity units” (psu). This unit is, for the purposes of this report, equivalent to “parts per thousand” (ppt). Unlike electrical conductivity (EC), salinity is a conservative tracer. Though salinity and EC are not linearly related, observed salinity is generally computed from observed electrical conductivity and temperature using standard formulas. For reference sake, ocean salinity is typically between 32 psu and 35 psu and 0.5 psu corresponds roughly to both the 250 mg/l Cl standard for Municipal and Industrial water use, and the 1.0 mS EC standard for Southern Delta agricultural use.

Figure H3.5-2 shows depth-averaged and tidally-averaged salinity at steady state conditions for baseline conditions (without sea level rise). Note that the predicted values represent salinity from seawater intrusion because local sources of salt (agricultural runoff etc.) are neglected in these simulations. The region shown includes San Pablo Bay, Carquinez Strait, Suisun Bay and a portion of the Delta. The effects of sea level rise on predicted salinity extend over a larger region, but the region of this figure was chosen to show a large area and still be legible. Figure H3.5-3 shows the predicted depth-averaged and tidally-averaged salinity at steady state conditions for the 20 cm MSL Rise scenario and the predicted depth-averaged and tidally-averaged salinity increase relative to the Baseline scenario. The predicted salinity increases are less than 1 psu in all portions of the region shown and greater than 0.5 psu only in a limited area. Figure H3.5-4 shows the predicted depth-averaged and tidally-averaged salinity at steady state conditions for the 50 cm MSL Rise scenario and the predicted depth-averaged and tidally-averaged salinity increase relative to the Baseline scenario. The predicted depth-averaged and tidally-averaged salinity increases are between 0.5 psu and 1 psu in most of the region shown in the figure and greater than 1 psu in some shoal and intertidal regions of San Pablo Bay and Suisun Bay. The 0.5 psu contour intrudes approximately 3 km further into the western Delta in the 50 cm MSL Rise scenario than the Baseline scenario. Figure H3.5-5 shows the predicted depth-averaged and tidally-averaged salinity at steady state conditions for 90 cm MSL Rise scenario and the predicted depth-averaged and tidally-averaged salinity increase relative to the Baseline scenario. Predicted salinity increases are in the range of 0.5 to 4 psu in Suisun Bay, Carquinez Strait and San Pablo Bay. The 0.5 psu contour intrudes approximately 7 km further into the western Delta in the 90 cm MSL Rise scenario than the Baseline scenario and much of the western Delta has predicted salinity higher than 0.1 psu. Figure H3.5-6 shows the predicted depth-averaged and tidally-averaged salinity at steady state conditions for 140 cm MSL Rise and the predicted depth-averaged and tidally-averaged salinity increase relative to the Baseline

scenario. Predicted salinity increases are in the range of 1 to 6 psu in Suisun Bay, Carquinez Strait and San Pablo Bay. The 0.5 psu contour intrudes more than 10 km further into the western Delta in the 140 cm MSL Rise scenario than the Baseline scenario and the 0.1 psu contour of predicted salinity from seawater intrusion extends into the central Delta.

The tidally-averaged salinity profiles along the two transects shown in Figure H3.5-7 are shown for each scenario in Figures H3.5-8 to H3.5-17. These figures indicate the vertical variability and longitudinal variability in predicted tidally-averaged salinity. The surface layers are only wet near high water, when salinity is at a maximum, and, therefore, the near surface region appears to have unstable stratification as an artifact of the tidal averaging. Unstable stratification is not present in the instantaneous salinity field during any part of the tidal cycle. The predicted tidally-averaged salinity profiles for the sea level rise scenarios shown in Figures H3.5-10 through H3.5-17, indicate increased salt intrusion with MSL rise, consistent with the salt intrusion noted in the salinity maps. Substantial vertical stratification is present in the Baseline scenario and all MSL rise scenarios. The degree of stratification is similar among the scenarios in Central Bay and San Pablo Bay, suggesting a similar degree of gravitational circulation among the scenarios. The predicted stratification in Suisun Bay and the western Delta increases with MSL rise, suggesting an increase in gravitational circulation. An increase in gravitational circulation was expected due to increased salinity gradients in these regions for the MSL rise scenarios and deeper water in these scenarios. Changes in transport processes with MSL rise will be discussed further in Section 7.

The salinity maps and profile figures discussed previously show tidally-averaged salinity. The temporal variability of predicted salinity can be explored at several locations using time series graphs. At the end of the simulation, tidally-averaged steady state conditions have been reached and, due to the idealized tides used to force the model, the same salinity pattern repeats each day. The four locations selected to examine tidal variability of predicted salinity are Martinez, Antioch, Jersey Point, and Emmaton. These locations, shown in Figure H3.5-18, were chosen primarily because they are important monitoring locations. Figure H3.5-19 shows the variability of predicted depth-averaged salinity at Martinez for each scenario. The salinity increases with increasing levels of sea level rise with salinity differences between scenarios that are fairly constant through the tidal cycle. Figure H3.5-20 shows the variability of predicted depth-averaged salinity at Antioch for each scenario. The salinity increases with increasing levels of sea level rise with the largest absolute salinity differences at high salinity values but very large relative differences at low salinity values. For example, at 4:00 am the predicted salinity for the Baseline scenario is 0.1 psu while the predicted salinity for the 140 cm MSL Rise scenario is 1 psu. At 10:00 am, the predicted salinity for the Baseline scenario is 1 psu while the predicted salinity for the 140 cm MSL Rise scenario is over 3 psu. Figure H3.5-21 shows the variability of predicted depth-averaged salinity at Jersey Point for each scenario. The predicted salinity increases with increasing levels of sea level rise with the largest absolute salinity differences at the end of flood tide, corresponding to the peak salinity values. For example, at 10:30 am the predicted salinity for the Baseline scenario is below 0.1 psu while the predicted salinity for the 140 cm MSL Rise scenario is 1 psu. Figure H3.5-22 shows the variability of predicted depth-averaged salinity at

Emmaton for each scenario. The predicted salinity increases with increasing levels of sea level rise with the largest absolute salinity differences at the end of flood tide, corresponding to peak salinity values. For example, at 10:00 am the predicted salinity for the Baseline scenario is less than 0.7 psu while the predicted salinity for the 140 cm MSL Rise scenario is 3 psu.

Abundance or survival of several estuarine biological populations in the San Francisco Estuary is positively related to freshwater flow (Jassby et al., 1995). These relationships have been described in terms of X2, the location of the 2 psu tidally-averaged bottom salinity. X2 is also used as a water quality standard, with requirements to maintain X2 less than specified values (e.g., seaward of Collinsville) during specified periods. Though this standard is complex, it is the water quality standard mostly likely to apply for the Net Delta Outflow of 260 m^3/s (9,182 cfs) used in the MSL rise scenarios. Therefore, a substantial increase in predicted X2 with MSL rise would suggest that substantially increased NDO may be required to meet the X2 standard as a result of sea level rise. The MSL rise scenarios all use constant Net Delta Outflow, and, therefore, a single X2 location is associated with the salinity field for each scenario at tidally-averaged steady state. Table H3-2 shows the computed X2 values for the MSL rise scenarios.

By making several approximations, the calculated increases in X2 for each MSL rise scenario can be related to an approximate compensating flow that would be required to return X2 to the value calculated for the Baseline scenario (83.4 km). The primary assumptions are that the X2 standard applies for the salinity conditions of the Baseline scenario and that the constant Net Delta Outflow of 260 m^3/s (9,182 cfs) used in this scenario is the minimum NDO that will meet this standard. Because X2 is near Collinsville for the Baseline scenario, this assumption is reasonable. An additional approximation is that the increase in flow required to move X2 a specified distance interval landward is the same for the MSL rise conditions as for historic conditions. This assumption will lead to an underestimate of required flow because the strength of salt intrusion processes increases with MSL rise, as will be shown in Section 7. Regression equations have been derived by Jassby et al. (1995) and Monismith et al. (2002) that relate X2 to NDO for historic conditions. The equations give significantly different X2 values for a given steady flow. Furthermore, several limitations and approximations are associated with the equations and the method and data used to derive the equations, as discussed by MacWilliams et al. (2005). Therefore, the flows calculated here are only rough estimates of additional NDO that may be required to meet the X2 standard. More precise flows could be estimated by integrating a water management model into UnTRIM, similar to the approach used to integrate a water management model into the WAM. Table H3-2 shows two rough estimates of additional NDO required to maintain X2 position at the Baseline X2 position for each MSL rise scenario. The first estimate is based on the relationship between X2 and NDO specified by the Jassby regression equation and the second is based on the Monismith regression equation. The Jassby regression equation yields larger flow values, but both flow values provided are quite substantial for the 90 cm MSL Rise scenario and the 140 cm MSL Rise scenario. The largest estimate of additional flow required to compensate for X2 increase due to sea level rise is 3,500 cfs estimated by the Jassby regression equation for the 140 cm MSL Rise scenario.

It should be noted that the fixed Net Delta Outflow of 260 m^3/s (9,182 cfs), corresponding to a typical summer NDO, was used in all simulations and that larger salt intrusion would occur during summer and fall conditions during a dry or critical year. In addition, while these scenarios span the likely range of sea level rise during the next 100 years, they almost certainly underestimate channel deepening that will occur as a cumulative effect of MSL rise, ongoing erosion, dredging activities, localized and larger scale scour from island flooding and restoration projects. Furthermore, the assumption of no island flooding and hardened shorelines outside of the Delta is also likely to lead to dramatic underestimation of effects of sea level rise, because sea level rise is likely to cause more frequent and severe flooding of Delta islands and tidal inundation of larger regions. The effect of tidal exchange with one flooded island in addition to MSL rise will be discussed in the following section.

Table H3-2 X2 location for MSL rise scenarios and estimates of additional Net Delta Outflow that would be required to return X2 to the value calculated for the Baseline scenario, based upon published regression equations for the estimation of X2

(The MSL rise scenarios assume a constant Net Delta Outflow of 260 m^3/s [9,182 cfs]. The actual X2 locations and additional NDO required to offset salt intrusion from sea level rise will depend upon Net Delta Outflow and other factors, including Delta island flooding.)

Scenario	MSL Rise (cm)	X2 Location (km)	Additional NDO Estimates (cfs)	
			Jassby	Monismith
Baseline	0	83.4	0	0
20 cm MSL Rise	20	84.3	470	360
50 cm MSL Rise	50	85.9	1,250	940
90 cm MSL Rise	90	88.6	2,420	1,730
140 cm MSL Rise	140	91.5	3,500	2,390

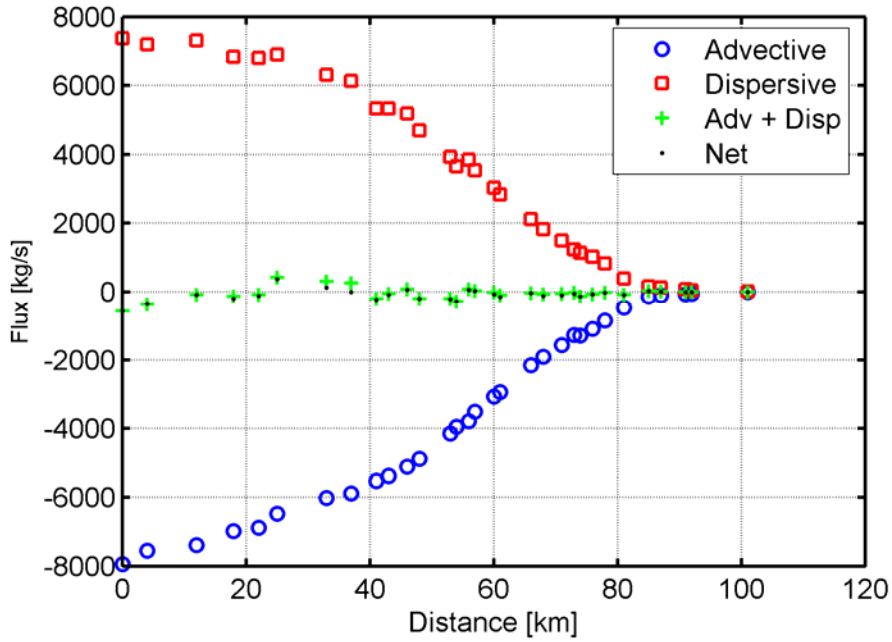

Figure H3.5-1 Predicted advective, dispersive and net (tidally-averaged) salt fluxes during the last day of the baseline scenario

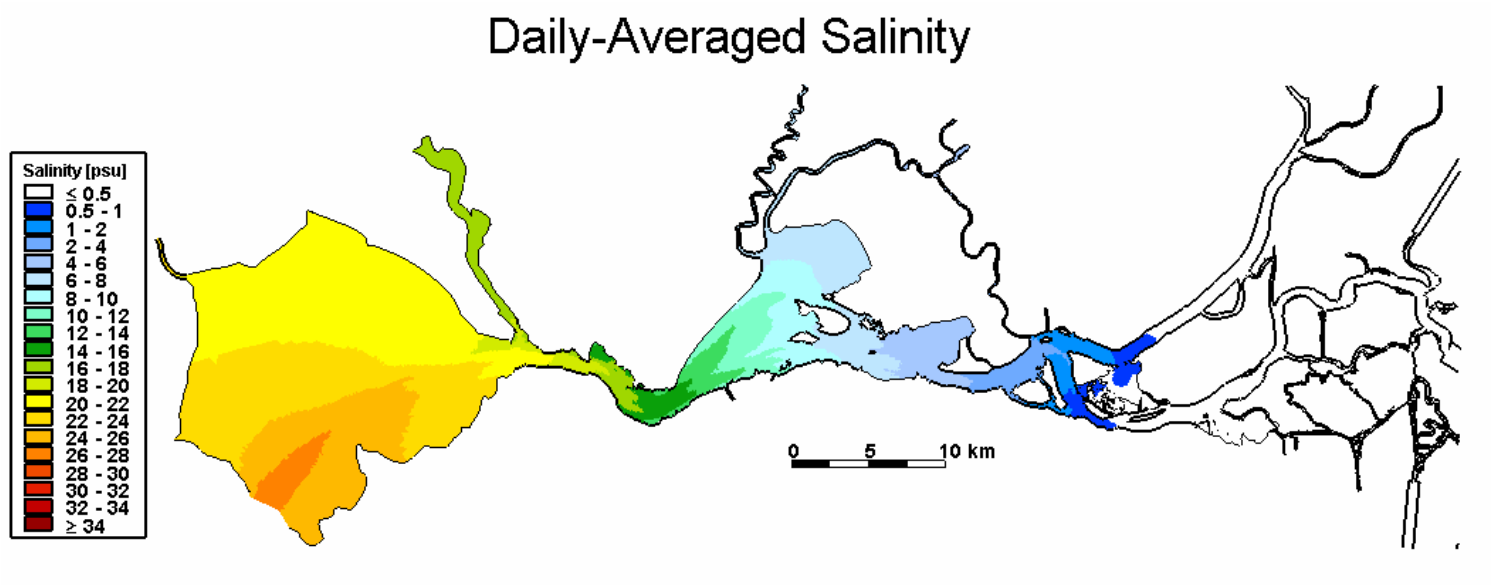

Figure H3.5-2 Depth-averaged and tidally-averaged salinity at tidally-averaged steady state conditions for the Baseline scenario

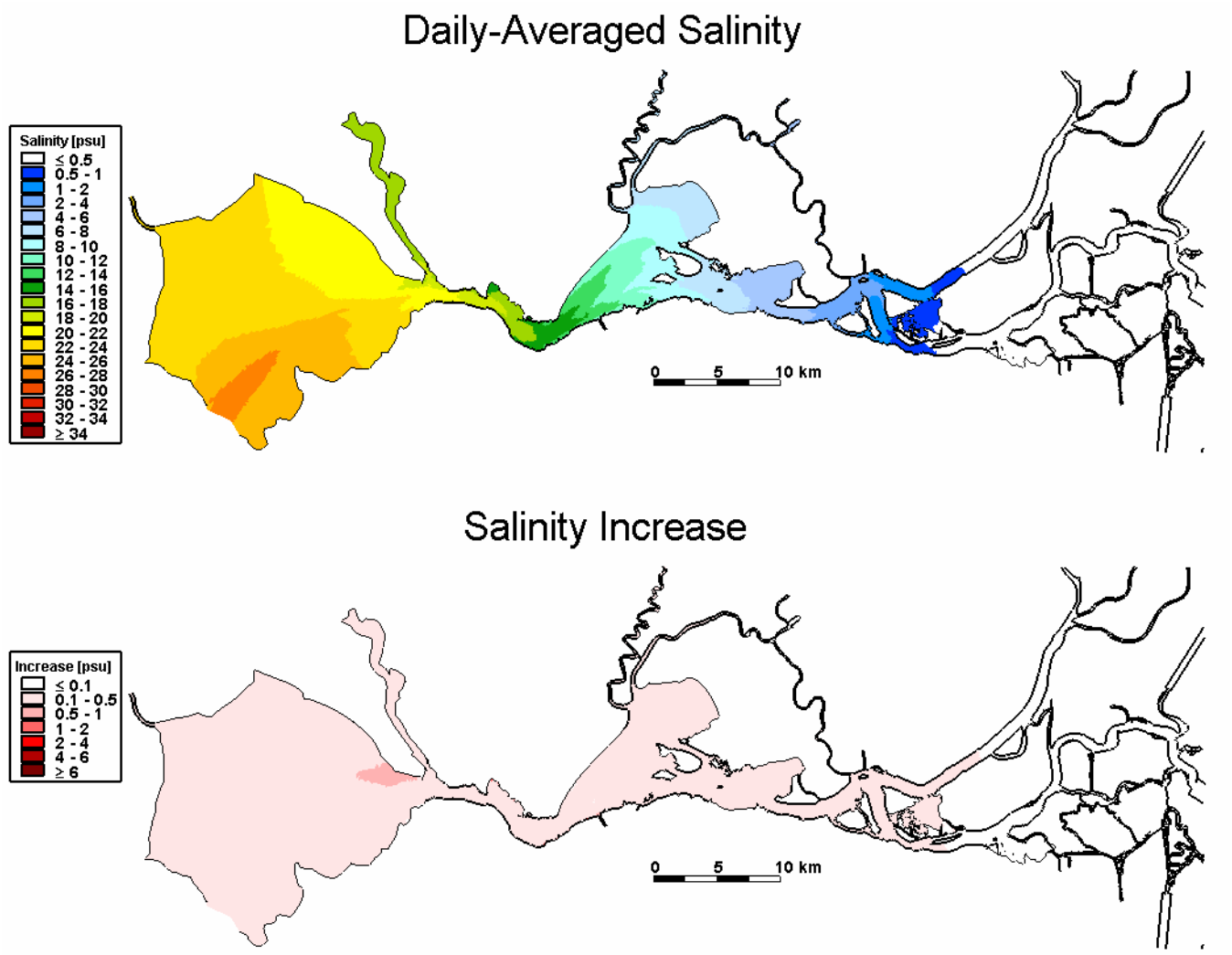

Figure H3.5-3Depth-averaged and tidally-averaged salinity at tidally-averaged steady state conditions for the 20 cm MSL Rise scenario and increase in salinity relative to the Baseline scenario

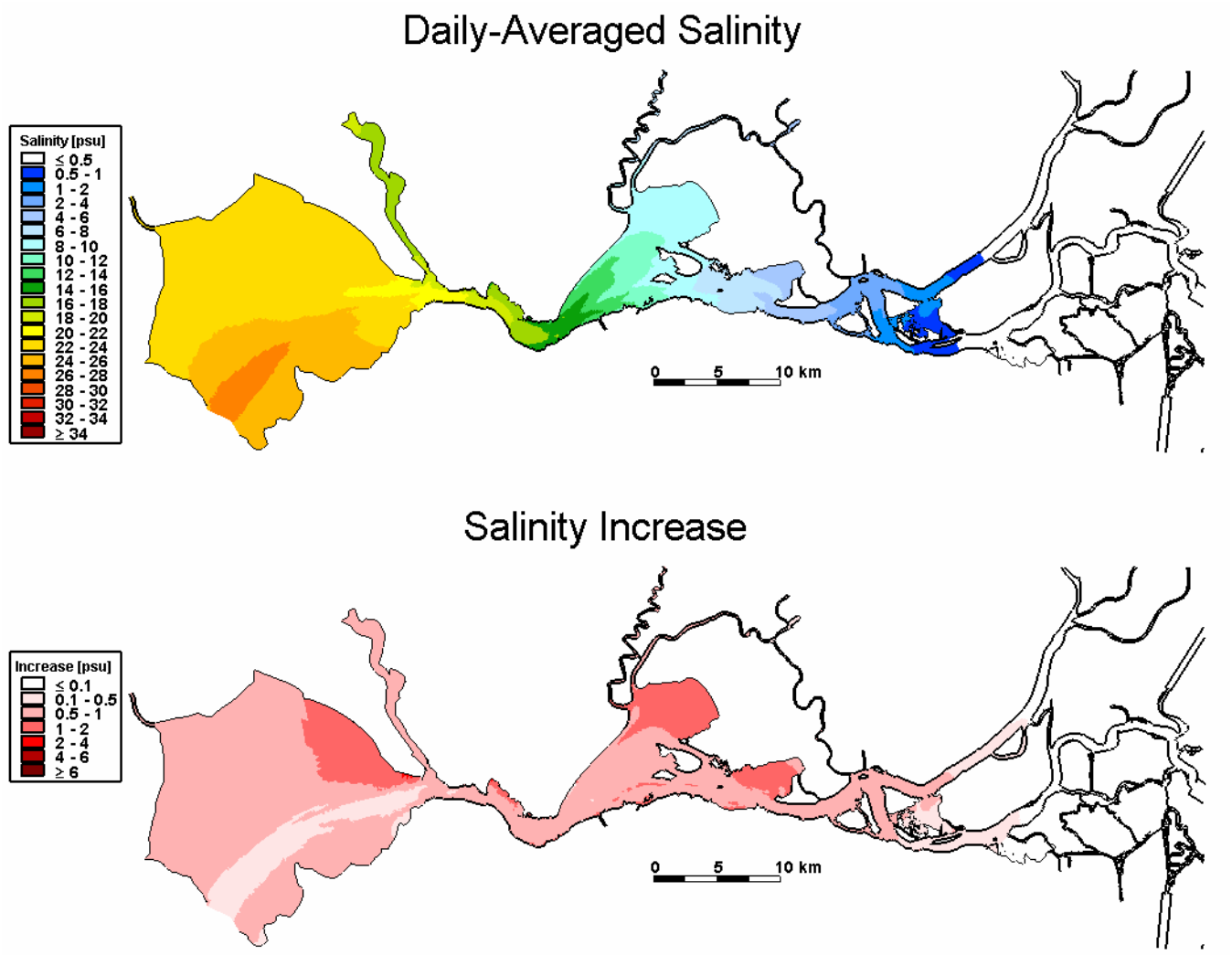

Figure H3.5-4Depth-averaged and tidally-averaged salinity at tidally-averaged steady state conditions for the 50 cm MSL Rise scenario and increase in salinity relative to the Baseline scenario

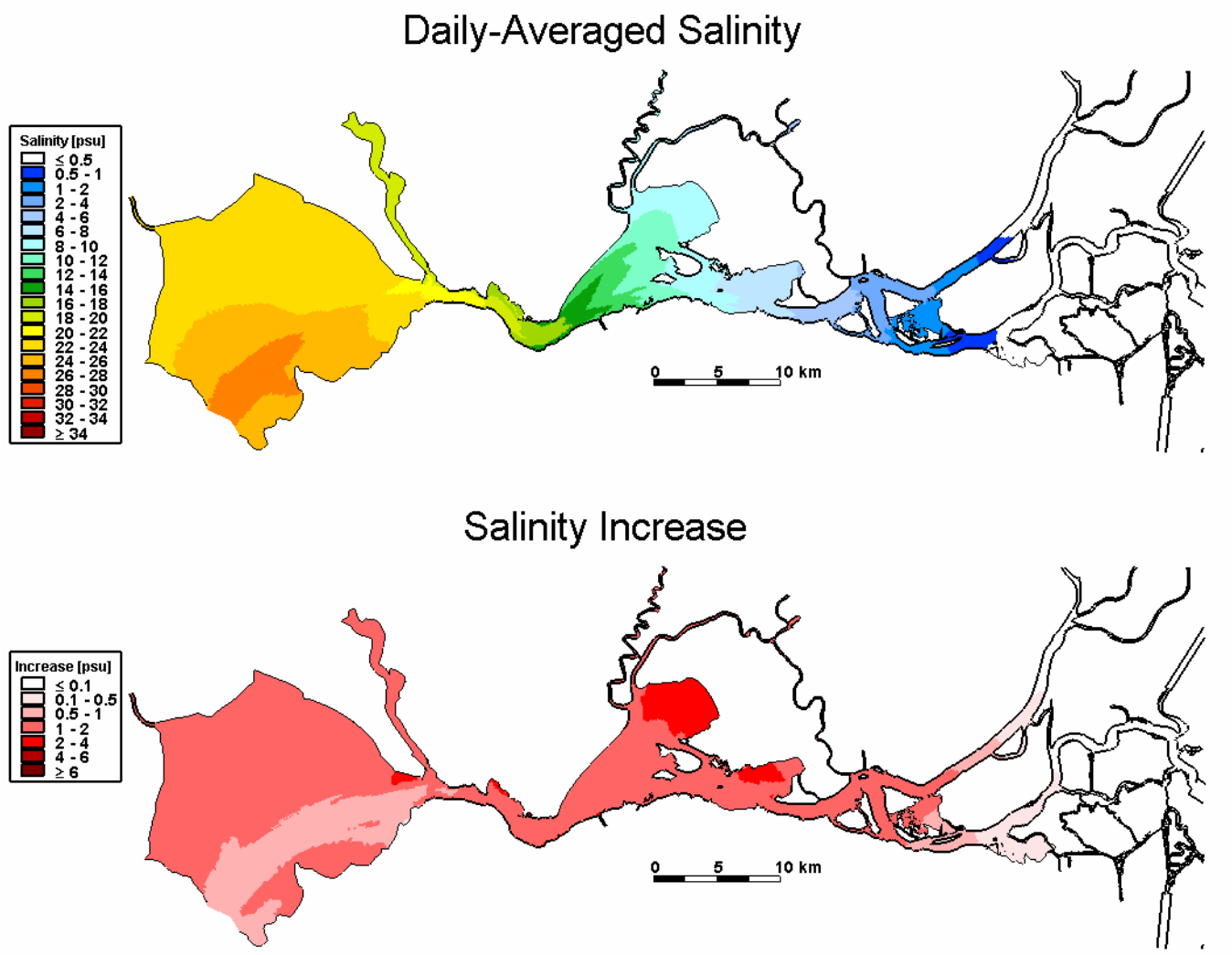

Figure H3.5-5 Depth-averaged and tidally-averaged salinity at tidally-averaged steady state conditions for the 90 cm MSL Rise and increase in salinity relative to the Baseline scenario

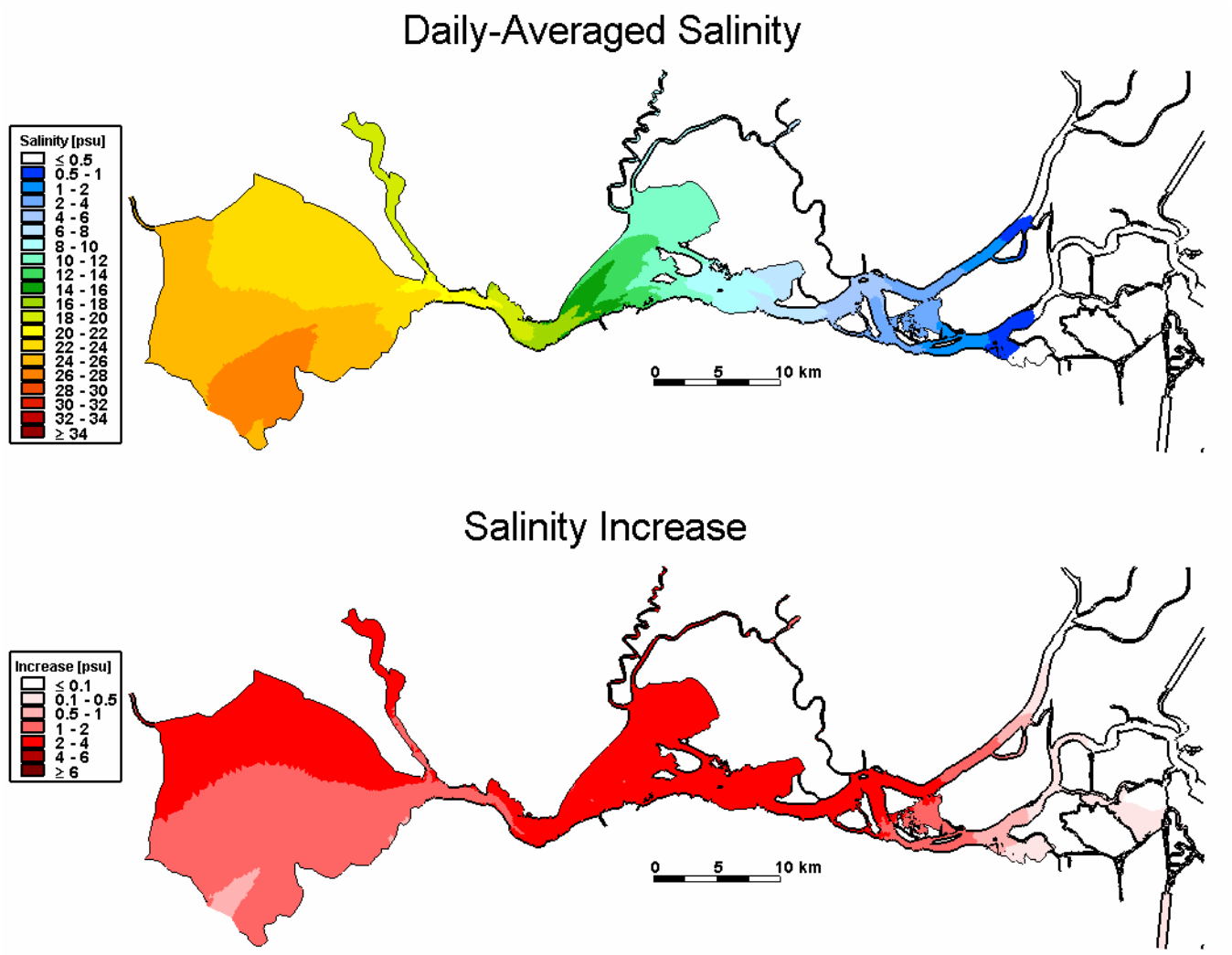

Figure H3.5-6 Depth-averaged and tidally-averaged salinity at tidally-averaged steady state conditions for the 140 cm MSL Rise scenario and increase in salinity relative to the Baseline scenario

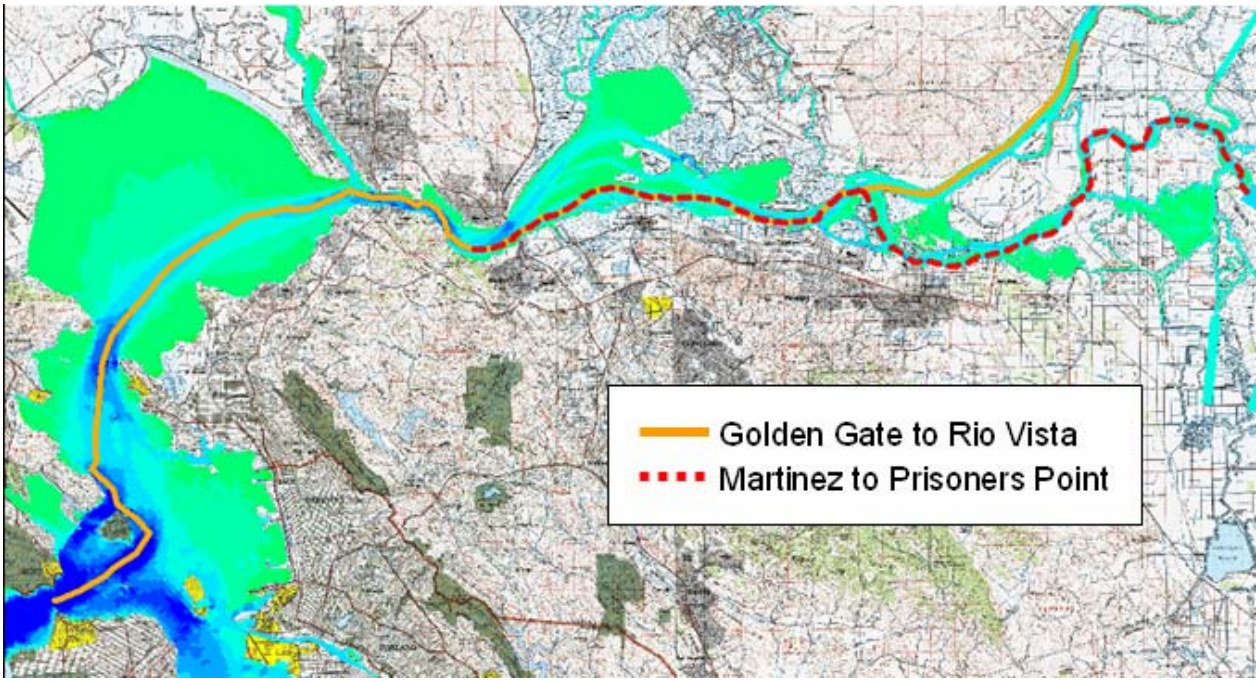

Figure H3.5-7The two channel centerline transects used for output of salinity data. The first transect extends from Golden Gate to Rio Vista while the second transect extends from Martinez to Prisoners Point, splitting from the first transect at the confluence of the San Joaquin River and the Sacramento River.

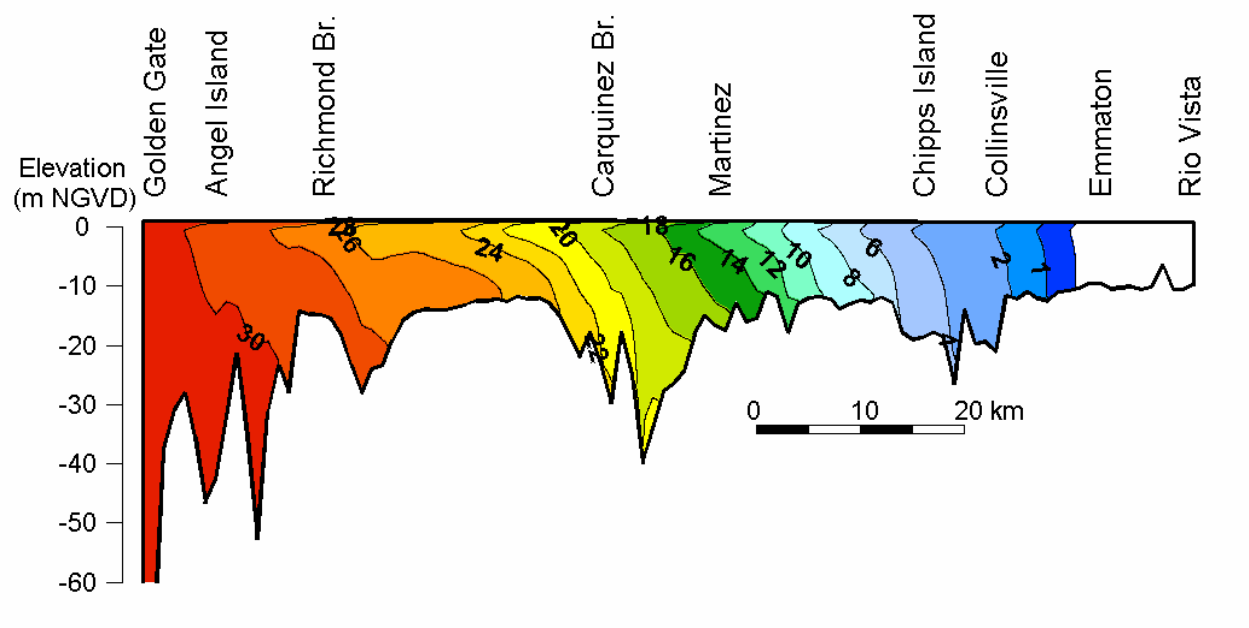

Figure H3.5-8 Tidally-averaged salinity along the centerline transect from the Golden Gate to Rio Vista at tidally-averaged steady state conditions for the Baseline scenario

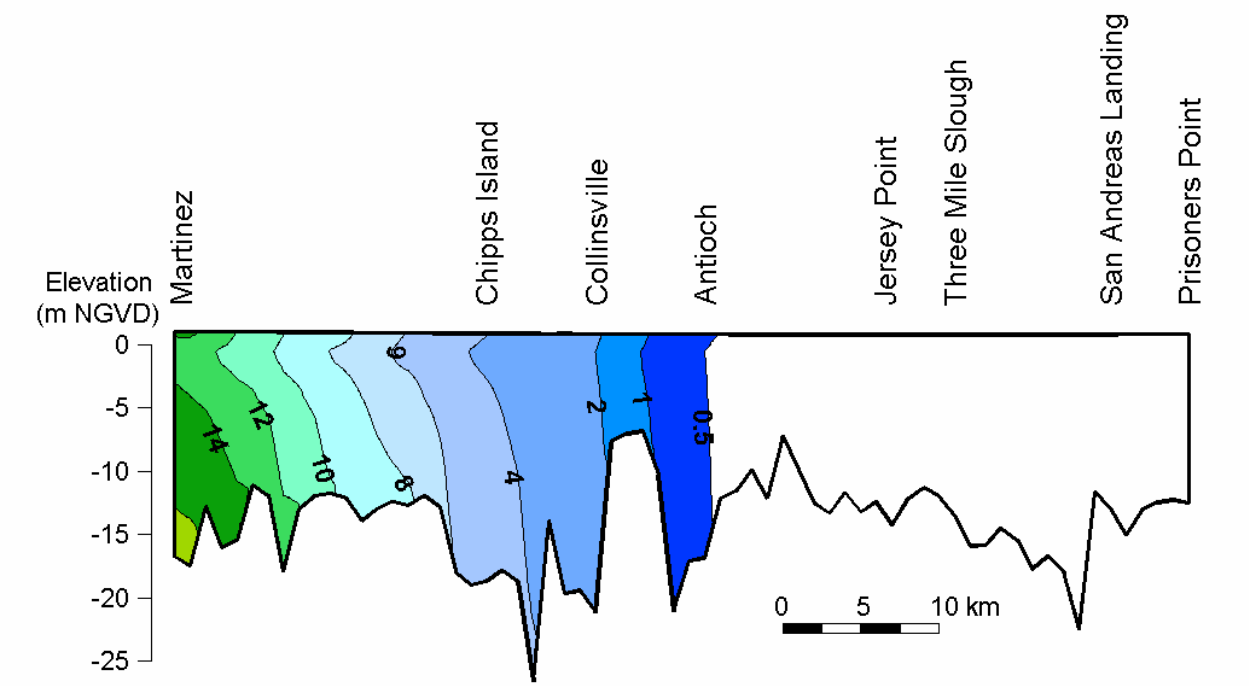

Figure H3.5-9 Tidally-averaged salinity along the centerline transect from Martinez to Prisoners Point at tidally-averaged steady state conditions for the Baseline scenario

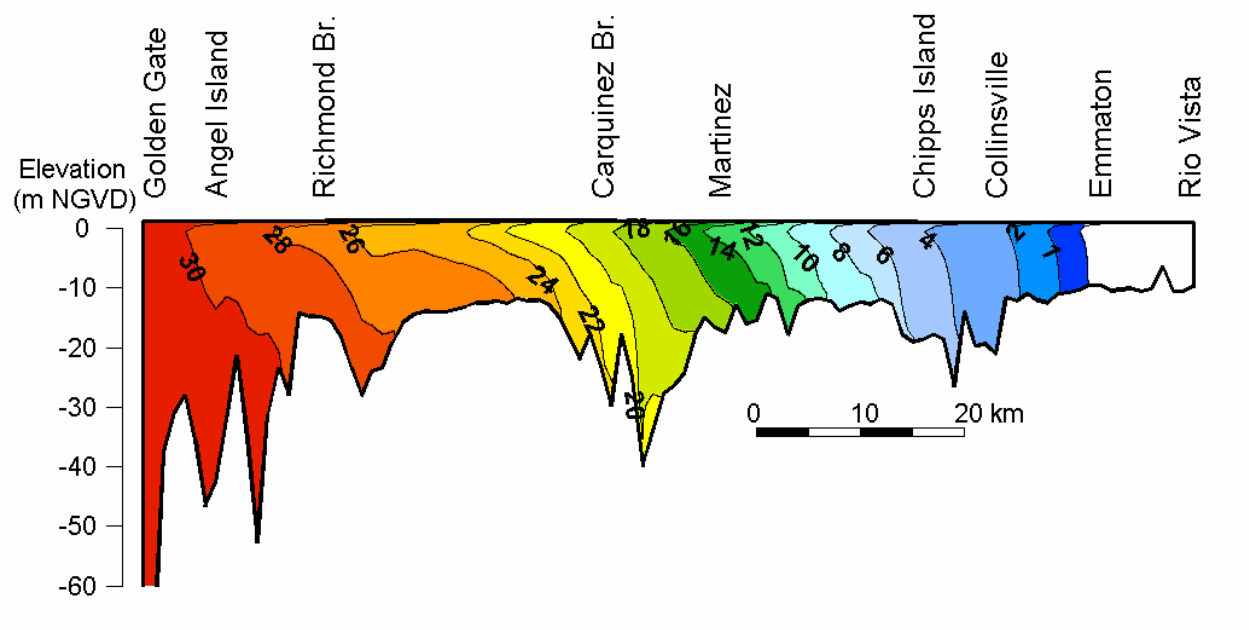

Figure H3.5-10 Tidally-averaged salinity along the centerline transect from Golden Gate to Rio Vista at tidally-averaged steady state conditions for the 20 cm MSL Rise scenario

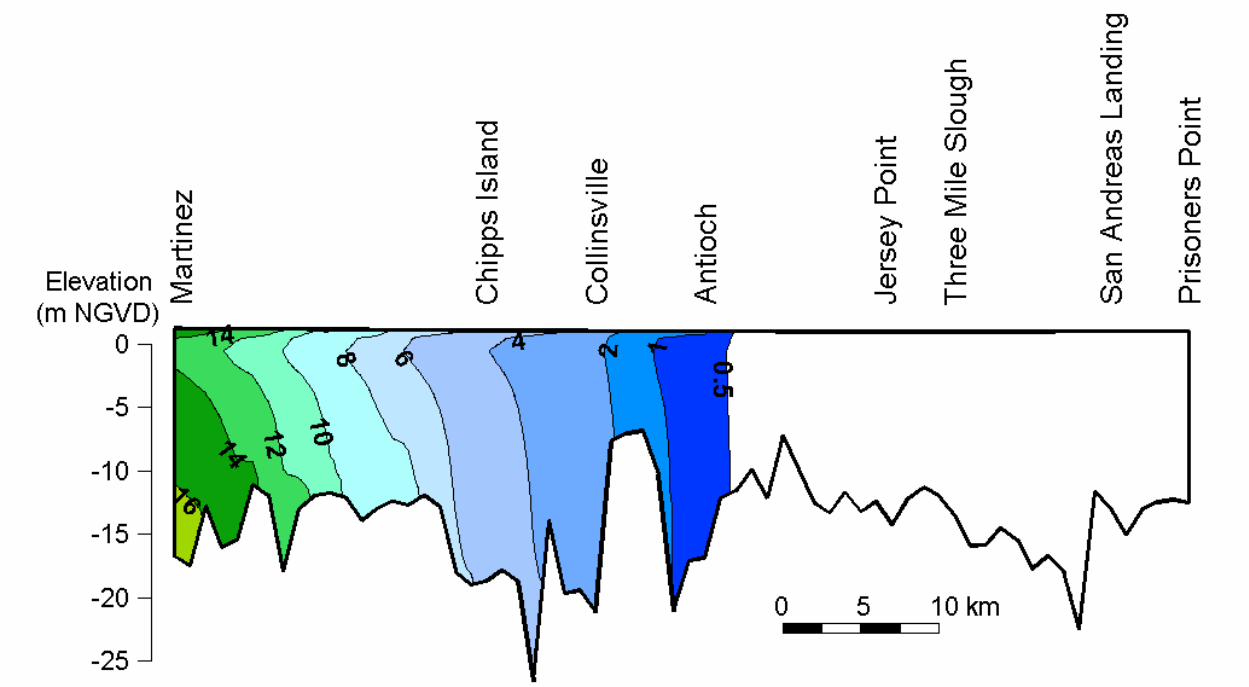

Figure H3.5-11 Tidally-averaged salinity along the centerline transect from Martinez to Prisoners Point at tidally-averaged steady state conditions for the 20 cm MSL Rise scenario

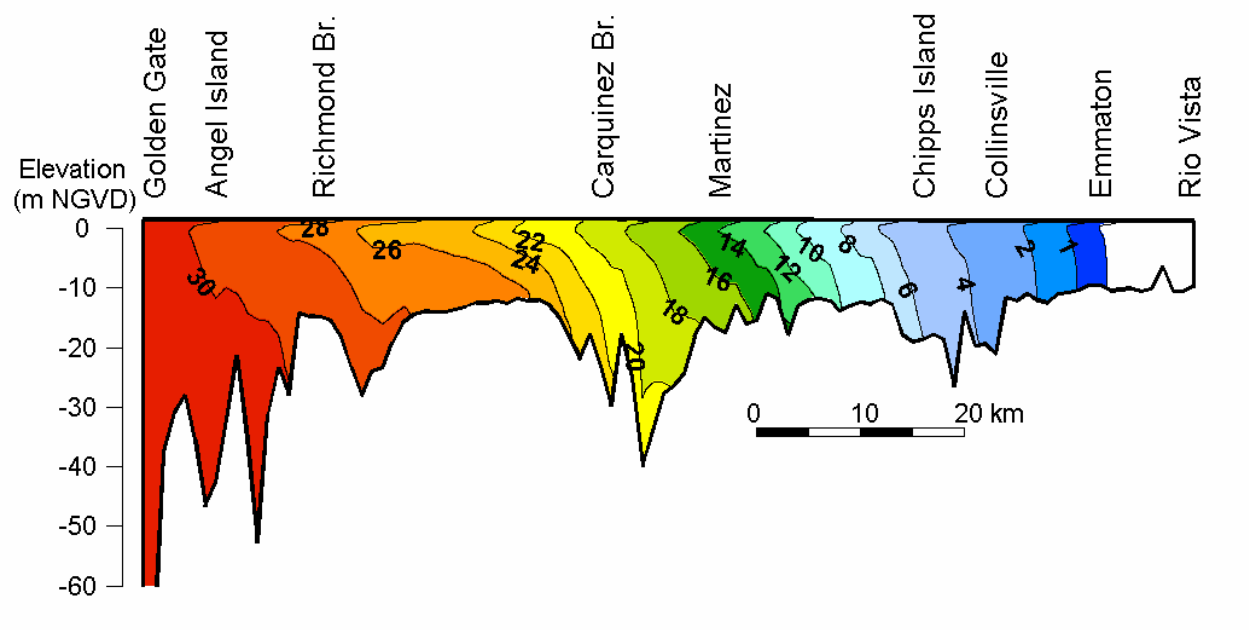

Figure H3.5-12 Tidally-averaged salinity along the centerline transect from Golden Gate to Rio Vista at tidally-averaged steady state conditions for the 50 cm MSL Rise scenario

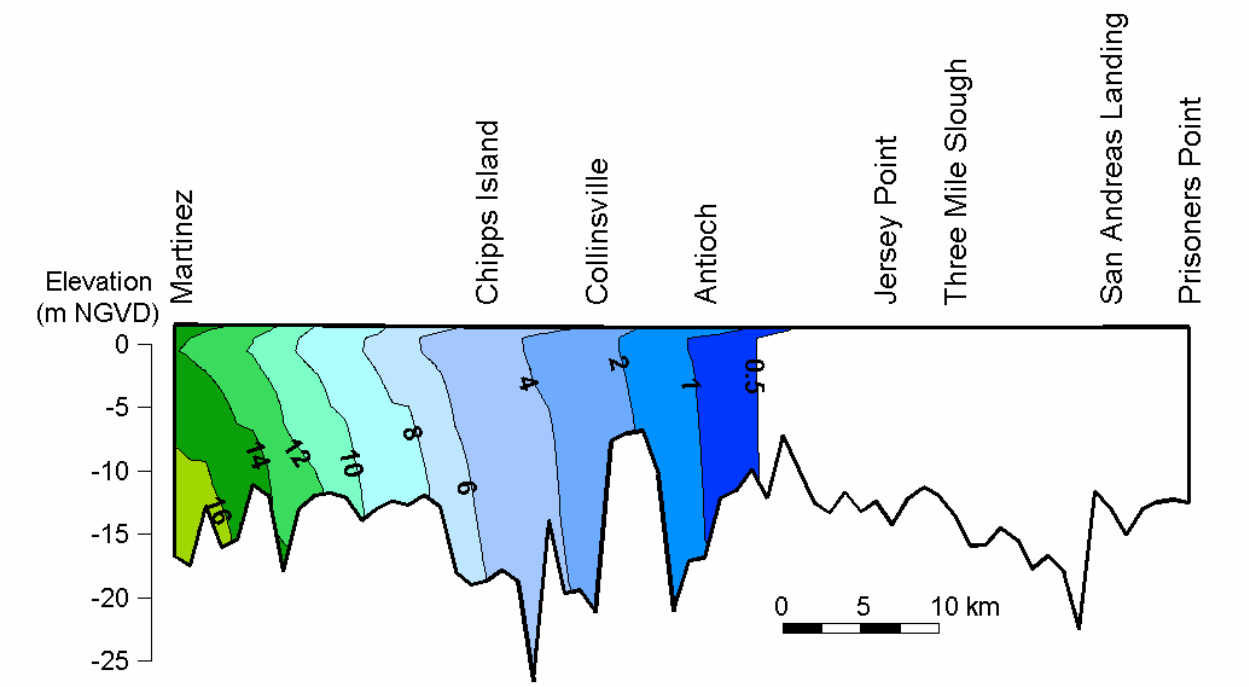

Figure H3.5-13 Tidally-averaged salinity along the centerline transect from Martinez to Prisoners Point at tidally-averaged steady state conditions for the 50 cm MSL Rise scenario

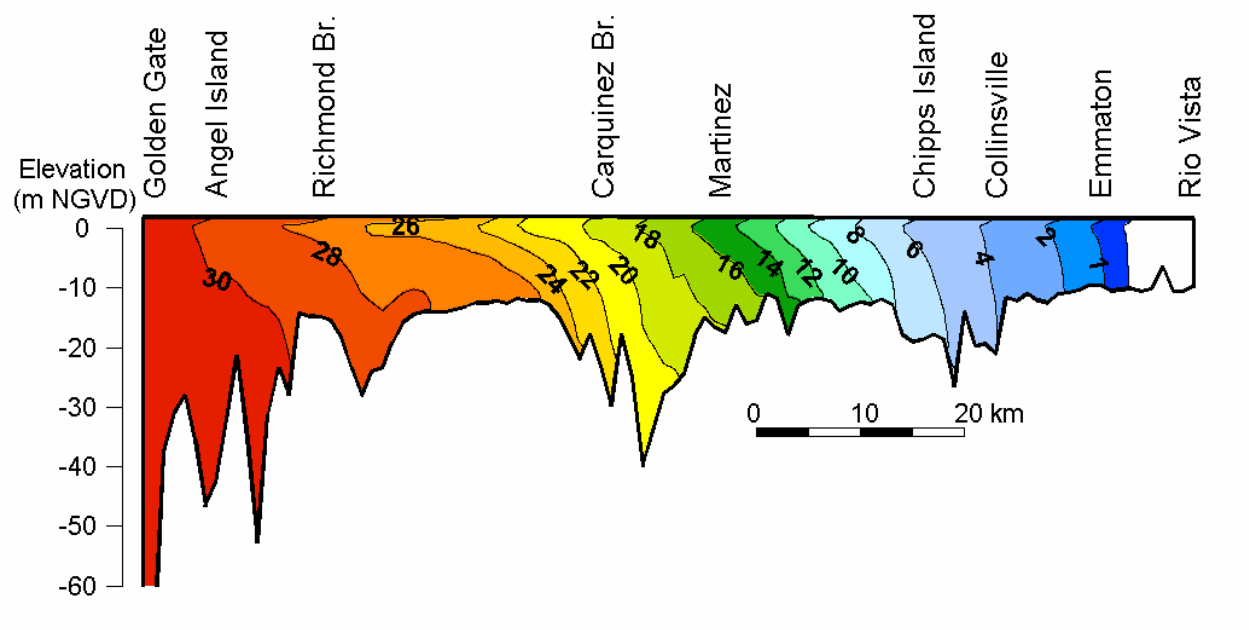

Figure H3.5-14 Tidally-averaged salinity along the centerline transect from Golden Gate to Rio Vista at tidally-averaged steady state conditions for the 90 cm MSL Rise scenario

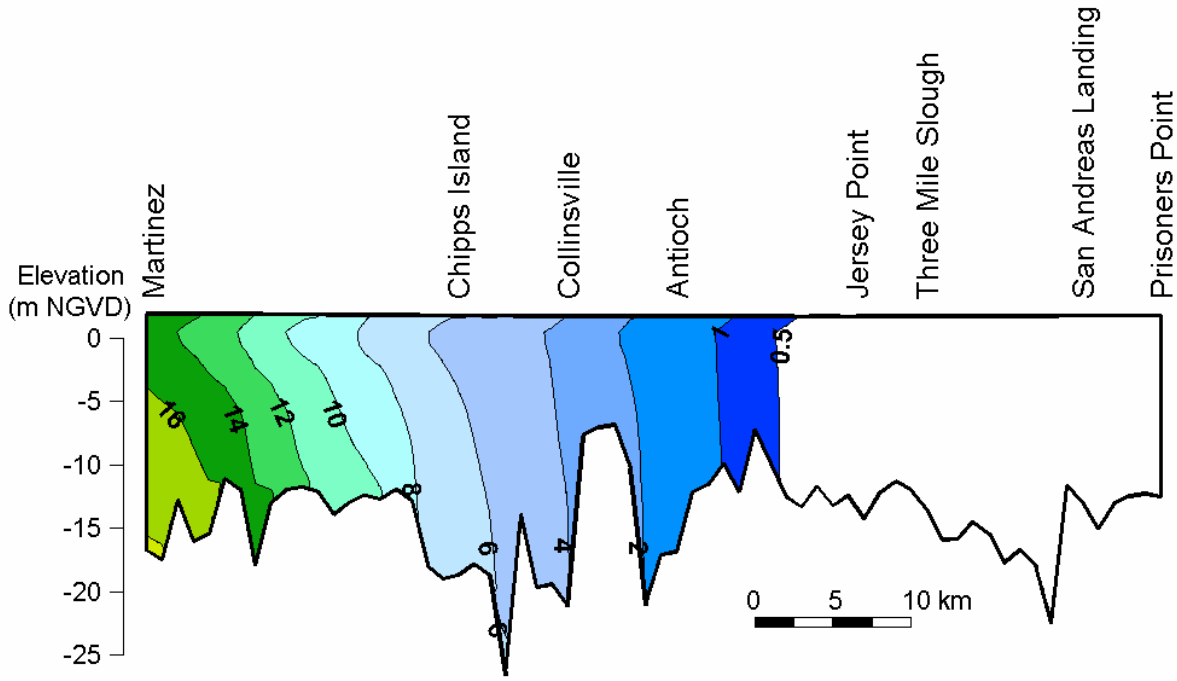

Figure H3.5-15 Tidally-averaged salinity along the centerline transect from Martinez to Prisoners Point at tidally-averaged steady state conditions for the 90 cm MSL Rise scenario

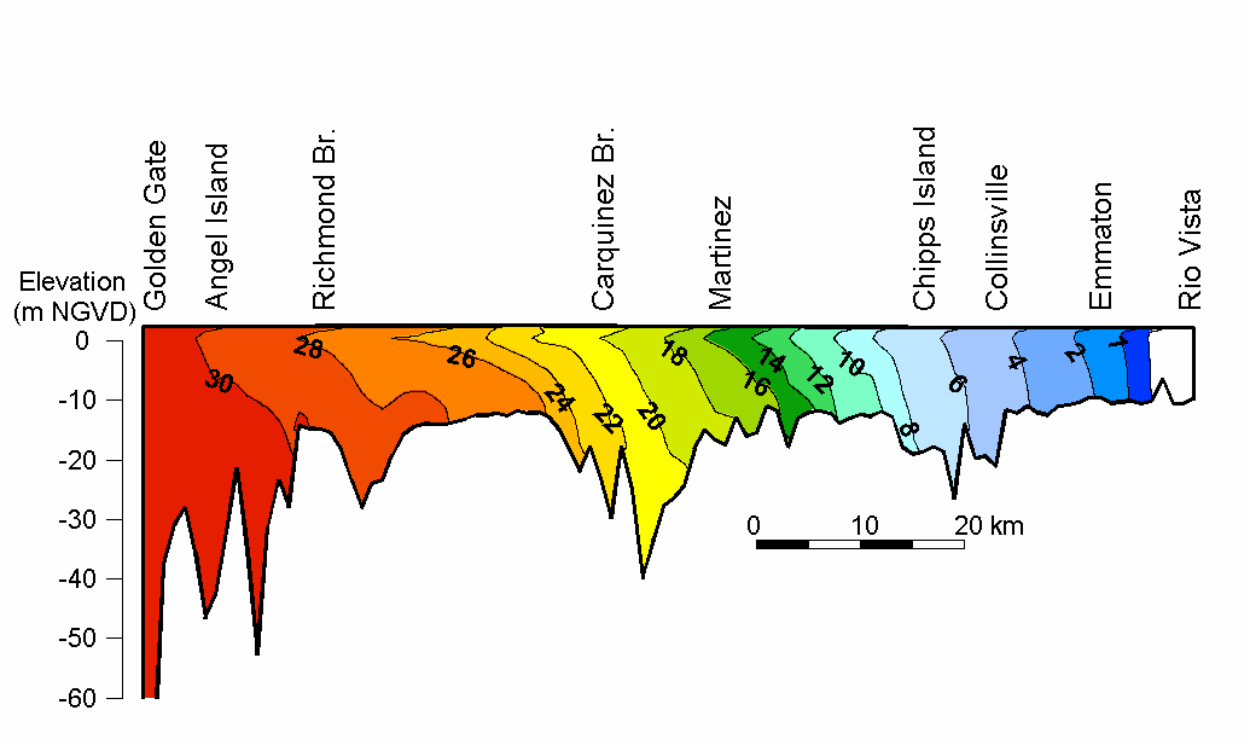

Figure H3.5-16 Tidally-averaged salinity along the centerline transect from Golden Gate to Rio Vista at tidally-averaged steady state conditions for the 140 cm MSL Rise scenario

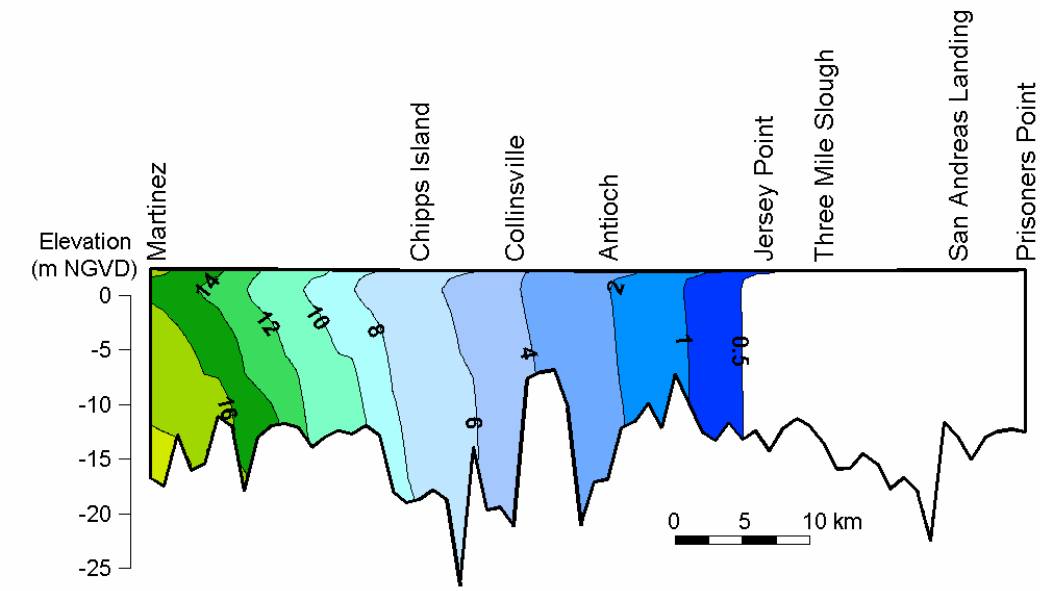

Figure H3.5-17 Tidally-averaged salinity along the centerline transect from Martinez to Prisoners Point at tidally-averaged steady state conditions for the 140 cm MSL Rise scenario

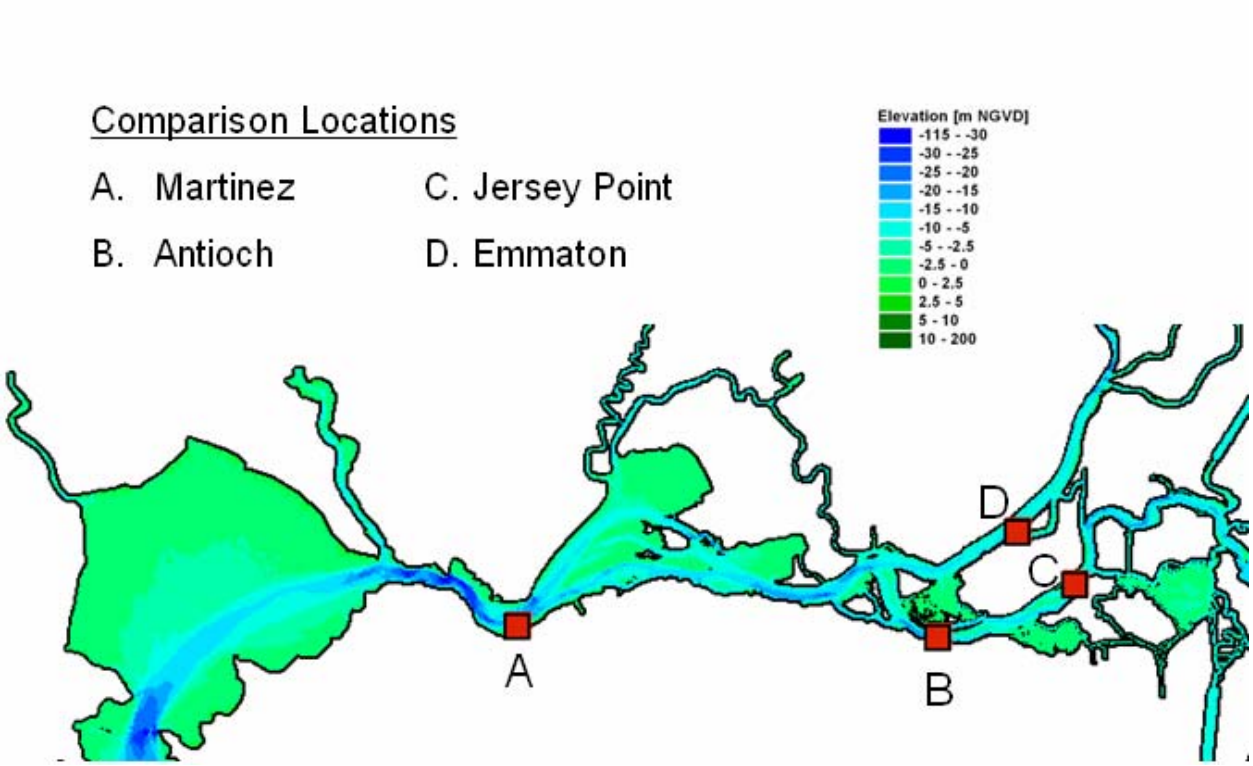

Figure H3.5-18 Locations used to compare tidal variability of salinity among scenarios

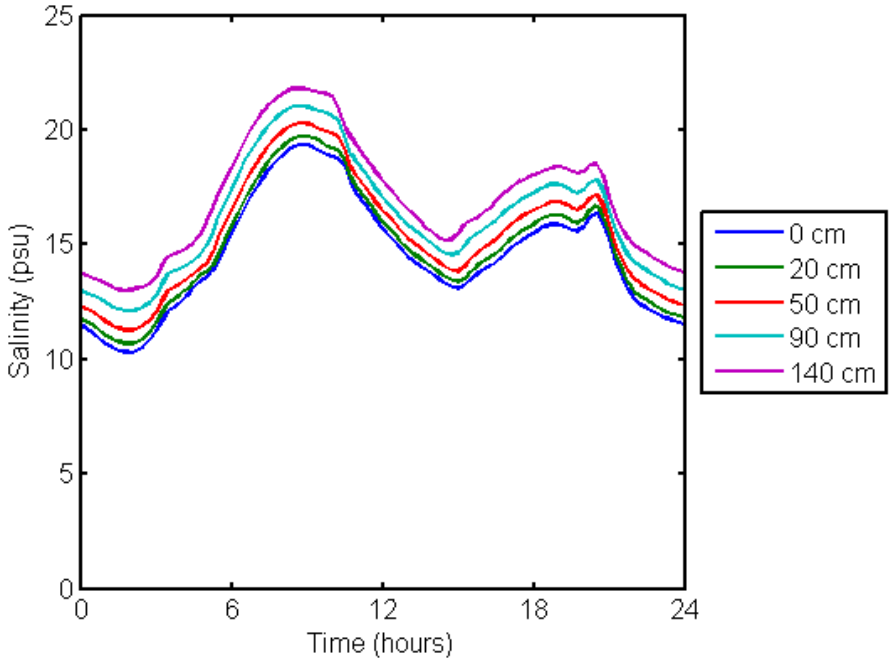

Figure H3.5-19 **Depth-averaged salinity at Martinez during the last day of each MSL rise scenario simulation**

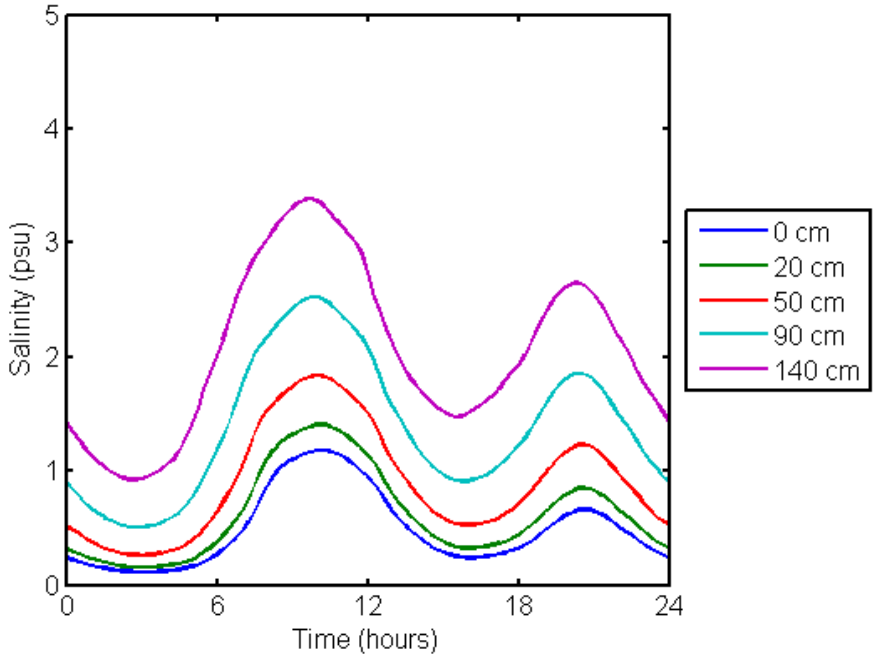

Figure H3.5-20 **Depth-averaged salinity at Antioch during the last day of each MSL rise scenario simulation**

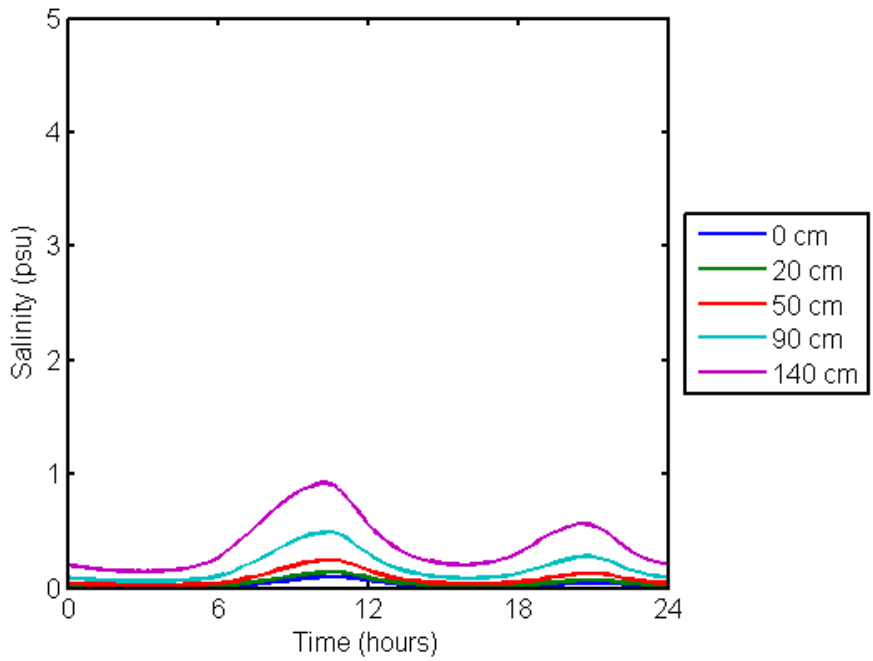

Figure H3.5-21 **Depth-averaged salinity at Jersey Point during the last day of each MSL rise scenario simulation**

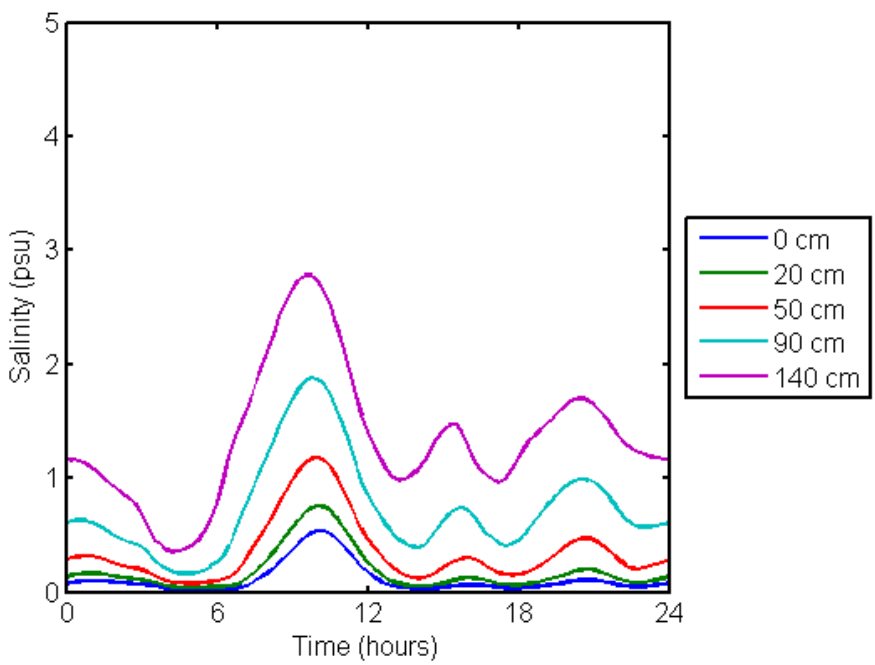

Figure H3.5-22 **Depth-averaged salinity at Emmaton during the last day of each MSL rise scenario simulation**

H3.6 Cumulative Effects of Sea Level Rise

In addition to the sea level rise scenarios, two supplemental scenarios are considered with 140 cm MSL rise. In the Perforated Sherman Island scenario, Sherman Island is considered with 20 breaches. In the Amplified Tides scenario, the tides are assumed to be amplified by 11 percent relative to existing tides. Each scenario simulation was run until tidally-averaged steady state salinity conditions were achieved. It was determined that tidally-averaged steady state conditions were achieved when the tidally-averaged salt flux past each cross-section was approximately zero. Figure H3.6-1 shows the predicted fluxes at the cross-sections indicated on Figure H3.3-1 at steady state conditions for the Baseline scenario. Note that the net salt flux over a tidal cycle is small because the advective and dispersive fluxes approximately balance. The analysis of salt fluxes and transport will be discussed in more detail in Section 7.

Figure H3.6-2 shows depth-averaged and tidally-averaged salinity at tidally-averaged steady state conditions for the Baseline scenario. Note that the predicted values represent salinity from seawater intrusion because local sources of salt (agricultural runoff etc.) are neglected in these simulations. The region shown includes San Pablo Bay, Carquinez Strait, Suisun Bay and a portion of the Delta. The effects of sea level rise on predicted salinity extend over a larger region, but the region of this figure was chosen to show a large area and still be legible. Figure H3.6-3 shows the predicted depth-averaged and tidally-averaged salinity at steady state conditions for the 140 cm MSL Rise scenario and the predicted salinity increase relative to the Baseline scenario. Both of these figures were included in the previous section, but are included here for easy reference.

The two cumulative effects scenarios considered here are compared against both the Baseline scenario and the 140 cm MSL Rise scenario. Figure H3.6-4 shows the predicted depth-averaged and tidally-averaged salinity at tidally-averaged steady state conditions for the Perforated Sherman Island scenario, and the predicted depth-averaged and tidally-averaged salinity increase relative to the Baseline scenario. The predicted salinity increases are between 1 psu and 4 psu in most of the region shown in the figure and greater than 4 psu in some intertidal regions of Suisun Bay. The 0.5 psu contour intrudes 10 to 15 km further into the western Delta in the Perforated Sherman Island scenario than the Baseline scenario and the 0.5 psu contour of predicted salinity from seawater intrusion extends into the central Delta.

The effects of Perforated Sherman Island alone are evaluated by subtracting the predicted depth-averaged and tidally-averaged salinity for the 140 cm MSL Rise scenario from the predicted depth-averaged and tidally-averaged salinity Perforated Sherman Island scenario. Because the Perforated Sherman Island scenario also assumes 140 cm of MSL rise, the calculated difference is the additional salt intrusion resulting from tidal exchange with Sherman Island and ranges from 0.1 psu up to 4 psu (Figure H3.6-5). Note that these effects are at steady state conditions, not transient effects associated with the initial flooding of Sherman Island. The increased salinity is particularly large near Sherman Island, in the range of 1 psu to 4 psu. Without sea level rise, the effects would have been lower, because less salt would have been present in the western Delta and Suisun Bay to mix into Sherman Island.

Figure H3.6-6 shows the predicted depth-averaged and tidally-averaged salinity at tidally-averaged steady state conditions for the Amplified Tides scenario, and the predicted depth-averaged and tidally-averaged salinity increase relative to the Baseline scenario. The predicted salinity increases are between 1 psu and 4 psu in most of the region shown in the figure and greater than 4 psu in some intertidal regions of Suisun Bay. The 0.5 psu contour intrudes approximately 10 further into the western Delta in the Amplified Tides scenario than the Baseline scenario and the 0.1 psu contour of predicted salinity from seawater intrusion extends into the central Delta.

The effects of tidal amplification alone are evaluated by subtracting the predicted depth-averaged and tidally-averaged salinity for the 140 cm MSL Rise scenario from the predicted depth-averaged and tidally-averaged Amplified Tides scenario. Because the Amplified Tides scenario assumes 140 cm of MSL rise, the calculated difference is the additional salt intrusion resulting from tidal amplification and ranges from 0.1 psu up to 1 psu (Figure H3.6-7).

The tidally-averaged salinity profiles along the transects shown in Figure H3.6-8 are shown for the Baseline scenario in Figures H3.6-9 and H3.6-10, and for the 140 cm MSL Rise scenario in Figures H3.6-11 and H3.6-12. These figures were also included in Section 5 and are reproduced here for easy comparison to the cumulative effects scenario results shown below. The surface layers are only wet near high water when salinity is at a maximum and, therefore, the near surface region appears to have unstable stratification as an artifact of the tidal averaging. Unstable stratification is not present in the instantaneous salinity field during any part of the tidal cycle. The predicted salinity profiles in Figures H3.6-13 and H3.6-14 show greatly increased salt intrusion due to tidal exchange with Sherman Island and Figures H3.6-15 and H3.6-16 show increased salt intrusion as a result of amplification of tides. Substantial vertical stratification in the predicted tidally-averaged salinity is present in the cumulative effects scenarios. The degree of predicted stratification is similar among the scenarios in Central Bay. In portions of San Pablo Bay and Carquinez Strait the predicted stratification decreases as a result of tidal amplification and tidal exchange with Sherman Island. This probably results because tidal currents increase in both cases, leading to more vigorous turbulent mixing. The predicted stratification in Suisun Bay and the western Delta increases as a result of exchange with Sherman Island. An increase in gravitational circulation was expected due to increased salinity gradients in these regions for this scenario.

The salinity maps and profile figures discussed previously show tidally-averaged salinity. The temporal variability of predicted salinity is shown at several locations in time series graphs. At the end of each simulation, tidally-averaged steady state conditions have been reached and, due to the idealized tides used to force the model, the same salinity pattern repeats each day. The four locations selected to examine tidal variability of predicted salinity are Martinez, Antioch, Jersey Point, and Emmaton. These locations, shown in Figure H3.6-17, were chosen primarily because they are important monitoring locations. Figure H3.6-18 shows the variability of depth-averaged salinity at Martinez for each scenario. The salinity increases slightly due to amplification of tides and due to tidal exchange with Sherman Island. Figure H3.6-19 shows the variability of depth-averaged salinity at Antioch for each scenario. The salinity increases due to amplification of tides

and due to tidal exchange with Sherman Island. Tidal exchange with Sherman Island causes large increases in salinity at Antioch and greatly decreases tidal variability, probably because Sherman Island is releasing salt to the San Joaquin River during ebb tides. For example, at 4:00 am the salinity for the Baseline scenario is 0.1 psu and the salinity for the 140 cm MSL Rise scenario is 1 psu, while the salinity for the Perforated Sherman Island scenario is 3 psu. Figure H3.6-20 shows the variability of depth-averaged salinity at Jersey Point for each scenario. The salinity increases significantly due to amplification of tides and greatly due to tidal exchange with Sherman Island. For example, at 4:00 am the salinity for the Baseline scenario is 0 psu and the salinity for the 140 cm MSL Rise scenario is 0.2 psu while the salinity for the Perforated Sherman Island scenario is nearly 2 psu. Figure H3.6-21 shows the variability of depth-averaged salinity at Emmaton for each scenario. The salinity increases significantly due to amplification of tides and greatly due to tidal exchange with Sherman Island. For example, at 5:00 am the salinity for the Baseline scenario is 0 psu and the predicted salinity for the 140 cm MSL Rise scenario is 0.4 psu while the predicted salinity for the Perforated Sherman Island scenario is nearly 3 psu.

Abundance or survival of several estuarine biological populations in the San Francisco Estuary is positively related to freshwater flow (Jassby et al., 1995). These relationships have been described in terms of X2, the location of the 2 psu tidally-averaged bottom salinity. X2 is also used as a water quality standard, with requirements to maintain X2 less than specified values (e.g., seaward of Collinsville) during specified periods. Though this standard is complex, it is the water quality standard mostly likely to apply for the Net Delta Outflow of 260 m^3/s (9,182 cfs) used in the MSL rise scenarios. Therefore, a substantial increase in predicted X2 from MSL rise would suggest that substantially increased NDO may be required to meet the X2 standard as a result of sea level rise. The MSL rise scenarios all use constant Net Delta Outflow, and, therefore, a single X2 location is associated with the salinity field for each scenario at tidally-averaged steady state. Table H3-3 shows the computed X2 values for the cumulative effects scenarios, with the Baseline and 140 cm MSL Rise values shown for reference. X2 values for the other MSL rise scenarios are provided in Table H3-2.

The estimated X2 increases for the cumulative effects scenarios are larger than the estimated X2 increases for the MSL rise scenarios. The X2 increase for each MSL rise scenario was related to an approximate compensating flow that would that would be required to return X2 to the value calculated for the Baseline scenario. However, this method to estimate compensating flow is probably not appropriate for the cumulative effects scenarios. Specifically, the regression equations used to relate X2 to NDO may not be appropriate for these scenarios, particularly the Perforated Sherman Island scenario, because the strength of dispersive transport increases substantially for these scenarios. Therefore, substantially more NDO would be required to maintain X2 than would be suggested by the regression equations. The WAM will be used to estimate flow required to meet relevant water quality standards for a large range of scenarios and will incorporate the effect of sea level rise on salt intrusion, as discussed in Section 7.

In summary, the simulations of the cumulative effects scenarios indicate increased Delta salinity from tidal amplification and greatly increased salinity from tidal exchange with

Sherman Island. The large increases noted in the Perforated Sherman Island scenario are consistent with the understanding that mixing in Franks Tract causes substantial mixing of salt into the central Delta (RMA 2005). Because Sherman Island is much larger than Franks Tract and closer to the large salinity gradients present in Suisun Bay during summer conditions, the effects of Sherman Island on salt intrusion should be much larger than those of Franks Tract. The simulation results suggest that the combination of large sea level rise and a modest extent of Delta island flooding would lead to large impacts on Delta water quality and water supply reliability.

It should be noted that the fixed Net Delta Outflow of 260 m^3/s (9,182 cfs) was used in all simulations and that larger salt intrusion would occur during summer and fall conditions during a dry or critical year. In addition, while 140 cm of MSL rise is on the high end of sea level rise predictions for the next 100 years, this scenario almost certainly underestimates channel deepening that will occur as a cumulative effect of MSL rise, ongoing erosion, dredging activities, localized and larger scale scour from island flooding and restoration projects. Furthermore, the assumptions of only one flooded island and hardened shorelines outside of the Delta are also likely to lead to dramatic underestimation of effects of sea level rise, because sea level rise is likely to cause more frequent and severe flooding of Delta islands and other regions.

Table H3-3 X2 Location for Baseline Scenario, 140 cm MSL Rise Scenario and the Two Cumulative Effects Scenarios

Scenario	MSL Rise (cm)	Cumulative Effects	X2 Location (km)
Baseline	0	none	83.4
140 cm MSL Rise	140	none	91.5
Perforated Sherman Is.	140	breached Sherman Island	97.5
Amplified Tides	140	tides amplified by 11%	93.5

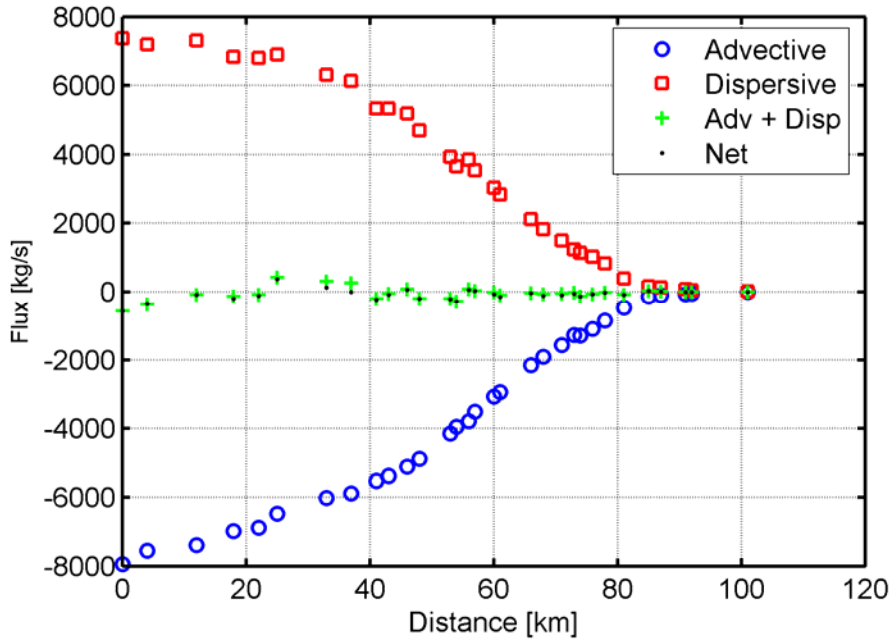

Figure H3.6-1 Predicted advective, dispersive and net (tidally-averaged) salt fluxes during the last day of the Baseline scenario

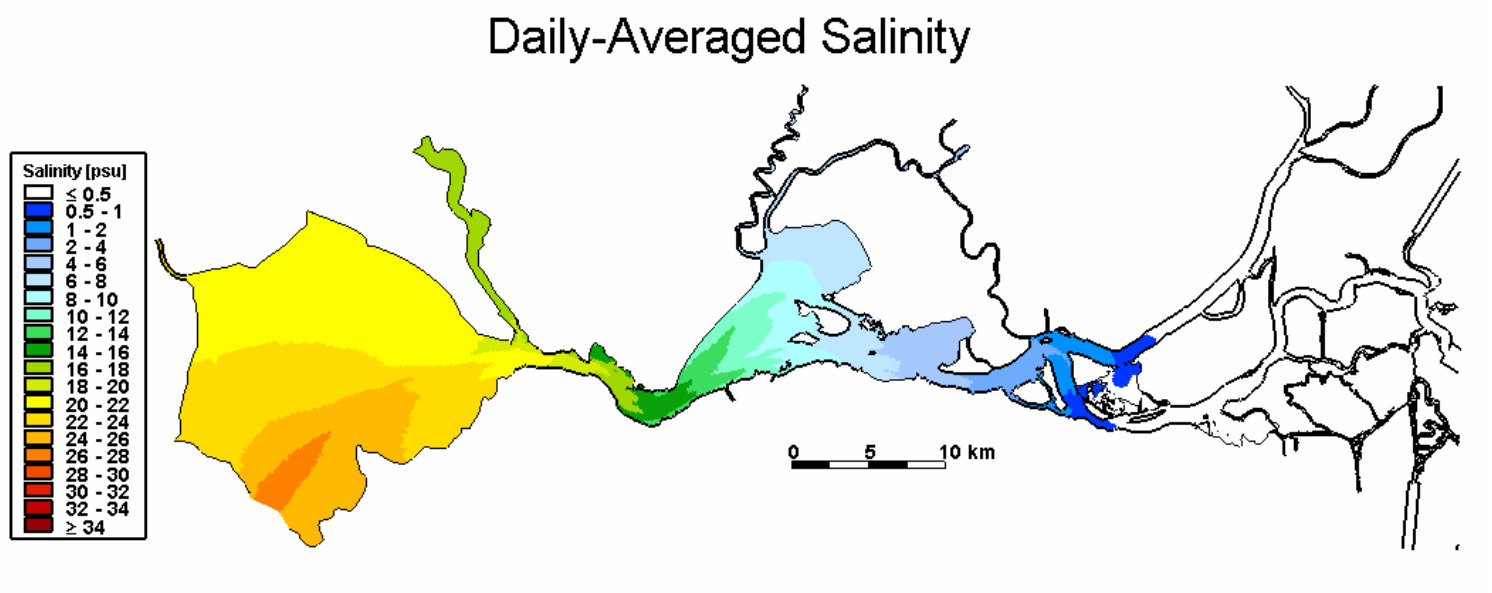

Figure H3.6-2 Depth-averaged and tidally-averaged salinity at tidally-averaged steady state conditions for the Baseline scenario

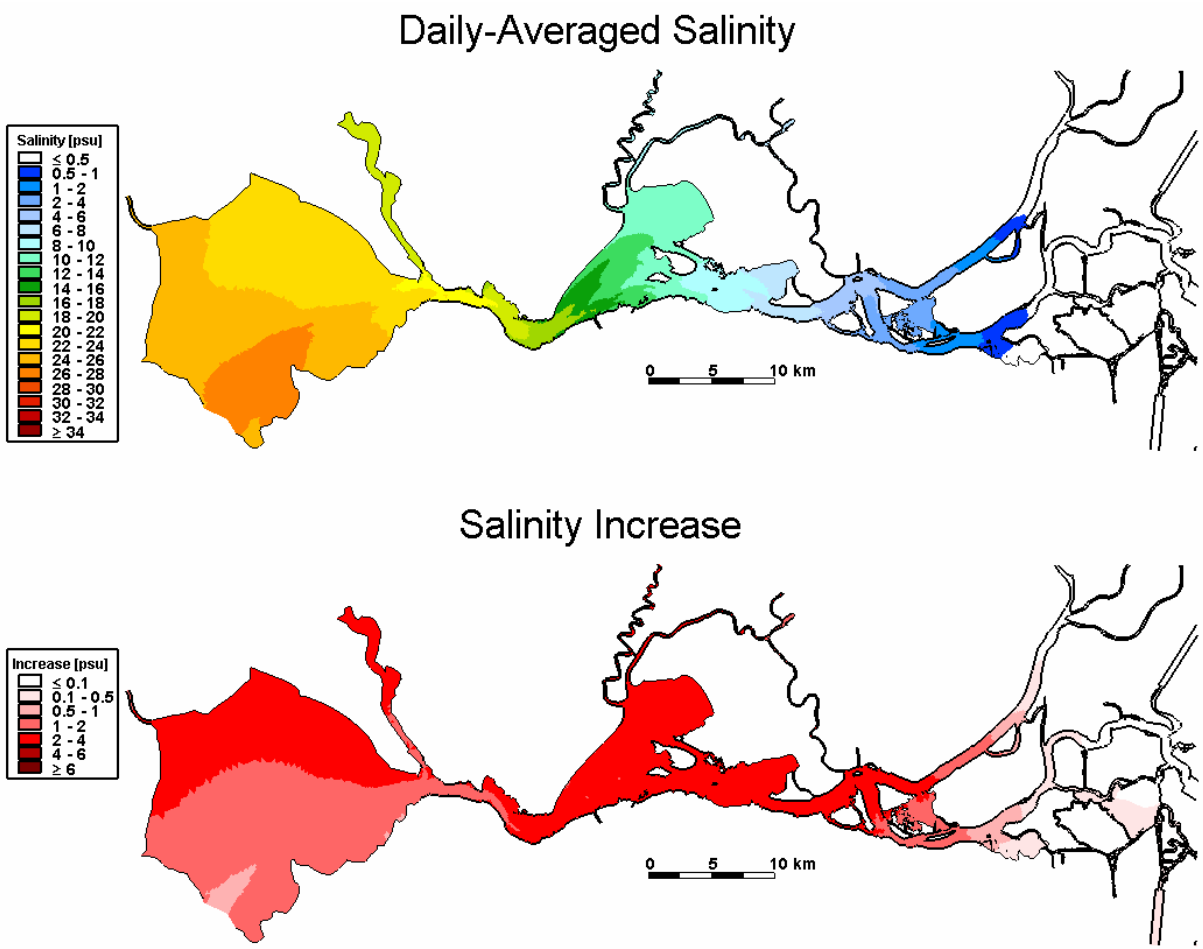

Figure H3.6-3Depth-averaged and tidally-averaged salinity at tidally-averaged steady state conditions for the 140 cm MSL Rise scenario and increase in salinity relative to the Baseline scenario

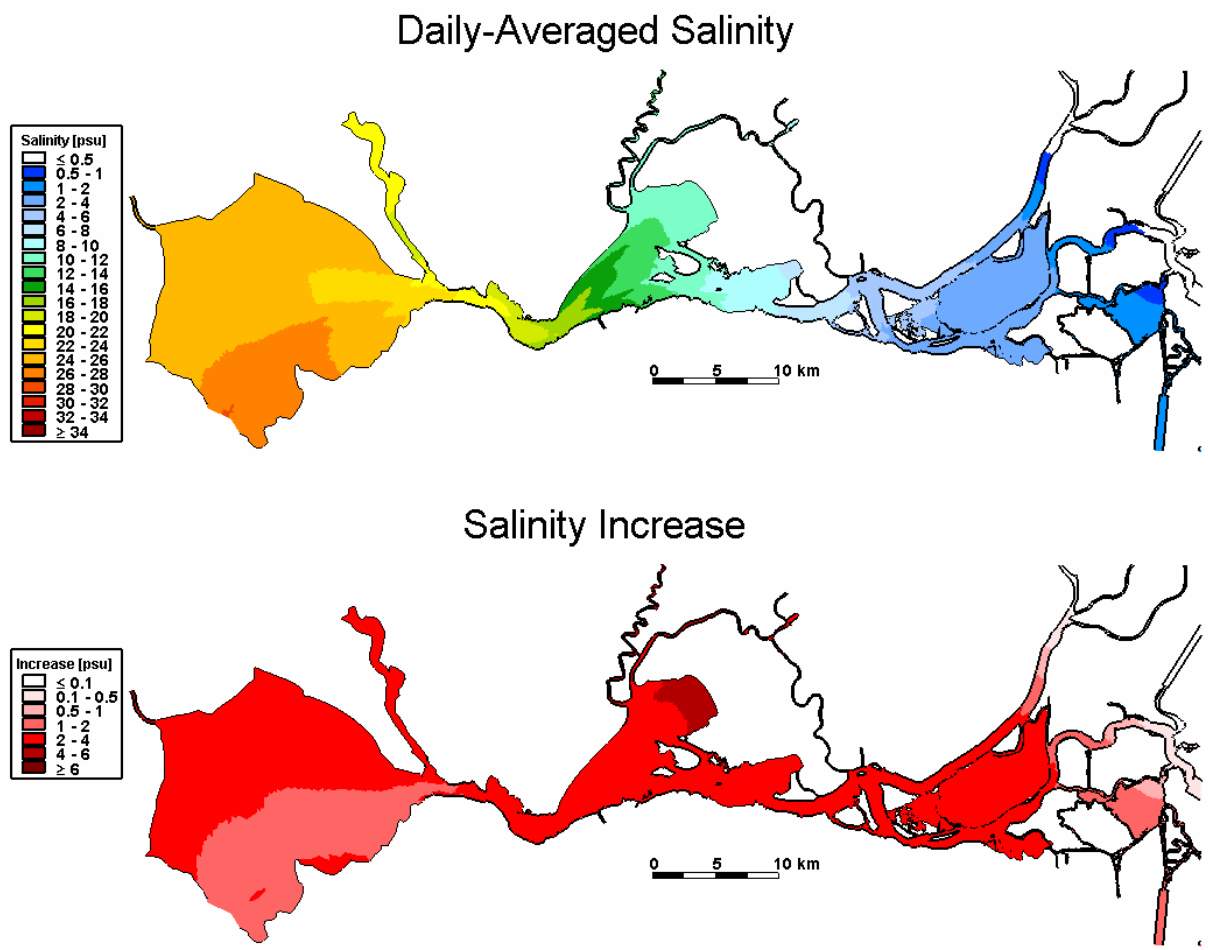

Figure H3.6-4Depth-averaged and tidally-averaged salinity at tidally-averaged steady state conditions for the Perforated Sherman Island scenario and increase in salinity relative to the Baseline scenario

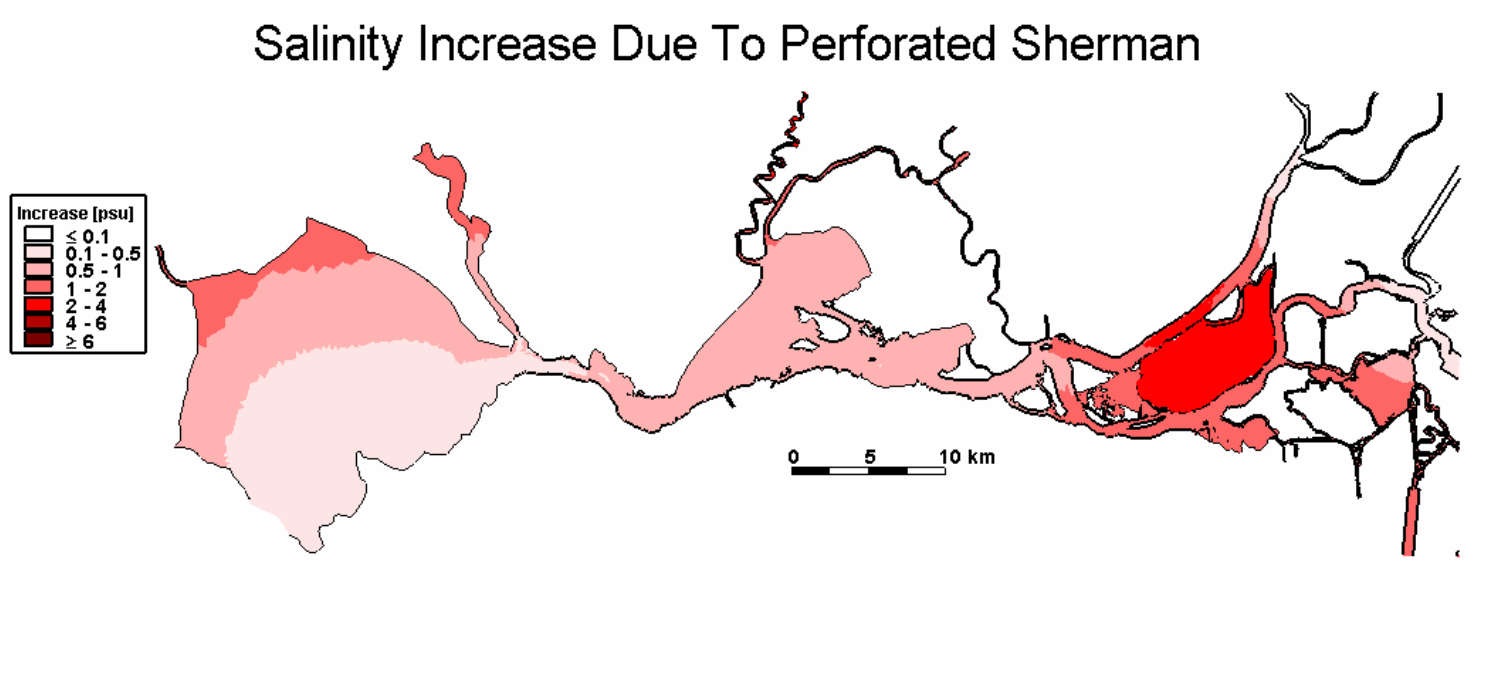

Figure H3.6-5Difference in depth-averaged and tidally-averaged salinity at tidally-averaged steady state conditions between the Perforated Sherman Island scenario and the 140 cm MSL Rise scenario

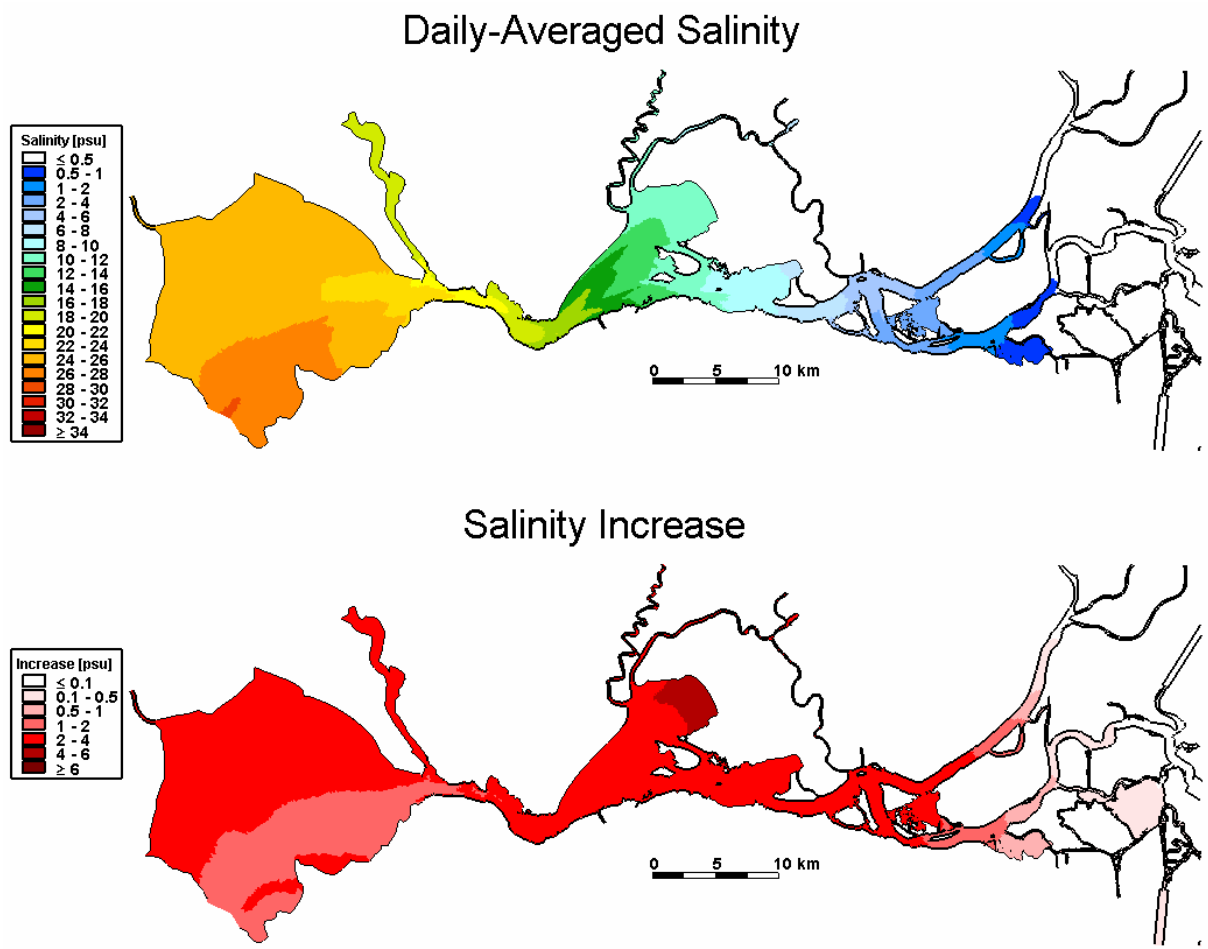

Figure H3.6-6Depth-averaged and tidally-averaged salinity at tidally-averaged steady state conditions for the Amplified Tides scenario and increase in salinity relative to the Baseline scenario

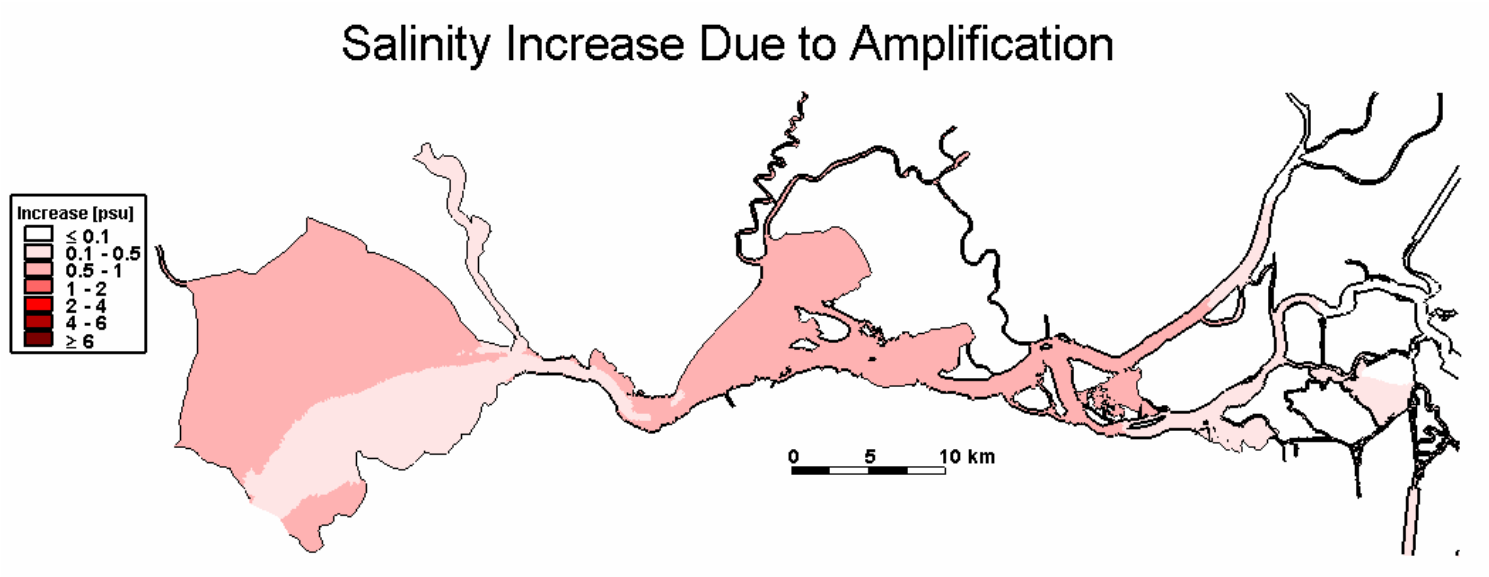

Figure H3.6-7Difference in depth-averaged and tidally-averaged salinity at tidally-averaged steady state conditions between the Amplified Tides scenario and the 140 cm MSL Rise scenario

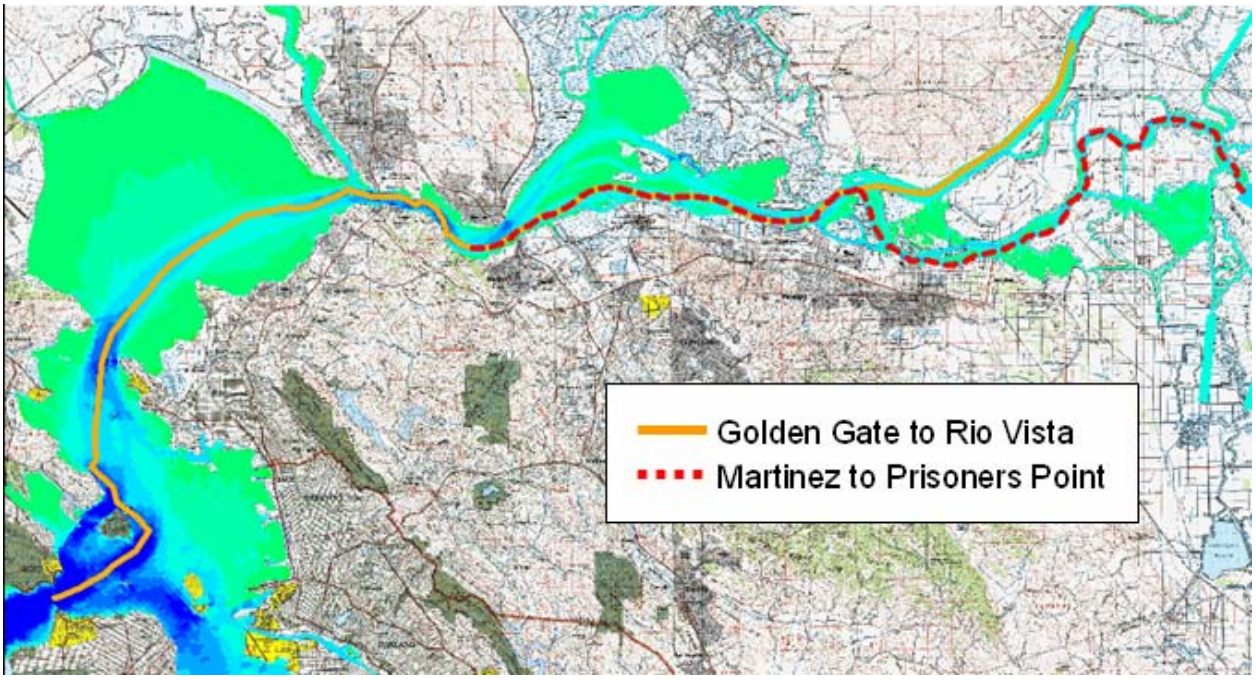

Figure H3.6-8The two channel centerline transects used for output of salinity data. The first transect extends from Golden Gate to Rio Vista while the second transect extends from Martinez to Prisoners Point, splitting from the first transect at the confluence of the San Joaquin River and the Sacramento River.

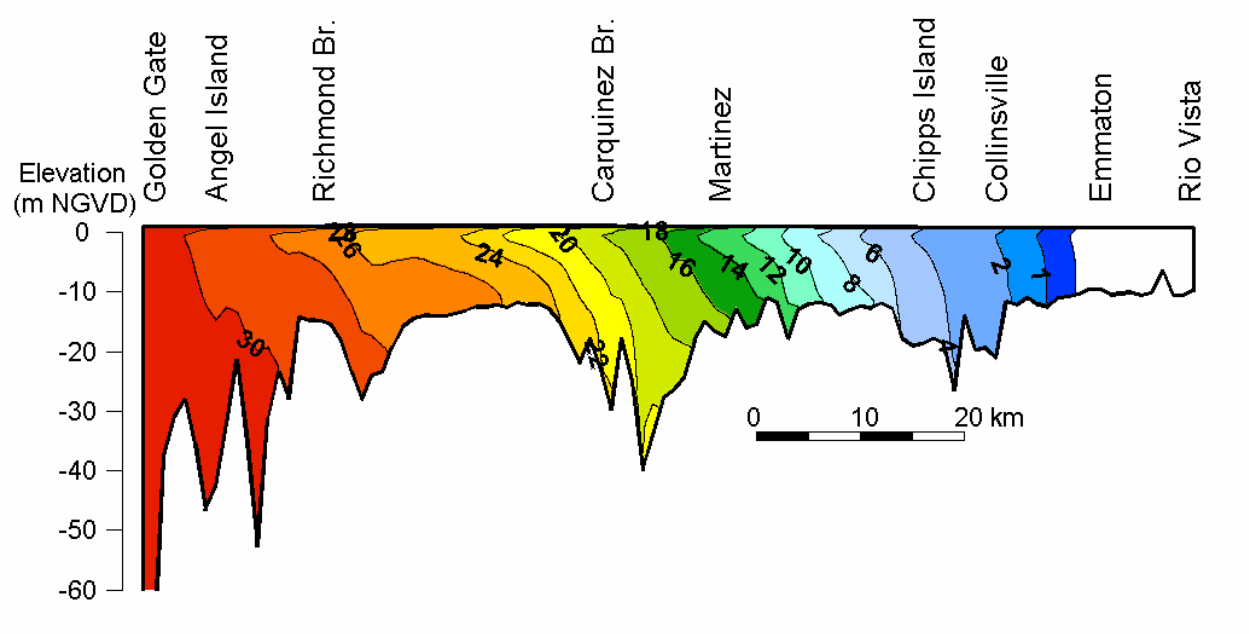

Figure H3.6-9 Tidally-averaged salinity along the centerline transect from Golden Gate to Rio Vista at tidally-averaged steady state conditions for the Baseline scenario

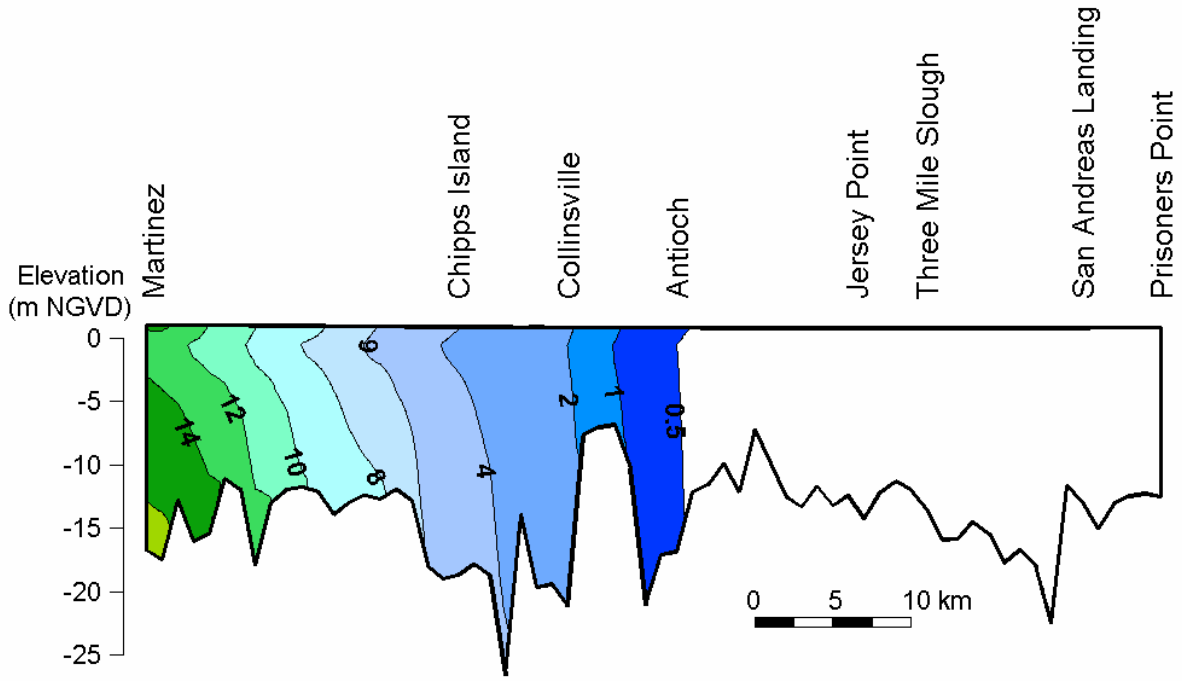

Figure H3.6-10 Tidally-averaged salinity along the centerline transect from Martinez to Prisoners Point at tidally-averaged steady state conditions for the Baseline scenario

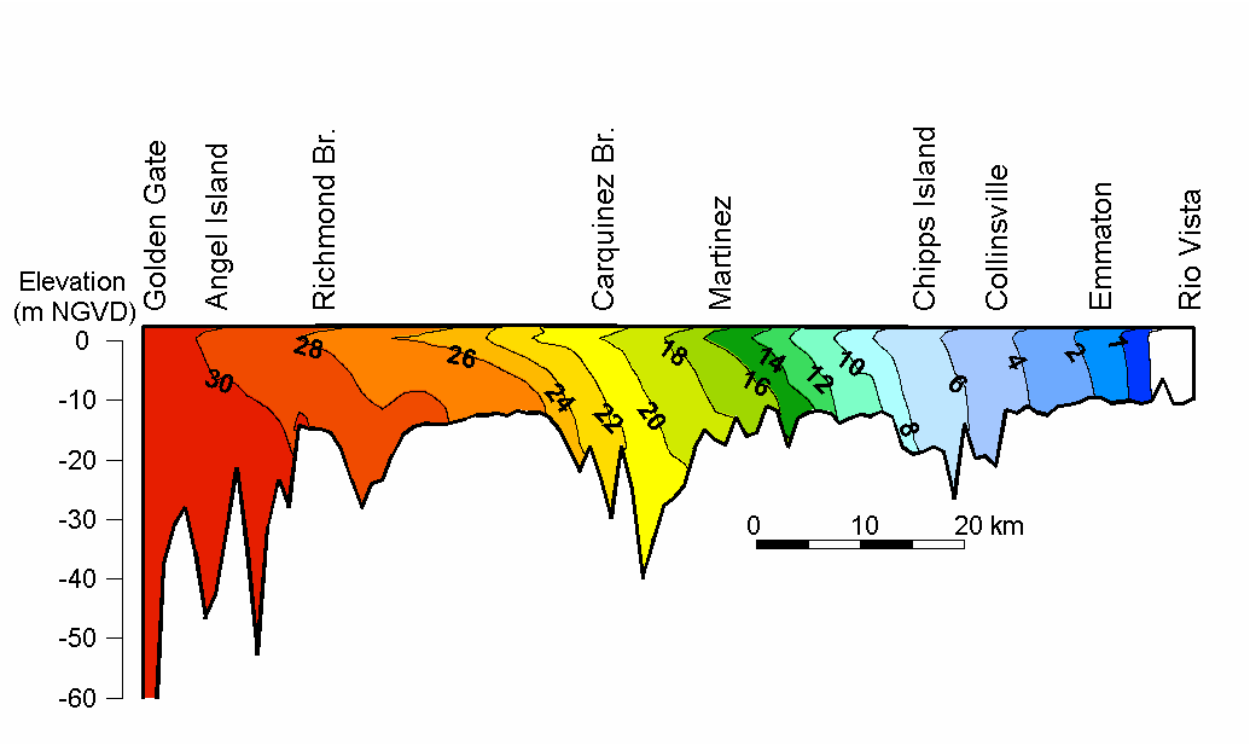

Figure H3.6-11 Tidally-averaged salinity along the centerline transect from Golden Gate to Rio Vista at tidally-averaged steady state conditions for the 140 cm MSL Rise scenario

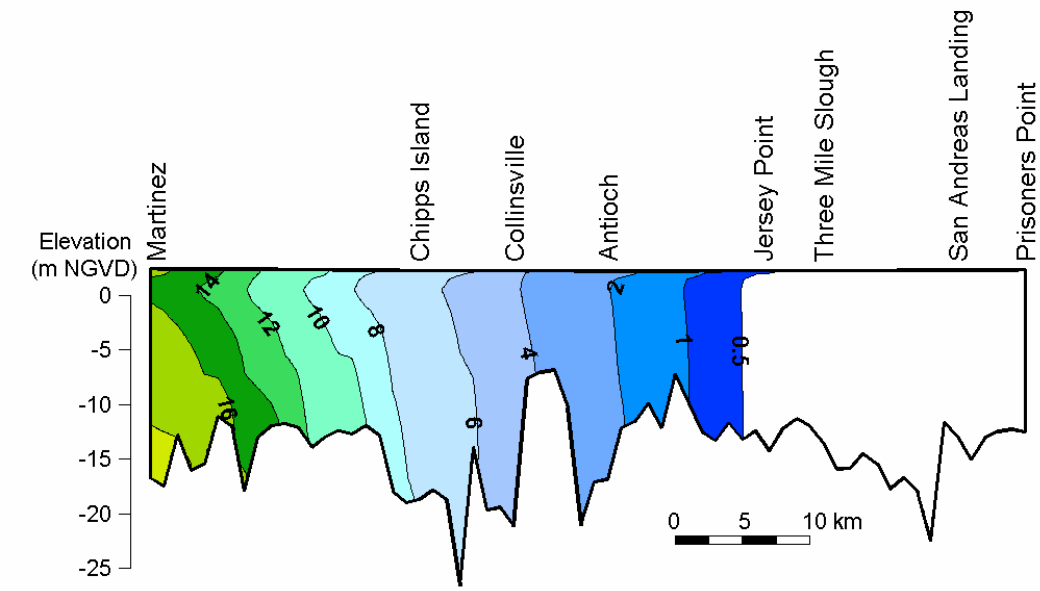

Figure H3.6-12 Tidally-averaged salinity along the centerline transect from Martinez to Prisoners Point at tidally-averaged steady state conditions for the 140 cm MSL Rise scenario

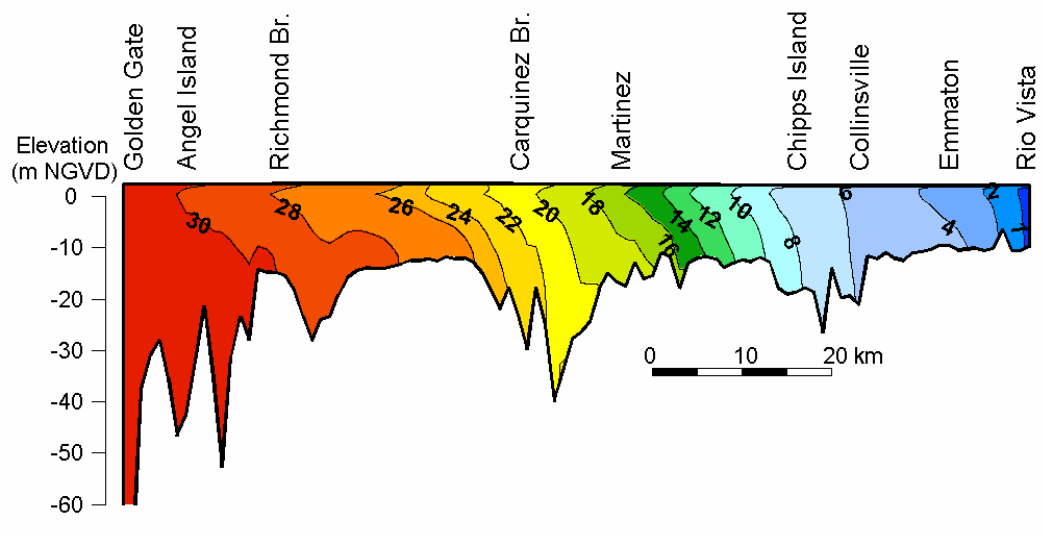

Figure H3.6-13 Tidally-averaged salinity along the centerline transect from Golden Gate to Rio Vista at tidally-averaged steady state conditions for the Perforated Sherman Island scenario

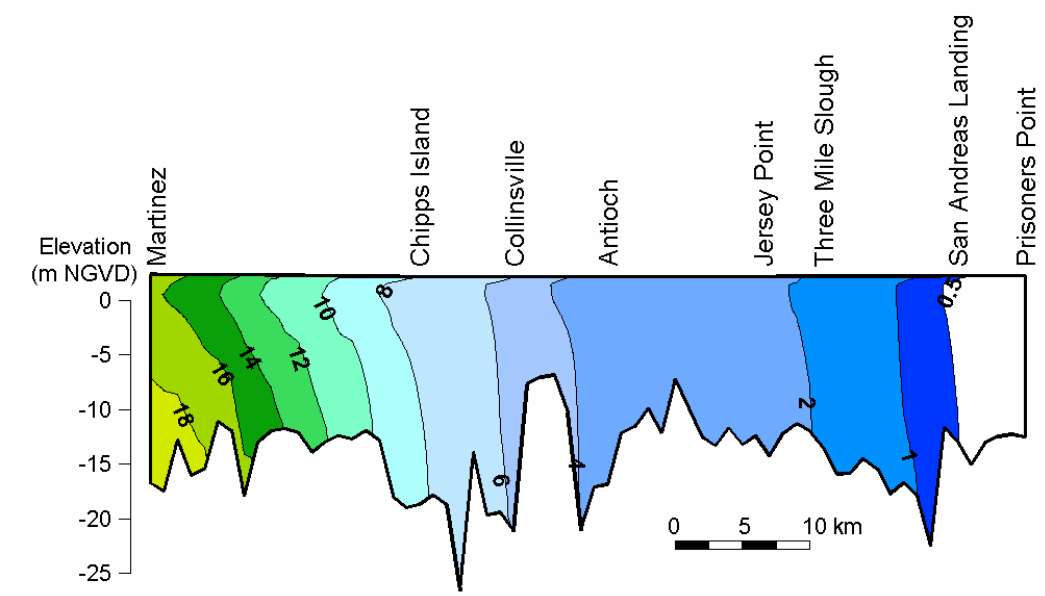

Figure H3.6-14 Tidally-averaged salinity along the centerline transect from Martinez to Prisoners Point at tidally-averaged steady state conditions for the Perforated Sherman Island scenario

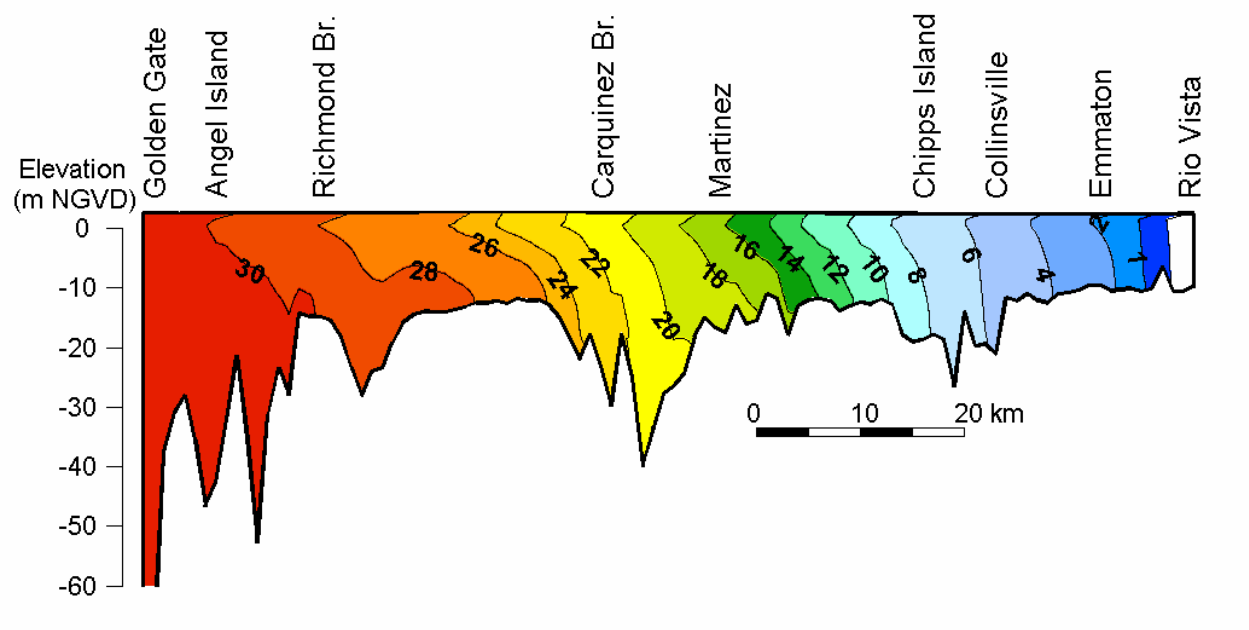

Figure H3.6-15 Tidally-averaged salinity along the centerline transect from Golden Gate to Rio Vista at tidally-averaged steady state conditions for the Amplified Tides scenario

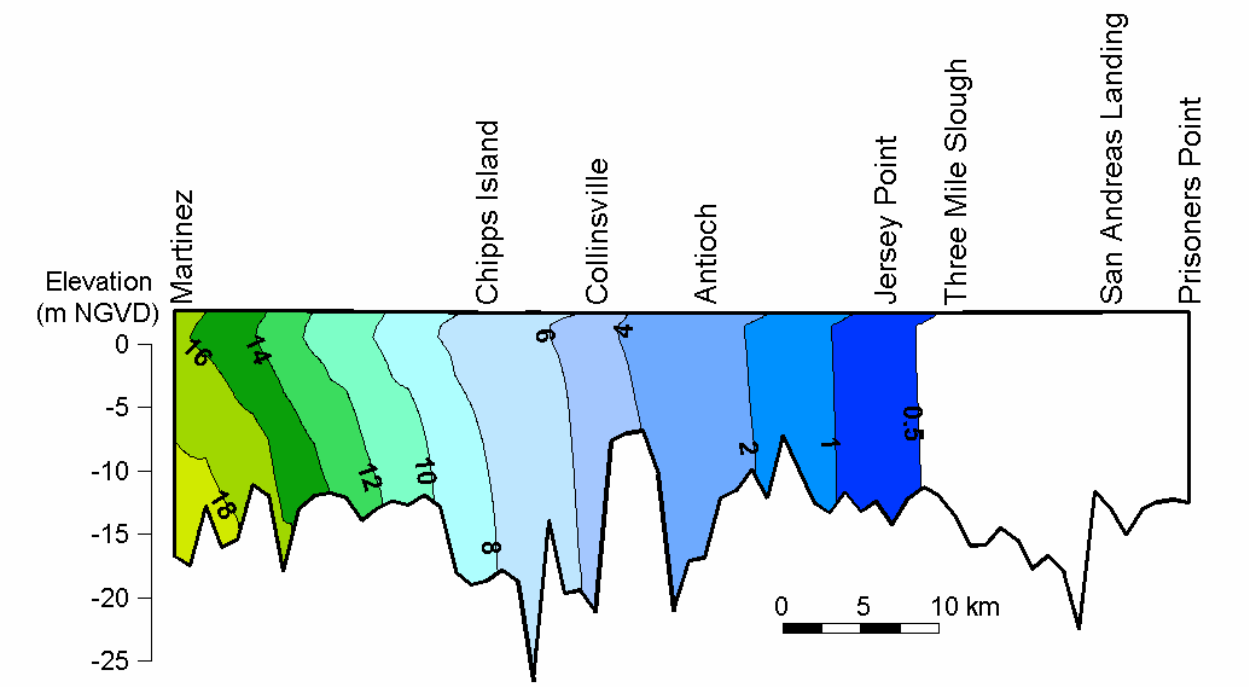

Figure H3.6-16 Tidally-averaged salinity along the centerline transect from Martinez to Prisoners Point at tidally-averaged steady state conditions for the Amplified Tides scenario

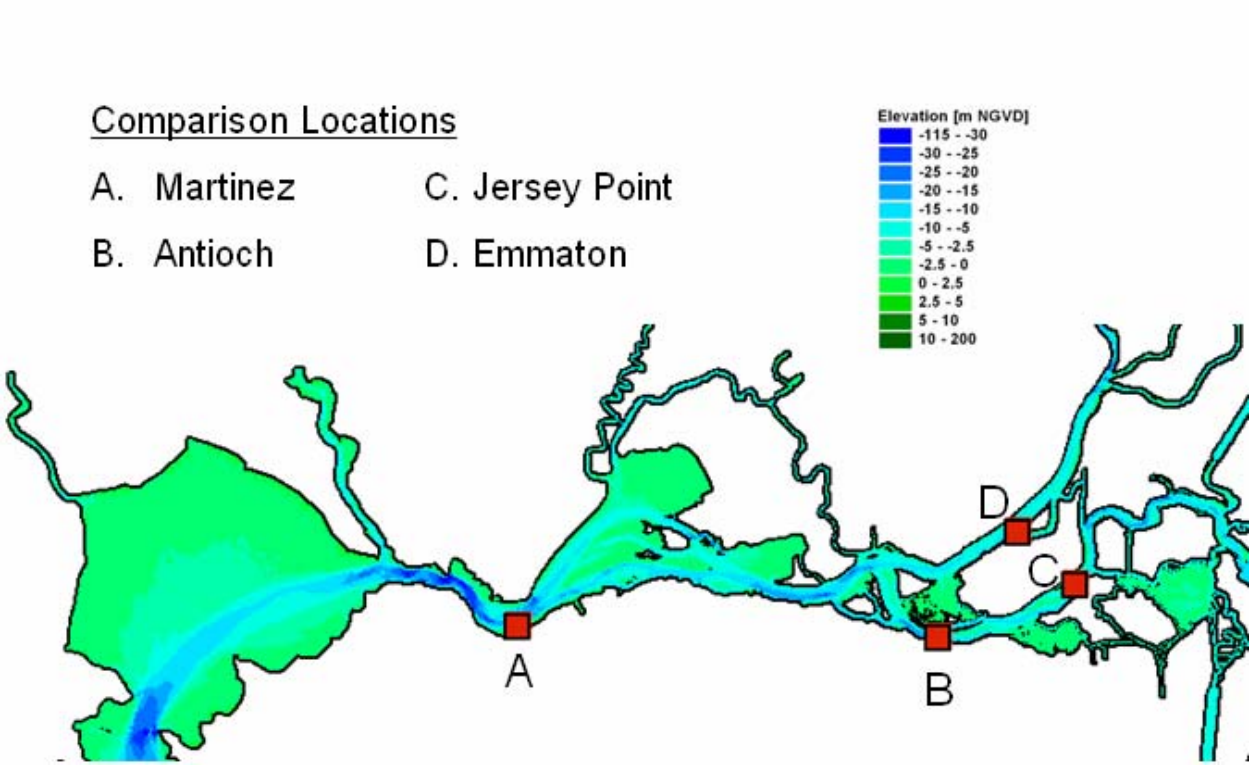

Figure H3.6-17 Locations used to compare tidal variability of salinity among scenarios

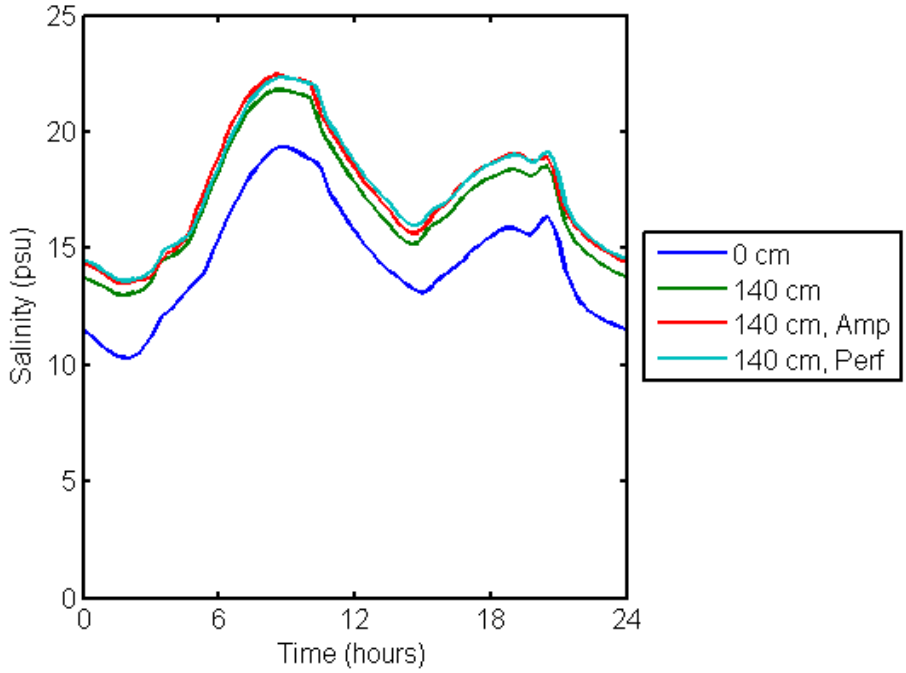

Figure H3.6-18 Depth-averaged salinity at Martinez during the last day of each cumulative effects scenario simulation

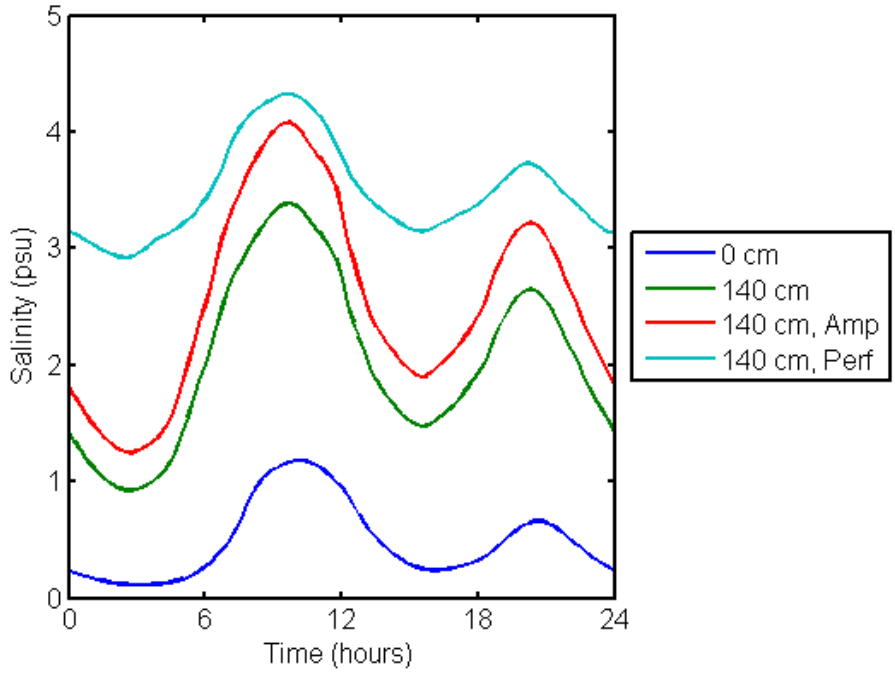

Figure H3.6-19 Depth-averaged salinity at Antioch during the last day of each cumulative effects scenario simulation

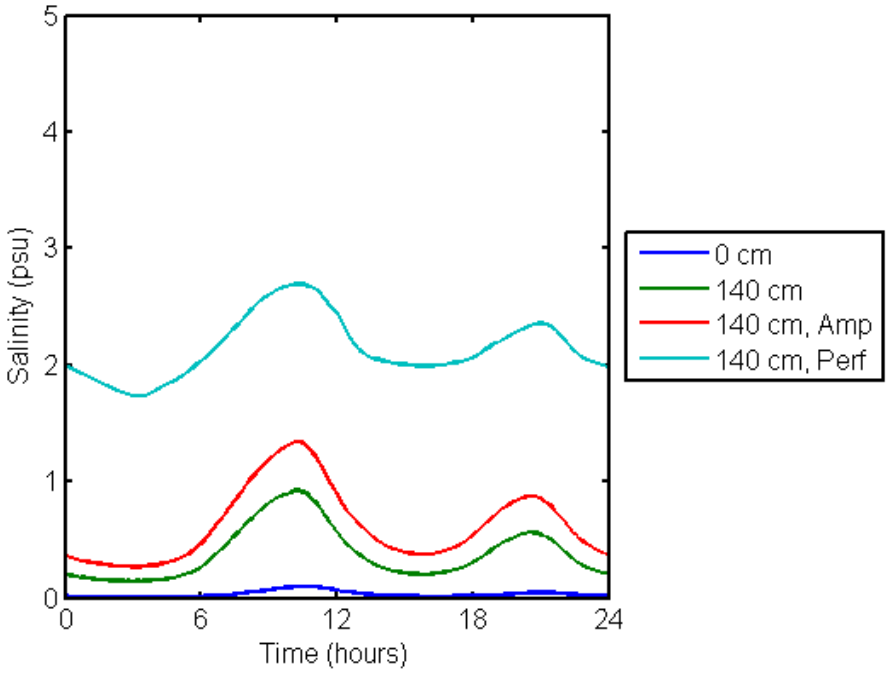

Figure H3.6-20 Depth-averaged salinity at Jersey Point during the last day of each cumulative effects scenario simulation

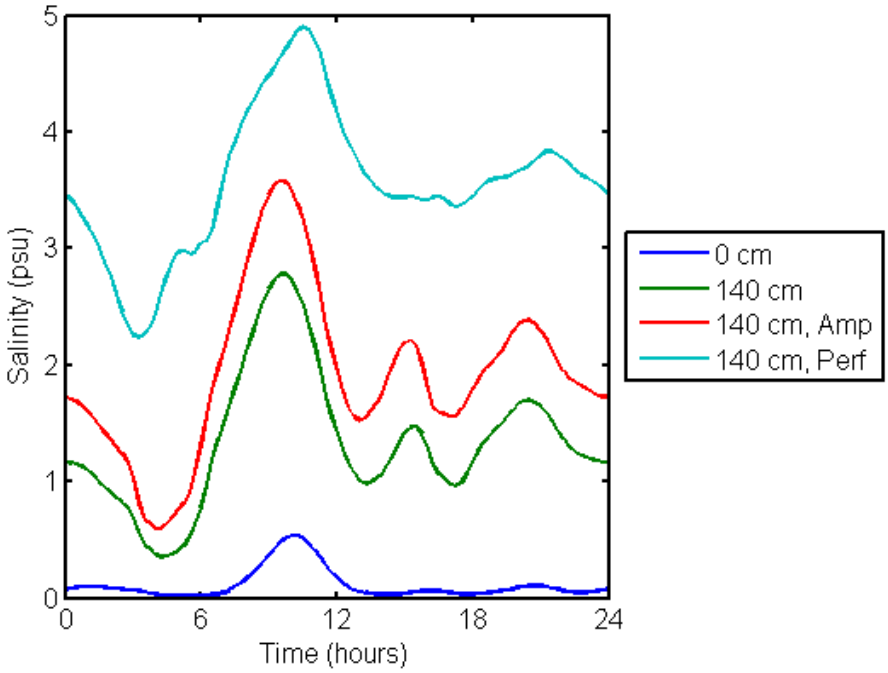

Figure H3.6-21 Depth-averaged salinity at Emmaton during the last day of each cumulative effects scenario simulation

H3.7 Effect of Sea Level Rise on Dispersive Transport

In this section, parameters representing the strength of salt intrusion (dispersive transport) processes are presented for each cross-section shown in Figure H3.3-1 and for each MSL rise scenario. The results of this analysis are a set of dispersion coefficients which indicate the variability of salt intrusion processes spatially and with MSL rise. Increases in dispersion coefficients with MSL rise indicate that additional Delta inflows will be required to meet salinity standards as a result of sea level rise. The dispersion coefficients are also directly useful in the WAM, where they will be used to account for the effect of MSL rise on salt intrusion processes.

The centerline transect used for the dispersion analysis is shown in Figure H3.3-2. The RMS depth-averaged velocity along this transect is shown in Figure H3.7-1. The RMS velocity generally increases with MSL rise in Carquinez Strait, Suisun Bay and the western Delta. The increase in RMS velocity with MSL rise is likely to explain several trends of variation of dispersion coefficient with MSL rise. The tidally-averaged salinity along the centerline transect is depth-averaged for each scenario at tidally-averaged steady-state conditions. The longitudinal salinity gradient at each point is determined by a linear fit to the depth-averaged salinity over roughly one tidal excursion (12 km) to determine the longitudinal salinity gradients shown in Figure H3.7-2. Note that the salinity gradient necessarily approaches zero when salinity approaches zero in the landward reaches of the domain. This predicted longitudinal salinity gradient was used, along with the estimated tidally-averaged cross-sectional area, salinity and flow at each cross-section and scenario to determine the dispersion coefficients shown in Figure H3.7-3. A different symbol color is used for each MSL scenario in Figure H3.7-3. The dispersion coefficients show large spatial variability. The calculated dispersion coefficients have limited variability with MSL at most cross-sections in Central Bay and San Pablo Bay. However, dispersion coefficients in Suisun Bay and the western Delta generally increase substantially with increased MSL.

The salt flux analysis described in the DRMS report “Parameterization of Mixing using a Three-Dimensional Hydrodynamic Model” was used to divide each dispersion coefficient into three components defined in Section 3: K_{gc}, $K_{us,}$ and K_{2D}. It should be noted that the dispersion coefficients presented here are independent from those in the DRMS report “Parameterization of Mixing using a Three-Dimensional Hydrodynamic Model” because different scenarios are considered, and the UnTRIM model was used in this analysis. Because the UnTRIM model uses an unstructured grid and the TRIM model uses a Cartesian grid, the orientation and location of the cross-sections are slightly different between the two models.

The estimated dispersion coefficients associated with gravitational circulation (K_{gc}) are shown in Figure H3.7-4. Note that this dispersion coefficient component is more variable with location than the overall dispersion coefficients, and a logarithmic vertical scale is used to capture the large variability of this estimated dispersion coefficient component. The dispersion coefficients associated with gravitational circulation drop substantially in Suisun Bay, relative to San Pablo Bay, starting at 55 km from the Golden Gate, near Benicia, and account for most of the drop in the overall dispersion coefficients in this region. These results are consistent with the findings of Burau et al. (1998) in the

Entrapment Zone Study. The interpretation in that study is that the reduced depth at the Benicia shoal reduced the strength of gravitational circulation. The dispersion coefficient component associated with gravitational circulation generally increases with increased MSL in Suisun Bay and the western Delta.

The dispersion coefficients associated with unsteady vertical shear (K_{us}) are shown in Figure H3.7-5. While the unsteady vertical shear component is smaller than the gravitational circulation component in Central San Francisco Bay and San Pablo Bay, it is of similar magnitude as the gravitational circulation component in Suisun Bay and the western Delta. Some of the dispersion associated with unsteady vertical shear is associated with the SIPS mechanism which is known to be active in portions of Suisun Bay (Stacey et al. 2001). The dispersion associated with unsteady vertical shear varies with sea level rise in Carquinez Strait, Suisun Bay and the western Delta. However, the trend of change in this component with sea level rise varies from cross-section to cross-section.

The dispersion coefficients associated with all other processes, termed K_{2D}, are shown in Figure H3.7-6. This dispersion is primarily associated with tidal dispersion. K_{2D} shows less spatial variability than the other components of dispersion. Since this component of the dispersion coefficient is not expected to have strong variation with stratification, the less pronounced spatial variability was expected. The dispersion coefficient component associated with tidal dispersion generally increases with increased MSL in Carquinez Strait, Suisun Bay and the western Delta. This increase is probably related to the increased RMS velocities shown in Figure H3.7-1.

In the following sections, the dispersion analysis results in each sub-embayment will be presented.

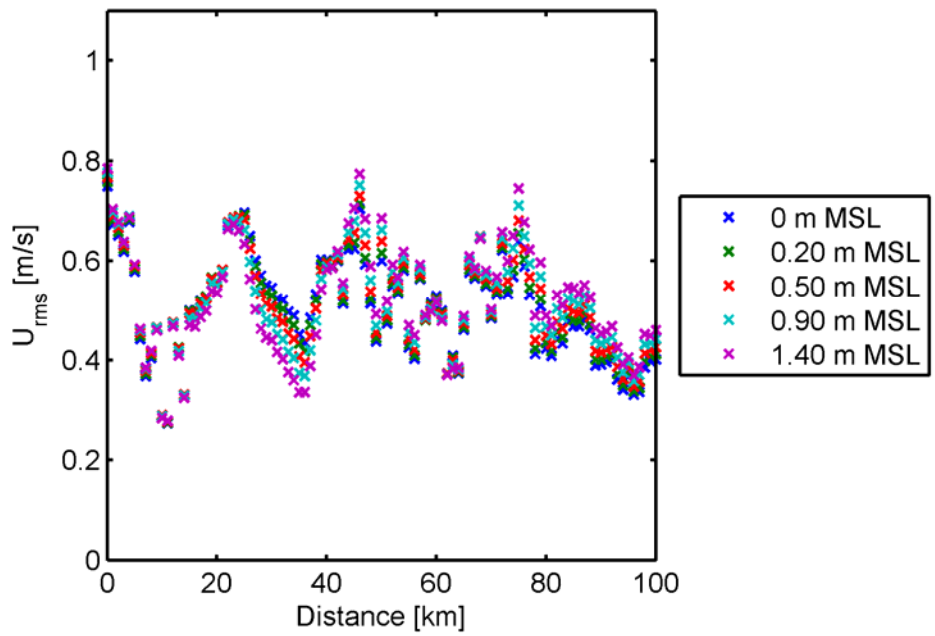

Figure H3.7-1Estimated root mean square depth-averaged velocity for all MSL rise scenarios. The horizontal scale is distance along the axis of the estuary from the Golden Gate

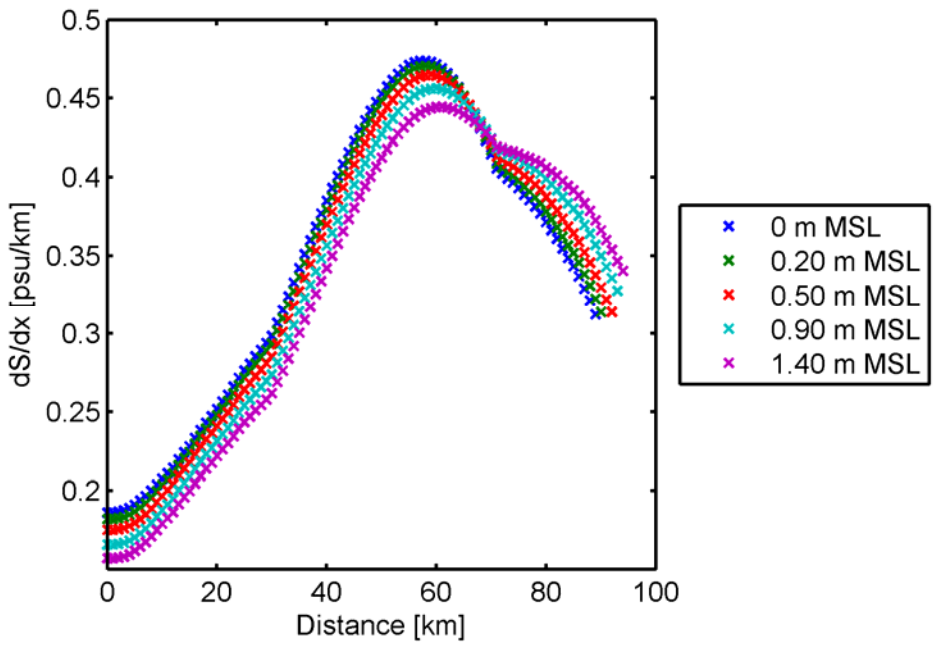

Figure H3.7-2Estimated depth-averaged salinity gradient for all MSL rise scenarios. The horizontal scale is distance along the axis of the estuary from the Golden Gate

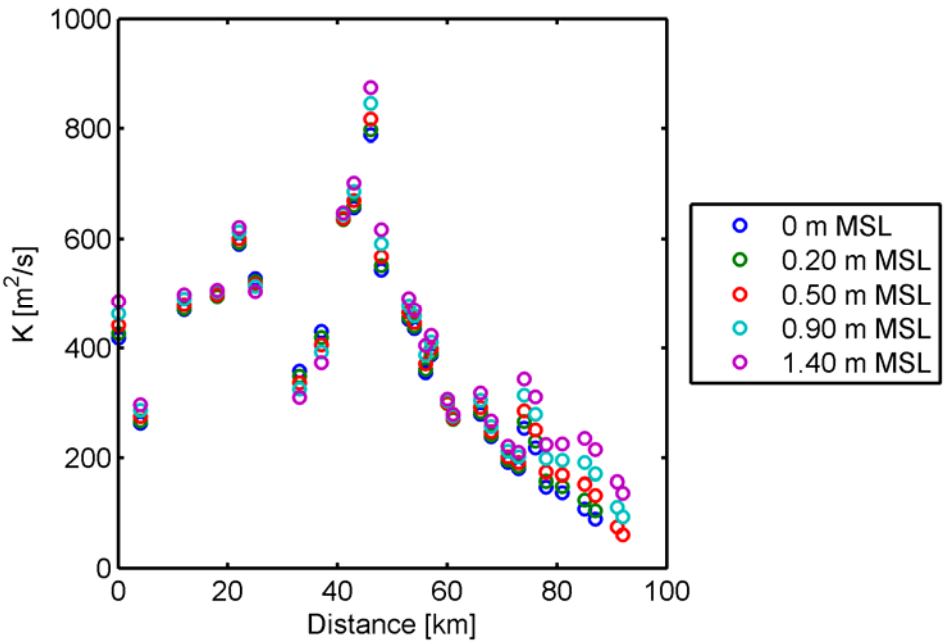

Figure H3.7-3Estimated dispersion coefficients for all MSL rise scenarios. The horizontal scale is distance along the axis of the estuary from the Golden Gate

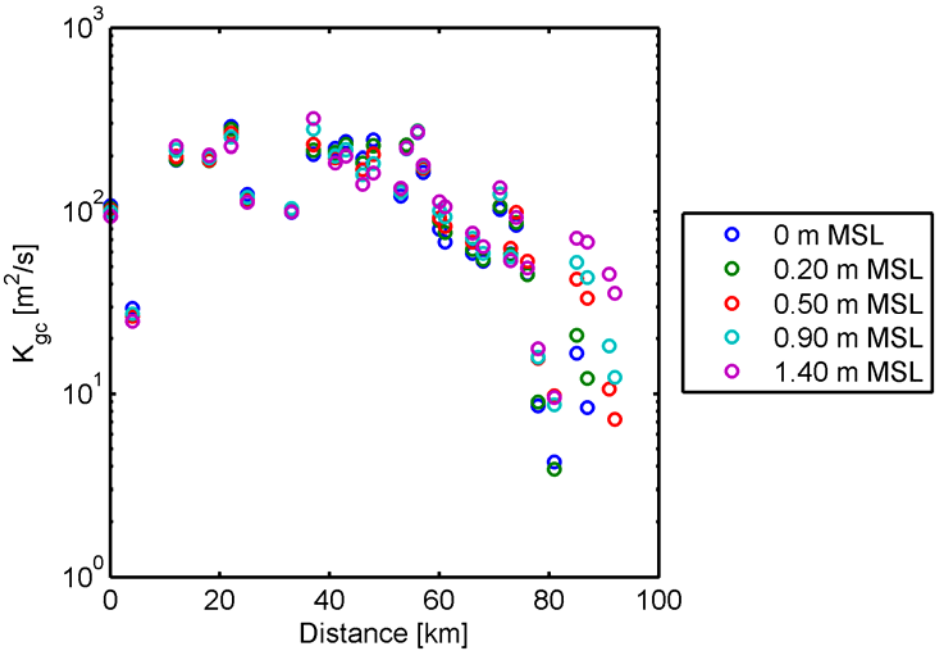

Figure H3.7-4Estimated dispersion coefficients associated with gravitational circulation for all MSL rise scenarios. The horizontal scale is distance along the axis of the estuary from the Golden Gate

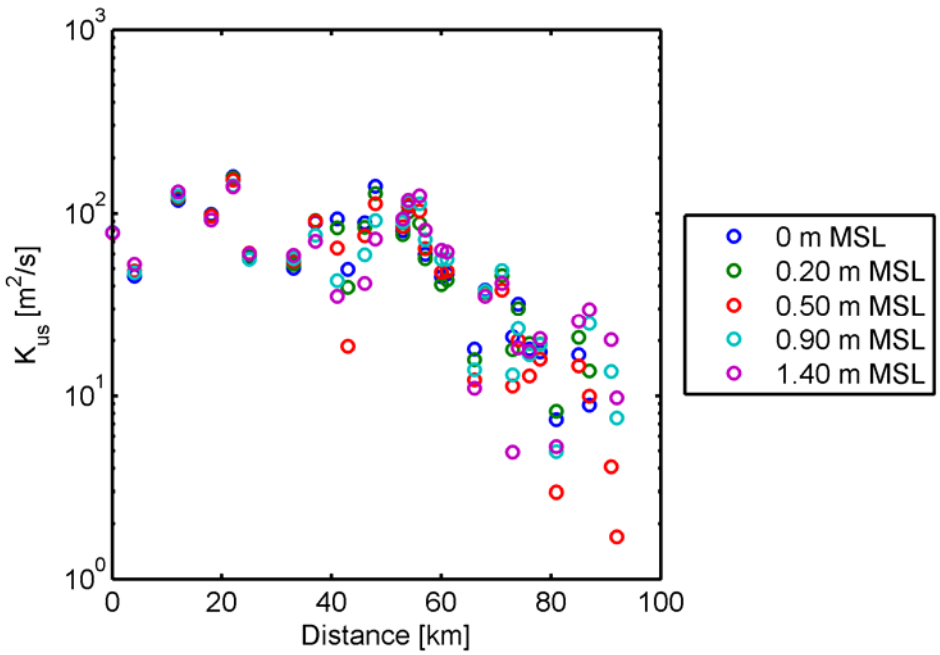

Figure H3.7-5Estimated dispersion coefficients associated with "unsteady vertical shear" for all MSL rise scenarios. The horizontal scale is distance along the axis of the estuary from the Golden Gate

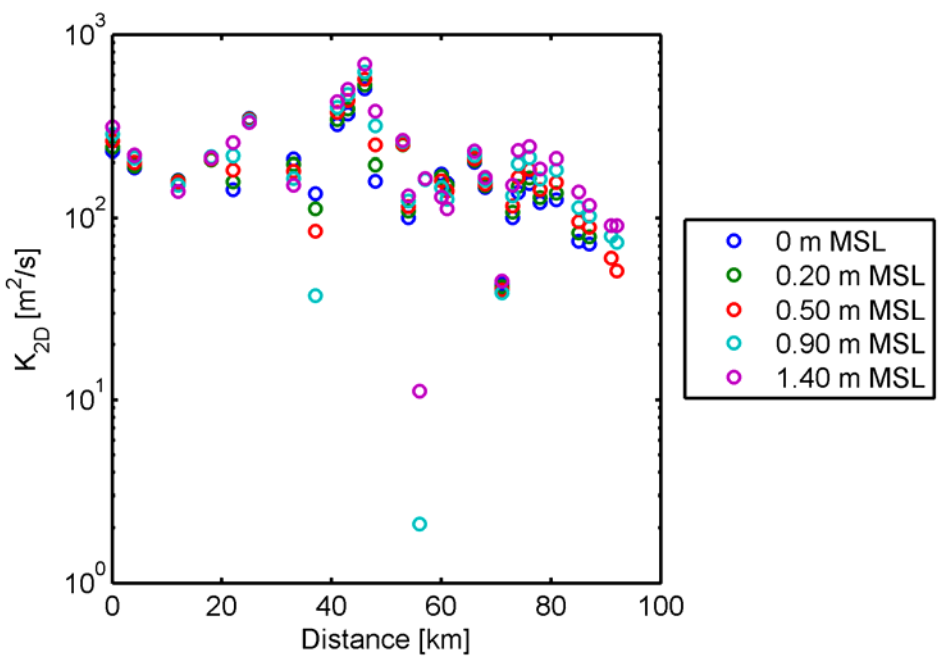

Figure H3.7-6Estimated dispersion coefficients associated with tidal dispersion for all MSL rise scenarios. The horizontal scale is distance along the axis of the estuary from the Golden Gate

H3.7.1 Central San Francisco Bay Cross-Sections

Dispersion coefficients and salt fluxes were estimated at the five cross-sections in Central Bay shown in Figure H3.3-1. In Figures H3.7.1-1 through H3.7.1-10, two figures are provided for each cross-section in order to summarize the results of the dispersion analysis at that location. The first type of figure shows each dispersion coefficient and the individual components of each dispersion coefficient for each MSL rise scenario. The second type of figure shows the overall dispersion coefficient and the dispersion coefficient associated with "three-dimensional processes" ($K_{gc} + K_{us}$) for each MSL rise scenario as well as linear fit equations that describe the variability of these dispersion coefficients with MSL rise.

The dispersion coefficients are generally large in Central Bay. Both tidal dispersion processes and gravitational circulation are important at all cross-sections in Central Bay. The dispersion coefficients increase weakly with MSL in Central Bay.

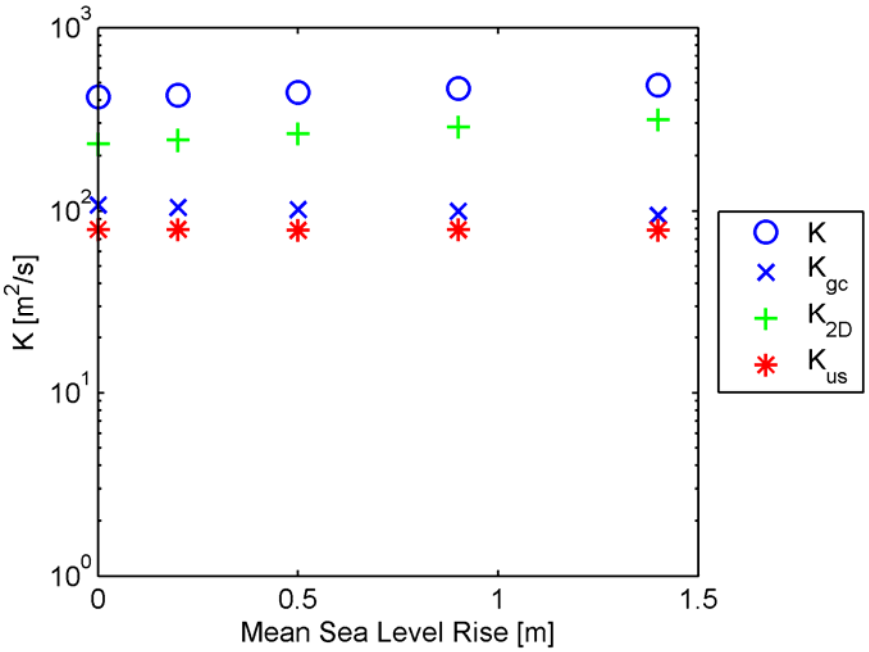

Figure H3.7.1-1 Dispersion coefficients and dispersion coefficient components calculated for each MSL rise scenario at cross-section 1, located at the Golden Gate

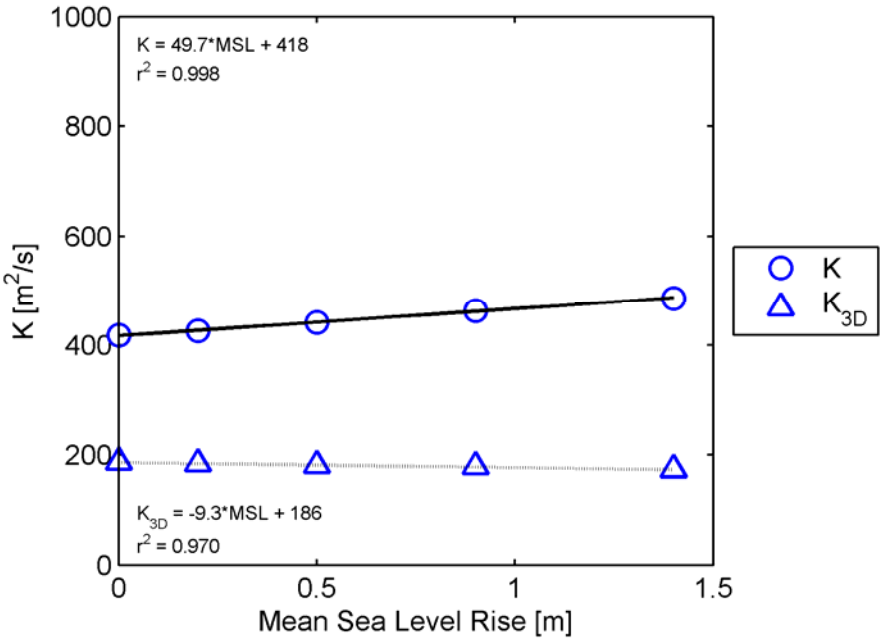

Figure H3.7.1-2 Total and three-dimensional dispersion coefficients calculated for each MSL rise scenario at cross-section 1, located at the Golden Gate. A best fit equation and r^2 value is shown for each set of coefficients

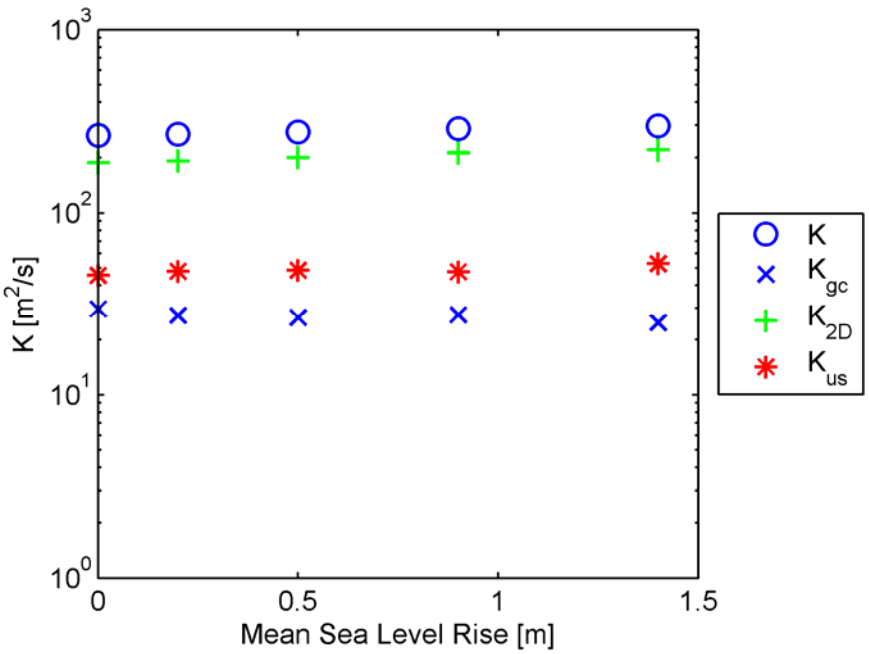

Figure H3.7.1-3 Dispersion coefficients and dispersion coefficient components calculated for each MSL rise scenario at cross-section 2, extending from San Francisco to Tiburon

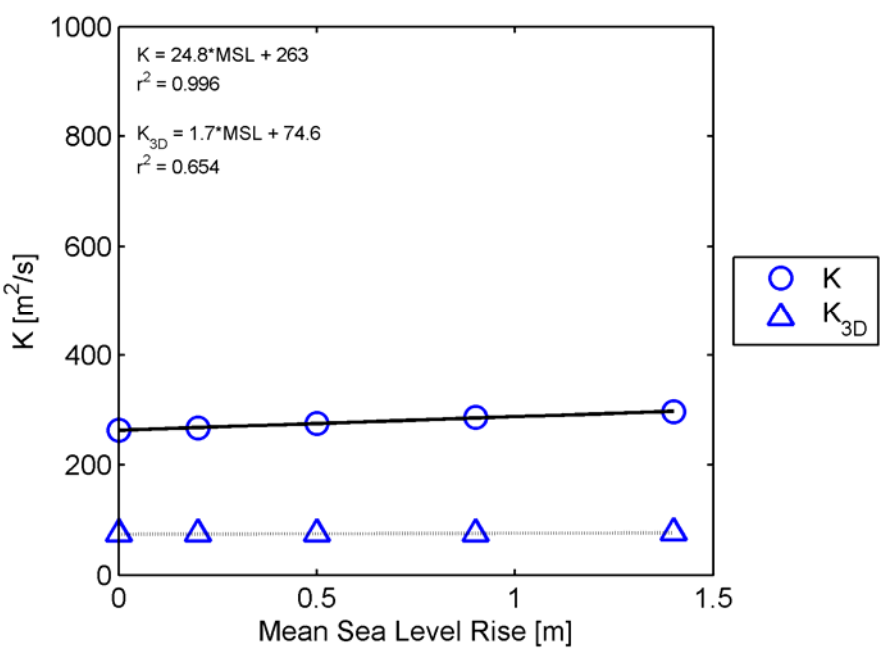

Figure H3.7.1-4 Total and three-dimensional dispersion coefficients calculated for each MSL rise scenario at cross-section 2, extending from San Francisco to Tiburon. A best fit equation and r^2 value is shown for each set of coefficients

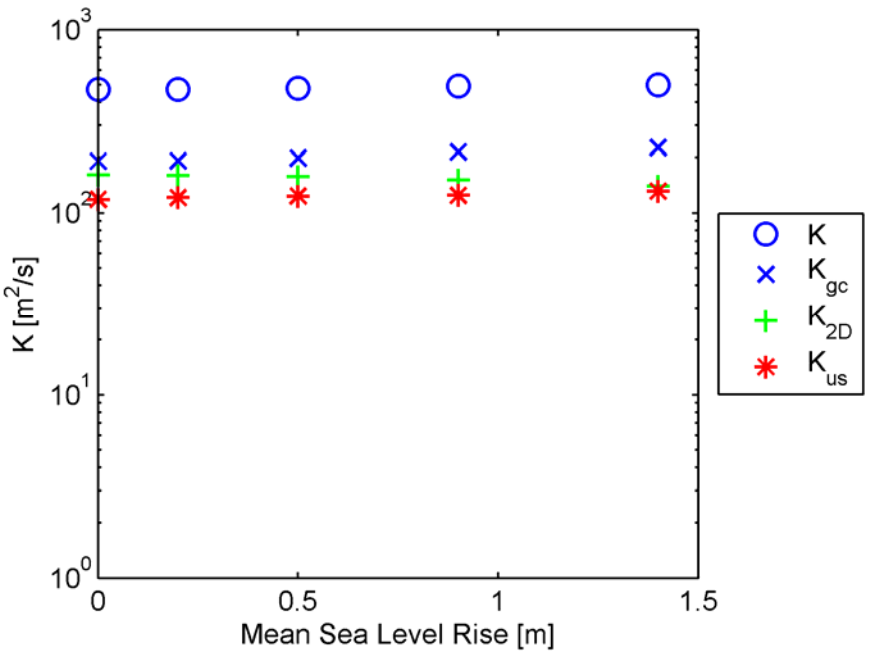

Figure H3.7.1-5 Dispersion coefficients and dispersion coefficient components calculated for each MSL rise scenario cross-section 3, extending from Point Richmond to Bluff Point

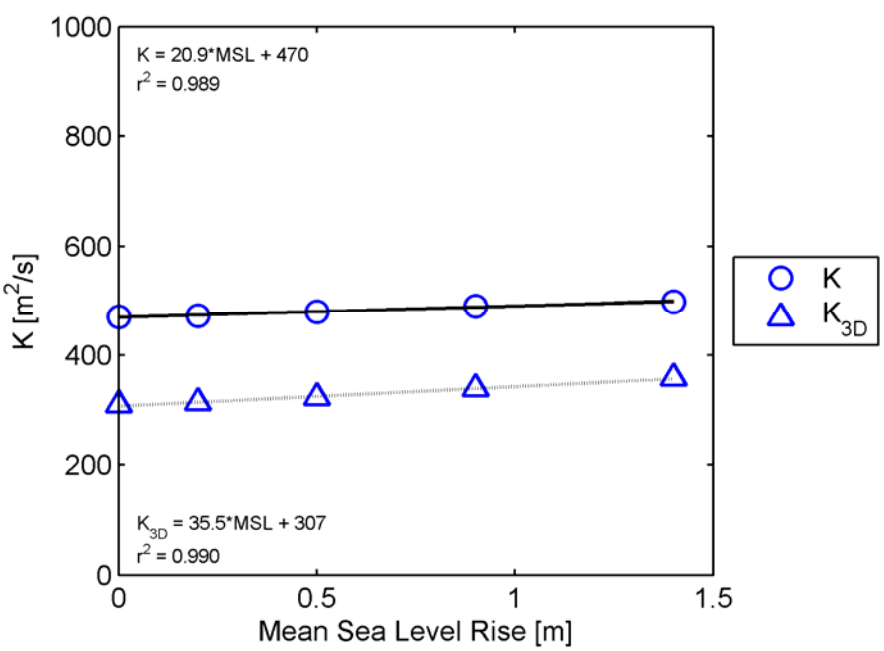

Figure H3.7.1-6 Total and three-dimensional dispersion coefficients calculated for each MSL rise scenario at cross-section 3, extending from Point Richmond to Bluff Point. A best fit equation and r^2 value is shown for each set of coefficients

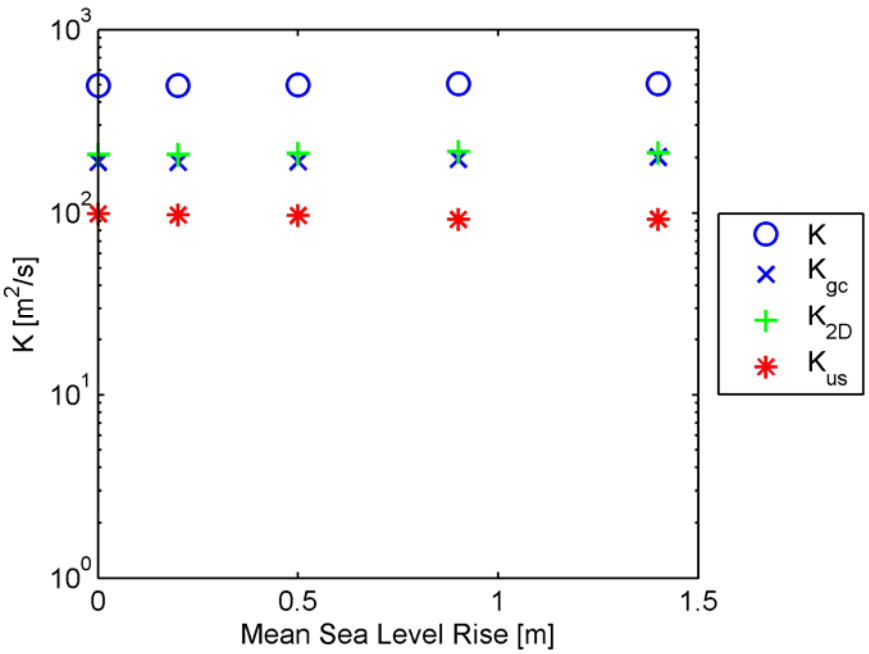

Figure H3.7.1-7 Dispersion coefficients and dispersion coefficient components calculated for each MSL rise scenario at cross-section 4, at the Richmond-San Rafael Bridge

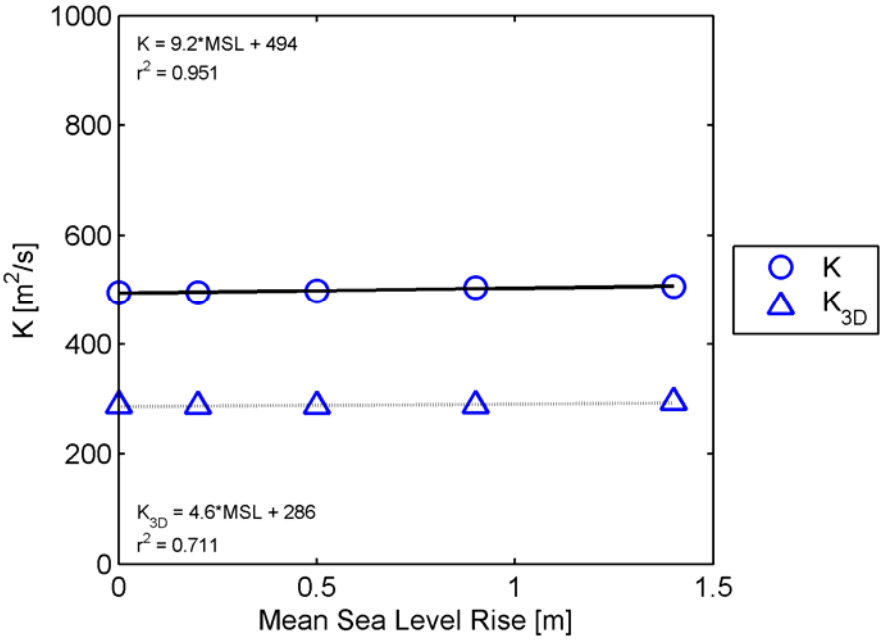

Figure H3.7.1-8 Total and three-dimensional dispersion coefficients calculated for each MSL rise scenario at cross-section 4, at the Richmond-San Rafael Bridge. A best fit equation and r^2 value is shown for each set of coefficients

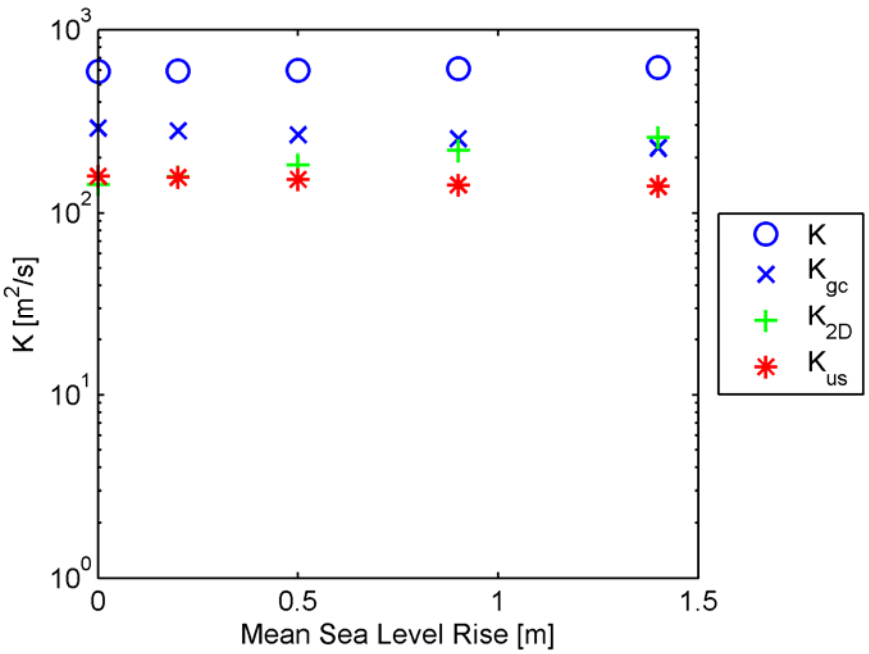

Figure H3.7.1-9 Dispersion coefficients and dispersion coefficient components calculated for each MSL rise scenario at cross-section 5, extending from Point San Pablo to Point San Pedro

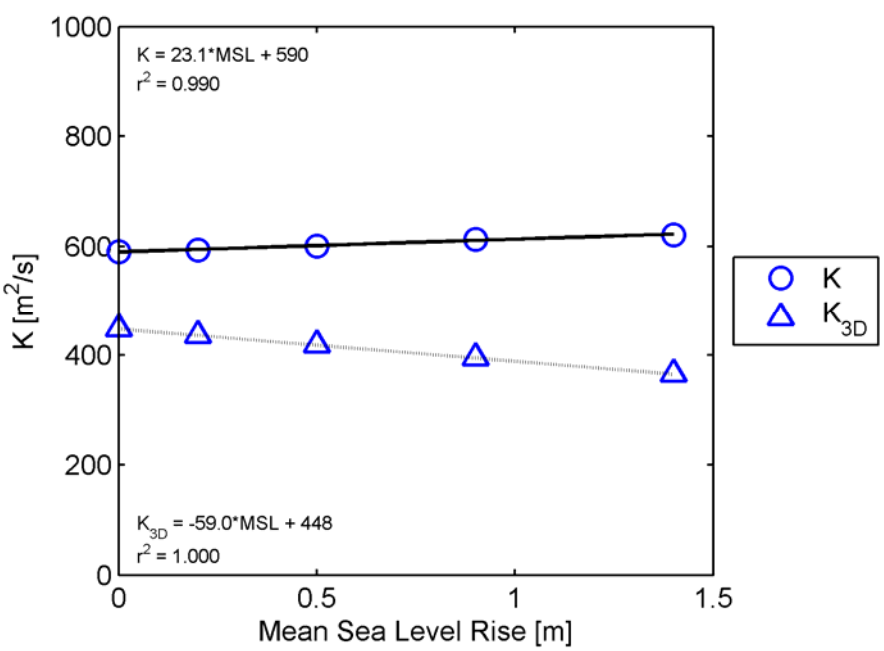

Figure H3.7.1-10 Total and three-dimensional dispersion coefficients calculated for each MSL rise scenario at cross-section 5, extending from Point San Pablo to Point San Pedro. A best fit equation and r^2 value is shown for each set of coefficients

H3.7.2 San Pablo Bay Cross-Sections

Dispersion coefficients and salt fluxes were estimated at the four cross-sections in San Pablo Bay shown in Figure H3.3-1. In Figures H3.7.2-1 through H3.7.2-8, two figures are provided for each cross-section in order to summarize the results of the dispersion analysis at that location. The first type of figure shows each dispersion coefficient and the individual components of each dispersion coefficient for each MSL rise scenario. The second type of figure shows the overall dispersion coefficient and the dispersion coefficient associated with "three-dimensional processes" ($K_{gc} + K_{us}$) for each MSL rise scenario as well as linear fit equations that describe the variability of these dispersion coefficients with MSL rise.

The dispersion coefficients are generally large in San Pablo Bay. Tidal dispersion processes and gravitational circulation are important at all cross-sections. As in Central Bay, the dispersion coefficient components show weak variability with MSL with a few exceptions. At cross-section 8, gravitational circulation increases with sea level rise and tidal dispersion decreases with MSL rise. The relatively large differences in dispersion coefficient components with MSL predicted here are probably associated with the particularly large shoal and intertidal extent in this cross-section. Because much of the cross-section is shallow, large changes in transport processes can be expected with changes in MSL. The K_{2D} value for the 140 cm MSL Rise scenario is negative at cross-section 8. The physical explanation for this negative value is not clear, but these unintuitive results emphasize that the actual transport processes are always three-dimensional. The physical mechanisms associated with different flux terms are conceptually distinct, but are all simplified conceptual representations that are useful in order to attempt to "untangle" the complex physics that result in dispersive transport.

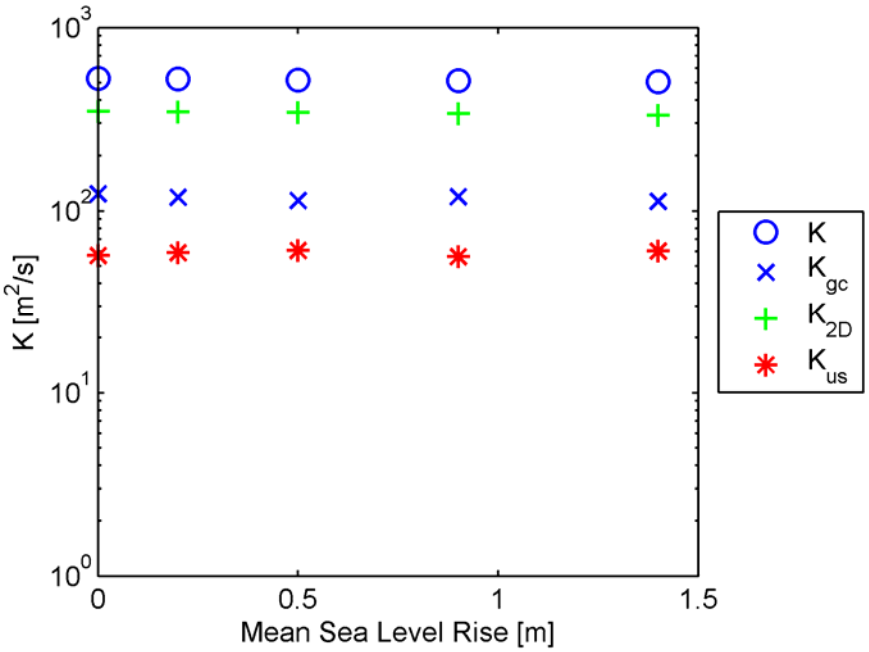

Figure H3.7.2-1 Dispersion coefficients and dispersion coefficient components calculated for each MSL rise scenario at section 6, extending from San Pablo to Point San Pedro

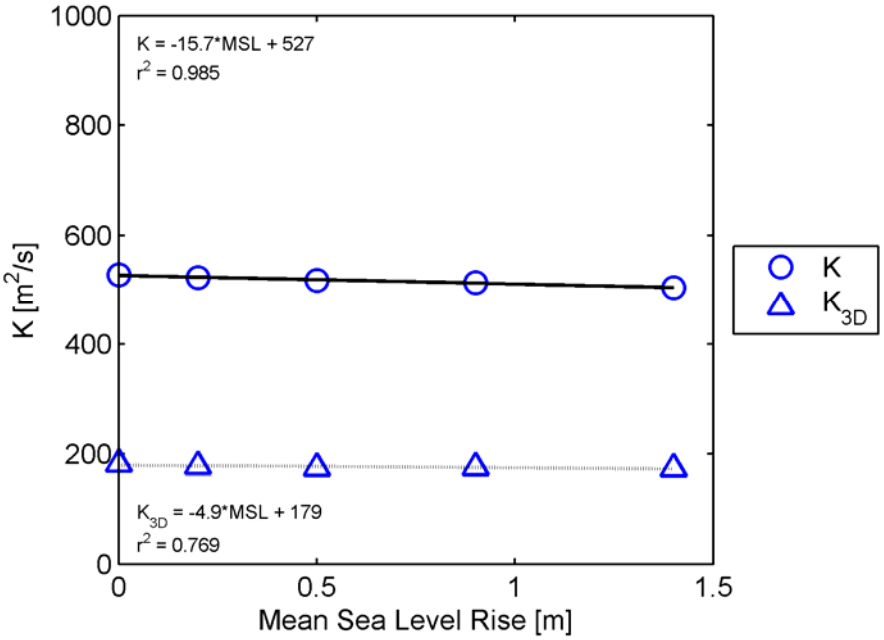

Figure H3.7.2-2 Total and three-dimensional dispersion coefficients calculated for each MSL rise scenario at cross-section 6, extending from San Pablo to Point San Pedro. A best fit equation and r^2 value is shown for each set of coefficients

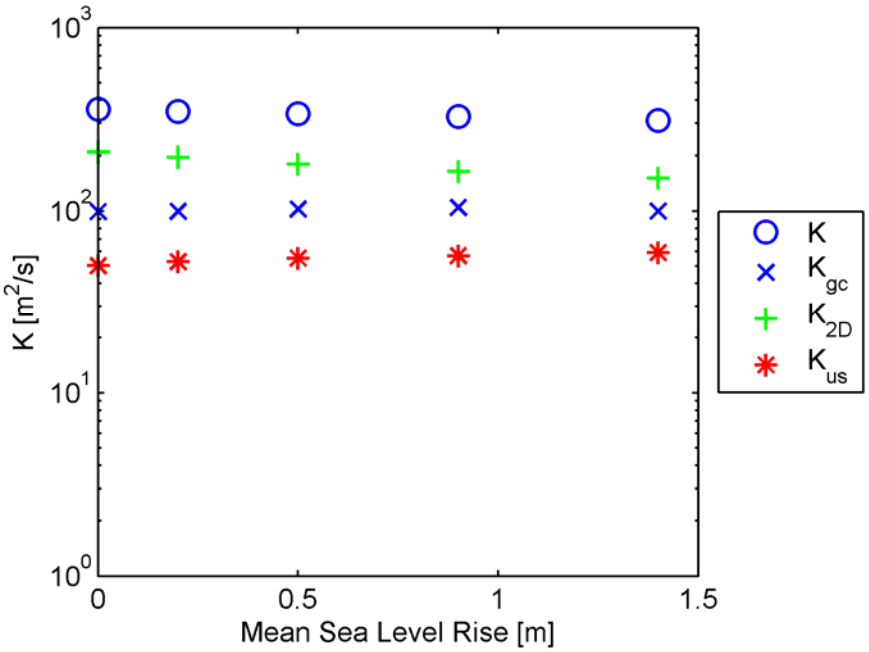

Figure H3.7.2-3. Dispersion coefficients and dispersion coefficient components calculated for each MSL rise scenario at cross-section 7, extending from Pinole Point to Sonoma Creek

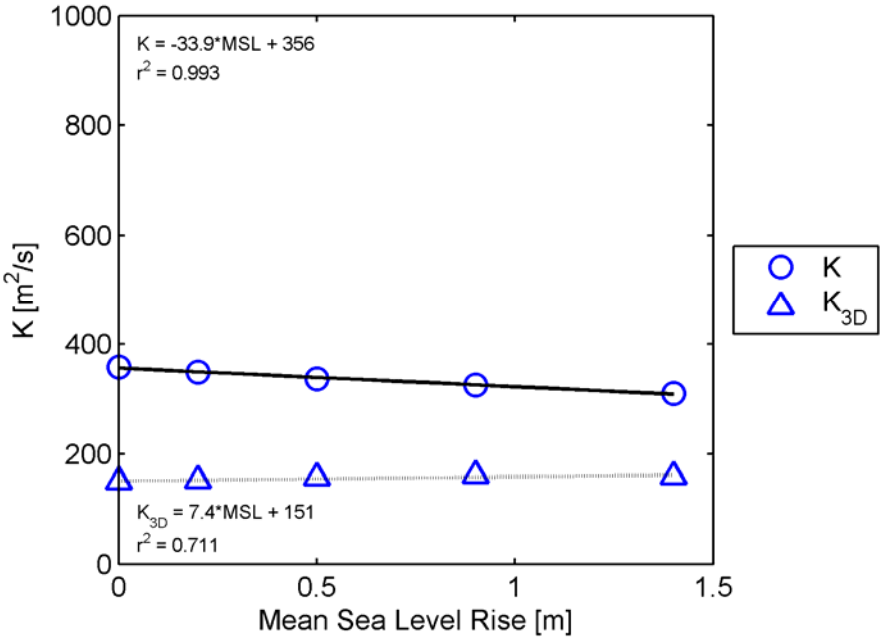

Figure H3.7.2-4 Total and three-dimensional dispersion coefficients calculated for each MSL rise scenario at cross-section 7, extending from Pinole Point to Sonoma Creek. A best fit equation and r^2 value is shown for each set of coefficients

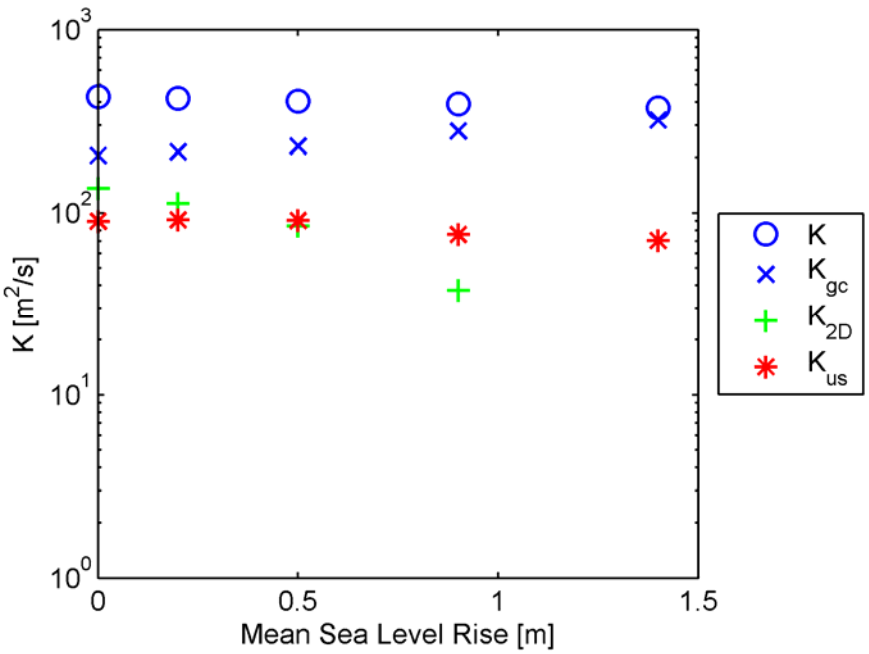

Figure H3.7.2-5 Dispersion coefficients and dispersion coefficient components calculated for each MSL rise scenario at cross-section 8, extending from Wilson Point to Mare Island

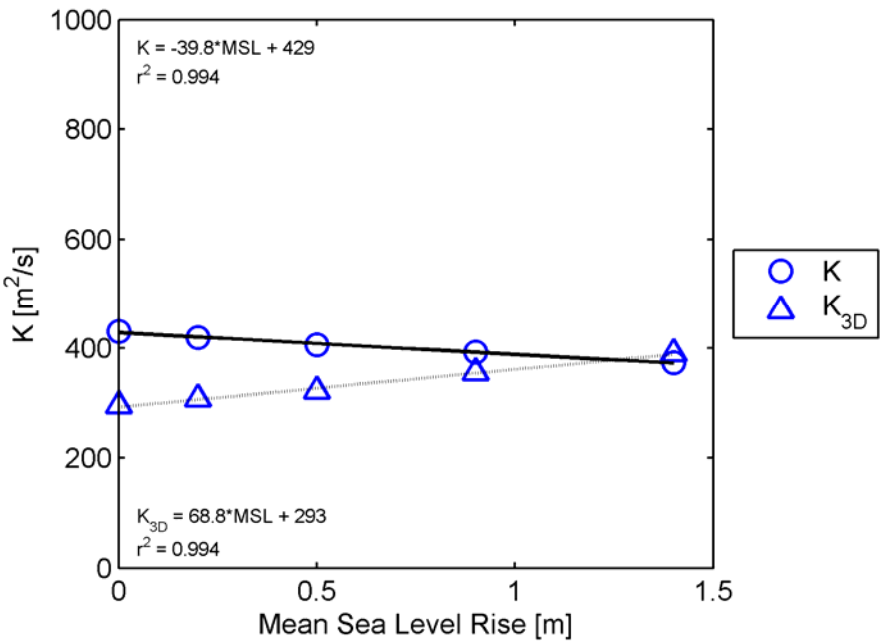

Figure H3.7.2-6 Total and three-dimensional dispersion coefficients calculated for each MSL rise scenario at cross-section 8, extending from Wilson Point to Mare Island. A best fit equation and r^2 value is shown for each set of coefficients.

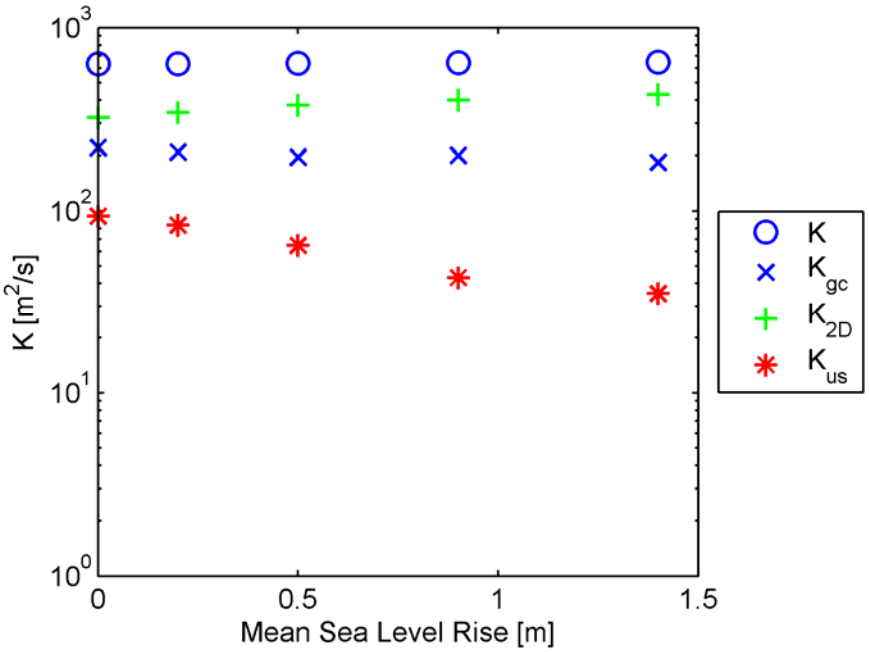

Figure H3.7.2-7 Dispersion coefficients and dispersion coefficient components calculated for each MSL rise scenario at cross-section 9, extending from Davis Point to Mare Island

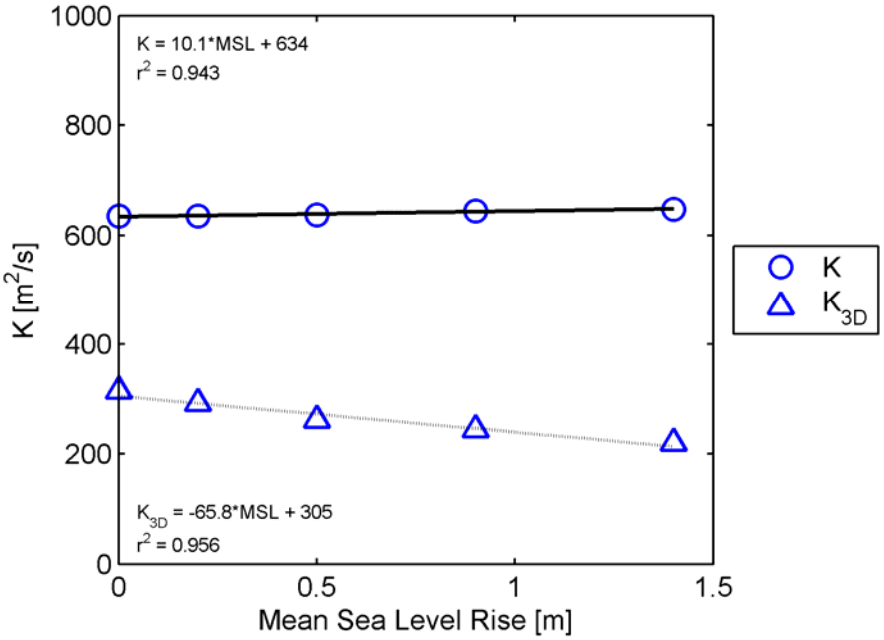

Figure H3.7.2-8 Total and three-dimensional dispersion coefficients calculated for each MSL rise scenario at cross-section 9, extending from Davis Point to Mare Island. A best fit equation and r^2 value is shown for each set of coefficients.

H3.7.3 Carquinez Strait Cross-Sections

Dispersion coefficients and salt fluxes were estimated at the six cross-sections in Carquinez Strait shown in Figure H3.3-1. In Figures H3.7.3-1 through H3.7.3-12, two figures are provided for each cross-section in order to summarize the results of the dispersion analysis at that location. The first type of figure shows each dispersion coefficient and the individual components of each dispersion coefficient for each MSL rise scenario. The second type of figure shows the overall dispersion coefficient and the dispersion coefficient associated with "three-dimensional processes" ($K_{gc} + K_{us}$) for each MSL rise scenario as well as linear fit equations that describe the variability of these dispersion coefficients with MSL rise.

The dispersion coefficients are large at the seaward end of Carquinez Strait and decrease with distance landward. Both tidal dispersion and gravitational circulation are important at all cross-sections, while unsteady vertical shear is smaller. Sea level rise has little effect on the overall predicted dispersion coefficient. The strength of tidal dispersion generally increases with increased sea level in the seaward portion of Carquinez Strait. The magnitude of the unsteady vertical shear component of dispersion decreases with increased MSL at several cross-sections. The reasons for these trends are not established but the trends may be partially attributed to increasing RMS velocity with sea level rise, indicated in Figure H3.7-1. The RMS velocity increase results partially from larger tidal prism due to less intertidal area as sea level rises and partially from decreased bottom friction due to deeper channels. Due to increased RMS velocity, tidal dispersion processes should strengthen and stratification, which is required for the SIPS process associated with unsteady vertical shear, should be less prevalent.

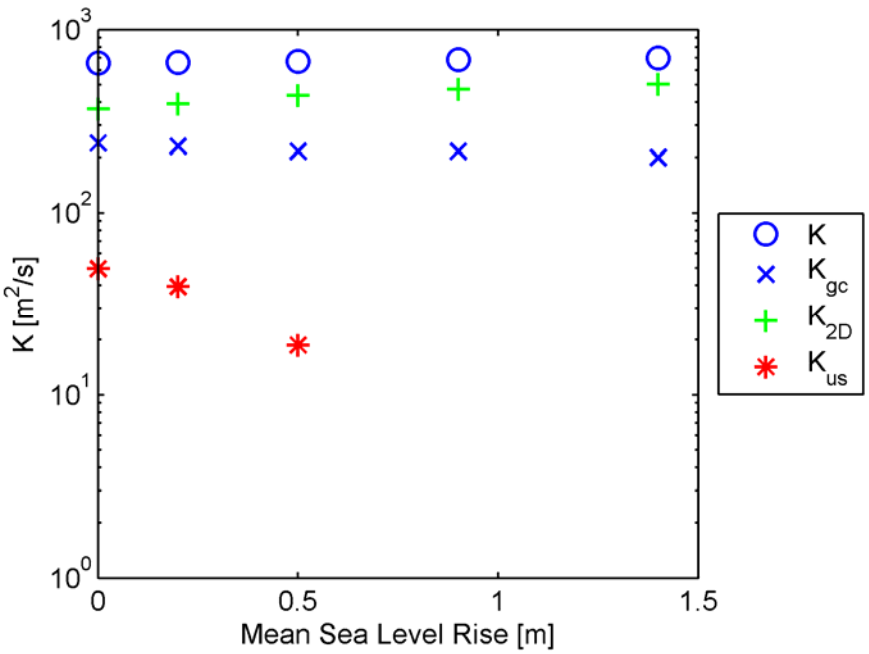

Figure H3.7.3-1 Dispersion coefficients and dispersion coefficient components calculated for each MSL rise scenario at cross-section 10, extending from Davis Point to Mare Island Straight

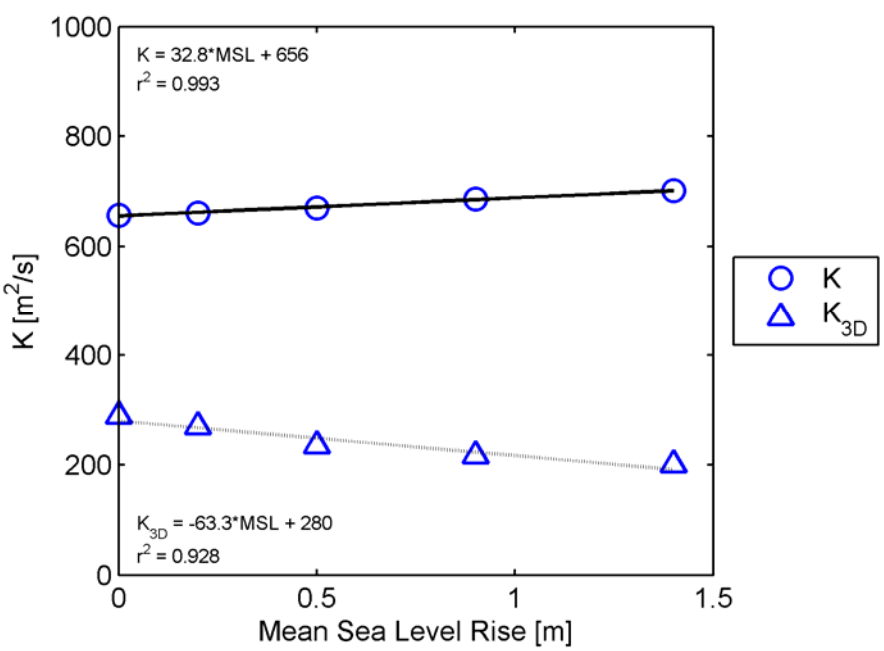

Figure H3.7.3-2 Total and three-dimensional dispersion coefficients calculated for each MSL rise scenario at cross-section 10, extending from Davis Point to Mare Island Straight. A best fit equation and r^2 value is shown for each set of coefficients

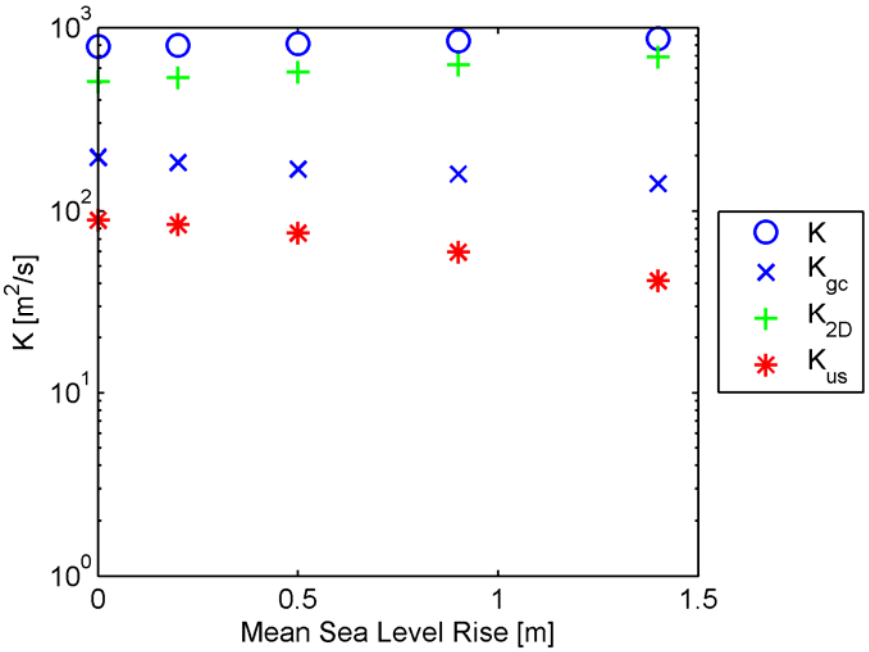

Figure H3.7.3-3 Dispersion coefficients and dispersion coefficient components calculated for each MSL rise scenario at cross-section 11, at the Carquinez Bridge

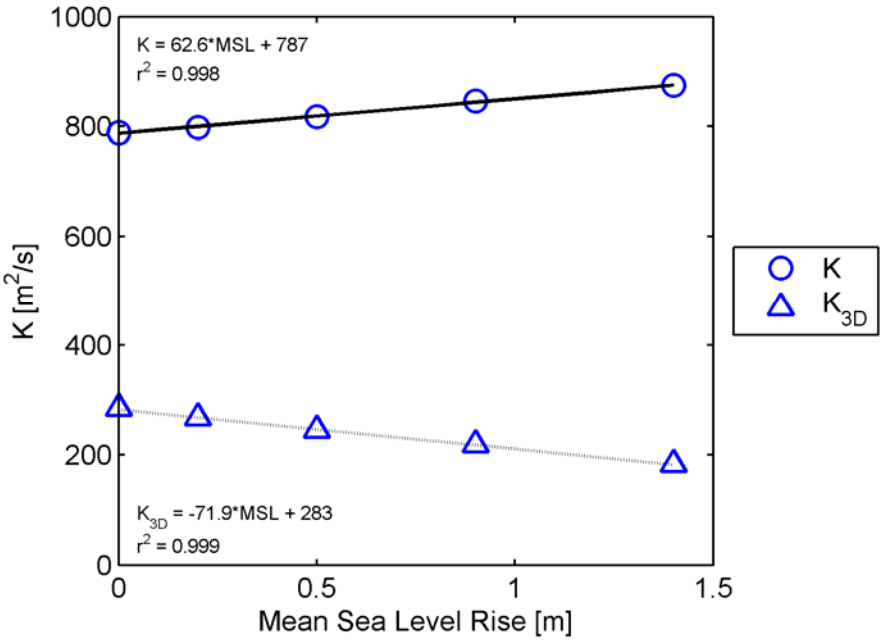

Figure H3.7.3-4 Total and three-dimensional dispersion coefficients calculated for each MSL rise scenario at cross-section 11, at the Carquinez Bridge. A best fit equation and r^2 value is shown for each set of coefficients

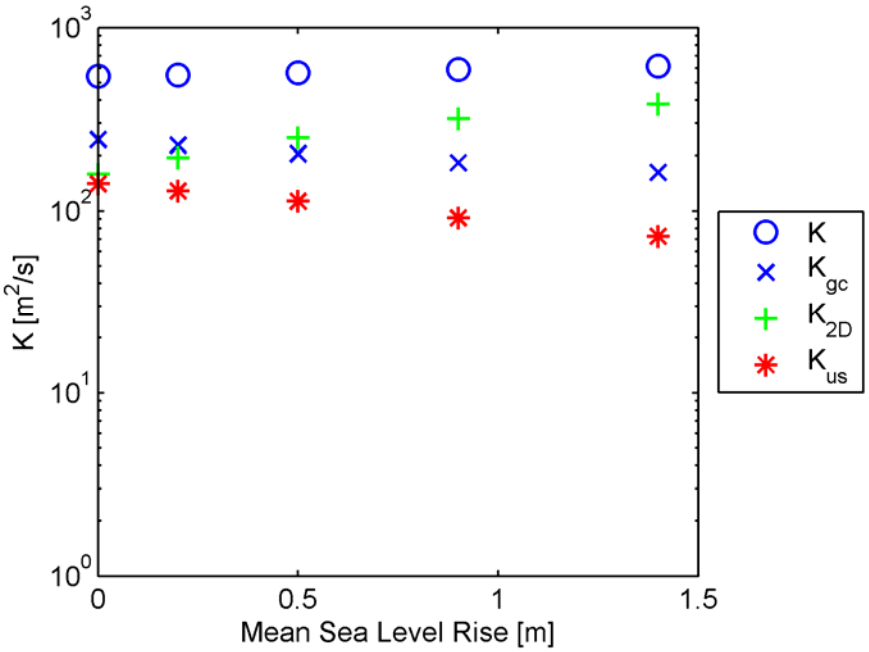

Figure H3.7.3-5 Estimated dispersion coefficients at cross-section 12, extending from Crockett to Dillon Point, as a function of MSL rise

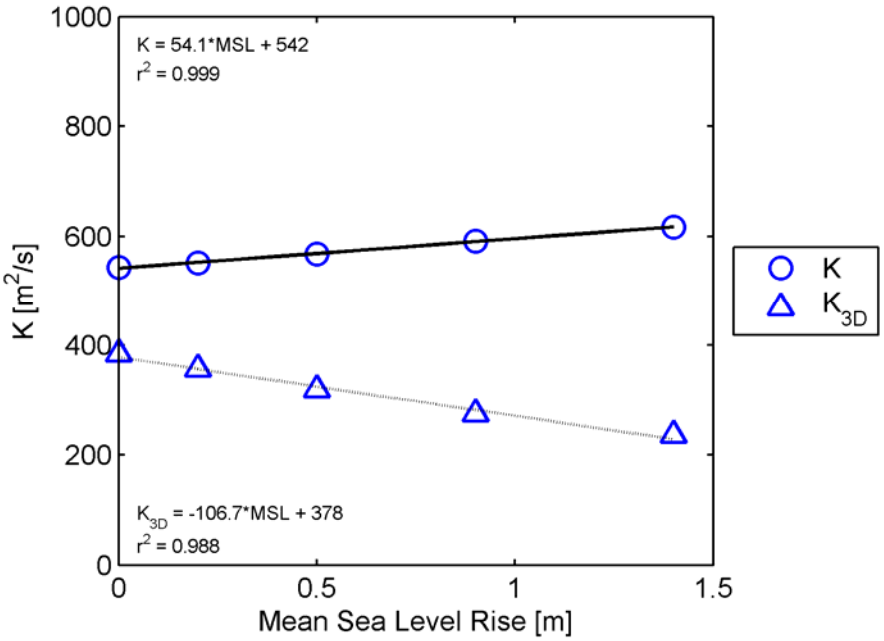

Figure H3.7.3-6 Total and three-dimensional dispersion coefficients calculated for each MSL rise scenario at cross-section 12, extending from Crockett to Dillon Point. A best fit equation and r^2 value is shown for each set of coefficients

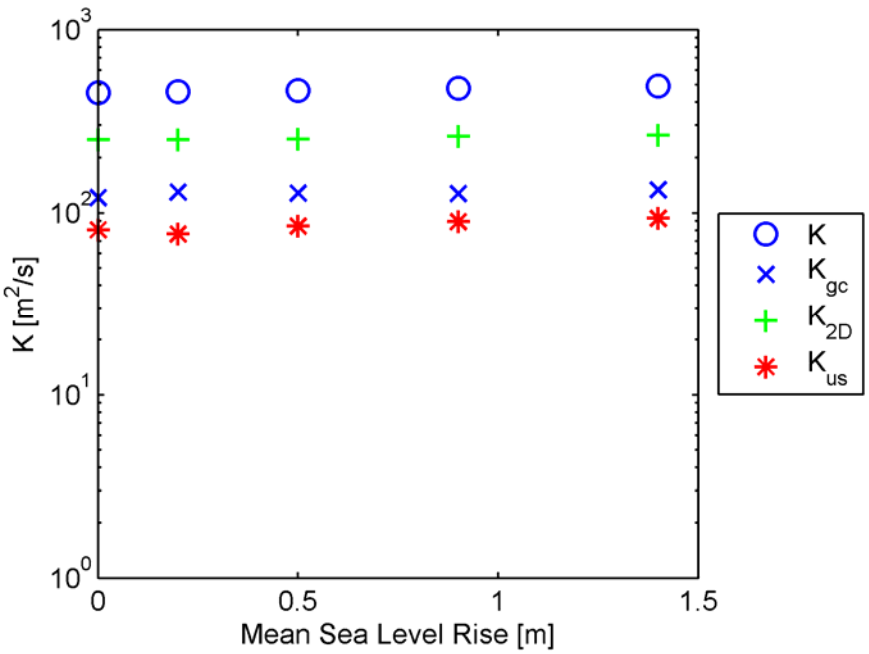

Figure H3.7.3-7 Dispersion coefficients and dispersion coefficient components calculated for each MSL rise scenario at cross-section 13, extending from Ozol to Benicia Point

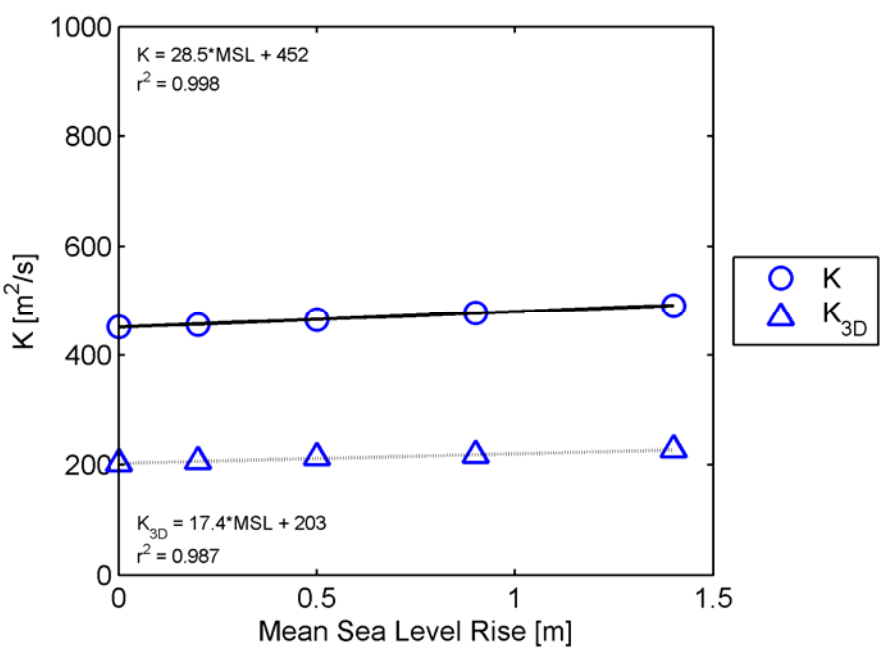

Figure H3.7.3-8 Total and three-dimensional dispersion coefficients calculated for each MSL rise scenario at cross-section 13, extending from Ozol to Benicia Point. A best fit equation and r^2 value is shown for each set of coefficients

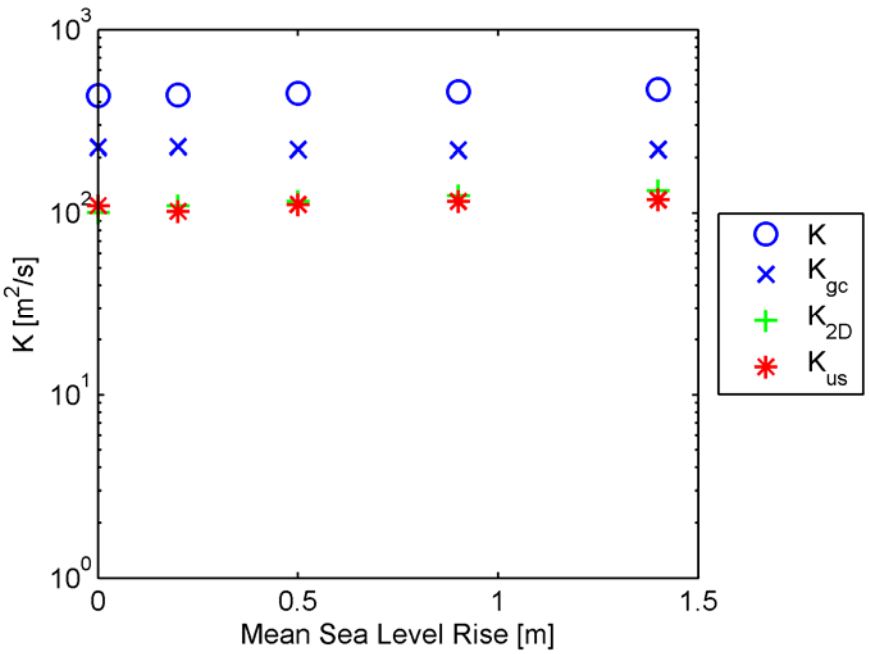

Figure H3.7.3-9 Dispersion coefficients and dispersion coefficient components calculated for each MSL rise scenario at cross-section 14, extending from Martinez to Benicia

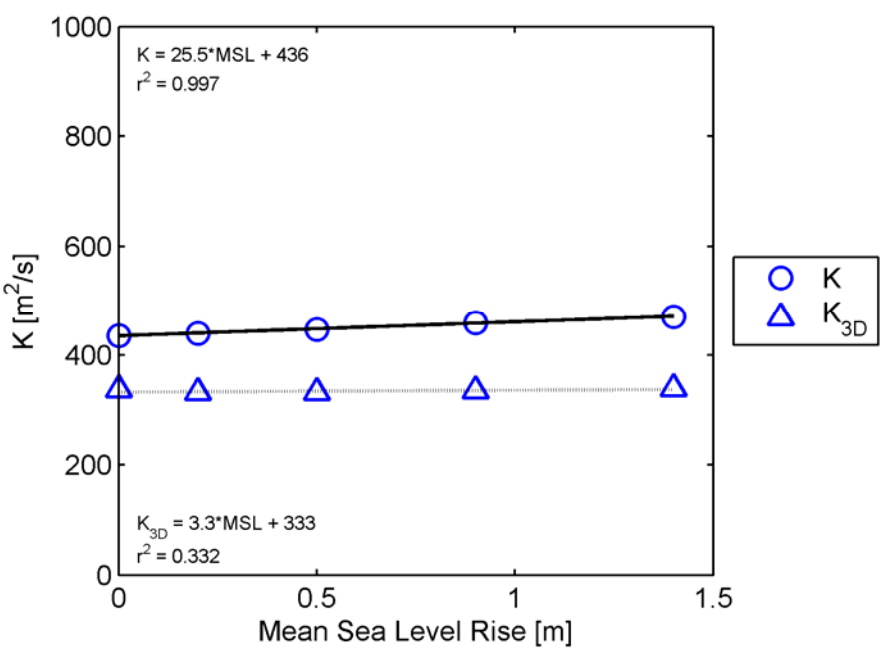

Figure H3.7.3-10 Total and three-dimensional dispersion coefficients calculated for each MSL rise scenario at cross-section 14, extending from Martinez to Benicia. A best fit equation and r^2 value is shown for each set of coefficients

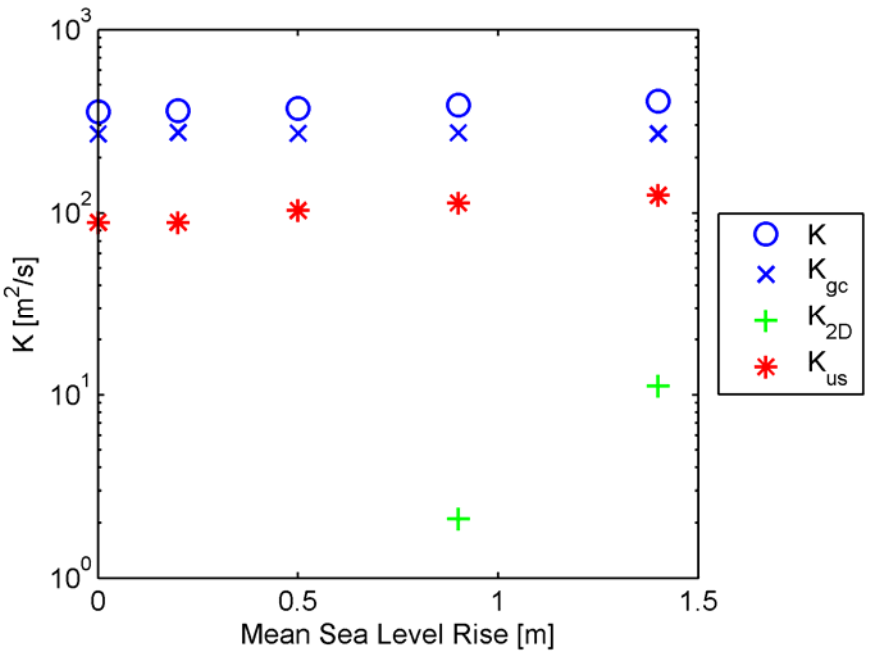

Figure H3.7.3-11 Dispersion coefficients and dispersion coefficient components calculated for each MSL rise scenario at cross-section 15, at the Benicia Bridge, as a function of MSL rise

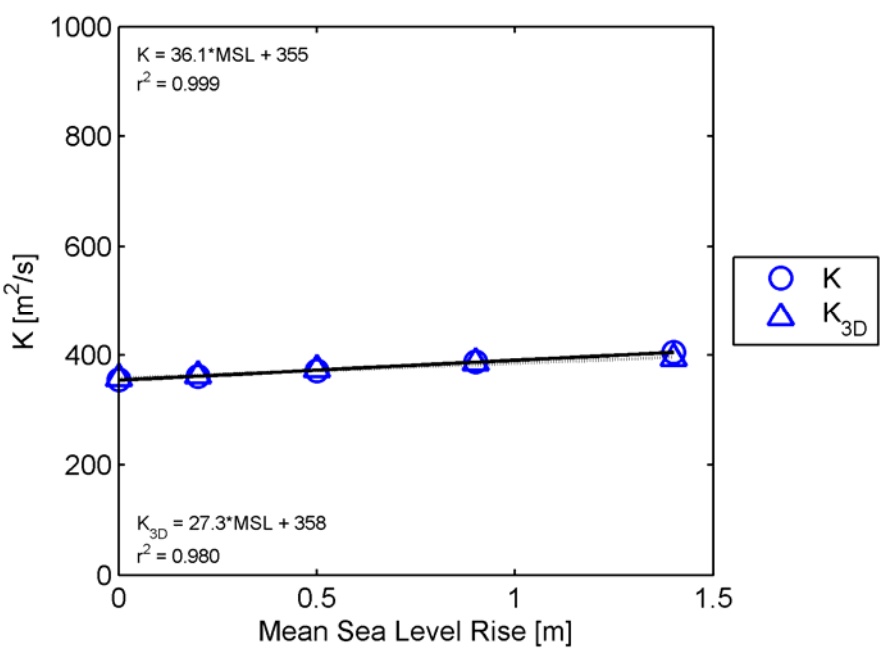

Figure H3.7.3-12 Total and three-dimensional dispersion coefficients calculated for each MSL rise scenario at cross-section 15, at the Benicia Bridge. A best fit equation and r^2 value is shown for each set of coefficients

H3.7.4 Suisun Bay Cross-Sections

Dispersion coefficients and fluxes were estimated at the eight cross-sections in Suisun Bay shown in Figure H3.3-1. In Figures H3.7.4-1 through H3.7.4-16, two figures are provided for each cross-section in order to summarize the results of the dispersion analysis at that location. The first type of figure shows each dispersion coefficient and the individual components of each dispersion coefficient for each MSL rise scenario. The second type of figure shows the overall dispersion coefficient and the dispersion coefficient associated with "three-dimensional processes" ($K_{gc} + K_{us}$) for each MSL rise scenario as well as linear fit equations that describe the variability of these dispersion coefficients with MSL rise.

The dispersion coefficients are small in Suisun Bay relative to those estimated in Central San Francisco Bay and San Pablo Bay. The dispersion coefficients are increase weakly with MSL in the seaward portion of Suisun Bay and increase with increased MSL in the western Delta. Tidal dispersion is the largest component of dispersion at most cross-sections but both gravitational circulation and unsteady vertical shear are important at some cross-sections.

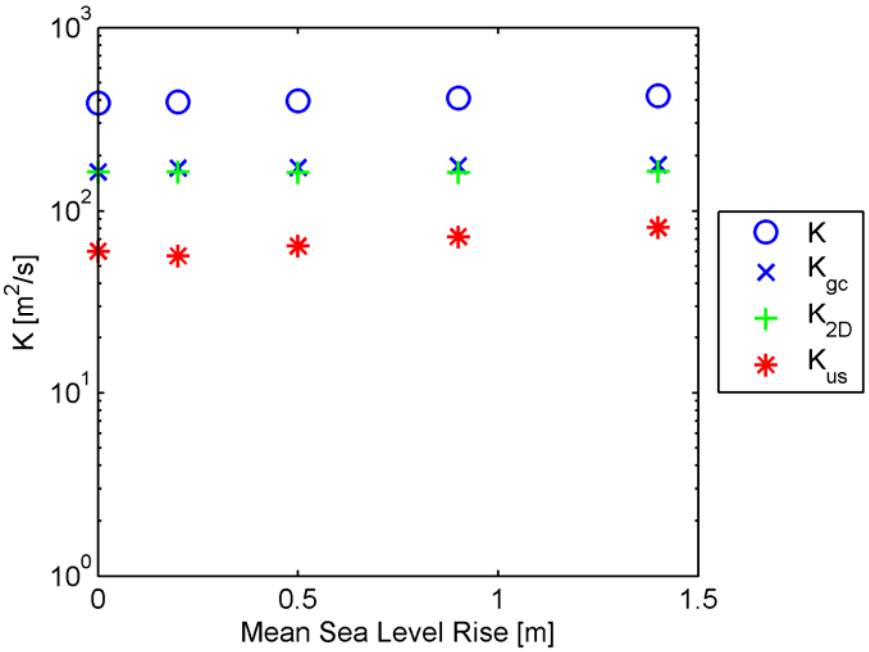

Figure H3.7.4-1 Dispersion coefficients and dispersion coefficient components calculated for each MSL rise scenario at cross-section 16, from Pacheco Creek to the Mothball Fleet

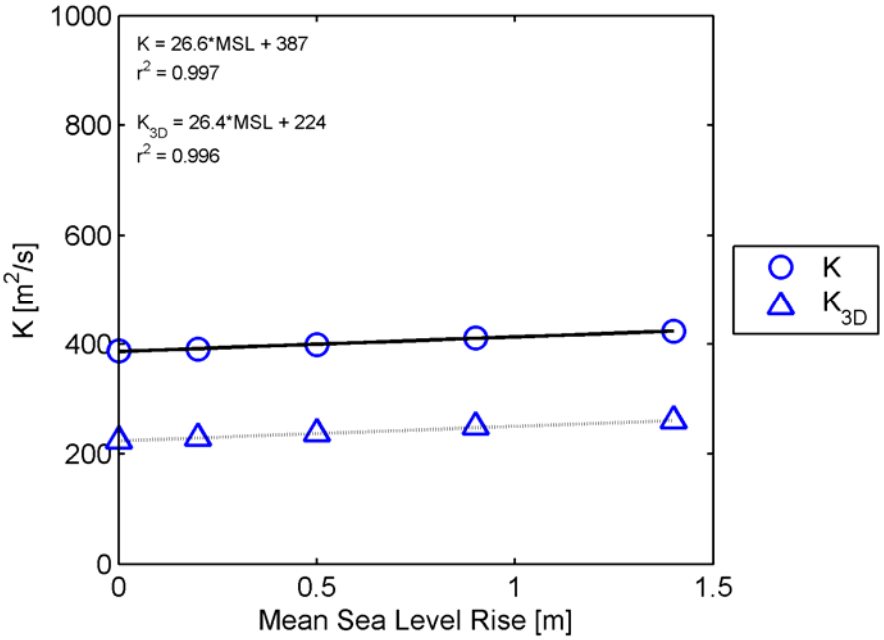

Figure H3.7.4-2 Total and three-dimensional dispersion coefficients calculated for each MSL rise scenario at cross-section 16, from Pacheco Creek to the Mothball Fleet. A best fit equation and r^2 value is shown for each set of coefficients

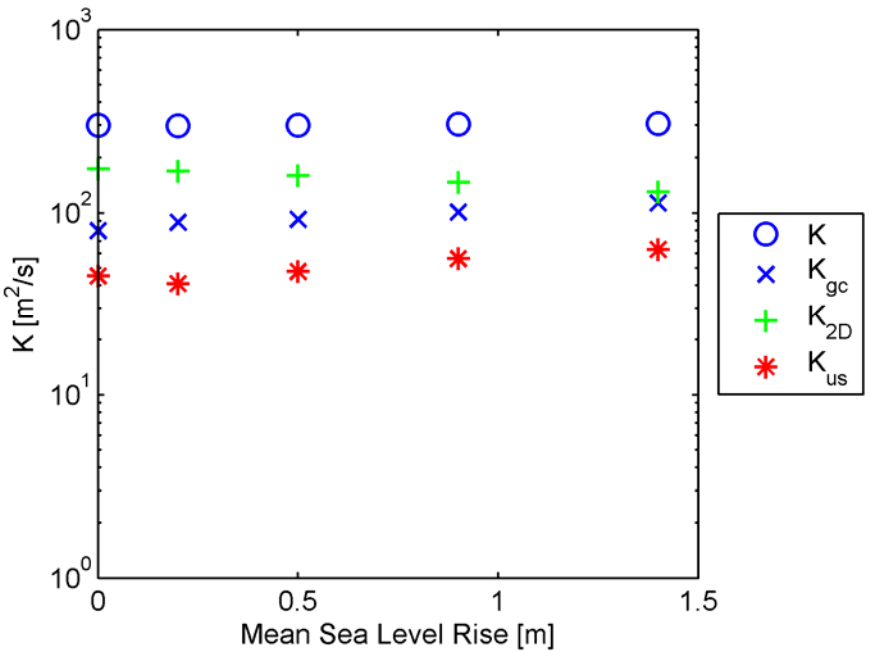

Figure H3.7.4-3 Dispersion coefficients and dispersion coefficient components calculated for each MSL rise scenario at cross-section 17, east of the Mothball Fleet

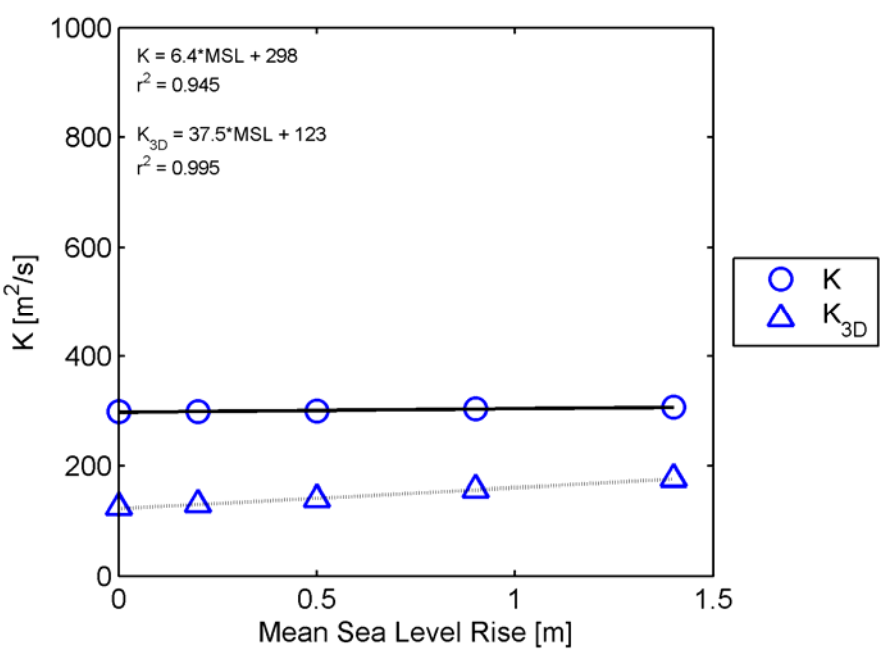

Figure H3.7.4-4 Total and three-dimensional dispersion coefficients calculated for each MSL rise scenario at cross-section 17, east of the Mothball Fleet. A best fit equation and r^2 value is shown for each set of coefficients

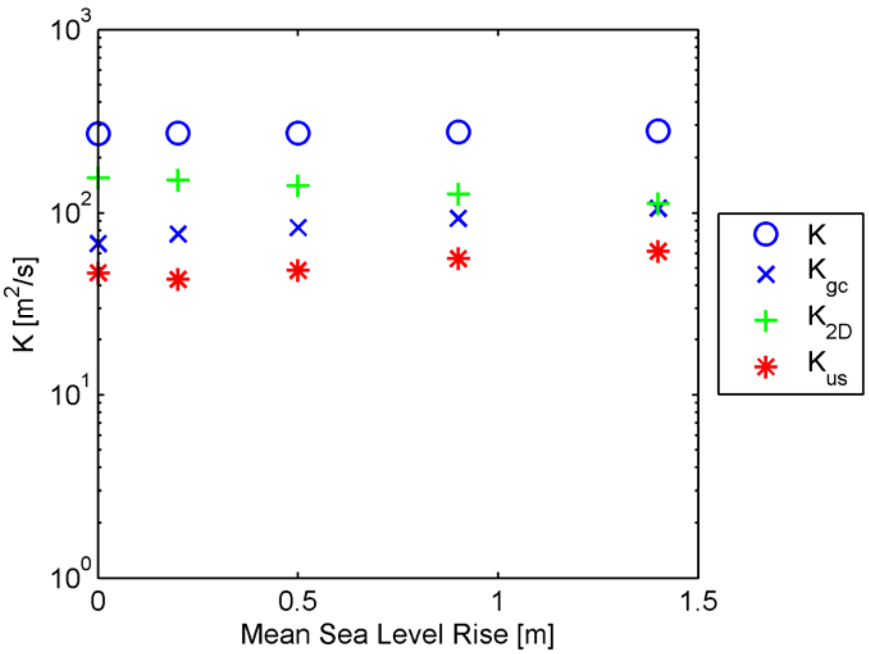

Figure H3.7.4-5 Dispersion coefficients and dispersion coefficient components calculated for each MSL rise scenario at cross-section 18, from Point Edith to Bahia

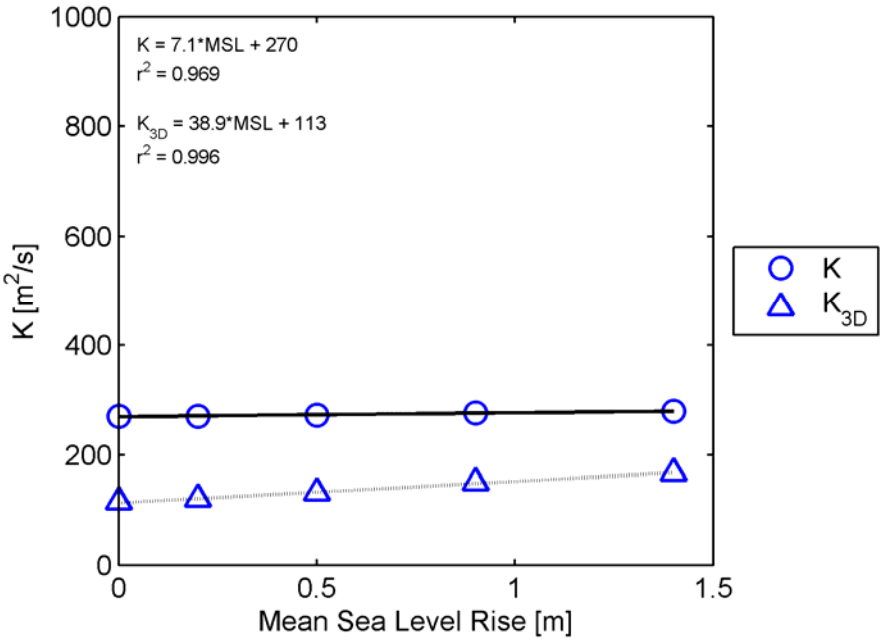

Figure H3.7.4-6 Total and three-dimensional dispersion coefficients calculated for each MSL rise scenario at cross-section 18, from Point Edith to Bahia. A best fit equation and r^2 value is shown for each set of coefficients

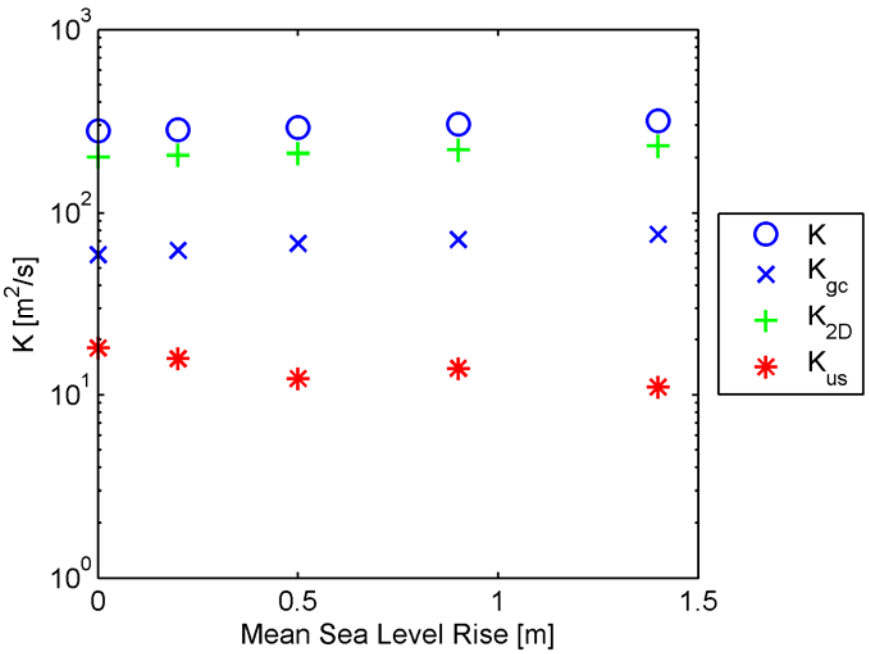

Figure H3.7.4-7 Dispersion coefficients and dispersion coefficient components calculated for each MSL rise scenario at cross-section 19, from Port Chicago to Grizzly Bay

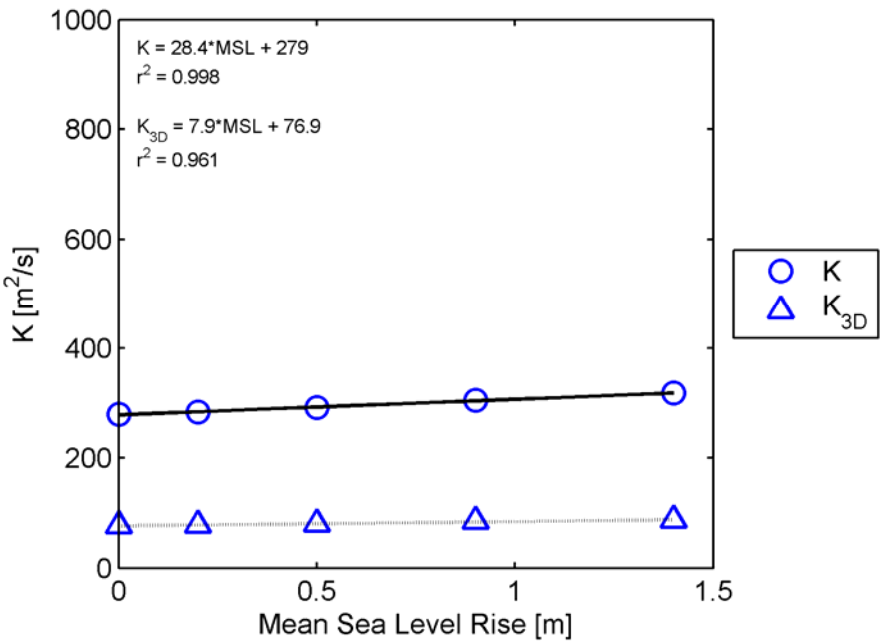

Figure H3.7.4-8 Total and three-dimensional dispersion coefficients calculated for each MSL rise scenario at cross-section 19, from Port Chicago to Grizzly Bay. A best fit equation and r^2 value is shown for each set of coefficients

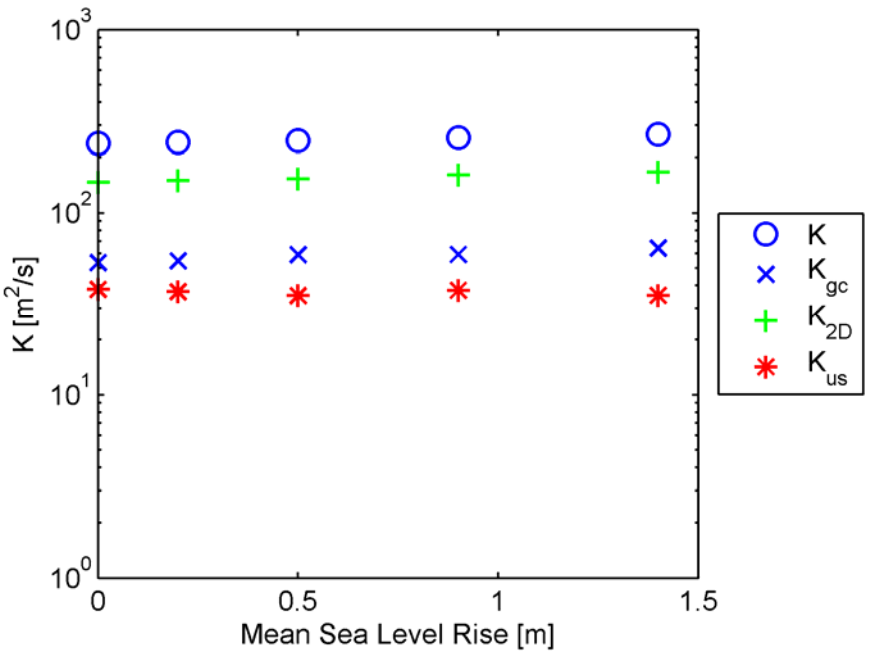

Figure H3.7.4-9 Dispersion coefficients and dispersion coefficient components calculated for each MSL rise scenario at cross-section 20, from Middle Point to Simmons Island

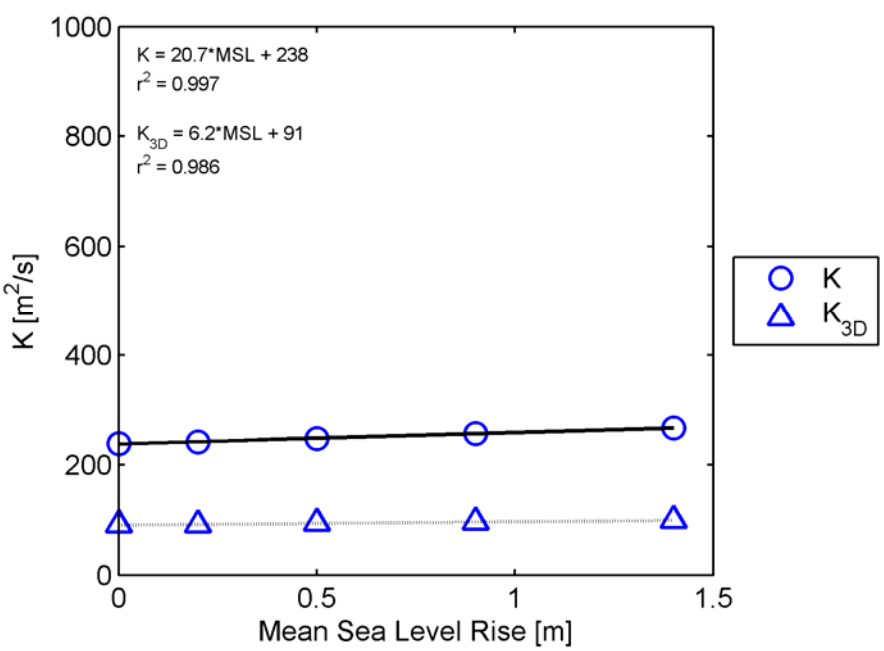

Figure H3.7.4-10 Total and three-dimensional dispersion coefficients calculated for each MSL rise scenario at cross-section 20, from Middle Point to Simmons Island. A best fit equation and r^2 value is shown for each set of coefficients

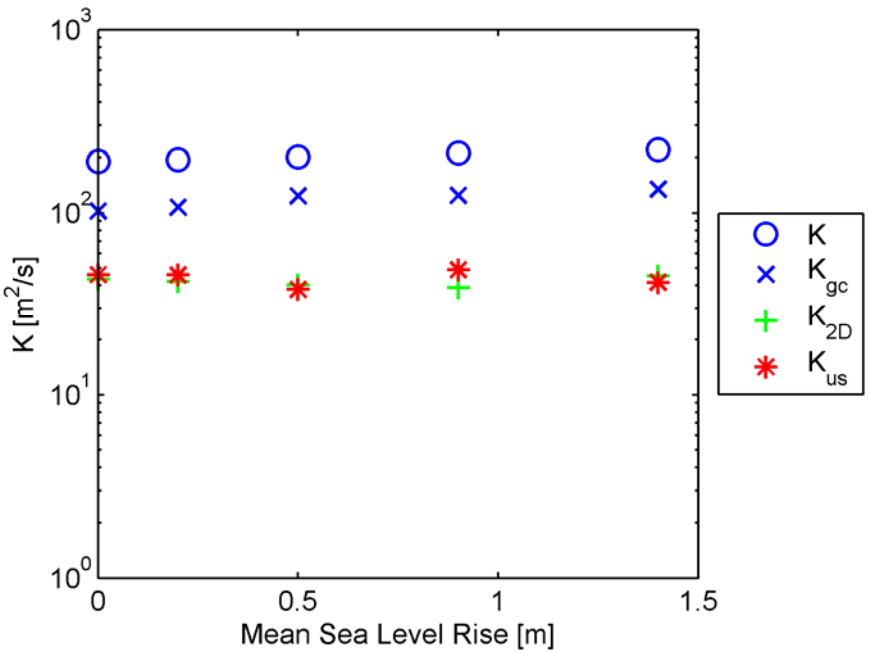

Figure H3.7.4-11 Dispersion coefficients and dispersion coefficient components calculated for each MSL rise scenario at cross-section 21, from Concord to Dutton Island

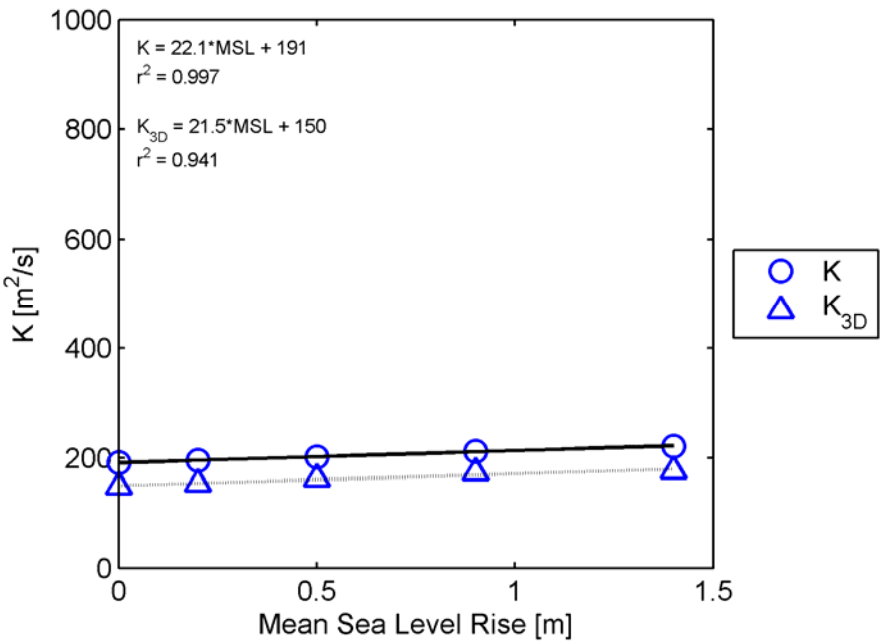

Figure H3.7.4-12 Total and three-dimensional dispersion coefficients calculated for each MSL rise scenario at cross-section 21, from Concord to Dutton Island. A best fit equation and r^2 value is shown for each set of coefficients

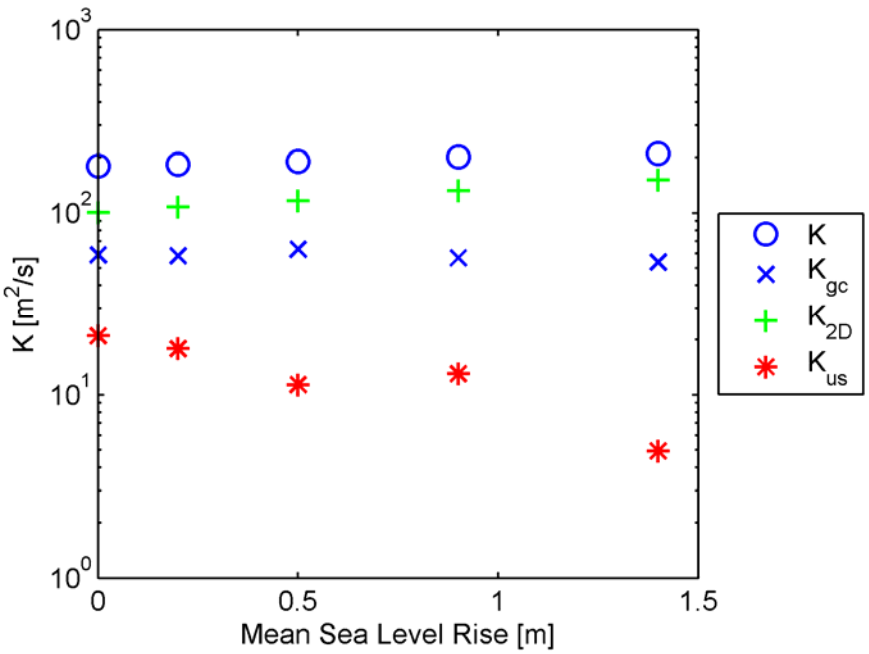

Figure H3.7.4-13 Dispersion coefficients and dispersion coefficient components calculated for each MSL rise scenario at cross-section 22, from Stake Point to Wheeler Island

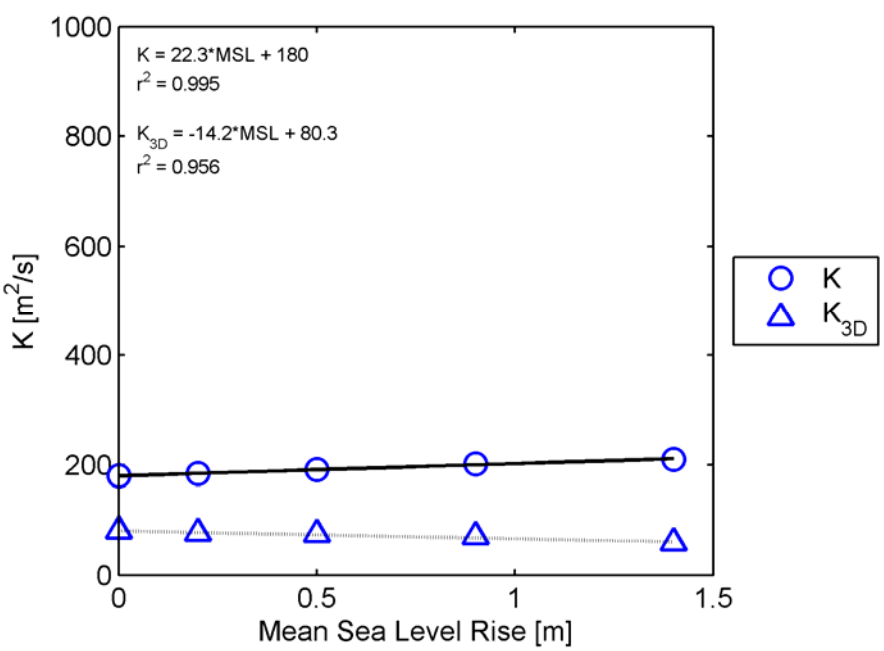

Figure H3.7.4-14 Total and three-dimensional dispersion coefficients calculated for each MSL rise scenario at cross-section 22, from Stake Point to Wheeler Island. A best fit equation and r^2 value is shown for each set of coefficients

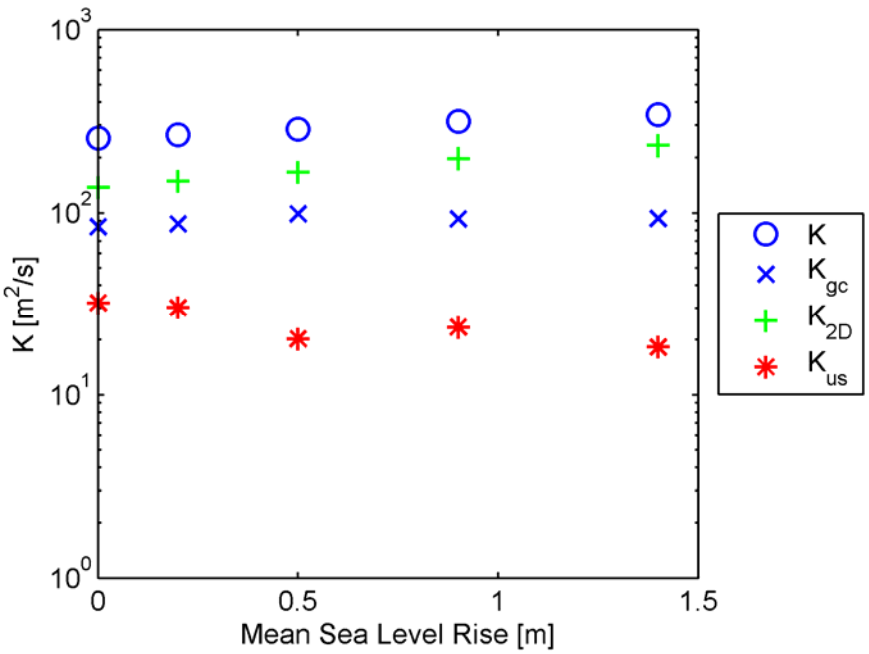

Figure H3.7.4-15 Dispersion coefficients and dispersion coefficient components calculated for each MSL rise scenario at cross-section 23, extending south from Simmons Point

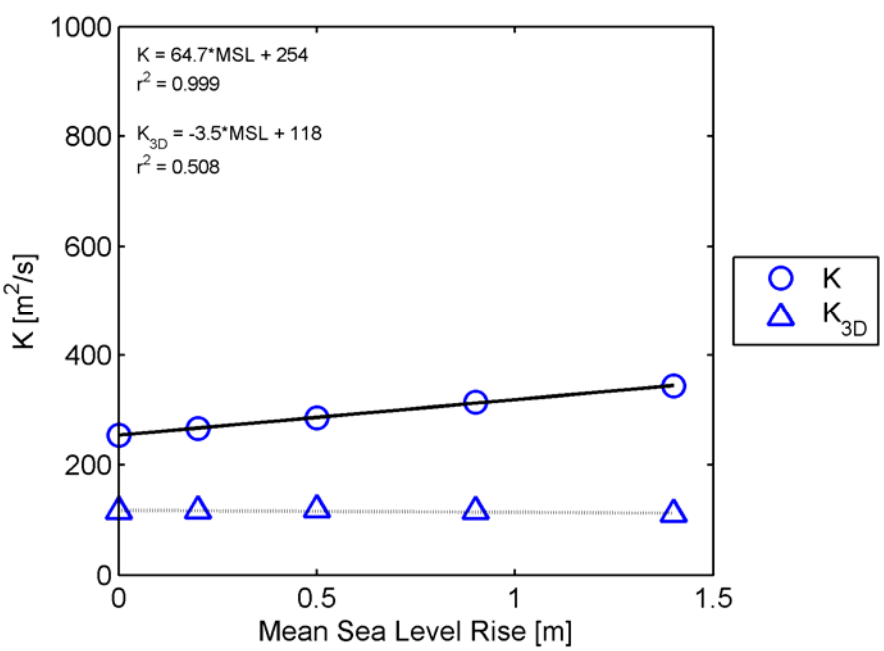

Figure H3.7.4-16 Total and three-dimensional dispersion coefficients calculated for each MSL rise scenario at cross-section 23, extending south from Simmons Point. A best fit equation and r^2 value is shown for each set of coefficients

H3.7.5 Western Delta Cross-Sections

Dispersion coefficients and fluxes were estimated at the five cross-sections in the western Delta shown in Figure H3.3-1. In Figures H3.7.5-1 through H3.7.5-10, two figures are provided for each cross-section in order to summarize the results of the dispersion analysis at that location. The first type of figure shows each dispersion coefficient and the individual components of each dispersion coefficient for each MSL rise scenario. The second type of figure shows the overall dispersion coefficient and the dispersion coefficient associated with "three-dimensional processes" ($K_{gc} + K_{us}$) for each MSL rise scenario as well as linear fit equations that describe the variability of these dispersion coefficients with MSL rise.

The dispersion coefficients are generally relatively small in the western Delta. Dispersion is dominated by tidal dispersion processes at most cross-sections. The dispersion coefficients increase substantially with increased MSL in the western Delta. The largest and most variable component of dispersion in this region is tidal dispersion. At cross-sections 27 and 28 the strength of gravitational circulation also increases with sea level rise. Note that the predicted salinity is too low in the Baseline and 20 cm MSL Rise scenarios to allow calculation of dispersion coefficients at cross-section 28.

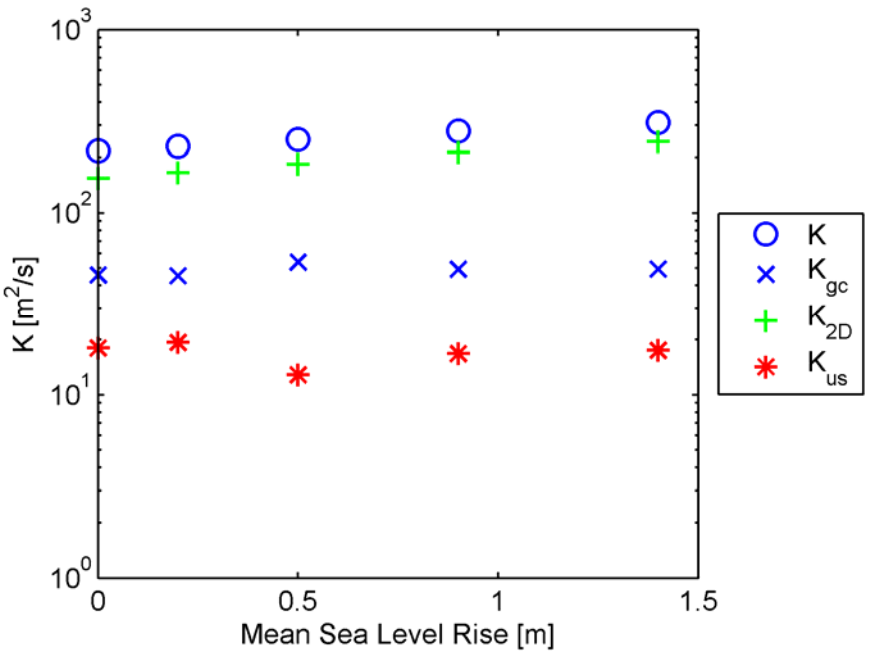

Figure H3.7.5-1 Dispersion coefficients and dispersion coefficient components calculated for each MSL rise scenario at cross-section 24, extending from Mallard Island to Chipps Island

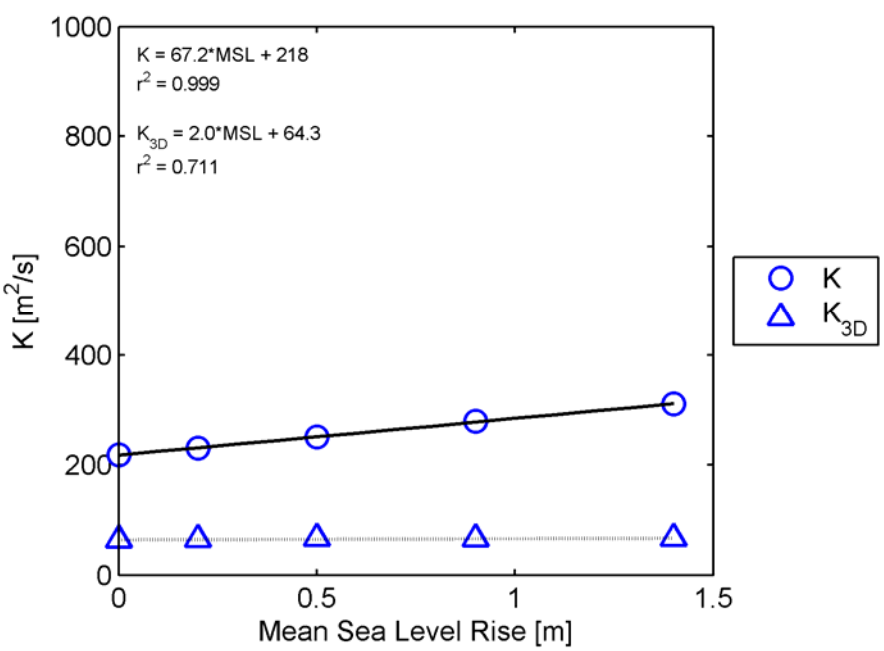

Figure H3.7.5-2 Total and three-dimensional dispersion coefficients calculated for each MSL rise scenario at cross-section 24, extending from Mallard Island to Chipps Island. A best fit equation and r^2 value is shown for each set of coefficients

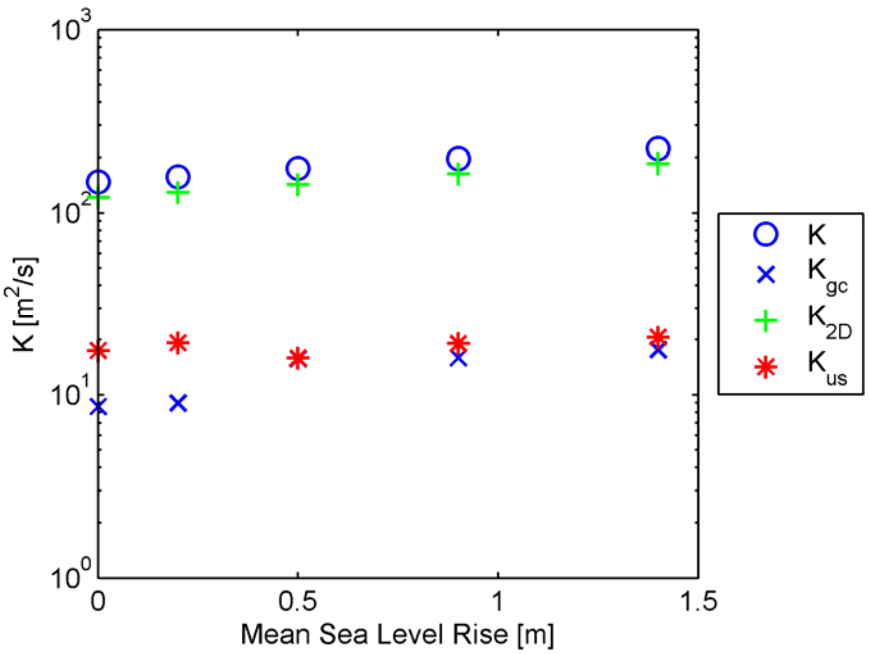

Figure H3.7.5-3 Dispersion coefficients and dispersion coefficient components calculated for each MSL rise scenario at cross-section 25, extending from Pittsburg to Chipps Island

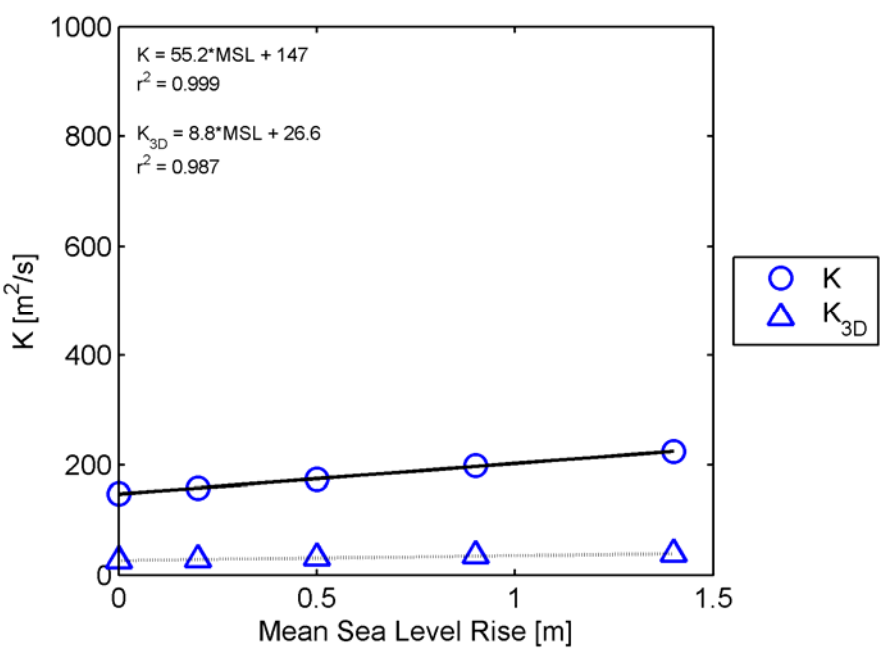

Figure H3.7.5-4 Total and three-dimensional dispersion coefficients calculated for each MSL rise scenario at cross-section 25, extending from Pittsburg to Chipps Island. A best fit equation and r^2 value is shown for each set of coefficients.

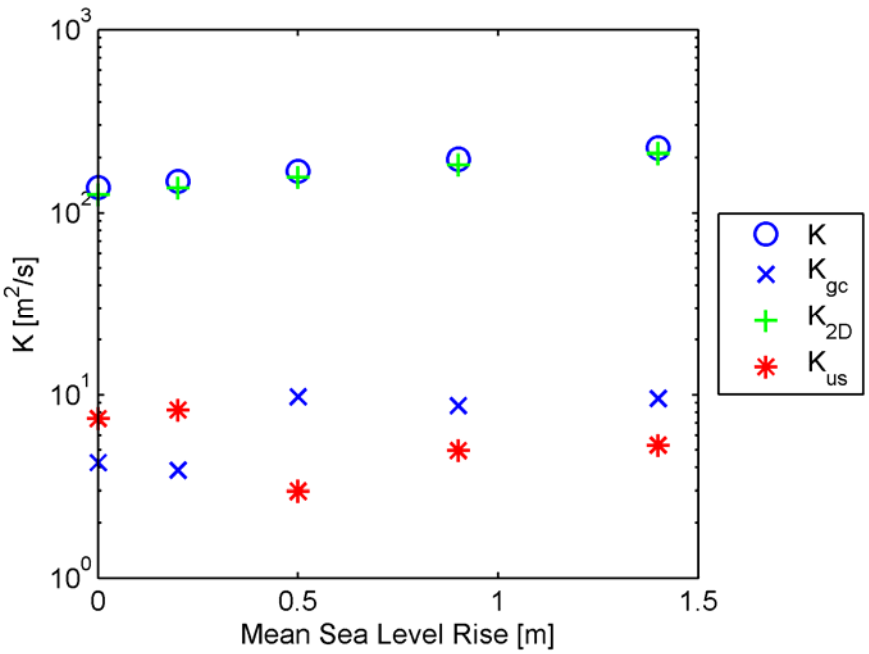

Figure H3.7.5-5 Dispersion coefficients and dispersion coefficient components calculated for each MSL rise scenario at cross-section 26, extending from Winter Island to Van Sickle Island

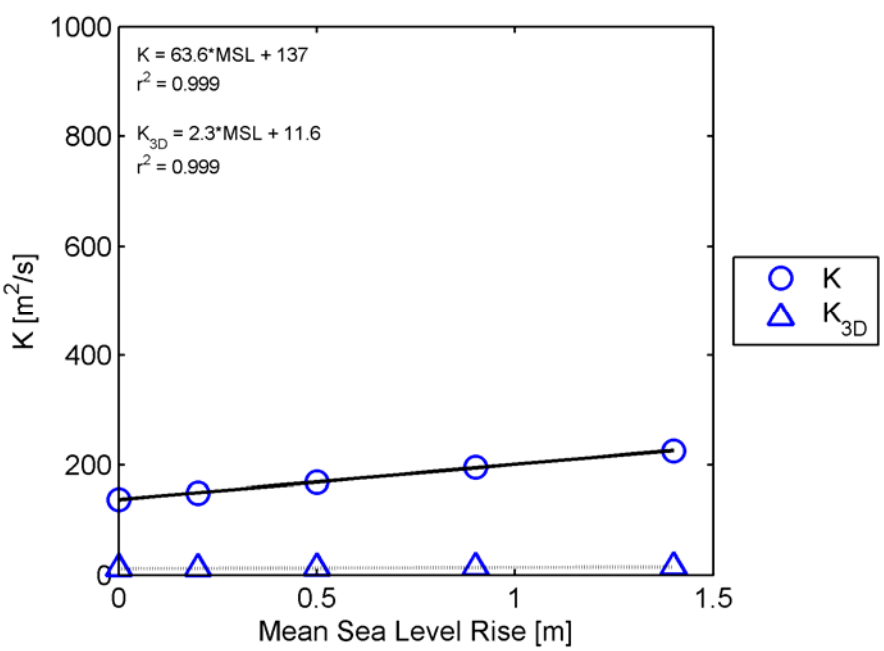

Figure H3.7.5-6 Total and three-dimensional dispersion coefficients calculated for each MSL rise scenario at cross-section 26, extending from Winter Island to Van Sickle Island. A best fit equation and r^2 value is shown for each set of coefficients

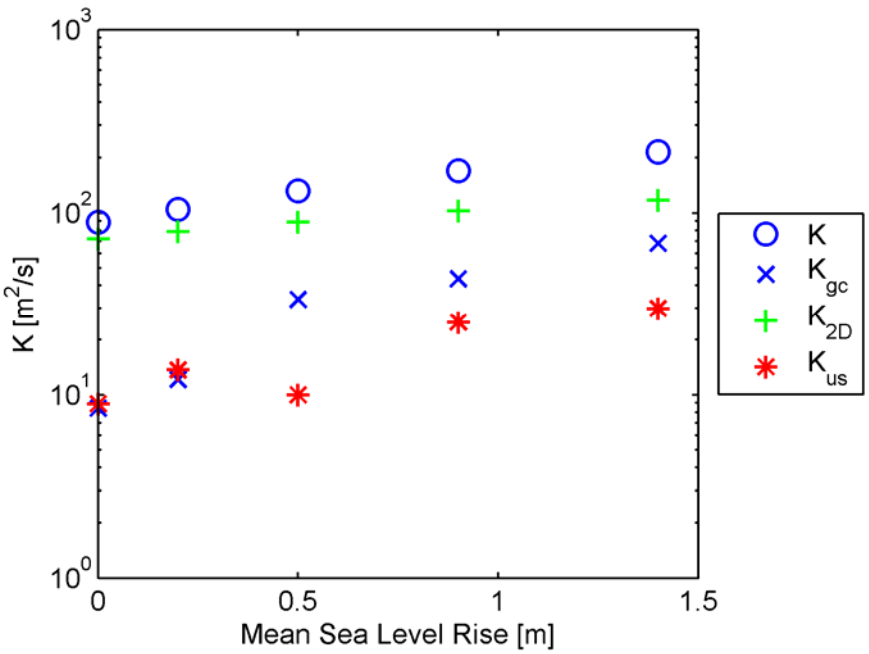

Figure H3.7.5-7 Dispersion coefficients and dispersion coefficient components calculated for each MSL rise scenario at cross-section 27, extending north from Sherman Island

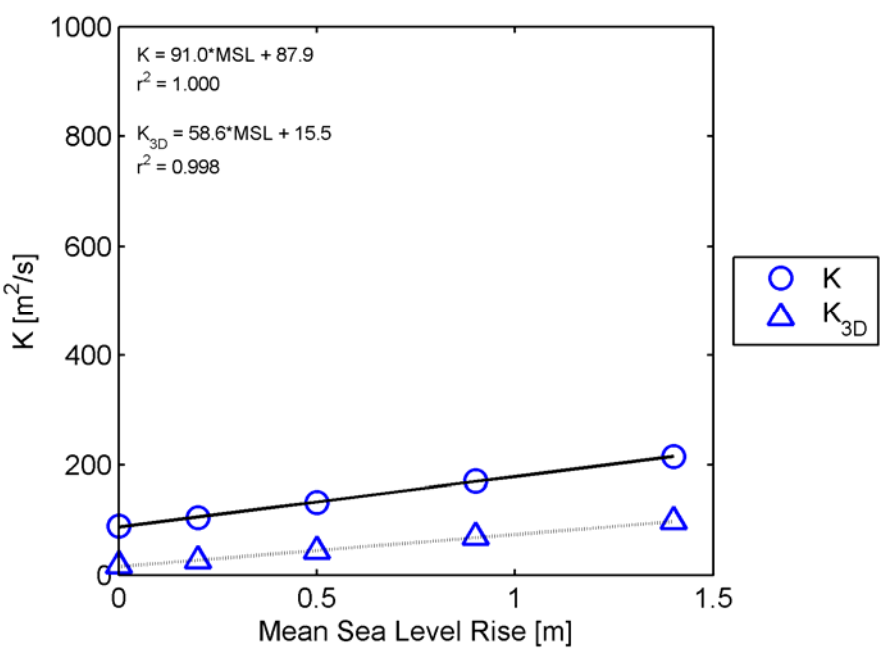

Figure H3.7.5-8 Total and three-dimensional dispersion coefficients calculated for each MSL rise scenario at cross-section 27, extending north from Sherman Island. A best fit equation and r^2 value is shown for each set of coefficients

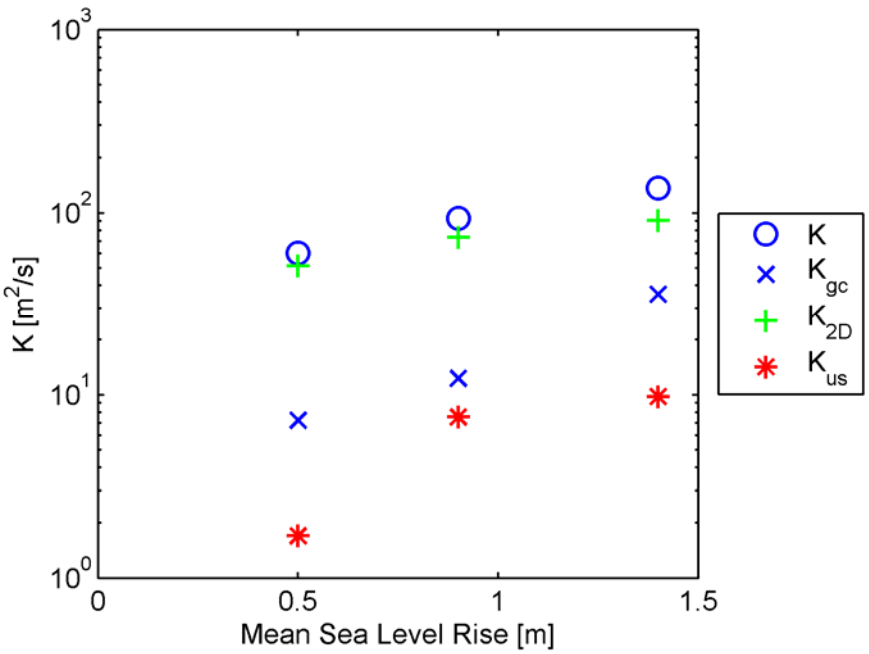

Figure H3.7.5-9 Dispersion coefficients and dispersion coefficient components calculated for each MSL rise scenario at cross-section 28, on Sacramento River near Emmaton

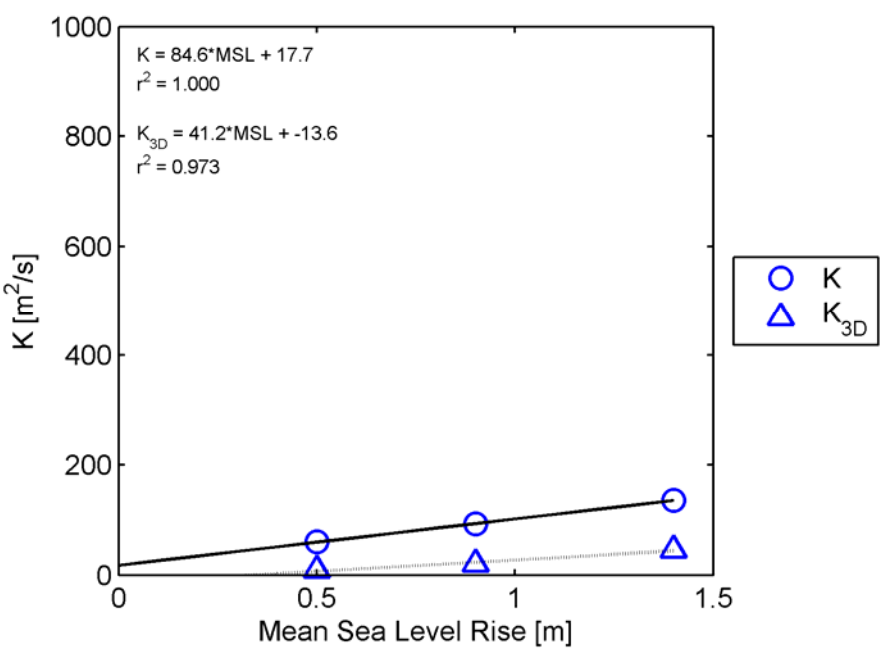

Figure H3.7.5-10 Total and three-dimensional dispersion coefficients calculated for each MSL rise scenario at cross-section 28, on Sacramento River near Emmaton. A best fit equation and r^2 value is shown for each set of coefficients

H3.7.6 Summary of Dispersion Coefficient Estimates

Dispersion coefficients have been estimated at 28 cross-sections in the San Francisco Estuary. At each cross-section, dispersion coefficients are estimated for 5 scenarios ranging from no sea level rise, to 140 cm MSL rise. These results are shown in Section 7.1 through Section 7.5. The calculated dispersion coefficients and the individual components of the dispersion coefficient (K_{gc}, K_{us}, and K_{2D}) vary strongly spatially. At each section the variability of K and K_{3D} ($K_{gc} + K_{us}$) with MSL rise is described by a linear curve fit. This form of equation is arbitrary but seems adequate given the high r^2 values of the linear fits at most cross-sections.

The values given in Table H3-4 are used in the WAM to modify the dispersion coefficients calculated in the DRMS report "Parameterization of Mixing using a Three-Dimensional Hydrodynamic Model." For each WAM scenario that incorporates sea level rise, the dispersion coefficients will be modified according to the linear fit information summarized in Table H3-4.

The dispersion analysis indicates that the strength of dispersive transport increase with MSL rise at all Carquinez Strait, Suisun Bay and western Delta cross-sections. In contrast, small changes are estimated in Central Bay and San Pablo Bay. Generally, the increases relative to dispersion coefficients for the Baseline scenario become larger with distance landward with generally small to moderate increases in Carquinez Strait, substantial increases in most of Suisun Bay, and large increases at all cross-sections in the Western Delta. The three-dimensional component of dispersion also increases at all Carquinez Strait, Suisun Bay and western Delta cross-section with the exception of two Suisun Bay cross-sections. A portion of the increase in total dispersion coefficients is associated with two-dimensional processes resulting from higher tidal currents and a portion is associated with three-dimensional processes, primarily associated with increased gravitational circulation.

As noted in Section 5, the increase in salt intrusion is substantial for 90 cm or more sea level rise. A portion of the increased salt intrusion is due to less effective flushing of the deeper channels by freshwater inflows. This is expected in the context of the salt balance equation

$$Q\,S = -K\,A(dS/dx)$$

From this equation, it is clear that if the cross-sectional area (A) increases without changes in K, Q or dS/dx, salinity (S) will increase. In portions of Suisun Bay and the western Delta K, A and dS/dx all increase with increased MSL, leading to multiplicative effects on salt intrusion.

Limited budget was provided for the parameterization analysis outlined here and in the DRMS report "Parameterization of Mixing using a Three-Dimensional Hydrodynamic Model." The apparent success of the simplified model in reproducing historic salinity conditions in the Estuary suggests that the parameterization approach is useful. It could be substantially improved by more detailed analysis of existing model results and by performing additional simulations. Most notably, dispersion processes could be analyzed much further into the Delta by considering low Net Delta Outflow conditions in additional UnTRIM model simulations. Furthermore, substantial improvements could be

made to both the three-dimensional model and the analysis technique used to estimate dispersion coefficients. Several uncertainties and proposed improvements are discussed in the Section 7.7.

Table H3-4 Results of parameterization of the effects of sea level rise on dispersive transport for use in WAM. The values listed are the slopes and intercepts of best fit lines for the variability of dispersion coefficients with Mean Sea Level rise

Section	K slope [m/s]	K int [m^2/s]	K r^2	K_{3D} slope [m/s]	K_{3D} int [m^2/s]	K_{3D} r^2
1	49.7	418	0.998	-9.3	186	0.970
2	24.8	263	0.996	1.7	75	0.654
3	20.9	470	0.989	35.5	307	0.990
4	9.2	494	0.951	4.6	286	0.711
5	23.1	590	0.990	-59.0	448	1.000
6	-15.7	527	0.985	-4.9	179	0.769
7	-33.9	356	0.993	7.4	151	0.711
8	-39.8	429	0.994	68.8	293	0.994
9	10.1	634	0.943	-65.8	305	0.956
10	32.8	656	0.993	-63.3	280	0.928
11	62.6	787	0.998	-71.9	283	0.999
12	54.1	542	0.999	-106.7	378	0.988
13	28.5	452	0.998	17.4	203	0.987
14	25.5	436	0.997	3.3	333	0.332
15	36.1	355	0.999	27.3	358	0.980
16	26.6	387	0.997	26.4	224	0.996
17	6.4	298	0.945	37.5	123	0.995
18	7.1	270	0.969	38.9	113	0.996
19	28.4	279	0.998	7.9	77	0.961
20	20.7	238	0.997	6.2	91	0.986
21	22.1	191	0.997	21.5	150	0.941
22	22.3	180	0.995	-14.2	80	0.956
23	64.7	254	0.999	-3.5	118	0.508
24	67.2	218	0.999	2.0	64	0.711
25	55.2	147	0.999	8.8	27	0.987
26	63.6	137	0.999	2.3	12	0.999
27	91.0	88	1.000	58.6	15	0.998
28	84.6	18	1.000	41.2	-14	0.973

H3.7.7 Uncertainty of Dispersion Coefficient Estimates

The dispersion analysis presented in this report was tailored to the needs of the WAM for the DRMS project. The UnTRIM model was calibrated for a large range of conditions, as documented in the DRMS report “UnTRIM San Francisco Bay-Delta Model Calibration.” This calibration provides confidence that physical processes responsible for salt transport are represented adequately. The method used for the calculation of dispersion coefficients is well established in many previous applications employing

salinity observations (e.g., Fischer et al. 1979). The method to distinguish fluxes from different physical processes is also well-established. One novel aspect of the analysis is the simplified forcing to reach a precise tidally-averaged steady state salinity field.

The results of the analysis are consistent with the conceptual model of transport developed through many field studies (e.g., Burau et al., 1998) and are consistent with the results of the TRIM model for current sea level documented in DRMS report "Parameterization of Mixing using a Three-Dimensional Hydrodynamic Model." The conceptual model is that gravitational circulation is the most important transport mechanism in San Pablo Bay and Carquinez Strait and that the importance of gravitational circulation decreases sharply at the Benicia shoal due to limited depth. In Suisun Bay, due to complex bathymetry as well as less pronounced gravitational circulation, tidal dispersion processes are the dominant transport processes.

Though the accuracy of the estimated dispersion coefficients is likely to be adequate for the DRMS project, several limitations and uncertainties limit confidence in the estimated dispersion coefficients. Some of this uncertainty is associated with the three-dimensional model predictions while additional uncertainty is associated with the analysis method. The three-dimensional model applied in this analysis provides a more detailed description of fluid motion in the San Francisco Estuary than depth-averaged or one-dimensional models. However, there are several sources of uncertainty inherent in the application of this model:

- Spatial resolution – the spatial resolution of the bathymetry of the model domain, and velocity and salinity distributions, is limited by the large computational expense associated with high-resolution models.
- Bathymetry data – limited spatial coverage and accuracy of bathymetry data can be a substantial source of error. Converting all data to a uniform vertical datum and horizontal datum can lead to some error. In particular, LiDAR data may have substantial errors in vertical datum and removing vegetation from the dataset can be difficult.
- Site-specific parameters – the TRIM model requires bottom friction coefficients to parameterize the resistance to flow at solid boundaries. These parameters are specified in model calibration by tuning to improve the calibration.
- Turbulence closure – the effect of turbulent motions on the tidal time scale motions is estimated by a turbulence closure. While many turbulence closures are available, this is an ongoing area of research and, particularly in stratified settings, the effect of turbulence on tidal flows and salinity is not easy to estimate accurately and different turbulence closures may give significantly different results (e.g., Celebioglu and Piasecki 2006).
- Numerical errors –a numerical method approximates the governing equations to some level of accuracy. The mathematical properties of the numerical method of the TRIM model are well understood due to detailed mathematical analysis presented in several peer reviewed publications. While the stability and conservation properties of the

method are ideal, a source of error in the numerical method is some degree of numerical diffusion of momentum and potential for damping of tidal propagation.

Though additional potential sources of uncertainty can be identified, the largest sources of uncertainty for hydrodynamic predictions are typically the accuracy and resolution of available bathymetry data and the grid resolution available to represent this bathymetry in the model. Every effort was made to minimize this uncertainty by making use of the best available bathymetric data and developing a high resolution grid. The model used for the scenarios documented in this report is expected to have improved accuracy relative to the TRIM model due to the use of a flexible unstructured grid which provides improved resolution of bathymetric features.

Additional uncertainty is associated with the simplified forcing used in the scenario simulations. As noted in Section 5, these approximations include:

- That tidal forcing is dominant relative to wind forcing and other environmental forcing.
- That a repeating M2 and K1 tide, with M2 period modified to 12 hours closely approximate “typical” tidal conditions
- That local tributary inflows do not affect tidal dispersion.
- That the average dispersion over a spring-neap tidal cycle is similar to the dispersion for average tidal amplitude.

Substantial uncertainty is also associated with the analysis technique. Sources of uncertainty include:

- The model cross-sections are not perfectly aligned normal to tidal flows.
- Precise tidally-averaged steady state conditions are approached asymptotically. Though advective and dispersive fluxes typically balance to within a 2% difference, precise tidally-averaged steady state conditions are not achieved.
- The salinity gradient is estimated based on centerline (“thalweg”) salinity, not cross-sectionally averaged salinity.
- Similarly, the depth value used to calculate horizontal Richardson number is the channel invert (“thalweg”) elevation and the friction velocity is also estimated at this location. Most previous uses of horizontal Richardson number assumed uniform depth.
- The depth and friction velocity in the Richardson number estimate are from a single point longitudinally while gravitational circulation requires a substantial distance to develop. Longitudinal variability in bathymetry is expected to be a primary reason for differences in the curve fit between different cross-sections.

Additional uncertainty is related to the use of the dispersion coefficient information in the WAM. One source of uncertainty is the limited number of sections provided by the dispersion analysis. Using this information in the WAM requires some spatial interpolation and extrapolation of dispersion coefficients. Most notably dispersion coefficients were not determined landward of the western Delta. In additional

simulations, dispersion coefficients could be estimated further into the Delta by considering very low Net Delta Outflow conditions.

Overall the WAM predicts salinity accurately for historic conditions suggesting that the parameterization approach is adequately accurate despite a large number of approximations and other sources of uncertainty. However, the uncertainty associated with DRMS scenarios is larger than the uncertainty/error in simulations of historic conditions because the approach here only captures a portion of the variability of transport processes with different conditions. With additional refinements of the hydrodynamic model and analysis method, it should be possible to improve the parameterization of dispersive mixing for future applications.

H3.8 Discussion

This report documents three-dimensional simulations of hydrodynamics and salinity for several sea level rise scenarios. These simulations supplement the large number of simulations performed with the WAM. The specific goals of the three-dimensional simulations are to:

- Estimate salinity for idealized sea level rise scenarios
- Quantify the strength of salt intrusion processes for different sea level rise scenarios
- Quantify the relative contribution of "three-dimensional transport processes," including gravitational circulation, to salt intrusion
- Account for sea level rise in the parameterization of dispersive transport for the WAM
- Inform uncertainty analysis of the WAM

The goals of the sea level rise scenario simulations were achieved, as is documented in this report. The only goal not explicitly addressed here is the uncertainty analysis of the WAM which will be discussed in a separate DRMS report.

Salinity was estimated for a total of 7 scenarios. The first five scenarios consist of a baseline scenario of no sea level rise and MSL increases of 20 cm, 50 cm, 90 cm and 140 cm. The next two scenarios also assume MSL rise of 140 cm and consider cumulative effects of MSL rise combined with additional changes. The Perforated Sherman Island scenario assumes 20 breach locations in Sherman Island. The Amplified Tides scenario assumes that tides are amplified by 11 percent relative to existing tides.

Idealized forcing was used in these scenarios, including repeating tides, consisting of an M2 constituent and a K1 constituent, a constant Net Delta Outflow of 260 m^3/s (9,182 cfs), and no salinity sources other than the coastal ocean boundary. This idealized forcing, used to simplify the analysis of dispersive transport, also limits the range of salinity conditions simulated by the model. The actual effects of sea level rise on salinity will vary with Delta outflow and during the spring-neap cycle.

The sea level rise scenario simulations indicate increasing Delta salinity with sea level rise. The 0.5 psu salinity contour is clearly indicated in the salinity maps and salinity profile figures because water at this salinity does not meet relevant municipal, industrial

and agricultural standards. The predicted tidally-averaged and depth-averaged salinity for the140 cm MSL Rise scenario exceeds 0.5 psu in a portion of the western Delta and the daily maximum salinity exceeds 0.5 psu in all 3 western Delta stations at which temporal variability was examined. If local sources of salt (e.g., agricultural drainage) were added to the simulation, the predicted salinity would increase further.

The cumulative effects scenario simulation results indicate increased Delta salinity with tidal amplification and greatly increased Delta salinity as a result of tidal exchange with Sherman Island. These predicted increases are consistent with the understanding that mixing in Franks Tract causes substantial mixing of salt into the central Delta (RMA 2005). Because Sherman Island is both much larger than Franks Tract and closer to the large salinity gradients present in Suisun Bay during summer conditions, the effects of Sherman Island on salt intrusion should be much larger than those of Franks Tract. The simulation results suggest that the combination of substantial sea level rise and a small degree of Delta island flooding could lead to large impacts on Delta water quality and water supply reliability.

The fixed Net Delta Outflow of 260 m^3/s (9,182 cfs) used in all simulations corresponds to typical summer flows. Larger salt intrusion would occur during summer and fall conditions during a dry or critical year. In addition, all sea level rise scenarios considered here are likely to greatly underestimate channel deepening that will occur as a cumulative effect of MSL rise, ongoing erosion, dredging activities, and scour from island flooding and restoration projects in the next century. Furthermore, substantial sea level rise would likely be accompanied by large scale island flooding and additional inundation both inside and outside of the Delta. Because the scenarios presented here consider only a portion of the direct and indirect effects sea level rise and do not address cumulative effects of many other expected changes to the estuary, they should be interpreted as a lower bound estimate of the potential effects of sea level rise. Future salt intrusion is likely to be much larger, primarily due to more frequent and severe flooding of Delta islands.

The analysis of dispersive transport quantified the expected strength of salt intrusion under a range of MSL rise. This analysis supplements the previous analysis of variability of dispersive transport with Net Delta Outflow described in the DRMS report "Parameterization of Mixing using a Three-Dimensional Hydrodynamic Model." The strength of predicted salt intrusion processes are represented by dispersion coefficients. The calculated dispersion coefficients are nearly constant with MSL in Central Bay and most of San Pablo Bay, increase slightly to moderately with MSL in Carquinez Strait and western Suisun Bay, and increase substantially with MSL in the eastern portion of Suisun Bay and in the western Delta. Three-dimensional processes are found to be significant throughout the estuary and dominant in some regions. The importance of three-dimensional processes increases with sea level rise in most of the Estuary, with large increases in the western Delta. The parameterization of dispersive transport could be improved in several ways that are discussed in Section 7.7. Most notably, dispersion coefficients could be estimated further into the Delta by considering very low Net Delta Outflow conditions in UnTRIM model simulations.

Several additional scenarios could better quantify the potential effects of sea level rise. The cumulative effects considered here were limited to a single flooded island and amplified tides. The WAM will consider many combinations of flooded islands and other changes to the estuary, but substantial uncertainty will be associated with these predictions. Several more flooded island scenarios should be simulated for a range of sea level rise with well calibrated two-dimensional and three-dimensional models in order to assess the uncertainty associated with the WAM and estimate economic costs associated with salt intrusion. In future applications, the two-dimensional and three-dimensional models should be coupled with a water management model, similar to the approach used to integrate a water management model into the WAM to account for reservoir operations, exports and other operations associated with management of the Delta. The cumulative effects of changes to hydrology from climate change, geomorphic change in the estuary, inundation of coastal areas from sea level rise and anticipated wetland restoration projects should be considered. Two-dimensional and three-dimensional scenario simulations that combine these and other expected changes should be performed for a range of MSL rise to estimate cumulative effects.

H3.9 Acknowledgements

We wish to thank the Department of Water Resources for funding this work, John DeGeorge and Richard Rachiele of RMA for general collaboration on the DRMS project, and Professor Mark Stacey for technical guidance.

H3.10 References

Burau, J.R., Gartner, J.W., and Stacey, M., 1998. Results for the hydrodynamic element of the 1994 Entrapment Zone Study in Suisun Bay. In Report of the 1994 Entrapment Zone Study, edited by Wim Kimmerer, 13-53. Interagency Ecological Program for the San Francisco Bay/Delta Estuary.

Casulli, V., 1999. A semi-implicit numerical method for non-hydrostatic free-surface flows on unstructured grid, in Numerical Modelling of Hydrodynamic Systems, ESF Workshop, pp. 175-193, Zaragoza, Spain.

Casulli, V. and R.A. Walters, 2000. An unstructured, three-dimensional model based on the shallow water equations, *International Journal for Numerical Methods in Fluids*, 32, 331-348.

Casulli, V. and Zanolli, P., 2002. Semi-Implicit Numerical Modelling of Non-Hydrostatic Free-Surface Flows for Environmental Problems, *Mathematical and Computer Modelling*, 36, 1,131-1,149.

Casulli, V. and Zanolli, P., 2005. High Resolution Methods for Multidimensional Advection- Diffusion Problems in Free-Surface Hydrodynamics, *Ocean Modelling*, 2005, 10, p.137-151.

Celebioglu, K., and Piasecki, M., 2006. Comparison of turbulence models with use of UnTRIM in the Delaware Bay, Proceedings of the Estuarine and Coastal Modeling Conference, ASCE, 2006.

Fischer, H.B., List, E.J., Koh, R.C.Y., Imberger, J., and Brooks, N.H., 1979. *Mixing in Inland and Coastal Waters*. New York: Academic Press

Hansen, D.V., and Rattray, M., 1965. Gravitational circulation in straits and estuaries, *Journal of Marine Research*, 23, 104-122.

Jassby, A. D., W. J. Kimmerer, S. G. Monismith, C. Armor, J. E. Cloern, T. M. Powell, J. R. Schubel, and T. J. Vendlinski, 1995. Isohaline position as a habitat indicator for estuarine populations, *Ecological Applications*, 5:272-289.

MacWilliams, M. L., E. S. Gross, and W. Kimmerer, 2005. Simulating salt intrusion into Suisun Bay and the Western Delta, http://www.rivermodeling.com/References/SaltIntrusionPoster.pdf, State of the Estuary Conference.

Monismith, S.G., Kimmerer, W., Burau, J.B., and Stacey, M.T., 2002. Structure and flow-induced variability of the subtidal salinity field in Northern San Francisco Bay, *Journal of Physical Oceanography*, 32, 3,003-3,019.

[RMA] Resource Management Associates, 2005. Flooded Islands Pre-Feasibility Study: Alternatives Modeling Report, prepared for CA Department of Water Resources for submittal to California Bay-Delta Authority, June 30.

Stacey, M.T., Burau, J.R, and Monismith, S.G., 2001. The creation of residual flows in a partially stratified estuary, *Journal of Geophysical Research*, 106(C8), 17,013-17,038.

Appendix I
Organic Carbon

Table of Contents

Executive Summary **I-1**
I.1 Introduction **I-1**
I.2 Purpose **I-2**
I.3 Approach **I-2**
I.4 Organic Carbon Models **I-3**
I.4.1 Island Production I-3
Quick Release I-3
Bacterial Mediated Long-term Production I-4
I.4.2 Scaling Factors I-5
Island Location / Distance from Southern Delta Pumps I-5
Island Production vs. Intake Water I-7
I.4.3 Assumptions I-7
I.5 Results **I-9**
I.6 Costs **I-23**
I.7 Conclusions **I-24**
I.8 References **I-25**

Tables

Table I-1 Seasonal Flux Rates (Year One), DWR Seasonal Flux Model
Table I-2 Estimated Costs Associated with Case 1 Through 6

Figures

Figure I-1 Yield factors for Central Delta islands due to net flow direction during exports/distance from Clifton Court Forebay.
Figure I-2 Case 1: One levee breach on Brannan-Andrus Island
Figure I-3 Case 2A: Three islands with one breach each (late spring event)
Figure I-4 Case 2B: Three islands with one breach each (summer event)
Figure I-5 Case 2C: Three islands with one breach each (early fall event)
Figure I-6 Case 3A: Three islands with one breach each, additional islands damaged but not flooded (late spring event)
Figure I-7 Case 3B: Three islands with one breach each, additional islands damaged but not flooded (summer event)

Figure I-8 Case 3C: Three islands with one breach each, additional islands damaged but not flooded (early fall event)

Figure I-9 Case 4A: Eleven levee breaches among ten Delta islands (late spring event)

Figure I-10 Case 4B: Eleven levee breaches among ten Delta islands (summer event)

Figure I-11 Case 4C: Eleven levee breaches among ten Delta islands (early fall event)

Figure I-12 Case 5A: Thirty-six levee breaches among twenty Delta Islands (late spring event)

Figure I-13 Case 5B: Thirty-six levee breaches among twenty Delta islands (summer event)

Figure I-14 Case 5C: Thirty-six levee breaches among twenty Delta islands (early fall event)

Figure I-15 Case 6A: Forty-six levee breaches among thirty Delta islands (late spring event)

Figure I-16 Case 6B: Forty-six levee breaches among thirty Delta islands (summer event)

Figure I-17 Case 6C: Forty-six levee breaches among thirty Delta islands (early fall event)

Acronyms and Abbreviations

BAU	Business as Usual
CalSim	California Water System Simulation Model (DWR & USBR)
cfs	cubic feet per second
CO_2	Carbon Dioxide
CVP	Federal Central Valley Project
DOC	dissolved organic carbon
DRMS	Delta Risk Management Strategy
DWR	California Department of Water Resources
dss	Data storage system
EC	Electrical Conductivity
HD	The WAM Hydrodynamic / Water Quality Submodel
ITF	Initial Technical Framework
JBA	Jack R. Benjamin & Associates, the DRMS risk analysis consultant
MWH	MegaWatt Hours
NDAL	Net Delta Area Losses (or Net Delta Consumptive Water Use)
OC	organic carbon
RMA	Resource Management Associates, the DRMS hydrodynamics consultant
SWP	State Water Project
SWRCB	State Water Resources Control Board
TAF	Thousand Acre-Feet
TM	Technical Memorandum
TOC	total organic carbon
µmhos/cm	Micro mhos per centimeter – Electrical Conductivity, a measure of salinity
URS	URS Corporation, the DRMS prime consultant
USBR	United States Bureau of Reclamation
WAM	Water Analysis Module or Model
WY	Water Year

Executive Summary

A preliminary analysis of total organic carbon (TOC) increases was conducted for six specific Delta levee breach scenarios. These scenarios also include variations in water year type and seasonality. The mass of TOC produced from the flooded peat islands as well as the increases in TOC concentrations at Clifton Court Forebay were modeled for the time period when salinity was restored enough to allow water exports to resume. Particle tracking hydrodynamic modeling was not used in the analysis.

Two critical drinking water quality thresholds were determined for TOC: the point at which additional treatment costs would be incurred, and the point at which current operations for organic carbon (OC) treatment (enhanced coagulation) was no longer effective.

The island inundation scenarios evaluated range from one breach on one island to forty-six breaches among thirty islands. The schedule to reclaim the islands ranges from 1.6 to 6.6 years. Enhanced coagulation is needed for 100 to 560 days with an estimated cost that ranging from $12 to 68 million. Water exports are interrupted due to salinity intrusion for 1 to 23 months. Additional decisions regarding water exports, prospective implementation of more advanced treatment, and/or potential interruptions of deliveries due to TOC range from 0 to 30 months. The problematic cases, based on this preliminary analysis, occur in major levee break events, with more than ten flooded islands. The problems take the form of periodic major spikes of TOC in exports that may last for three to nine months.

Drinking water can be reliably treated with enhanced coagulation in the 1 and 3 flooded islands scenarios evaluated, and in one of the 10 flooded islands scenarios. More substantial problems occur in the 20 and 30 flooded island scenarios. With sustained TOC concentrations greater then 6 mg/L, the Delta water may not be usable for municipal and industrial purposes however it may be suitable for agriculture. Decisions must then be made regarding water exports that impact potability in downstream reservoirs, storage, and drinking water treatment facilities.

More detailed modeling and an evaluation of dewatering locations and rates can be used to refine the predicted magnitude and duration of TOC spikes. However, additional treatment options may also be needed to address periods when TOC concentrations are above 6 mg/L. Thus, more detailed modeling and management of island dewatering to lessen TOC concentrations is recommended. Development of contingency plans for more advanced treatment is also recommended.

I.1 Introduction

Water exported from the Sacramento-San Joaquin river delta (Delta) is an important drinking water source for more then 20 million people in California. Dissolved organic carbon (DOC) is a disinfection byproduct precursor for chlorinated drinking water. It is estimated that 20 to 50 percent of Delta water trihalomethane precursors originate from drainage water from Delta islands peat soil (Fujii et al. 1998).

The high organic matter content of peat is associated with high DOC concentrations in the soil pore water. DOC production within peat soil and sediment is a result of microbial activities that break down complex organic compounds in decaying plant matter to simpler compounds. These low molecular weight compounds then undergo a series of condensation reactions to recombine into higher molecular weight compounds such as fulvic acids and humic substances which make up DOC (Thibodeaux and Aguilar 2005). When inundated, the DOC will move from the bed layer into the overlaying water.

The organic matter fraction of peat soils in the central Delta is particularly high. Jersey Island, Orwood Tract, Sherman Island, and Twitchell Island have soil organic matter fractions that range from 18 to 37 percent (Aguilar and Thibodeaux 2005). Muck, which primarily consists of decomposed peat, is the predominant soil type in the central Delta (Delta Protection Commission 2002).

Delta water exporters are concerned about the potential impact of organic carbon on drinking water intakes due to flooded peat islands.

I.2 Purpose

The purpose of this memorandum is to address the concerns raised by drinking water exporters regarding total organic carbon increases and the resulting water quality treatment cost increases that would occur from Delta island flooding in the event of multiple island/multiple levee breaches.

I.3 Approach

The Department of Water Resources (DWR) conducted measurements and modeling of organic carbon releases as part of the 2004 Jones Tract levee failure and response. We have adapted the organic carbon model created by the DWR to predict the mass of organic carbon produced and released for the six levee failure cases described in the Phase 1 DRMS report. This includes both a quick release fraction and sustained production due to microbial mediated production.

The Jones Tract report also presents a fingerprint for DOC at Clifton Court Forebay during dewatering at Upper and Lower Jones Tract. This fingerprint was based on output from the DWR Delta Simulation Model (DSM2). The mass of DOC in the fingerprint that is attributed to Jones Tract was calculated and compared to the mass of DOC released during dewatering. This comparison was used to create a global scaling factor that accounts for the difference between the amount of organic carbon produced and the amount of organic carbon that reaches Clifton Court Forebay. Scaling factors were then assigned to each of the islands based upon this factor as well as island location/net flow direction during exports.

The water treatments costs associated with organic carbon removal, as provided by Delta exporters, was then used to develop an order of magnitude cost estimate for the increase in water treatment costs due to the increases in organic carbon at the southern Delta drinking water intakes for each of the six cases.

I.4 Organic Carbon Models

I.4.1 Island Production

Several factors can influence the release of organic carbon from island peat soil due to island inundation. The quick release fraction of DOC comes from a finite amount of readily available material. This fraction becomes suspended on the time scale of hours to days. When a Delta levee is breached, the water that fills the island is turbulent and has high velocity flows. Particle suspension occurs during filling. Shear forces may release colloids that were previously attached to soil surfaces. The inundation also gives rise to flows within the pore spaces of the soil. This may cause colloids to become detached from soil particles within the bed and will also cause unassociated organic carbon material to enter the overlaying water.

Another portion of the DOC is generated by microbial processes in the peat sediment and is produced nearly continuously and is subsequently released from the bed. This long-term fraction can be generated on the time scale of years to decades. The release rate is dependent on the organic fraction in the soil and on temperature/seasonal variations. As time increases the percent organic carbon in the bed soil slowly decreases, as does the release rate (Aguilar and Thibodeaux 2005). The DOC is transported from sediment pore water to the overlying water through molecular diffusion or advection.

The conversion between DOC and TOC is necessary for calculations. Operationally DOC is defined as non-settleable organic matter in the <0.45 μm size range (Aguilar and Thibodeaux 2005). TOC includes both particulate organic carbon and DOC. In the flooded peat soils at Jones Tract, DOC comprised an average of 85 percent of the TOC (DuVall et al. 2005); this conversion factor was assumed for all Delta islands.

Quick Release

DuVall et al. (2005) estimated the initial release DOC concentration at Jones Tract by multivariate regression analysis. Upper Jones had a quick release concentration (as determined by wet oxidation analysis) of 2.22 mg/L, and Lower Jones had a quick release concentration of 5.78 mg/L. Assuming that Jones Tract had an average depth of 3.7 meters, the initial release is 8.2 g/m^2 of DOC for Upper Jones and 21.4 g/m^2 of DOC for Lower Jones.

Thibodeaux and Aguilar (2005) developed a model that predicts both the quick release fraction and the bacterial mediated long-term release fraction for DOC. For a hypothetical enclosed reservoir, with a depth of 3 meters, a peat bed consisting of 15% organic carbon, and inundation flows which disturb 10 cm of soil and release the associated pore water DOC content, the initial average DOC concentration in the reservoir is 3.53 mg/L with a reported range of uncertainty between 2.65 and 4.39 mg/L. This is equivalent to an initial release of 10.6 g/m^2 of DOC, with a range of 8 to 13.2 g/m^2 of DOC.

It is interesting to note some of the experimental differences behind these quick release estimates. The Jones Tract estimates represent actual field data from a dynamic system. Upper Jones was an open system that was in contact with fresher river water through the

unrepaired levee for three weeks. During this time there was potential DOC loss into the channels and dilution by the channel water at the sampling location. Lower Jones was connected to Upper Jones via a passage under a railroad trestle, opposite to and nearly five miles away from the levee breach. Any DOC loss or dilution was by water from Upper Jones and not directly by channel water. The quick release estimate for Lower Jones would be less confounded by freshwater dilution and DOC lost from the system.

The Thibodeaux and Aguilar model was calibrated by laboratory scale experimentation. They simulated the organic carbon flux from bed sediment pore water for three peat soils with different percent organic matter. As part of the experimental design, soil samples were homogenized and sieved prior to subsampling, and water was placed on sediment so as to avoid particle suspension in the jar reactors. The sample preparation for the experiment potentially contributed to an increase in the amount of readily available organic carbon in the pore water; the experimental design potentially decreased the amount of organic carbon flux due to colloid detachment from suspended sediments. The Thibodeaux and Aguilar model quick release estimate does not fully account for field conditions which occur during Delta island inundation.

The quick release estimate for Lower Jones derived from the multivariate regression analysis was chosen to determine the quick release fraction for the six levee failure cases. Section I.4.3 contains the quick release organic carbon production (by mass in kg) for each of the islands in each three DRMS scenarios.

Bacterial Mediated Long-term Production

DuVall et al. (2005) developed a monthly average organic carbon flux rate in their seasonal flux model. This rate varies between 0 and 0.5 g/m^2-d of TOC depending on time of year. A monthly flux rate from this model and a monthly time step was used to determine the organic carbon areal flux for each of the islands in the DRMS scenarios. The monthly flux rates used in the calculations for the DRMS scenarios are as follows.

Table I-1 Seasonal Flux Rates (Year One), DWR Seasonal Flux Model

Month	Flux rate for TOC (g/m^2-d)	Month	Flux rate for TOC (g/m^2-d)
January	0	July	0.5
February	0.04	August	0.47
March	0.13	September	0.38
April	0.25	October	0.25
May	0.38	November	0.13
June	0.47	December	0.04

Experimental data and other model values have similar flux rates as the seasonal flux model. The time dependent portion of the by multivariate regression analysis for DOC at Jones Tract is 0.118 mg/L-d (DuVall et al. 2005), which is calculated from field scale data acquired from Jones Tract. Assuming that Jones Tract had an average depth of 3.7

meters, the equivalent long-term release flux rate is 0.44 g/m^2-d of DOC or 0.51 g/m^2-d of TOC, when DOC is assumed to account for 85% of the TOC. A multi-year mesocosm experiment, performed by the DWR, had tanks with flooded peat soil that yielded a TOC flux rate of 0.41 to 0.45 g/m^2-d in warmer months and 0.12 to 0.15 g/m^2-d in cooler months (DuVall et al. 2005). The model developed and presented by Thibodeaux and Aguilar (2005) predicts the microbial produced DOC concentration from a hypothetical reservoir, which has a depth of 3 meters and a peat bed consisting of 15% organic carbon, to be 0.241 mg/L-d. This is equivalent to an areal flux rate of 0.72 g/m^2-d of DOC or 0.85 g/m^2-d of TOC.

The carbon flux model developed by the DWR in DuVall et al. 2005 was chosen for the long-term release of organic carbon. This model is consistent with field scale measurements and accounts for season variation, but does not account for variation in peat bed percent organic carbon.

I.4.2 Scaling Factors

Scaling factors were applied to each of the Delta islands to account for the difference between the amount of organic carbon that was produced on each island and the amount of organic carbon from that island that is expected to reach south Delta drinking water intakes. These scaling factors are based upon the assumed net flow direction during exports and a global scaling factor that accounts for additional loss.

Island Location / Distance from Southern Delta Pumps

Yield factors were applied to each island based on net flow direction during water exports and the distance from southern Delta drinking water intakes. Each island is assigned a zero percent, fifty percent, or one hundred percent yield factor. Figure I-1 shows the location of central Delta islands and the assigned yield factors.

It is assumed that all of the organic carbon that is produced on Sherman Island would be swept into the bay, and away from the southern Delta drinking water intakes by the Sacramento River. Jersey Island, Bradford Island, Twitchell Island, Brannon-Andrus Island, and Grand Island were assigned a 50 percent scaling factor to account for the influence of both water exports and the Sacramento River on net flow direction. Bethel Island, Webb Tract, Staten Island, Bouldin Island, Venice Island, Empire Tract, Medford Island, Mandeville Island, Quimby Island, Holland Island, Hotchkiss Tract, Veale Tract, Palm Tract, Bacon Island, McDonald Tract, Rindge Tract, Upper and Lower Jones Tract, Woodward Island, Orwood Tract, Victoria Island, Byron Tract, Middle Roberts Island, Union Island, and Fabian Tract are assumed to be close enough to Clifton Court Forebay to have pumping activities dominate the net flow direction of the surrounding channels.

0%
Sherman

50%
Brannon-Andrus Island
Twitchell Island
Bradford Island
Jersey Island

100%
Webb Tract
Bethel Island
Holland Tract
Quimby Island
Mandeville Island
McDonald Tract
Venice Island
Bouldin Island
Bacon Island
Palm Tract
Upper and Lower Jones Tract
Orwood Tract
Woodward Island
Byron Tract
Victoria Island

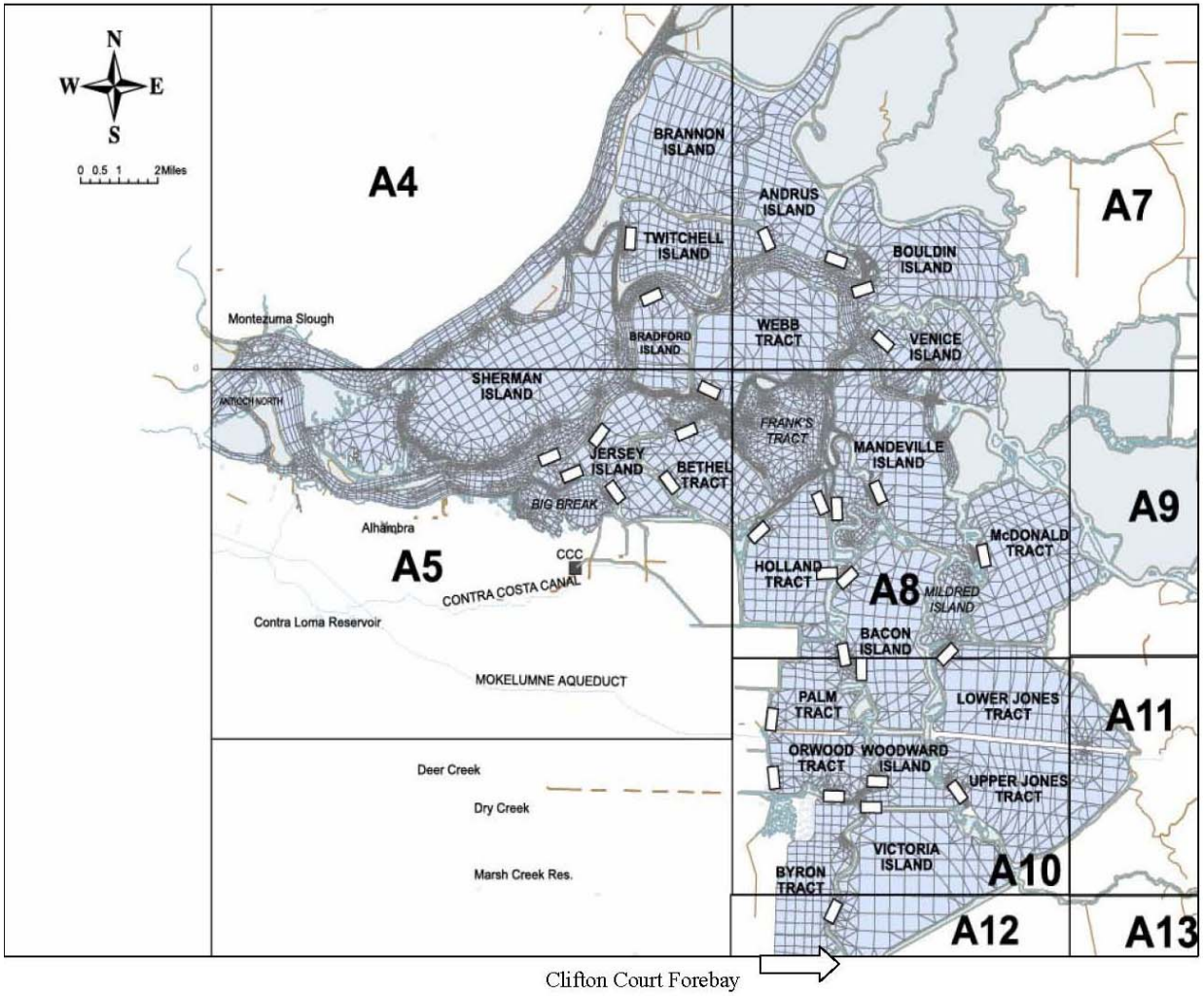

Figure I-1 Yield factors for Central Delta islands due to net flow direction during exports/distance from Clifton Court Forebay.

Island Production vs. Intake Water

A global scaling factor of 50 percent was applied at each island regardless of location to account for the difference between the amount of organic carbon produced at Jones Tract and the amount of Jones Tract organic carbon found at the Banks Pumping Plant drinking water intakes.

DuVall et al. (2005) presents the DSM2 modeled fingerprint for DOC at Clifton Court Forebay, developed by the Bay Delta Office, during dewatering at Jones Tract. In this model, the sources that contribute DOC include the Sacramento River, the San Joaquin River, the east side tributaries, the Delta, and Jones Tract. Jones Tract contributed approximately 1.5 mg/L of DOC to Clifton Court Forebay in the last two months of the island pump-out. During this time the water intake volume ranged from 2,968 to 14,237 acre-feet per day (USBR 2005).

The DSM2 fingerprint indicates approximately a week delay between completion of the island pumping at Lower Jones Tract and the last of the Jones tract DOC to arrive at Clifton Court Forebay. This indicates a travel time on the order of days to weeks for organic carbon from Jones Tract pump-out water to travel to Clifton Court Forebay.

From 10/25/04 to 12/20/04, Jones Tract contributed approximately 1.7 million kilograms of organic carbon to its adjacent channel through water pump-out in the final stage of repairs. This estimate is based upon information provided in DuVall et al. (2005), which includes the DOC linear regression equations, the average Jones Tract island depth that was used in DSM2 model, and the area of Upper and Lower Jones.

Approximately 0.9 million kilograms of organic carbon originating from Jones Tract arrived at the drinking water intakes at Clifton Court Forebay from 10/31/04 to 12/26/04. This estimate was calculated using information contained in the DSM2 fingerprint and from published intake volumes at Clifton Court Forebay.

The 50 percent scaling factor accounts for the difference between these calculations. The loss could be due to uptake, settling and burial, other water exports, tidal outflow to the Bay, and unknown processes.

I.4.3 Assumptions

The assumptions used in the models, the scaling factors, and in the calculations that predict the amount of TOC that potentially impacts drinking water treatments costs are discussed below.

Information from the Jones Tract levee failure and response was generalized to create the organic carbon quick release and long term flux calculations. There is an implicit assumption that the general flooded island scenario will have conditions similar to Jones Tract. In the flooded peat soils at Jones Tract, DOC contributed an average of 85 percent of the TOC; this conversion factor was assumed for all Delta islands. The quick release production seen at Upper Jones (21.4 g/m^2 of DOC) was the assumed areal production for all islands; this is potentially a lower end estimate because it does not account for possible dilution at Upper Jones. The long term TOC flux rates from the DWR seasonal

flux model was the assumed production rate for all islands. These flux rates were calibrated with Jones Tract data but not experimentally derived.

Organic carbon production and transport can vary by island. The organic carbon flux rate would be influenced by the percent organic matter content in peat soil, which varies among islands and decays over time. Management decisions such as above Delta releases, i.e. reservoir releases north of the Delta, would influence the transport of organic carbon to southern Delta intakes. Additional factors that may be important include hydraulic exchange, organic carbon content of the channel water, and dispersion of organic carbon prior to levee repair.

Hydrodynamic modeling was not used for the transport of organic carbon from the islands to the Banks pumping plant. Instead, scaling factors were used based on general categorizations, which might not reflect actual flow dynamics.

The contribution of island TOC mass to southern Delta intakes was calculated after exports had resumed. These calculations account for the amount of mass predicted in the pump-out water and dewatering schedule and duration. Half of the island produced TOC was assumed to be transported from the island into the adjacent channels through open levees. This was modeled to occur until the breach repair was complete. For islands that had unrepaired levees during water exports, the TOC released from the open island contributed to the TOC loading at Clifton Court Forebay. The amount of TOC in the pump-out water was assumed to equal half of the initial “quick release” and long term TOC flux produced by that island prior to the completion of levee repair and all of the long term production thereafter.

The increase in TOC concentration at the southern Delta intakes due to flooded islands and dewatering repairs was also calculated. To model these increases the organic carbon contribution from Jones Tract was scaled. Jones Tract pump-out water was estimated to contribute 1.8 mg/L and approximately 15,000 kg/d of TOC to Clifton Court Forebay. (An increase of 1.5 mg/L of DOC was associated with Jones Tract pump-out water as seen in the DSM2 fingerprint for Clifton Court Forebay from 10/31/04 to 12/20/04, and it is assumed that DOC contributed an average of 85 percent of the TOC.)

There are several assumptions implicit in the scaling of Jones Tract organic carbon concentrations and the distribution of organic carbon loads over the pump-out stage. Assumptions include the following.

- The TOC released while the water exports are interrupted does not contribute to the organic carbon loading at Clifton Court Forebay after the exports have resumed. This assumes that the processes that pushed back the salinity also pushed back the organic carbon. (For example, this could occur when the Delta is flushed prior to resuming exports.)
- There are similar amounts of dispersion and dilution of organic carbon in the modeled breach scenarios as seen by Jones 2004. This implies a similar amount of above Delta releases during the pump-out phase.
- The mass of organic carbon produced prior to the start of dewatering is evenly distributed over the pump-out duration. This would imply a constant pump-out rate.
- Organic carbon impacts from multiple islands are additive.

I.5 Results

The CALFED Water Quality Program Record of Decision water quality goal for Clifton Court Forebay and other southern and central Delta drinking water intakes is 3.0 mg/L TOC (Brown and Caldwell 2005). Background concentrations of TOC and DOC in the Delta are typically between 3-4 mg/L, but are often higher during winter storm events (DWR 2007).

The Metropolitan Water District of Southern California provided a cost associated with the treatment of Delta water for organic carbon concentrations up to 6 mg/L of TOC. (Delta water is treated by Metropolitan to ensure a total organic carbon concentration of less then 4 mg/L.) A cost increase of $18 per acre-foot is associated with enhanced coagulation (operations and maintenance costs, not capital investments). At a high enough concentration over a prolonged period of time, additional capital investment would be required to reliably treat the water. For example, a combined background and additional island TOC concentration that is greater then 6 mg/L for a duration greater than one month would not be reliably treated by enhanced coagulation.

If elevated TOC concentrations are sustained (greater the 6 mg/L for more than one month), the Delta water could be considered non-potable. (Short duration spikes of TOC are diluted during transport and storage of the State Water Project water.) Water exports could then be used for agricultural use but not for urban drinking water use, resulting in loss of drinking water supply during portions of the island dewatering.

The additional TOC concentrations due to the flooded peat islands were estimated at Clifton Court Forebay and modeled for Cases 1 through 6. Cases 1 through 6 are described in the Delta Risk Management Strategy (DRMS) Phase 1 draft Risk Analysis Report (URS/JBA 2007). Input was acquired from the Emergency Response and Repair model and the Water Analysis Module. Water export interruption durations were determined based on salinity.

Cases 2A, 3A, 4A, 5A, and 6A represent a late spring event with a levee failure date of June 1, 1927. Cases 2B, 3B, 4B, 5B, and 6B represent a summer event with a levee failure date of August 1, 1972. Cases 2C, 3C, 4C, 5C, and 6C represent an early fall event with a levee failure date of October 1, 1930. Case 1 had an indeterminate start date; it was modeled with a June 1, 1927 levee failure date.

Two critical thresholds are determined for the model -- the level for which water treatment for TOC is necessary and the level for which water treatment by enhanced coagulation is no longer effective for TOC. In the model, the background TOC concentration for the Delta was assumed to be 3 mg/L. (A variable background concentration was not modeled.) Therefore an addition of 1 mg/L TOC would increase water treatment costs and a sustained increase of more then 3 mg/L TOC would not be able to be reliably treated by enhanced coagulation.

Cases 1 through 6 had minor to severe impacts due to increases in TOC concentrations at Clifton Court Forebay. Figures I-2 to I-17 illustrate the additional TOC concentrations expected at Clifton Court Forebay in Cases 1 through 6.

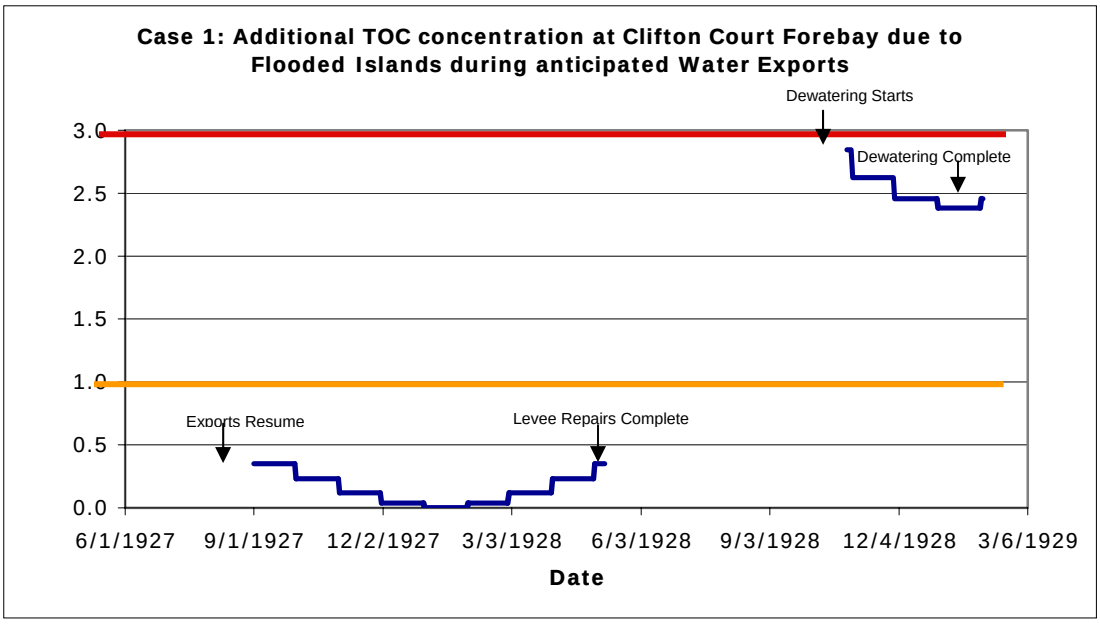

Figure I-2 Case 1: One levee breach on Brannan-Andrus Island

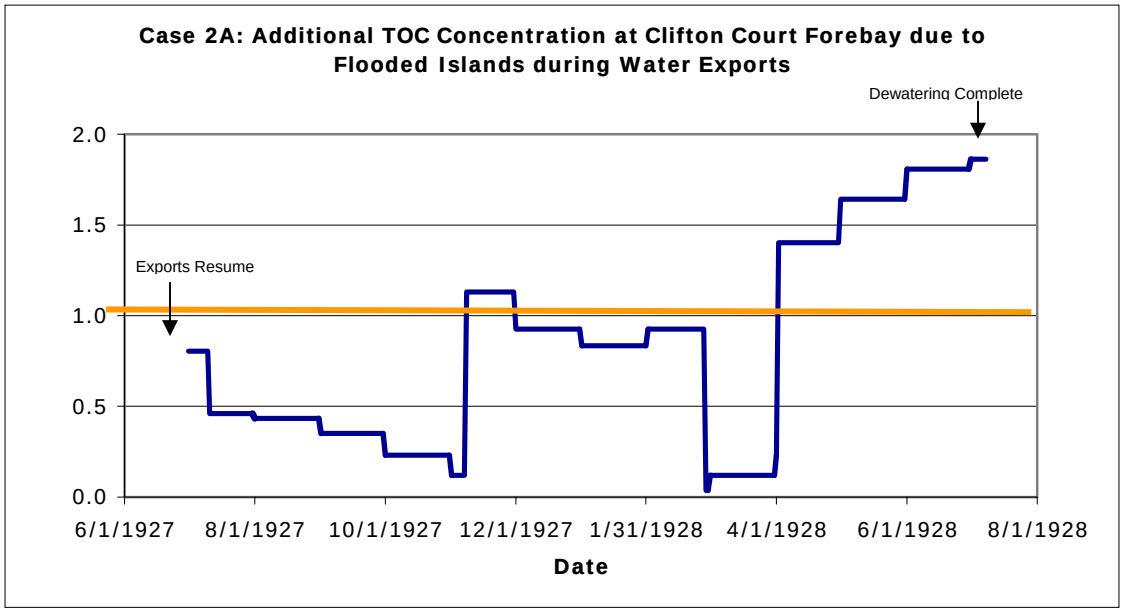

Figure I-3 Case 2A: Three islands with one breach each (late spring event)

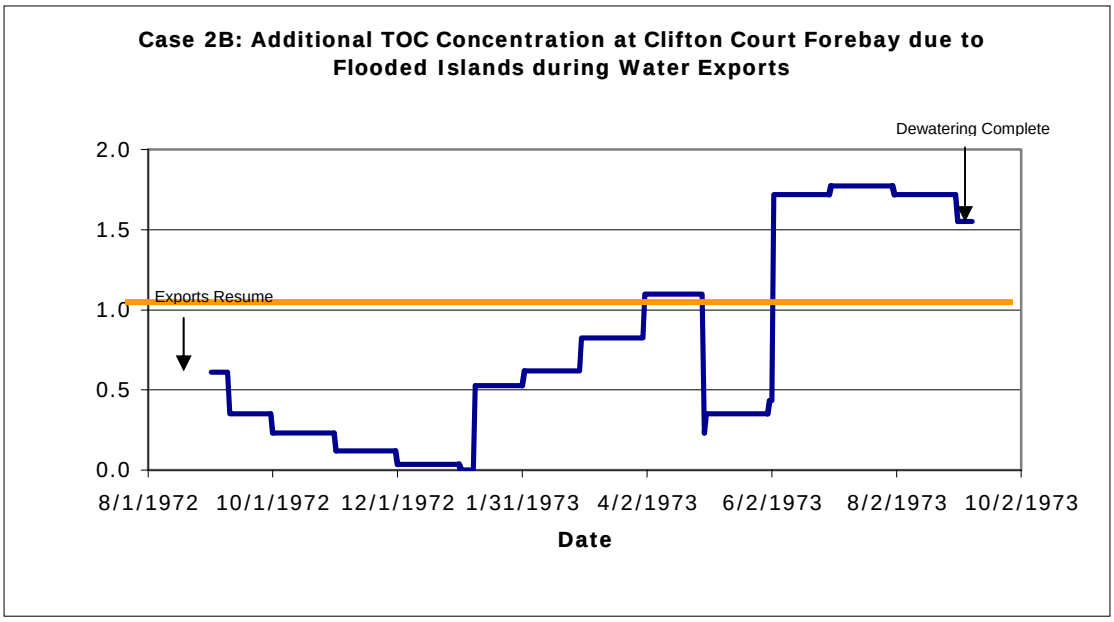

Figure I-4 Case 2B: Three islands with one breach each (summer event)

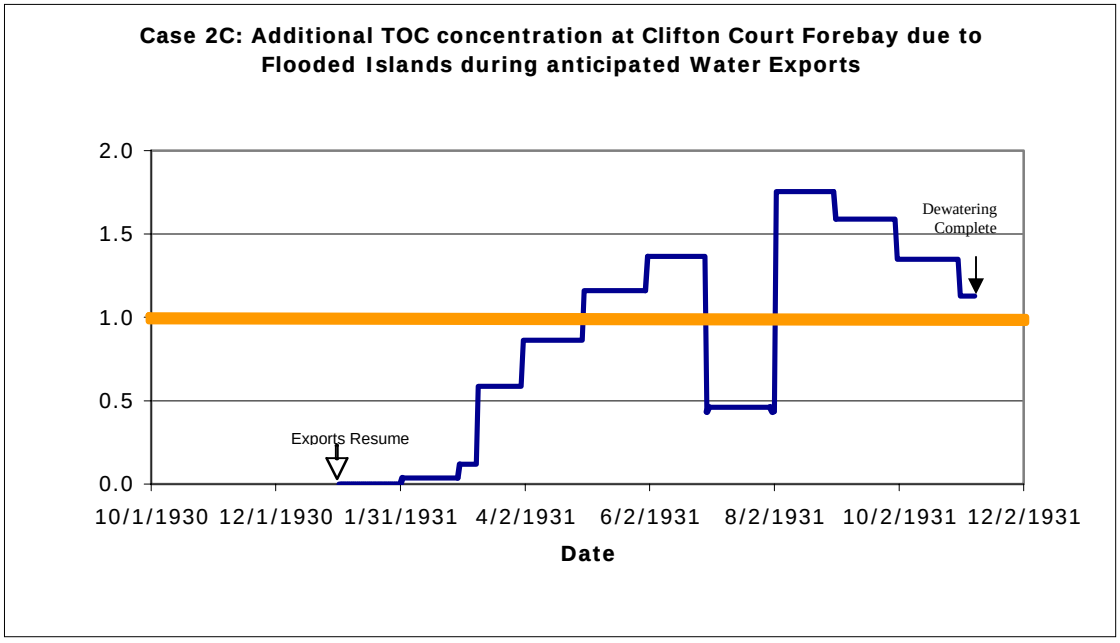

Figure I-5 Case 2C: Three islands with one breach each (early fall event)

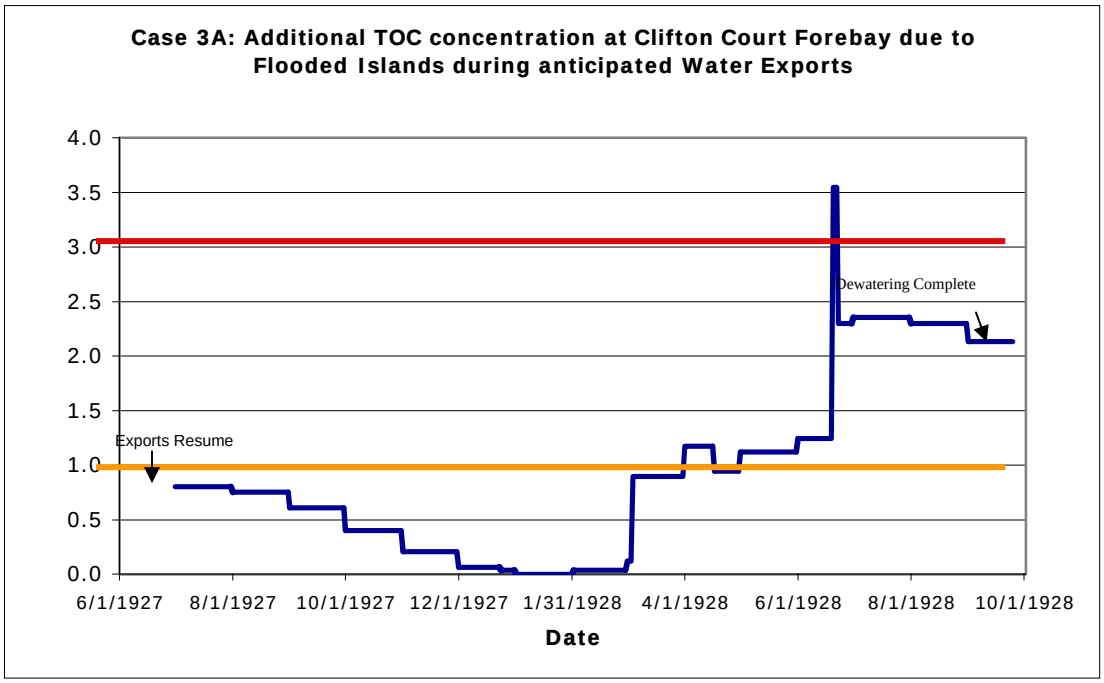

Figure I-6 Case 3A: Three islands with one breach each, additional islands damaged but not flooded (late spring event)

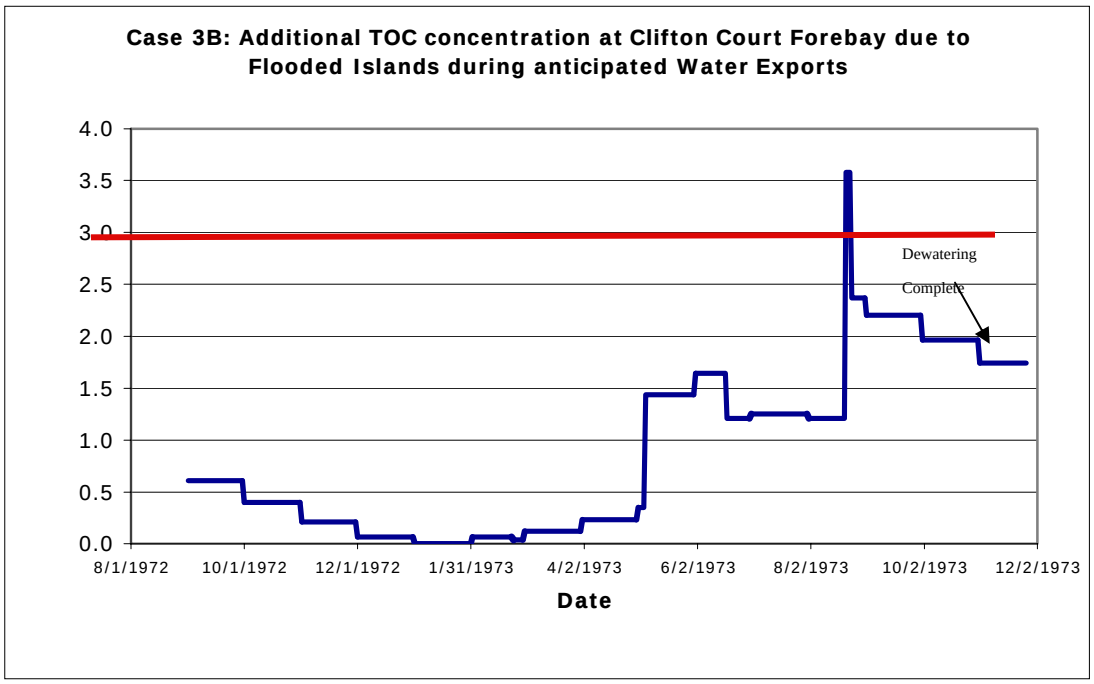

Figure I-7 Case 3B: Three islands with one breach each, additional islands damaged but not flooded (summer event)

Dewatering
Complete

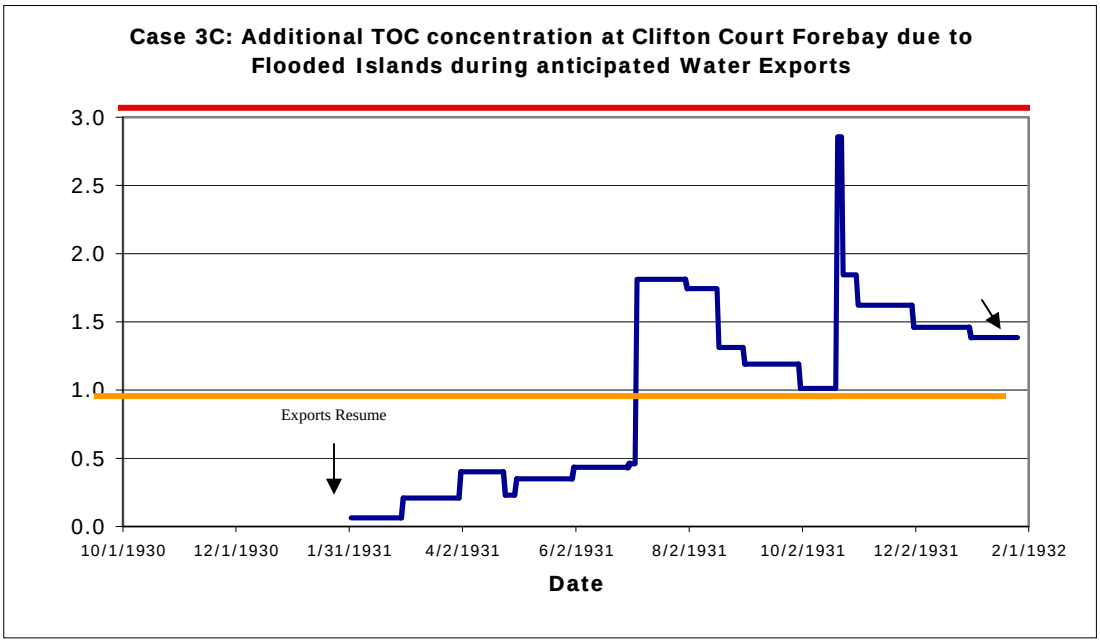

Figure I-8 Case 3C: Three islands with one breach each, additional islands damaged but not flooded (early fall event)

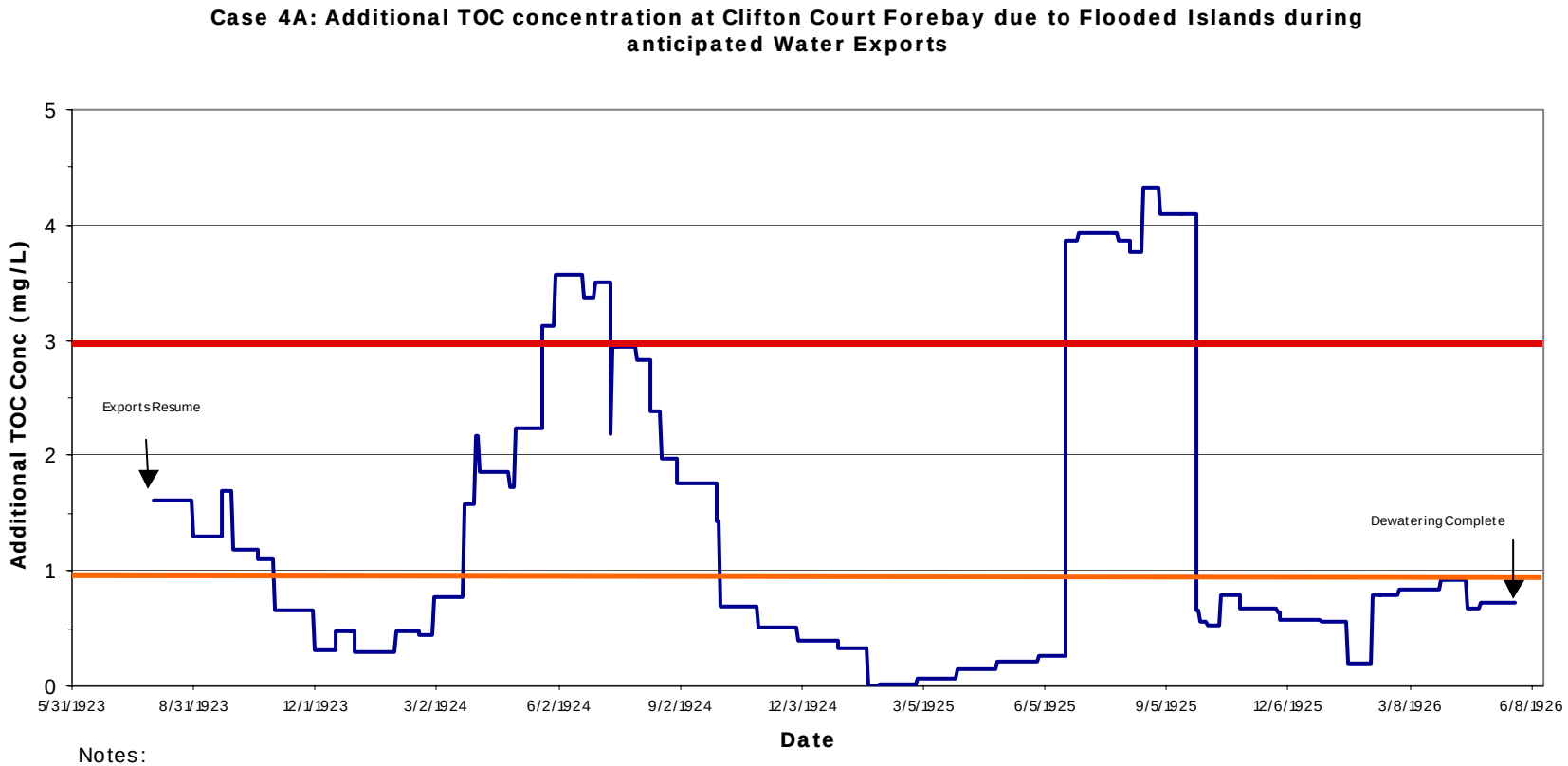

Notes:
Assumed background TOC concentration for Delta water is 3 mg/L. Higher background concentrations may occur during winter storm events. Treatment costs are associated with a TOC increase of 1 mg/L (orange line). Treatment goal is less then 4 mg/L TOC from all sources. Exports are potentially curtailed when additional TOC is greater then 3 mg/L (red line). Treatment by enhanced coagulation is effective up to a combined background and additional TOC concentration of 6 mg/L.

Figure I-9 Case 4A: Eleven levee breaches among ten Delta islands (late spring event)

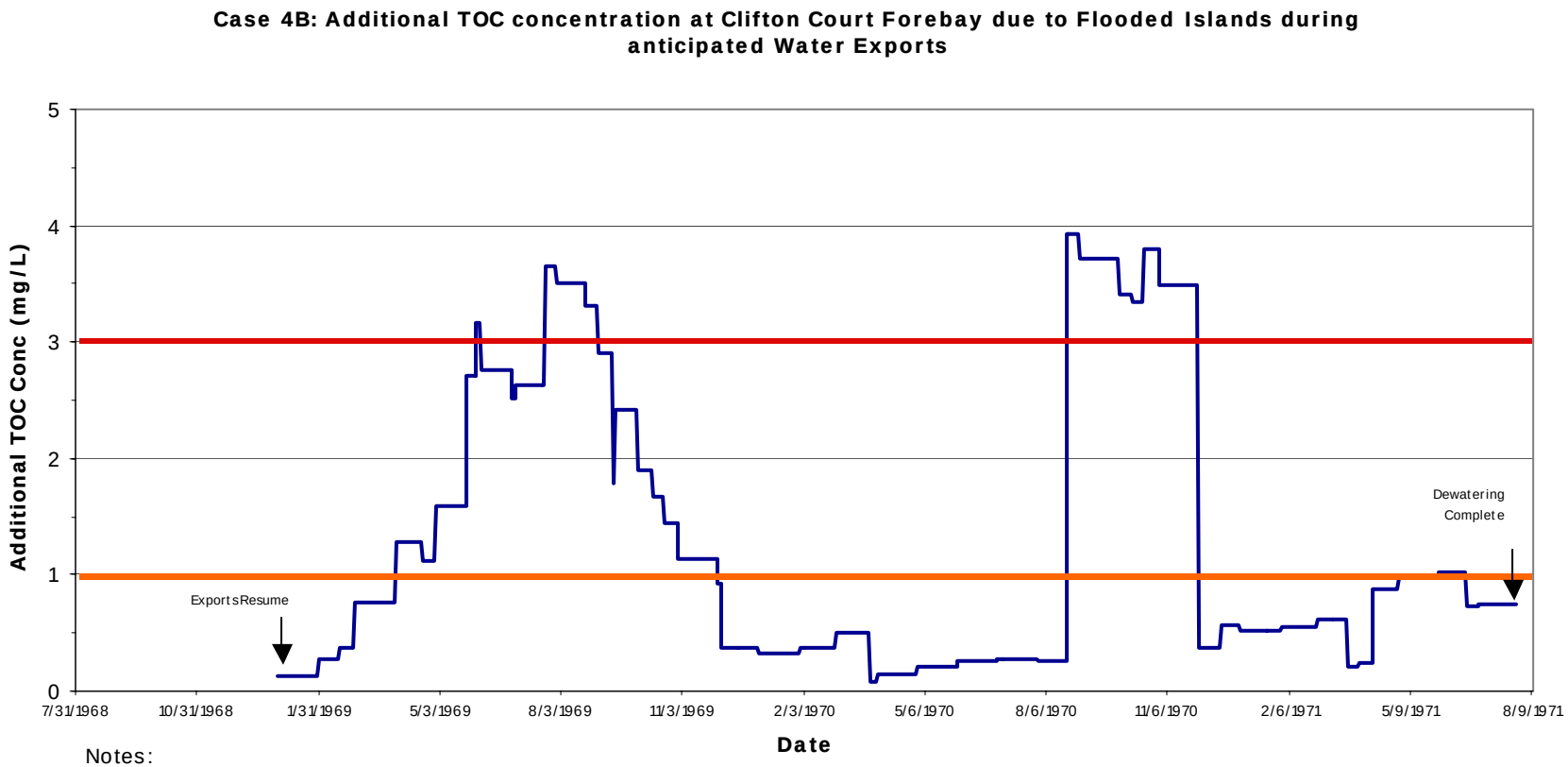

Notes:
Assumed background TOC concentration for Delta water is 3 mg/L. Higher background concentrations may occur during winter storm events
Treatment costs are associated with a TOC increase of 1 mg/L (orange line). Treatment goal is less then 4 mg/L TOC from all sources.
Exports are potentially curtailed when additional TOC is greater then 3 mg/L (red line). Treatment by enhanced coagulation is effective up to a combined background and additional TOC concentration of 6 mg/L.

Figure I-10 Case 4B: Eleven levee breaches among ten Delta islands (summer event)

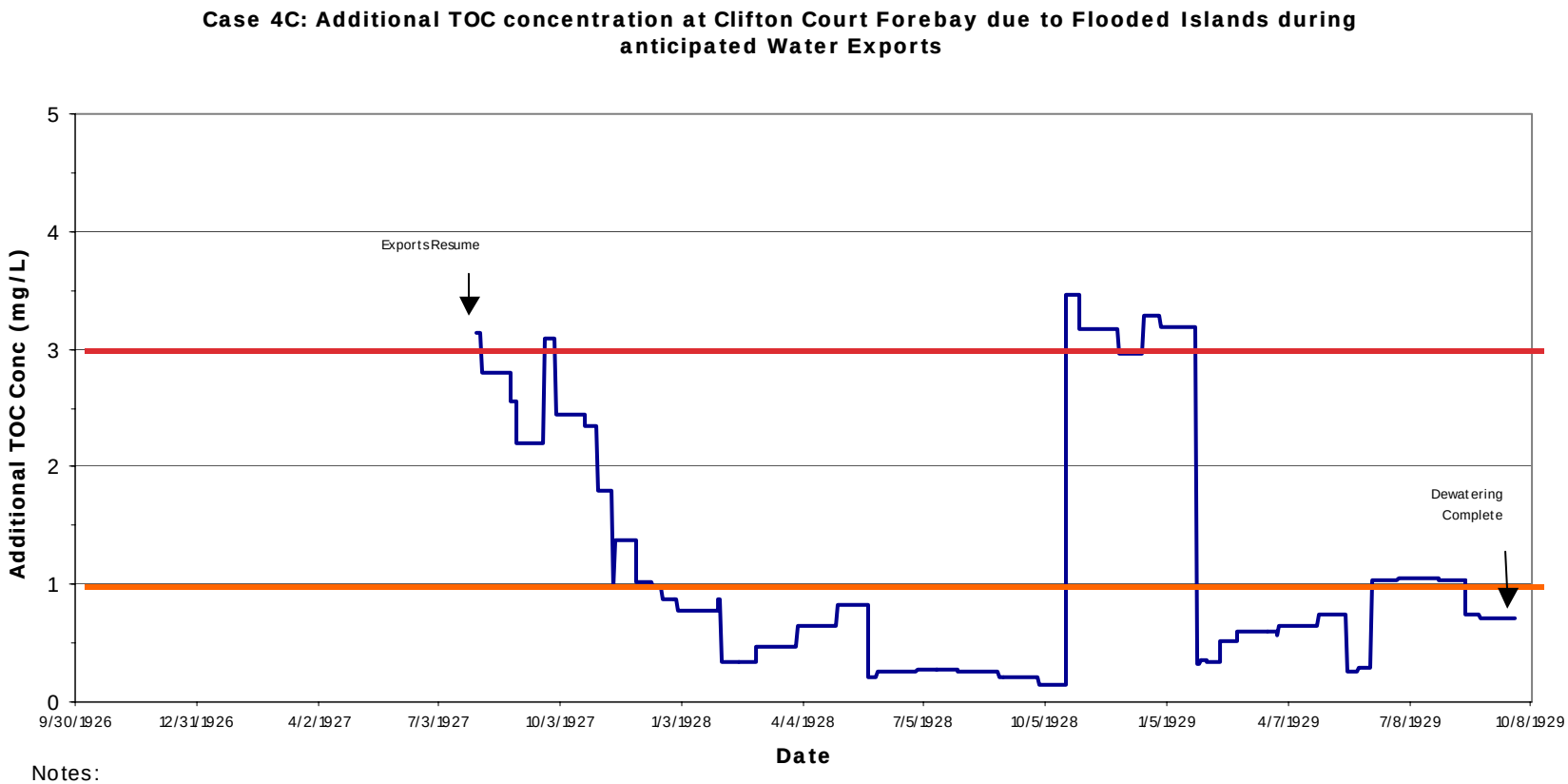

Notes:
Assumed background TOC concentration for Delta water is 3 mg/L. Higher background concentrations may occur during winter storm events. Treatment costs are associated with a TOC increase of 1 mg/L (orange line). Treatment goal is less then 4 mg/L TOC from all sources. Exports are potentially curtailed when additional TOC is greater then 3 mg/L (red line). Treatment by enhanced coagulation is effective up to a combined background and additional TOC concentration of 6 mg/L.

Figure I-11 Case 4C: Eleven levee breaches among ten Delta islands (early fall event)

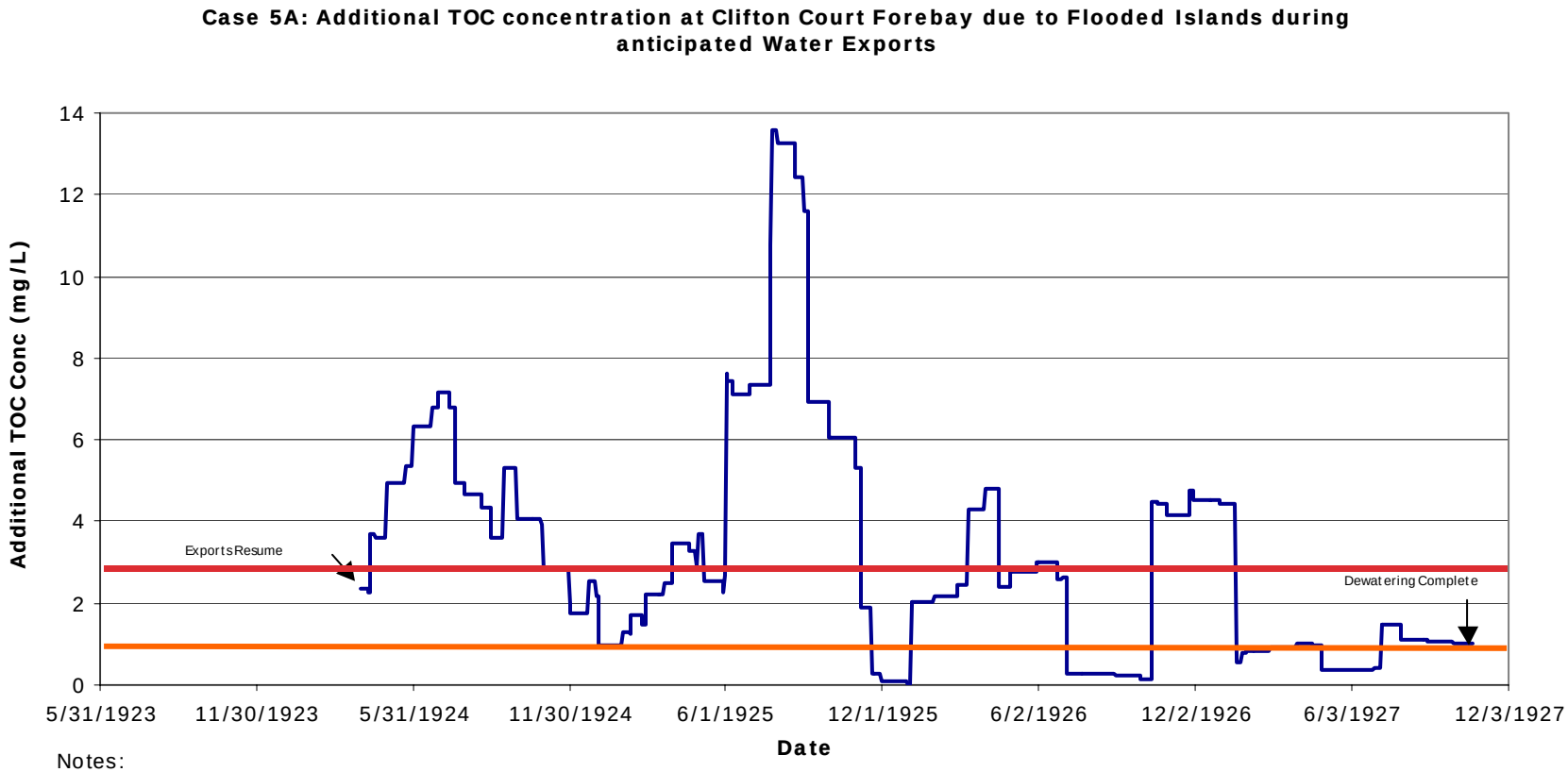

Notes:
Assumed background TOC concentration for Delta water is 3 mg/L. Higher background concentrations may occur during winter storm events. Treatment costs are associated with a TOC increase of 1 mg/L (orange line). Treatment goal is less then 4 mg/L TOC from all sources. Exports are potentially curtailed when additional TOC is greater then 3 mg/L (red line). Treatment by enhanced coagulation is effective up to a combined background and additional TOC concentration of 6 mg/L.

Figure I-12 Case 5A: Thirty-six levee breaches among twenty Delta Islands (late spring event)

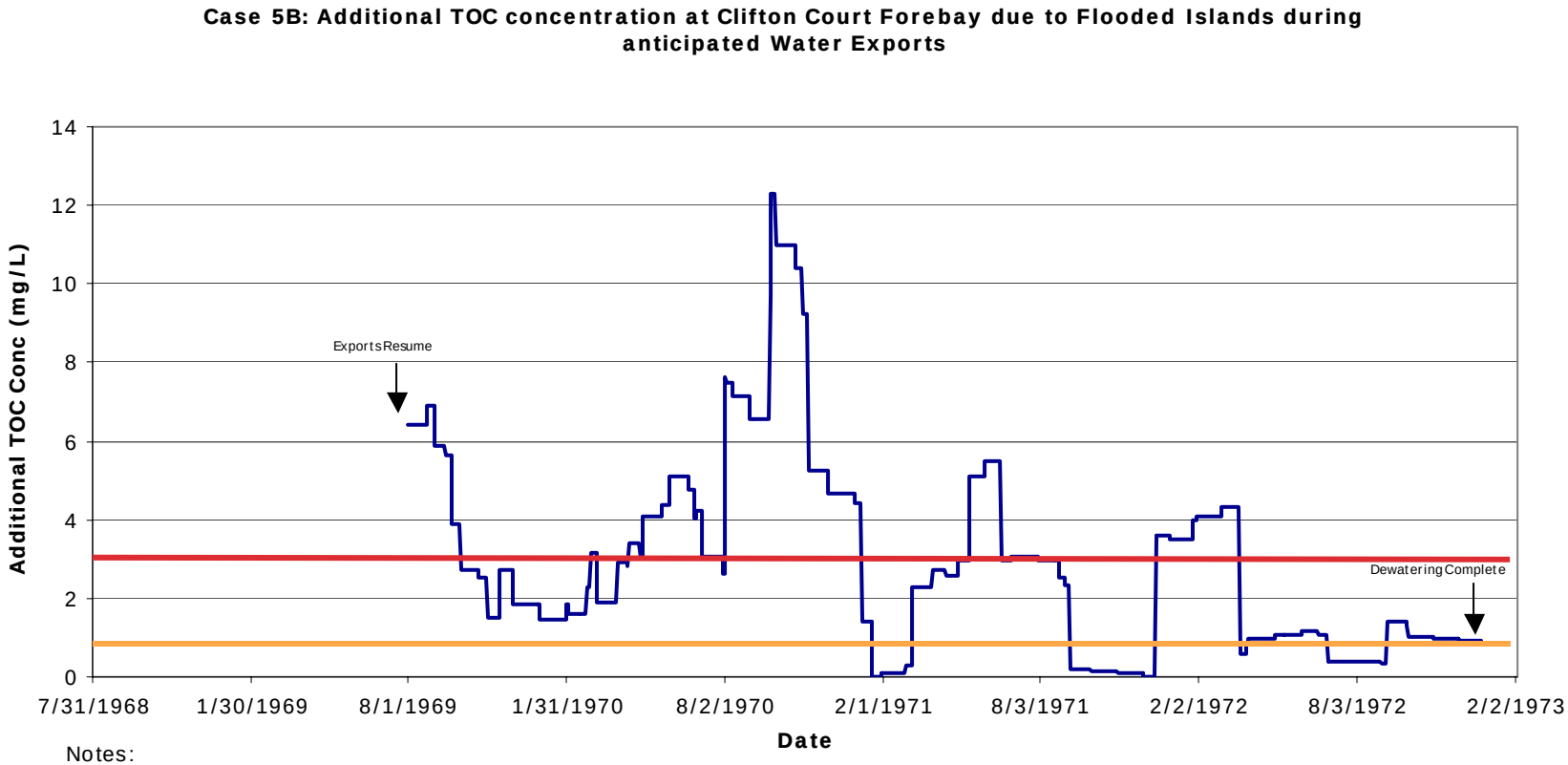

Notes:
Assumed background TOC concentration for Delta water is 3 mg/L. Higher background concentrations may occur during winter storm events. Treatment costs are associated with a TOC increase of 1 mg/L (orange line). Treatment goal is less then 4 mg/L TOC from all sources. Exports are potentially curtailed when additional TOC is greater then 3 mg/L (red line). Treatment by enhanced coagulation is effective up to a combined background and additional TOC concentration of 6 mg/L.

Figure I-13 Case 5B: Thirty-six levee breaches among twenty Delta islands (summer event)

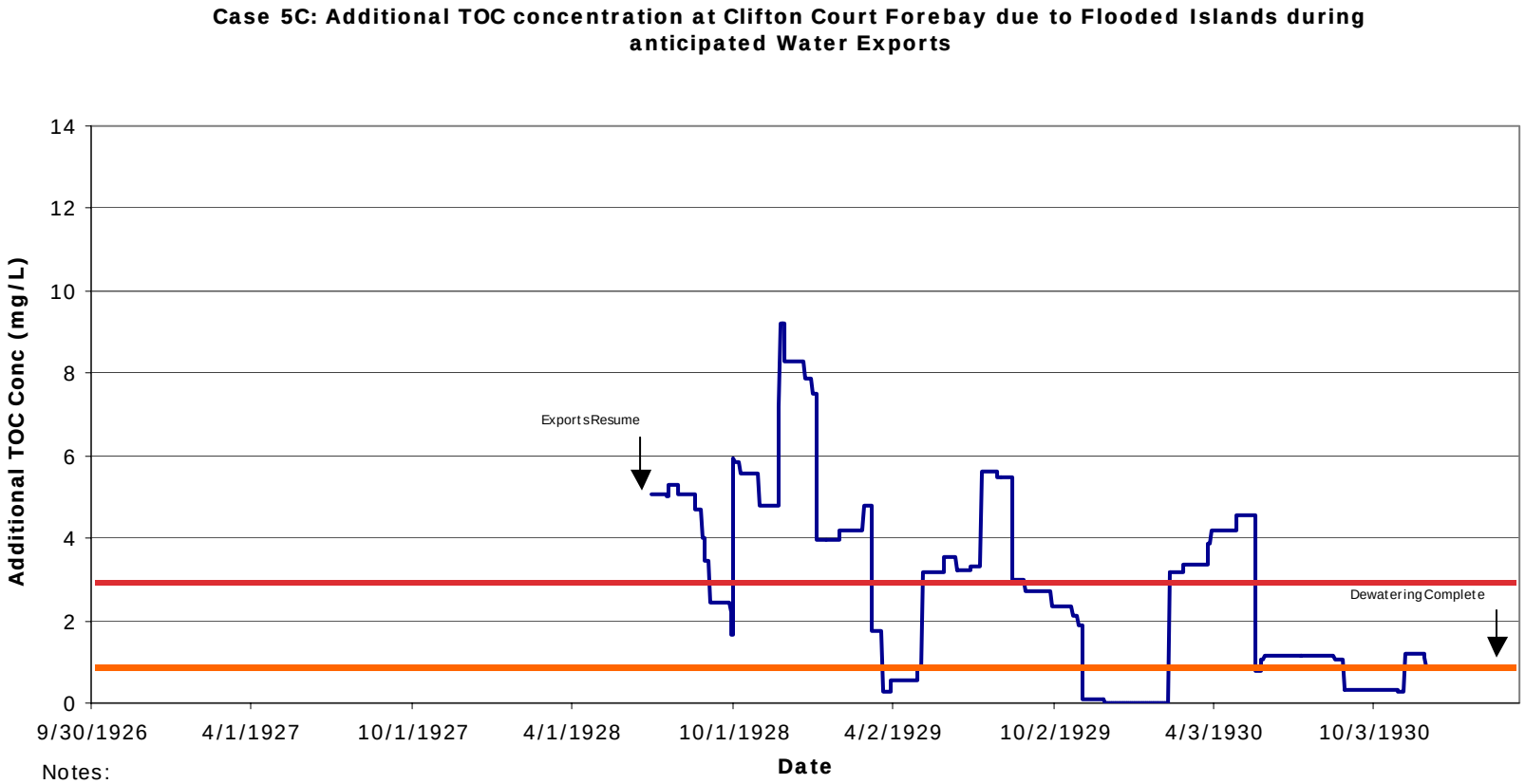

Notes:
Assumed background TOC concentration for Delta water is 3 mg/L. Higher background concentrations may occur during winter storm events. Treatment costs are associated with a TOC increase of 1 mg/L (orange line). Treatment goal is less then 4 mg/L TOC from all sources. Exports are potentially curtailed when additional TOC is greater then 3 mg/L (red line). Treatment by enhanced coagulation is effective up to a combined background and additional TOC concentration of 6 mg/L.

Figure I-14 Case 5C: Thirty-six levee breaches among twenty Delta islands (early fall event)

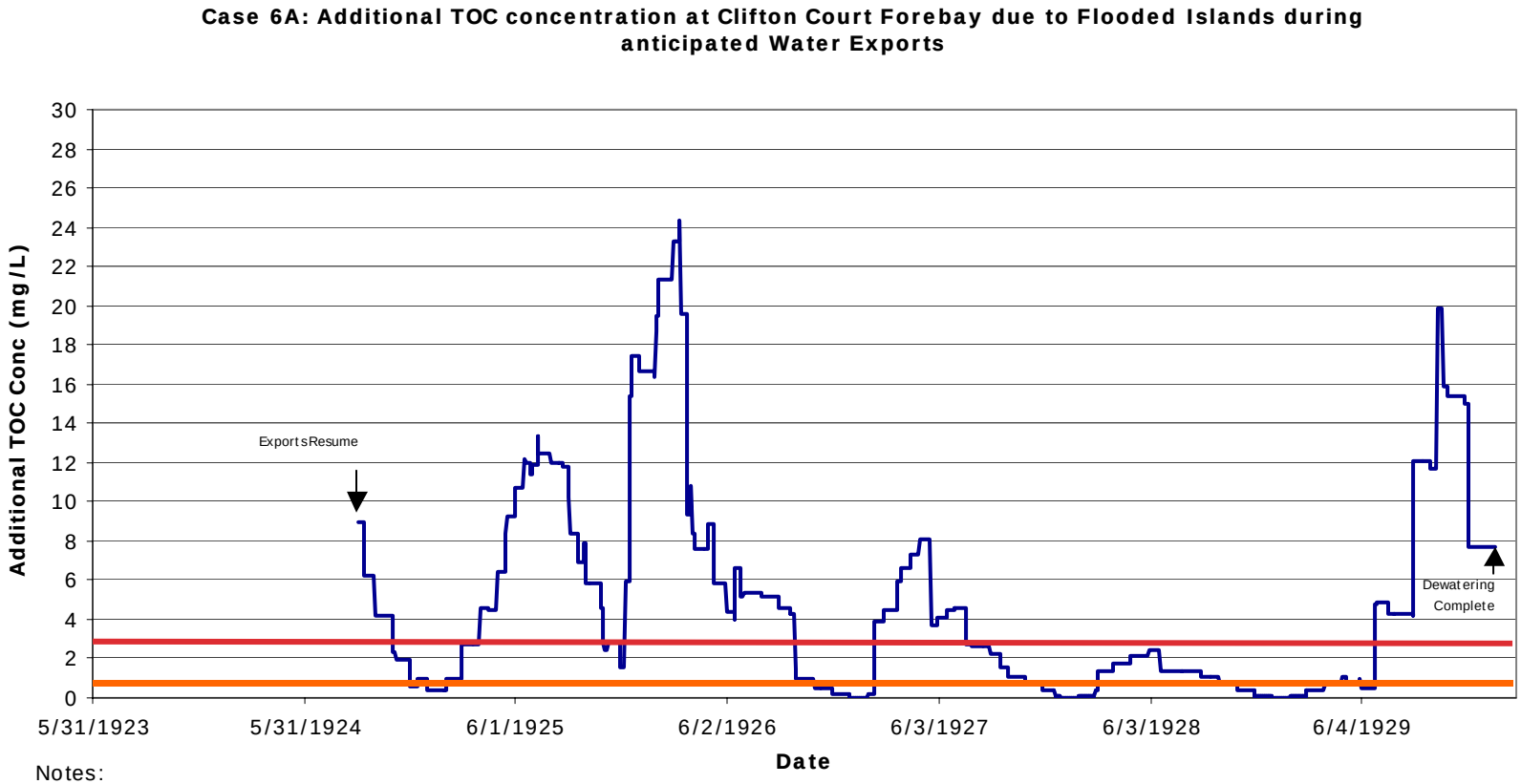

Notes:
Assumed background TOC concentration for Delta water is 3 mg/L. Higher background concentrations may occur during winter storm events. Treatment costs are associated with a TOC increase of 1 mg/L (orange line). Treatment goal is less then 4 mg/L TOC from all sources. Exports are potentially curtailed when additional TOC is greater then 3 mg/L (red line). Treatment by enhanced coagulation is effective up to a combined background and additional TOC concentration of 6 mg/L.

Figure I-15 Case 6A: Forty-six levee breaches among thirty Delta islands (late spring event)

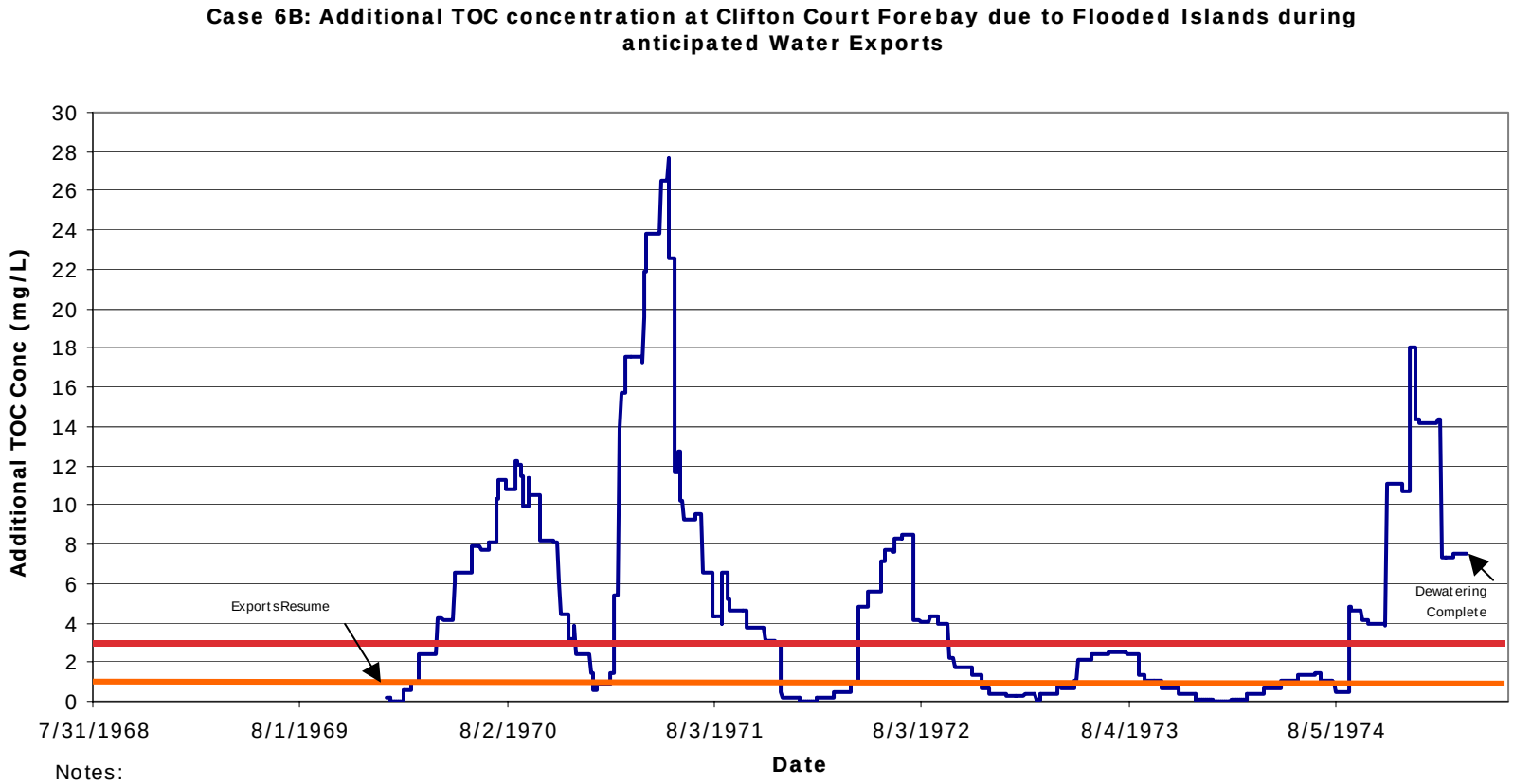

Notes:
Assumed background TOC concentration for Delta water is 3 mg/L. Higher background concentrations may occur during winter storm events. Treatment costs are associated with a TOC increase of 1 mg/L (orange line). Treatment goal is less then 4 mg/L TOC from all sources. Exports are potentially curtailed when additional TOC is greater then 3 mg/L (red line). Treatment by enhanced coagulation is effective up to a combined background and additional TOC concentration of 6 mg/L.

Figure I-16 Case 6B: Forty-six levee breaches among thirty Delta islands (summer event)

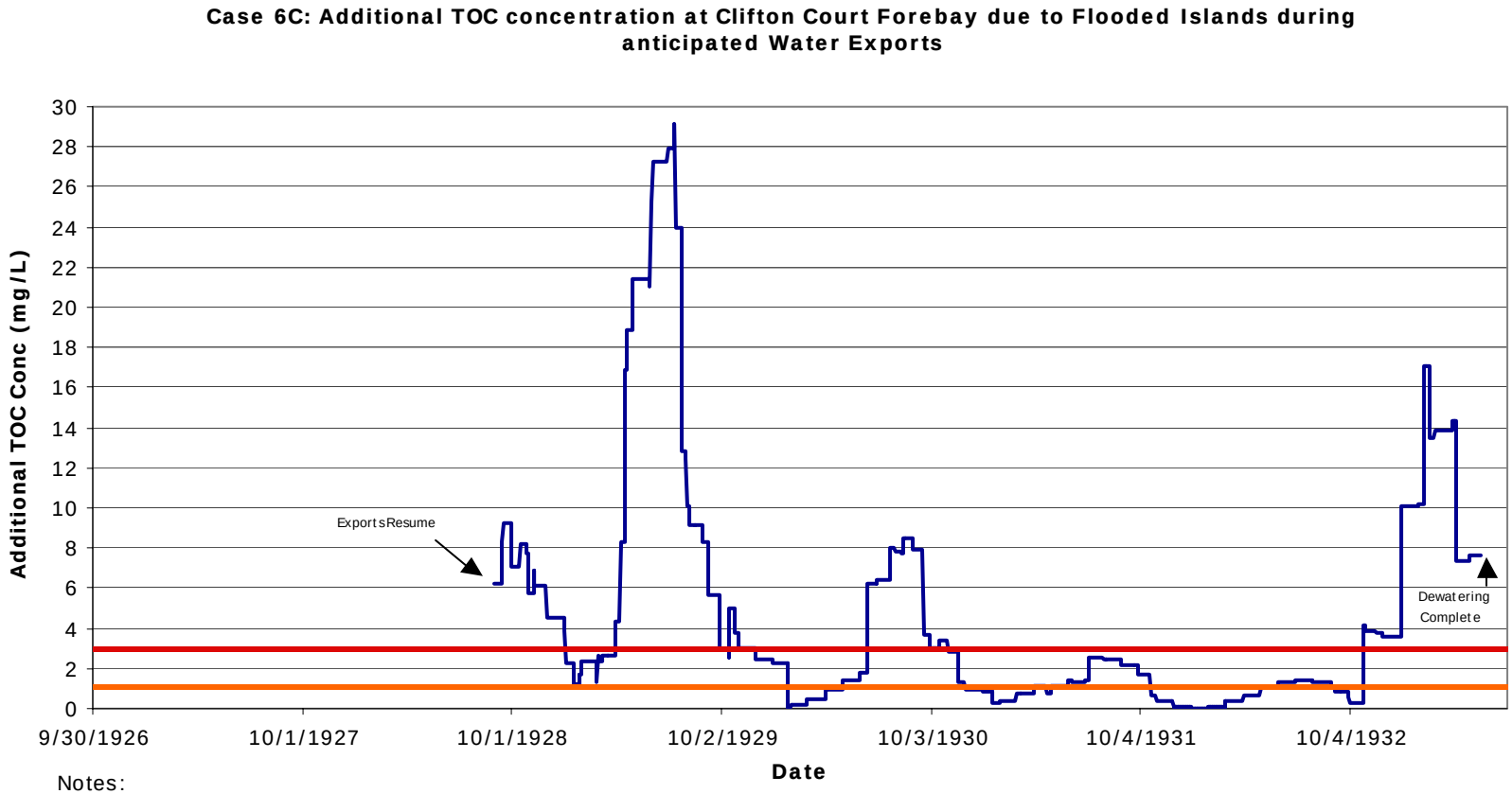

Notes:
Assumed background TOC concentration for Delta water is 3 mg/L. Higher background concentrations may occur during winter storm events. Treatment costs are associated with a TOC increase of 1 mg/L (orange line). Treatment goal is less then 4 mg/L TOC from all sources. Exports are potentially curtailed when additional TOC is greater then 3 mg/L (red line). Treatment by enhanced coagulation is effective up to a combined background and additional TOC concentration of 6 mg/L.

Figure I-17 Case 6C: Forty-six levee breaches among thirty Delta islands (early fall event)

I.6 Costs

The water treatment costs for excess organic carbon was provided by the Metropolitan Water District of Southern California. For a TOC concentration of 6 mg/L, the cost for enhanced coagulation is $18 per acre-foot. This cost is for enhanced coagulation operations and maintenance only, since Metropolitan has already made these capital investments. Enhanced coagulation operation and maintenance costs include chemical costs (coagulant and polymer) and solid handling.

A TOC concentration of 6 mg/L is considered very high and is at the upper end of the range of TOC concentrations that Metropolitan has historically observed in treatment plant influent. This cost was derived from actual treatment operations at Metropolitan's Mills treatment plant in Riverside, which treats 100% State Water Project water. If organic carbon concentrations were to occur above 6 mg/L for a sustained period of time (more than a month), additional capital investment would be required to reliably treat the water. Sustained TOC concentrations are less likely to be diluted during transport.

Table I-2 shows the water treatment costs associated with Delta water that has an additional 1-3 mg/L TOC at Clifton Court Forebay. The number of days associated with the possibility of additional export interruptions is also included. Water treatment costs were not estimated for additional TOC concentrations greater then 3 mg/L. Additional water treatment costs may occur if water is exported during this time. Costs associated with additional export interruptions were not quantified.

Table I-2 Estimated Costs Associated with Case 1 Through 6

Case	Possible Export Interruption (days)	Increases treatment due to TOC loading		
		Additional treatment needed (days)	Estimated Volume (acre-feet)	Estimated Treatment Cost
1	0	100	660,000	$12,000,000
2A	0	120	820,000	$15,000,000
2B	0	130	860,000	$15,000,000
2C	0	160	1,100,000	$19,000,000
3A	3	160	1,100,000	$20,000,000
3B	3	200	1,400,000	$25,000,000
3C	0	210	1,400,000	$25,000,000
4A	150	230	1,600,000	$28,000,000
4B	140	220	1,500,000	$27,000,000
4C	90	210	1,400,000	$25,000,000
5A	550	400	2,700,000	$49,000,000
5B	500	430	2,900,000	$53,000,000
5C	430	240	1,600,000	$29,000,000

Table I-2 Estimated Costs Associated with Case 1 Through 6

Case	Possible Export Interruption (days)	Increases treatment due to TOC loading		
		Additional treatment needed (days)	Estimated Volume (acre-feet)	Estimated Treatment Cost
6A	940	450	3,000,000	$54,000,000
6B	900	380	2,600,000	$47,000,000
6C	700	560	3,800,000	$68,000,000

Notes:

Cost is $18/acre-foot for enhanced coagulation operations and maintenance only.

Assumes that 50% of the combined SWP (Banks Pumping Plant) and CVP exports would be treated with enhanced coagulation when the additional island derived TOC is greater then 1 mg/L and less then 3 mg/L at Clifton Court Forebay.

Assumes an average annual intake of 4,927 TAF from Clifton Court Forebay (DWR 2005).

I.7 Conclusions

A simplified model was used to estimate the amount of organic carbon production for each island in the six cases described in the DRMS Phase 1 report. Scaling factors were then applied to estimate the amount of TOC that originated from the islands and was transported to southern Delta water export facilities. The increases in water treatment costs associated with enhanced coagulation were calculated to provide an order of magnitude cost estimate for water treatment due to organic carbon increases at drinking water intakes. Additional costs would be incurred to treat the sustained increases predicted by the model in Cases 4, 5, and 6. These additional costs could include additional capital improvements by drinking water treatment facilities or the costs related to additional water export interruptions.

Repair schedules could be modified to reduce the predicted magnitude and duration of TOC concentrations. The following factors contributed to a greater organic carbon impact at Banks Pumping Plant.

- Longer duration between levee repair and island pump-out.
- Several islands pumped during the same time period.
- Accelerated island pump-out rates.
- Larger island size.
- Closer distance between the flooded island and Clifton Court Forebay (with a net flow direction to the pumps).

Hydrodynamic modeling was not used for the transport of organic carbon from the islands to the Banks pumping plant. Particle tracking would decrease the amount of uncertainty associated with the dispersion and dilution of TOC.

I.8 References

Aguilar, L., and L. J. Thibodeaux. 2005. Kinetics of peat soil dissolved organic carbon release from bed sediment to water. Part 1. Laboratory simulation. Chemosphere 58:1309-1318.

Brown and Caldwell. 2005. CALFED Water Quality Program Assessment Report. Developed for the CALFED Bay-Delta Program. June. Access online at http://calwater.ca.gov/Programs/DrinkingWater/adobe_pdf/Initial_Assessment/WQP_Initial_Assessment_6_2005.pdf

Bureau of Reclamations (USBR). 2005. 2004 Water Accounting Reports. Federal-State Operations. Central Valley Project. U.S. Department of the Interior. January. Online at: http://www.usbr.gov/mp/cvo/pmdoc.html

Delta Protection Commission. 2002. Land Use and Resource Management Plan for the Primary Zone of the Delta. Regional Location Maps – Delta Atlas. Soils. May. Soils map online at: http://www.delta.ca.gov/atlas/soil.pdf

Department of Water Resources (DWR). 2005. California Water Plan Update 2005. Sacramento-San Joaquin Delta Region. Bulletin 160-05. Volume 3, Chapter 12. December.

Department of Water Resources (DWR). 2007. Water Data Library (WDL) Water Quality Data. Clifton Court Intake. Access online at http://wdl.water.ca.gov/includes/station_details.cfm?qst_id=10

DuVall, R. et al. 2005. Jones Tract Flood Water Quality Investigations. Municipal Water Quality Investigations Program. Division of Environmental Services. Department of Water Resources. Draft Report. October.

Fujii, R. Ranalli, A.J., Aiken, G.R., and B.A. Bergamaschi. 1998. Dissolved Organic Carbon Concentrations and Compositions, and Trihalomethane Formation Potentials in Waters from Agricultural Peat Soils, Sacramento-San Joaquin Delta, California: Implications for Drinking-Water Quality. Water-Resources Investigation Report 98-4147. U.S. Geological Survey. Prepared in cooperation with the California Department of Water Resources.

Thibodeaux, L. J., and L. Aguilar. 2005. Kinetics of peat soil dissolved organic carbon release to surface water. Part 2. A chemodynamic process model. Chemosphere 60:1190-1196.

URS/JBA. 2007. Delta Risk Management Strategy (DRMS) Phase 1 Draft Risk Analysis Report. URS Corporation and Jack R. Benjamin & Associates, Inc., April.